Docetaxel Nanostructured lipid carrier with enhanced blood brain barrier permeability for targeted glioblastoma therapy

By

Tamara Zwain

A thesis submitted in partial fulfilment of the requirements for the degree of Doctor of Philosophy at the University of Central Lancashire

October 2018

University of Central Lancashire

STUDENT DECLARATION FORM

Concurrent registration for two or more academic awards

I declare that while registered as a candidate for the research degree, I have not been a registered candidate or enrolled student for another award of the University or other academic or professional institution

---

Material submitted for another award

I declare that no material contained in the thesis has been used in any other submission for an academic award and is solely my own work

---

Collaboration

Where a candidate's research programme is part of a collaborative project, the thesis must indicate in addition clearly the candidate's individual contribution and the extent of the collaboration. Please state below:

Signature of Candidate ________________ Tam

Type of Award _________**PhD**_______________

School ________**School of Pharmacy and Biomedical Sciences**____________

Abstract

The major clinical challenge in the treatment of glioblastoma is the inability of chemotherapeutic agents to pass the blood-brain barrier (BBB). Docetaxel a hydrophobic anticancer drug used alone and in combination with other drugs to treat tumours is a P-glycoprotein substrate and suffers from the drawback of non-specific cytotoxicity and limited accumulation in the brain. To address these clinical challenges and enhance therapeutic potential for glioblastoma treatment and penetration of BBB, the project investigated nanostructured lipid carrier (NLC) for encapsulation of docetaxel and explored two polyunsaturated fatty acids (PUFAs) gamma-linolenic acid (GLA) and Alpha-linolenic acid (ALA), and a novel selective aptamer (SA43) as targeting ligands for specific glioblastoma targeting.

A novel, simple and sensitive HPLC method was developed and validated for quantification of docetaxel from BBB cell culture medium. The method exhibited high precision and accuracy with sample recovery ranging from 90.03- 100.02% and was used to determine the permeated drug in the 3D *in-vitro* BBB model. Validated HPLC methods with high precision and accuracy were also developed for quantification of docetaxel from the NLCs and release media. Docetaxel-NLC were formulated using biodegradable materials combining Dynasan 114 as solid lipid with three liquid lipids and surfactants employing hot homogenisation technique on probe sonicator. A 3^2 factorial design was used for optimisation of critical factors to get docetaxel-NLCs with particles size (136.8 nm), relatively low polydispersity index (PDI 0.231), high entrapment efficiency (99.1%) and high total drug content (80.6%) with zeta potential of -32.4 mV contributing to the stability of the docetaxel-NLC over a six months period. Docetaxel-NLCs was successfully lyophilised with an only a small increase in particle size (13nm) using 10% trehalose as a cryo-protectant. All three ligands (GLA, ALA and SA43) were successfully conjugated to Docetaxel-NLCs and covalent bonding was confirmed with reduction of surface free amines, FTIR and Raman spectroscopy. DSC and XRD confirmed the presence of docetaxel in an amorphous state within the NLCs.

In-vitro cell lines studies revealed the high efficacy of PUFAs surface modified docetaxel-NLCs (GLA-docetaxel-NLC and ALA-docetaxel-NLC) where IC_{50} showed ~ 6.5 fold increase in docetaxel activity at 24h towards glioblastoma (U87MG) cells and ~ 10 fold higher cytotoxicity in patient-derived short-term culture obtained from Brain Tumour North West organisation (BTNW911) glioblastoma cells at 24 and 48 h. Aptamer surface modified docetaxel-NLC (SA43-docetaxel-NLC) showed high selectivity towards glioblastoma cell lines with high potency as compared to non-cancerous brain cells (SVG P12) with a preferable lower toxicity. Moreover, all developed formulations showed significantly higher cellular uptake by U87MG and BTNW911 cells as compared to SVG P12 cells. Active transport through endocytosis was determined as the internalisation mechanism for the all surface modified docetaxel-NLCs. Furthermore, bare and surface modified docetaxel-NLCs exhibited cell cycle arrest at G2/M phase with the highest percentage of distribution in G2/M phase obtained with SA43-docetaxel-NLCs. Docetaxel-NLC also showed high toxicity and penetration in 3D U87MG spheroids in comparison to native docetaxel though surface modification of docetaxel-NLCs did not enhance the uptake by 3D U87MG spheroids.

Docetaxel encapsulation within the NLCs exhibited enhanced permeability when studied in all human 3D *in-vitro* BBB model. Notably, functionalisation of docetaxel-NLC with GLA and ALA further enhanced the permeation across the BBB while SA43-docetaxel-NLC displayed similar permeability as docetaxel-NLC. Distinctive increase in the apparent permeability through the BBB and uptake by U87MG cells was observed for all the surface modified docetaxel-NLCs when studied in diseased *in-vitro* BBB model in the presence of a tumour monolayered cell line (U87MG).

The aforementioned research has demonstrated that docetaxel-NLCs is a viable potential product for use in the treatment of glioblastoma, exhibiting selective uptake and BBB permeability when conjugated with appropriate targeting ligands. This research could contribute widely to treating and targeting brain tumour.

Acknowledgement

I would like to acknowledge with sincere appreciation my director of study Professor Kamalinder Singh and co-supervisor Dr Jane Alder for excellent scientific guidance, advice, support, and encouragement throughout my research. Working with you both was an amazing experience, you have made me become a better researcher and hopefully in the future a successful academic.

I would like to express my gratitude and special thanks to my father Dr Akeel Zwain. I could never reach this far without your support in every possible way, you are my role model. To my mother and aunt Wedad, you both are amazing and supportive, and I am so lucky to have such wonderful people in my life. Thank you for your prayers and Duaa.

To my sweet husband and love of my life Ali Al-Janabi, I am really lucky to have such a thoughtful person. Thank you for your support, love and understanding. You are an amazing person and a wonderful husband.

I would also like to thank Dr Lisa Shaw and Dr Clare Lawrence for a valuable project related advise, Dr Mohamed Alhnan, Dr Abdullah Israb and Dr Timothy Snape for their help in analytical interpretation, Dr Julie Burrows for her excellent training and support, Dr Sarah Dennison, Dr Izabela Stasik and Dr Enoche Oga for always helping out and encouraging me during my research, Dr Tim Dawson and Kate Ashton from the BTNW team for providing samples used in my research. Professor Jai Singh for his continuous advice and support.

My sincere admiration and appreciation for my friends, Dr Tanem Garanti, thank you so much for being there for me and supporting me during my research and beyond, and also, I would like to thank Dr Canras Batunlu. I would like to thank Dr Noorhan Sabah, my sweet and faithful friend you are my hero. Dr Zena Sabah and Dr Karawan Ali, I am so grateful for everything you have done for me and for encouraging me during my research. A special thanks to my friends Vicky Metcalfe, Zenab Butt, Mehak, Dr Swati Kumar, Dr Saurabh Prabhu, Dr Manar Hameed and Dr Sura Nomaan for their support and encouragement.

I would like to thank my family and especially my youngest brother Dr Ahmed Zwain, for their help, encouragement and support. Finally, I would like to Thank Allah for this great opportunity and wonderful blessings.

Contents

list of Figures

Figure number **Page number**

Chapter one

Chapter two

Chapter three

Chapter four

Chapter five

List of Tables

Tables **Page number**

Chapter one

Chapter two

Chapter three

Chapter four

Abbreviations

3D	Three dimensional
ABC	ATP-binding cassette
ALA	Alpha-linolenic acid
AP	Ascorbyl Palmitate
Apo-E	Apo-lipoproteins
AUC	Area under the curve
B	Batch
BBB	Blood-brain barrier
BCRP	Breast cancer resistance protein
BSA	Bovine serum albumin
BT	Brachytherapy
BTNW	Brain Tumour North West
CD36	Fatty acid translocases
CNS	Central nervous system
CPGMC	Capryol propylene glycol monocaprylate
Cyto. B	Cytochalasin B
D114	Dynasan 114
DC	Drug content
DCM	Dichloromethane
DL	Drug loading
DMSO	Dimethyl sulphoxide
DNA	Deoxyribonucleic acid
DSC	Differential scanning calorimetry
DTX	Docetaxel
EBD	Evans blue dye
EDC	1-Ethyl-3-(3-dimethylaminopropyl) carbodiimide
EE	Entrapment efficiency
EMA	European Medicines Agency
EMEM	Eagle's minimal essential medium
EPR	Enhanced Permeation and Retention
EVOM-2	Epithelial Voltohmmeter
FABPs	Fatty acid binding proteins
FAGs	Free amino groups
FBS	Foetal bovine serum
FD	Free (unentrapped) drug concentration
FDA	Food and Drug Administration
FR	Flow Rate
FTIR	Fourier-Transform Infrared Spectroscopy
GB	Glioblastoma multiforme
GLA	Gamma linolenic acid
GLU	Glucose transporters
GSCs	Glioblastoma stem cells
Gy	Gray
HS	Human serum albumin
Temp	Temperature
HBMEC	Human microvascular endothelial cells
HBSS	Hank’s balanced salt solution
HBVP	Human brain vascular pericytes
HCL	Hydrochloric acid

HDL	High-density lipoprotein
HPH	High-pressure homogeniser
HPLC	High-performance liquid chromatography
HS	Human serum
HSH	High-speed homogeniser
IC_{50}	Inhibition concentration 50%
ICH	International Conference on Harmonization
IDH	Isocitrate dehydrogenase
IS	Internal standard
IV	Intravenous injection
L.L	Liquid lipid
LB	Labrasol
LDL	Low-density lipoproteins
LE80	Lipoid E80
LG90	Lauroglycol 90
LOD	Limit of detection
LOQ	Limit of quantification
LS75	Lipoid S75
LV	L-valine
MG	Miglyol 812N
MP	Mobile phase
MDR	Multidrug resistance
MFI	Mean fluorescence intensity
MRPs	Multidrug resistance-associated proteins
MS	Multiple sclerosis
NEAA	Non-essential amino acid
NHA	Normal human astrocytes
NHS	N-hydroxysuccinimide
NICE	UK National Institute of Clinical Excellence
NLCs	Nanostructure lipid carrier
NPs	Nanoparticles
Ntd	Nitrendipine
OATPs	Organic anion transporting polypeptides
OCTs	Organic cation transporters
OFAT	One factor at a time
P188	Poloxamer188
P407	Poloxamer407
Papp	Apparent permeability
PBS	Phosphate buffered saline
PCS	Photon correlation spectroscopy
PDI	Polydispersity index
PEG	Polyethyleneglycol
PEI	polyethyleneimine
PFD	paraformaldehyde
Pg-p	P-glycoprotein
PH90	Phospholipon H90
PPARs	Peroxisome proliferator-activated receptors
PS	Particle size
PTX	Paclitaxel
PUFAs	Polyunsaturated fatty acids
R123 or R	Rhodamine123
RES	Reticuloendothelial system
RFU	Relative fluorescent units

RHB	Ringer HEPES buffer
ROS	Reactive oxygen species
RSD	Relative standard deviation
RT	Retention time
S HS15	Soultol HS15
S.L	Solid lipid
SC	Sodium Cholate
SD	Standard deviation
SDS	Sodium Dodecyl Sulphate
SELEX	Systematic evolution of ligands by exponential enrichment
SEM	Scanning electron microscopy
SFEE	Supercritical fluid extraction of emulsions
SLNs	Solid lipid nanoparticles
SPSS	Statistical Package for the Social Sciences
SRS	Stereotactic radiosurgery
T80	Tween 80
TCAA	Trichloracetic acid
TD	Total drug
TEER	Trans endothelial electrical resistance
TfR	Transferrin receptor
TGA	Thermogravimetric analysis
THF	Tetrahydrofuran
TJs	Tight junctions
TMZ	Temozolomide
TNBS	Trinitrobenzene sulfonic acid
TPGS	Tocopheryl polyethene glycol
Ultra-S	Ultra-sonication
VEGF	Vascular endothelial growth factor
Vit E.	Vitamin E
VLDL	Very low-density lipoprotein
WHO	World Health Organisation
XRD	X-ray diffractometer
ZP	Zeta potential

Chapter One

Introduction

1.1. Brain tumour

A brain tumour is a disease in which cells grow uncontrollably in the brain. Brain tumours can be broadly categorised into two types, benign and malignant. First, benign tumours are unable to spread beyond the brain, itself. It is not essential for benign tumours in the brain to be treated and progress is often self-limited. Sometimes benign tumours can progress to malignant brain tumours or cause complications because of the position but surgery or radiation can be helpful. Second, malignant tumours are typically called brain cancer. These tumours can extend outside of the brain (Abinaya *et al.,* 2017).

Malignant brain tumours represent some of the most devastating diagnoses a clinician may ever deliver to a patient. There are over 130 different types of brain tumours, but the most common malignant tumours of the brain are glioblastomas, accounting for over 80% of all primary brain malignancies (Ostrom *et al.,* 2015; Osswald *et al.,* 2015). These cancers are aggressive, invasive, and destructive tumours, considered among the deadliest forms of human cancers (Maher *et al.,* 2001).

1.2. Glioblastoma

Glioblastoma (GB) is a general term used to characterise a tumour that originates from glial brain cells that represent a heterogeneous group of malignancies of the central nervous system (Hands *et al.,* 2014). Approximately 50% of primary brain tumours are GBs (Louis *et al.,* 2007).

There are three main cell types of glial origin with the potential to produce tumours. These include astrocytes leading to astrocytomas (including glioblastomas), oligodendrocytes giving rise to oligodendrogliomas, and ependymal cells forming ependymomas. Recent advances have rendered this method of classification obsolete, and the World Health Organisation (WHO) 2016 4th edition classification standards include further separation of the subsections based on molecular and genetic traits (Louis *et al.,* 2016).

1.2.1. Glioblastoma classifications and grades

Pre-2016 literature, the classification of tumours of the central nervous system (CNS), according to WHO 2007, was largely based on histological concepts, where tumours were classified according to microscopic similarities with different putative cells of origin and presumed levels of differentiation (Louis *et al.,* 2007). At present, glioblastomas are classified by cell type, location, grade, and molecular markers according to updated 2016 WHO guidelines.

Recently, many subtypes of glioblastomas were categorised by distinct molecular markers and graded by clinical, histological and molecular appearance as defined (Louis *et al.,* 2016). The molecular characterisation and the presence of isocitrate dehydrogenase (IDH) mutation and 1p/19q (codeletion of chromosome arms 1p for petite, small arm of the chromosome and the 19q for chromosome arm 19) codeletion were included and reported by Louis *et al.,* (2016). In this new classification, the histologic subtype of grade II mixed oligoastrocytoma has also been eliminated. Now, the genotype plus phenotype is used to define these tumours (Louis *et al.,* 2016).

Glioblastomas that has progressed from lower grade diffuse or anaplastic astrocytomas is now identified as IDH mutants (Louis *et al.,* 2016; Ohgaki and Kleihues, 2013; Ohgaki *et al.,* 2014). IDH sequencing is recommended for distinguishing glioblastomas, if immunohistochemistry for mutant R132H IDH1 protein and sequencing for *IDH1* codon 132 and *IDH2* codon 172 gene mutations are both negative, or if sequencing for *IDH1* codon 132 and *IDH2* codon 172 gene mutations alone is negative, then the lesion can be diagnosed as IDH-wildtype (Louis *et al.,* 2016). The classification of diffuse glioblastomas was based on both phenotype and genotype expressed in a number of ways (Figure 1.1). Grading a glioblastoma biopsy by a neuropathologist is the most important classification for determining the overall severity of malignancy. Generally, low-grade glioblastomas (WHO Grade I and II) are slower growing and are associated with better prognosis, while a high-grade glioblastoma (WHO Grade III or IV) grow faster and have a poor prognosis (Louis *et al.,* 2016). In this project grade III and IV of GBs were chosen for the study due to the patient outcome since it is the most common and aggressive grades.

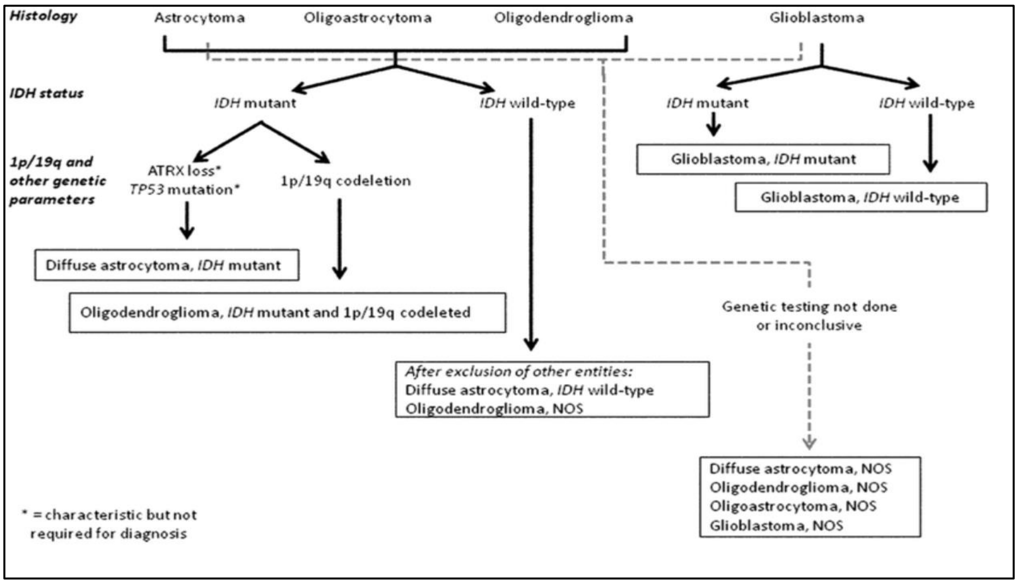

Figure 1.1 Classification of the glioblastomas based on histological and genetic features (Louis et al., 2016).

1.2.2. Glioblastoma incidence and survival rates

Glioblastoma is the most common primary malignant brain tumour among the adult population, making up 46% of all the malignant brain and central nervous system tumours and 15% of all primary brain tumours (Ostrom *et al.,* 2015). It is almost always fatal in adults (Khan *et al.,* 2009). Patients with GBs have a life expectancy of six to four months after diagnosis (Brodbelt *et al.,* 2015). The median life expectancy for patients with GB is in the range of 12-15 months, dropping to 3-5 months in older patients > 70 years old (Brodbelt *et al.,* 2015). Reasons, for decreased life expectancy with age are probably multi-factorial, including aggressive tumour biology, under-treatment and co-morbidities and frailty reducing treatment tolerance.

There were 10,743 patients registered with GBs in England from 2007 to 2011 (6451 male, 4292 female), giving an overall national incidence of 4.64/100,000/year. Incidence increases with age. One, two and five-year survivals, were 28.4%, 11.5% and 3.4% respectively. Age-stratified median survivals decreased significantly ($p < 0.0001$) with increasing age from 16.2 months for the 20–44-year age group, to 7.9 months for the 45–69 years, and 3.2 months for 70+ years. In the maximal treatment subgroup, patients aged up to 69 years had a median survival of 14.9 months. Patients over 60 years were less likely to receive maximal combination treatment, but median survival was better with a maximal treatment at all ages (Brodbelt *et al.,* 2015).

1.2.3. Glioblastoma treatment

Treatment for GB and its histological variants typically involves radiation and chemotherapy using temozolomide (TMZ) (Stupp *et al.,* 2005; Karsy *et al.,* 2012). High-grade glioblastomas are particularly insensitive to radiation and genotoxic drugs (Mehta *et al.,* 2011). Therapeutic effect of glioblastoma is often limited due to the low permeability of delivery systems across the blood-brain barrier (BBB) and poor penetration into the tumour tissue (Xin *et al.,* 2012). Moreover, drug penetration is only one of several major challenges (Preusser *et al.,* 2011). GB is a grade IV brain tumour characterised by a heterogeneous population of cells that are highly infiltrative, angiogenic and resistant to chemotherapy (Alves *et al.,* 2011), also the presence of GB stem cells (GSCs) is another cause of GB heterogeneity (Jiang *et al.,* 2017). GSCs are highly resistant to current cancer treatments, which ultimately fail in GB treatment because they do not eliminate GSCs, which survive to regenerate new tumours (Alves *et al.,* 2011).

1.2.3.1. Surgical intervention

Surgery is the first-line therapy for glioblastoma, however, glioblastomas recur in the resection margins of 90% of patients (Hamard *et al.,* 2016). Surgical intervention is essential for the initial treatment of GB. The surgery, ranging from biopsy to subtotal resection to gross-total resection, can affect overall patient survival (Anton *et al.,* 2012; Urbanska *et al.,* 2014). Although surgical resection can greatly reduce tumour bulk, complete excision is virtually impossible due to the infiltrative nature of these tumours (Venkatesh *et al.,* 2015; Price *et al.,* 2012).

1.2.3.2. Chemotherapy treatment

Chemotherapy is the most common treatment option for recurrent malignant glioblastomas (Kreisl 2009; Combs *et al.,* 2005). Although traditionally reserved for treatment of recurrent GB, chemotherapy agents such as temozolomide and carboplatin have shown a wide range of efficacy, either when administered alone or as a supplement to cytoreductive surgery (Karsy *et al.,* 2012).

To treat the infiltrating tumour cells, there has been much interest in using local therapies inserted at the time of surgery. Carmustine wafers (Gliadel®) are biodegradable polymers that release 7.7 mg of carmustine over a few weeks directly into the resection cavity. A phase III study in patients, which were newly diagnosed with high-grade glioblastomas showed that carmustine wafers were well tolerated and associated with a survival advantage (Westphal *et al.,* 2003). Guidelines were developed according to the UK National Institute of Clinical Excellence (NICE) for people with brain and other CNS tumours (NICE, 2006). NICE issued guidance and recommended the use of carmustine wafers as an option for the treatment of newly diagnosed high-grade glioblastomas (WHO Grade III and IV) (NICE Technology Appraisal Guidance TA121, NICE 2007). The NICE 2016 recommendation has been updated and reviewed in March 2016, the NICE technology appraisal guidance TA23 on carmustine implants and temozolomide for the treatment of newly diagnosed high-grade glioblastoma (NICE 2016).

1.2.3.3. Radiation

Radiotherapy has emerged as an indispensable component of therapy to overcome the limitation of other treatments. It is delivered primarily by external-beam radiotherapy to treat glioblastoma (Snider and Mehta, 2016). To improve local control and limit toxicity to normal brain tissue with these infiltrating tumours, novel imaging techniques such as (CT, augmented frequently with MRI and PET) are actively being explored to better define tumour extent and to map associated radiotherapy treatment fields (Dawson and Sharpe, 2006). Hyper fractionated radiotherapy has been associated with a survival detriment. Current standard-of-care treatment involves the concurrent use of temozolomide and radiotherapy to 6,000 c Gy over 30 days, photon radiation therapy is measured in gray (Gy) followed by adjuvant temozolomide treatment for 6 months (Barani and Larson 2015). Radiotherapy and chemotherapy improve survival, but death is inevitably from either recurrent or progressive disease (Stephen *et al.,* 2012).

1.2.3.4. Stereotactic radiosurgery and brachytherapy

Stereotactic radiosurgery (SRS) is a non-invasive method of localised irradiation, particularly for smaller recurrent GB lesions (Combs *et al.,* 2005; Minniti *et al.,* 2011), using iodine-125 seeds in anaplastic astrocytoma, oligoastrocytoma or oligodendroglioma (Suchorska *et al.,* 2016). SRS has gained widespread popularity in part because of its use as an outpatient procedure and its relatively decreased recovery period. In a study by Combs *et al.,* (2005) the median survival of patients undergoing single-fraction SRS (median dose of 15 Gy) for recurrent GB was 10 months (Combs *et al.,* 2005). Brachytherapy (BT) for glioblastoma, involves the use of radioactive isotopes to deliver ionizing radiation directly into the tumour bed. It was introduced as a therapy to prolong survival in GB patients, but over the past few decades, it has come with variable success (Barbarite *et al.,* 2017). It was reported that brachytherapy and stereotactic radiosurgery are effective therapies for relapsed GB but tend to be associated with notable toxicity (Barani and Larson 2015).

Due to unsuccessful current GB treatments including limitation of drug penetration to the BBB, recurrence, toxicity and inability to remove a tumour completely by surgical intervention, it was essential for the research here in this thesis, to investigate a new approach for chemotherapeutic formulation treatment and to overcome some of the side effects that prevent maximal treatment in the elderly population in particular. This thesis will focus on developing nanoparticles for chemotherapeutic delivery to glioblastoma that potentially can penetrate and pass through the BBB, also the mechanism of internalisation and uptake will be explored.

1.3. Blood-brain barrier

The BBB acts as a physical barrier, regulating the passage of molecules from the bloodstream to the brain, making it impossible for some types of drugs to reach the brain upon systemic administration. More than 98% of potential new therapeutic molecules are unable to cross the BBB (Pardridge 2002). The BBB consists of endothelial cells connected together by tight junctions (TJ), in contact with the pericytes as well as astrocytes (Pardridge 2005) (Figure 1.2).

If there were no BBB, the brain microvasculature would provide an extraordinary way to access the brain. This microvasculature has a total surface area of 20 m^2 and a total length of 640 km. This massive vascularisation theoretically would give the brain the possibility to be permeated by small molecules (by simple diffusion) in half a second (Pardridge 2003), however, unlike peripheral capillaries, those of the brain present no fenestrae. In addition, few pinocytosis vesicles, and tight junctions, also known as zonula occludens closely regulate the movement of molecules through the paracellular pathway comprising of an almost impermeable barrier for drugs administered through the peripheral circulation (Blasi *et al.,* 2007). A further contribution to the BBB functions is given by the astrocytes. These have a multitude of functions important for brain homeostasis (maintenance of potassium ion levels, inactivation of neurotransmitters, regulation and production of growth factors and cytokines) (Blasi *et al.,* 2007).

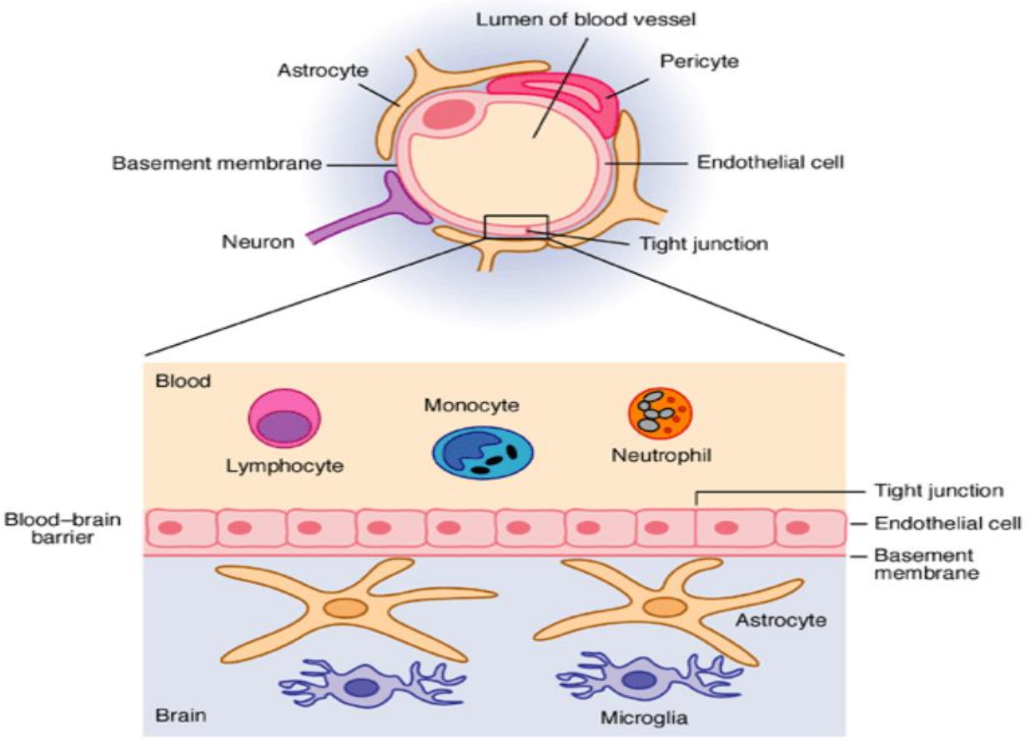

Figure 1.2 The neurovascular unit of the Blood-brain barrier (BBB) (Cambridge University 2003/ Source: **http://www-ermm.cbcu.cam.ac.uk/03006264h.htm*).***

1.3.1. Transport mechanisms across the blood-brain barrier

The transport of solute molecules across the BBB membrane takes place by four different mechanisms (Georgieva *et al.,* 2014). The proposed mechanisms are shown in Figure 1.3.

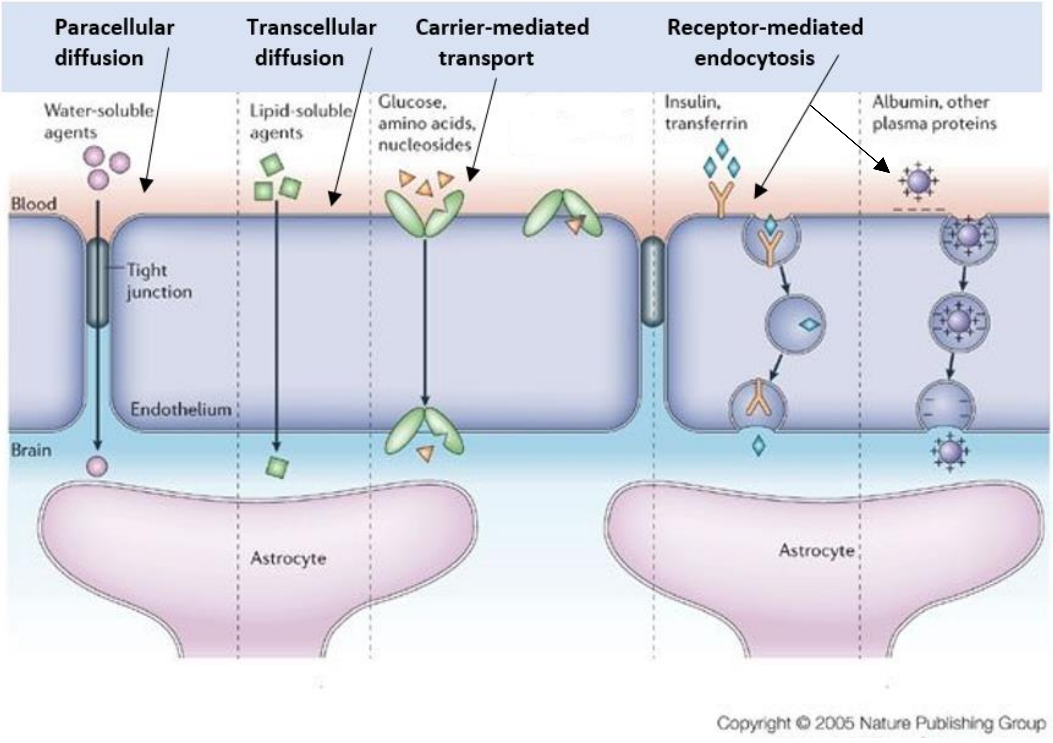

Copyright © 2005 Nature Publishing Group

Figure 1.3 Potential transport mechanisms across the blood-brain barrier, diffusion and active transport are the main transport mechanisms. Adapted and modified from Nature Publishing group (2005).

1.3.1.1. Paracellular diffusion

Paracellular diffusion is a non-saturable and non-competitive process occurring between cells, the presence of TJs in brain endothelial cells greatly affects para-cellular diffusion, only small size, water-soluble molecules can diffuse through the BBB, apparently by passing through the tight junctions (Patel *et al.,* 2013; Yuan *et al.* 1995; Georgieva *et al.,* 2014).

1.3.1.2. Transcellular diffusion

Transcellular diffusion takes place across cells and is a non-saturable and non-competitive process. The properties of the substances required for trans-cellular transport are high lipophilic nature and low molecular weight (around < 450 Da) that will facilitate transport of the molecule into the brain (Patel *et al.,* 2013), and not be a substrate for active efflux transporters (Pardridge 2012). The efflux transporters at the BBB, ATP-binding cassette (ABC) transporters (ABCB1 or P-glycoprotein (P-gp), that includes the multidrug resistance-associated proteins (MRPs or ABCC), and ABCG or breast cancer resistance protein (BCRP) (Qosa *et al.,* 2015) play a crucial role by limiting the brain tissue exposure to a variety of therapeutic agents, including compounds that are highly lipophilic and would easily permeate through the BBB in the absence of efflux transport (Loscher and Potschka, 2005) (Figure 1.3).

1.3.1.3. Carrier-mediated transport

The exchange of substances between the blood and the brain, including nutrients, occurs actively by selective membrane-bound carrier systems. This process of active carrier-mediated transport involves the development of transient narrow pores, induced by binding the substrate to the carrier. These, in turn, allow the passage of specific substrate molecules (Blasi *et al.,* 2007). Several carrier systems have been described in brain capillaries enabling the specific transport to facilitate the transfer of nutrients, including glucose, galactose, amino acids, nucleosides, lactates and pyruvates, adenine and guanine, choline, vitamins and hormones (Ricci *et al.,* 2006). Glucose provides the main energy source for the brain and glucose transporters (GLUT1 and GLUT3) are of great significance as mediated transporters (Zlokovic 2008). Equally important is the mono-carboxylate (lactate; pyruvate) transporter system (MCT1) (Ohtsuki and Terasaki 2007). Moreover, specialised carriers exist for essential amino acids and vitamins (Zlokovic 2008). The protein transporters organic anion transporting polypeptides (OATPs) are expressed in a variety of different tissues including the brain (König 2010). It is thought to be involved in the cellular uptake of various organic compounds (Kovacsics *et al.,* 2016). And organic cation transporters (OCTs) achieve important function within the brain for drug transportation (Couroussé and Gautron, 2015).

1.3.1.4. Receptor-mediated endocytosis

Some large endogenous proteins and hormones are able to cross the BBB by endocytosis, mediated by certain receptors present on the luminal side of the barrier. Specific receptors have been identified for insulin, insulin-like growth factors, angiotensin II, folates and transferrin (Bickel *et al.,* 2001). Lipids can also be internalised in the brain in the form of low-density lipoproteins (LDL), which are recognised and endocytosed by the endothelial cells, due to the expression of various apo-lipoproteins (especially ApoE) on the surface of the LDL (Blasi *et al.,* 2007).

Poly-cationic proteins (e.g. cationised albumins or immunoglobulin) can be transported across the BBB by means of absorptive transcytosis, without the plasma-membrane receptors involvement. In this situation, endocytosis is initiated through the association of poly-cationic substances with the negative charges present on the plasma membrane of endothelial cells (Smith and Gumbleton 2006) (Figure 1.3).

1.4. Nanotechnology for brain drug delivery

In recent years, with the advent of nanomedicine, engineered tunable devices with a size in the order of a billionth of meters have been proposed as an intriguing tool, potentially able to solve the unmet problem of drug transport across the BBB (Holmes 2013). Among other devices, nanoparticle (NPs) technology is rapidly advancing. NPs are objects sized between 1 and 100 nm (Youns *et al.,* 2011). Different types of NPs have been introduced as a carrier system (Agrahari 2017). (Figure 1.4).

What makes NPs even more attractive for medical applications is the possibility of conjoining features such as high chemical and biological stability, lipophilic nature enabling disposition across membranes, feasibility of incorporating both hydrophilic and hydrophobic pharmaceuticals and the ability to be administered by a variety of routes (including oral, inhalational, and parenteral) (Petkar *et al.,* 2011).

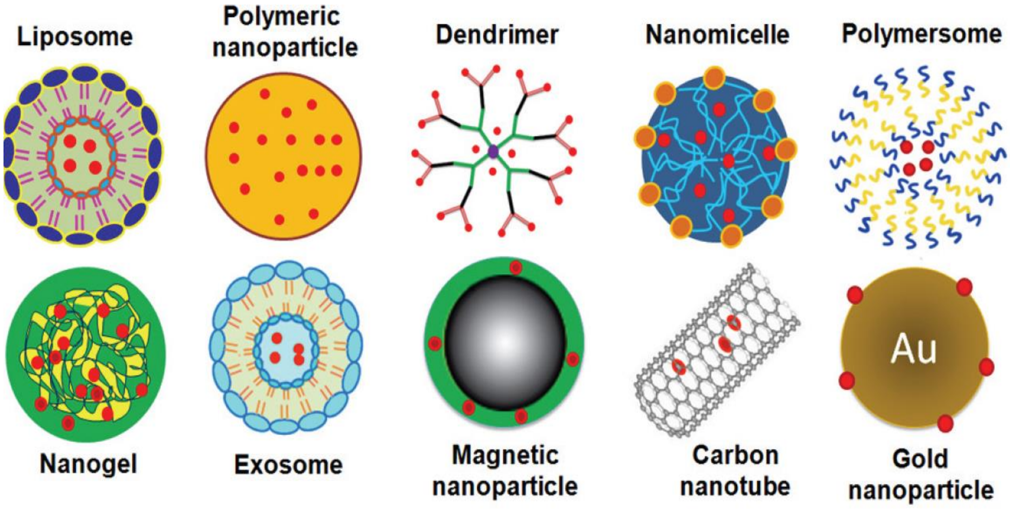

Figure 1.4 Schematic illustration of various nanoparticles classified based on their building components and characteristic structure (Agrahari 2017).

Moreover, NPs can be functionalised by covalent conjugation to various ligands (such as antibodies, proteins, or aptamers) for targeted delivery to the site of action. The large surface-area-to-volume ratio of NPs permits multiple copies of a ligand to be attached, to dramatically increase binding affinity via the multivalent functionalisation (Montet *et al.,* 2006). The tailoring of NPs to enhance drug delivery to the brain does not necessarily imply an ability to cross the BBB. It is predictable that NPs could play the role of increased brain permeation in at least in two ways:

1. By increasing the drug concentration inside, or at the luminal surface of BBB cells, thereby establishing a locally high concentration gradient between blood and brain, higher than that obtainable after systemic administration of the free drug. The gradient should then favour the enhanced passive diffusion of the free drug (Figure 1.3). This task could be realised by synthesising NPs functionalised to target brain capillary endothelial cells. This feature can be followed or not by measuring subsequent uptake of free drug from targeted cells (Haque *et al.,* 2012).

2. By transport of the NPs into the CNS, together with drug cargo. This task can be realised by enabling NPs to target brain capillary endothelial cells and measure the subsequent trans-cellular passage of NPs across the BBB (Martin-Banderas *et al.,* 2011), as previously explained in section 1.3 and as shown in Figure 1.3.

Some examples of nanomedicines for cancer treatment approved by the Food and Drug Administration FDA and those undergoing clinical trials are listed in table 1.1.

Table 1.1 Examples of Nanomedicines for cancer treatment approved by FDA and those undergoing clinical trials (Pillai 2014).

Drug product	Active ingredient	Manufacturer	Indications	FDA approved date/clinical trial status
Doxil (Caelyx)	Liposomes-doxorubicin	Orth biotech, Schering-Plough	Ovarian/breast cancer	November 1995
Abraxane **(Taxol)**	Albumin-bound Paclitaxel, Nanospheres.	Abraxis Bioscience, AstraZeneca	Various Cancers	Jan-05
	Nab-paclitaxel in combination with gemcitabine	Celgene	Metastatic pancreatic cancer	September 2013
Myocet	Liposome-encapsulated Doxorubicin	Elan/Sopherion therapeutics	Breast cancer	2000, Approved in Europe and Canada
DepoCyt	Liposomal Cytarabine	Skye Pharma, Enzon	Lymphomatous meningitis	Apr-99
LEP-ETU	Liposomal Paclitaxel	Neopharma	Ovarian/breast/lung cancers	In a clinical phase I/II

Drug product	Active ingredient	Manufacturer	Indications	FDA approved date/clinical trial status
EndoTAG-I	Paclitaxel	Medigene /SynCore Biotechnology	Breast cancer/Pancreatic cancer	In clinical phase II
Marqibo	Vincristine liposome	Talon Therapeutics	Philadelphia chromosome- negative lymphoblastic leukaemia	Aug-12
Thermodox	Doxorubicin-liposome	Celsion	Hepatocellular carcinoma	In clinical phase III
Lipoplatin	Liposomal Cisplatin	Regulon	Pancreatic/ Head and Neck/breast cancer	In clinical phase III
Aurimmune **(CYT-6091)**	TNF-α bound to colloidal Gold nanoparticles	Cytimmune Sciences	Head and Neck Cancer cancer	In clinical phase IIphase II
Auroshell	Gold Nanoshells	Nano spectra Biosciences	Aurolace therapy for cancer	In clinical Phase I
General-PM	Paclitaxel-loaded polymeric micelle	Samyang	Breast cancer/small cell lung cancer	Marketed in Europe, Korea
Paclical	Paclitaxel micelles	Oasmia Pharmaceutical AB	Ovarian cancer	Phase III
NKTR-105	PEG-Docetaxel	Nektar Therapeutics	Solid tumours	Phase I

1.5. NPs can cross the BBB

Many medicines are not able to reach the brain due to the lack of drug-specific transport systems through the BBB (Miller 2010). The development of new strategies based on NPs to enhance the brain drug delivery is of great importance in the therapy and diagnosis of CNS diseases and it is based on the interactions between NPs and the BBB and on their intracellular traffic pathways (Jain 2012).

1.5.1. Crossing the BBB without functionalisation

Although almost all nanomaterials fall into the class of BBB impermeable, some exceptions have been reported in recent years. For instance, gold and silica NPs have been shown to reach the brain and accumulate in neurons even in the absence of any specific functionalisation, with a mechanism that substantially is still unknown (Wu *et al.,* 2011). It was reported that gold NPs mainly accumulate in the hippocampus, thalamus, hypothalamus, and the cerebral cortex. The same finding was reported for titanium dioxide NPs, furthermore, these NPs were found to cross the BBB in mice particularly when smaller than 40 nm in diameter (Ze *et al.,* 2013).

1.5.2. Adsorptive-mediated transcytosis

The concept of adsorptive-mediated transcytosis through the BBB was originally suggested by the observation that cationic proteins can bind to the endothelial cell surface but also cross the BBB (Broadwell 1989) (Figure 1.3). The mechanism applied to NPs is based on the proper functionalisation of their surface allowing electrostatic interaction with the luminal surface of BBB due to the presence of negative charges on endothelial cells (Masserini 2013). This interaction can be promoted by NPs bearing a positive surface charge.

Different procedures can be followed to measure this phenomenon. The first is developing NPs made of components that bear a positively charged surface at physiological pH (7.4). This is the case of nano-sized vesicles made of bola amphiphilic molecules that, following intravenous administration to mice, showed a marked accumulation in the encapsulated fluorescent cargo, whereas the non-encapsulated probe was detected only in peripheral tissues but not in the brain (Dakwar *et al.,* 2012).

A second procedure is to functionalised the NPs surface with positively charged biomolecules combining the physicochemical features with biological activity, which have been extensively used for NPs decoration, facilitating the BBB passage of drugs (Tian *et al.,* 2012).

1.5.3. Receptor-mediated transcytosis

One of the most recently applied strategies for drug delivery across the BBB endothelium using functionalised NPs is the exploitation of the transcytosis physiological mechanism of transport of macromolecules, relying on the presence of specific receptors on the luminal surface of cells. Transcytosis is the process by which extracellular cargo internalised at the apical plasma membrane domain of a polarised cell is transported via vesicular intermediates to the contralateral (basolateral) plasma membrane. For example, transferrin, apolipoproteins, and 2-macroglobulin are some of the proteins that reach the brain following the path across endothelial cells (Muro *et al.,* 2004).

1.5.3.1. Lipoprotein receptors

Apolipoprotein E (Apo-E) is a 34- kDa protein constituent of both very low-density lipoprotein (VLDL) and high-density lipoprotein (HDL), which transports cholesterol and other lipids in the plasma and in the CNS (Laskowitz *et al.,* 2001). The lipoproteins were taken up by the brain through the recognition of apo E by specific receptors at the BBB, which include the low-density lipoprotein receptor (LDLR) and the LDLR-related protein (LRP). Taking into consideration that LRP has been reported to be highly expressed on endothelial brain microvessels, the LDLR is an ideal target to exploit for transport into the brain (Bell *et al.,* 2007).

1.5.3.2. Transferrin receptor (TfR)

The transferrin receptor (TfR) is the most widely studied receptor for BBB targeting. TfR is a transmembrane glycoprotein, consisting of two linked 90-kDa subunits, each one binding a transferrin molecule. The receptor is highly expressed on hepatocytes, immature erythroid cells, placental tissue, and rapidly dividing cells, both normal and malignant (Ponka and Lok 1999). Furthermore, it is expressed on endothelial cells of the BBB. The role of the receptor is the regulation of cellular uptake of iron via transferrin; a plasma protein which transports iron in the circulation. Cellular uptake starts with the binding of transferrin to the transferrin receptor followed by endocytosis (Moos *et al.,* 2007). Ironbound transferrin has a high affinity for the TfR, therefore it has been used with success as a ligand for functionalisation and targeting of liposomes to cultured brain endothelial cells (Visser *et al.,* 2005; Chang *et al.,* 2009).

1.5.4. Retrograde transport

Trans-synaptic retrograde transport could enable some types of nanocarriers to travel from peripheral nerve terminals to neuronal cell bodies in the CNS (Cui *et al.,* 2007). Studies in this regard have shown that NPs modified with polyethyleneimine (PEI) and other polyplexes display active retrograde transport along neurites but are unable to mediate efficient biological actions upon reaching the neuronal body (Bergen and Pun 2008).

1.5.5. BBB breakdown

BBB breakdown occurs in neuroinflammatory diseases (Vries *et al.,* 1997). NPs can transiently and reversibly open the tight junctions located at the BBB and other sites, thus, increasing paracellular permeability (Sadekar and Ghandehari 2012). Using intra-arterial injection of mannitol arabinose, lactamide, saline, urea and several radiographic contrast agents were found to be conventional for reversibly disrupt the BBB (Bellavance *et al.,* 2008). These agents are hyperosmolar in nature and cause shrinkage of the endothelial cells, thus causing a transit opening of tight junction (TJ). The BBB disruption therapy is an intensive and effective way of delivering medication to brain tumours (Treat *et al.,* 2012). Nevertheless, it is known that tight junctions can be opened only to a limited extent (Adamson *et al.,* 2004) making only small NPs 20nm in diameter use this pathway to penetrate the brain through the BBB (Adamson *et al.,* 2004).

1.5.6. Exploiting Monocyte/Macrophage Infiltration in the CNS

Monocyte/macrophage infiltration in the CNS plays a key role in neuroinflammation, as well as in lesion development and brain injury in neurological diseases such as multiple sclerosis (MS) and stroke (Adamson *et al.,* 2004). The role of active phases of cell infiltration during CNS disorders is important because anti-inflammatory treatments can target cell adhesion molecules and chemokines guiding cellular trafficking (Stoll *et al.,* 1998). This strategy could be realised at least in two ways as listed below.

1.5.6.1. Trojan monocytes for NPs delivery to the brain

NPs drug delivery systems have been used to avoid the reticuloendothelial system (RES) clearance and achieve longer circulation time for enhanced tissue uptake. After phagocytosis of NPs, monocytes work just like Trojan horses, may transport their cargo into the brain (Afergan *et al.,* 2008). This technique has been used for serotonin, a BBB impermeable neurological drug, by embedding it into negatively charged liposomes and its brain uptake was analysed in rats and rabbits. The performance of liposomal serotonin was significantly better, leading to two-fold higher drug concentration in brain than the free drug. The Trojan monocyte approach provides a new possibility of more effective treatment of brain-associated inflammatory disorders, including multiple sclerosis and Alzheimer's disease, which are characterised with increased passage of immune cells across the BBB (Park 2008).

1.5.6.2. NPs mimicking activated monocytes

The therapeutic efficacy of drug loaded NPs systemically administered depends on the ability to attack the immune system, to cross the biological barriers of the body, and to localise at target tissues. (Parodi *et al.,* 2013). The nano-porous silicon particles can successfully perform all these actions when they are coated with cellular membranes purified from leukocytes, avoiding being cleared by the immune system. Furthermore, they can be attached to endothelial cells through receptor-ligand interactions and transport and release a doxorubicin payload across an inflamed endothelial barrier in an *in-vitro* study (Parodi *et al.,* 2013).

1.6. Solid Lipid Nanoparticles

Solid lipid nanoparticles (SLNs) are nanospheres made from solid lipids, with a diameter of approximately 50–1000 nm. SLNs consist of a solid lipid matrix, for example, glycerides, fatty acids, or waxes stabilised by physiologically compatible emulsifiers (e.g. phospholipids, bile salts, Tween_80, polyoxyethylene ethers, or polyvinyl alcohol (Battaglia and Gallarate 2012; Lasa-Saracibar *et al.,* 2012).

SLNs are usually produced by the hot homogenisation method, which generally entails using high-pressure homogenisation (HPH) (Müller *et al.,* 2000; Joshi and Müller 2009; Souto *et al.,* 2004). SLNs have been reported as a promising anticancer drug delivery system to the brain after IV injection. This is due to the ability of SLNs to cross the blood-brain barrier and deliver drugs to the brain when coated with proper surfactants, such as polysorbates (Blasi *et al.,* 2007). Thus, SLNs have high potential in brain tumour treatment. The advantages of SLN are the ability to immobilise hydrophilic or hydrophobic drugs in the solid matrix (Figure 1.5), sustain the drug release, and the prevention of premature degradation of the incorporated drug. In addition, the matrix is composed of physiological components and/or excipients of accepted status (FDA-approved constituents), decreasing the risk of acute and chronic toxicity (Joshi and Müller 2009; Souto *et al.,* 2004).

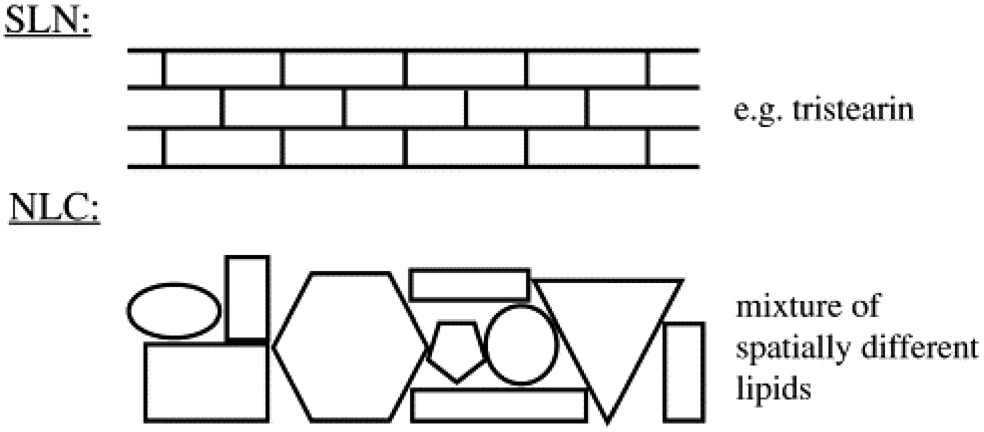

Figure 1.5 Nanostructure of SLN compared with the nanostructured lipid carrier (NLC), taken from (Radtke and Müller 2001).

1.6.1. Nanostructure lipid carrier (NLC)

NLCs were introduced as the next generation of SLNs at the end of the 1990s, to overcome the difficulties of previous SLNs (Mehnert *et al.,* 2001; Müller *et al.,* 2014) NLCs improve the stability, capacity of drug loading and prevent the drug expulsion during storage. They are distinguished from SLNs by the composition of the solid matrix. Lipidic phase in NLCs contains both solid and liquid lipids at the ambient temperature (Pardeike *et al.,* 2009). Formless, imperfect and multiple types are the three forms of NLCs (Kaur *et al.,* 2015), as shown in (Figure 1.6).

The drug re-partitions into the lipids while the lipids increase structural perfection during the cooling, leading to the embedding of drug molecules onto the particle surface and formation of a drug-enriched shell. This unfavourable drug incorporation mode limits the drug loading capacity and leads to drug expulsion during storage and burst release. To overcome this potential issue, Muller *et al*., (2002) proposed a novel lipid nano-system called “nanostructured lipid carriers” (NLC) (Muller *et al.,* 2002). The NLC is a modification of the conventional SLN by making the solid lipid core a less organised nanostructure. The lipid cores with imperfect crystal structure can be realised by either using spatially different lipids, such as mono-, di-, triglycerides with different chain lengths, or mixing some liquid lipids (oils) with the solid lipid. The space between different fatty acid chains and crystal imperfections provide more accommodation for drug molecules. In addition, some drugs have higher solubility in oils than in solid lipids, therefore, the NLC as a new generation of SLN increases the drug payload and decreases drug expulsion and burst release. Besides the lipid matrix, it is also possible to tune the release profile by adopting different production method (warm or cool) or modifying surfactant concentration. (Muller *et al.,* 2002).

There are several production techniques for SLNs such as high-pressure homogenization (HPH), solvent emulsification /evaporation, supercritical fluid extraction of emulsions (SFEE), ultra-sonication or high-speed homogenization (Blasi *et al.,* 2007; Naguib *et al.,* 2014) and spray drying (Kakadia and Conway, 2014). Two processes of the HPH, hot and cold processes have been developed. These are two basic production methods in which, the drug is dissolved or solubilised in the lipid being melted at around 5-10 °C above its melting point (Blasi *et al.,* 2007).

1.6.1.1. NLC classes

NLCs differ from SLNs by the following: more drug loading capacity, less water in the dispersion, prevention or minimization of the drug expulsion during storage. No significant difference between the bio-toxicity of SLNs and NLCs has been reported (Tamjidi *et al.,*2013; Doktorovova *et al.,* 2014a). The different classes of NLCs are summarised in the sections below and Figure 1.6.

1.6.1.2. Class one imperfect

The class one NLCs are formed when solid and liquid fats (oil) are mixed in various lipid structures. Specific conditions in the crystallisation procedure lead to an extremely disordered structure. Imperfect lipid matrix structures present a gap between triglyceride fatty acid chains in crystal and thus increase the ability of the drugs to enter the matrix (Kaur *et al.,* 2015).

1.6.1.3. Class two formless

Non-crystalline matrix is a type of NLCs that has no crystalline structure and thus prevents the expulsion of the loaded drug, which is known as an amorphous type (Kaur *et al.,* 2015).

1.6.1.4. Class three multiple types

In class three multiple types of NLCs, drug solubility in liquid lipid is greater than in solid lipid, thus it is present as a dissolved drug in nano-compartments of oil in solid lipid thus preventing it from decomposition. This form of NLCs is similar to w/o/w emulsions (Feng and Mumper 2013).

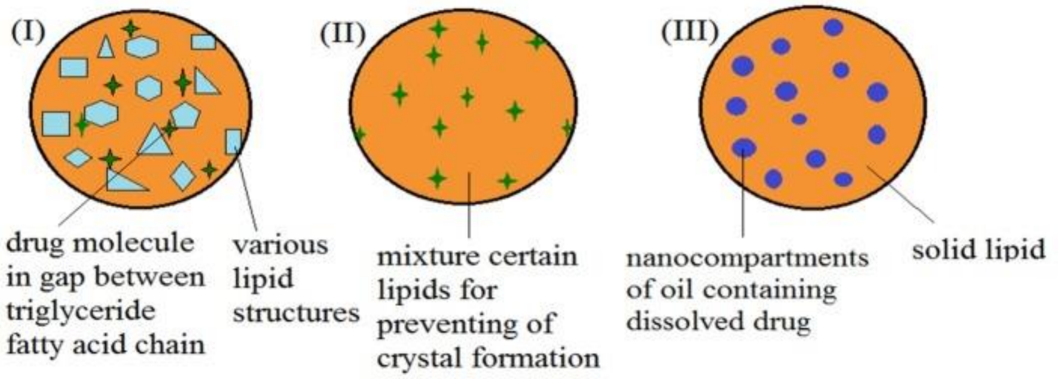

Figure 1.6 Structures of NLCs Class I (imperfect type), class II (formless type), class III (multiple types). (Selvamuthukumar and Velmurugan 2012).

1.7. Targeted drug delivery using NPs

Delivering effective quantities of the drug into the right target cells through clinically feasible methods represents a major challenge for the successful development of cancer nanomedicines (Alonso 2004). Nano-delivery platforms were designed to overcome such barriers and can be divided into two ways: passive targeting and active targeting.

1.7.1. Passive targeting

Blood vessels in tumours may have a leaky endothelium, failing the normal barrier function thus allowing entry of macromolecules up to 400 nm in size (Yuan *et al.,* 1995). NPs passively diffuse into tumour tissue through the leaky vasculature, accumulate in a tumour, and release therapeutic payloads into the tumour cells. This process is known as the enhanced permeability and retention (EPR) effect (Matsumura and Maeda 1986). A limitation of the passive targeting is that it is dependent on the diffusion of drugs (Jain 1994).

1.7.2. Active targeting

To overcome the limitation of EPR, active targeting strategies were incorporated into NPs using affinity molecules such as antibodies, peptides, or aptamers that bind to antigens or receptors on the target cells to enhance the therapeutic efficacy by increasing cellular uptake and accumulation (Peer *et al.,* 2007; Bamrungsap *et al.,* 2012).

1.8. Evaluation of permeation of NPs through the BBB

Crossing the BBB is a very challenging goal in drug delivery. Different methods have been proposed to assess whether a drug or a formulation is suitable for brain delivery. Some of these methods involve the use of *in vitro* models, while others use *in vivo* models in rats or mice. Among *in vitro* methods, the most important are models of the BBB (Grant *et al.,* 1998). These generally comprise of cultured brain microvasculature, which can be grown in either the absence or in the presence of glial cells. Although primary cultures of brain endothelium alone may form tight intercellular junctions, co-culture with astrocytes generally leads to increased formation and complexity of endothelial tight junctions (Gastaldi *et al.,* 2014). In turn, these induce expression of specific BBB markers. Currently, the development of immortalised endothelial cell lines that preserve a stable BBB phenotype is of great interest.

The trans-well system consists of cultured brain microvessel endothelial cell monolayers, grown on a microporous membrane submerged in culture medium. Cultured cortical astrocytes are compartmentalised below the endothelial monolayer, and they release soluble factors, which preserve the BBB properties. This system affords the study of bidirectional transport across the BBB. It is an advantageous and well-established way of artificially evaluating the crossing of NPs across the BBB *in-vitro* (Smith 1996).

1.9. Cellular uptake pathways

After crossing the blood-brain barrier the next important question is whether the SLNs/NLCs can be internalised by the tumour cell and whether anticancer drugs are released from the SLNs/NLCs intracellularly. Nano-particles located in the external environment of a cell can interact with the plasma membrane. This can lead to the uptake of these nanoparticles by the cells through a process named “endocytosis” (Sahay *et al.,* 2010). If the nanoparticles cannot be internalised, the drug can still enter cells after being released from the nanoparticles, however, the drug can also disperse to the surrounding normal tissues rather than be delivered mainly to the cancer cells. In fact, *in-vitro* and *in-vivo* studies reveal that the intracellular concentration of the drug is much higher when it is released from nanoparticles into the cytoplasm than from the concentration of non-capsulated drug with nanoparticles after internalisation (Chen *et al.,* 2004; Jain *et al.,* 2010). The form of endocytosis involved in nanoparticles uptake can be expected to affect the nanoparticles intracellular localisation and trafficking, understanding endocytic mechanisms is then crucial for the development of nanoparticles for clinical therapies (Martins *et al.,* 2012).

Furthermore, most nanoparticles have been shown to exploit more than one pathway to gain cellular entry (Sahay *et al.,* 2010). The endocytosis of nanoparticles also depends on the cell type treated (Thurn *et al.,* 2007), bearing in mind that cell type could be critical in defining the nanoparticle entry and its destination in the cells. Endocytosis is known as a general entry mechanism for various extracellular materials. It is divided into two main categories, phagocytosis (uptake of large particles) and pinocytosis (uptake of fluids and solutes) (Doherty and McMahon 2009; Sahay *et al.,* 2010). Phagocytosis is followed by specialised professional phagocytes, such as macrophages, monocytes, or dendritic cells. The phagocytic pathway of cellular entry consists of recognising the particles followed by the adhesion of the opsonised particles onto the cell membrane and ingestion of the particle by the cells. Pinocytosis, in contrast, is present in all types of cells and has multiple forms depending on the cell origin and function. Pinocytosis can be classified as clathrin-mediated endocytosis, caveolae-mediated endocytosis, clathrin- and caveolae-independent endocytosis, and macropinocytosis (Conner and Schmid 2003). Internalisation through clathrin-dependent endocytosis normally happens when the clathrin coat on the plasma membrane develops invaginations in the membrane leading to the budding of clathrin-coated vesicles (Figure 1.7), (Sahay *et al.,* 2010). Nano-particles localised on the cell membrane could be trapped within the vesicles and brought within the cells. Receptor-mediated endocytosis through clathrin-coated pits is the most common pathway of endocytosis (Martins *et al.,* 2012).

Alternatively, clathrin-independent endocytosis can happen through the caveolae or lipid-raft pathway. Caveolae are flask-shaped membrane invaginations on cell surfaces that have high amounts of cholesterol and sphingomyelin. Caveolae are found in muscle, endothelial cells, fibroblasts and adipocytes and absent in neurons and leukocytes (Conner and Schmid 2003; Sahay *et al.,* 2010). In the macro-pinocytosis, the macro-pinosomes are larger (0.5–10 µm) and distinct from other vesicles formed during pinocytosis (Figure 1.7). This pathway is possible for virtually any cell (such as macrophages and brain microvessel endothelial cells) with only a few exceptions. Macropinocytosis can internalise large particles with submicron and greater sizes in cells, which lack phagocytosis (Sahay *et al.,* 2010).

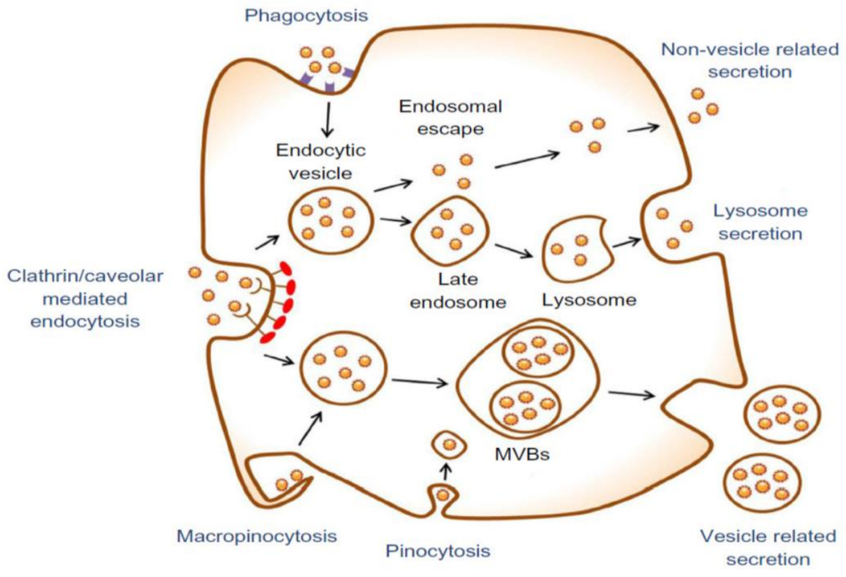

Figure 1.7 Endocytosis mechanism and pathway mediators (Oh and Park, 2014).

Attempt to clarify endocytic uptake mechanisms have been published (Conner and Schmid 2003). Coumarin-6 marked SLNs were internalised into A30 cells at 37 °C. The uptake was decreased, but not completely stopped at 4°C incubation. This suggested that energy-dependent processes (endocytosis) might be involved in SLNs uptake (Rivolta *et al.,* 2011). By pre-incubation with specific uptake mechanism inhibitors, two independent research groups have specified that clathrin-mediated endocytosis might be the preferential uptake mechanism of SLNs, while caveolae-mediated endocytosis seems to play an only minor role or not involved at all (Martins *et al.,* 2012; Zhang *et al.,* 2012). Martins *et al*., (2012) also found out that macro-pinocytosis might be involved to a smaller extent in some cell types.

1.10. Docetaxel

Docetaxel (DTX) is a second-generation taxane derived from the needles of the European yew tree, Taxus baccata (Bissery *et al.,* 1995). Early *in vitro* studies revealed that docetaxel has a wide spectrum of antitumor activity (Bissery *et al.,* 1995). It was demonstrated that DTX could significantly inhibit brain tumour growth by local injection (Sampath *et al.,* 2006). Docetaxel (Taxotere) is a novel, semi-synthetic, the anticancer agent, structurally related to paclitaxel (Taxol) (Figure 1.8) (Musumeci *et al.,* 2006). Unlike paclitaxel, docetaxel exhibits linear pharmacokinetics and, due to differences in drug efflux, is retained intracellularly for a longer period (Bissery *et al.,* 1995). DTX has shown efficacy in clinical trials against a variety of human tumours (Kaye and Vase 2002). It has also been reported to act as a potent radiosensitiser against systemic malignancies (Baker *et al.,* 2006). The anti-proliferation effect of DTX may have antitumor effects on brain cancer.

Sampath *et al.,* (2006) found that following local injection in a mouse brain tumour model, only low levels were found in the brain.

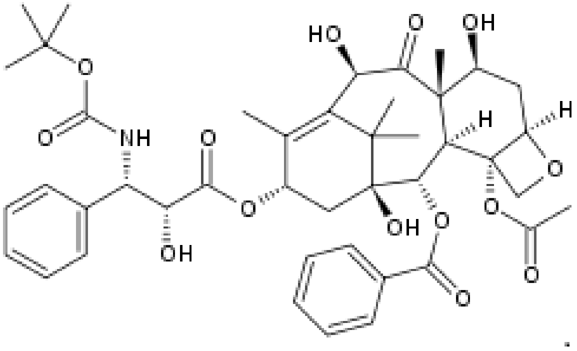

Figure 1.8 The chemical structure of docetaxel (Musumeci et al., 2006).

1.10.1. Mechanism of action of DTX

DTX mechanism of action is through inhibition of tubulin depolymerisation resulting in microtubule aggregation and cell death (Sparreboom *et al.,* 1998). The central role of microtubules in cell division and other relevant cellular functions makes it a target for anticancer drug development (Fanale et al., 2015). The primary mechanism of action for the taxanes (docetaxel and paclitaxel) is to promote microtubulin assembly and stabilise the polymers against depolymerisation, thereby inhibiting microtubule dynamics (Ringel *et al.,* 1991). This mechanism of action employed by taxanes is distinct from that of other anti-microtubule agents, which prevent microtubule assembly (Rowinsky, Donehower, 1996). The consequences of blocking microtubule dynamics are complex; a number of vital cellular functions in which microtubules play a critical role are compromised. Impairment of mitotic progression leading to cell cycle arrest is considered to be a principal component of docetaxel's mechanism of action. This blocks the progression of a cell through its natural division cycle and, consequently, inhibits cell proliferation (Herbst and Khuri, 2003). Disruption of microtubules not only affects progression through the cell cycle but may also alter signalling pathways involved in processes such as apoptosis (Wang *et al.,* 1999). Apoptosis, also known as 'programmed cell death, is a physiologic process involving the activation of certain signalling pathways and genetic programs. Defects in this process are believed to contribute to a number of human diseases and decreased or inhibited apoptosis is a feature of many malignancies (Renehan *et al.,* 2001). Several studies have demonstrated that docetaxel and other microtubule-targeting agents promote apoptosis in cancer cells (Schimming *et al.,* 1999).

1.11. Aim and objectives of the project

1.11.1. Aim

The aim of this thesis was to enhance selectivity and therapeutic efficacy of an anticancer drug docetaxel (DTX) for targeting and treating glioblastomas, by examining the glioblastoma cell lines proliferation, internalisation, uptake, cell cycle distribution and permeation through 3D *in-vitro* BBB model that was set up from human origin cell lines.

This was achieved by enhancing permeation through the BBB of the poorly water-soluble drug DTX, by incorporating it into nanostructure lipid carrier (NLC) as a delivery system composed of biodegradable excipients and increasing its selective uptake by glioblastoma cells by use of novel aptamer and polyunsaturated fatty acids (PUFAs) as targeting ligands.

1.11.2. Specific objectives:

- To develop and validate a high-performance liquid chromatography method for quantification of DTX from NLC, release media and a biological matrix.
- To develop NLC with high drug content and entrapment efficiency of DTX.
- To study the physicochemical characterisation of the developed DTX-NLCs.
- To functionalise DTX-NLC with two PUFAs (Gamma-linolenic acid (GLA) and Alpha-linolenic acid (ALA) and one novel aptamer SA43 as ligands for enhancing DTX-NLC selectivity and efficacy.
- To examine the potential effects of DTX-NLC and functionalised DTX-NLCs in an *in-vitro* study of treatment of glioblastoma cell lines, non-cancerous brain cells, and short-term culture glioblastoma cells.
- To explore the anti-cancer efficiency and uptake of DTX-NLC and functionalised DTX-NLCs using a diseased/tumour 3D *in-vitro* BBB model in the presence of monolayer glioblastoma cell line (U87MG).
- To evaluate the potential mechanism of cellular uptake for DTX-NLC and functionalised DTX-NLCs.
- To investigate the potential permeation of DTX-NLC and functionalised DTX-NLCs using 3D *in-vitro* BBB model.

Chapter Two

Analytical methods development and validation

2.1. Introduction

2.1.1. High-performance liquid chromatography (HPLC)

HPLC is a fast, reliable and commonly used technique for qualification and quantification of pharmaceutical and biological materials (Bansal *et al.,* 2010; Shabir 2003; Rao *et al.,* 2006). One of the most critical factors in developing pharmaceutical drug substances and drug products today is ensuring that the analytical test methods that are used to analyse the products generate reliable and meaningful data, therefore this chapter reports development and validation of separate analytical methods for quantification of DTX in the DTX-NLCs to determine drug loading (DL), entrapment efficiency (EE), and *in-vitro* drug release in these formulations to provide assurance on the quality of products.

2.1.2. HPLC method for analysing sample permeation through a physiological *in-vitro* BBB model

Assessing BBB penetration is an essential and evaluative step at the early phase of the CNS drug discovery process and formulation development for CNS therapeutics (Doan *et al.,* 2002; Kikuchi *et al.,* 2013). As DTX-NLCs have been developed for brain targeting, it is necessary to evaluate their performance and determine their BBB permeability which was carried out by using a 3D *in-vitro* BBB model. Previous examples of HPLC analysis of various drugs permeation across an artificial BBB (human and animal) have been reported in the literature (Nakagawa *et al.,* 2009; Jahne *et al.,* 2014; Moradi-Afrapoli *et al.,* 2016).

A quantitative analytical HPLC method was developed and validated to assess the DTX in the biological media to determine drug permeated across the *in-vitro* BBB model derived from cells of human origin.

In addition, prior to HPLC analysis, an extraction procedure was developed to separate the drug of interest from biological media based on previously published protocols (Jahne *et al.,* 2014; Moradi-Afrapoli *et al.,* 2016).

2.1.3. HPLC validation

The US Food and Drug Administration (FDA, 1995 and 2001) recognised the importance of HPLC to the drug development process and have increased validation requirements in recent years. Moreover, the International Conference on Harmonization (ICH 1996), has added to the FDA requirements to create an acceptable and professional validation process for all developed drug as detailed in this section (Shabir 2003; Polagani *et al.,* 2013; Patel *et al.,* 2011).

Analytical method validation is created to ensure that the analytical methodology is accurate, specific, reproducible and robust over the duration of time in which the product will be usually analysed. All laboratories must perform the method of validation, at least every 3-months to be in line with the US FDA regulation and the ICH guidelines. In addition, for analytes that need to be resolved from a biological matrix need additional validation to be performed according to the European Medicines Agency (EMA). The following sections summarise all the validation requirements from the regulatory agencies FDA, ICH and EMA.

2.1.3.1. Specificity

Specificity involves separation and correct identification of a specific analyte from all potential sample components. It is very important in the chromatographic method development to demonstrate the ability of the method to accurately measure the analyte response and give a specific peak.

2.1.3.2. Precision

Precision is the measure of the degree of repeatability of an analytical method under normal operation and is normally expressed as the percent relative standard deviation (RSD %) for a statistically significant number of samples, for example, three levels, three repetitions each. Precision may be performed at three different levels: repeatability, intermediate precision, and reproducibility.

2.1.3.2.1. Repeatability

Repeatability (intra-day precision) is the measure of variation of the method operating over a short time interval under the same conditions. It should be determined from a minimum of nine determinations covering the specified range of the procedure (for example three levels, three repetitions each). The acceptable precision criterion for an assay method is that the instrument precision (RSD) will be ≤ 1%, and for the impurity assay and biological samples, at the limit of quantitation, the instrument precision (repeatability) will be ≤ 5%.

2.1.3.2.2. Intermediate precision

Intermediate precision means inter-day variation and is the measure of variation within laboratories, due to random events, such as different days, analysts and equipment. In determining intermediate precision, experimental design should be employed, so that the effects (if any) of the individual variables can be monitored. Precision criteria for an assay method are that the inter-assay precision will be ≤ 2%, and for impurity assay, at the limit of quantitation, and the inter-assay precision will be ≤ 10%.

2.1.3.2.3. Reproducibility

Reproducibility is normally not expected if intermediate precision was previously performed. Reproducibility is determined by testing homogeneous samples in multiple laboratories, where the mean results will be within 2% of the value obtained by the primary testing lab. For an impurity method, the mean results will be within 10%.

2.1.3.3. Accuracy

The accuracy of an analytical method is the closeness of the measured results to the actual value (normally a reference standard). Accuracy criteria for an assay method (FDA) are that the mean recovery will be 100 ± 2% at each concentration over the range of 80 -120% of the target concentration. The ICH recommends collecting data from a minimum of nine determinations over a minimum of three concentration levels covering the specified range (for example three concentrations, three replicates each), and for extraction of an analyte from a biological matrix, the acceptable limit of accuracy should be within 10 % RSD.

2.1.3.4. Recovery

Recovery is defined as comparing the ratio of mean peak area obtained from a biological sample spiked with the analyte of interest before the extraction process, with those mean peak areas from the biological sample to which the analyte of interest was added after the extraction process, this ratio should be less than 15%.

2.1.3.5. Matrix effect

Matrix effect defined for the analyte extraction from different types of biological media, by comparing peak area of the analyte of interest in the presence of the biological media with the peak area in absence of the biological media (reference standard). This ratio will be defined as a matrix factor, this ratio should be less than 15%.

2.1.3.6. Limit of detection and quantification

The HPLC Limit of detection (LOD) is the lowest amount of analyte that can be detected above baseline noise; typically, three times the noise level. And the limit of quantitation (LOQ) is defined as the lowest amount of analyte which can be reproducibly quantitated above the baseline noise.

2.1.3.7. Samples stability

Samples and standards should be tested over at least a 48 h period (depends on intended use), and quantitation of components should be determined by comparison to freshly prepared standards. A stability criterion for assay methods is that sample and standard solutions and the mobile phase will be stable for 48 hours under defined storage conditions. Stability is acceptable when the change in the standard or sample response is within 2 % relative to freshly prepared standards, and within 15 % according to EMA guidelines for biological samples.

2.2. Aim and Objectives

The aim of this Chapter was to develop and validate HPLC methods for the quantification of DTX. This was achieved by the following objectives:

2.2.1. Objective 1

Quantification DTX in DTX-NLCs and surface modified DTX-NLCs, to determine DTX loading and entrapment efficiency of DTX in all developed formulations.

2.2.2. Objective 2

Quantification of DTX that is been released from DTX-NLC and DTX-NLC surfaced modified formulations in two release media to study the kinetics of DTX release over a period of time in an *in-vitro* environment.

2.2.3. Objective 3

Extraction and quantification of DTX in a biological matrix comprising a mixture of three primary cell media consisting of proteins and human serum. This analytical method enabled quantification of DTX and DTX-NLC that permeated through the physiological *in-vitro* BBB model. This method will contribute to access the ability to use DTX-NLCs as a delivery system for brain-targeted therapy.

2.3. Materials and equipment

2.3.1. Equipment

High-Performance Liquid Chromatography (HPLC) analysis was performed using the Agilent HPLC 1260 Infinity from Agilent Technologies, USA and data were studied with Agilent's software OpenLAB CDS CS Workstation (Agilent Technologies, USA). Reversed-phase HPLC C18 column (Luna 5µm, PFP(2), 100Å, 250 x 4.6 mm (Phenomenex, UK). Benchtop centrifuge (Spectrafuge 24D, Jencons-Pls, UK).

2.3.2. Materials

Tetrahydrofuran (THF), methanol, acetonitrile, acetone, ethanol, dichloromethane, dimethyl sulfoxide (DMSO) and chloroform were of HPLC grade and purchased from Fisher Scientific, UK. Transparent and amber HPLC glass vials; orthophosphoric acid and Amicon 3 kDa molecular cut-off centrifugal filters were purchased from Fisher Scientific, UK. Docetaxel (DTX) and paclitaxel (PTX) were purchased from Kemprotec, UK. Phosphate buffer saline (PBS) 1 tablet dissolved in 200 ml water yields buffer containing 0.1 M phosphate buffer, 0.0027 M potassium chloride (KCl), and 0.137 M sodium chloride (NaCl), pH 7.4 at 25°C (Fisher, UK). Endothelial Basal Medium (EBM) and the following growth supplements: 0.5 ml rhEGF, 0.2 ml Hydrocortisone, 0.5 ml GA-1000 (Gentamicin, Amphotericin-B), 0.5 ml VEGF, 2ml rhFGF-B, 0.5 R^3-IGF-1, 0.5 ml Ascorbic Acid, 0.5 ml Heparin, and 2% human serum (HS)/ 1 ml to form EGM-2; Astrocyte Basal Medium (ABM™) and the following growth supplements: rhEGF, 0.5 ml; Insulin, 1.25 ml; Ascorbic Acid, 0.5 ml; GA-1000, 0.5 ml, L Glutamine, 5.0 ml and 3 % HS/ 1 ml to form AGM-2 purchased from Lonza, UK and Pericyte Basal Medium (PM) with growth supplements of 5 ml of Pericyte Growth Supplement (PGS), 5 ml of penicillin/streptomycin solution (P/S) and 2% HS/1 ml (Caltag Medsystems, UK).

2.3. Methods

2.4.1. HPLC method for quantification of DTX from NLCs

Drug content and drug entrapment are important pharmaceutical parameters to evaluate the success of NLCs as drug delivery systems. Therefore, a rapid and efficient analytical method is essential for the evaluation of these parameters. To quantify DTX, reversed phase HPLC was used which is a bonded phase chromatographic technique that uses water as the base solvent. Separation of compounds is based on solvent strength and selectivity and may also be affected by column temperature and pH. In general, the more polar components elute faster than the less polar components (Loffe *et al.,* 2002). The method that has been used in this study was adopted and modified from previous literature (Muthu *et al.,* 2011). Chromatographic conditions for DTX quantification were adjusted to an isocratic mobile phase, which consisted of acetonitrile and water (50:50, v/v). The mobile phase flow rate (FR) was 1.0 ml/min, the sample injection volume was 20 µl and the UV detection wavelength was 230 nm. A Phenomenex column Luna 5µm, PFP(2), 100Å, 250 x 4.6 mm (Phenomenex, UK) was used throughout the experiment. The column temperature adjusted to 40 °C for the total analytical period of 15 min. A standard reference sample of DTX at 4 µg/ml was injected for all analytical studies to ensure that the HPLC system was working properly. All samples were injected three times, and experiments were carried out in triplicate. The mean and standard deviation were calculated, and standard calibration curves were generated.

2.4.1.1. Organic solvents used for dissolving DTX-NLC

Before the method validation, it was necessary to prove that an appropriate and optimised method had been used for the separation of DTX from other sample components by dissolving the sample appropriately. Ideally, the mobile phase should be used to dissolve the samples, however, if the sample is not soluble in the mobile phase a different solvent should be tested (ICH guidelines, 1996). In this experiment, to determine the DTX encapsulation efficiency, DTX loading and total DTX entrapped in the DTX-NLC accurately, it was essential to dissolve the formulation completely to overcome interference, peak tailing and poor symmetry in the HPLC chromatogram. However, as the NLCs were not soluble in the mobile phase, further optimisations were carried out.

For dissolving the DTX-NLC formulation, the following organic solvents were evaluated in different ratios, acetone: ethanol (4.5:4.5, v/v); THF: DCM (7:2, v/v); THF: chloroform (5:5, v/v); THF: acetonitrile (3:7, v/v); methanol: THF (4.5:5.5; 5.5:5.5; 5.5:7.5; 4:6; 7:3; 7:4; 7:5; 3:9 and 2:10, v/v). Moreover, ethanol: THF (5:5; 5:7; 7:3; 9:9; 3:7 and 6:14 v/v), respectively were also evaluated. Only completely soluble samples were injected and analysed by the HPLC system as described in section 2.4.1.

2.4.1.1.1. Sample preparation

Once the solubility of DTX-NLC was achieved using THF and acetonitrile: water mixture (50:50, v/v) as solvents of choice, then samples were tested for the specificity of the method to quantify DTX. For DTX detection and quantification, DTX (20 µg/ml) concentration was prepared in a mixture of (20: 80 v/v) THF then injected into the HPLC system to confirm that there was no interference with DTX peak.

A standard stock solution of DTX (100 µg/ml) was prepared in THF. Six working standards (ICH guidelines) were prepared by dilution of the stock in THF: mobile phase (20:80, v/v) to give DTX concentrations of 10, 8, 6, 4, 2 and 1 µg/ml. Samples were vortexed for 1 min, and a 1 ml solution of each sample was placed in an HPLC vial for analysis. All samples were injected three times, and the experiment was carried out in triplicate.

2.4.1.2. HPLC method validation for quantification of DTX from NLCs

The validation of the analytical methods for DTX quantification in DTX-NLC was carried out as per FDA and ICH regulations. The following validation parameters were addressed: specificity, linearity, precision, accuracy, LOD, LOQ, and stability.

2.4.1.2.1. Specificity

A 20 µg/ml DTX was prepared as described in section 2.4.1.1.1, and injected into the HPLC system, along with three other samples M.P, THF, and Blank-NLC (B-NLC). All samples were examined for DTX peak presence and symmetry.

2.4.1.2.2. Linearity

A linear regression analysis was achieved by examining a range of DTX concentrations (1, 2, 4, 6, 8, 9, 10 µg/ml) that were prepared as described in section 4.2.1.1.1, and a linear calibration plot was acquired.

2.4.1.2.3. Precision

2.4.1.2.3.1. Repeatability

As per the FDA and ICH guidelines, one level concentration was examined for the repeatability test. DTX at 4 µg/ml concentration was prepared as described in section 2.4.1.1.1 and injected ten times, then the percentage relative standard division (% RSD) was calculated.

2.4.1.2.3.2. Intra-day and inter-day precision

The intra-day analysis was carried out by preparing three concentrations with three injections under the same experimental conditions. 4, 6, and 10 µg/ml DTX concentrations were prepared as described in section 2.4.1.1.1 and examined for their standard deviation (SD) and % RSD, while for inter-day precision, one concentration of DTX (2 µg/ml) was prepared as described in section 2.4.1.1.1 and injected on three different days and the SD and % RSD were calculated.

2.4.1.2.4. Accuracy

Three DTX concentrations (6, 8, 10 µg/ml) were prepared as described in section 2.4.1.1.1 and examined for their accuracy and % RSD.

2.4.1.2.5. LOD and LOQ

The LOD and LOQ were obtained by examining one concentration of DTX (10 µg/ml) prepared as detailed in section 2.4.1.1.1, and LOD and LOQ were calculated.

2.4.1.2.6. Solution stability

One level concentration of DTX 3.5 µg/ml was prepared as described in section 2.4.1.1.1 and evaluated for its stability for up to six weeks, and the mean, SD, and %RSD were calculated.

2.4.2. HPLC method for quantification of DTX in two release media

In-vitro drug release studies were performed to quantify DTX released from the developed DTX-NLCs at 37 °C into two different release media, release medium I consisted of absolute ethyl alcohol and phosphate buffer saline (PBS), pH 7.4) (30:70, v/v) (Zhang *et al.,* 2017), while release media II consisted of 0.1 M PBS at pH 7.4 (Tan *et al.,* 2017). Chromatographic conditions were used for the HPLC were as detailed in section 2.4.1.

2.4.2.1. Sample preparations

For quantification of DTX in the release medium I, a standard stock solution of DTX (100 µg/ml) was prepared in ethanol. Five working standards were prepared by dilution with a mixture of (30:70, v/v) of ethanol and PBS pH 7.4 (release media I) to give a DTX concentration of 5, 2.5, 1, 0.5 and 0.25 µg/ml. For the release medium II, a standard stock solution of DTX (100 µg/ml) was prepared in ethanol. Five working standards were prepared by dilution with PBS, pH7.4 (release media II) to give DTX concentrations of 5, 2.5, 1, 0.5 and 0.25 µg/ml. All samples were vortexed for 1 min, and a 1 ml solution of each sample was placed in an HPLC vial for analysis.

2.4.2.2. HPLC method validation for quantification of DTX from release media

The validation of the analytical methods for DTX quantification in release media was carried out as per FDA and the ICH regulations. The following validation parameters were addressed: specificity, linearity, precision, accuracy, LOD, LOQ, and stability.

2.4.2.2.1. Specificity

A 1 µg/ml DTX was prepared in both the release media as described in section 2.4.2.1. and injected into the HPLC system, along with blank release media. All samples were examined for the presence of DTX peak and its symmetry.

2.4.2.2.2. Linearity

A linear regression analysis in two different media was achieved by examining a range of DTX concentrations (0.25, 0.5, 1, 2.5, and 5) µg/ml that were prepared as described in section 2.4.2.1. and linear calibration plots were acquired.

2.4.2.2.3. Precision

2.4.2.2.3.1. Repeatability

As per the FDA and ICH guidelines, one concentration was examined for the repeatability test. DTX at 0.25 µg/ml concentration was prepared in the two-release media as described in section 2.4.2.1 and injected ten times, then the percentage relative standard deviation (% RSD) was calculated.

2.4.2.2.3.2. Intra-day and inter-day precision

The intra-day analysis was carried out by preparing three concentrations with three injections under the same experimental conditions. Three DTX concentrations (0.25, 1, and 2.5 µg/ml) were prepared in both the media as described in section 2.4.2.1 and examined for their SD and % RSD, while for inter-day precision, one concentration of DTX 5 µg/ml was prepared in both the media as described in section 2.4.2.1, and injected in three different days, and the SD and % RSDs were calculated.

2.4.2.2.4. Accuracy

Three DTX concentrations (0.25, 2.5, and 5 µg/ml) were prepared in two different media as described in section 2.4.2.1 and examined for their accuracy and % RSD.

2.4.2.2.5. LOD and LOQ

The LOD and LOQ were obtained by examining one concentration of DTX (1 µg/ml) prepared in both the different media as detailed in section 2.4.2.1 and LOD and LOQ were calculated.

2.4.2.2.6. Solution stability

One concentration of DTX (2.5 µg/ml) was prepared as described in section 2.4.2.1 and evaluated for its stability for up to three days for the purpose of this analytical method, and the mean, SD, and %RSD were calculated.

2.4.3. HPLC method development for DTX quantification and extraction from biological matrices

Only a few HPLC methods for drug quantitation after permeation through a physiological *in-vitro* BBB model have been reported in the literature. In previous studies, the drug of interest was extracted and quantified from Ringer HEPES buffer (RHB) and/or Hank's balanced salt solution (HBSS, pH7.4) plus bovine serum albumin (BSA) as corresponding matrices (Jahne *et al.,* 2014; Moradi-Afrapoli *et al.,* 2016). To our knowledge, no method has been developed for DTX quantification in a biological matrix consisting of a mixture of biological media and human serum (HS). As the *in-vitro* BBB model comprised of three type of cells (endothelial, astrocytes and pericytes) and therefore a combination of three media along with human serum is required for their growth. Our study aimed to quantify DTX permeated in this biological matrix consisting of a mixture of three biological media and their growth supplements in equal ratio (1:1:1) as follows, EBM+ 2% HS/ 1 ml, ABM +3 % HS/ 1 ml PM+ 2% HS/1 ml. The serum addition is essential as a source of growth and adhesion factors and plays a crucial role as a cell membrane permeability regulator, and serves as a carrier for lipids, enzymes, micronutrients and trace elements for a basic cell culture environment (Invitrogen, Life Technologies). Therefore an HPLC method was developed and optimised specifically for DTX quantification in biological media consisting of serum. Isocratic and gradient mobile phases were explored, and mobile phase pH was adjusted to 5 by using orthophosphoric acid as recommended in the literature (Choudhury *et al.,* 2013).

2.4.3.1. HPLC Method optimisation

Various combinations of different reversed-phase columns flow rates and different mobile phases were evaluated to achieve a good resolution, symmetrical peaks, shorter retention time and better peak shape by improving peak separation of the drug of interest from sample components peaks (Rigo-Bonnin *et al.,* 2016).

2.4.3.1.1. Stationary phase optimisation

For the stationary phase optimisation, the methods by Schmidt *et al.,* (2017) and Khan *et al.,* (2016) were adapted for the DTX quantification. Four commercially available silica columns were utilised during method development: Kromasil 3.9 x 150 mm, (Waters, UK); Kinetex, 2.64 x B-C18 100Å, 75x4.60 mm, (Phenomenex, UK) and Luna 5µm, PFP(2) 100Å, 250 x 4.6 mm (Phenomenex, UK), under the same chromatographic conditions with mobile phase acetonitrile: water (50:50, v/v) at 1 ml/min flow rate.

2.4.3.1.2. Flow Rate (FR)

The method of Khan *et al.,* (2016) was adopted and optimised further. Mobile phase flow rates at 0.8, 0.9, and 1 ml/min were examined under the same experimental conditions acetonitrile: water (50:50, v/v) mobile phase and C18 Luna Column 5u PFP (2) 100A, 250 x 4.6 mm (Phenomenex) was selected for further studies. The flow rate that showed the best peak shape, symmetry and resolution were selected for validation studies.

2.4.3.1.3. Mobile phase

Isocratic and gradient mobile phase were tested using varying ratios of acetonitrile: water as shown in Table 2.1. The mobile phase that gave the target peak of DTX with no peak interference, acceptable peak symmetry and good separation from the sample component was selected for further validation according to ICH and FDA guidelines.

2.4.3.1.3.1. Isocratic mobile phase

Different mobile phases were tested (Table 2.1), for quantification of DTX in a biological sample.

Table 2.1 Isocratic mobile phase used for quantification of DTX in a biological sample.

Solvent A	Solvent B	Solvent C	pH	Ratio
Acetonitrile	H_2O	-	-	50:50
Acetonitrile	H_2O	-	-	40:60
Acetonitrile	H_2O	-	-	60:40
Acetonitrile	H_2O	-	-	70:30
Acetonitrile	H2O	-	-	65:30
Acetonitrile	1% acetic acid in H_2O	-	5	60:40
Acetonitrile	1% acetic acid in H_2O	-	5	40:60
Acetonitrile	The orthophosphoric acid in H_2O	THF	5	40:50:10

2.4.3.1.3.2. Gradient mobile phase

A gradient mobile phase was evaluated, and the pH was adjusted to 5 by using orthophosphoric acid (Choudhury *et al.,* 2013) as shown in Table 2.2. According to Rigo-Bonnin *et al.,* (2016) when a gradient mobile phase was used with lower pH it gave better peak separation.

Table 2.2 Table showing a gradient mobile phase with pH 5.

Time (min)	%B H2O	%C THF	%D Acetonitrile	FR (ml/min)
0	50	10	40	1
10	20	10	70	1
10	50	10	40	1
12	50	10	40	1

2.4.3.2. Optimisation of DTX extraction from biological samples and sample preparation

Precipitation of biological proteins by using acetonitrile prior to bioanalysis has been widely reported (Khan *et al.,* 2016; Jahne *et al.,* 2014; Moradi-Afrapoli *et al.,* 2016). Acetonitrile was therefore used to evaluate its suitability to extract DTX from biological samples in a combination with two other organic solvents THF and DMSO.

2.4.3.2.1. THF/acetonitrile for DTX extraction

DTX standard stock (100 µg/ml) was prepared in THF. Five working standards were prepared by diluting with (20: 80, v/v) THF: M.P (water: acetonitrile) to give a DTX concentration of 5, 4, 3, 2 and 1 µg/ml. A volume of 50 µl was placed in a 1.5 ml tube (Eppendorf) from each working standard, and 450 µl of biological media mixture was added to the working standard solution. A volume of 500µl of ice-cold acetonitrile was added to the mixture. All samples were vortexed for 1 min, the samples were centrifuged at 16300 x g for 30 min, then 800 µl supernatant was transferred to an HPLC vial for analysis. A further 300 µl supernatant was diluted with 200 µl acetonitrile and transferred to the HPLC for analysis.

2.4.3.2.2. DMSO/ acetonitrile for DTX extraction

A standard DTX stock solution concentration (500 µg/ml) was prepared in DMSO. Six working standards were prepared by dilution with a mixture of (20:80, v/v) of DMSO: M.P (acetonitrile: water, 50:50, v/v) to give DTX concentrations 40, 30, 20, 15, 10 and 4 µg/ml respectively. Samples were vortexed for 1 min and a volume of 50 µl was taken from each working standard and placed in a 1.5 ml tube (Eppendorf), 450 µl of primary cells media mixture was added to the working standard solution. The samples were vortexed for 1 min. Finally, 500 µl of ice-cold acetonitrile was added to give a DTX concentration of 2, 1.5, 1, 0.75, 0.5, and 0.2 µg/ml that contain 1% DMSO. The samples were centrifuged at 16300 x g for 30 min and 800 µl supernatant was placed in an HPLC vial and analysed.

2.4.3.2.3. DMSO/ acetonitrile for DTX extraction by using paclitaxel as an internal standard

A similar extraction method was used as detailed in section 2.4.3.2.2, with the presence of 0.1 µg/ml paclitaxel (PTX) as an internal standard (IS). After samples were vortexed for 1 min, 50 µl was taken from each working standard and placed in a 1.5 ml tube (Eppendorf), then 50 µl of PTX (0.1 µg/ml) was added, followed by addition of 400 µl of biological media. Finally, the samples were vortexed for 1 min and 500 µl of ice-cold acetonitrile was added to give a DTX concentration of 2, 1.5, 1, 0.5, 0.25, 0.1 and 0.05 µg/ml) that contained 1% DMSO. The samples were centrifuged at 16300 x g for 30 min and 800 µl was taken from the supernatant solution from each sample and placed in an HPLC vial and analysed.

2.4.3.3. HPLC method validation for DTX quantification and extraction from biological matrices

There are separate EMA and FDA guidelines for validation of the analytical methods for analytes that need to be resolved from a biological matrix. The validation was therefore performed considering these guidelines, whereby the following validation parameters were addressed: specificity, linearity and range, precision, accuracy, recovery, LOD, LOQ, matrix effect and stability and freeze throwing stability evaluation.

2.4.3.3.1. Specificity

DTX at 2 µg/ml and PTX (IS) at 0.1 µg/ml were prepared separately and in combination (2 µg/ml DTX and PTX 0.1 µg/ml) as described in section 2.4.3.2.3 and injected into the HPLC system along with two other samples M.P and blank-biological matrix (without DTX and PTX) to examine for any peak interference.

2.4.3.3.2. Linearity

A linear regression analysis was achieved by examining a range of DTX concentrations (0.05, 0.1, 0.25, 0.5, 1, 1.5, and 2) µg/ml that were prepared as described in section 2.4.3.2.3 and a linear calibration plot was acquired.

2.4.3.3.3. Precision

2.4.3.3.3.1. Repeatability

As per the FDA and ICH guidelines, one concentration of DTX 2 µg/ml was prepared as described section 2.4.3.2.3 and examined for repeatability by injecting nine times and the % RSD was calculated.

2.4.3.3.3.2. Intra-day and inter-day precision

The intra-day analysis was carried out by preparing three concentrations of DTX 0.05, 0.5, and 1 µg/ml (section 2.4.3.2.3) with three injections under the same experimental conditions and examined for their SD and % RSD; while for inter-day precision, one concentration of DTX 1.5 µg/ml was prepared and injected on three different days and the SD and % RSD were calculated.

2.4.3.3.4. Accuracy

Three DTX concentration 0.05, 0.5, and 1 µg/ml were prepared as described in section 2.4.3.2.3 and examined for their accuracy and % RSD.

2.4.3.3.5. Recovery

For evaluation of the extraction recovery method from biological matrices, a method was adopted and modified from Moradi-Afrapoli *et al.,* (2016). Four sets of standards were prepared as described in section 2.4.3.2.3, where: (set I) included DTX concentrations (low 0.05 µg/ mL, medium 0.5 µg/ mL and high 2 µg/ mL) extracted, then spiked with IS (0.1 µg/ mL PTX); (set II) a batch of blank samples were extracted and then afterwards were spiked with IS plus and DTX concentrations (low, medium and high). The absolute recovery of the extraction process was calculated by comparing the ratio of peak area obtained in the set I to peak area obtained from set II. Moreover, to calculate the absolute recovery for the IS, set III was prepared by extracting the IS with 0.1 µg/ml medium concentration and then afterwards was spiked with DTX (high concentration). Later, set IV was prepared by taking a blank sample replicate and extracting, then afterwards was spiked with IS plus high DTX concentration. By comparing the ratio of peak area for those of set III to those of set IV, an absolute recovery of the IS was calculated.

2.4.3.3.6. Matrix effect

DTX concentration of 1 µg/ml was prepared as described in section 2.4.3.2.3 in the presence and absence of a biological matrix and injected to determine the matrix factor.

2.4.3.3.7. LOD and LOQ

The LOD and LOQ were obtained by examining DTX at 2 µg/ml as detailed in section 2.4.3.2.3.

2.4.1.2.8. Solution stability

Three level concentrations of DTX (0.05, 0.5, and 2 µg/ml) were prepared as described in section 2.4.3.2.3 and stored at -20 °C and evaluated for their stability for up to 21 days and one concentration of DTX (0.5 µg/ml) was examined for its stability during three cycles of freeze/thawing then mean, SD and %RSD were calculated.

2.5. Results and Discussion

2.5.1. HPLC method development for DTX quantification in DTX-NLC

The key objective of the chromatographic method is to achieve separation of the impurity from the peak of interest (ICH guidelines). Well-separated peaks are essential for quantitation. This is a very useful parameter if potential interference peak(s) may be of concern. Previous studies have attempted to dissolve DTX from lipid microspheres using a combination of acetonitrile, water and methanol, where methanol was reported as the solvent of choice (Du *et al.,* 2013). In the present study, DTX-NLC solubility was investigated in a combination of the common organic solvents where the formulation failed to dissolve in the listed solvents (Table 2.3).

Table 2.3 DTX-NLC dissolved in variable ratios of organic.

DTX-NLC (ml)	**Organic solvent**	**Composition**	**Findings**
1	Ethanol: acetone	4.5: 4.5	Lipid does not dissolve.
1	DMC: THF	2: 7	Lipid does not dissolve.
1	Chloroform: THF	5: 5	Lipid does not dissolve.
1	Acetonitrile: THF	3: 7	Not clear.

It was found out that a combination of THF with either methanol or ethanol dissolved DTX-NLC samples successfully (Tables 2.4 and 2.5). Including methanol/ ethanol as solvents resulted in dissolving DTX-NLC yielding a clear solution. However, the chromatograms were causing a split in the DTX peak. Furthermore, when the volume of THF was increased to more than twice than ethanol a single sharp peak with good symmetry was obtained. Therefore, THF was used to dissolve the DTX-NLC and then a serial dilution with a combination of THF and mobile phase (acetonitrile: water 50:50, v/v) proved to be the best solvent for preparation of DTX-NLC samples.

Table 2.4 DTX-NLC dissolved in Methanol and THF in a different ratio.

DTX-NLC (ml)	**Methanol (ml)**	**THF (ml)**	**Findings**
1	4.5	5.5	Clear solution and peak splitting
1	5.5	5.5	Clear solution and peak splitting
1	5.5	7.5	Clear solution and peak splitting
1	4	6	Clear solution. Peak splitting
1	7	3	Lipid does not dissolve
1	7	4	Not Clear solution
1	5	7	Clear solution and peak splitting
1	3	9	Clear solution and peak splitting
1	2	10	Clear solution and peak splitting

Table 2.5 DTX-NLC formulation dissolved in Ethanol and THF with different ratios.

DTX-NLC (ml)	**Ethanol (ml)**	**THF (ml)**	**Findings**
1	5	5	Clear solution. Peak splitting
1	5	7	Clear solution. Peak splitting
1	7	3	Clear solution. Peak splitting
1	9	9	Clear solution. Peak splitting.
1	3	7	Clear solution. Peak splitting
1	6	14	Clear solution

2.5.1.1. HPLC method validation for quantification of DTX from NLCs

2.5.1.1.1. Specificity

As per ICH guidelines method, specificity and peak separation is a critical step for developing a new method for quantification of an analyte. A well separated DTX peak with good shape and symmetry were obtained when 20 µg/ml DTX was prepared in (20: 80, v/v) THF: M.P and the DTX peak was detected at a retention time (RT) of 8.6 min (Figure 2.1 a). Moreover, the absence of any peak at RT of 8.6 min confirmed that there was no excipient or impurity interference at the RT of DTX as is evident from chromatograms of B-NLC in M.P and THF (Figures 2.1 b, 2.1 c and 2.1 d). This method was found to be specific for DTX quantification in DTX-NLC and was further validated.

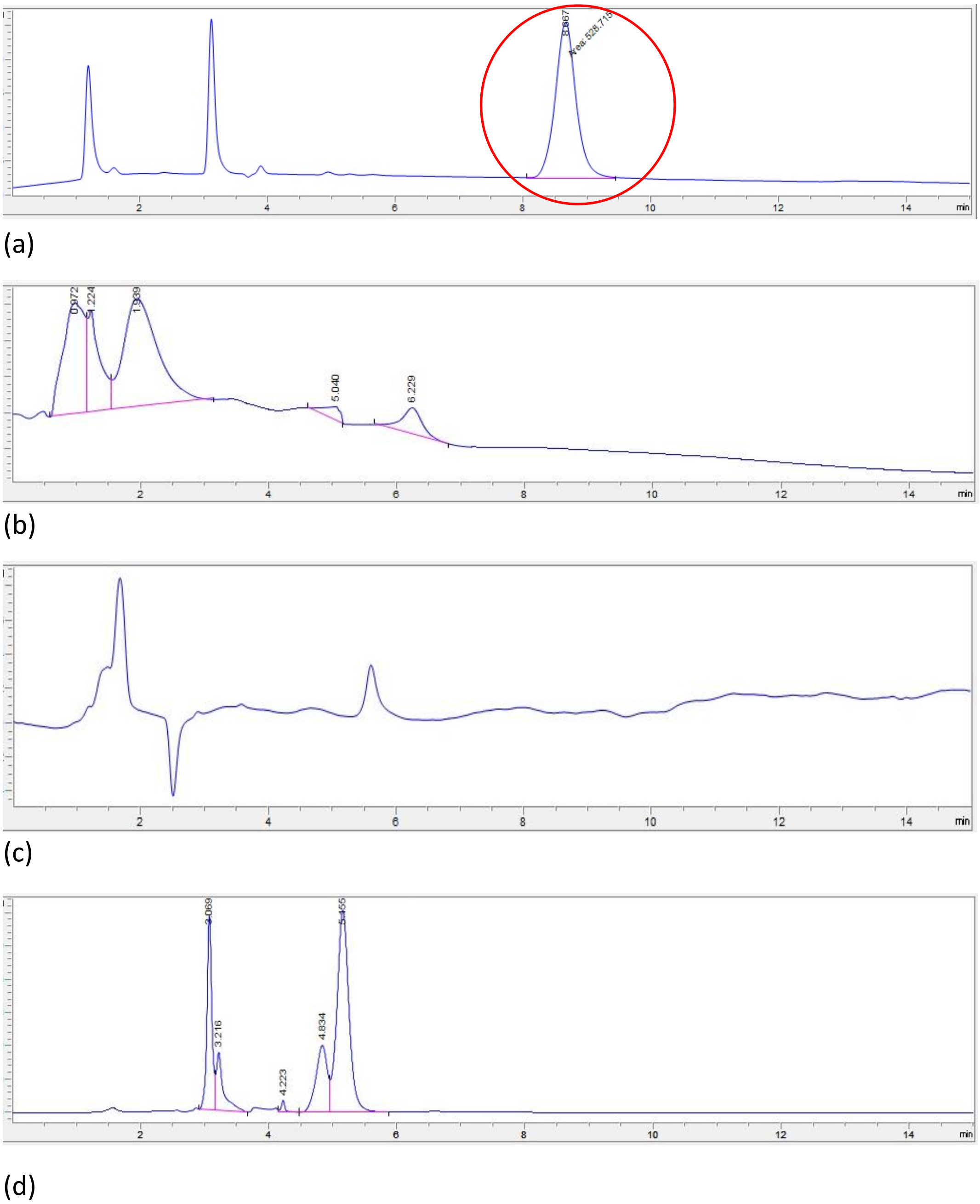

Figure 2.1 HPLC chromatograms (a) concentration 20 µg/ml of DTX dissolved in THF: M.P; (b) B-NLC dissolved in THF: M.P. (c) M.P peak; (d) THF peak. The peak of interest DTX had a retention time of 8.6 min.

2.5.1.1.2. Linearity

A linear calibration curve was acquired by plotting the mean area under the curve (MAUC) against DTX concentrations ranging from 1 to 10 µg/ml (Figure 2.2). The assessment of linearity was achieved by linear regression analysis using R^2 values. A correlation coefficient R^2 of 0.9994 was obtained demonstrating linearity of DTX for the studied concentration range. Similar findings were reported in the literature, where a standard plot was considered acceptable when the R^2 value is closer to 1 (Shabir 2004). An R^2 >

0.999 (Kumar *et al.,* 2010) and $R^2 > 0.990$ (Muthu *et al.,* 2011) were considered an excellent demonstration of the relationship between peak area and drug concentration. The respective linear regression was calculated by the equation below:

$Y = 21.504x+0.2972$ (Equation 2.1)

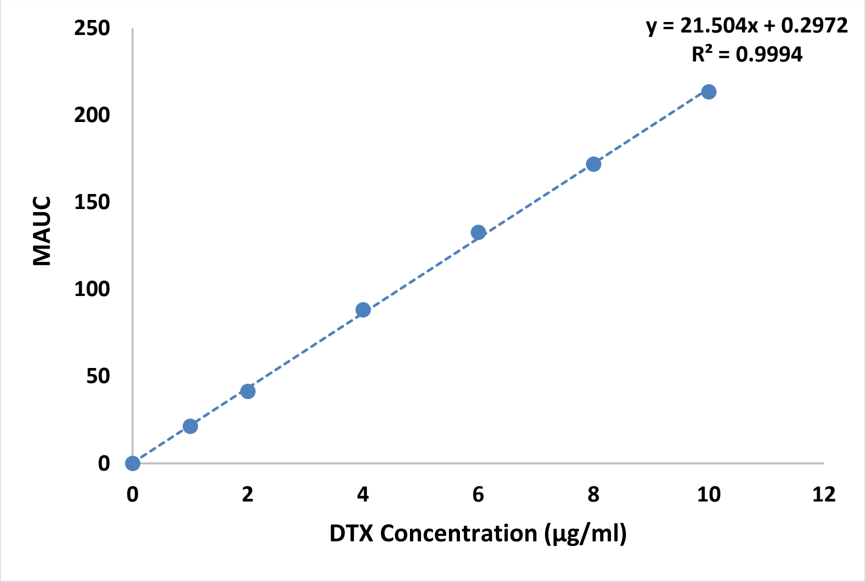

Figure 2.2 DTX standard plot showing a linear relationship between DTX concentration and average AUC obtained by HPLC analysis. Data are mean ± SD, (N=3).

2.5.1.1.3. Precision

The injection (system) precision of an analytical method is related to the repeatability and reproducibility of the technique and can be represented as % RSD.

2.5.1.1.3.1. Repeatability

The ICH and FDA guidelines propose injection of the same sample ten times under the same chromatographic conditions. This experiment established repeatability by performing ten replicates for independently prepared DTX concentration (4 µg/ml) where RSD was 0.709 % (Table 2.6). All data were considered acceptable for the injection repeatability when the % RSD ≤ 1 % (ICH and FDA guidelines).

Table 2.6 HPLC data obtained for the injection repeatability (instrumental precision) using the same concentration of DTX.

DTX labelled concentration (µg/ml)	DTX actual concentration (µg/ml)
4	3.606
	3.643
	3.620
	3.624
	3.638
	3.583
	3.615
	3.559
	3.615
	3.578
Average	3.608
SD	0.025
RSD (%)	0.709

2.5.1.1.3.2. Intra-day and Inter-day precision

Intra-day precision was established by analysing three concentrations with three injections under the same experimental conditions following the ICH guidelines. The % RSD values for the nominated three DTX concentrations 4, 6 and 10 µg/ml were 1.497, 0.470 and 0.088 % respectively (Table 2.7). Intra-assay precision was considered acceptable when the % RSD ≤ 2. The ICH guidelines suggest inter-day precision should be determined by the injection of one sample on three different days. A 2µg/ml was the nominated DTX concentration for this experiment. The obtained % RSD was (0.753 %) (Table 2.8) which was well within the acceptable limits of ≤ 2 %. All generated data were within the acceptable limits of the ICH guidelines.

Table 2.7 HPLC data obtained for intra-day method precision.

DTX labelled concentration (µg/ml)	DTX actual concentration (µg/ml)	SD	%RSD
4	4.047	0.060	1.479
	4.075		
	4.163		
6	6.147	0.028	0.470
	6.189		
	6.133		
10	9.911	0.008	0.088
	9.909		
	9.895		

Table 2.8 HPLC data obtained for inter-day method precision.

DTX labelled concentration (µg/ml)	Time (day)	DTX actual concentration (µg/ml)
2	Day 1	2.01
	Day 2	1.997
	Day 3	1.980
Mean	1.995	
SD	0.015	
% RSD	0.753	

2.5.1.1.4. Accuracy

The accuracy of an analytical method is the closeness of the measured results to the actual concentration of the standard. The following equation was used to calculate the accuracy:

Accuracy = 100*(calculated data/ actual data) (Equation 2.2)

For DTX concentrations, 6, 8 and 10 µg/ml, the recovery of DTX in samples ranged from 99 % to 100.6 % (Table 2.9). The method was found to be accurate as the % RSD was well within the acceptable limits 100 ± 2 % following ICH and FDA guidelines.

Table 2.9 Results obtained for method accuracy.

DTX labelled concentration (µg/ml)	DTX actual Concentration (µg/ml)	Accuracy (%)	RSD (%)
6	6.15	100.6	0.090
8	7.97	99.6	1.069
10	9.90	99.0	0.099

2.5.1.1.5. LOQ and LOD

The LOQ is the lowest quantity that can be quantified by HPLC system; while the LOD is the lowest quantity that can be detected (ICH and FDA guidelines). The two parameters were calculated as described in the equations below:

LOQ= (10X % SD)/Slope (Equation 2.3)

LOD= (3.3x % SD)/Slope (Equation 2.4)

The LOQ of DTX was obtained at 0.041 µg/ml and the LOD was 0.013 µg/ml under the same conditions.

2.5.1.1.6. Solution stability

The RSD of the assay of DTX during solution stability experiments was < 1.0 % (Table 2.10). No change was observed in the content of the solution during stability experiments. The experimental data confirmed that sample solutions used during the assay were stable up to six weeks and were suitable for the intended purpose of the developed HPLC method (ICH guidelines).

Table 2.10 Sample stability.

DTX labelle Concentration (µg/ml)	Time (day)	DTX actual Concentration (µg/ml)
3.5	1	3.52
	2	3.52
	3	3.58
	7	3.57
	14	3.52
	28	3.54
	35	3.54
	42	3.53
Mean	3.54	
SD	0.023	
% RSD	0.658	

The development and validation of this HPLC method according to ICH and FDA guidelines for the DTX quantification, demonstrated the HPLC method was suitable for measurement of DTX content, encapsulation efficiency and total DTX entrapped in DTX-NLC.

2.5.2. HPLC method for quantification of DTX from release media

2.5.2.1. HPLC method validation for quantification of DTX from release media

2.5.2.1.1. Specificity

The chromatographic separation was achieved by using the HPLC method as described 2.3.1. An acceptable DTX peak with good shape and symmetry were obtained in both release media. The DTX peak was detected at RT of 8.9 min (Figure 2.3 a and b). Moreover, the absence of the peak at RT of drug (8.9 min) when only blank release media was injected (Figure 2.3 c and d) confirmed that there was no interference of release media components with the DTX peak demonstrating the specificity of the method and was considered to be acceptable and serve its purpose for quantification of DTX in release media.

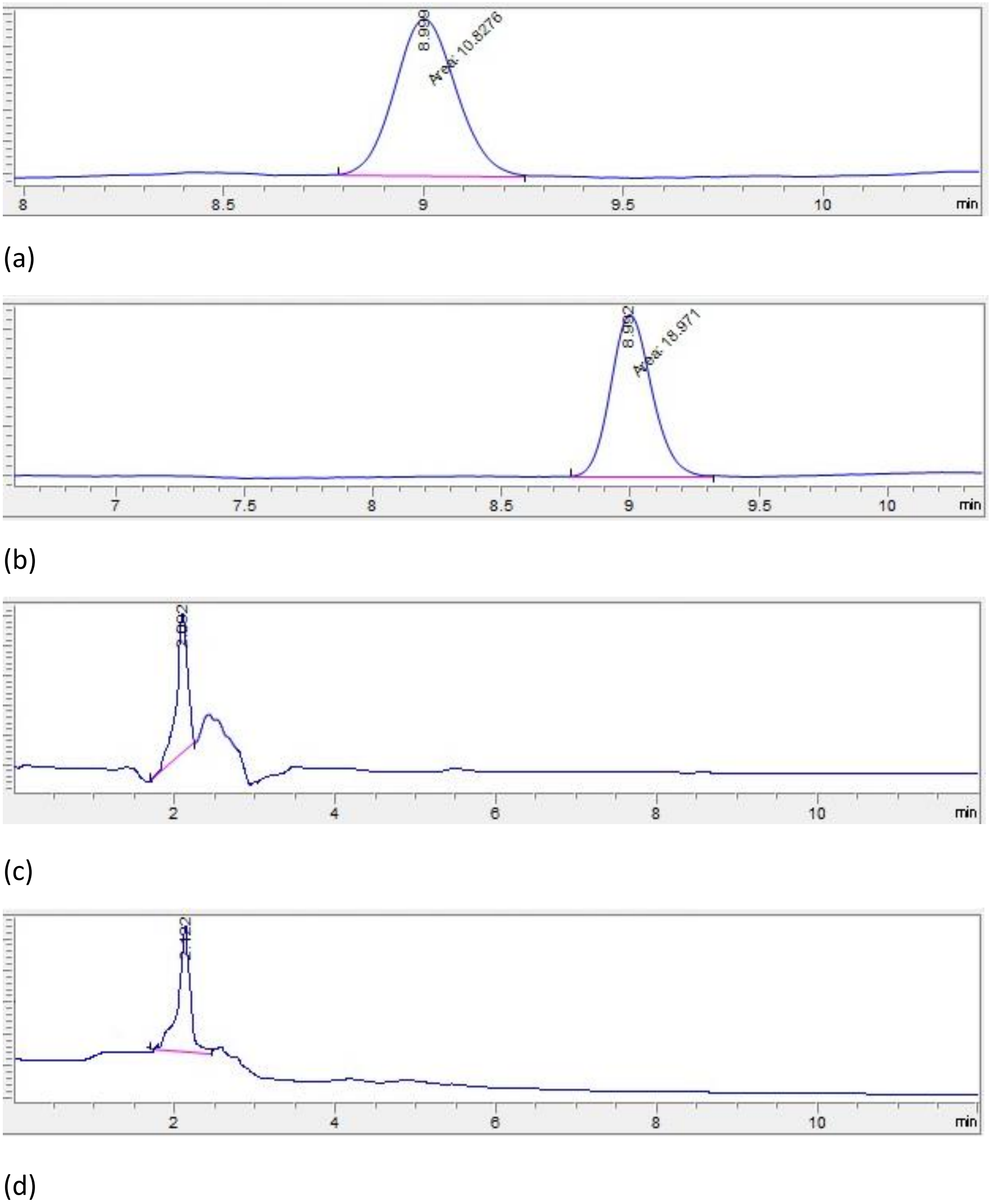

Figure 2.3 HPLC chromatograms (a) concentration 1 µg/ml of DTX dissolved in release media (30:70, v/v, ethanol: PBS pH7.4) (b) concentration 1 µg/ml of DTX dissolved in release media (100%, PBS pH7.4), (c) blank release media (30:70, v/v, ethanol: PBS pH7.4), (d) blank release media (100%, PBS pH7.4).

2.5.2.1.2. Linearity

Linear calibration curves were acquired by plotting the mean area under the curve (MAUC) against DTX concentrations ranging from 5 to 0.25µg /ml (Figure 2.4 a, b) for the two-release media respectively. The assessment of linearity was achieved by linear regression analysis using R^2 values.

The correlation coefficients R^2 obtained were 0.9999 for the release media I and II. This demonstrated that the linearity for DTX quantification from both the release media within the studied concentrations range was acceptable (Muthu *et al.,* 2011; Shabir 2004) as ICH guidelines recommend when the value of R^2 is close to or equal to 1, the developed HPLC method is within the acceptable limits. The equations of the linear curves were as below:

$Y=20.687x-0.2672$ (Equation 2.5)
$Y=20.994x-0.1584$ (Equation 2.6)

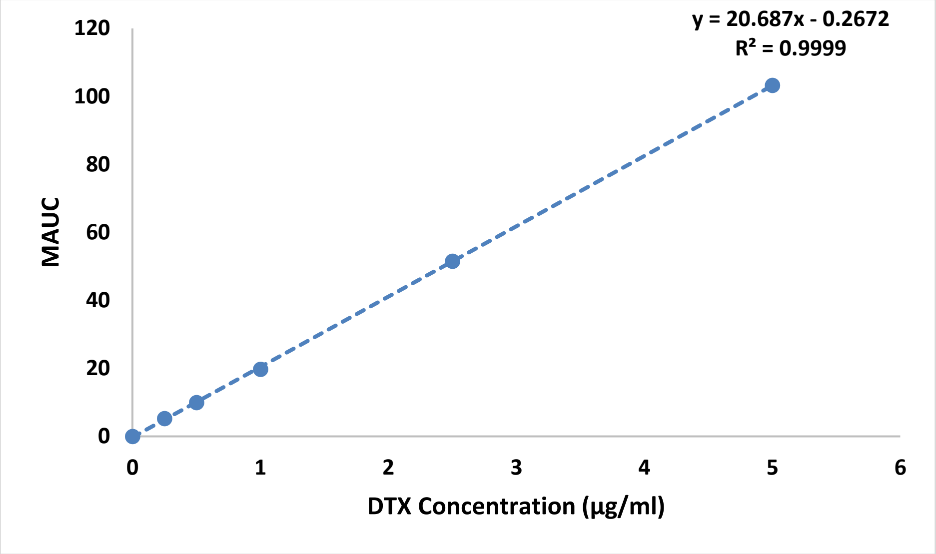

(a)

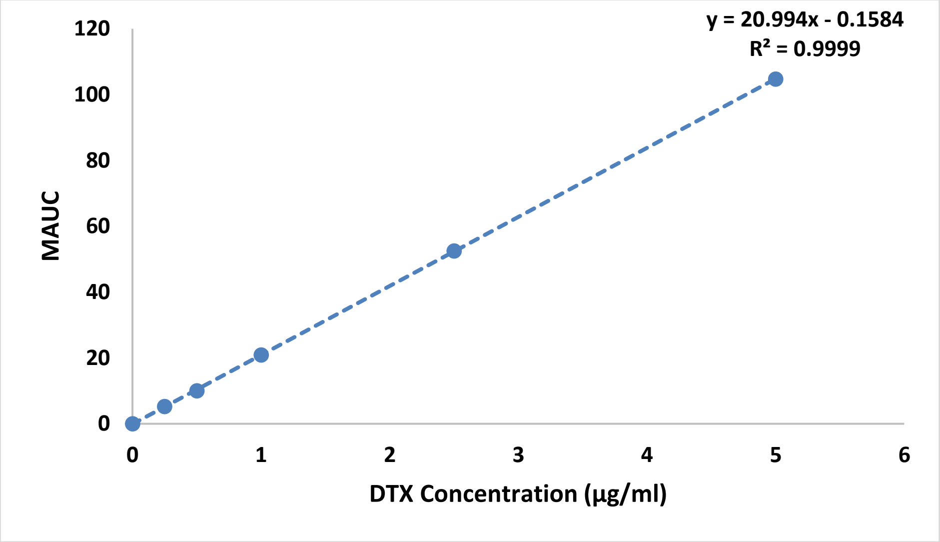

(b)

Figure 2.4 DTX standard plots showing (a) linear relationship of DTX concentration and average AUC obtained for the release media I (30:70, v/v, ethanol: PBS pH7.4) and (b) linear relationship of DTX concentration and average AUC obtained for the release media II (100 % PBS pH7.4) HPLC analysis. Data are mean ± SD, (N=3).

2.5.2.1.3. Precision

2.5.2.1.3.1. Repeatability

The ICH and FDA guidelines propose injection of the same sample ten times under the same chromatographic conditions. This experiment established repeatability by performing the ten replicates for independently prepared DTX concentration (0.25 µg/ml) for both the release media. A low % RSD (0.741 % and 0.907 %) was obtained for both release media respectively (Table 2.11). All data were considered acceptable for the injection repeatability when the % RSD ≤ 1 % (ICH and FDA guidelines).

Table 2.11 HPLC data obtained for the injection repeatability (instrumental precision) using same concentration of DTX for release media (30:70, v/v ethanol: PBS pH7.4) I and II (100 % PBS pH7.4) release media II.

DTX labelled Concentration (µg/ml)	DTX actual Concentration (µg/ml) Release Media I	DTX actual Concentration (µg/ml) Release Media II
0.25	0.251	0.251
	0.255	0.256
	0.252	0.251
	0.255	0.248
	0.256	0.249
	0.253	0.252
	0.251	0.251
	0.255	0.252
	0.253	0.252
	0.252	0.252
Average	0.253	0.251
SD	0.001	0.002
RSD (%)	0.741	0.907

2.5.2.1.3.2. Intra-day and Inter-day precision

Intra-day precision was established by analysing three concentrations with three injections under the same experimental conditions following the ICH guidelines. The % RSD values for nominated DTX concentrations 0.25, 1 and 5 µg/ml were 0.84, 0.446 and 0.79 % (Table 2.12) for the release media I, and 0.624, 0.881 and 0.264 % for release media II respectively (Table 2.12). Intra-assay precision was considered acceptable when the % RSD ≤ 2 (ICH and FDA guidelines). The ICH guidelines suggest the injection of one sample on three different days for inter-day precision. A 5 µg/ml was used in both release media as the nominated DTX concentration for this experiment. The % RSD obtained were (0.718 and 0.313 %) for the two-release media respectively (Table 2.13). The % RSD values were well within the acceptable limits of ≤ 2 % (ICH and FDA guidelines).

Table 2.12 HPLC data obtained for intra-day method precision for release media I (30:70, v/v, ethanol: PBS Ph7.4) I and release media II (100 % PBS Ph7.4) II.

DTX labelled concentration (µg/ml)	DTX actual concentration (µg/ml) Release media I	SD	%RSD	DTX actual concentration (µg/ml) Release media II	SD	%RSD
0.25	0.256	0.002	0.840	0.253	0.001	0.624
	0.252			0.250		
	0.253			0.252		
1	0.959	0.004	0.446	0.991	0.008	0.881
	0.952			0.993		
	0.960			1.007		
2.5	2.505	0.019	0.790	2.507	0.006	0.264
	2.479			2.510		
	2.518			2.498		

Table 2.13 HPLC data obtained for inter-day method precision for release media (30:70, v/v ethanol: PBS Ph7.4) I and for the release media (100 % PBS Ph7.4) II.

DTX labelled concentration (µg/ml)	Time (day)	DTX actual concentration (µg/ml)	Time (day)	DTX actual concentration (µg/ml)
5	Day 1	5.050	Day 1	5.007
	Day 2	4.993	Day 2	4.981
	Day 3	4.984	Day 3	5.010
Mean	5.00		4.99	
SD	0.035		0.015	
% RSD	0.718		0.313	

2.5.2.1.4. Accuracy

The accuracy of an analytical method is the closeness of the measured results to the actual data; equation 2.2 was used to calculate the accuracy. For DTX concentrations 0.25-5 µg/ml, the recovery of DTX in samples was ranging from 100 % to 101.6 % (Table 2.14) for the release media I, and 99.99 % to 100.7 % for the release media II (Table 2.14). The method was found to be accurate as the % RSD values were well within the acceptable limits 100 ± 2 % of the ICH and FDA guidelines.

Table 2.14 Results obtained for method accuracy for release media (30:70, v/v and ethanol: PBS Ph7.4) I and for release media (100% PBS Ph7.4) II.

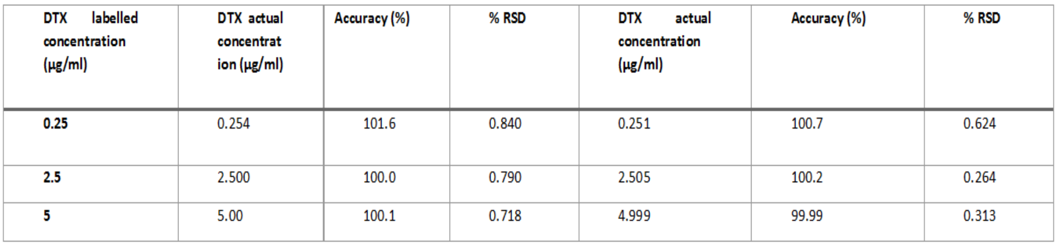

DTX labelled concentration (µg/ml)	DTX actual concentration (µg/ml)	Accuracy (%)	% RSD	DTX actual concentration (µg/ml)	Accuracy (%)	% RSD
0.25	0.254	101.6	0.840	0.251	100.7	0.624
2.5	2.500	100.0	0.790	2.505	100.2	0.264
5	5.00	100.1	0.718	4.999	99.99	0.313

2.5.2.1.5. LOQ and LOD

The LOQ and LOD were calculated as described in equations 2.3 and 2.4, respectively. The LOQ of DTX was obtained at 0.216 and 0.42 µg/ml for release media I and II respectively while LOD was 0.071 and 0.138 µg/ml respectively for the two media under the same conditions.

2.5.2.1.6. Solution stability

The RSD of the assay of DTX during solution stability experiments were 0.872 and 0.275 % for the first and second release media, respectively when 2.5 µg/ml was assessed as nominated concentration to test the stability of both release media (Table 2.15). No changes were observed in the content of the solution during stability experiments. The experimental data confirmed that sample solutions used in the assay were stable up to three days and were suitable for the intended purpose of the developed HPLC method.

Table 2.15 Sample stability for release media (30:70, v/v and ethanol: PBS pH7.4) I and release media (100% PBS pH7.4) II.

DTX labelled concentration (µg/ml)	Time (day)	DTX actual concentration (µg/ml)	DTX labelled concentration (µg/ml)	Time (day)	DTX actual concentration (µg/ml)
2.5	1	2.494	**2.5**	1	2.208
	2	2.514		2	2.210
	3	2.470		3	2.219
Mean	2.493		2.212		
SD	0.021		0.006		
% RSD	0.872		0.275		

The HPLC methods developed and validated according to ICH and FDA guidelines for quantification of free DTX in release media were thus found suitable for the purpose.

2.5.3. HPLC method development for quantification of DTX from the biological matrix

HPLC method for the extraction and quantification of DTX from the biological sample was established as described in section 2.4.3.2.3. This method was required to quantify a low concentration of DTX in the biological matrix when samples were collected from the basolateral side of a physiological 3D *in-vitro* BBB model. This matrix consisted of a combination of three primary cells media prepared as per recommended manufacturer directions (supplements, protein and human serum) (Lonza, UK). No previous method has been reported DTX quantification after collecting a sample from a physiological *in-vitro*

BBB model. Earlier methods have employed, RHB and HBSS as matrices for such quantification (Jahne *et al.,* 2014; Moradi-Afrapoli *et al.,* 2016).

2.5.3.1. HPLC method optimisation

2.5.3.1.1. Optimisation of stationary phase

The selection of a suitable HPLC column is a major step to achieve a good analyte peak. Four reversed phase C18 columns were investigated, shows that DTX could not be detected at a low concentration of 1 µg/ml when HPLC was performed using Kinetex, 2.64 x B-C18 100A, 75x4.60 mm column (Phenomenex), the peak tailing and poor symmetry was the reason behind disregarding this column. The high concentration of DTX at 10 and 100 µg/ml were quantified by using the C18, 150 mm, Kromasil column, but there was an interference between the diluent and the DTX peak. In addition, the peak symmetry was not acceptable. A high concentration of DTX at 10 and 100 µg/ml were quantified using C18, 3.9 x 150 mm, Waters column, but this column was not used due to peak interference with the diluent. According to ICH guidelines the accuracy of quantification decreases with increase in peak tailing because of the difficulties encountered during integration in determining where and when the peak ends, hence the calculation of the area under the peak will not be accurate. All columns described above have very short column length, which may have contributed to peak tailing and/or peak interference. Column choice is a critical step in acquiring a good shape peak with no interference (Schmidt *et al.,* 2017; Khan *et al.,* 2016). Moreover, a new column with longer length and presence of pentafluoro phenyl (PFP) in column packing, Luna 5u PFP(2) 100A, C18, 250 x 4.6 mm (Phenomenex) was used specifically for separation of hydrophobic compounds. The chromatogram (Figure 2.5 c, d, e) reveals an acceptable peak with good symmetry and no interference. Also, a lower concentration could be detected using this particular column after further optimisation. This column was therefore used for quantification of DTX in biological matrices.

2.5.3.1.2. Optimisation of flow rate (FR)

Three mobile phase flow rates were explored, as described in section 2.4.3.1.2. The FR of 0.8 and 0.9 ml/min did not show any peak at lower DTX concentration of 1 µg/ml. Poor peak symmetry and peak tailing were obtained with this FR at high concentrations of DTX. The HPLC chromatogram obtained at a flow rate of 1 ml/ min (figure 2.5 c, d, e), showed acceptable DTX peak with good peak symmetry and no interference. Importantly, lower concentration could be detected using this specific flow rate. This FR was selected for further HPLC method development for quantification of DTX in biological matrices. This finding was in line with another previous study (Sathyamoorthy *et al .,* 2014).

2.5.3.1.3. Optimisation of mobile phase

Different mobile phases were examined for quantification of DTX in a biological matrix as described in section 2.4.3.1.3. Initially, isocratic mobile phases were investigated for quantification of DTX, which caused interference of the diluent with the DTX peak, unacceptable peak tailing, the peaks symmetry was not acceptable. According to Agilent technical support, a lower pH might improve the peak shape and symmetry, further orthophosphoric acid was used (Choudhury *et al.,* 2014) to bring the preferred pH in a gradient mobile phase as described in Table 2.2. Chromatogram (figure 2.5 d) displayed DTX peak with good shape, by using this M.P a low DTX concentration (0.2 µg/ml) was quantified with acceptable peak symmetry and no peak tailing when ortho-phosphoric acid was selected to bring the preferred pH to the gradient mobile phase. This gradient mobile phase was used for the quantification of DTX in biological matrices. Further optimisation was carried out for the quantification of DTX from the biological matrix.

2.5.3.2. Optimisation of sample preparation

Extraction of DTX from the biological matrix was carried out investigating acetonitrile with two organic solvents THF and DMSO as described in section 2.4.3.2. only the use of DMSO/acetonitrile and extracting the DTX using ice-cold acetonitrile were found to be a suitable method, as no peak interferences from the biological matrix with the DTX peak were found and the peak symmetry was found to be acceptable with no peak tailing (Figure 2.10 c and d). This method was therefore selected for the DTX extraction and quantification of biological matrices in the presence of PTX, which was used as IS and validated according to ICH, FDA and EMA guidelines.

2.5.3.3. HPLC method validation for DTX extraction and quantification from the biological matrix

2.5.3.3.1. Specificity

This method demonstrated specificity for quantification of DTX in a biological matrix, due to the absence of any interfering peak at RT of DTX (7.2 min) when blank biological matrix and gradient mobile phase were injected in HPLC as evident by chromatograms shown in figure 2.5 a and b. DTX peak eluted at RT 7.2 min (Figure 2.5 c and d) when extracted from biological samples with symmetrical peak shape and good baseline resolution. The PTX (IS) peak eluted at RT 7.7 min (Figure 2.5 c and e). Moreover, there was no peak interference from other sample components (Figure 2.5 c, d and e). The absence of any interfering peaks from the blank biological matrix and gradient mobile phase (Figure 2.5 a and b) at RTs of the analyte and internal standard highlights the specificity of this method.

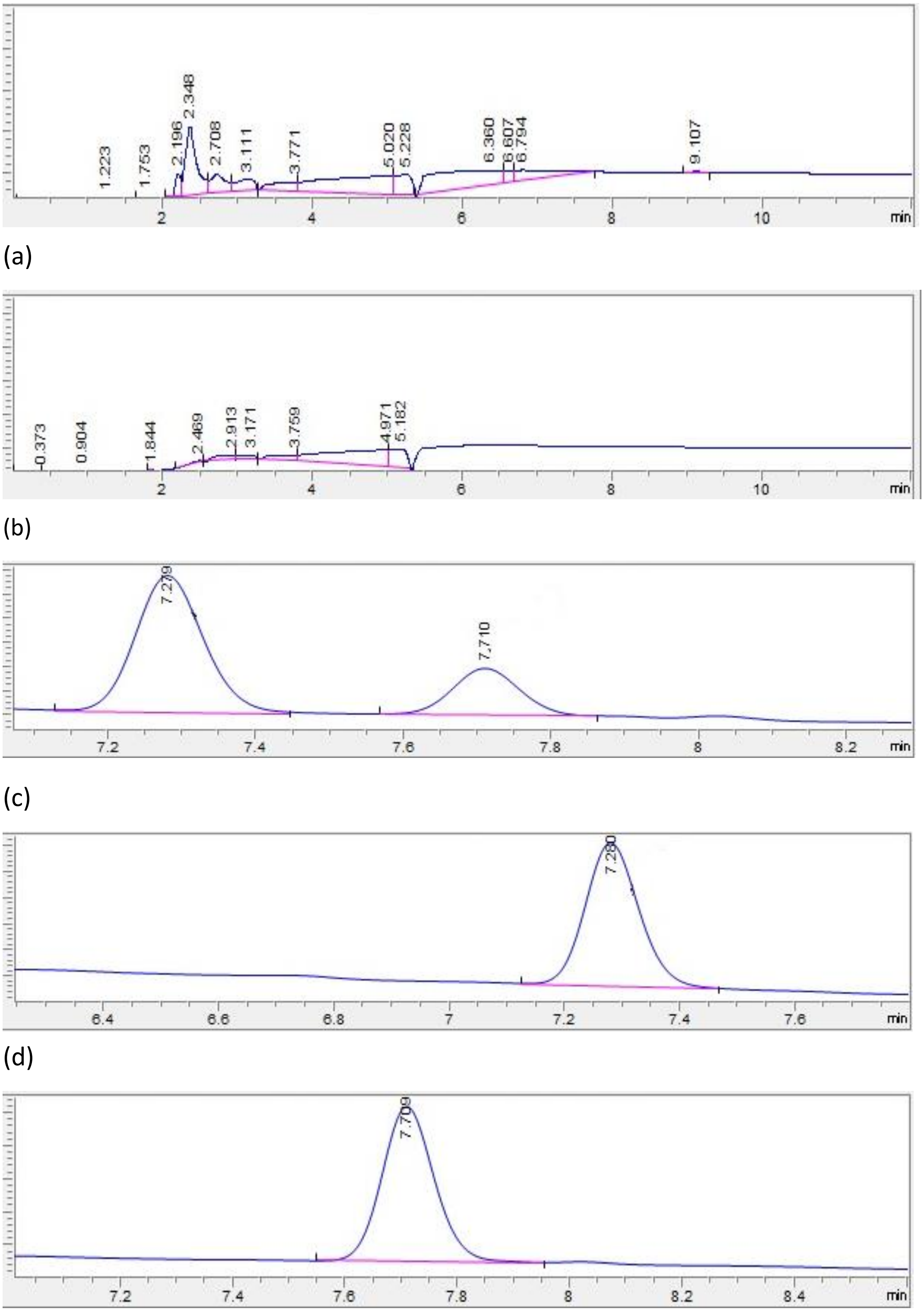

Figure 2.5 HPLC chromatograms (a) blank biological matrix, (b) gradient mobile phase, (c) docetaxel and internal standard paclitaxel extracted from the biological matrix, (d) docetaxel peak in a biological matrix, (e) paclitaxel peak in the biological matrix.

2.5.3.3.2. Linearity

A linear calibration curve was acquired (Figure 2.6), using the standard solutions ranging from 0.05 to 2 µg/ml. The calibration curve was generated by a linear fit of the DTX/PTX standard area ratio versus DTX concentration. The assessment of linearity was performed by linear regression analysis using R^2 values.

In this study, the correlation coefficient R^2 obtained was 0.9987. Similar results were obtained previously (Moradi-Afrapoli *et al.,* 2016). Since the acquired R^2 value was acceptable, this demonstrated that the linearity of the DTX quantification within the studied concentration range for the newly developed method was acceptable. It was calculated according to the following equation:

$Y = 3.4588x-0.0247$ ***(Equation 2.8)***

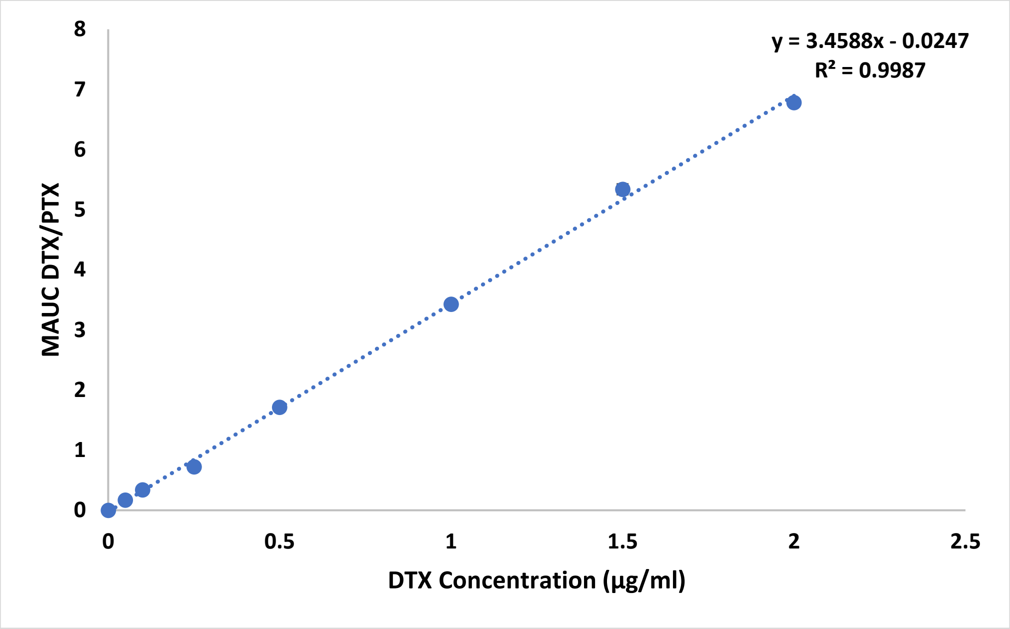

Figure 2.6 DTX standard plot for DTX from the biological matrix. Data are mean ± SD, (N=3).

2.5.3.3.3. Precision

The % RSD was generated by calculating the DTX/PTX ratio as described below:

2.5.3.3.3.1. Repeatability

Repeatability precision was evaluated by injecting one concentration nine times. The % RSD value obtained for the instrumental precision for DTX at a nominated concentration of 2 µg/ml was 2.099 % (Table 2.16). Samples were acceptable if the assay value was within the acceptable limits (±5 % RSD) following EMA guidelines, it is worth to mention that this result is in line with the FDA and ICH guidelines as well.

2.5.3.3.3.2. Intra and inter-day precision

Intra-day precision was assessed by three injections for three different concentrations. The % RSD values for the nominated three DTX concentrations of 0.05, 0.5 and 1 were 1.081, 1.890 and 0.988 % respectively (Table 2.17). Moreover, the ICH guidelines suggest the injection of one sample on three different days to examine the inter-day precision. The % RSD value was 1.615 % for the nominated concentration of DTX 1.5 µg/ml (Table 2.18). Acceptable limits within the % RSD values ≤ 10% according to EMA guidelines, FDA and ICH guidelines as well. Thus, the newly developed method for DTX quantification from the biological sample was within the acceptable limits.

Table 2.16 HPLC data obtained for the injection repeatability (instrumental precision) using the same concentration of DTX.

DTX labelled concentration (µg/mL)	DTX/PTX actual concentration (µg/mL)
2	1.977
	1.948
	2.010
	2.006
	1.908
	1.979
	1.938
	2.006
	2.012
Average	1.970
SD	0.041
RSD (%)	2.099

Table 2.17 HPLC data obtained for intra-day method precision.

DTX labelled concentration (µg/mL)	DTX/PTX actual concentration (µg/mL)	SD	RSD%
0.05	0.049	0.0005	1.081
	0.048		
	0.049		
0.5	0.493	0.009	1.890
	0.489		
	0.507		
1	0.985	0.009	0.988
	0.995		
	1.005		

Table2.18 HPLC data obtained for inter-day method precision.

DTX labelled Concentration (µg/ml)	Time (day)	DTX/PTX Actual concentration (µg/ml)
1.5	Day 1	1.528
	Day 2	1.546
	Day 3	1.578
Mean	1.551	
SD	0.025	
% RSD	1.615	

2.5.3.3.4. Accuracy

The accuracy of an analytical method is the closeness of the measured results to the actual data. It can be calculated using accuracy method equation 2.2.

The % accuracy for DTX in samples ranging from 0.05 to 1 µg/ml ranged from 98.6 to 99.5 % with RSD in range of 0.988 to 1.890 (Table 2.19). These findings were in line with the ICH, FDA and EMA guidelines. Acceptable limit of accuracy is ±10 % RSD. Therefore, the method can be said to be accurate

Table 2.19 Results obtained for method accuracy.

DTX labelled concentration (µg/ml)	DTX/PTX actual concentration (µg/ml)	Average accuracy (%)	Average RSD (%)
0.05	0.049	98.6	1.081
0.5	0.497	99.41	1.890
1	0.995	99.5	0.988

2.5.3.3.5. Recovery

The extraction recovery was determined as described in section 2.4.3.3.5 for three nominated DTX concentrations 0.05, 0.5 and 1 µg/ml, in three replicates plus medium concentration of PTX as IS 0.1 µg/ml by comparing the ratio of the set I (Figure 2.7 a) to the ratio of set II (Figure 2.7 b). The obtained % recovery was 100.02 %, 101.90 % and 90.03 % for the nominated DTX concentrations (Table 2.20) and the % recovery for the IS was 99.59 %, by calculating the ratio when peak area from set III (Figure 2.7 c) was compared to those peak area obtained in set IV (Figure 2.7 d) as tabulated in table 2.21.

All obtained data showed acceptable extraction recovery with respect to ICH, FDA and EMA guidelines, which mention that RSD must be less than ±15%, which was achieved in this experiment. Moreover, the obtained extraction recovery % were better than data reported by Jahne *et al.,* (2014) and Moradi-Afrapoli *et al.,* (2016). This might be due to their method employs buffers as a matrix, and lower centrifugation time and speed during the extraction. We have used a centrifugation time of 30 min at 16300 x g to ensure high extraction of DTX and PTX resulting in their high recovery.

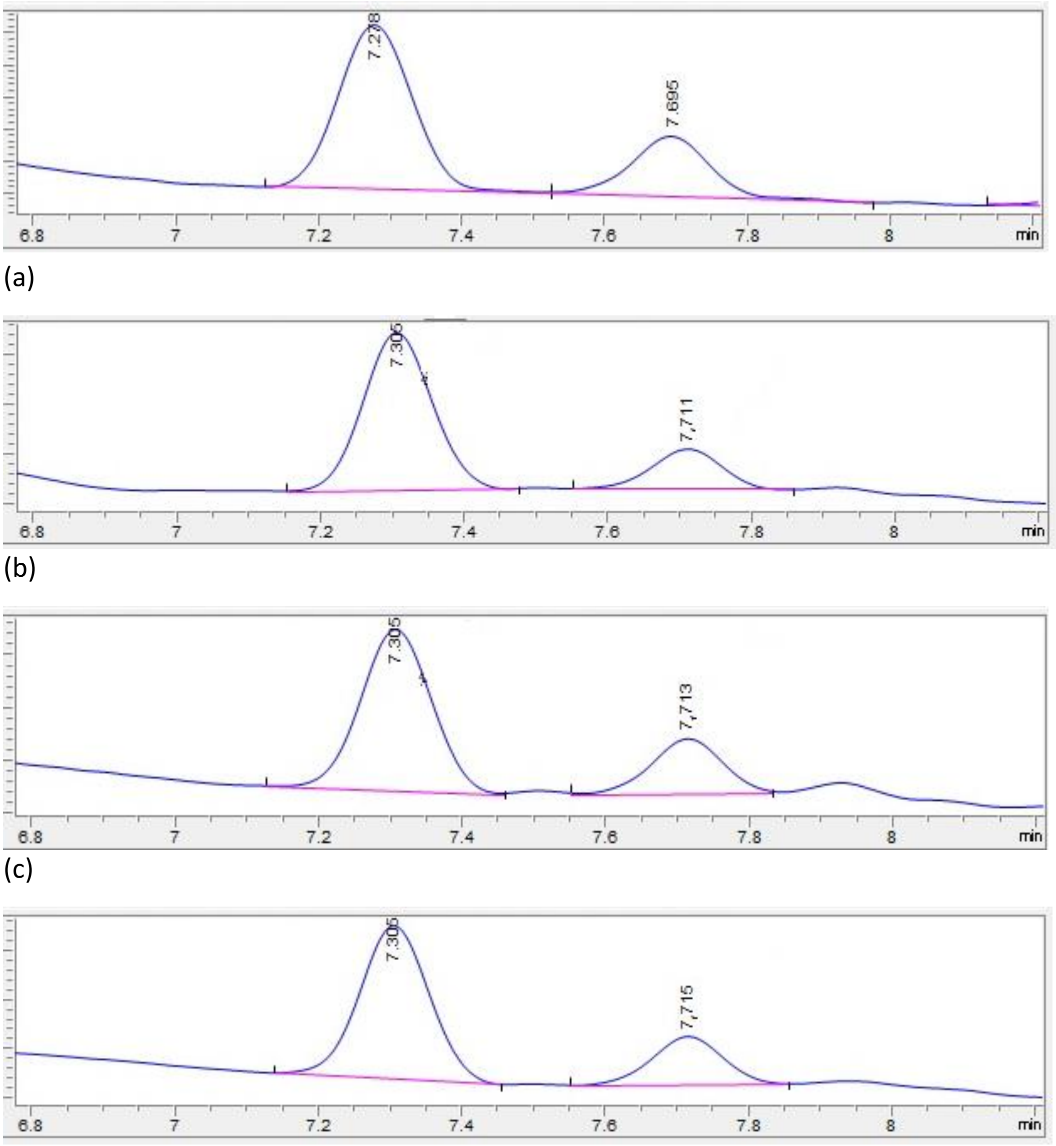

(a)

(b)

(c)

(d)

Figure 2.7 HPLC chromatogram showing the peak resolution for (a) 1 µg/ml docetaxel extracted and then unprocessed IS added in biological matrix (set I), (b) extraction of blank biological matrix then adding unprocessed 1µgm/ml docetaxel and IS 0.1 µg/ml (set II), (c) 0.1 µg/ml IS extracted and then unprocessed 1µg/ml docetaxel was added in biological matrices (set III), (d) extraction of blank biological matrices then adding unprocessed 1µgm/ml docetaxel and IS 0.1 µg/ml (set IV).

Table 2.20 Results obtained for method recovery for DTX.

DTX labelled concentration (µg/ml)	Set I	Set II	% Recovery
0.05	0.279	0.245	100.02
	0.273	0.281	
	0.236	0.266	
Average	0.2634	0.264	
SD	12.944		
%RSD	12.941		
0.5	1.524	1.557	101.90
	1.729	1.582	
	1.578	1.600	
Average	1.610	1.580	
SD	6.392		
%RSD	6.273		
1	2.959	3.656	90.03
	2.920	3.115	
	2.722	2.852	
Average	2.867	3.208	
SD	7.934		
%RSD	8.812		

Table 2.21 Results obtained for method recovery for IS.

DTX labelled concentration (µg/ml)	Set III	Set IV	% Recovery
0.1	2.861	2.837	99.59
	2.889	2.716	
	2.942	2.96	
Average	2.898	2.838	
SD	3.69		
%RSD	3.711		

2.5.3.3.6. Matrix effect

To determine the effect of the presence of biological matrix on the DTX concentration, it was essential to measure the matrix factor by comparing peak area response for DTX in the presence of matrix to the peak area in the absence of the biological matrix. In this experiment, the obtained matrix factor was equal to 1.130 for the nominated DTX concentration (Table 2.22).

If the factor is greater than 1 it might be due to ion enhancement, and less than 1 might be due to ion suppressant (Rigo-Bonnin *et al.,* 2016). Our results reveal ion enhancement in the tested biological matrix. Also, the results fall well within the acceptable values given by EMA guidelines, whereby the variation must be less than 15 %.

Table 2.22 Results obtained for matrix effect for DTX.

DTX labelled concentration (µg/ml)	Peak area in the presence of matrix	Peak area in the absence of matrix	Matrix factor
1	96.5	87.7	1.137
	97.7	86.6	1.151
	105.0	90.5	1.102
AV	99.73	88.26	1.130
SD	4.60	2.010	0.025
% RSD	4.612	2.278	2.258

2.5.3.3.7. LOQ and LOD

LOQ is the lowest value that can be quantified. In this study, the LOQ of DTX was 0.04 µg/ml Furthermore, the LOD was explained as the lowest value that can be detected by the HPLC system. In this experiment, the LOD was 0.01 µg/ml. The LOQ and LOD were both calculated using equations 2.3 and 2.4, respectively. These findings were similar to a previous study (Patel *et al.,* 2011) where acceptable LOQ and LOD must be within ±20 % of the nominal concentration.

2.5.3.3.8. Solution stability

The % RSD values of DTX nominated concentrations 0.05, 0.5 and 2 µg/ml during solution stability experiments carried out for 21 days at -20 °C was well within the acceptable limits 15 % of EMA guidelines (Table 2.23). No changes were observed in the content of the solution during stability experiments. Moreover, the experimental data confirmed that sample solutions used during the assay for three freeze/thaw cycles were stable for DTX nominated concentration 0.5 µg/ml according to EMA guidelines as reported in table 2.24 the % RSD equal to 7.720 %, the result was within 15 %. These results demonstrated the stability of DTX within the chosen biological matrices.

Table 2.23 Sample stability at -20 °C.

DTX labelled Concentration (µg/ml)	Time (day)	DTX actual Concentration (µg/ml)
0.05	1	0.052
	7	0.039
	14	0.039
	21	0.041
Mean	0.043	
SD	0.006	
% RSD	14.811	
0.5	1	0.495
	7	0.432
	14	0.341
	21	0.431
Mean	0.425	
SD	0.063	
% RSD	14.927	
2	1	2.014
	7	1.950
	14	1.848
	21	1.427
Mean	1.810	
SD	0.264	
% RSD	14.605	

Table 2.24 Sample stability at -20 ° for three freeze/thaw cycles.

DTX labelled concentration (µg/ml)	Freeze/thaw cycle	DTX actual Concentration (µg/ml)
0.5	Fresh sample	0.052
	Cycle 1	0.497
	Cycle 2	0.470
	Cycle 3	0.425
Mean	0.472	
SD	0.036	
% RSD	7.720	

Hence to summarise the HPLC method to quantify free DTX in a biological matrix comprising a combination of three cell growth media and serum could be successfully developed and validated. This method would be useful to quantify DTX during permeability studies of DTX and DTX-NLC through a physiological 3D *in-vitro* BBB model to determine the potential of DTX-NLC for brain-targeted delivery.

In summary, for quantification of DTX concentration within the NLCs a serial dilution of acetonitrile and THF were used to dissolve the DTX-NLCs and an isocratic mobile phase consisting of acetonitrile and water (50:50, v/v) was used throughout this method wherein the HPLC method developed was found to be acceptable and accurate. Another HPLC method was developed with the same isocratic mobile phase for quantification of DTX in two release media consisting of PBS 100% and PBS 70%+ 30% Ethanol, this method was found to be precise. Both HPLC methods were validated according to the FDA and ICH guidelines. Additionally, for quantification and extraction of DTX in a biological matrix, a third HPLC method was developed where a gradient mobile phase with pH 5 was used throughout this method and an ice-cold acetonitrile was used as a solvent of choice to extract the DTX from the biological matrix, this method was also validated according to the FDA, ICH and EMA guidelines.

Chapter Three

DTX-NLCs development, functionalisation and characterisation

3.1. Introduction

3.1.1. Docetaxel for brain cancer treatment

Docetaxel has long been used to treat various types of cancers (Breast, head and neck, prostate and gastric carcinoma) with the commercial dosage form Taxotere® licensed by Sanofi-Aventis and approved by the FDA (Fauzee *et al.,* 2011). However, DTX has not been applied to treat brain metastases or primary tumours as it is subject to P-gp efflux at the BBB and consequently it is unable to accumulate in the brain at adequate concentrations (Loscher and Potschka, 2005)

Moreover, DTX is practically insoluble in water and thus the clinically used product Taxotere® is formulated with ethanol and Tween 80 to solubilise the drug as described by the manufacturer (Sanofi-Aventis, Canada), the high content of polysorbate 80 is believed to cause hypersensitivity hemolysis and cholestasis (Ten *et al.,* 2003). It has been reported that DTX inhibits brain tumour growth following local injection in a mouse brain tumour model (Sampath *et al.,* 2006). Thus, a novel formulation of DTX, which would permit BBB permeation and avoid usage of polysorbate 80 in such high concentration, would be a useful alternative for treatment of brain tumours.

3.1.2. Nanostructure lipid carrier

Nanostructure lipid carrier (NLC) is a new generation of solid lipid carrier (SLN), was proposed to overcome the limitations of SLN (Muller *et al.,* 2002a) by making the structure of solid lipid core less organised by mixing a variety of liquid lipid with solid lipid as previously discussed in chapter one. Higher drug payloads could be incorporated in these amorphous structures with decreased drug expulsion upon storage (Radtke and Muller, 2001). Moreover, the non-uniform structure of NLCs might contribute to why NLCs have a more controlled drug release than SLNs (Muller *et al.,* 2002a). It was reported that entrapment of PTX in solid NPs significantly increased the PTX brain uptake, by either shielding the drug from direct interaction with P-gp by the encapsulation inside the NPs or by modulating of BBB P-gp function by the surfactant (Koziara *et al.,* 2004). These data open the potential for brain delivery of chemotherapeutic drugs loaded in lipid NPs. The aim of this study was to determine whether NLCs could be used as a delivery system for DTX for treatment of a brain tumour and whether anticancer properties are achieved with a minimal side effect.

3.1.2.1. Influence of surfactants on NPs brain drug delivery

A major obstacle for drug delivery to treat diseases of the CNS is the inability of the drug to reach the site of action due to the presence of BBB. The BBB prevents most treatments from entering brain tissue because of its tight junctions (Masserini 2013; Tunblad 2004). Surface properties of nanoparticles have a great impact on their interaction with living cell and tissues, previous studies have shown successful BBB passage of NPs when fabricated with cationic stabilisers and/or non-ionic surfactants, but not when anionic compounds were used. Interestingly, the size and surface charge of NPs have shown little influence on BBB permeation (Voigt *et al.,* 2014).

Improved brain uptake after an intravenous (IV) administration has been reported for nitrendipine (Ntd) loaded SLNs prepared from triglycerides and surfactants (soy lecithin and poloxamer188) as compared to Ntd suspension. This might be attributed due to the encapsulation of Ntd within the SLN, which makes it consequently delivered to the brain bypassing the BBB by endocytosis pathway (Manjunath and Venkateshwarlu 2006). Incorporation of soy lecithin probably improved brain therapeutic uptake for the drug loaded in the SLNs and it showed effective targeting for the brain drug delivery by enabling the SLNs passing through the BBB. Also, NLC developed by Miglyol 812 increased the drug level in the brain due to fast onset of action (Singh *et al.,* 2013). Another surfactant Solutol® HS15 which is a mixture of free PEG 660 and PEG 660 hydroxy stearate has been recently approved as novel and a safe parenteral excipient for human use. It has been used as a solubiliser for poorly soluble drugs (Kasongo *et al.,* 2011). Moreover, Solutol® HS15 improved neuronal immune response when combined with soy lecithin (Singh *et al.,* 2013).

An important requirement for all NPs chosen for brain delivery system is that NPs should be prepared from rapidly biodegradable particles, as the non-degradable particles might cause a potential risk to the delivery system (Wohlfart *et al.,* 2012). Tween 80 (T80), lecithin, poloxamer 188 (P188) and sodium glycocholate are all considered as acceptable surfactants for IV route (Muller *et al.,* 2000). Additionally, surfactants can overcome drug resistance by inhibition of P-gp as has been demonstrated by the previous study whereby edelfosine-loaded SLN coated with T80 showed higher uptake by C6 glioblastoma cells (Mendoza *et al.,* 2011). Surfactants, therefore, play a fundamental role in the development of formulations intended for brain delivery (Olbrich *et al.,* 2002a; Olbrich *et al.,* 2002b).

3.1.3. Surface modification for selective and enhanced docetaxel delivery

Functionalisation of NPs surface with different types of ligands is usually desirable to achieve selective cellular binding and internalisation through receptor-mediated endocytosis. There some challenges of targeting cancers and tumours, as defective cells often have similar characteristics to the surrounding non-cancerous cells, to overcome this feature the ligands can be designed to have specificity and selectivity for some receptors that are overexpressed on cancerous cells but are less expressed on non-cancerous cells. Ligands that have been widely used for functionalisation of NPs include antibodies, small molecules, peptides and aptamers (Wang *et al.,* 2008). In the present work, two polyunsaturated fatty acids (PUFAs) gamma-linolenic acid (GLA) and alpha-linolenic acid (ALA) and one novel aptamer SA43 have been explored as ligands for functionalisation of NLC for better targeting and enhanced efficacy.

3.1.3.1. Polyunsaturated fatty acids and their tumoricidal effect on glioblastomas

It has been reported in the previous literature that gamma-linolenic acid (GLA) an omega 6 fatty acid has a potential anticancer effect, GLA demonstrated tumoricidal action towards glioblastoma cells with less or no neurotoxicity towards non-cancerous brain cells. GLA's tumoricidal effect is due to the induced apoptotic effect on of glioblastoma cells (Bell *et al.,* 1999; Madhavi and Das 1994). The study by Bell *et al.,* (1999) also involved evaluating the effect of GLA on glioblastoma spheroids cells e.g C6 (rodent glioblastoma cell line), U373 and U87MG (glioblastoma) and MOG human cell lines. These studies demonstrated the antiproliferation effect on tumour; invasion and impaired spheroid growth, suggesting that local delivery of GLA could reduce tumour size and growth. In addition, Alpha-linolenic acid (ALA) an omega 3 fatty acid has much potential for improving the therapeutic efficacy of anti-cancer drugs for the treatment of breast cancer when MCF7 cells were treated with ALA conjugated with doxorubicin (Huan *et al.,* 2009). Several studies have demonstrated that ALA sensitises tumour cells to effects of anti-cancer drugs either in tumour-bearing animals or *in-vitro* cell culture where ALA can play an important role in cancer prevention/progression. These PUFAs induced changes in tumour fatty acid composition resulting in increased sensitivity to chemotherapy, especially in tumour lines that are resistant to chemotherapy, and cause high cytotoxicity to tumour cells and protection of normal cells (Horia and Watkins 2005).

FABPs are intracellular fatty acid binding proteins involved in the binding and the intracellular trafficking of fatty acids and retinoids to different subcellular compartments:

cytoplasmic, for metabolism and energy production, or nuclear, for regulation of gene transcription via activation of peroxisome proliferator-activated receptors (PPARs) (Forman *et al.,* 1997). The previous literature showed that FABP or FABP7 are involved in the internalisation and intracellular transport of PUFAs which are highly up-regulated in glioblastoma cells in comparison with normal brain cells (Liang *et al.,* 2005; Mita *et al.,* 2007). GLA and other PUFAs also produce mitochondrial depolymerisation, lipid accumulation and overexpression of P_{53} and GMYC, by forming various lipid peroxidase (Chung *et al.,* 2003; Cury-Boaventura *et al.,* 2005; Chi *et al.,* 2004). To the best of our knowledge there are no reports of these PUFAs being used as ligands for targeting glioblastoma cells, therefore in the present work DTX-NLCs are functionalised with GLA and ALA for their potential effect on enhancing the anti-cancer effect of the chemotherapeutic drug and brain-targeted therapy.

3.1.3.2. Aptamers are the new trend in selective targeting of glioblastomas

Aptamers are short single-stranded DNA, RNAs, or modified nucleic acids that can fold into complex three-dimensional structures and specifically bind to their targets (Dausse *et al.,* 2009; Nimjee *et al.,* 2005). Aptamers can be selected from randomly synthesised and easily modified oligonucleotide libraries through the systematic evolution of ligands by exponential enrichment (SELEX) (Gopinath, 2007). Their advantages can be due to ease of selection and synthesis, high binding affinity and specificity, low immunogenicity and versatile synthetic accessibility with high purity (Zhang *et al.,* 2011; Zhou and Rossi 2011). Moreover, NPs significantly enhanced intracellular drug delivery and tumour spheroid penetration when functionlised with aptamers and could target glioblastoma and accumulate at the tumour site (Gao *et al.,* 2012b). Aptamers have also been demonstrated to have more specific and higher affinity for the intended target than other ligands for example antibodies (Sun *et al.,* 2014).

Recent studies showed DTX-encapsulated NPs formulated with PLGA-b-PEG copolymer and surface functionalised with the A10 RNA aptamers could recognise the extracellular domain of the prostate-specific membrane antigen (Chen *et al.,* 2016). Moreover, Gao *et al.,* (2012a) found that DTX-loaded PEG-PCL NPs functionalised with GMT8, an aptamer with the highest affinity for U87MG cells was used for targeted glioblastoma therapy. In addition, SA43-aptamer which has high specificity to glioblastoma cell (U87MG) has been demonstrated for its binding to Ku 70 and Ku 80 which probably was responsible for its selectivity to cancerous glioblastoma cells rather than non-cancerous cell lines (Aptekar *et al.,* 2015). SA43-aptamer also showed potential to permeate through *in-vitro* BBB model due to a transient opening of the TJ as determined by a temporary reduction in the trans-endothelial electrical resistance (TEER) and good apparent permeability (Papp of 4.32 ± 3.90 x10^{-9} cm/ min) (Aptekar *et al.,* 2015). Due to the selectivity of SA43-aptamer towards glioblastoma cells and its ability to permeate through an *in-vitro* BBB model, SA43 was selected as a selective ligand for functionalisation of DTX-NLC in the present study.

3.2. Aim and objectives

The main aim of this chapter was to develop NLC, that have high encapsulation efficiency to incorporate chemotherapeutic drug docetaxel (DTX), and further functionalised the DTX-NLC with GLA, ALA, and SA43-aptamer.

3.2.1. Objective 1

Development and optimisation of NLC loaded with DTX, and to evaluate the effect of process and product parameters on critical quality attributes of NPs, the particle size, polydispersity index (PDI), zeta potential (ZP), entrapment efficiency (EE), total drug (TD), and drug loading (DL), using one factor at a time and factorial design approach.

3.2.2. Objective 2

Functionalisation of DTX-NLCs with three ligands; two PUFAs, (GLA and ALA), and one selective aptamer SA43 for the potential effect on targeted brain delivery and enhanced selectivity for glioblastoma cells.

3.2.3. Objective 3

To carry out the physicochemical characterisation of the developed bare and functionalised DTX-NLCs.

3.2.4. Objective 4

To assess the stability of the bare DTX-NLC and study the effect of storage temperature on different parameters DTX-NLC.

3.3. Equipment and materials

3.3.1. Equipment

Probe sonicator (Vibra Cell Sonics, USA), Sigma Centrifuge (Germany). Malvern Zetasizer Nano (Malvern Instalment Ltd, Uk). Centrifuge (Spectrafuge 24D, Jencons-Pls, UK). Bruker powder X-ray diffractometer (XRD). Differential scanning calorimetry (DSC) Q2000 TA (Thermal Analysis Instruments, Elstree, Hertfordshire, UK). Nicolet iS 10 Fourier transform infrared spectroscopy (Thermo Scientific, UK). Horiba HR800 Raman with a green detector. Centrifuge (3-16PK SCIQUIP). High-Pressure Liquid Chromatography (HPLC) system (Agilent 1260 Infinity HPLC instrument Agilent Technologies, USA). Nano-Drop, Spectrophotometer (Thermo Scientific, UK).

3.3.2. Materials

Docetaxel (DTX) and Paclitaxel (PTX) were purchased from Kemprotec company, UK. Dynasan114 (D114) and Miglyol 812N were given as a free sample from CREMER OLEO, company, Germany. Sodium cholate was purchased from Sigma Aldrich, UK. Phospholipon 90H (PH90), Lipoid S75 and E80 were free samples from Lipoid, Germany. Poloxamer188 (P188) was given as a free sample from BASF company, Germany. Solutol HS15 (S HS15) was purchased from Sigma. Labrasol (LB), Lauroglycol 90 (LG90) and Capryol propylene glycol monocaprylate (CPGMC) were given as a free sample from Gattefossé company, France. 1-Ethyl-3-(3-dimethylaminopropyl) carbodiimide (EDC), N-hydroxysuccinimide (NHS) were purchased from (Fisher, UK). Dimethyl sulfoxide (DMSO), Tetrahydrofuran (THF), Methanol, Acetonitrile, and ethanol were purchased from Fisher Scientific, UK (all solvents were used were HPLC grade). Ortho-phosphoric acid (Fisher Scientific, UK). Amicon 3 kDa molecular cut-off centrifugal filters purchased from (Fisher Scientific, UK). Spectra/Por® dialysis membrane (3.5K Da MWCO) was obtained from Spectrum Labs, USA. Phosphate buffer saline (PBS) 0.1 M (pH 7.4), purchased from Sigma Aldrich. SA43-Aptamer was synthesised by Integrated DNA Technologies (IDT) and conjugated at the 5’ end with-COOH functional group (IDT, Glasgow, UK and IDT, US). RNase free water purchased from Fisher, UK. Ascorbyl palmitate (AP), and α-Tocopherol (Vit E), sodium chloride, and dextrose were purchased from (Sigma, UK). Eagle’s minimum essential medium (EMEM) was purchased from Lonza. Double distilled water was used throughout these experiments unless otherwise indicated.

3.4. Methods

3.4.1. Preparation of Docetaxel-loaded nanostructure lipid carrier (DTX-NLC)

NLC loaded with DTX were prepared by hot homogenisation technique (Naguib *et al.,* 2014). High melting point triglyceride Dynasan 114 (D114) (55-58 °C) as solid lipid (S.L) and four liquid lipids (L.Ls), Miglyol 812 N (MG), Labrasol (LB), Lauroglycol 90 (LG90) and Capryol propylene glycol monocaprylate (CPGMC) were investigated for fabrication of the DTX-NLCs.

Briefly, anticancer drug DTX (1 mg/ml), solid lipid D114 (4 g), lipophilic surfactant Phospholipon 90 H (PH90) (300 mg), three liquid lipids (L.Ls): LB, LG90, and CPGMC (150 mg each) to give a total 450 mg of L.Ls, and non-ionic solubiliser and an emulsifying agent Solutol HS15 (S HS15) (300 mg) were placed in a beaker and dissolved in ethanol (250 µl). Lipid-drug mixture was melted using a water bath. The temperature was brought to 65 °C (ten degrees higher than the melting point of the solid lipid). Another lipophilic surfactant Lipoid S75 (LS75) (2.4 g) was then added to the mixture (lipid phase). The aqueous phase, composed of an anionic static bio-surfactant sodium cholate (SC) (374 mg) and any other surfactant used during the optimisation in a (100 ml) water, was placed in another beaker with continuous stirring using magnetic stirrer, and kept at the same temperature (65°C ±5) as the lipid phase temperature by using a water bath. The aqueous phase was added to the lipid phase under continuous stirring for 20 min to form a pre-emulsion. The subsequent oil-in-water pre-emulsion was placed in a glass vial under the controlled condition of temperature (ice-bath) and the mixture was sonicated using the probe sonicator for an overall time of 40 min at a sonication intensity of 40 %. The hot nano-emulsion was left to cool down at room temperature to form DTX-NLC. For the blank NLC (B-NLCs) the same procedure was followed but DTX was not added during the preparation.

To prepare a Rhodamine123 (R) labelled NLCs, R was added in the lipid phase to form R-DTX-NLC. To remove the titanium particles (that originated from the titanium probe of the ultrasonicator) from the NLC suspensions, nanoparticle formulations were centrifuged (Garanti *et al.,* 2016) at a low rotation speed at 179 x g for 5 min.

3.4.1.1. Optimisation of NLCs

In order to prepare a uniform stable formulation with a low particle size (PS) and polydispersity index (PDI), various parameters affecting the NLCs preparation were investigated. The product parameters including surfactant types and their concentrations in the aqueous phase, the concentration of solid lipid (S.L) and liquid lipids (L.Ls) in the lipid phase were evaluated. Moreover, the process parameters included sonication time, and mixing time under high-speed homogeniser (HSH) Ultra-turax were also assessed. Previous studies have shown these parameters to have a critical effect on NPs production (Zirak and Pezeshki, 2015; Keum *et al.,* 2011). In addition, the effect of process temperature was also studied. Various experiments were designed altering one factor at a time and their effect on the PS and PDI of the NLCs were observed.

3.4.1.2. Optimisation of NLCs by 3^2 factorial design

After the preliminary optimisation and changing one factor at the time, a final optimisation was performed by factorial design adopted and modified from Gao *et al.,* (2011). In this study two factors, three-level central composite rotatable design 3^2 was used to study the effect of two independent variables, surfactant concentration (A) and lipid concentration (B), on the five response variable PS, PDI, entrapment efficiency (EE), total drug (TD) and drug loading (DL) of DTX-NLCs. Factorial designs generate polynomial equations comprised of interacting terms and regression coefficients, which together assist in evaluating the responses. An initial 3^2 full factorial design was created (Table 3.1). A total of nine experiments were carried out. Design-Expert® Software was used to design this experiment and ANOVA was used for statistical analysis. The data were considered as significant when p values were < 0.05. The Design Expert software generates two basic models, the particularly full model in which non-significant terms are included and reduced model in which non-significant terms are excluded.

Table 3.1 Independent variables in 3^2 factorial design and the actual concentrations used.

Batch number	**Surfactant (A)**	**Conc. (mg/100 ml)**	**Lipid (B)**	**Conc. (g/100 ml)**
B38	-1	250	-1	3
B41	0	375	-1	3
B43	+1	500	-1	3
B39	-1	250	0	4
B20	0	375	0	4
B44	+1	500	0	4
B40	-1	250	+1	5
B42	0	375	+1	5
B45	+1	500	+1	5

3.4.2. Functionalisation of DTX-NLCs with PUFAs

DTX-NLC was prepared as described in section 3.4.1. and it was surface modified with either gamma-linolenic acid (GLA) or alpha-linolenic acid (ALA). The coupling process was adopted and modified from, Yang and Hu (2015) through forming amide linkage by a covalently coupling free amino group of DTX-NLC to the carboxylic acid group of GLA or ALA, using EDC and NHS as coupling agents. Briefly, 1 mg/ml of GLA or ALA were placed in a glass container and dissolved in ethanol, vortexed for 1 min and then mixed with EDC (1:1 molar ratio, PUFA: EDC, pH 7.4,) EDC was dissolved in water (1mg/ml), the mixture was flushed with nitrogen gas to maintain the stability of PUFAs. This mixture was stirred for 30 min at room temperature. Then NHS (1:1 molar ratio, NHS: EDC) was added, NHS was dissolved in H_2O (1mg/ml) and stirred with the mixture for 30 min at room temperature. 1 ml DTX-NLC formulation was added to the mixture under a stream of nitrogen gas and then allowed to stir for 12 h under the same conditions to form GLA-DTX-NLC and ALA-DTX-NLC respectively (Figure 3.1). Excessive unbound materials were removed from GLA-DTX-NLC and ALA-DTX-NLC using dialysis bag. Briefly, 1 ml formulation was placed in a dialysis bag (3.5K Da MWCO), then transferred into a beaker containing 100 ml of water and stirred for 15 min for two purification cycles. Particle size (PS), PDI and zeta potential (ZP) were measured before and after conjugation using Malvern Zetasizer Nano.

As PUFAs are known to oxidise, a combination of antioxidant 0.02%, w/v of Vit.E + 0.05%, w/v of AP (Bvg 2009; Pharmaceutical Excipients, 7th edition, 2012), were added and evaluated. Both Vit E and AP were added into the lipid phase during the DTX-NLC preparation as described in section 3.4.1. When the antioxidants were employed, nitrogen flushing was not done during the coupling process, of GLA and ALA.

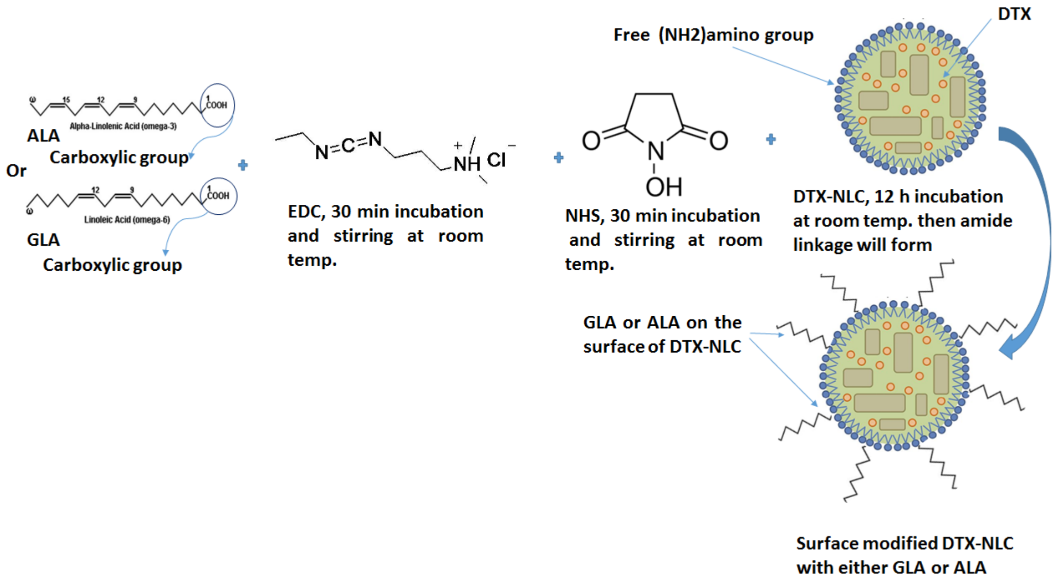

Figure 3.1 Schematic diagram showing the crosslinking of DTX-NLC with PUFAs by covalent bonding in the presence of EDC and NHS to form an amide linkage between a free amino group of DTX-NLC and PUFAs carboxylic group. This reaction was carried out at room temperature (Chemical structures were adopted from Fisher and Sigma, Uk websites, and NLC picture was adopted and modified from Yingchoncharoen et al., 2016).

3.4.2.1. Optimisation of DTX-NLC functionalised with PUFAs

DTX-NLCs have free amino groups (FAG) available on their surface due to the presence of phospholipids (LS75 and PH90) incorporated in the formulation. The FAG was quantified with Trinitrobenzene sulfonic acid (TNBS) reaction as described in section 3.4.4. The ligands density might affect the PS and PDI of the NPs (Zupančič *et al.,* 2017;

Bandyopadhyay *et al.,* 2011). Therefore, various ratios of PUFAs to FAG available on the DTX-NLC were investigated (1:1, 1:1/2, 1:1/3, 1:1/4, 1:1/5, 1:1/6 and 1:1/7, FAG: PUFAs ratio) to prepare varied batches of both GLA-DTX-NLC and ALA-DTX-NLC and their effect on PS and PDI were observed. EDC and NHS coupling agents were used equally to the molar ratio of the PUFAs in this process (Figure 3.1).

3.4.3. Functionalisation of DTX-NLCs with SA43-aptamer

SA43-aptamer was synthesised by IDT company and conjugated at the 5' end with -COOH functional group and was used for functionalisation with DTX-NLC through covalent bonding, due to the presence of FAG on the surface of the DTX-NLCs; an amide linkage was formed when DTX-NLC was linked with free -COOH group on the SA43-aptamer (Farokhzad *et al.,* 2004; Yang and Hu 2015).

Briefly, 250 µl of RNase free water was added to the SA43 freeze-dried sample to give a concentration of 24.73 µM (Stock 1) as measured by Nanodrop. This stock was then either freshly used or stored at -20° C for later experiments. From stock 1 a final 1:1/8 ratio (FAG: SA43, ratio) was prepared by covalent bonding using coupling agents EDC and NHS in equal molar ratios 1:1/8 molar, (SA43: EDC/NHS, ratio), modified from previously published methods (Medley *et al.,* 2012). An appropriate volume of stock 1 was placed in a glass container and diluted up to 100 µl with RNase free water, then EDC was added to the SA43 solution (1:1 molar ratio, SA43: EDC), where EDC was dissolved in RNases free water (2mg/ 1ml) the mixture was left stirring for 30 min at room temperature. Then NHS (1:1 molar ratio, EDC: NHS) were added (NHS was dissolved in RNases free water 2mg/1ml) and stirred with the mixture for 30 min under the same conditions. 1 ml DTX-NLC formulation was added to the mixture (DTX-NLC was prepared with RNase free water in all experiments included with SA43-aptamer). This mixture was allowed to stir for 12 h under the same conditions to form SA43-DTX-NLC (Figure 3.2). Excessive unbound materials were removed by purification of SA43-DTX-NLC using dialysis bag as detailed in section 3.4.2. Particle size, PDI and ZP were measured before and after conjugation.

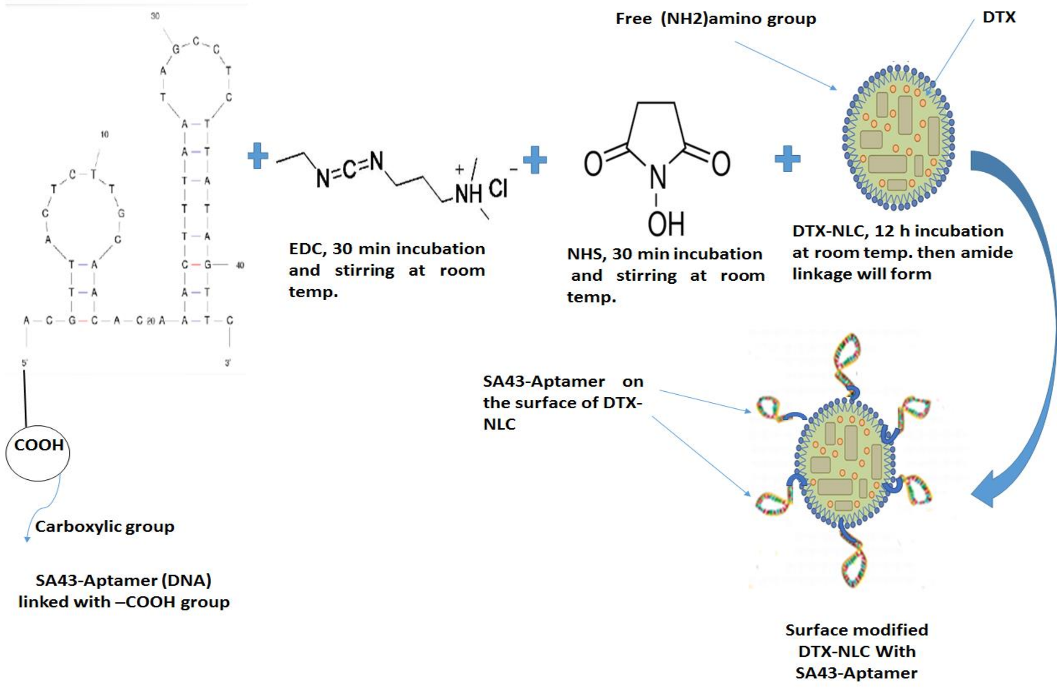

Figure 3.2 Showing crosslinking of DTX-NLC with SA43-Aptamer by covalent bonding in the presence of EDC and NHS to form an amide linkage between a free amino group of DTX-NLC and SA43 carboxylic group. This reaction was carried out at room temperature (Chemical structures were adopted from Fisher and Sigma, Uk websites, the SA43 structure adopted and modified from Aptekar et al., 2015 and NLC picture was adopted and modified from Yingchoncharoen et al., 2016).

3.4.3.1 Optimisation of DTX-NLC functionalised with SA43-aptamer

The SA43-DTX-NLC formulation was optimised by testing different ratios of SA43 to the FAG available on the surface of the DTX-NLCs that was quantified by TNBS (section 3.4.4). The FAG: SA43 ratios that have been assessed in this experiment were (1:1/70, 1:1/35, 1:1/23, 1:1/12, and 1:1/8, FAG: SA43 ratio), and their effect on PS, PDI, and ZP were studied. Appropriate volume of stock 1 (4.04, 8.08, 12.12, 24.27, and 36.4 µl), respectively for each ratio was taken and diluted up to 100 µl with RNAs free water, and further functionalised with DTX-NLC through forming an amide bond by using EDC and NHS mixture equal to the SA43 molar ratio (1:1 ratio, SA43: EDC/NHS) as detailed in section 3.4.3 (Figure 3.2) to give a range of SA43-DTX-NLC formulations.

3.4.4. Conjugation efficiency

Conjugation efficiency was calculated by determining free amino groups (FAG) on DTX-NLC pre- and post-conjugation with ligands (GLA, ALA, and SA43-aptamer). As FGA react with Trinitrobenzene sulfonic acid (TNBS) therefore this assay was used to determine FGA on DTX-NLC surface. Excess TNBS is added to the formulation and the reacted TNBS gives a measure of the FAG in the tested samples (Gao *et al.,* 2011).

Initially, calibration curves were obtained to measure the unreacted TNBS, by modification Gao *et al.,* (2011) method, then reacted TNBS was calculated as described in equation 3.1. To prepare the calibration curve, TNBS was diluted with a $NaHCO_3$ solution (4%, pH8.5) to give a concentration of 4 µmol/ml (Stock1). Two sets were prepared from stock1, first set was the active set and samples were prepared by placing 50, 100, 125, 150, 200, 250 µl of the solution in a 10 ml volumetric flask to give a final concentration of 0.2, 0.4, 0.6, 0.8 and 1 µmol/ml, respectively. To each volumetric flask, 100 µl of 1% trichloracetic acid (TCAA) was added, then 100 µl of L-valine (LV) (40 µmol/ml) was added, samples were vortexed for 1 min (Figure 3.3 a). The second set was the blank set, the samples were prepared exactly like the first set, but without adding LV to the blank samples (Figure 3.3 b). Both sets were then kept in dark to react for 1 h at 40 °C, the reaction was terminated by adding 0.5 µmol/ml HCl solution to make the volume up to 10 ml in each volumetric flask in both sets. The absorbance of all samples was measured at 410 nm. For each concentration first, the absorption of the blank sample was measured, and the equipment settings auto-zeroed followed by measuring the absorption of the active sample. Data were collected, and this experiment was carried out in triplicate, mean and SD was calculated, and a calibration curve (concentration of TNBS vs. Absorbance) was generated. The unreacted TNBS was quantified from the calibration curve. From there, the reacted TNBS was calculated (equation 3.1) which was equivalent to the FAG in the tested formulation.

$$Reacted\ TNBS = Total\ TNBS - Unreacted\ TNBS \qquad \textbf{(Equation 3.1)}$$

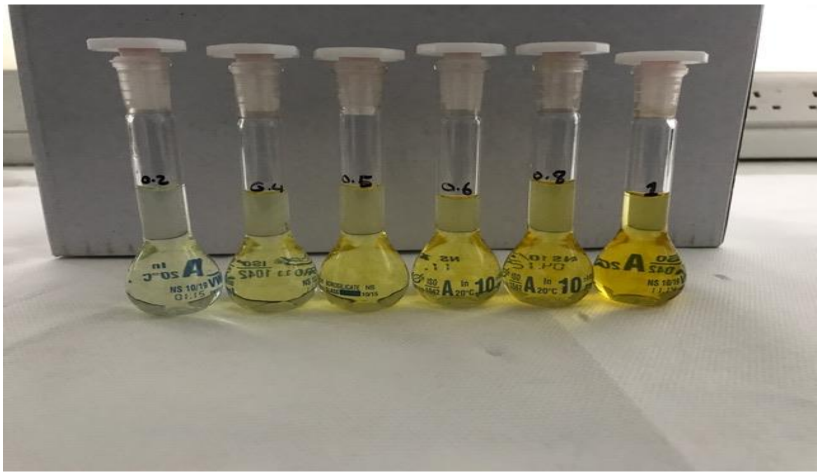

(a)

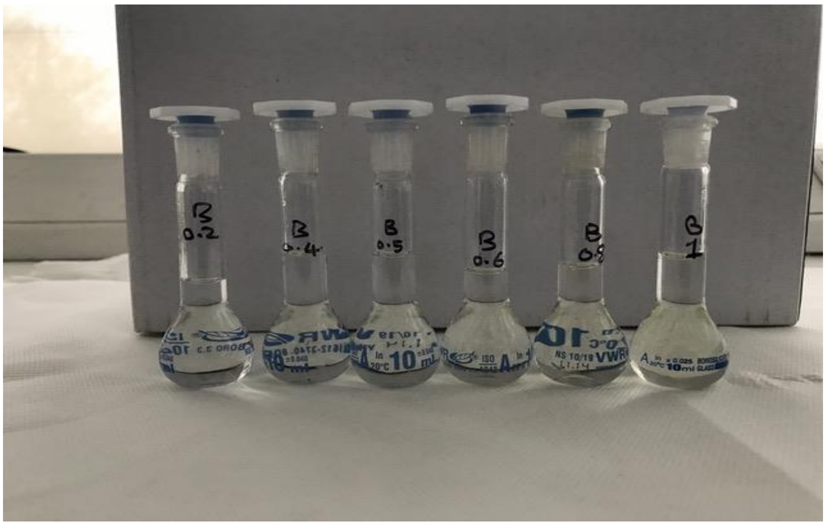

(b)

Figure 3.3 Showing different concentrations of TNBS for the preparation of the standard plot (a) first set was the active set and samples (50, 100, 125 150, 200, 250) µl of TNBS solution placed in a 10 ml volumetric flask to give a final concentration of 0.2, 04, 0,6, 0,8 and 1 µmol/ml, to each volumetric flask 100 µl of 1% trichloracetic acid (TCAA) was added to each sample and then 100 µl of L-valine (LV) (40 µmol/ml), (b) the second set was the blank set, the samples were prepared exactly like the first set, but without adding LV to the blank samples, then 0.5 µmol/ml HCl solution was added to make the volume up to 10 ml in each volumetric flask.

The process to determine FAG in DTX-NLC is shown schematically in Figure 3.4. For DTX-NLC formulation, briefly, 0.5 ml of each formulation was placed in a glass container and 4 ml of TNBS (4 µmol/ml) was added (Total TNBS in this case 16 µmol/4ml). All samples were transferred to the incubator, kept in dark for 1 h at 40 °C. Following incubation, 2ml was transferred to a centrifuge tube and centrifuged for 30 min at 16300 x g. Then 900 µl of the supernatant was placed in two individual 10 ml volumetric flasks one was labelled as the active sample, and the second was labelled as a blank sample. For each active sample, a 100 µl of 1% TCAA was added followed by adding 100 µl of L-valine (LV) (40 µmol/ml), samples were then vortexed for 1 min. The blank samples were prepared exactly like the active sample, but with one difference in step as the LV was not added to the blank samples. Both active and blank samples were transferred to the incubator, kept in dark for 1 h at 40 °C for the reaction to take place. Samples were removed from the incubator, and the reaction was terminated by adding 0.5 µmol/ml HCl solution to make the volume up to 10 ml for each sample. Absorbance then measured using spectrophotometer at 410 nm wavelengths. The blank sample was measured first followed by its active sample for each specific formulation and the quantity of unreacted TNBS was measured using the calibration curve from the equation of the curve. From calculated unreacted TNBS, the reacted TNBS was determined using equation 3.1.

The % ligand conjugation to DTX-NLC was calculated using the following equation

$$\% \, Conjugation = \left\{ \frac{Total\ FAG\ before\ conjugation - FAG\ after\ conjugation}{Total\ FAG\ before\ conjugation} \right\} * 100$$

(Equation 3.2)

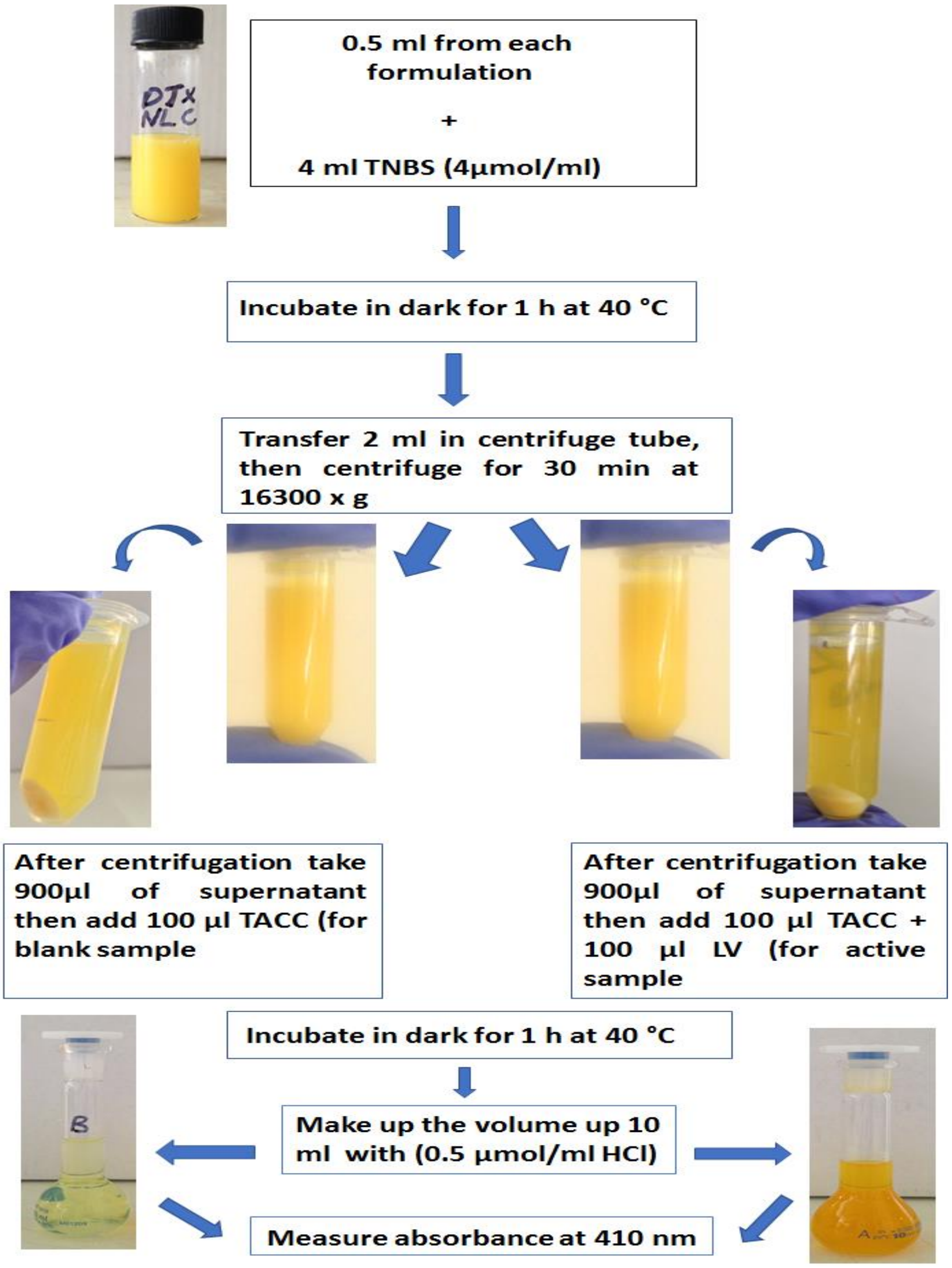

Figure 3.4 Schematic diagram showing the preparation of the blank and active samples to measure the unreacted TNBS of DTX-NLC.

3.4.5. Freeze-drying of NLCs

NLCs were freeze-dried using two cryoprotectant agents sucrose and trehalose (Li *et al.,* 2009; Sun *et al.,* 2016). Both the cryoprotectants were examined in different percentages and in combination to achieve a formulation with small particle size without alteration in the particle size distribution after reconstitution with water. The studied sucrose percentages were (1, 2, 3, 5, 10, 15 and 20 %). Furthermore, trehalose was assessed in different percentages (3, 5, 10, 15, and 20) %. Additionally, sucrose and trehalose were used in combination with a 1:1 ratio by using 2.5% of each agent (Sun *et al.,* 2016). 1 ml of NLC was placed in a glass container and mixed properly with the cryoprotectant agent then covered with parafilm and transferred to -80 °C freezer to be stored for 24 h. A number of small holes were made into the parafilm to help water evaporation then all glass containers were placed inside the freeze drier for 96 h of the main drying cycle and 24 h of secondary drying (over all five days freeze drying period).

3.4.6. Physicochemical characterisation

Appropriate characterisation of NLCs is crucial for the management of product quality, stability, and drug release (Das and Chaudhury, 2011; Mehnert and Mader, 2001). There are several important parameters such as particle size (PS), particle distribution (PDI), zeta potential (ZP), drug content, drug entrapment efficiency (EE), morphology, crystallinity and structural compositions that were evaluated for DTX-NLC formulations are as detailed below.

3.4.6.1. Particle size, polydispersity index and zeta potential of NLCs

Photon correlation spectroscopy (PCS) was used to obtain the PS, PDI and zeta potential (ZP) of all bare and surface-modified DTX-NLCs using Zeta Sizer Instrument at 25° C. PCS measures the fluctuation of the intensity of the scattered light caused by particle movement (Iqbal *et al.,* 2012; Yoon *et al.,* 2013). Size measurements were obtained by measuring 1.5 ml of formulation. The formulations placed in a zeta sizer transparent cuvette. All measurements were repeated at least three times from three different samples. Mean and standard deviations were calculated.

3.4.6.2. DTX-NLC Total Drug (TD) and Drug Loading (DL)

In order to measure the DTX content and loading concentration in DTX-NLC and surface modified DTX-NLCs with PUFAs and SA43-aptamer, a specific HPLC method was developed and validated with respect to ICH and FDA guidelines. HPLC method was used as described in section 2.4.1. After several steps of optimisation, the best organic solvent was chosen to completely dissolve DTX-NLC formulations as described in section 2.4.1.1. This method was modified from Garanti *et al.,* (2016). A serial dilution of THF and mobile phase (acetonitrile and water, 50:50, v/v) were chosen to carry out this experiment. 1 ml of each formulation was placed in a 5 ml volumetric flask and the volume made up to 5 ml with THF to give 200 µg/ml concentration (stock 1). Further dilution of this stock with

THF was carried out to generate 20 µg/ml concentration (stock 2). From stock 2 a final concentration of 4 µg/ml was prepared by placing 1 ml of stock 2 in a volumetric flask, and further diluting with mobile phase up to 5 ml. All samples were vortexed for 1 min. 1 ml of each sample was taken from the final concentration and placed in HPLC vials for analytical study. The samples were injected three times and a reference sample of DTX (4 µg/ml) was injected during all analytical experimentation, as recommended by ICH and FDA guidelines. The mean and SD were calculated for the area under the curve. The equations below were used to calculate the DL and TD %, respectively.

$$\% \, DL = \left\{ \frac{Mass\ of\ DTX}{Mass\ of\ Lipids\ in\ the\ NLCs + Mass\ of\ DTX} \right\} * 100 \qquad \textbf{(Equation 3.3)}$$

$$\% \, TD = \left\{ \frac{DTX\ concentration\ after\ processing}{DTX\ added\ concentration\ before\ processing} \right\} * 100 \qquad \textbf{(Equation 3.4)}$$

3.4.6.3. DTX Entrapment Efficiency

Entrapment efficiency (EE) of all DTX-NLC and surface modified DTX-NLCs were determined by quantifying free DTX concentration, the un-entrapped drug in nanoparticles and is separated from NLCs following protocols adopted and modified from previous literature (Kasongo *et al.,* 2011; Garanti *et al., 2016)* by using Amicon 3 kDa molecular cut-off centrifuge filters. Briefly, 0.5 ml of each formulation was placed in the centrifuge filter and centrifuged at 15600 x g for 60 min. The lipid nanoparticles with entrapped drug remained on top of the filter while aqueous phase with the unentrapped free drug (FD) passed through the filter membrane as shown in (Figure 3.5). The filtrate was used for DTX quantification, by placing 100 µl of the filtrate and the volume made up to 1 ml with 100% acetonitrile. Samples were subsequently injected into HPLC and analysed, using the HPLC method as described 2.4.1. Entrapment efficiency (%EE) was determined by the equation below:

$$\% \, EE = \left\{ \frac{TD - FD}{TD} \right\} * 100 \qquad \textbf{(Equation 3.5)}$$

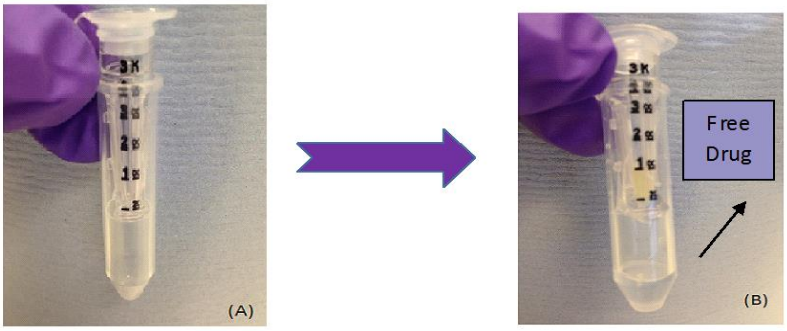

Figure 3.5 Separation of unentrapped drug (free drug) from drug loaded NLCs using centrifugal filters (A) Before spinning the filters; (B) After spinning the filters.

3.4.6.4. *In-vitro* DTX-NLCs release study

The release of DTX from DTX solution (DTX prepared in ethanol 2mg/2ml), Taxotere ® and DTX-NLC were evaluated in a pH7.4 PBS. Typically, dialysis bag was used to carry out this experiment (dialysis membranes molecular weight cut-off 3.5 kDa). The dialysis bag was cut into appropriate sizes, then were kept in water for 1 h prior to the experiment in accordance with manufacturer's instructions; then 2ml samples were placed in the dialysis membranes and both ends of the membrane were securely tied with knots and thread to prevent any possible leakage of the samples. All samples were immersed in 400 ml of release media pH7.4 PBS solution at 37 °C under horizontal shaking (100rpm/min) (Tan *et al.,* 2017). Samples (1ml) were withdrawn at the predetermined time points (0.5, 1, 2, 4, 6, 8 and 24) h respectively, and replaced with 1 ml of fresh release media. The amount of DTX released was tested using HPLC method that was specifically developed and validated for this purpose.

Another release media (PBS pH 7.4 containing 30 % (v/v) ethanol) was used to evaluate the DTX release from DTX solution, DTX-NLC, GLA-DTX-NLC and ALA-DTX-NLC at 37 °C (Zhang *et al.,* 2017) respectively. The same method mentioned above was employed, then samples were analysed by HPLC method developed and validated as described in section 2.4.2 and 2.5.2.

3.4.6.5. Scanning electron microscopy (SEM)

DTX-NLC particle morphology was observed via scanning electron microscopy (SEM) (Melzig *et al.,* 2018) using freeze-dried powder sample. DTX-NLC sample was spread evenly on a metallic stub before the analysis with SEM. JFC, the sample was coated with 1200 Fine Coater that was used to coat the sample with gold for 2 min under vacuum. Samples were then studied with SEM microscope at 20 Kv.

3.4.6.6. X-ray diffractometer (XRD)

Crystalline structures were tested for surfactants SC and PH90, solid lipid D114, drug DTX, physical mixture (DTX+ D114), and DTX-NLC (Freeze Dried). Samples were placed into the sample holders and scanned from 5° to 50° with a scanning rate of 5°/minute, with a scan type coupled two theta/theta using Scintillation counter and 1-dimensional LYNXEYE detector, A Cu-Kα radiation source-detector was used exposing samples to Cu Kα radiation (30 kV, 10 mA) (Shi *et al.,* 2012; Garanti *et al.,* 2016).

3.4.6.7. Thermogravimetric analysis (TGA)

DTX and D114 pure powdered forms were tested against B-NLC and DTX-NLC in freeze-dried form, and DTX-NLC in suspension form and was investigated for their thermal behaviour. Stability of GLA-DTX-NLC, ALA-DTX-NLC, and SA43-DTX-NLC, was also determined, where each sample was heated from 25-500 °C using TGA Q500. Approximately 10 mg of each sample was placed in a platinum pan and analysed for weight % loss as a function of temperature. The collected data were analysed using TA Universal Analysis software (TA Instruments, Elstree, Hertfordshire, UK).

3.4.6.8. Differential scanning calorimetry (DSC)

Thermal behaviour study was employed to evaluate the crystallization and melting behaviour of various samples. To identify and determine the possible difference between D114 and DTX pure drug in comparison to freeze-dried. DTX-NLC and B-NLC DSC thermograms were run for each of these samples. In addition, DTX-NLC, GLA-DTX-NLC, ALA-DTX-NLC and SA43-DTX-NLC were also evaluated. A sample of approximately 5mg was placed in a hermetically sealed Tzero pan, and an empty pan was used as a reference. Samples were analysed using heat/cool/heat run. The heating rate used was 10 °C /min and the temperature was cycling between 0-240 °C. Samples were measured under a nitrogen purge of 50 ml/min. The collected data were analysed using TA Universal Analysis software (TA Instruments, Elstree, Hertfordshire, UK).

3.4.6.9. Fourier-Transform Infrared Spectroscopy (FTIR)

The interaction between the materials and the polymorphic state was measured using FTIR. Pure powdered DTX was investigated against DTX-NLC and B-NLC in freeze-dried forms. Moreover, the suspension form of DTX-NLC was compared to GLA-DTX-NLC, ALA-DTX-NLC and SA43-DTX-NLC in suspension forms, and GLA and ALA pure materials were also analysed. Samples were measured for % transmittance ranging between 400-4000 cm^{-1} using diamond crystal and a resolution of 0.5 cm^{-1} and accumulation of 150 scan. The data were analysed using the OMNIC software (Thermo Scientific, UK).

3.4.6.10. Raman spectroscopy

For further characterisation, DTX pure drug was compared with DTX-NLC as a freeze-dried form by Raman spectroscopy. The Raman spectroscopy machine was calibrated using high purity silica wafer with a distinguishable scattering and at 520 cm^{-1}. The drug and DTX-NLCs were analysed using the following settings: green laser was used in the analysis (532 nm) with a grating of 600, 50X magnification was used for the objective lens and laser intensity of 0.01 %. The powdered samples were placed evenly on a slide wrapped with aluminium tin and for the NLCs suspension (DTX-NLC, GLA-DTX-NLC, and ALADTX-NLC) they were measured using the accessory liquid sample holder with a quartz cuvette objective range of 400- 2000 cm^{-1}. All samples were analysed under the same settings and parameters. LabSpec 6 software was used to analyse the data.

3.4.7. Stability study

DTX-NLCs stability were evaluated in suspension and freeze-dried form using various protocols as detailed below:

3.4.7.1. Colloidal stability

Colloidal stability was performed on DTX-NLC in different physiological media (PBS, EMEM, Dextrose 5%, NaCl 0.9 % and H_2O) to assess their stability by placing 1 ml of DTX-NLC into five individual glass containers and added 30 ml of each of the tested media into the containers. Samples were mixed properly then transferred the mixture to the incubator and stored all five containers at 37°C. Then 1.5 ml was withdrawn from each container at different time intervals (0.5, 1, 2, 4, 6, 8 and 24) h, and evaluated for the changes in PS and PDI, as per method modified from Sun *et al.,* (2016).

3.4.7.2. Short-term stability

The stability of the developed DTX-NLC and B-NLC samples in suspension form were evaluated by storing samples at room temperature for three months. Samples were withdrawn periodically after one, two and three months and were compared to the freshly prepared samples and characterised for their PS, PDI, ZP, %EE, %TD and % DL. This method was adopted and modified from literature (Gao *et al.,* 2008).

3.4.7.3. Long-term stability

Freeze dried DTX-NLC where stored at -20, 4, 25, and 40 °C, for up to six months in a glass container, sealed properly, and the formulations were assessed and characterised periodically after 0, 1, 3 and 6 months for their PS, PDI, ZP, %EE, %TD and % DL after reconstitution with water.

3.4.8. Statistical analysis

The statistical analysis was performed using the Kolmornov-Smirnov test for normality followed by ANOVA (with post-hoc analysis Tukey and Dunnett test) by using statistical analyses using the Statistical Package for the Social Sciences SPSS Version 20 software (IBM company, USA) and the Microsoft Excel software for Microsoft office 360 (Microsoft Corporation, USA). The analysis of variance was statistically significant difference when (*) $P < 0.05$ with (95% confidence), (**) $P < 0.001$ (99% confidence), and (***) $P < 0.000$. The data are presented as the mean ± standard deviation for N=3 experiments in triplicate (n=9).

3.5. Results and discussion

3.5.1. Preparation of NLCs

B-NLCs and DTX-NLCs were prepared using the probe sonicator/hot homogenisation technique (Naguib *et al.,* 2014) as described in section 3.4.1. The probe sonicator has the limitation of heat being released during the sonication process. This heat could affect the stability of the drug. Therefore, the temperature was controlled between 50-70 °C, by placing the vial that contained DTX-NLC or B-NLC in an ice bath during the sonication process and the sonication was carried out alternatively every 5 min with a total processing time of 40 min.

3.5.2. Optimisation of Blank-NLC

The surface charge of the NPs has been reported to play a critical role in stabilisation of NPs, as well as successful passage through the BBB when fabricated with non-ionic and cationic surfactants (Voigt *et al.,* 2014). In the present study, various surfactants were explored, and initial optimisation was carried out with B-NLCs and then further optimisation was performed on DTX loaded NLCs as various product and process parameters were studied to shed light on their effect on the PS and PDI of the NLCs.

3.5.2.1. Effect of high-speed homogenisation (HSH)

High-speed homogenisation (HSH) has been used for size reduction of NLCs (Singh *et al.,* 2015). Combining HSH with probe sonication would probably result in obtaining a lower particle size of the NLCs. Three different batches (B4, B6 and B7) with varying ration of surfactants were fabricated (Table 3.2), to study the effect of HSH time on PS and PDI. All three formulations were prepared with and without 15 min of HSH prior to the probe sonicator.

B4 showed a significant difference in both PS and PDI when HSH was used prior to the ultra-sonication compared to when HSH was not employed during the fabrication of the batch (Figure 3.6 a and b). While B6 showed a significant difference in PS, no significant difference on PDI was observed when HSH was used prior to sonication process. Moreover, when HSH was used in B7 prior to ultra-sonication, it showed a no significant difference in PS as compared to the batch prepared without HSH prior to the ultra-sonication. It was found that the effect of HSH was variable depending upon the formulation composition than the HSH time (Figure 3.6 a and b).

Table 3.2 Compositions of three B-NLCs batches B4, B6, B7, and HSH time.

Batch Number	HSH Time (min)	D114 (g)	PH90 (mg)	L.Ls (mg)	P188 (g)	SC (mg)	LS75 (g)	LE80 (g)	S HS15 (mg)
B4	15 -	5	300	450	-	250	1.2	1.2	300
B6	15 -	5	300	450	1.2	-	1.2	1.2	300
B7	15 -	5	300	450	1.2	250	1.2	-	300

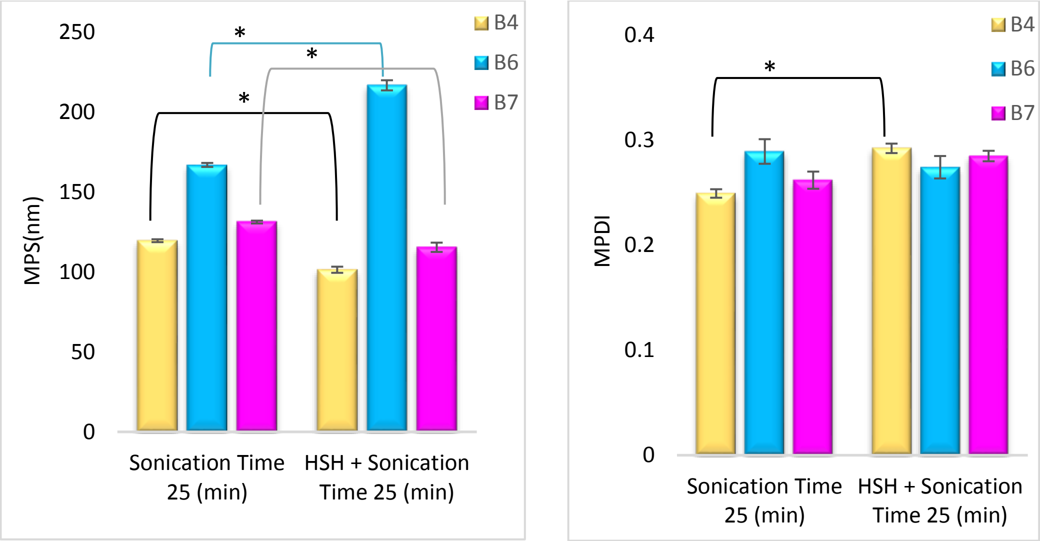

(a) (b)

Figure 3.6 (a) Effect of HSH time on PS for (B4, B6, and B7); (b) Effect of HSH time on PDI for (B4, B6 and B7). Data are mean ± SD, N=3, * P < 0.05 refers to the significant difference.

3.5.2.2. Effect of surfactants

According to Voigt *et al.,* (2014), a successful BBB passage could be achieved if NPs were fabricated with non-ionic surfactants. To achieve our goal of stable NLCs formulation with low PS and uniform distribution that might have a potential to pass the BBB, optimisation was carried out with different surfactants. Initially, B-NLCs were prepared with several types of anionic and non-ionic surfactants to assess their effect on PS and PDI.

3.5.2.2.1. Effect of Sodium cholate (SC) on B-NLCs

As surfactants play an important role to prevent aggregation and reduce the surface tension between particles (Blasi *et al.,* 2007), in this study to understand the role of sodium cholate SC, an anionic static bio-surfactant B-NLCs were prepared (B31, B4, B5, B6, and B7) as per table 3.3. It was observed that SC as a surfactant played an important role in the stabilisation of B-NLCs. This is line with a previous study which has reported SC as a better stabiliser than Sodium Dodecyl Sulphate (SDS), which result from higher repulsive energy barrier and a shallower attractive energy which could be attributed to rigid, bean-like structure of SC (2010; Wei *et al.,* 2016). This could be inferred as formulation B6 that did not contain SC showed large particle size with a wide particle size distribution in the range of 20-700 nm (Figure 3.7 a). Formulations containing SC (B31, B4, B5, and B7) revealed lower PS with a uniform distribution (Figure 3.7 b and c).

Table 3.3 Compositions of B-NLCs batches B31, B4, B5, B6 and B7 at 30 min sonication time.

Batch number	**D114 (g)**	**PH90 (mg)**	**L.L (mg)**	**P188 (g)**	**SC (mg)**	**LS75 (g)**	**LE80 (g)**	**S HS15 (mg)**
B31	5	300	450	1.2	250	1.2	1.2	300
B4	5	300	450	-	250	1.2	1.2	300
B5	5	300	450	1.2	250	-	1.2	300
B6	5	300	450	1.2	-	1.2	1.2	300
B7	5	300	450	1.2	250	1.2	-	300

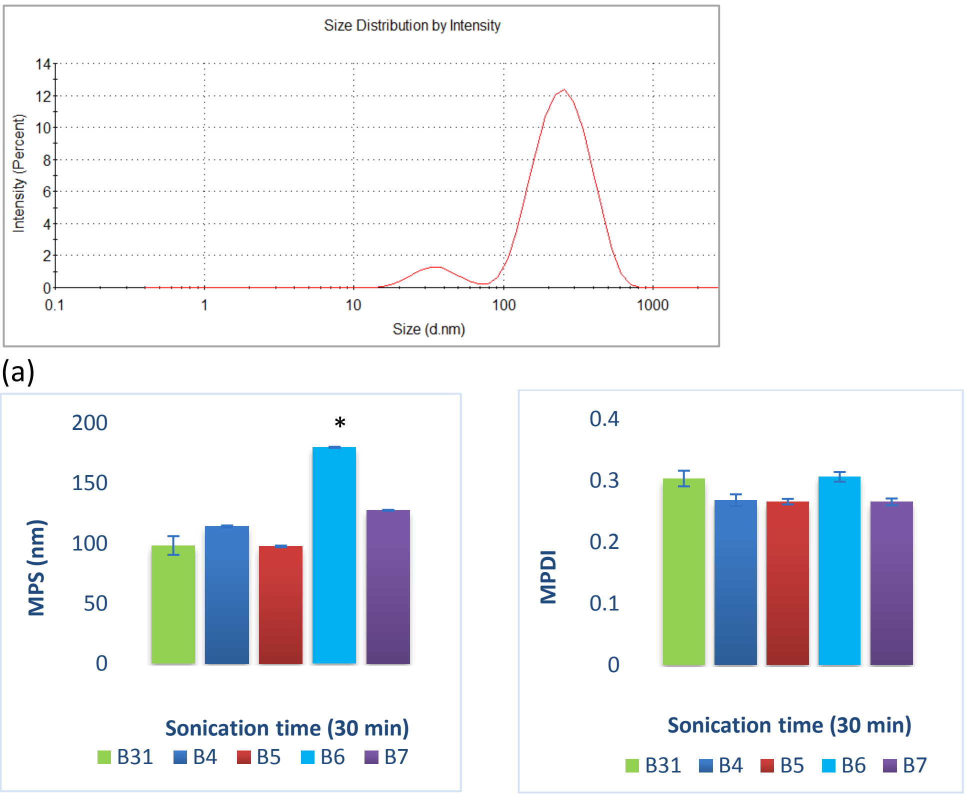

(a)

(b)

(c)

Figure 3.7 Particle size distribution for (a) B6 and effect on PS distribution, Bar charts showing the Sodium Cholate (SC) and surfactants (b) effect on PS, (c) effect on PDI. Data are mean ± SD, N=3, * $P < 0.05$ refers to the significant difference in particle size for B6 when compared to all the other batches, and no significant difference in the PDI for all tested batches.

3.5.2.2.2. Effect of Poloxamer188 (P188) on B-NLCs

Poloxamer188 is a non-ionic surfactant and previously reported to facilitate the drug delivery to the brain (Blasi *et al.,* 2007). In this study, the presence and absence of P188 were evaluated (Table 3.4), showing a significant increase in PS but reduced PDI when P188 was not added (Batch B4) as compared to B31 (Figure 3.8 a and b), indicating that through inclusion of P188 might aid in achieving NLCs with lower PS but at the cost of wider particle size distribution.

Table 3.4 Compositions of two B-NLCs batches B4 and B31.

Batch number	**D114 (g)**	**PH90 (mg)**	**L.Ls (mg)**	**SC (mg)**	**LS75 (g)**	**LE80 (g)**	**S HS15 (mg)**	**P188 (g)**
B4	5	300	450	250	1.2	1.2	300	-
B31	5	300	450	250	1.2	1.2	300	1.2

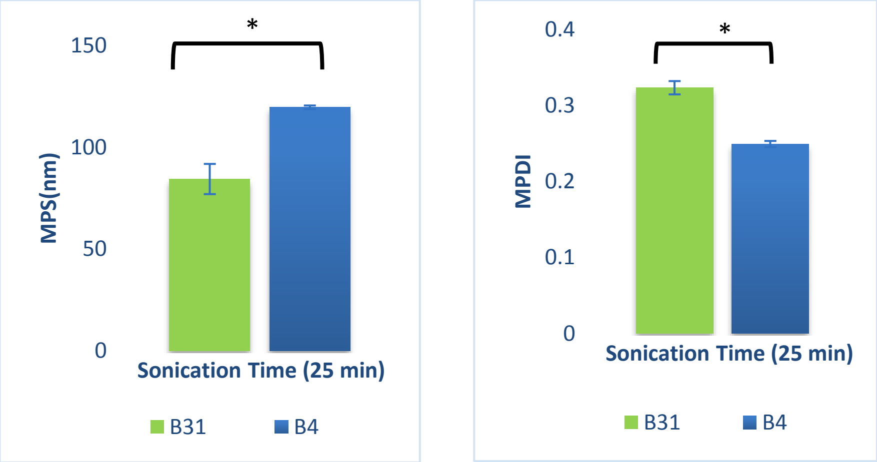

(a) (b)

Figure 3.8 Bar charts demonstrating the effect of Poloxamer188 on (a) PS and (b) PDI. Data are mean ± SD, N=3, * $P < 0.05$ refers to the significant difference in PS and PDI for B31 when compared with B4.

Further, the concentration of P188 was explored to find if the concentration had any role on PS and PDI; therefore, the P188 concentration was reduced from 1.2 g (B31) to 0.3 g (B8) and evaluated for its effect on PS and PDI (Table 3.5). Notably, the reduction in P188 concentration showed no effect on both PS and PDI (Figures 3.9 b and c), which remained the same as in the one containing higher concentration. Therefore, P188 was not considered suitable and was not considered for further optimisation. Though P188 has been widely used as an efficient stabiliser for lipid NPs (Olbrich *et al.,* 2004), our studies gave contrary results (figure 3.9 a).

Table 3.5 Composition of two B-NLCs batches B8 and B31.

Batch number	D114 (g)	PH90 (mg)	L.Ls (mg)	SC (mg)	LS75 (g)	LE80 (g)	S HS15 (mg)	P188 (g)
B8	5	300	450	250	1.2	1.2	300	0.3
B31	5	300	450	250	1.2	1.2	300	1.2

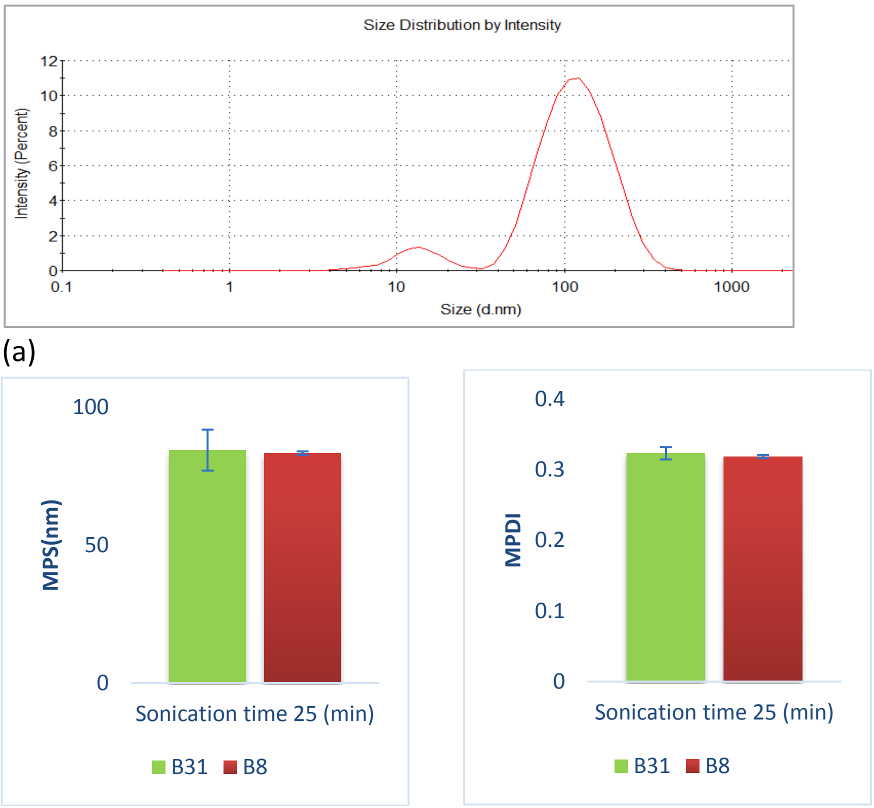

(a)

(a) (c)

Figure 3.9 Poloxamer 188 (P118) effect (a) particle distribution B31, bar charts showing Effect of P188 concentration on (b) PS, (c) PDI. Data are mean ± SD, N=3, * P < 0.05 refers to significant difference. In this case, there was no significant difference between B31 and B8 when compared with respect to PS and PDI.

3.5.2.2.3. Effect of Phospholipon H90 (PH90) on B-NLCs

Phospholipon H90 (PH90) is a widely used lipophilic surfactant in NPs preparation (Blasi *et al*., 2007). The effect of PH90 was investigated by comparing B31 (0.3 g of PH90) with B13 (without PH90) (Table 3.6). Though addition of PH90 did not significantly lower the PS but notably it did not cause any increase in PS or had any negative impact on the PDI (Figure 3.10 a and b), therefore, it was retained as part of the surfactants system as several reports have shown PH90 to facilitate the transport of the drug to the brain (Blasi *et al.,* 2007; Girotra and Singh, 2017).

Table 3.6 Compositions of two B-NLCs batches B31 and B13.

Batch number	**D114 (g)**	**PH90 (mg)**	**L.Ls (mg)**	**SC (mg)**	**LS75 (g)**	**LE80 (g)**	**S HS15 (mg)**	**P188 (g)**
B31	5	300	450	25the 0	1.2	1.2	300	1.2
B13	5	-	450	250	1.2	1.2	300	1.2

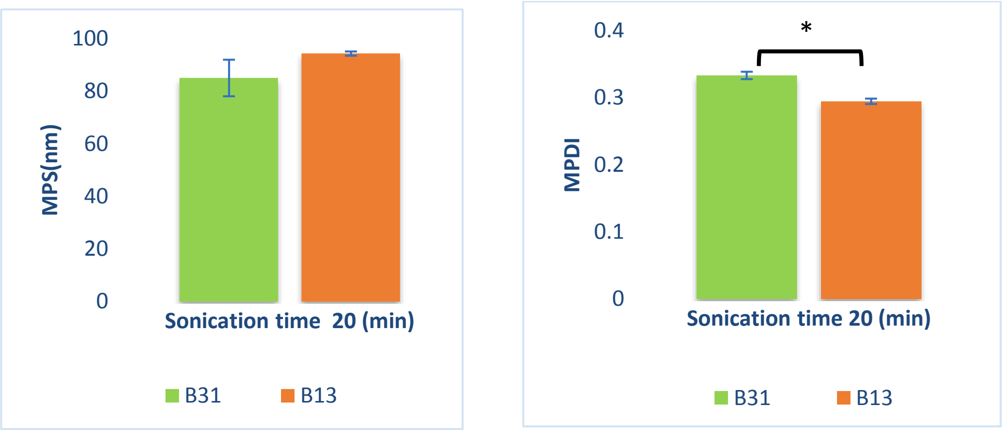

(a) (b)

Figure 3.10 B-NLCs with PH90 0.3 % and without PH90 (a) effect of PH90 on PS; (b) effect of PH90 on PDI. Data are mean ± SD, N=3, * P < 0.05 refers to significant difference. In this case, there was no significant difference between B31 and B13 when compared with respect to PS and PDI.

3.5.3. Optimisation of DTX-NLCs

To evaluate the effect of excipients on PS and PDI when the drug was loaded, further optimisations were carried out with DTX loaded NLCs as follows:

3.5.3.1. Effect of surfactants

3.5.3.1.1. Effect of Tween 80 (T80) on DTX-NLCs

Tween 80 (T80) is a well-known non-ionic hydrophilic surfactant and it is widely employed in NP fabrication either alone or in combination with lipophilic surfactants (Voigt *et al.,* 2014). T80 was incorporated with other non-ionic surfactants to assess its effect on both PS and PDI (Table 3.7). The presence of T80 in B23 was found to give a very wide particle size distribution with two peaks, (Figure 3.11 a). Even after 15 min of sonication (Figure 3.11 b and c), PS remained high, therefore, T80 was not continued as part of the surfactants combination in our formulation. It is worth mentioning that T80 has previously reported enhancing BBB drug delivery though we could not use it to our advantage (Voigt *et al.,* 2014). T80 is also used in the formulation of the FDA approved DTX formula

(Taxotere®) which is believed to cause hypersensitivity (Sanofi-Aventis, Canada, 2015) and suffer from limitations due to hemolysis effect (Ellis *et al.,* 1996).

Table 3.7 Compositions of two DTX-NLCs batches B23 and B36.

Batch number	**DTX (mg)**	**D114 (g)**	**PH90 (mg)**	**L.Ls (mg)**	**SC (mg)**	**LS75 (g)**	**LE80 (g)**	**S HS15 (mg)**	**T80 (g)**
B23	100	4	300	450	375	1.2	1.2	300	1
B36	100	4	300	450	375	1.2	1.2	300	-

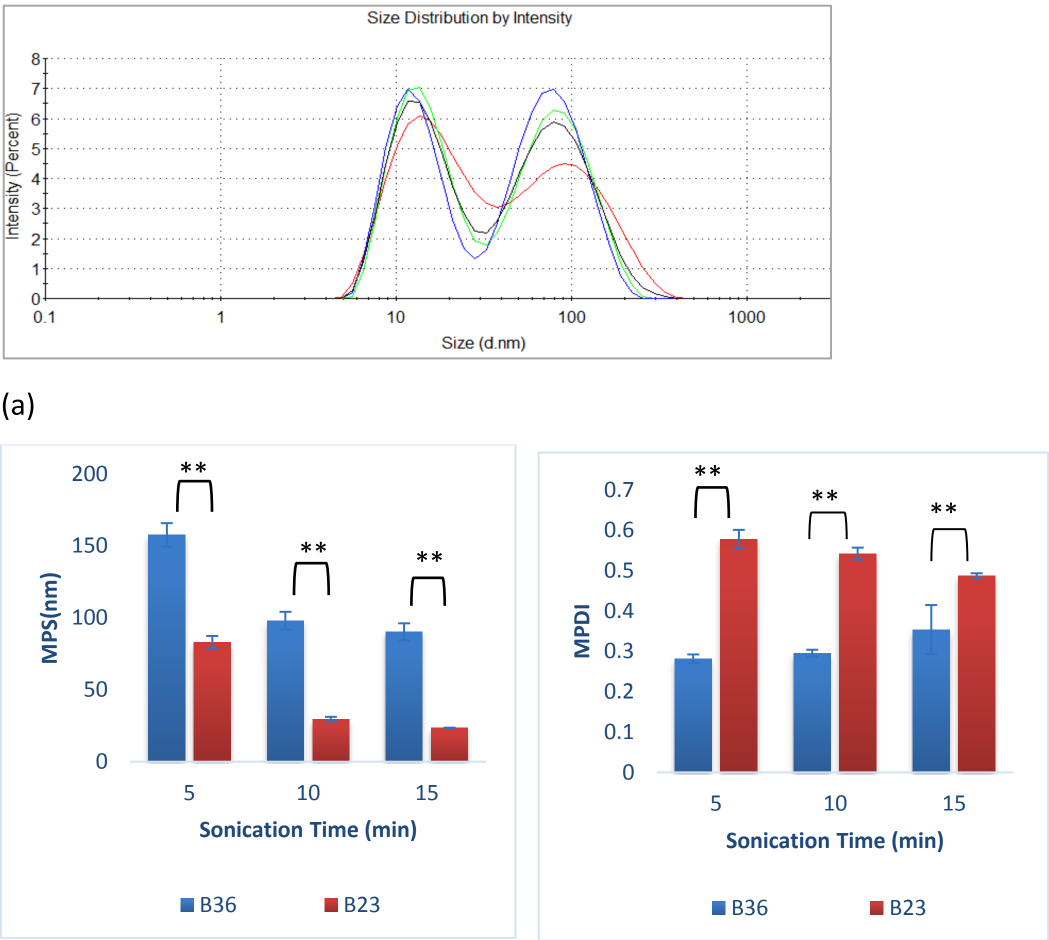

(a)

(b) (c)

Figure 3.11 Size and distribution data (a) mean data showing the effect of T80 on particle distribution at 15 min sonication time (b) bar chart showing effect of T80 on MPS at 5,10, 15 min sonication time; (c) bar chart showing effect of T80 on MPDI at 5, 10, and 15 min sonication time. Data are mean ± SD, N=3, ** P < 0.001 refers to the significant difference in PS and PDI when B36 compared to B23 at 5, 10, 15 min.

3.5.3.1.2. Effect of Vitamin E TPGS (d-alpha tocopheryl polyethene glycol 1000 succinate) on DTX-NLCs

TPGS is a non-ionic surfactant that enables delivery to the brain (Keum *et al.,* 2011). TPGS was used to evaluate its effect on both PS and PDI (Table 3.8). A significant reduction in

PS for B17 (containing 0.5 g of TPGS) was noticeable when compared with the PS of B33 (without TPGS) at all examined sonication time intervals (Figure 3.12 b). However, PDI of the formulations remained high even after 15 min of sonication (Figure 3.12 c). As TPGS affected the particle distribution of DTX-NLCs (Figure 3.12 a), therefore it was not used for further optimisation.

Table 3.8 Compositions of two DTX-NLCs batches B17 and B33.

Batch number	**DTX (mg)**	**D114 (g)**	**PH90 (mg)**	**L.Ls (mg)**	**SC (mg)**	**LS75 (g)**	**LE80 (g)**	**SHS15 (mg)**	**TPGS (mg)**
B17	100	5	300	450	250	1.2	1.2	300	500
B33	100	5	300	450	250	1.2	1.2	300	-

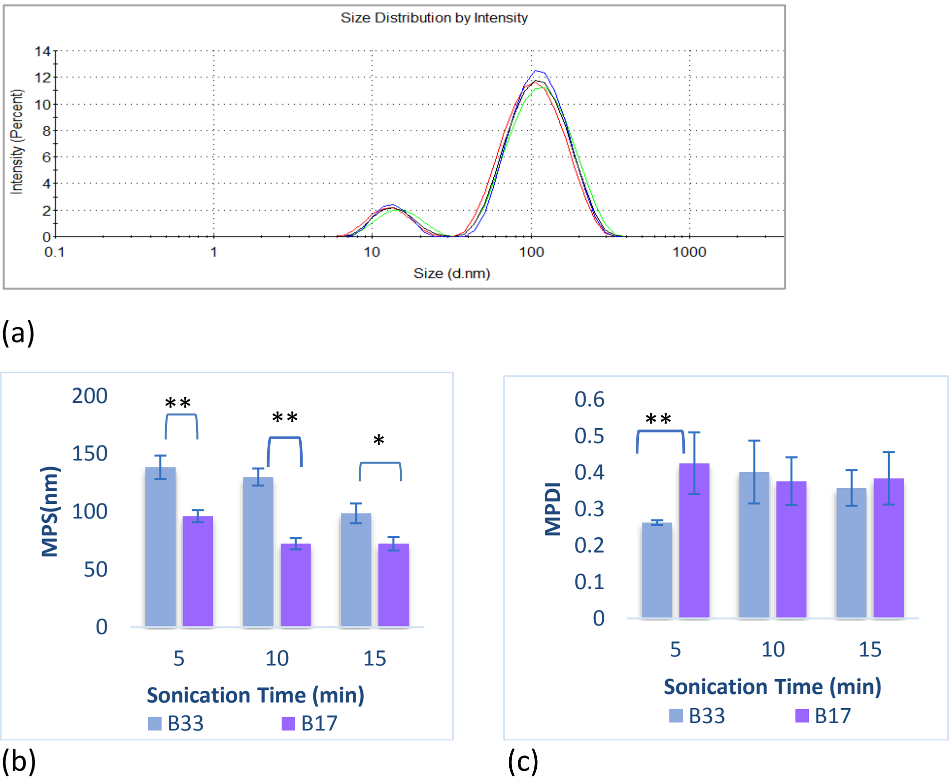

Figure 3.12 DTX-NLCs composed of 0.5 % of TPGS and no TPGS (a) mean data showing B17 particles distribution effect of TPGs on PS at 15 min sonication time (b) effect of TPGs on PDI at 5, 10, and 15 min sonication time. Data are mean ± SD, N=3, * $P < 0.05$, ** $P < 0.001$ refers to the significant difference in PS for B33 when compared with PS of B17 at 5, 10, 15 min. A significant difference was observed for the PDI in B33 when compared to the PDI of 17 at 5 min sonication time.

3.5.3.1.3. Effect of Poloxamer407 (P407) on DTX-NLCs

Poloxamer407 (P407) is a hydrophilic non-ionic surfactant, which is adsorbed onto hydrophobic NPs providing stability for the NPs preventing opsonisation and macrophages uptake through prolonged blood circulation (Moghimi and Szebeni, 2003).

Additionally, Blasi *et al.,* (2007) have reported high brain uptake by P407 coated NPs. Two batches B21 (contain 2 g of P407), and B34 (without P407) were prepared as summarised in Table 3.9 and evaluated for their effect on PS and PDI after 15 min sonication. No significant effect on PS was observed on the incorporation of P407 (Figure 3.13 b), though a significant increase in particle distribution was obtained in the presence of P407 (Figure 3.13 c). Due to the wide particle distribution (Figure 3.13 a) P407 was also not included in the surfactant combination of DTX-NLCs fabrication.

Table 3.9 Composition two DTX-NLCs batches B21 and B34.

Batch number	**DTX (mg)**	**D114 (g)**	**PH90 (mg)**	**L.Ls (mg)**	**SC (mg)**	**LS75 (g)**	**LE80 (g)**	**S HS15 (mg)**	**P407 (g)**
B21	100	5	300	450	375	0.8	0.8	300	2
B34	100	5	300	450	375	0.8	0.8	300	-

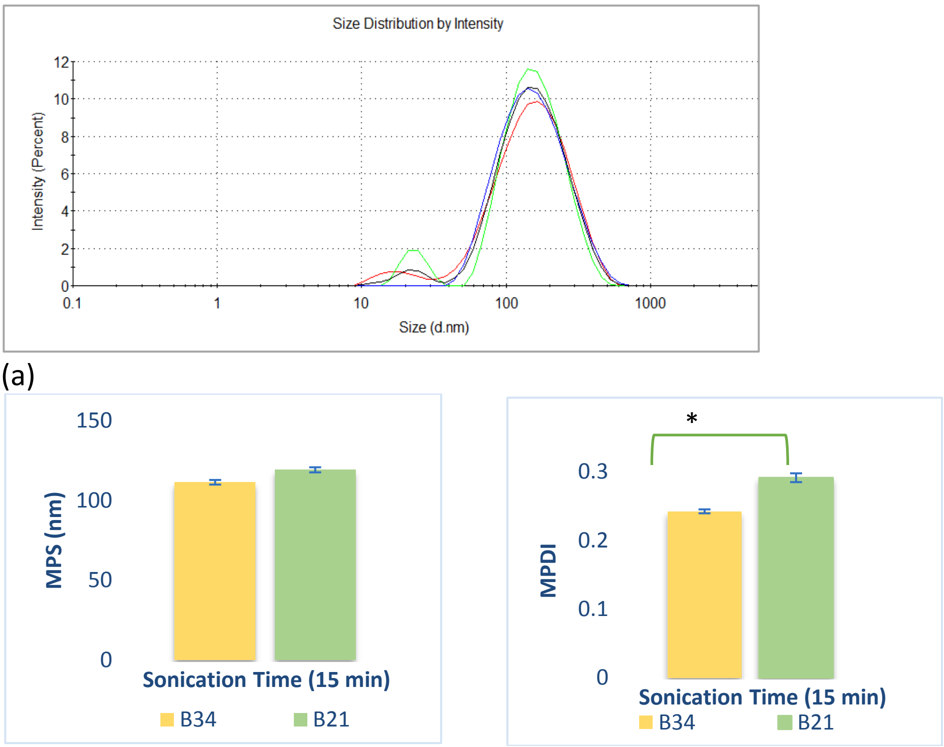

(a)

(b) (c)

Figure 3.13 Size and particle distribution (a) mean data showing the DTX-NLC prepared with P407 and its effect on particle distribution after 15 min sonication time. DTX-NLCs composed of 2 % P407 and without P407 to assess their effect on (b) PS, (c) effect of P407 on PDI. Data are mean ± SD, N=3, * P < 0.05 refers to the significant difference. In this case, no significant difference was observed in the PS for B21 when compared with B34, and a significant increase in the PDI of B21 when compared with the PDI of B34.

3.5.3.1.4. Effect of Sodium cholate (SC) on DTX-NLCs

As incorporation of SC showed a significant reduction in particle size when incorporated with surfactant combination for the preparation of B-NLC formulations, it was worth investigating SC effect on DTX-NLCs size and distribution. Two percentages were considered, B16 (contains 0.5 % of SC) and B32 (contains 0.375 % of SC) (Table 3.10). SC at lower concentration showed a significant reduction in PS, with no effect on particle distribution (Figure 3.14 a and b) indicating the vital role of SC in obtaining lower PS of DTX-NLC formulation. It is worth mentioning that a previous report has shown egg lecithin-SC form a mixed micellar state, which resulted in better stability of nanostructure (Walter *et al.,* 1991). Thus, SC was included in the DTX-NLC formulation and further optimisation was carried out.

Table 3.10 Compositions of two DTX-NLCs batches B16 and B32.

Batch number	DTX (mg)	D114 (g)	PH90 (mg)	L.Ls (mg)	SC (mg)	LS75 (g)	LE80 (g)	S HS15 (mg)
B16	100	4	300	450	500	1.2	1.2	300
B32	100	4	300	450	375	1.2	1.2	300

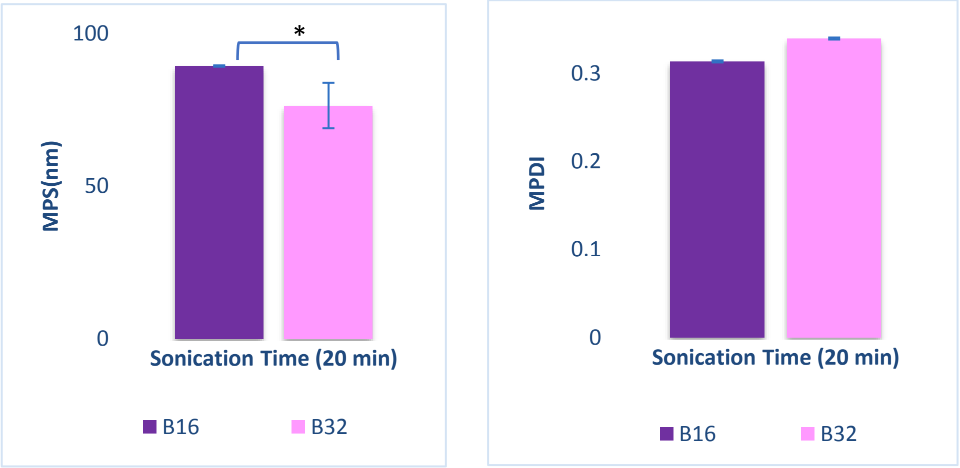

(a) (b)

Figure 3.14 DTX-NLCs composed of Sodium cholate 0.5 % and 0.375% respectively (a) effect of hydrophilic surfactant SC on PS, (b) effect of hydrophilic surfactant SC on PDI. Data are mean ± SD, N =3, * P < 0.05 refers to the significant increase in PS for B16 when compared to PS of B32, and no significant difference in PDI.

3.5.3.1.5. Effect of Solutol HS15 (S HS15) on DTX-NLCs

DTX a highly insoluble drug which faces some challenges during incorporation in the lipid matrix (Yin *et al.,* 2009; Kintzel *et al.,* 2006; Persohn *et al.*, 2005). S HS15 is a potent non-ionic solubiliser and an emulsifying agent which has low toxicity and is approved by FDA for parenteral application. S HS15 was used in the fabrication of DTX-NLC (Table 3.11). High concentration of S HS15 in B22 (600 mg/100 ml) though had limited effect on the PS, increased the PDI significantly (Figure 3.15 a and b) in comparison to the lower concentration B35 (300 mg/100 ml). Therefore, S HS15 was used in lower concentration

(300 mg/100 ml). This concentration was suitable for incorporation of DTX at (1mg/1ml) concentration, to enhance the DTX solubility.

Table 3.11 Compositions of two DTX-NLCs batches B22 and B35.

Batch number	**DTX (mg)**	**D114 (g)**	**PH90 (mg)**	**L.Ls (mg)**	**SC (mg)**	**LS75 (g)**	**LE80 (g)**	**S HS15 (mg)**
B22	100	4	300	450	250	1.2	1.2	600
B35	100	4	300	450	250	1.2	1.2	300

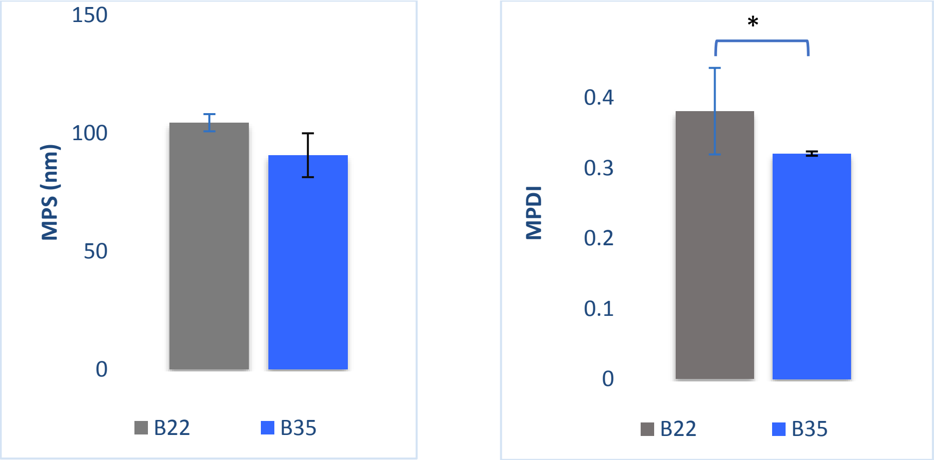

(a) (b)

Figure 3.15 DTX-NLCs composed of 0.6% and 0.3 % of S HS15 (a) effect of S HS15 on PS; (b) effect of S HS15 on PDI. Data are mean ± SD, N =3, * P < 0.05 refers to the significant increase in PDI of B22 when compared to B35. While no significant difference was observed in PS when B22 compared to B35.

3.5.3.2. Effect of Liquid lipids (L.Ls) on DTX-NLCs

It is well known that liquid lipids (L.Ls) are present in the NLC as oil nano-compartments that enhance the solubility of the drug and also prevent drug leakage (Muller *et al.,* 2002a; Das *et al.,* 2012) on storage. The content of the liquid lipid phase incorporated can influence the size and surface morphology of the particles (Zhuang *et al.,* 2010). Therefore, the effect of four L.Ls was studied. Figure 3.16 a and b demonstrate the effect on PS and PDI when three L.Ls in combination were used for fabrication of B20 showing not only low PS, but also led to high incorporation of DTX as revealed by high entrapment efficiency, total drug (Figure 3.17 a), and high loading capacity (Figure 3.17 b) as compared to three other batches prepared with individual L.Ls, B25 contains Miglyol 812 N (MG), B26 contains Labrasol (LB), and B27 contains Capryol propylene glycol monocaprylate (CPGMC), B30 contains Lauroglycol 90 (LG90), B20 contains a combination of

LB:CPGMC:LG90 in equivalent ratio and SLN formulation B29 (without L.Ls) (Table 3.12). DTX showed good solubility in all the selected L.Ls (Quan *et al.,* 2013), but only B20 resulted in high drug content as well as better stability and uniform particle distribution. Three L.Ls were therefore used in combination with the production of the DTX-NLC (B20) formulation.

Table 3.12 Compositions of six DTX-NLCs batches B20, B25, B26, B27, B29, and B30.

Batch number	DTX (mg)	D114 (g)	L90 (mg)	LG90. (mg)	LB. (mg)	CPGMC (mg)	MG. (mg)	SC. (mg)	LS75 (g)	S HS15 (mg)
B20	100	4	300	150	150	150	-	375	2.4	300
B25	100	4	300	-	-	-	150	375	2.4	300
B26	100	4	300	-	150	-	-	375	2.4	300
B27	100	4	300	-	-	150	-	375	2.4	300
B29	100	4	300	-	-	-	-	375	2.4	300
B30	100	4	300	150	-	-	-	375	2.4	300

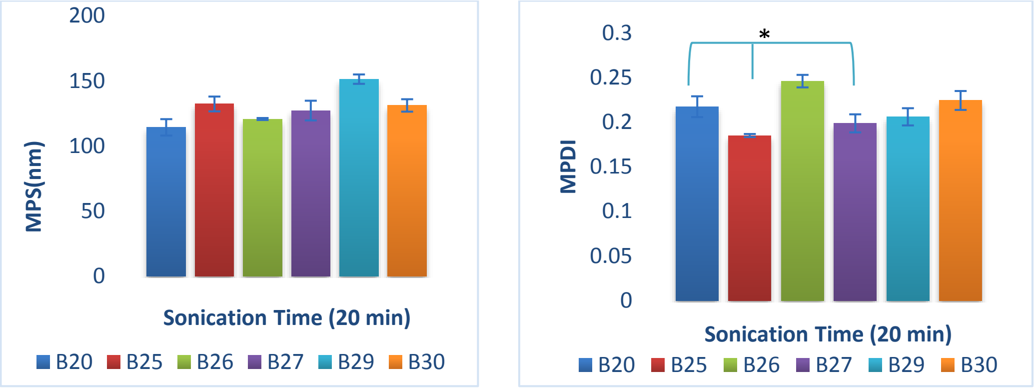

(a) (b)

Figure 3.16 Solid lipid and liquid lipids effect on the preparation of DTX-NLCs (a) effect of S.L and L.L on PS, (b) effect of S.L and L.L on PDI. Data are mean ± SD, N =3, * P < 0.05 refers to the significant difference. In this case, there was no significant difference in PS when B20 compared to all the other batches. While a significant reduction observed in PDI when B20 compared to B25 and B27.

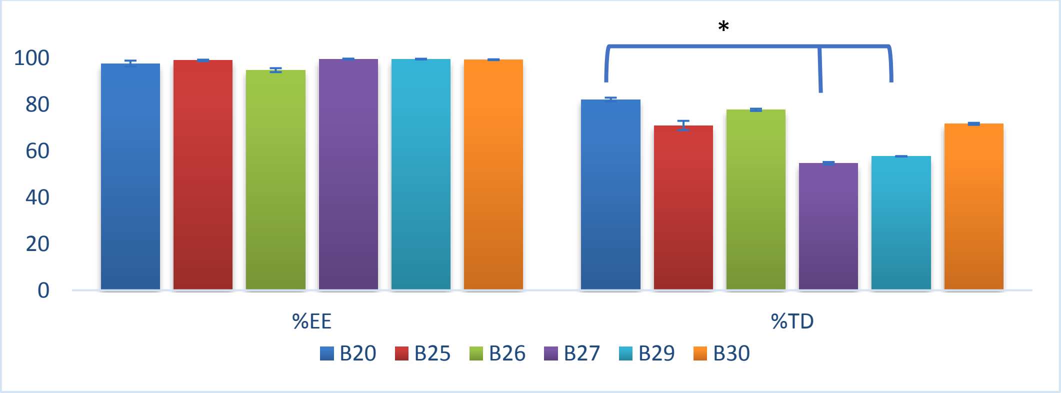

(a)

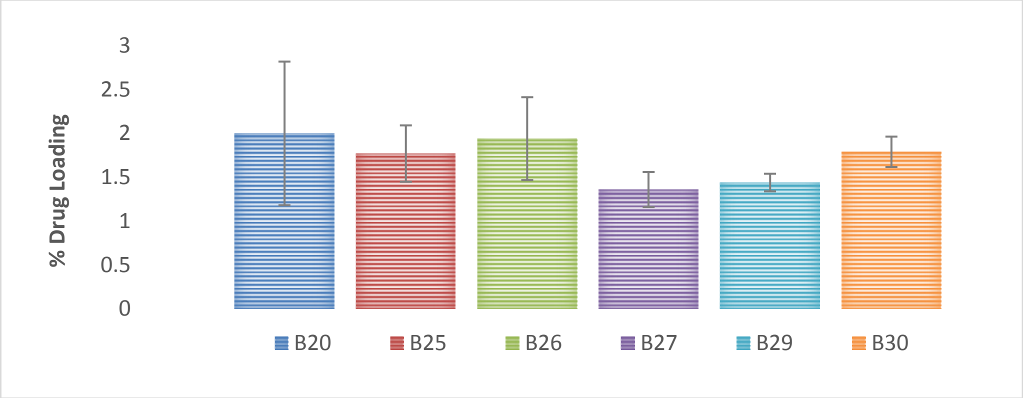

(b)

Figure 3.17 Solid lipid and liquid lipids effect on the preparation of DTX-NLCs (a) effect of S.L and L.L on %EE and %TD, and (b) effect of S.L and L.L on %DL. Data are mean ± SD, N=3, * $P < 0.05$ refers to the significant difference. In this study, there was no significant difference in % EE and % DL when B20 compared to all the other batches, and a significant reduction in % TD when B20 compared to B27 and B29.

3.5.4. Optimisation of process parameters on the selected DTX-NLC

From the above experiments, a prototype composition of DTX-NLC was achieved (Table 3.12). It was found to be that B20 was the most stable amongst all studied formulations with respect to PS and PDI, therefore the process parameters, temperature and sonication time were further investigated to evaluate their effect on PS, PDI, %EE, %TD and %DL for the selected DTX-NLC formulation (B20).

3.5.4.1. Effect of process temperature on DTX-NLCs

Process temperature has a large impact on the stability of the NLCs, DTX is heat sensitive drug and therefore processing temperature could affect its stability during DTX-NLC fabrication. Probe sonication, when used for a continuous period of time, can lead to a rise in sample temperature. This is because, during sonication, the extreme local heating cycles that take place on microscale bubble interface due to cavitation results in bulk heating of the liquid over time (Hielscher 2005). Excessive bulk heating can cause substantial liquid evaporation resulting in a change in sonicated volume or degradation of the material. A simple approach to minimise temperature driven heat effect is to avoid substantial high-temperature excursion by immersing the container in a cooling ice-bath. Additionally, operating pulse mode, ultrasonication intervals are alternated with static (sonication off) intervals. Duration of on and off intervals can be regulated. Operating in pulse mode reduced the temperature increase, minimising unwanted side effect and allowing better control over temperature than continuous mode operation.

It was observed that when the temperature was not controlled during DTX-NLC (Table 3.13), the drug content resulted in a lower percentage of TD (Figure 3.18 c and d). Controlling the temperature was considered important to get the desired drug content in the formulation. Not only TD of the DTX-NLC was affected by temperature control, but it had an effect on PS and PDI also (Figure 3.18 a and b). Low PS and uniform distribution could be obtained when the formulations were prepared under controlled temperature environment, which avoided the rise in sample temperature during sonication. Thus a significant reduction in PS and PDI were obtained when B20 was prepared by controlling the temperature by using an ice bath as compared to uncontrolled or pulsed control conditions, Our results are in line with a previous report by Singh *et al.,* (2015).

Table 3.13 DTX-NLC B20 compositions and temperature variation assessment.

Batch number	**Temperature (°C)**	**DTX (mg)**	**D114 (g)**	**PH90 (mg)**	**L.Ls (mg)**	**SC (mg)**	**LS75 (g)**	**S HS15 (mg)**
B20: **DTX-NLC**	Ice Bath control (50-70) °C	100	4	300	450	375	2.4	300
	1 min on/1 min off (50-75) °C							
	No control (70-82) °C							

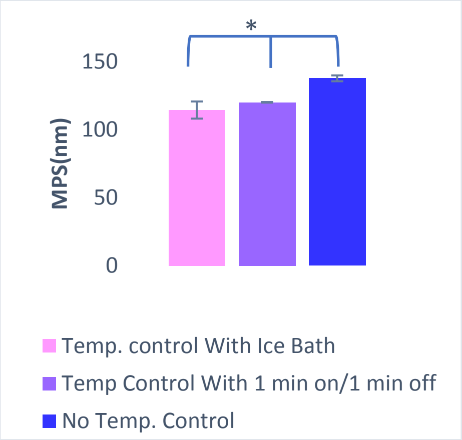

(a)

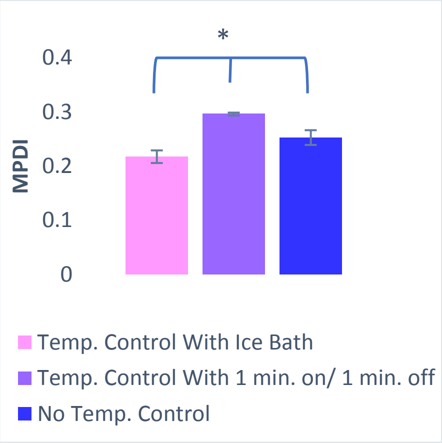

(b)

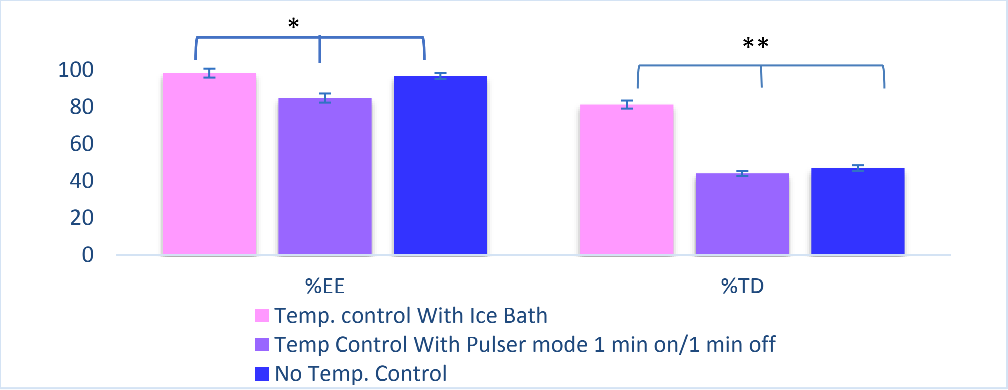

(c)

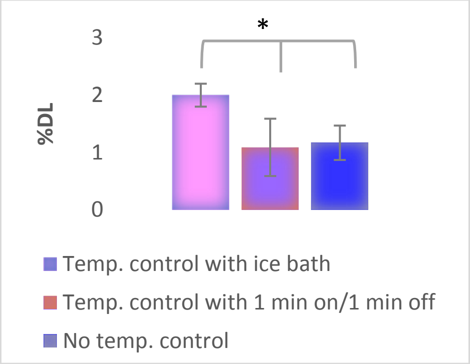

(d)

Figure 3.18 Temperature effect on DTX-NLCs B20 (a) effect on PS; (b) effect on PDI; (c) %EE and %TD; (d) %DL. Data are mean ± SD, N =3, * P < 0.05 and ** P < 0.001 refers to the significant difference in PS, PDI, % EE, % TD and % DL for B20 controlled by ice bath when compared to similar batches with two temperature studies.

3.5.4.2. Effect of sonication time and drug loading on B-NLC (B28) and DTX-NLCs (B20)

The total energy delivered to a dispersion during sonication is not only dependent on the applied power but also on the total time that the dispersion is subjected to an ultrasonication treatment (Hielscher 2005).

$E = P \ x \ t$ **(Equation 3.6)**

Where E = energy, P = Power, and t = time

The increase in sonication time resulted in lower particles size and PDI, that could be achieved at 25 min of sonication (under controlled temperature by ice-bath). It was interesting to note that drug-loaded NLCs (Table 3.14) resulted in smaller PS than B-NLCs when sonicated for 25 min (Figure 3.19).

Table 3.14 Compositions of DTX-NLCs B20 and B-NLCs B28, and their effect on PS and PDI.

Batch number	**Ultra-S Time (min)**	**DTX (mg)**	**D114 (g)**	**PH90 (mg)**	**L.L (mg)**	**SC (mg)**	**LS75 (g)**	**S HS15 (mg)**
B20: DTX-NLC	5	100	4	300	450	375	2.4	300
	10							
	15							
	20							
	25							
B28: B-NLC	5	-	4	300	450	375	2.4	300
	10							
	15							
	20							
	25							

High sonication time beyond 20 min resulted in high PDI, therefore 20 min was considered optimum for processing DTX-NLCs. Keum *et al.,* (2011) reported similar findings, where the PS increased at higher sonication intervals.

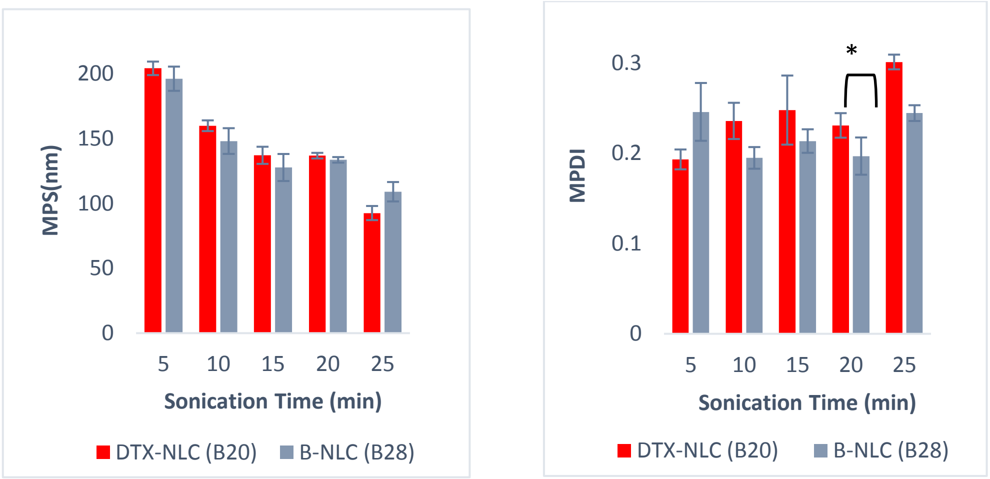

(a) (b)

Figure 3.19 Drug loading DTX-NLC B20 and B-NLC B28 (a) effect on PS; (b) effect on PDI. Data are mean ± SD, N =3, * P < 0.05 refers to the significant difference in PS and PDI for both batches when compared with respect to the sonication time. A significant increase observed in the PDI and no significant difference in PS between B20 and B28 when compared at 20 min sonication time.

3.5.5. DTX-NLCs optimisation by factorial design

Following the preliminary optimisation studies whereby the effect of various process and product parameters were investigated, DTX-NLC (B20) showed desired characteristics and was therefore taken up for final optimisation using 3^2 factorial design. Sodium cholate (SC) as a surfactant in the NLC formulation was found to critically impact the size and PDI, and the lipid concentration Daynasn 114 (D114) is well documented to affect the performance of lipid structure (Naguib *et al.,* 2014). Therefore, those two critical input variables were studied on five response variables PS, PDI, %EE, %TD, and %DL. Nine formulations were prepared, and the data were statistically analysed by using ANOVA (Table 3.15). The contour plots and response surface graphs are given in figures (3.20, 3.21, 3.22, 3.23, and 3.24).

Table 3.15 Coefficient Estimate, p-value, Model p-value, for two factors.

Response	Factors	p-value	Model p-value	F value
PS	A-surfactant concentration B-lipid concentration AB A^2 B^2	0.0003 <0.0001 0.0374 0.0003 0.0006	* <0.0001	138.11
PDI	A-surfactant concentration B-lipid concentration AB A^2 B^2	0.0913 < 0.0001 0.1154 0.2564 0.0145	0.0001 *	32.48
%EE	A-surfactant concentration B-lipid concentration AB A^2 B^2	0.4385 0.0639 0.0513 0.0653 0.9843	0.0750 ns	3.31
%TD	A-surfactant concentration B-lipid concentration	0.0032 0.5502	0.0097 *	7.64
%DL	A-surfactant concentration B-lipid concentration	0.0034 < 0.0001	<0.0001 *	28.26

(*) Refers to a significant difference when the p-value ≤ 0.05 and (ns) refers to non-significant results.

3.5.5.1 Effect of inputs variables (surfactant and lipid) on response variables

3.5.5.1.1. Particle size

For PS response a quadratic model was indicated by Design-Expert software, F-value of 138.11 implies that the model was significant. There is only 0.01% chance that an F-value this large could occur due to noise. Values of "Prob > F" < 0.05 indicate model terms are significant. In this case, A, B, AB, A^2, B^2 are significant model terms. The model P-value <0.0001 implies that the model is significant (Table 3.15).

The final polynomial equation generated by the software, representing the effect of both variables on particle size in terms of coded factors is as follows:

$$\text{Particle size} = +109.27 - 7.84A + 27.16B - 3.76AB + 11.85A^2 + 10.40B^2 \quad \textbf{(Equation 3.7)}$$

The equation in terms of coded factors can be used to make predictions about the response for given levels of each factor (Figure 3.20 a). The coded equation is useful for identifying the relative impact of the factors by comparing the factor coefficients. Positive sign before the factor in the polynomial equation suggests a synergistic effect, signifying that the response increase with the factor, whereas for the negative sign, it means response and factor have a reciprocal relation. The magnitude of the coefficient indicates the degree of contribution of the factor to the response (Esim *et al.,* 2018). The lipid concentration had a positive impact on the particle size, implying increasing the lipid concentration lead to increase in PS. In contrast, high surfactant concentration would lead to lowering in the PS (Figure 3.20 b and c). Higher concentration of surfactant would result in a reduction in the surface tension and production of particles with small sizes whereas the lower concentration of surfactant would be insufficient to reduce the interfacial tension yielding larger size particle (Landfester *et al.,* 1999; Van Zyl *et al.,* 2004).

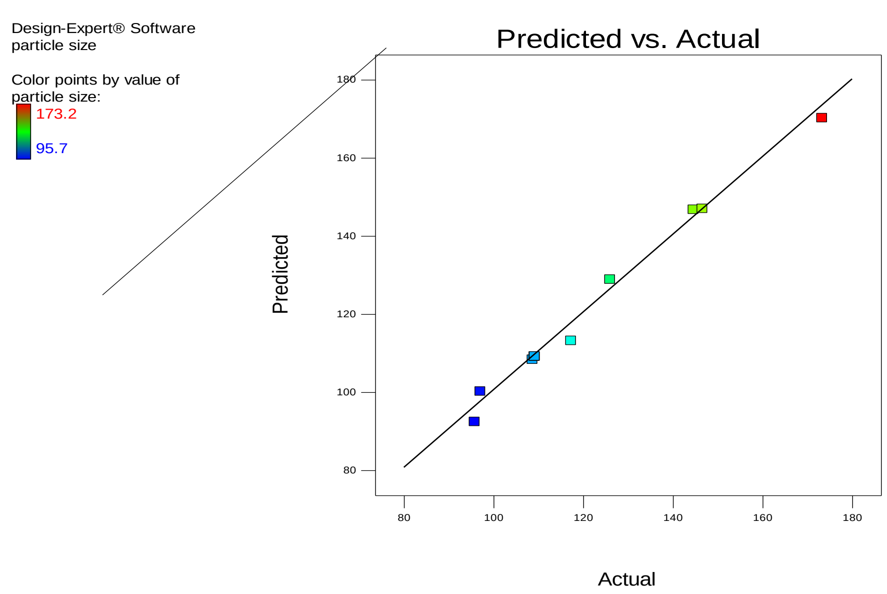

(a)

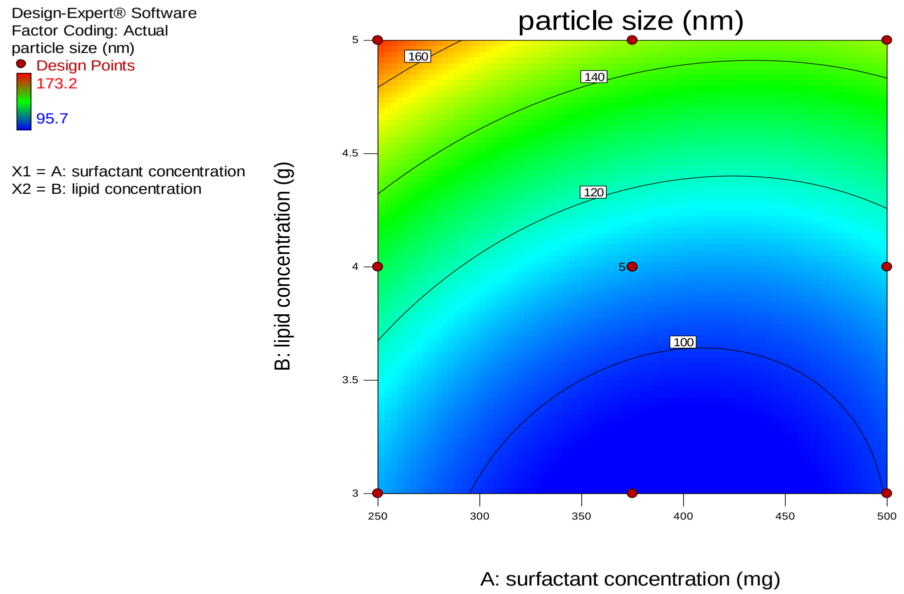

(b)

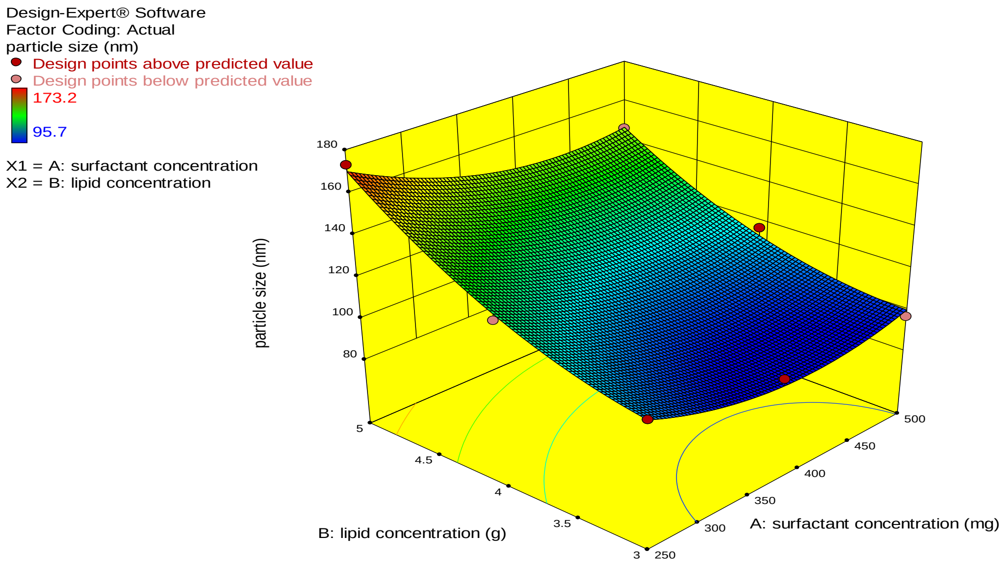

(c)

Figure 3.20 (a) PS response for 3^2 factorial design predicted VS actual values, (b) PS response for 3^2 factorial design actual values 2D contour plot, (c) PS response for 3^2 factorial design response surface 3D graph.

3.5.5.1.2. Polydispersity index

PDI response is shown in (Figure 3.21 a, b, c). The model F-value of 32.48 implies that the model is significant. There is only a 0.01% chance that an F-value this large could occur due to noise. Values of "Prob > F" < 0.05 indicate model terms are significant. In this case B, B^2 are significant model terms. While values greater than 0.1 indicate the model terms are not significant. If there are many insignificant model terms not counting those required to support hierarchy. The model reduction may improve the model. the model P-value less than 0.05 indicate model terms are significant (Table 3.15).

The final equation representing the effect of both variables on PDI in terms of coded factors is as follows:

$$\text{Polydispersityindex}=+0.23+6.667*A-0.040B-7.500*AB+6.207*A^2+0.016B^2$$

(Equation 3.8)

Lipid concentration had a negative impact on the PDI. High concentration would lead to better homogeneity of PS. The blue rejoins (Figure 3.21 b) shows the presence of homogeneous particles. The equation in terms of coded factors can be used to make predictions about the response for given levels of each factor. The equation in terms of actual factors can be used to make predictions about the response for given levels of each factor (Figure 3.21 a).

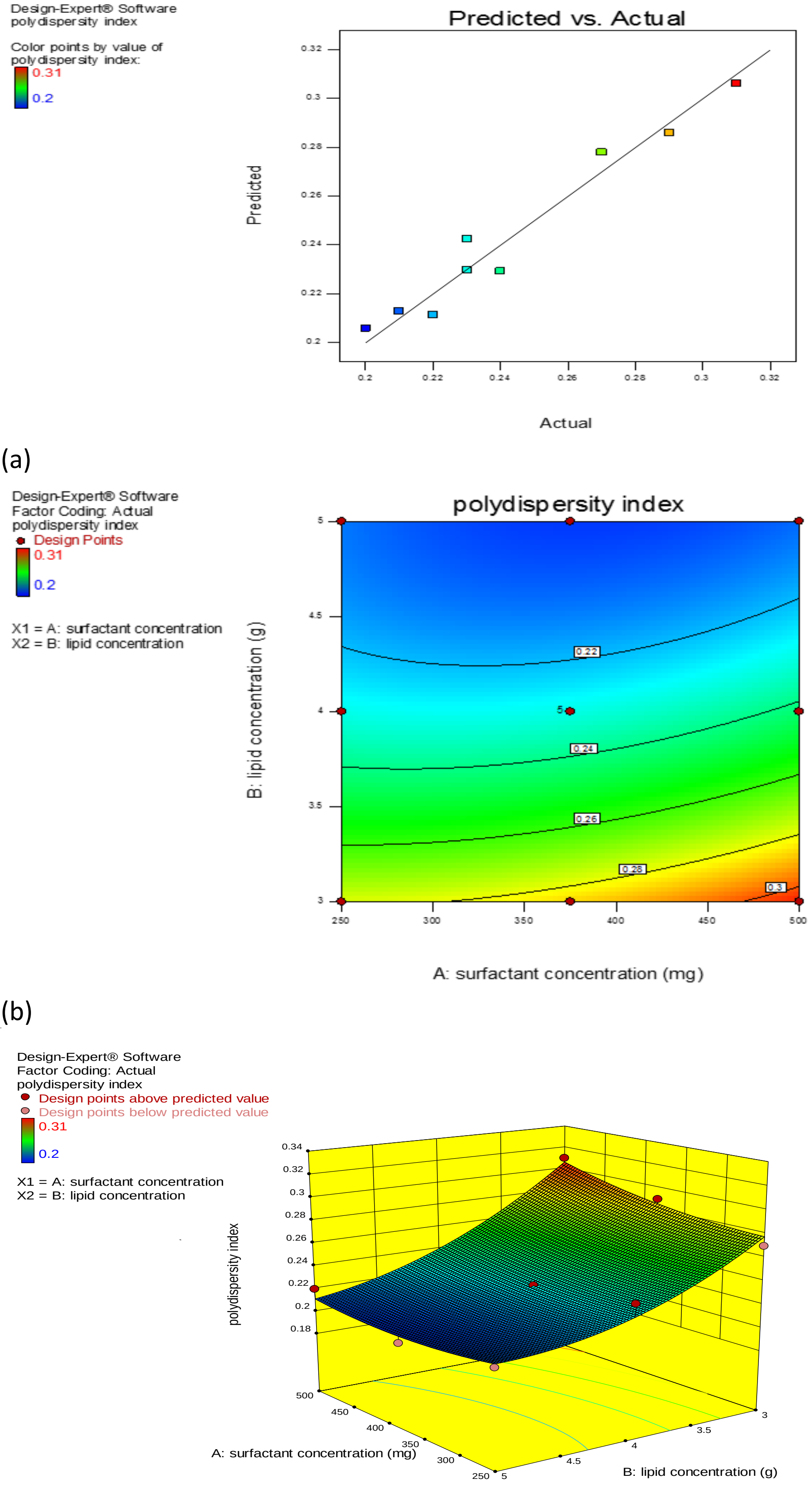

(a)

(b)

(c)

Figure 3.21 (a) PDI response for 3^2 factorial design predicted vs actual values, (b) PDI response for 3^2 factorial design actual values 2D contour, (c) PDI response for 3^2 factorial design response surface 3D graph.

3.5.5.1.3. Entrapment efficiency

For % EE response, the model F-value of 3.31 implies that there is a 7.50% chance that an F-value this large could occur due to noise. Values of "Prob > F" < 0.05 indicate that the model terms are significant. Values greater than 0.1 indicate the model terms are not significant, the model reduction may improve the model. The p-value of the surfactant concentration and the quadric effect of the lipid concentration were not significant (Table 3.15).

The final equation representing the effect of both variables on EE in terms of coded factors is as follows:

$$\% \text{ EE} = +98.36+0.56A+1.50B-1.96AB-2.19A^2+0.021B^2 \qquad \textbf{(Equation 3.9)}$$

Both surfactant and lipid concentration had a positive impact on %EE, though the coefficient values suggested the lipid concentration have a higher impact on the % EE than the surfactant concentration (Figures 3.22 a, b, c).

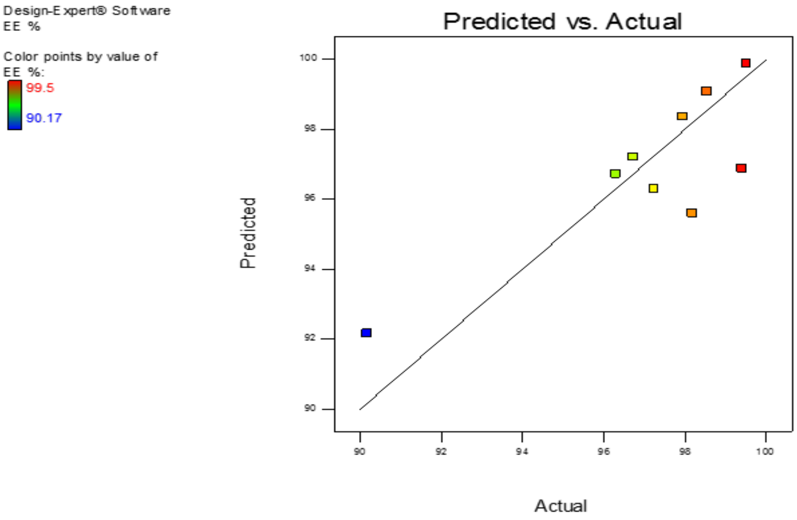

(a)

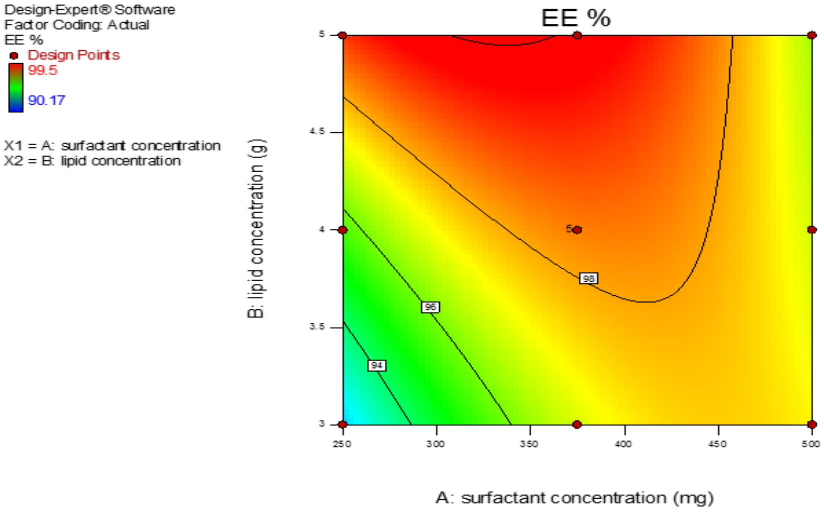

(b)

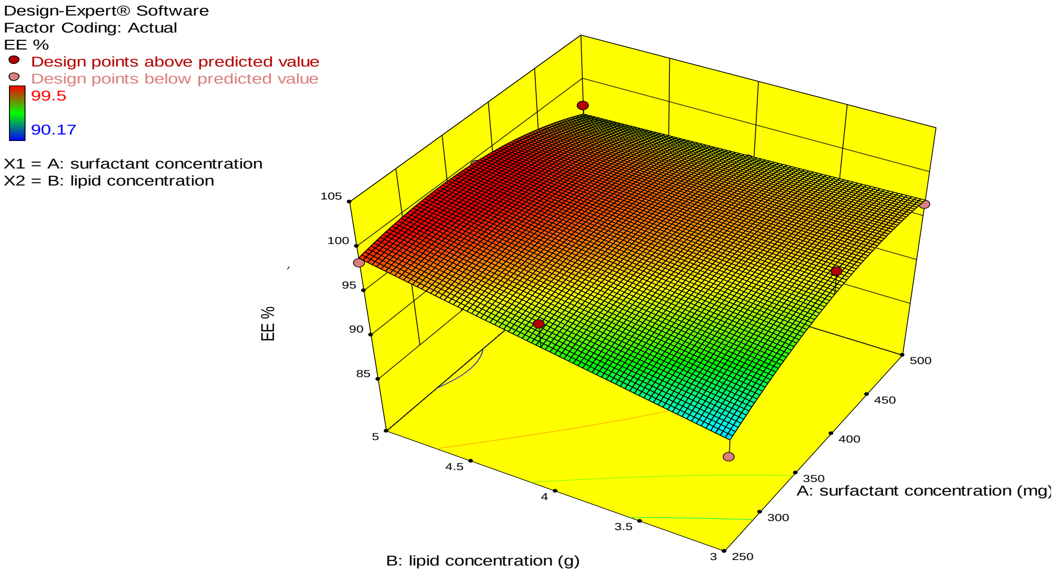

(c)

Figure 3.22 (a) % EE response for 3^2 factorial design predicted vs actual values, (b) %EE response for 3^2 factorial design actual values 2D contour, (c) %EE response for 3^2 factorial design response surface 3D graph.

3.5.5.1.4. Total drug

For the TD%, the model F-value of 7.64 implies that the model is significant. There is only a 0.97% chance that an F-value this large could occur due to noise. Values of "Prob > F" < 0.05 indicate that the model terms are significant. In this case, A is a significant model term. Values > 0.1 indicate the model terms are not significant. If there are many insignificant model terms (not counting those required to support hierarchy), the model reduction may improve the model (equation 3.10).

TD model P-value < 0.05 indicate model terms are significant. In this case, only surfactant concentration was a significant model term. Values > 0.1 indicate the model terms are not significant (Table 3.15). The final reduced equation representing the effect of both variables on TD in terms of coded factors is as follows:

$\% \text{ TD} = +78.18 - 10.53A + 1.69B$ (Equation 3.10)

From the above equation, it can be concluded that the higher lipid concentration in NLC would lead to higher TD content in the NLCs. This could be due to the fact that the increased lipid concentration would give more opportunity for the drug to be loaded into the lipid matrix. For the surfactant concentration, high concentration causes a negative relation with % TD, this might be due to the fact high surfactant concentration might lead to high dispersion of the surfactant on the interphase of water and lipid phase, thus reducing the interfacial tension resulting in smaller droplet, and consequently lower PS and reduction in the drug content (Figures 3.23 a, b, c).

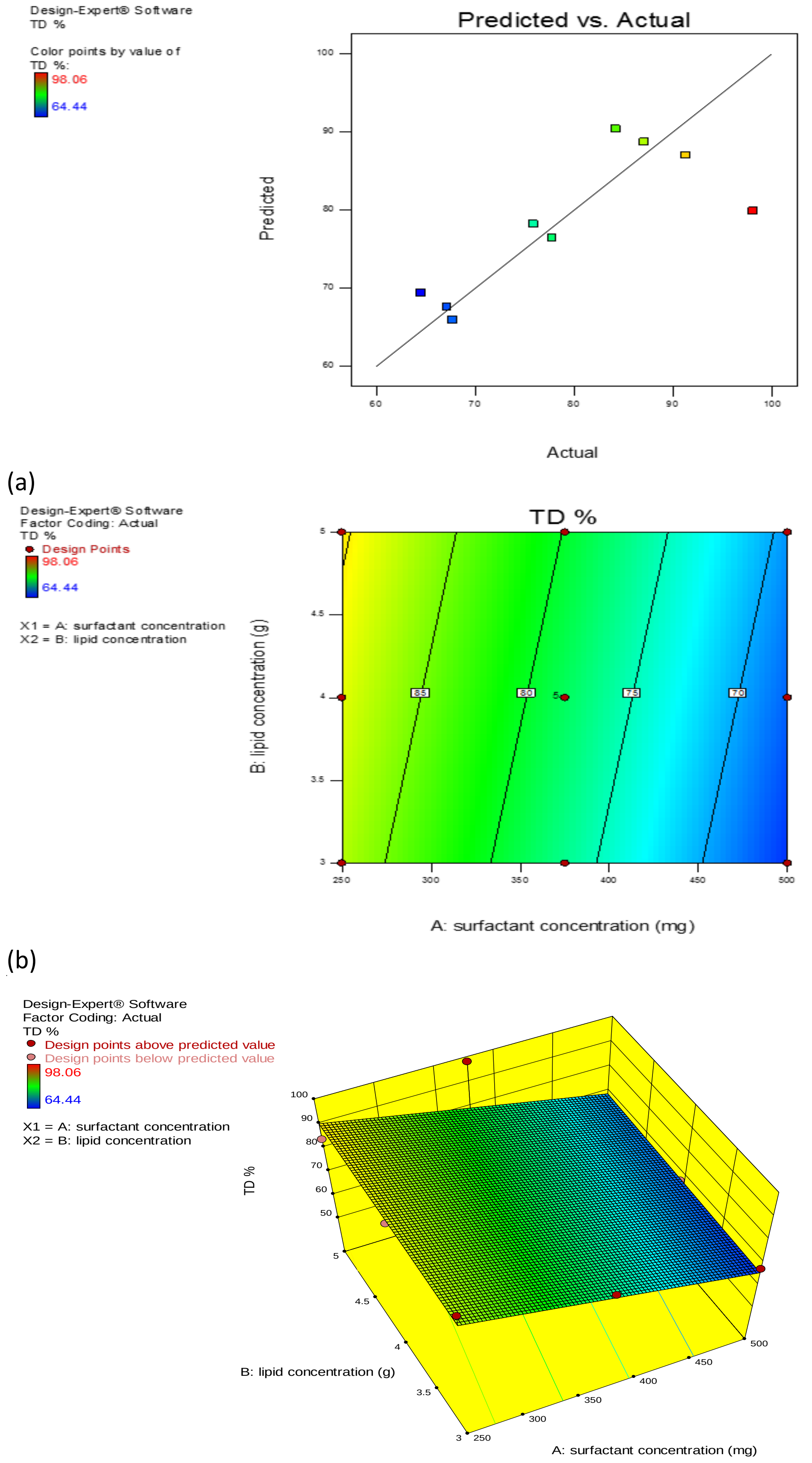

(c)

Figure 3.23 (a) %TD response for 3^2 factorial design predicted vs actual values, (b) %TD response for 3^2 factorial design actual values 2D contour, (c) % TD response for 3^2 factorial design response surface 3D graph.

3.5.5.1.5. Drug loading

The % DL response model F-value of 28.26 implies that the model is significant. There is only a 0.01% chance that an F-value this large could occur due to noise. Values of "Prob > F" < 0.05 indicate that the model terms are significant. In this case A, B are significant model terms. Values > 0.1 indicate the model terms are not significant. If there are many insignificant model terms (not counting those required to support hierarchy).

The final reduced equation representing the effect of both variables on DL in terms of coded factors is as follows:

$\% DL=+1.41-0.098A-0.17B$ **(Equation 3.11)**

From the above equation, factors, lipid and surfactant concentration had a negative impact on DTX loading. This means higher lipid concentration would lead to lower drug loading. For calculation of drug loading as lipid content of NLCs is in denominator its higher value will lead to lower drug loading value. Response model p-value < 0.05 indicate model terms are significant (Table 3.15). both input factors surfactant and lipid concentrations had a significant impact on the % DL (Figures 3.24 a, b, c).

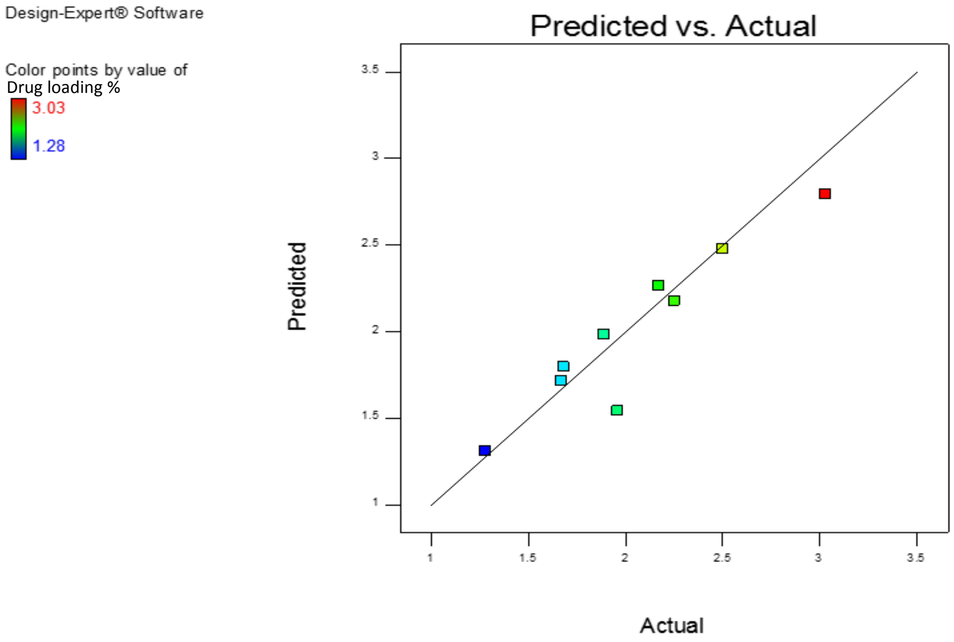

(a)

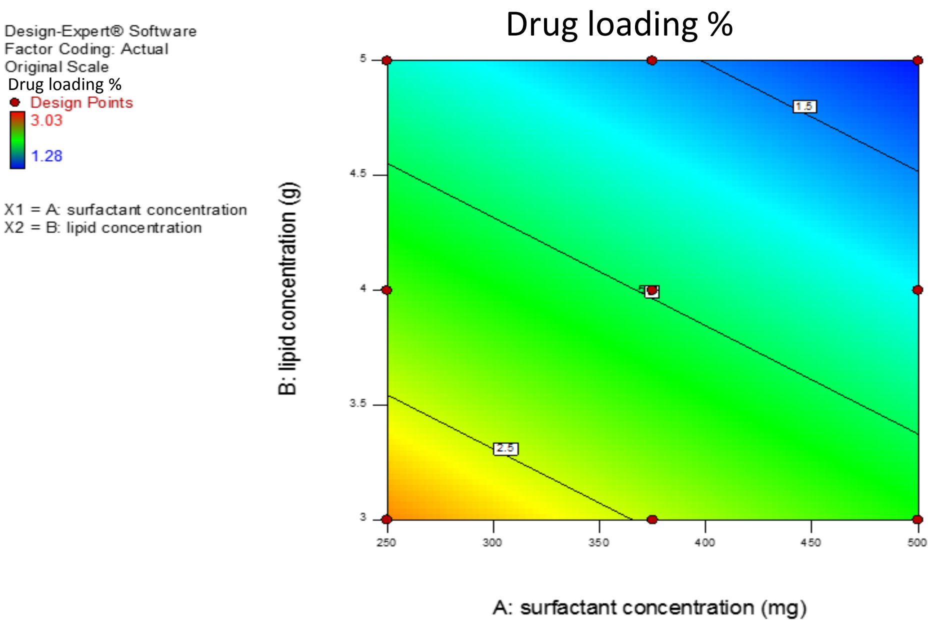

(b)

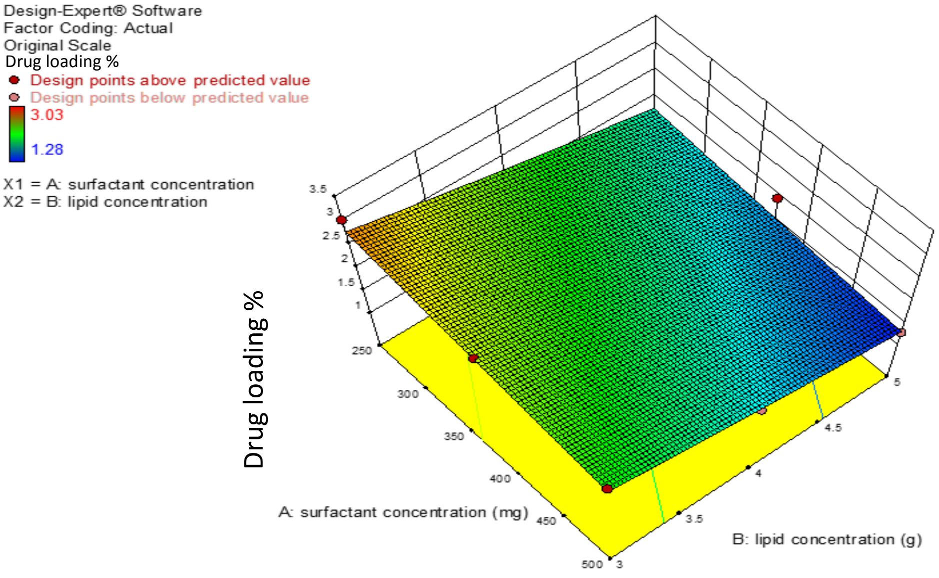

(c)

Figure 3.24 (a) % DL response for 3^2 factorial design predicted VS actual values, (b) % DL response for 3^2 factorial design actual values 2D contour, (c) % DL response for 3^2 factorial design response surface 3D graph.

In this study, lower PS and PDI were achieved with surfactant and lipid concentration of 3.5 g and 375 mg, respectively. Moreover, high %EE, %TD, and %DL were obtained with lipid and surfactant concentration > 4.5g and 375 mg, 4g and 375 mg, 3g and 250 mg, respectively. From the factorial design B20 of the DTX-NLC formulation was selected as the optimum formulation. The chosen final formulation had lipid and surfactant content at 4g and 375 mg respectively. And they were incorporated with 100 mg DTX, 2.4 g lipoid S75 (LS75), 300 mg of Solutol HS15 (S HS15), 300 mg Phospholipon 90 H (PH90) and 450 mg of three liquid lipids Labrasol (LB), CPGMC, and Lauroglycol 90 (LG90) in a 1:1:1, ratio to obtain DTX-NLC formulation with a stable, uniform distribution and high %EE, %TD, and %DL.

3.5.6. Functionalisation of DTX-NLCs with PUFAs

DTX-NLCs were functionalised with either GLA and ALA as described in section 3.4.2. through amide bond formation (Figure 3.1). Different ratios of each ligand were evaluated for their suitability depending on the effect of the presence of PUFAs ligands and the availability of FAG on the surface of the DTX-NLC for conjugation. The ligand density is known to impact the PS, particle geometry and surface property (charge and hydrophobicity) (Bertrand *et al.,* 2014; Valencia *et al.,* 2011). Therefore, the effect of ligand density in terms of different ratios of ligand to FAG was investigated on PS, PDI, and ZP of GLA-DTX-NLC and ALA-DTX-NLC.

3.5.6.1. Functionalisation of DTX-NLCs with GLA

In this experiment the FAG determined for DTX-NLC was 5.91 ± 0.181 µmol/ml pre-conjugation with GLA, so different ratios were evaluated for GLA functionalisation with DTX-NLC (1:1, 1:1/2, 1:1/3, 1:1/4, 1:1/5, 1:1/6 and 1:1/7 ratio, FAG: PUFAs), respectively. The data clearly shows that the particle size is significantly higher when GLA was conjugated to DTX-NLC as compared to bare DTX-NLC (Figure 3.25 a). Additionally, no significant difference in PDI values was observed on conjugation with different GLA ratios as compared to bare DTX-NLC (Figure 3.25 b). The data verified the influence of the conjugation on PS, notably, when the FAG: GLA ratio increased the PS increased as well. For GLA-DTX-NLCs when FAG: GLA, ratio increased 1:1/4 1:1/3, 1:1/2, and, 1:1, PS increased from 160-452 nm (Figure 3.26 a). The ligand density had a high impact on the PS with almost a linear increase in the PS from lower to higher ratios (1:1/4, 1:1/3, 1:1/2, and 1:1 ratio, FAG: GLA). Large PS is known to be opsonised and uptake by macrophages and removed from the circulatory system (Liu *et al.,* 2017). Therefore though high ligand density is desirable as high ligand concentration can lead to efficient binding to the target due to high avidity (Cao *et al.,* 2018; Elias *et al.,* 2013), but not at the cost of very high particle size as that would lead to opsonisation of particles. As the following ratios of FAG: GLA (1:1/5, 1:1/6 and 1:1/7) had limited effect on the PS ranging from 153 to 160 nm (Figures 3.26 a and b), therefore these formulations with two ratios 1:1/5 and 1:1/6 were selected for proliferation study.

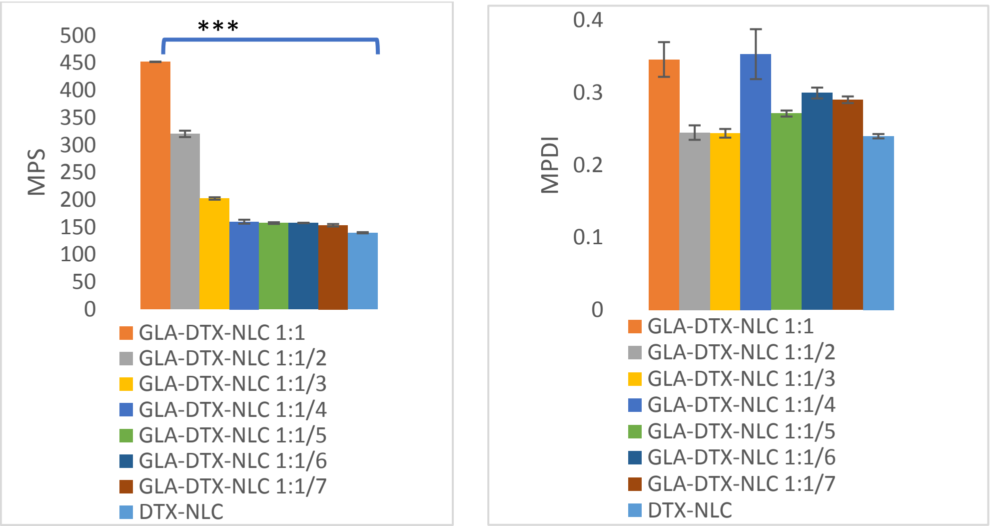

(a) (b)

Figure 3.25 DTX-NLCs formulation pre- and post-conjugation with GLA when different ratios were used to form GLA-DTX-NLCs (a) effect on PS, (b) effect on PDI. Data are mean ± SD, N=3, * P < 0.05 and *** p < 0.000 refers to the significant increase in PS in all GLA-DTX-NLCs formulation in all examined ratios when compared to DTX-NLC, while no significant difference in PDI was obtained after GLA conjugation to DTX-NLCs in all examined ratios.

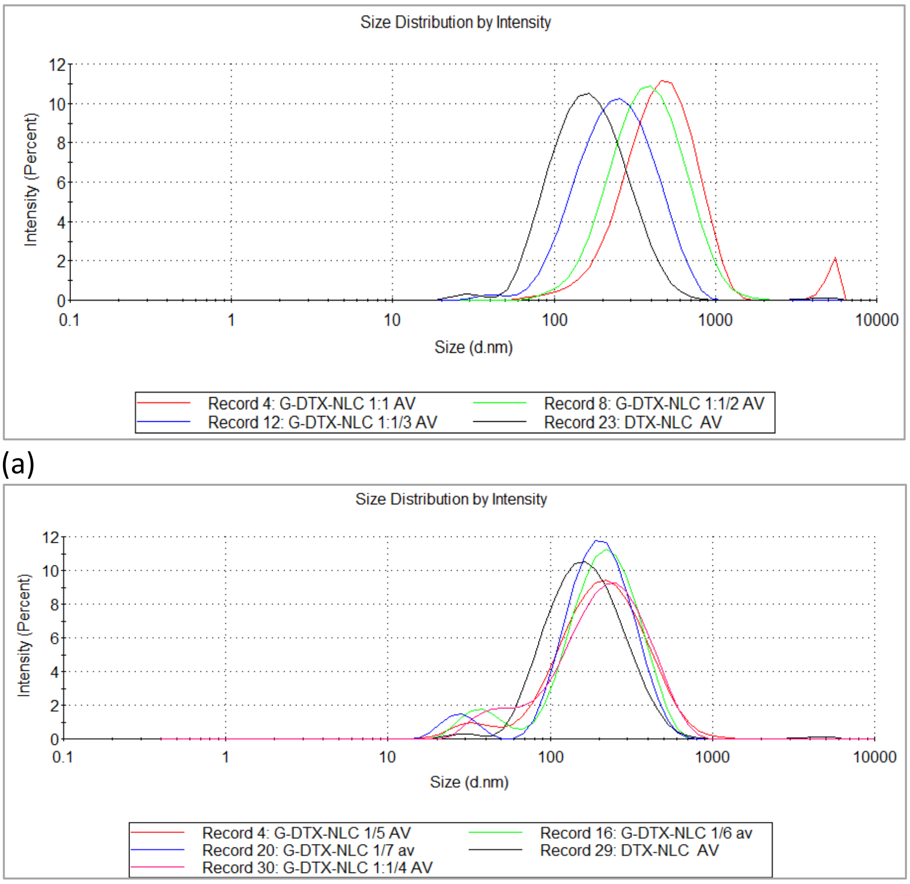

(a)

(b)

Figure 3.26 Particle size distribution data showing DTX-NLCs compared to GLA-DTX-NLCs in different ratios and their effect on PS and PDI (a) DTX-NLC compared with 1:1, 1:1/2 and 1:1/3 GLA ratios, (b) DTX-NLC compared with 1:1/4, 1:1/5, 1:1/6, and 1:1/7 GLA ratios.

The ligand density not only affects the PS but also the surface charge of the DTX-NLCs, where a significant reduction was observed with GLA-DTX-NLC 1:1/5 ratio ZP as compared to the ZP of DTX-NLC (Figure 3.27). From the above data we can conclude that when GLA is conjugated to DTX-NLC, the PS and ZP can be used as indicating parameters for conjugation due to the significant change they bring about on formation of GLA-DTX-NLC.

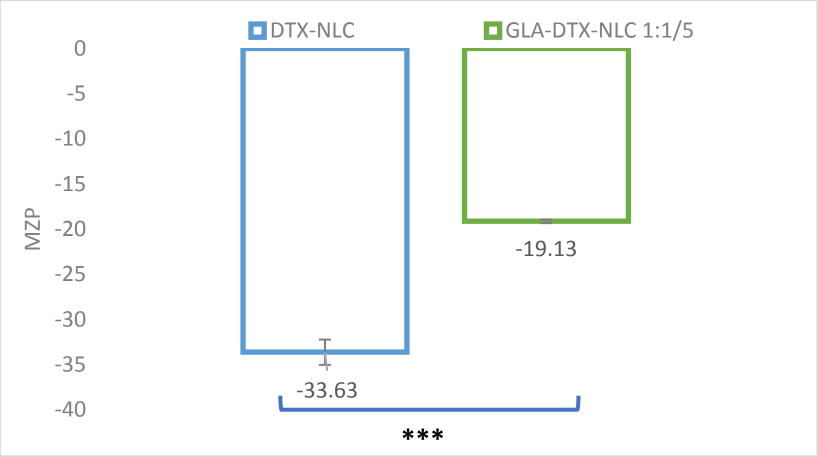

Figure 3.27 DTX-NLCs conjugation with 1:1/5 GLA (FAG: GLA, ratio) to form GLA-DTX-NLCs and their effect on ZP. Data are mean ± SD, N =3, *** p < 0.000 refers to the significant reduction in ZP for GLA-DTX-NLCs formulation when compared to DTX-NLC ZP.

3.5.6.1.1. Functionalisation of DTX-NLCs with GLA in the presence of antioxidants

As GLA is highly prone to oxidation, a combination of two antioxidants 0.02 % of α-Tocopherol (Vit E) and 0.05 % of Ascorbyl palmitate (AP) in a total percentage of 0.07% was used to protect the GLA-DTX-NLC from oxidation. Antioxidants were added in the lipid phase during the fabrication of DTX-NLC. The formulation of GLA-DTX-NLC in the following ratio of FAG: GLA 1:1/5 and 1:1/6 ratio, was studied in the presence of antioxidants and their effect on PS and PDI was investigated (Figure 3.28). Figures 3.29 a and b show a significant increase in PS and PDI when DTX-NLC prepared with antioxidants Vit. E+ AP and then conjugated with GLA in both the tested ratios. As the chosen antioxidants combination had an impact on both PS and PDI, these two ratios were further tested on glioblastoma cell lines to examine their effect on proliferation of cells (Chapter Four, section 4.5.2.2.1).

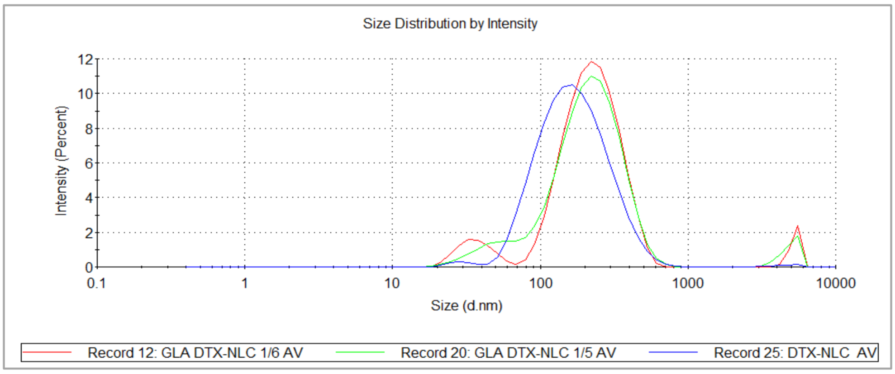

Figure 3.28 Size distribution data showing DTX-NLC prepared with antioxidants Vit.E+AP and compared to GLA-DTX-NLCs in different ratios and their effect on PS and PDI. DTX-NLC compared with 1:1/5 and 1:1/6, GLA ratios.

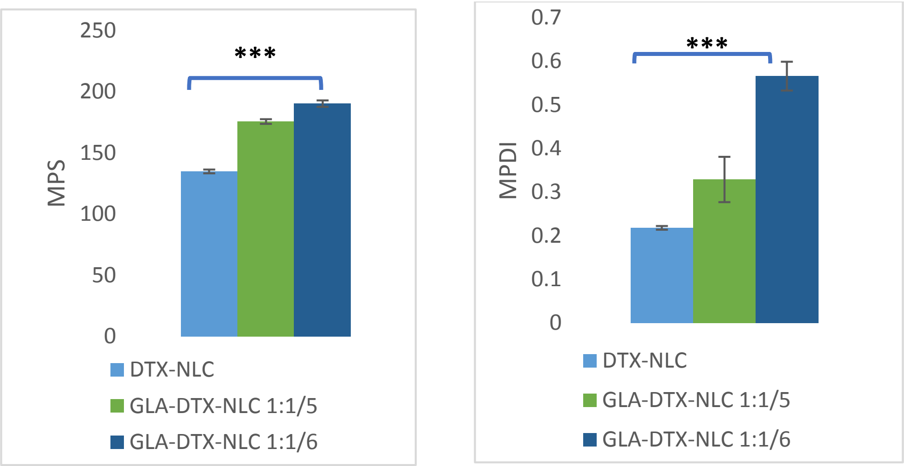

(a) (b)

Figure 3.29 DTX-NLCs prepared with antioxidants Vit.E+AP then conjugation with GLA when 1:1/5 and 1:1/6, ratios were used to form GLA-DTX-NLCs (a) effect on PS, (b) effect on PDI. Data are mean ± SD, N=3, *** $P < 0.000$ refers to the significant increase in PS and PDI for both GLA-DTX-NLC formulations in both examined ratios when compared to DTX-NLC pre-conjugation.

Out of the all studied ratio, 1:1/5 (FAG: GAL, ratio) was showing acceptable particle size and distribution (Figure 3.30), and was further taken up for detailed characterisation as it also showed a high tumoricidal activity towards glioblastoma cells as detailed in Chapter Four. The inclusion of antioxidants hindered the cell proliferation, therefore the addition of antioxidants was not included in the preparation of GLA-DTX-NLC, and the entire process of surface functionalisation was carried out under nitrogen environment.

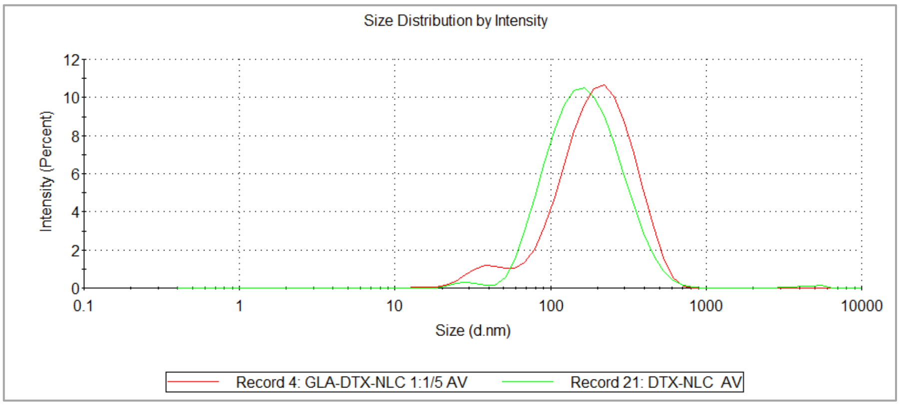

Figure 3.30 Particle size distribution of DTX-NLC and GLA-DTX-NLC in 1:1/5 ratio and its effect on PS and PDI.

3.5.6.2. Functionalisation of DTX-NLCs with ALA

As high ratio of the ligand GLA resulted in high particle size, therefore, lower ratios of FAG: ALA was investigated for their effect on PS and PDI in ALA-DTX-NLC formulations. In this experiment, the FAG for bare DTX-NLC was 5.91 ± 0.181 µmol/ml and it was used for conjugation with ALA in the following ratios (1:1/5, 1:1/6 and 1:1/7 ratio, FAG: ALA) respectively, and their effect on PS and particle distribution was evaluated (Figure 3.31). As anticipated 1:1/6 and 1:1/7 ratios showed less effect on PS, while 1:1/5 ratio showed a notable increase in the PS. The data demonstrated a significant increase in PS of ALA ratios 1:1/5 and 1:1/6 and no significant effect on PS for ALA ratio 1:1/7 when all ratios were compared to the PS of bare DTX-NLC. Additionally, the PDI showed a significant effect between bare DTX-NLC, and ALA conjugated formulation prepared with three FAG: ALA ratios (Figure 3.32 a and b).

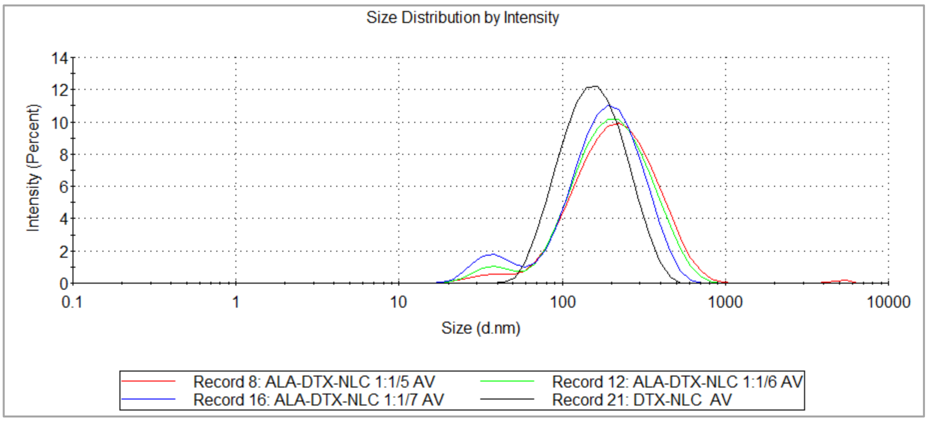

Figure 3.31 Size distribution data showing DTX-NLC compared to ALA-DTX-NLC in 1:1/5, 1:1/6 and 1:1/7 ratios and their effect on PS and PDI.

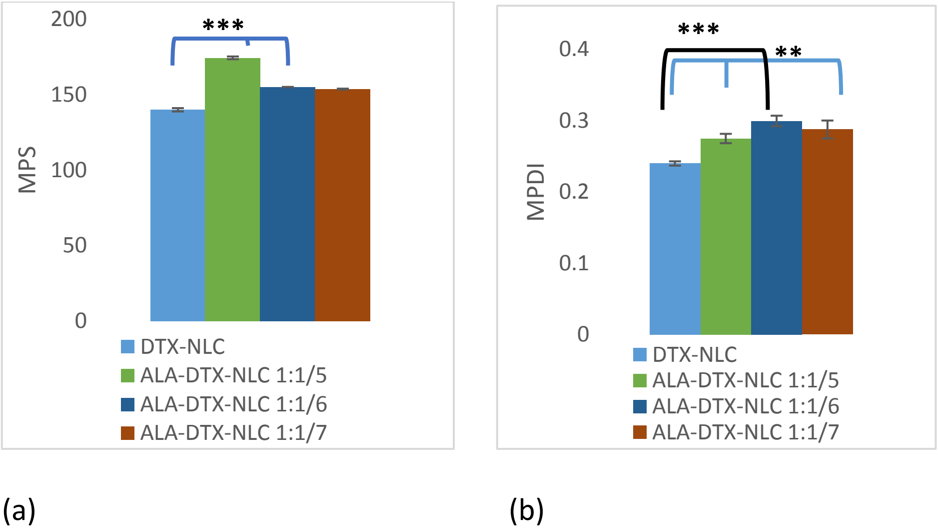

(a) (b)

Figure 3.32 DTX-NLCs compared to conjugation with ALA when different ratios were used to form ALA-DTX-NLCs (a) effect on PS, (b) effect on PDI. Data are mean ± SD, N=3,* P < 0.05, ** P < 0.001 and *** P < 0.000 refers to significant difference in PS and PDI for DTX-NLC when compared to all ALA-DTX-NLCs formulation in all examined ratios, except 1:1/7 ALA ratio when there was no significant difference in PS when compared to DTX-NLC pre-conjugation.

The ALA 1:1/6 ratio (FAG: ALA) was selected as this formulation has a high ligand density with minimal increase in PS (Figure 3.32 a). The surface functionalisation of DTX-NLC with ALA showed a significant reduction of charge at the particle surface due to the presence of hydrophobic ALA on the surface of DTX-NLC (Figure 3.33). The 1:1/6 ratio (FAG: ALA) formulation was taken up for detailed characterisation due to reasonably low PS and particles distribution (Figure 3.34). Additionally, to evaluate the effect of different ratios of ALA on glioblastoma cell lines, 1:1/5 and 1:1/6 ratios, (FAG: ALA) were examined for their proliferation impact on glioblastoma cells (Chapter Four, section 4.5.2.2.2).

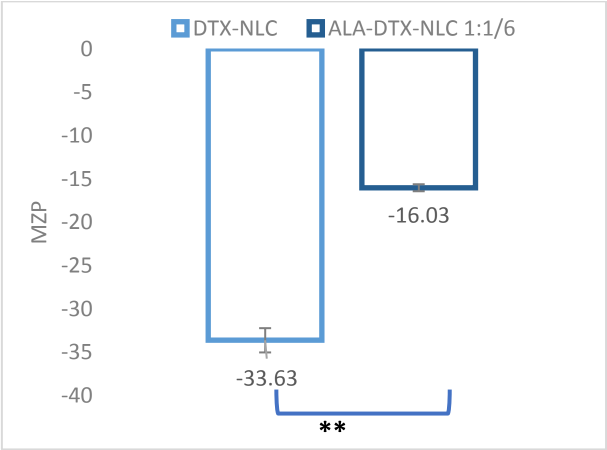

Figure 3.33 ZP of DTX-NLCs compared to ZP of ALA-DTX-NLCs when ALA 1:1/6 ratio was used to form ALA-DTX-NLC. Data are mean ± SD, N=3,** P < 0.001 refers to the significant difference in ZP for DTX-NLC when compared to ZP of ALA-DTX-NLCs formulation when 1:1/6 ALA ratio was examined.

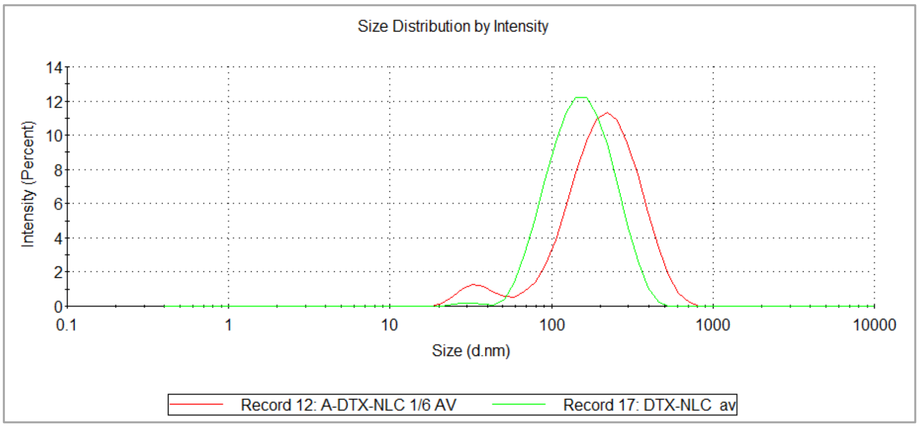

Figure 3.34 Size distribution data showing DTX-NLC and compared to ALA-DTX-NLC when 1:1/6 ALA ratios were used, and their effect on PS and PDI.

3.5.6.2.1. Functionalisation of DTX-NLCs with ALA in the presence of antioxidant

To evaluate the effect of the presence of antioxidants in DTX-NLC on PS and PDI Vit E and AP were used during DTX-NLC fabrication, then DTX-NLC were conjugated with ALA. Different ratios of ALA were examined (1:1/4, 1:1/5, 1:1/6 and 1:1/7) to produce ALA-DTX-NLCs (Figure 3.35). A significant increase was obtained in both PS and PDI when DTX-NLC (prepared with Vit E and AP) compared to ALA-DTX-NLC formulation when different ALA ratios were conjugated (Figure 3.36 a and b). These data showed the impact of antioxidants presents on both PS and PDI, further studies were vital to evaluate the effect of the presence of antioxidants on the glioblastoma cells, two ratios 1:1/5 and 1:1/6 were chosen for proliferation test with glioblastoma cells (Chapter Four, section 4.5.2.2.1). Similar to GLA, ALA is prone to oxidation, so the functionalisation of DTX-NLC with ALA was carried out completely under nitrogen environment when no antioxidants were used.

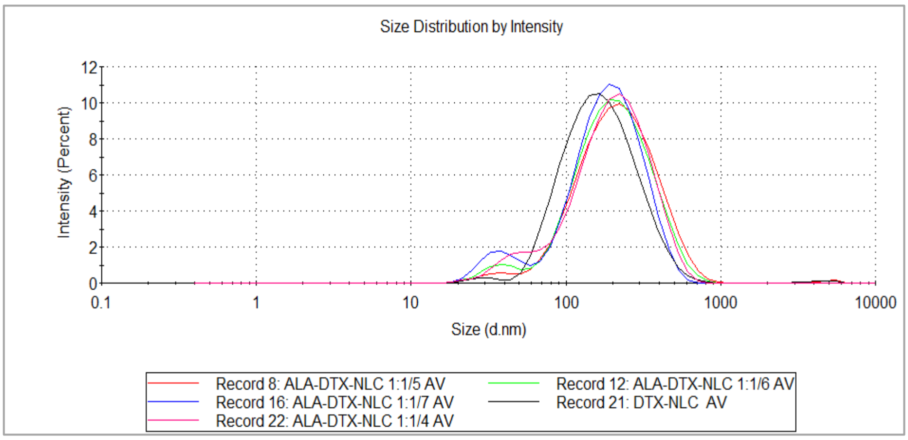

Figure 3.35 Particle Size distribution data showing DTX-NLC prepared with Vit E and AP and compared to ALA-DTX-NLCs when different ratios of ALA were used 1:1/4, 1:1/5 and 1:1/6 ratios DTX-NLC compared with 1:1/7 ALA ratio, and their effect on PS and PDI.

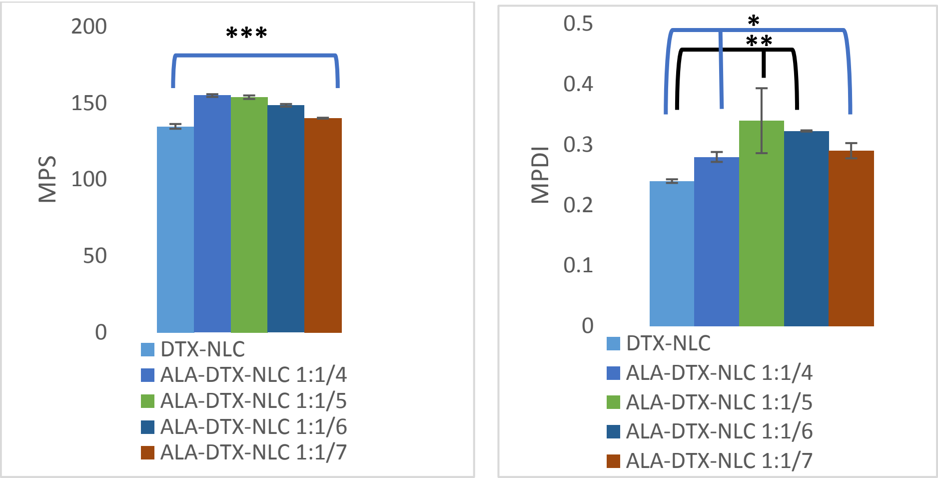

(a) (b)

Figure 3.36 DTX-NLCs prepared with Vit E and AP compared to conjugation with ALA when different ratios (1:1/4, 1:1/5, 1:1/6 and 1:1/7) were used to form ALA-DTX-NLCs (a) effect on PS, (b) effect on PDI. Data are mean ± SD, N =3,* P < 0.05, ** P < 0.001 and *** P < 0.000 refers to the significant difference in PS and PDI for DTX-NLC when compared to all ALA-DTX-NLCs formulation in all examined ratios.

3.5.7. Functionalisation of DTX-NLCs with SA43-aptamer

SA43 is a novel selective aptamer. To the best of our knowledge, there are no previous reports in the literature of conjugation SA43-aptamer with NPs. SA43 was conjugated to DTX-NLC to improve its selectivity towards glioblastoma cells. The FAG for DTX-NLC was 7.04 ±0.18 µmol/ml prior to conjugation with SA43. Five ratios of FAG: SA43 were assessed (1:1/8, 1:1/12, 1:1/23, 1:1/35, and 1:1/70) respectively for preparation of SA43-DTX-NLC. Significant effects on PS, PDI, and ZP were obtained when DTX-NLC was compared to SA43-DTX-NLC formulations (Figure 3.37 a, b, and 3.39). Moreover, the data showed a uniform distribution with PDI ranging from 0.23-0.27 in all developed SA43-DTX-NLCs (Figure 3.38 a). The FAG: SA43 1:1/8 ratio was chosen due to uniform distribution of the SA43-DTX-NLC and PS < 93 nm, and high ligand density (Figure 3.38 b). These findings were within the PS range of previous literature for Anti-PSMA aptamer that was reported by Chen *et al.,* (2016). Notably, ZP of surface modified NPs with aptamers have a negative surface charge > -32 mV, as it was anticipated due to aptamers negative charge. So successful modification of NPs with the aptamer was indicated using the PS and ZP as reported by previous researchers Modrejewski *et al.,* (2016).

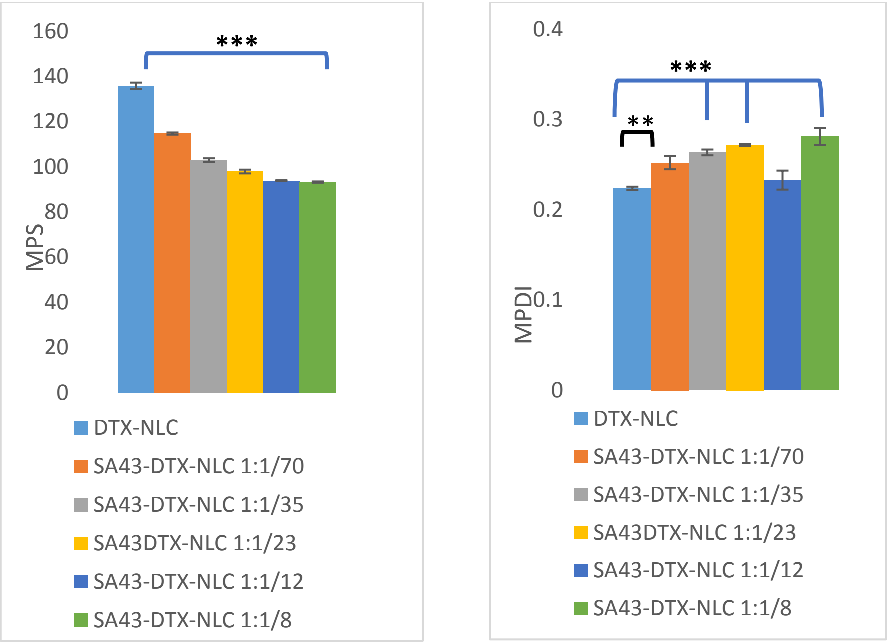

(a) (b)

Figure 3.37 DTX-NLCs compared to conjugation with SA43 when different ratios (1:1/8, 1:1/12, 1:1/23, 1:1/35, and 1:1/70) were used to form SA43-DTX-NLCs (a) effect on PS, (b) effect on PDI. Data are mean ± SD, N=3,** P < 0.001 and *** P < 0.000 refers to the significant difference in PS and PDI for DTX-NLC when compared to all SA43-DTX-NLCs formulation in all examined ratios. Except there was no significant difference in the PDI when 1:1/12 SA43 used to prepare SA43-DTX-NLC and compared with DTX-NLC.

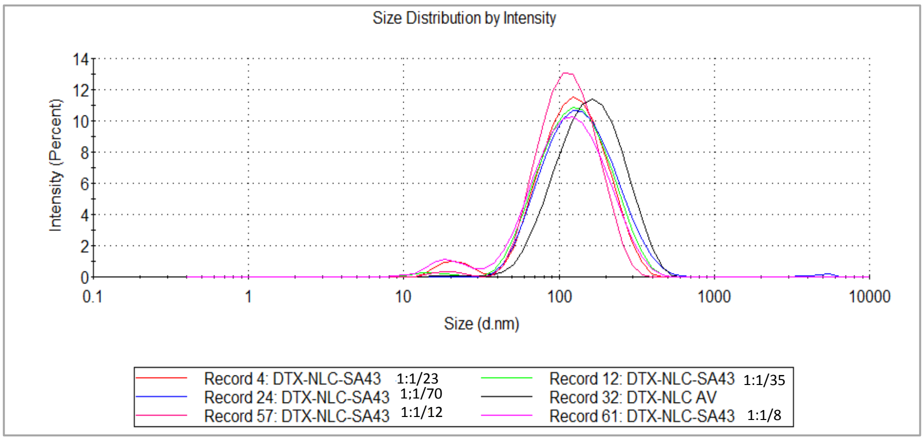

(a)

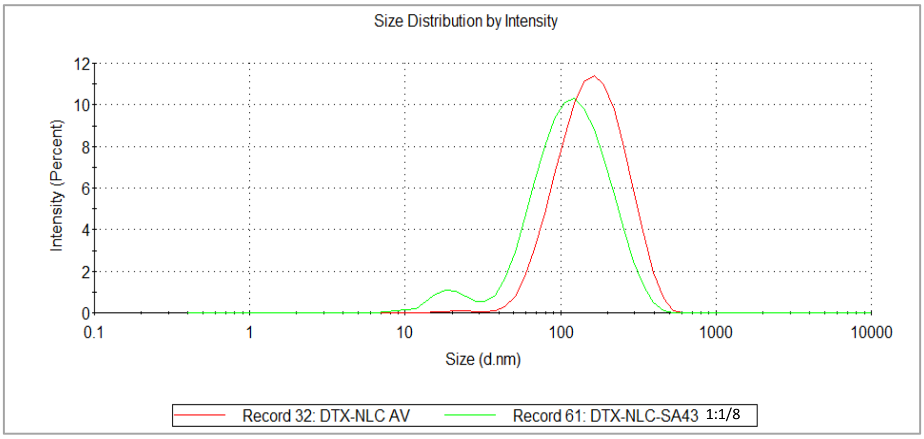

(b)

Figure 3.38 Size distribution data showing DTX-NLC and compared to SA43-DTX-NLCs when (a) (1:1/8, 1:1/12, 1:1/23, 1:1/35, and 1:1/70) ratios of SA43 were used, (b) the ration of 1:1/8 of SA43 was chosen. Their effect on PS and PDI were demonstrated in comparison with DTX-NLC pre-conjugation.

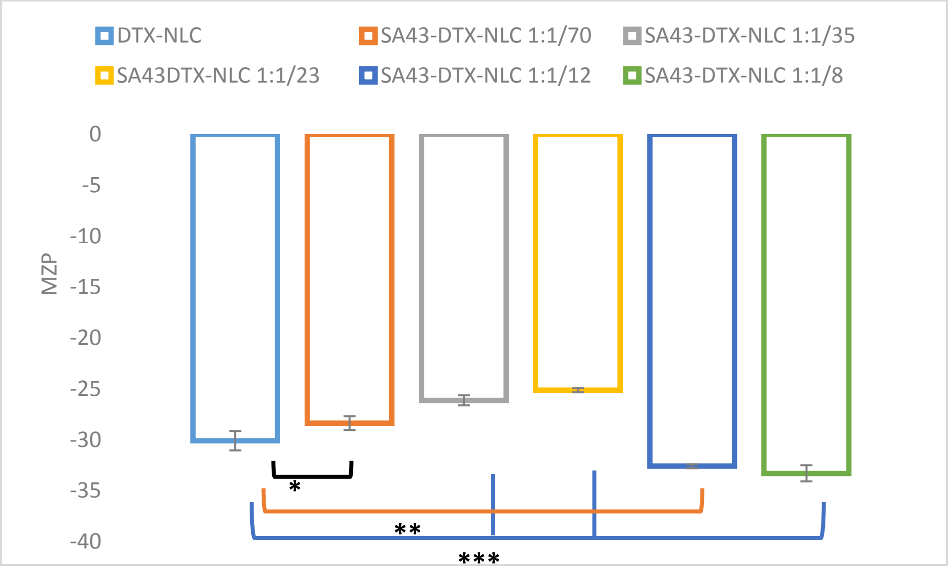

Figure 3.39 DTX-NLCs compared to conjugation with SA43 when different ratios (1:1/8, 1:1/12, 1:1/23, 1:1/35, and 1:1/70) were used to form SA43-DTX-NLCs and their effect on ZP. Data are mean ± SD, N =3, *P < 0.05, ** P < 0.001 and *** P < 0.000 refers to the significant difference in ZP for DTX-NLC when compared to all SA43-DTX-NLCs formulation in all examined ratios.

3.5.8. Conjugation efficiency

As described in section 3.4.4, and explained in the schematic diagram (figure 3.5) the FAG was calculated for all formulation pre and post conjugation with GLA, ALA and SA43 ligands. The TNBS concentration was calculated by generating a calibration for TNBS (Figure 3.40) as described in section 3.4.4, and equation 3.12 was used to calculate the unreacted TNBS and then equation 3.1 was used to obtain the reacted TNBS which correlates to FAG that is available on DTX-NLCs formulation pre and post conjugation with ligands (Table 3.16).

$Y=1.1307x - 0.1366$ (Equation 3.12)

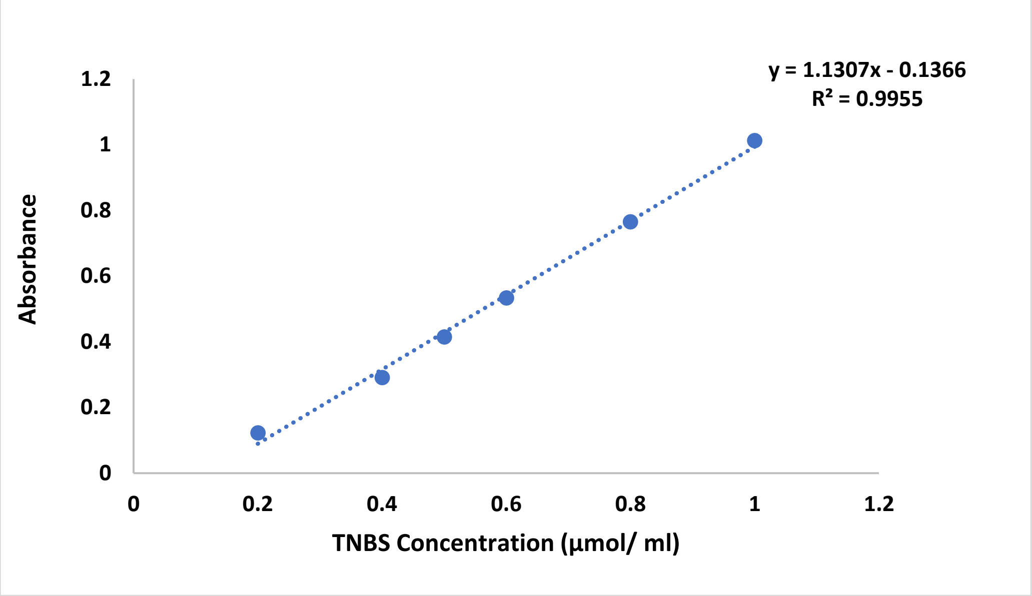

Figure 3.40 TNBS standard plot, prepared by using active known concentrations of TNBS and their blank samples. Data are mean ± SD, N=3.

Table 3.16 Ratios for different ligands used for surface modification of DTX-NLC, and FAG availability for pre and post conjugation.

Name of formulations	**The ratio of FAG: ligands**	**FAG concentration µmol/ml**
DTX-NLC	-	6.23± 0.69
GLA-DTX-NLC	1:1/5	3.38± 0.51
	1:1/6	4.44± 0.16
ALA-DTX-NLC	1:1/5	2.32± 0.33
	1:1/6	4.025± 0.27
SA43-DTX-NLC	1:1/8	2.93± 0.03
	1:1/12	4.04 ±0.76
	1:1/23	6.19± 1.07
	1:1/35	6.8± 0.32
	1:1/70	6.85± 0.59

Covalent bonding of ligands on the DTX-NLC surface decreased the free amino groups available, confirming the conjugation of ligands to DTX-NLCs. For all three ligands it was observed that as the ligand density was increased (as indicated by the higher FAG: ligands ratio), the FAG present on the surface of the DTX-NLC decreased.

For GLA-DTX-NLCs there was almost 10 folds increase in % conjugation when the FAG: GLA ratio increased from 1:1/7 to 1:1 (Figure 3.41 a). For ALA-DTX-NLCs similar pattern was found (Figure 3.41 b), while SA43 with low ligand density 1:1/70 showed only 2.6 % conjugation which could be increased to 50 % by increasing the SA43 ratio up to 1:1/8 (FAG: SA43, ratio) (Figure 3.41 c).

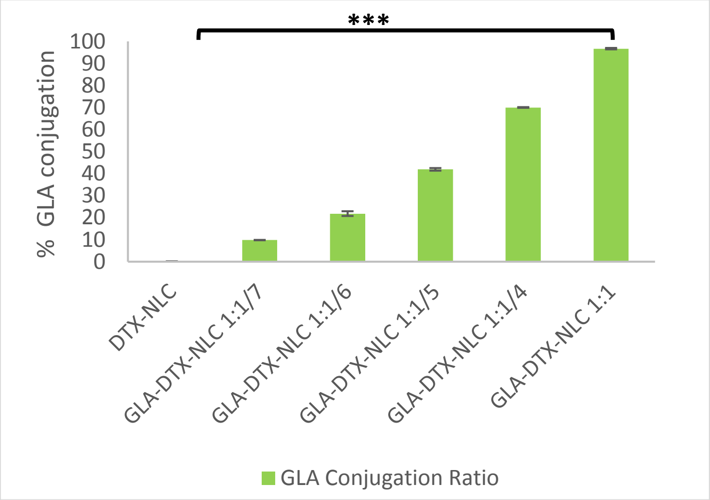

(a)

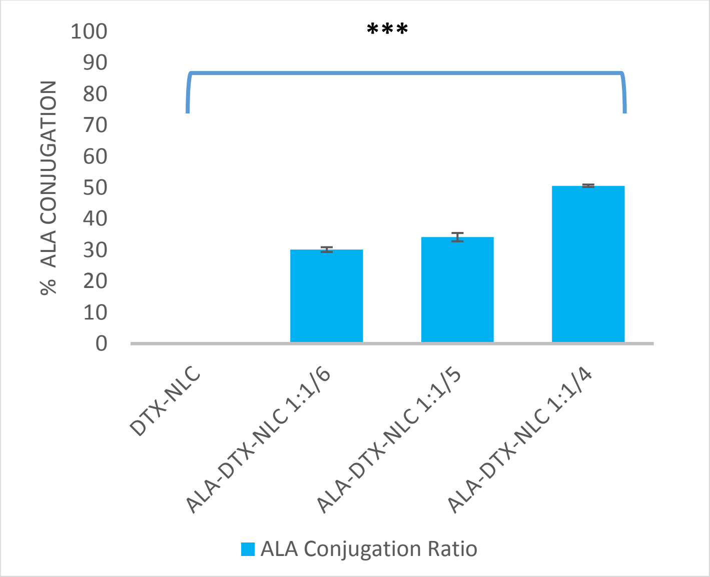

(b)

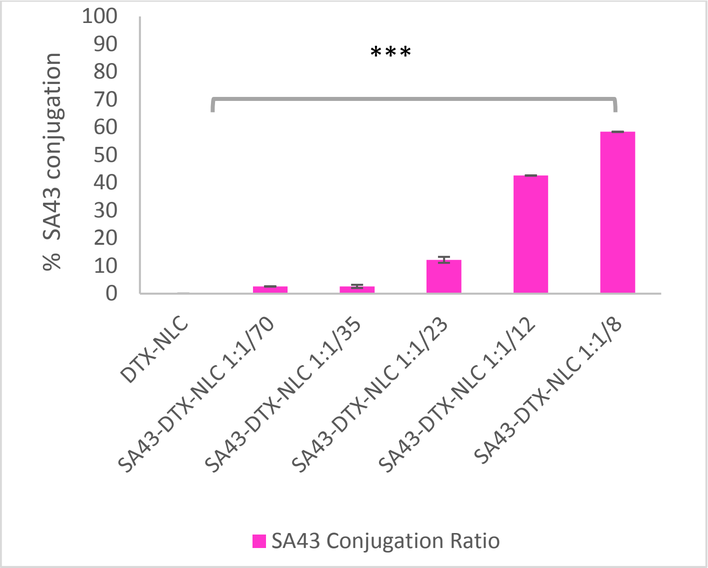

(c)

Figure 3.41 The % conjugation of DTX-NLCs with ligands (a) GLA-DTX-NLCs when different GLA ratios were evaluated, (b) ALA-DTX-NLCs when different ALA ratios were evaluated, (c) SA43LA-DTX-NLC when different SA43 ratios were evaluated. Data are mean ± SD, N=3 and *** P < 0.000 refers to the significant difference in % conjugation.

3.5.9. Freeze drying

The freeze-drying process for DTX-NLC was carried out in presence of two cryoprotective agents. Low percentage 1-10 % of sucrose did not provide sufficient cryoprotection and resulted in aggregation with a highly significant increase in both PS and PDI as compared to the DTX-NLC before freeze-drying (Figure 3.42 a and b); while for higher percentage of sucrose 15 and 20 %, the PS > 397 and wide range of particle distribution was observed. A combination of 1:1 ratio of trehalose and sucrose were used at concentration of 5% cryoprotective, that resulted in no significant difference in the PDI in comparison to the PDI of the DTX-NLC pre-freeze drying (Figure 3.42 c and d) even though a lower % of sucrose was used, that might be attributed to the presence of trehalose.

Further, trehalose was investigated in variable percentages 3, 5, 10, 15, and 20 %. Trehalose was investigated. 10% trehalose was found to be acceptable as a cryoprotectant for DTX-NLC as it resulted in the free-flowing stable product (Figure 3.42 e) which could be reconstituted to give a dispersion with uniform particle distribution PS 140.4 ± 2.25 and PDI 0.238 ± 0.023. It is worth noting that there was only 13 nm increase in PS as compared to original DTX-NLC before freeze drying. This is quite remarkable as previous reports have shown 50-100 nm increase in PS on reconstitution after freeze-drying when 10% trehalose was used as a cryoprotectant (Lozano *et al.,* 2013). Trehalose preserves Lipid NPs during freeze-drying as it forms an amorphous glass, additionally, physical isolation of NPs due to the glassy cryoprotectant reduces the freeze-drying stress on the NPs, thus, maintaining the PS during the freeze-drying (Beloqui *et al.,* 2016).

Additionally, the PDI of 3, 5, and 10 % trehalose exhibited no significant difference when compared to the PDI of DTX-NLC before freeze drying. Meanwhile, a higher % of trehalose 15 and 20 % displayed a significant increase in the PDI (Figure 3.42 c and d). It is worth mentioning that our findings showed better PS after freeze-drying when compared to previous literature by Li *et al.,* (2009) as SLNs suffer from challenges of high PS (245.3± 13.6 nm) after reconstitution. Thus 10% was chosen to freeze dry the DTX-NLCs.

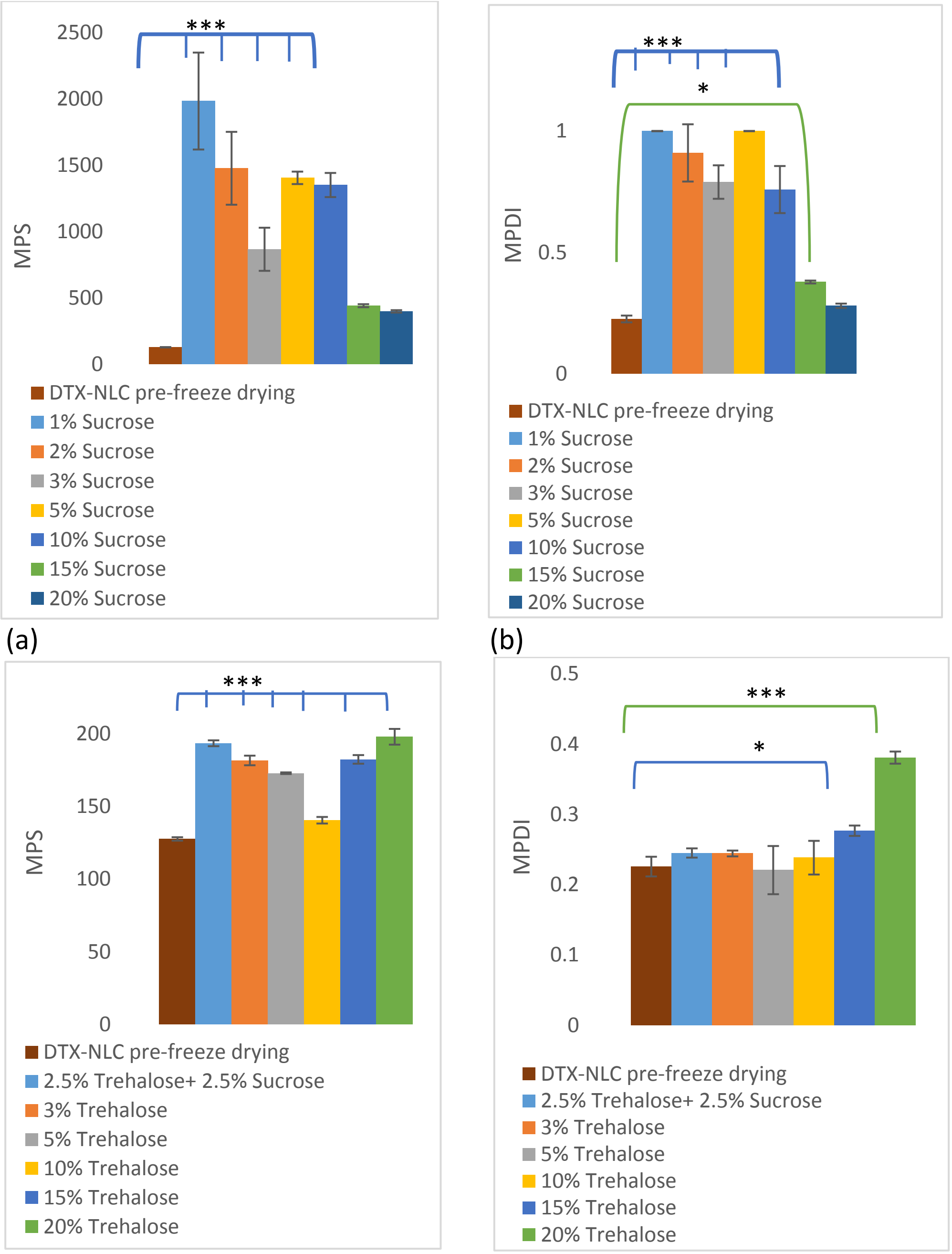

(a) (b)

(c) (d)

(e)

Figure 3.42 Effect of cryoprotective agents on DTX-NLCs (a) effect on PS when 1, 2, 3, 5, 10, 15, and 20 % of sucrose was used, (b) effect on PDI PS when 1, 2, 3, 5, 10, 15, and 20 % of sucrose was used, (c) effect on PS when 2.5% of sucrose and 2.5 % trehalose were used as combination, and 3, 5, 10, 15, and 20 % of trehalose was used, (d) effect on PDI when 2.5% of sucrose and 2.5 % trehalose were used as combination, and 3, 5, 10, 15, and 20 % of trehalose was used, (e) DTX-NLC picture showing DTX-NLC pre and post-freeze drying with 10% trehalose. Data are mean ± SD, N=3, * P < 0.05 and *** P < 0.000 refers to the significant difference when all examined percentages were compared with respect to PS and PDI of DTX-NLC pre-freeze drying.

3.5.10. Physicochemical characterisation

A detailed characterisation was carried out for final optimised B-NLC, DTX-NLC, GLA-DTX-NLC, ALA-DTX-NLC and SA43-DTX-NLC formulations.

3.5.10.1. Size, polydispersity index, zeta potential, %TD, %DL and % EE

Particles generally affect the biodistribution and pharmacokinetics of NPs (Mehnert and Mader, 2001; Xie *et al.,* 2010). It also has an impact on extravasation to the leaky vasculature of a tumour, and the BBB passage of the NPs is critically affected by PS apart from other factors (Modarres *et al.,* 2018; Patel *et al.,* 2013). It is also important that particles should be monodispersed with low PDI (Zhang *et al.,* 2009).

The B-NLC showed no significant difference in PS in comparison to PS of DTX-NLC, indicating that loading DTX into the NLCs had no impact on the PS, and only caused a slight increase in PDI (Table 3.17). DTX-NLC of average PS 136.8 ±2.165 nm was achieved with low PDI 0.231 ±0.0136 (Table 3.17) indicating a fairly uniform particle distribution. PDI values ranging from 0-0.5 are considered to be monodisperse and homogenous, and PDI values < 0.3 are accepted as a homogenous sample (Zhang *et al.,* 2009; Anton *et al.,* 2007). The low PS of DTX-NLC could be attributed to the inclusion of L.Ls and surfactants which reduce the interfacial tension and lower the particle size. Previous reports of DTX lipid NPs have shown PS ranging from 150-182, and a PDI < 0.2 (Naguib *et al.,* 2014).

Functionalisation of DTX-NLC with PUFAs (GLA and ALA) resulted in approximately 20 nm increase in PS (Table 3.17), confirming the interaction and conjugation of PUFAs with DTX-NLC. On the contrary, SA43-DTX-NLC PS was lower than DTX-NLC due to the SA43 -ve charge that might have resulted in stronger attraction to the shell and led to smaller PS, or simply due to the folding of the aptamer on the DTX-NLC surface as previously suggested by Modrejewski *et al.,* (2016).

The presence of surface charge on the NPs resulted in repulsion and avoid aggregation of NPs, ZP > ± 30 mV inputs good stability of the NPs (Caddeo *et al.,* 2008; Mukherjee *et al.,* 2008). The ZP for B-NLC and DTX-NLC were -34.4 ±0.742 mV and -32.4 ±0.967 mV, respectively, indicating that surface charge did not affect by the addition of DTX since DTX does not contain functional groups that can ionize in NLCs as in line with the previous report by Gao *et al.,* (2008). Conjugation of DTX-NLC with PUFAs resulted in significant reduction in ZP as demonstrated in table 3.17, confirming the conjugation of ligands on the surface of the DTX-NLCs. The capping of NPs with fatty acids resulted in a reduction of the surface charge (Jaimes-Aguirre *et al.,* 2017). A high %EE were achieved for all tested DTX-NLC and surface modified DTX-NLCs. Acceptable %TD and %DL were determined with DTX-NLC, while lower % TD were encountered for all surface modified DTX-NLC due to dilution of the DTX-NLC during the conjugation process.

Table 3.17 DTX-NLCs, B-NLCs, DTX-NLCs surface modified formulations mean particle size (PS), polydispersity index (PDI), zeta potential (ZP), %EE, %TD, and %DL.

Batches	**PS (nm)**	**PDI**	**ZP(mV)**	**%EE**	**%TD**	**%DL**
B-NLC	133.56 ±2.150	0.179 ±0.020	-34.4 ±0.742	-	-	-
DTX-NLC	136.8 ±2.165	0.231 ±0.0136	-32.4 ±0.967	99.13 ± 1.2	88.6 ±1.37	2.01 ±0.034
GLA-DTX-NLC	157.36 ± 1.53	0.271 ±0.004	-19.13 ±0.208	98.67 ±0.2	66.98 ±7.733	1.35 ±0.178
ALA-DTX-NLC	155 ±0.1	0.289 ±0.007	-16.03 ±1.205	99.21 ±0.42	62.415 ±4.70	1.257 ±0.089
SA43-DTX-NLC	93.25 ±0.277	0.281 ±0.009	-33.3 ±0.793	98.9 ±0.9	42.384 ±2.434	0.85 ±0.036

3.5.10.2. *In-vitro* drug release

The cumulative release profiles of DTX from different samples over 24 h at 37° C and the drug release from all tested formulations were calculated using a calibration curve generated through a validated HPLC method as explained in Chapter two (sections 2.4.2 and 2.5.2).

The release of DTX from DTX solution, DTX-NLCs and Taxotere, was achieved in a controlled pH close to the physiological environmental conditions by assessing all three samples in release media PBS, pH7.4 (Figure 3.43 a). All three tested samples suffered from delayed release in the buffer due to the absence of the sink condition. Therefore, DTX release from NLCs was assessed in 30% ethanol+70% PBS, at pH7.4 to achieve sink conditions (Zhang *et al.,* 2017). DTX release from DTX-NLC was faster than the release from GLA-DTX-NLC and ALA-DTX-NLC, due to more than 40% of DTX was released from DTX-NLC at 2 h presenting a biphasic profile with the initial fast burst release followed by a slow sustained release (Lozano *et al.,* 2013) that could be due to diffusion of drug (DTX) molecules on the surface of the DTX-NLCs as previously reported by Koopaei *et al.,* (2014). While in case of GLA-DTX-NLC and ALA-DTX-NLC their release pattern showed more than 12% of DTX released from each formulation under the same conditions followed by very slow release profile where more than 40 % was released at 24 h (Figure 3.43 b), demonstrating sustained release effect when DTX-NLC were surface modified with GLA and ALA, a sustained release effect is more favourable than faster drug release particularly for IV.administration. In addition, the slower DTX release when the NLCs were surface modified might be attributed to the higher PS of the formed GLA-DTX-NLC and ALA-DTX-NLC in comparison to PS of the bare DTX-NLC, and that might lead to increasing the distance between the surface and the lipid core of the NLCs as previously reported by Xu *et al.,* (2009).

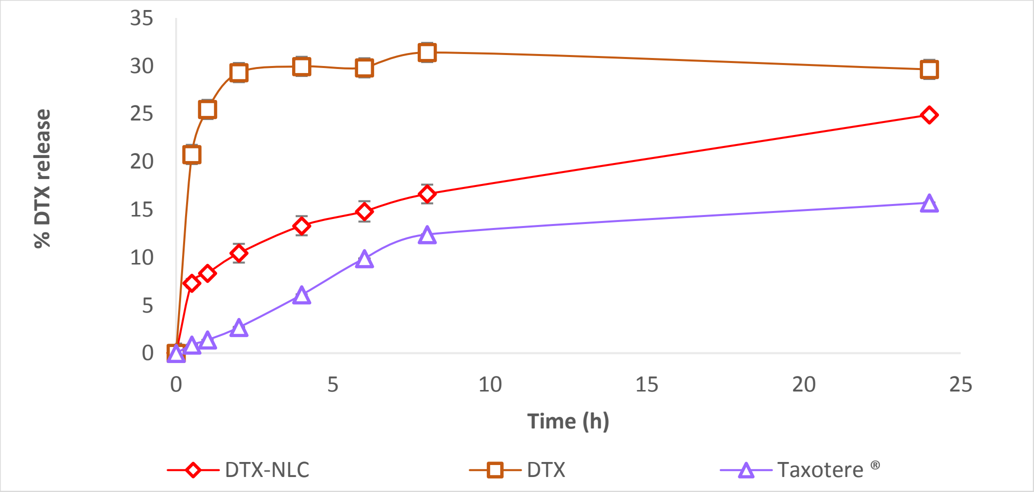

(a)

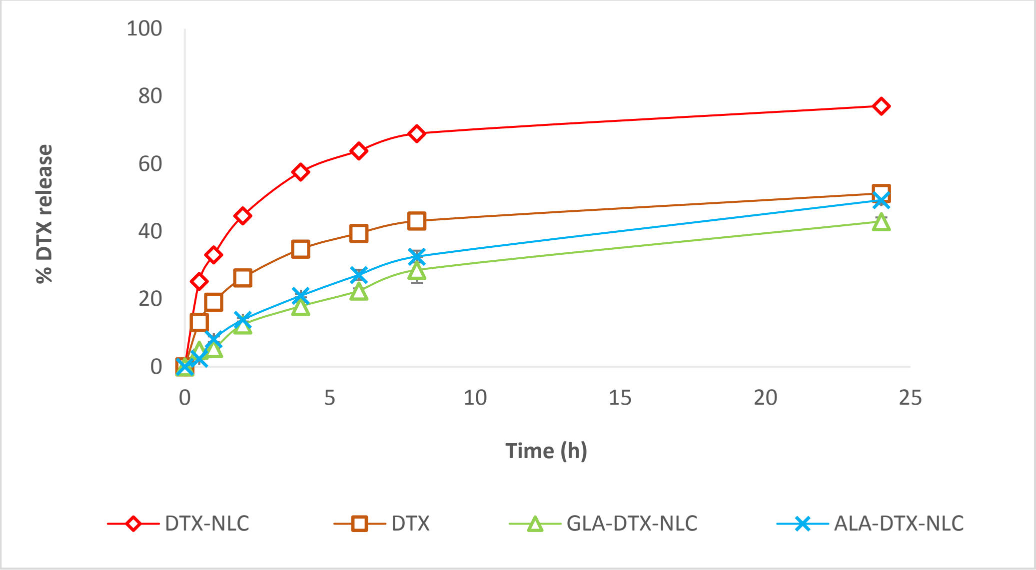

(b)

Figure 3.43 DTX release profile from NLCs over 24 h at 37° C (a) when 100 % PBS, (pH7.4) was used as release media to study the release of DTX from DTX, DTX-NLCs and Taxotere, (b) when 30% Ethanol+70% PBS, (pH7.4) was used as release media to study the release of DTX from DTX, DTX-NLCs, GLA-DTX-NLC, and ALA-DTX-NLC. Data are mean ± SD, N=3.

3.5.10.3. Scanning electron microscopy

SEM images for the freeze-dried DTX-NLC (Figure 3.44) illustrated spherically shaped particles and a PS >288 nm that might be attributed to the protection effected by trehalose as a cryo-protectant. Our finding showed DTX-NLC freeze-dried in nanometre range compared to previous results showing increased PS in micrometre range after freeze-drying (Doktorovova *et al.,* 2014).

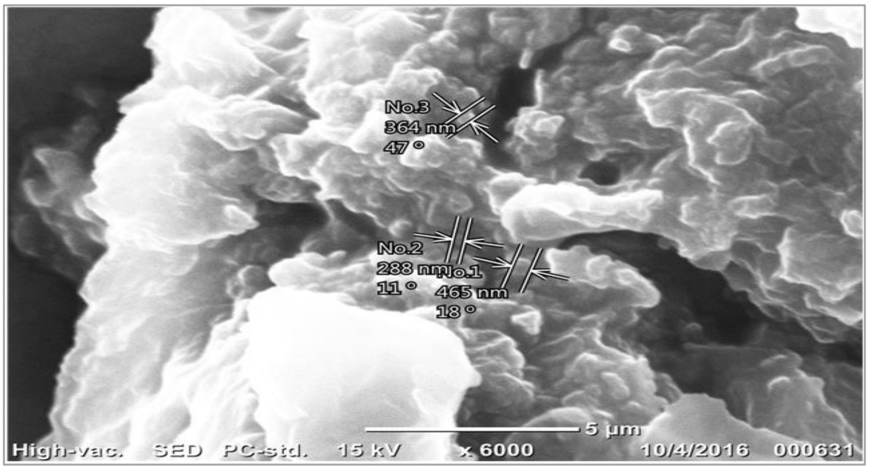

Figure 3.44 SEM images showing freeze dried DTX-NLC in different magnifications (a) X6000 magnifications, and (b) X17000 magnification with zooming mood.

3.5.10.4. X-ray diffractometer

The X-ray diffractometer (XRD) was used to investigate the crystalline structure of DTX and further confirm the status of DTX in NLCs formulation. Figure 3.45 shows the XRD pattern of all tested samples where the surfactants SC showed one peak at 2ϴ value of 14.36 and PH90 showed a high-intensity peak at 6.29° and medium intensity peaks at 9.5°, 12.8°, 14.4°, 16.1°, 17.7°, 19.3°, 20.2°, 21,09°, 22.2° and 23.05°. The lipid D114 demonstrated peaks of low-intensity at 35.06°, the medium intensity at 7.4°, 10.2°, 15.3°, 16.6°, 17.05°, 17.6° and very high-intensity peak at 19.3°, 22.5°, 24.06°, 24.10°, D114 obtained diffraction peaks were in line with Severino *et al.,* (2012). Moreover, DTX powdered sample showed usual peaks at 2ϴ values of 5.4°, 8.1°, 10.18°, 11.4°, 12.7°, 14.2° and 17.17° in line with previous reports by Fang *et al.,* (2014). In the physical mixture, the peaks at 2ϴ were at 7.4°, 16.7°, 17.3°, 17.9°, 19.4°, 23.29° and 24.14° which could be attributed to solid lipid D114. The DTX fingerprint peaks were absent from the physical mixture due to the low concentration of DTX used as compared to the D114. DTX-NLC diffraction pattern showed peaks appearing at 2ϴ of 7.8°, 15.05°, 15.68°,16.8°, 17.4°, 19.5°, and 24,2° attributed to D114 diffraction peaks, and 9.4°, 12.8°, 18.1°, 17.4°, 19.5° and 21.5° which could be attributed to PH90 diffraction peaks. The SC peak did not appear in the DTX-NLC due to its low concentration present in DTX-NLC. The absence of DTX characteristic peaks in the DTX-NLC formulation might suggest that DTX was in an amorphous state within the NLCs (Figure 3.45).

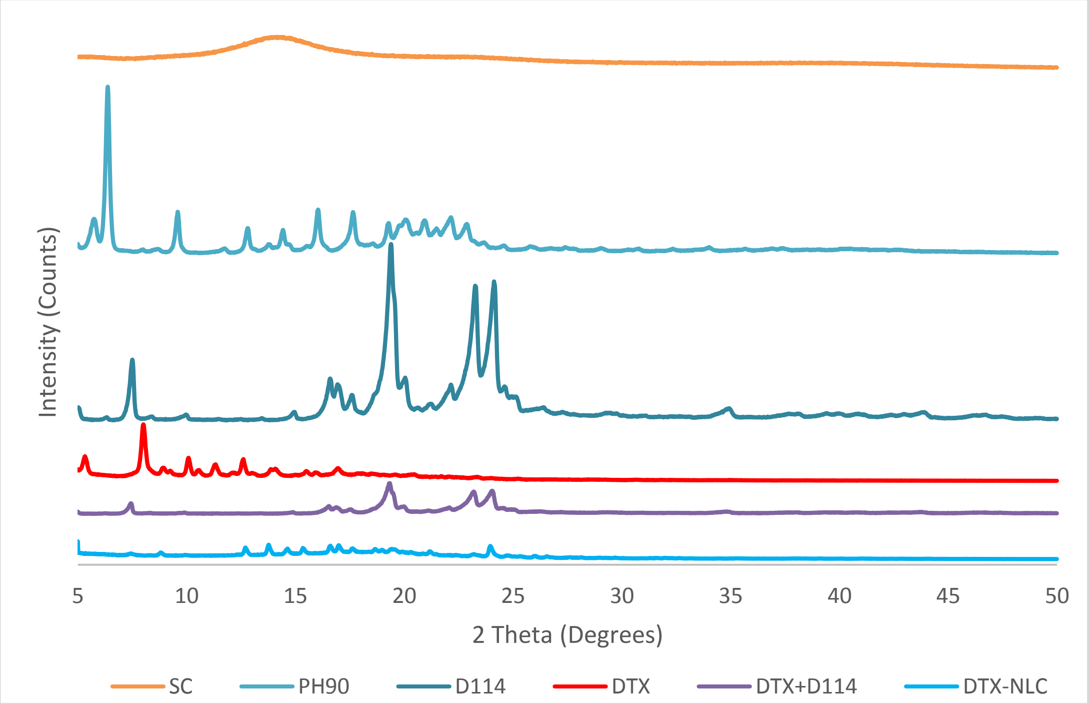

Figure 3.45 XRD structure of SC, PH90, D114, DTX, a physical mixture of DTX and D114, and DTX-NLC, expressed in 2ϴ°.

3.5.10.5. Thermogravimetric analysis

The TGA was performed for thermal stability analysis for DTX, D114, B-NLC, DTX-NLC, GLA-DTX-NLC, ALA-DTX-NLC and SA43-DTX-NLC. The TGA of DTX showed major degradation started at around 204°C with 6% weight loss, our data was in line with Kulhari *et al.,* (2014) findings, though mild degradation with approximately 2% loss was observed at initial temperature around 53°C, and at 110 °C around 3% loss was observed, revealing the importance of controlling the temperature during the processing of DTX-NLC (Figure 3.46). D114 is relatively stable lipid as shown in Figure 3.46 where a stable degradation pattern with 8% weight loss at 320° was notable. The B-NLC showed an early degradation at 204 °C, as compared to D114 degradation, that could be due to presence of L.Ls and surfactants apart from solid lipid (D114) in the B-NLC structure, followed by increase in degradation around 260 °C with 10% weight loss, while DTX-NLC showed higher degradation 15% loss at 204 °C in comparison to the B-NLC (8% lost) at 204 °C (Figure 3.46). The functionalised DTX-NLCs demonstrated an equal stability as compared to DTX-NLC, where ALA-DTX and SA43-DTX-NLC started degradation around 280 °C and almost 30% of weight loss, apart from GLA-DTX-NLC which indicated a faster degradation at temperature 84.8°C and almost 60% weight loss, that might be attributed to the high water content in this formulation or instability of the formulation during extensive heat (Hénon *et al.,* 1997; Won *et al.,* 2008) (Figure 3.46). Individual TGA thermographs for each sample in Appendix I.

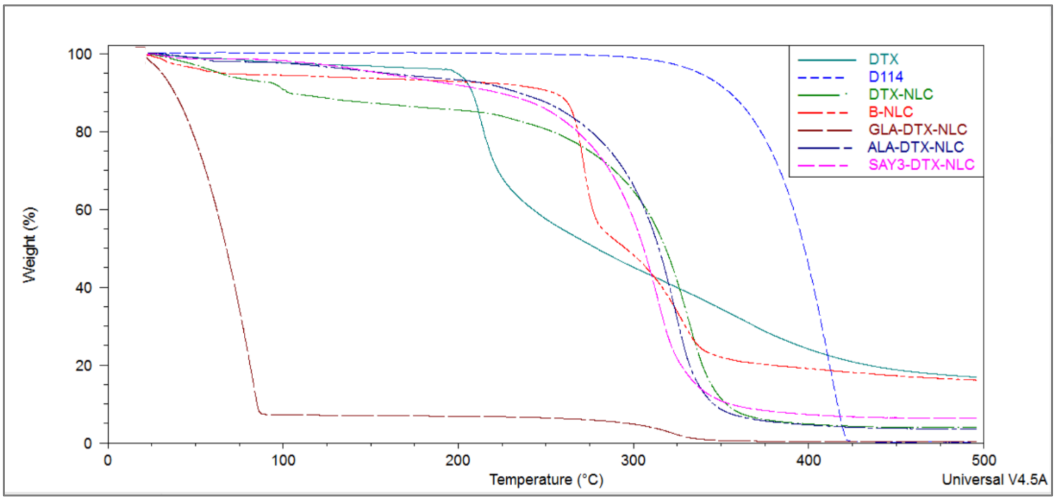

Figure 3.46 TGA thermographs using heat ranging from 25-500 °C for overlay of DTX, D114, DTX-NLC, B-NLC, GLA-DTX-NLC, ALA-DTX-NLC, and SA43-DTX-NLC degradation pattern.

3.5.10.6. Differential scanning calorimetry

To further investigate the physical state of D114, DTX in B-NLC, DTX-NLC, GLA-DTX-NLC, ALA-DTX-NLC, and SA43-DTX-NLC, DSC studies were performed. The D114 demonstrated a melting endothermic peak at 59.33 °C (Figure 3.47 a), and recrystallisation of lipid during the cooling cycle as shown by the exothermic peak detected at 28.57 °C (Figure 3.47 b) as demonstrated by (Naguib *et al.,* 2014). The melting endothermic peak for pure DTX was observed at 170.46 °C (Figure 3.47 a). This finding was in line with Singh *et al.,* (2015). Shifting of D114 was observed in the B-NLC, which exhibited a characteristic lipid D114 melting peak at 55.61 °C in the first heat cycle (Figure 3.47 a), that might be due to incorporation of L.Ls in addition to the D114 (impurity effect), additionally, B-NLC exhibited lipids recrystallises during cooling as evident from the exothermic peaks detected at 25.18 °C (Figure 3.47 b). DTX-NLC showed melting peak at 54.42° C attributed to D114, however, no DTX peaks were observed at 170°C demonstrated that DTX in the NLC formulations might be in an amorphous state or in the solid-solution state after encapsulation into the NLCs (Figure 3.47 a), and recrystallisation during the cooling cycle at 25.4 °C (Figure 3.47 b). A similar finding has been obtained by Tao *et al.*, (2013) and Naguib *et al.,* (2014).

Surface modified formulations GLA-DTX-NLC, ALA-DTX-NLC, and SA43-DTX-NLC showed melting peaks at 55.37, 56.08 and 55.34 °C characteristic of D114. It is worth to mention that the intensity of the lipid melting endothermic peaks for surface modified NLCs were very low in comparison to B-NLC and DTX-NLC peaks that might be attributed to fact that the surface modified NLCs have been diluted during the coupling process. These formulations also showed recrystallisation of lipid during the cooling cycle as evident by peaks detected at 27.84, 27.61 and 27.39 °C for GLA-DTX-NLC, ALA-DTX-NLC, and SA43-DTX-NLC, respectively (Figure 3.47 b).

Similarly, to DTX-NLC thermal behaviour, DTX melting endotherm was absent in the surface-modified formulations suggesting the amorphous nature of drug in the formulations. D114, B-NLC, DTX-NLC, GLA-DTX-NLC, ALA-DTX-NLC, and SA43-DTX-NLC were demonstrating melting endothermic peaks at 59.04, 55.05, 55.34, 55.05, 55.91, and 54.20 °C, respectively as observed in Figure 3.47 c, for the second heat cycle.

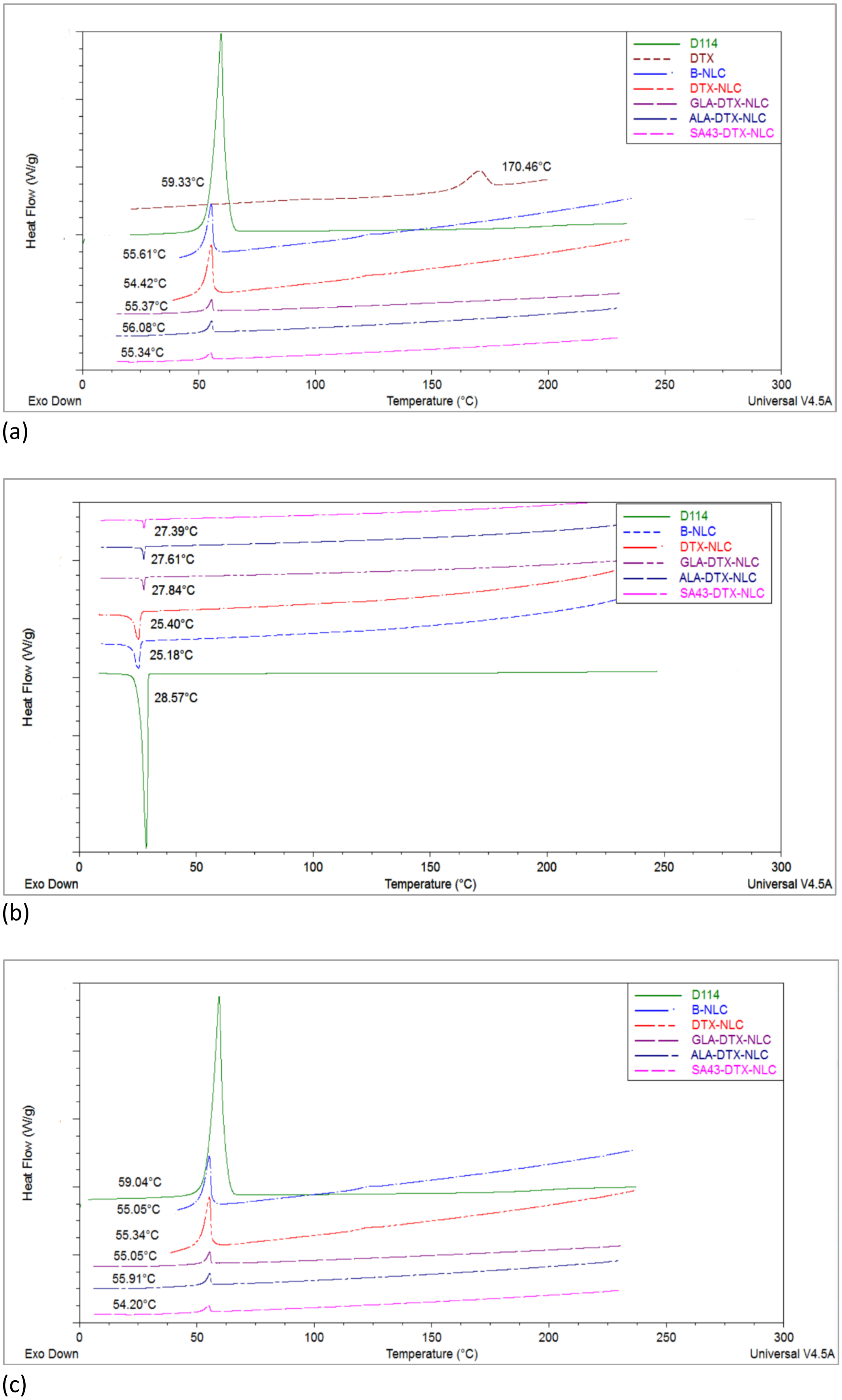

Figure 3.47 DSC thermograph using method heat/cool/heat, for D114, DTX, DTX-NLC, B-NLC, GLA-DTX-NLC, ALA-DTX-NLC, and SA43-DTX-NLC (a) first heat phase, (b) cool phase (c) second heat phase.

3.5.10.7. Fourier-transform infrared spectroscopy

Fourier-transform infrared spectroscopy (FTIR) involves energy transferred to molecules by absorption of IR radiation and this result in covalent bond stretching, twisting, and bending in the stationary phase states of the molecule. Each molecule has its own characteristic IR spectra, thus changes in structure can be detected by IR (Cantor and Schimmel, 1980). FTIR spectroscopy of DTX, B-NLC, DTX-NLC and surface modified DTX-NLCs was carried out and the vibrational band's assignments are summarised in tables 3.18, 3.19, 3.20 and 3.21. All band assessments were confirmed with previous literature (Shabani *et al.,* 2016; Fang *et al.,* 2014; Rusu and Rusu 2010; Venishetty *et al.,* 2013; Singh *et al.,* 2015; Seçilmi and Bardakç, 2011; Mushtaq *et al.,* 2014; Bright *et al.,* 2010; Tugarova *et al.,* 2018).

DTX, DTX-NLC, and B-NLC

DTX demonstrated the characteristic vibrational band assignments, which are in conformation with previous reports (Shabani *et al.,* 2016; Fang *et al.,* 2014) as shown in Figure 3.48. DTX-NLC showed the characteristic peaks of DTX positions at (3688, 1700, 1457 and 1368) cm^{-1} that correlates to OH stretching, C=O stretching, N-H diffraction and C-H bending respectively, indicating the presence of DTX within the DTX-NLC (Table 3.18 and Figure 3.48), however, some DTX peaks are absent due to the interaction between DTX and DTX-NLC.

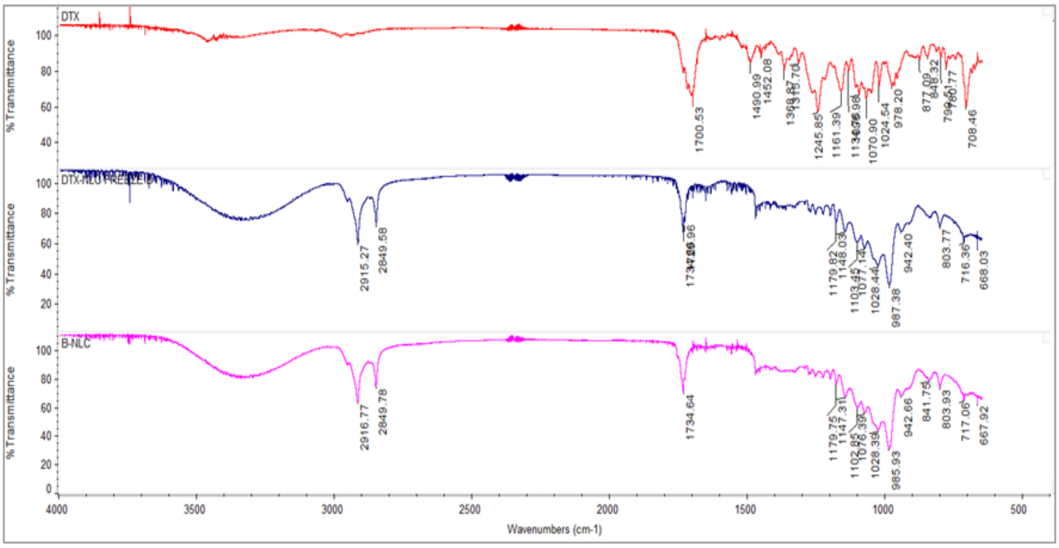

Figure 3.48 FTIR spectrum overlay of DTX, DTX-NLC and B-NLC, and their band assignments.

The DTX-NLC had all the characteristic peaks that were present in the B-NLC (Figure 3.48 and Table 3.18), which could be due to the presence of same excipients used in the formulations apart from the drug, which includes (solid lipid, liquid lipids, and surfactants). A detailed FTIR spectrum in Appendix I.

Table 3.18 FTIR Vibrational band assignment for DTX, DTX-NLC, and B-NLCs.

FTIR frequency (cm^{-1})	**Vibrational band assignment**	**DTX**	**DTX-NLC**	**B-NLC**
3688	O-H stretching	√	√	
3459	N-H/ O-H stretching	√		
3326	N-H stretching		√	√ shift to 3351
2979	C-H stretching	√		
2915 and 2849	CH$_2$ asymmetrical and symmetrical stretching		√	√
1734	C=O stretching		√	√
1718	C=O stretching	√		
1700	C=O stretching	√	√	
1490	C=C stretching	√		
1472	CH$_2$ / CH$_3$ asymmetrical stretching		√	√
1457	N-H, CH$_3$, O-H diffraction	√	√	
1452	C-H bending	√		
1368	C-H bending/C-C stretching	√	√	
1273	C-O stretching		√	√
1254	C-O stretching		√	√
1245	C-O stretching	√		
1228	C-O stretching		√	√
1201	C-O stretching		√	√
1179	S=O stretching		√	√
1161	C-O stretching	√		
1148	S=O stretching		√	√
1103	C-N stretching		√	√
1077	CH$_2$ twisting/ aromatic ring stretching		√	√
1070	C-O stretching/ Aromatic ring stretch/CH$_2$ twisting	√		
1028	C-N /C-O stretching		√	√
1024	C-O stretching	√		
987	C=C bending		√	√
978	C-S stretching	√		
942	C-H twisting		√	√
848	C-H out of plane bending	√		
803	C=C bending		√	√
780	C-H bending	√		
716	C-H bending		√	√
708	C-H out of plane bending	√		
668	C=C bending/ Aromatic ring stretch		√	√

DTX-NLC, GLA, and GLA-DTX-NLC

GLA-DTX-NLC retained all characteristic peaks of DTX-NLC, GLA-DTX-NLC also showed characteristic peaks of GLA at (1772, 1775, 1506, 1419, and 917) cm^{-1} that were related to (C=O, C=O, N-H bending, CH_2 symmetrical, and C=C), respectively, which were absent in the DTX-NLC. Additionally, GLA-DTX-NLC showed new peaks at (2991, 1085, 1044 and 882) cm^{-1} that were characterisation for (N-H stretching, C-O stretching, Aromatic deformation, C-O-C and C-H bending) respectively, which were not seen in spectrums of either in GLA or DTX-NLC, suggestive of GLA interaction with DTX-NLC, and indicating the GLA functionalisation with DTX-NLC. However, the characteristic peaks of amide bond formation at C=O at 1653 cm^{-1} and N-H bend at 1558 cm^{-1} (Rusu and Rusu 2010; Venishetty *et al.,* 2013; Singh *et al.,* 2015) were masked due to overlapping with the DTX-NLC carbonyl group (Figure 3.49 and Table 3.19). A detailed FTIR spectrum is given in Appendix I.

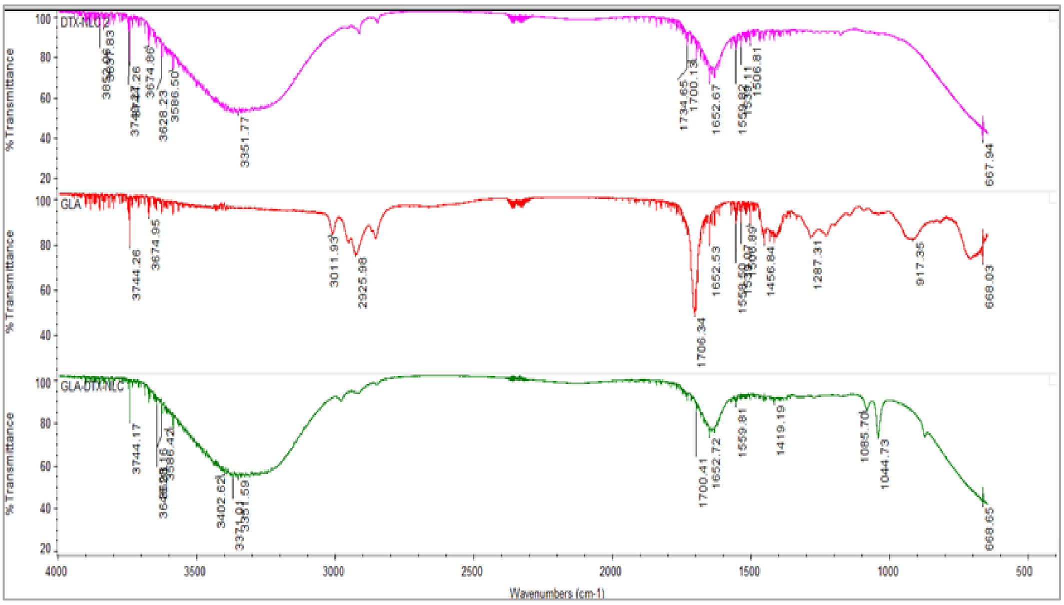

Figure 3.49 FTIR spectrum overlay of DTX-NLC, GLA and GLA-DTX-NLC, and their band assignments.

Table 3.19 FTIR Vibrational band assignment for DTX-NLC, GLA and GLA-DTX-NLC.

FTIR frequency (cm^{-1})	**Vibrational band assignment**	**DTX-NLC**	**GLA**	**GLA-DTX-NLC**
3011	C-H stretching		√	
2991	N-H stretching			√
2915	CH_2 asymmetrical and symmetrical stretching	√		√
2849	CH_2 asymmetrical and symmetrical stretching	√	√	√
1772	C=O stretching		√	√
1751	C=O stretching		√	√
1734	C=O stretching	√		√
1700	C=O stretching	√		
1653	C=C/ C=O amide I stretch	√		√
1558	N-H bending	√		√
1506	N-H bending / N-O stretching		√	√
1455	N-H, CH_3, OH detraction	√		√
1419	CH_2 symmetrical scissoring		√	√
1085	C-O stretching			√
1044	Aromatic ring deformation/C-O-C			√
917	C=C bending		√	√
882	C-H bending			√
711	C=C bending		√	

DTX-NLC, ALA, and ALA-DTX-NLC

ALA-DTX-NLC also showed the formation of new peaks at 2991, 1085, 1044 and 882) cm^{-1} that were characteristics for N-H stretching, C-O stretching, Aromatic deformation, C-O-C and C-H bending respectively, which were absent in both ALA and DTX-NLC, indicating the interaction and conjugation of ALA to the DTX-NLC. Additionally, some of the ALA peaks were present in ALA-DTX-NLC, to further suggest the confirmation of the functionalisation of DTX-NLC with ALA. Similar observation to GLA-DTX-NLC, the ALA-DTX-NLC characteristic amide bond formation at C=O at 1653 cm^{-1} and N-H bend at 1558 cm^{-1} (Rusu and Rusu 2010; Venishetty *et al.,* 2013; Singh *et al.,* 2015; Seçilmi and Bardakç, 2011) were masked due to overlapping with the DTX-NLC carbonyl group (Figure 3.50 and Table 3.20). A detailed FTIR spectrum in Appendix I.

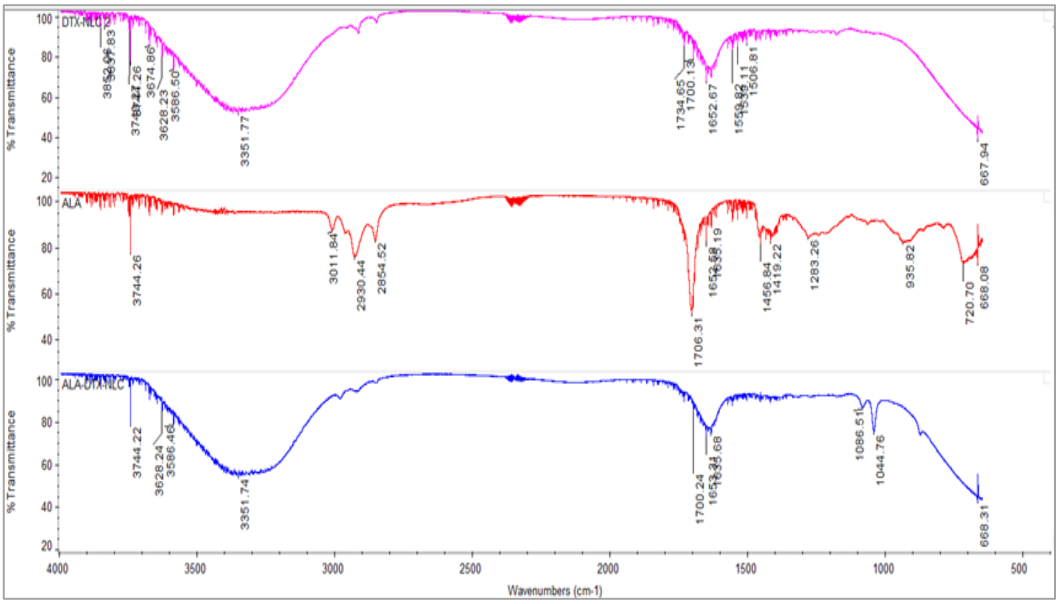

Figure 3.50 FTIR spectrum overlay of DTX-NLC, ALA and ALA-DTX-NLC, and their band assignments.

Table 3.20 FTIR Vibrational band assignments for DTX-NLC, ALA and ALA-DTX-NLC.

FTIR frequency (cm⁻¹)	**Vibrational band assignment**	**DTX-NLC**	**ALA**	**ALA-DTX-NLC**
3011	C-H stretching		√	
2991	N-H stretching			√
2915	CH_2 asymmetrical and symmetrical stretching	√		√
2849	CH_2 asymmetrical and symmetrical stretching	√	√	√
1734	C=O stretching	√	√	√
1700	C=O stretching	√	√	√
1653	C=C stretching	√	√	√
1635	Cis C=C /C=O amide I stretch		√	√
1558	N-H bending	√	√	√
1455	N-H, CH_3, OH detraction	√	√	√
1419	CH_2 symmetrical scissoring		√	√
1085	C-O stretching			√
1044	Aromatic ring deformation/ CO-O-CO stretching			√
935	O-H out of the plane of the carbonyl group		√	
917	C=C bending			
882	C-H bending			√

DTX-NLC, SA43 and SA43-DTX-NLC

As seen in figure 3. 51 and band assignment given in table 3.21, the appearance of two bands SA43-DTX-NLC at 1772 cm^{-1} (C=O stretching) and 1505 cm^{-1} (N-H bending) might provide a preliminary proof for the amide bond formation. Also, it was noted some mutual peaks between SA43-DTX-NLC and the DTX-NLC demonstrating the interaction of SA43-aptamer with the DTX-NLC. A detailed FTIR spectrum in Appendix I.

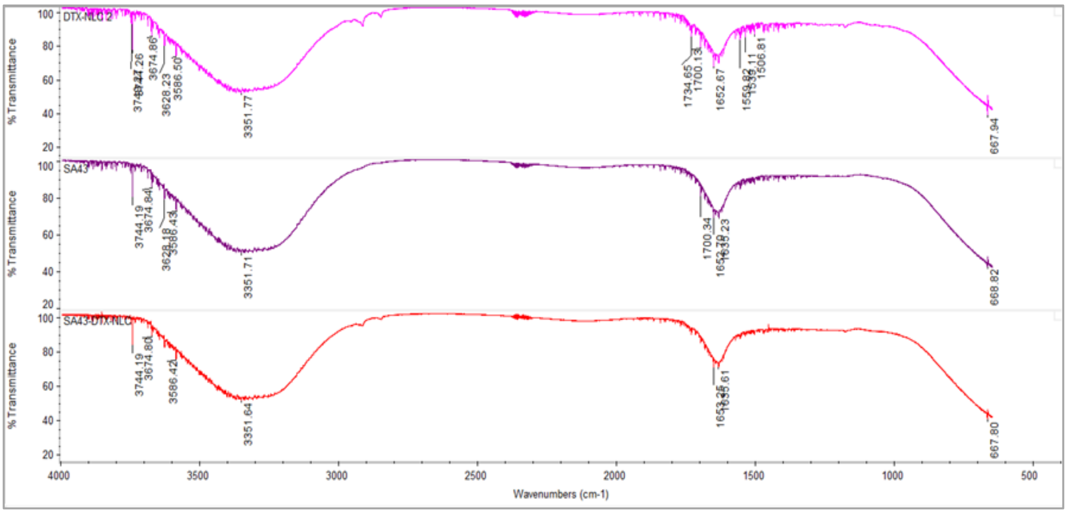

Figure 3.51 FTIR spectrum overlay of DTX-NLC, SA43 and SA43-DTX-NLC, and their band assignments.

Table 3.21 FTIR Vibrational band assignments for DTX-NLC, SA43 and SA43-DTX-NLC.

FTIR frequency (cm^{-1})	**Vibrational band assignment**	**DTX-NLC**	**SA43**	**SA43-DTX-NLC**
2915	CH_2 asymmetrical and symmetrical stretching	√		√
2849	CH_2 asymmetrical and symmetrical stretching	√		√
1772	C=O stretching		√	√
1734	C=O stretching	√	√	√
1700	C=O stretching	√	√	√
1684	C=O stretching, I or III amide	√	√	√
1653	Cis C=C stretching	√	√	√
1635	C=C/ C=O stretching	√	√	√
1558	N-H bending	√	√	√
1505	N-H bending		√	√
1455	N-H, CH_3, OH detraction	√		
1181	C-H bending	√		√

3.5.10.8. Raman spectroscopy

Raman spectroscopy is a highly informative nondestructive method of analysis to determine the structural and compositional properties of NPs (Gopal *et al.,* 2016). In NPs the crystalline Raman peak position is usually downshifted and asymmetrically broadened with respect to bulk material (Meilakhs and Koniakhin, 2017). All Raman vibrational band assignments summarised in tables 3.22, 3.23 were compared with previous published literature (Torres *et al.,* 2007; Ansari *et al.,* 2018; Yamini *et al.,* 2014; Lo *et al.,* 2009; Schaffer *et al.,* 1991) and with the company data analysis handbook for Raman band assignment positions by Horiba (2017).

DTX and DTX-NLC

Table 3.22 showed band shifting at (1783, 1658, 1626, 1605, 1533, 1261, 1079, 1061, 908, and 842) cm^{-1} as evident in Raman spectrum (Figure 3.52) confirmed the encapsulation of DTX within the DTX-NLC due to appearing of DTX corresponding peaks in the DTX-NLC spectrum.

Table 3.22 Raman Vibrational band assignments for DTX and DTX-NLC.

Raman shift (cm^{-1})	Vibrational band assignment	DTX	DTX-NLC Freeze dried
1813	C=O stretching	√	√
1793	C=O	√	√
1786	C=C/C=O stretching	√	√ shifted to 1783
1651	C=O/ C=C stretching	√	√ shifted to 1658 high intensity
1631	C=O/C=C/ C=N stretching	√	√ shifted to 1626
1601	C=N/C=C stretching	√	√ shifted to 1605
1530	C-N stretching	√	√ shifted to 1533
1357	C-(NO2)	√	√
1346	C-(NO2) (phospholipids)	√	√
1275	C=O stretching	√	√ shifted to 1261
1230	C-N stretching/CH_2 twisting	√	√
1026	C=S	√	√ shifted to 1079
1003	C=S	√	√ shifted to 1061
960	C=O stretching	√	√
950	C-C stretching/ CH_2 rocking	√	√
894	C-C stretching	√	√ shifted to 908
849	C-C stretching	√	√ shifted to 842
702	C-N stretching	√	√
694	C-C/C=O deformation	√	√

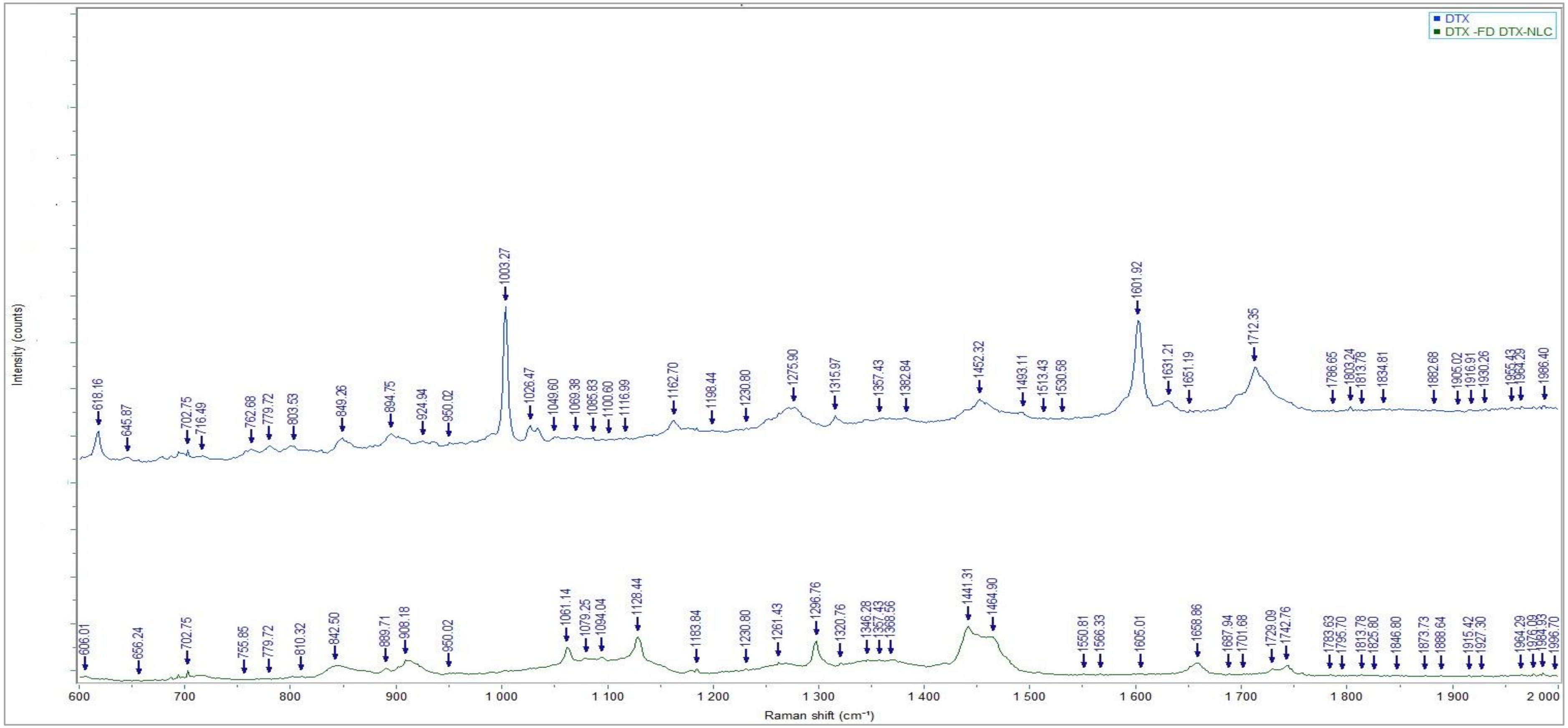

Figure 3.52 Raman overlay spectrum of DTX and DTX-NLC their characteristic peaks.

DTX-NLC, GLA-DTX-NLC, and ALA-DTX-NLC

Raman spectrum of functionalised GLA-DTX-NLC and ALA-DTX-NLC were obtained and the Raman shift of the main bond are summarised in table 3.23, together with their corresponding band assignments.

GLA-DTX-NLC demonstrated a Raman shift at (1737, 1883, 1937, 1440, 1399, 1383, 1262, 1207, 1161, 1104, 1017, 980, 967, 920, 586, and 530) cm^{-1} which were a characteristic of (C=O stretching, C=O stretching, C=O/ C=N stretching, CH_3/CH_2 stretching, N-H stretching, N-H stretching, C=O stretching/N-H bending, C-N stretching, C-N stretching, C-N stretching/CH_3 twisting, C=O, C=O stretching, C-C stretching, and C=O bending), respectively.

Raman shift was also used to evaluate the amide bond formation and any changes in the Raman spectrum after ligands been linked to the DTX-NLC as shown in Figure 3.53 and Table 3.23 that indicates some characteristic peaks that only appeared in the GLA-DTX-NLC and ALA-DTX-NLC at Raman shifts (1451, 1189, 1101, 945, 905, 773, and 684) cm^{-1} assigned for (CH_3 asymmetrical deformation, C-C/C-N stretching, C-C/C-N stretching/ CH_3 twisting, C-C stretching, , C-C stretching, C-N stretching/ C-H out of plane bend, and C-C stretching), respectively, those bands were absent in DTX-NLC, that might suggest the interaction and conjugation between the two PUFAs ligand and the DTX-NLC. Though some of the amide bond characteristics peaks (C=O at 1653 cm^{-1} and N=H at 1246 cm^{-1}). were present in both surface modifieds DTX-NLCs and the DTX-NLC pre-conjugation, that might be attributed to peaks overlapping in all tested samples.

Table 3.23 Raman Vibrational band assignments for DTX-NLC, GLA-DTX-NLC, and ALA-DTX-NLC suspension form.

Raman shift (cm^{-1})	**Vibrational band assignment**	**DTX-NLC**	**GLA-DTX-NLC**	**ALA-DTX-NLC**
1853	C=C	√	√	
1844	C=C	√		
1828	C=C	√	√	
1793	C=O	√		
1773	C=O	√	√	
1761	C=O	√	√	
1755	C=O			√
1741	C=O stretching	√		√ shifted to 1743
1730	C=O stretching	√	√ sifted to 1737	
1712	C=O stretching		√	
1706	Ketone	√	√ shifted to 1702	
1688	C=O/C=C/C=N stretching	√	√ shifted 1883 Amide band	√
1674	C=O/ C=N stretching	√		√ shifted to 1676
1666	C=O stretching/amide I		√	
1653	C=O/C=C stretching (amide I)	√	√	√
1639	C=O/C=C/C=N stretching	√	√ shifted 1937	√
1625	C=O N-H stretching amide bond formation		√	
1608	Amide	√		√
1600	Amide		√	
1596	C-C / Amide			√
1559	Amide		√	
1543	C-N stretching		√	
1521	C-N stretching	√	√	Shifted to 1529
1509	C-N stretching		√	
1496	Aromatic ring	√		
1451	CH_3 asymmetrical deformation		√	√
1441	CH_3 asymmetrical /CH_2/ring stretching	√	√ Shifted to 1440	
1416	CH_3/CH_2		√	
1396	N-H stretching	√	√ shifted to 1399	√ shifted to 1399
1386	N-H stretching	√	√shifted to 1383	
1367	CH_3 umbrella mode (phospholipids)		√	
1299	CH_2 twisting/	√	√	√ shifted to 1294
1266	C=O stretching/N-H bending	√	√ shifted to 1263	
1252	C-N stretching/ N-H bending		√	
1246	C-N stretching/ N-H bending amide III stretch	√		
1233	C-N/C-O stretching, C-H in-plane bend	√		√ shifted to 1231
1228	C-N stretching/CH_2 twisting		√	
1200	C-N stretching	√	√ shifted to 1207	
1191	C-N / C-C stretching	√		
1189	C-N/ C-C stretching		√	√

Raman shift (cm^{-1})	Vibrational band assignment	DTX-NLC	GLA-DTX-NLC	ALA-DTX-NLC
1163	C-N/ C-C stretching/CH_3 rocking	√ very sharp and high-intensity peak	√ shifted to 1161, low intensity	√ shifted to 1169, low intensity
1124	C-N stretching/CH_2 twisting	√		
1112	C-N stretching	√		
1101	C-N/C-C stretching/ CH_3 twisting		√ shifted to 1104	√ shifted to 1109
1075	C-C stretching	√	√	√ high intensity
1033	Sulfonic acid	√		
1020	Aromatic ring	√	√ shifted to 1017	√
995	Aromatic ring breathing	√	√	√ high intensity
977	C=O	√	√ shifted to 980	√
962	C=O	√	√ shifted to 967	√ shifted to 964
945	C-C stretching/ CH_2 rocking		√	√ shifted to 940
925	C-C stretching	√	√ shifted to 920	√ shifted to 920
905	C-C stretching		√	√
895	C-C stretching	√		
878	C-C stretching	√	√	√ high intensity
868	C-C ending/ CH_2 twisting	√		
856	C-C stretching	√	√	
773	C-N stretching/ C-H out of plane bend		√	√
724	C-N stretching III amide		√	
707	C-N stretching III amide	√	√	√ high intensity
695	C-C/C=O deformation		√	
684	C-C		√	√
679	C-C out of the plane	√ high intensity		
645	C-C	√		
633	C-C stretching / C-H out of plane bend	√	√	
595	C=S		√	√ shifted to 598
582	C=S	√	√ shifted to 586	√ shifted to 580
577	C-Cl		√	
528	C=O bending	√	√ shifted to 530	
503	O-H torsion	√	√	√ high intensity
475	S-S	√		

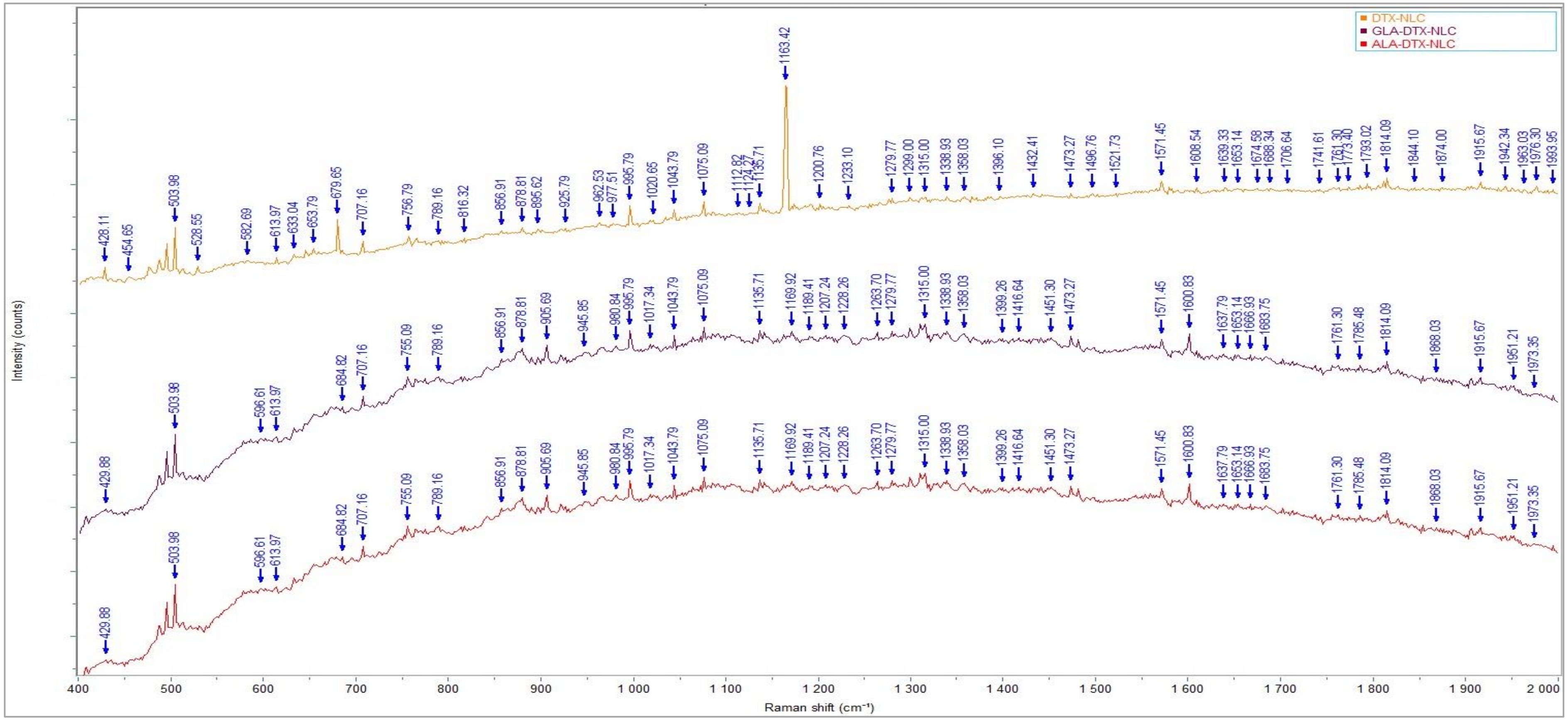

Figure 3.53 Raman overlay spectrum of DTX-NLC, GLA-DTX-NLC and ALA-DTX-NLC, and their characteristic peaks.

3.5.11. Stability studies

3.5.11.1. Colloidal stability

DTX-NLC maintained good stability in water, as well as dextrose 5% over a period of 24 h as seen by no significant change in PS and uniform distribution, maintained during this study (Figure 3.54 a and b). These results were in agreement with the previous study by Rohiwal *et al.,* (2015) when BSA NPs were examined in similar media. However, in the presence of NaCl 0.9 % and PBS a drastic increase in both PS and PDI were observed (Figure 3.54 a and b), that might be attributed to both NaCl 0.9 % and PBS have anionic moieties which might result in changes in the surface charge of DTX-NLC and consequently led to DTX-NLC aggregation or due to potential formation of insoluble salts that might lead to precipitation from the colloidal dispersion and co-precipitate colloidal particles along with it (Rohiwal *et al.,* 2015). Thus, H_2O and dextrose 5% could be a good media for reconstitution of freeze-dried NPs and avoiding of anionic physiological solution would be preferable.

EMEM was used during cell culture biology work, involving incubation of EMEM with NLCs, thus, it was considered for investigating its effect on the DTX-NLC colloidal stability. In the initial time period up to 6 h there was a slight increase in PS, however, beyond 6 h, an increase in PS and PDI were observed (Figure 3.54 a and b), that might be due to the presence of amino acids, glucose, and FBS. As it is well known that proteins and vitamins might adsorb onto the NPs (Goppert *et al.,* 2005), and lead to the formation of a corona on the surface resulting in an increase in PS (Barbero *et al.,* 2017). These results were in line with Rohiwal *et al.,* (2015) findings.

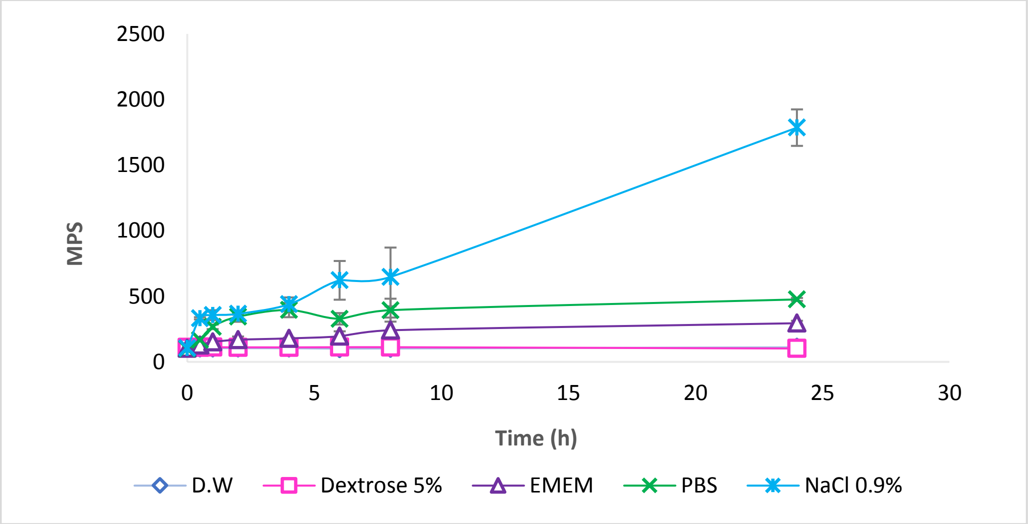

(a)

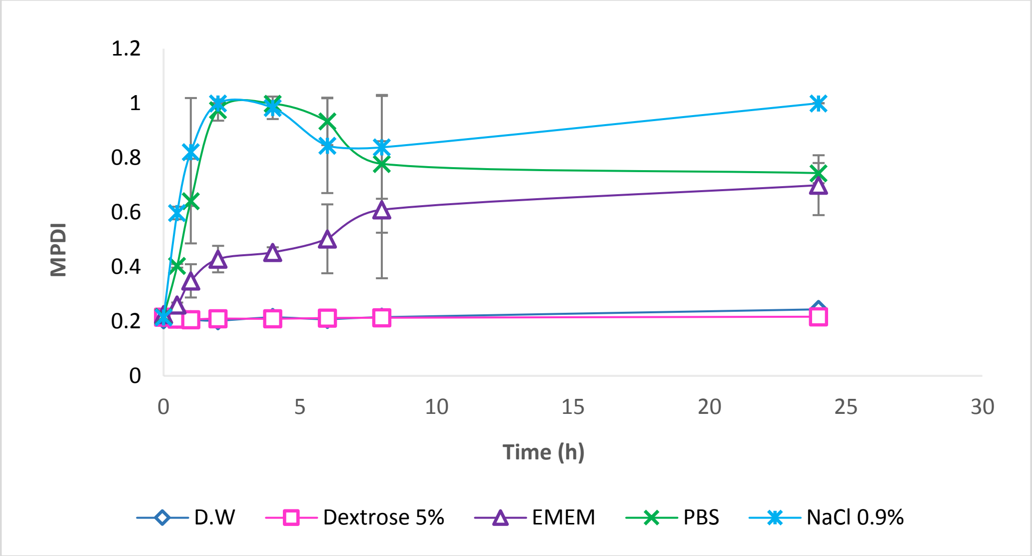

(b)

Figure 3.54 Effect of physiological media on DTX-NLCs over 24 h during different time intervals at 37°C (a) effect on PS when PBS, EMEM, Dextrose 5%, NaCl 0.9 % and H2O (D.W) were used, (b) effect on PDI when PBS, EMEM, Dextrose 5%, NaCl 0.9 % and H2O (D.W) were used. Data are mean ± SD, N=3.

3.5.11.2. Short-term stability

Stability studies were performed on the liquid dispersion of DTX-NLCs and B-NLCs for up to three months at room temperature (Tables 3.24 and 3.25). Both formulations demonstrated stable features for all investigated parameters (Figure 3.55 a and b). There was no change observed on PS and PDI due to high ZP more than -30 mV which was maintained over a period of three months. These findings were in line with Radomska-Soukharev (2007) and, Radomska-Soukharev and Muller (2006). High ZP plays a crucial role to prevent drug aggregation, as the electrostatic repulsion prevents aggregation of particles might lead to colloidal stability (Caddeo *et al.,* 2008). Moreover, 15 % reduction in TD was obtained over the same period. Lyophilisation (freeze-drying) of the formulation might result in better drug stability with DTX-NLC and overcome drug loss.

Table 3.24 DTX-NLCs in liquid dispersion stability study for three months at room temperature.

DTX-NLCs	PS (nm)	PDI	ZP (mV)	%EE	%TD	%DC
Day 0	136.8 ±2.94	0.231 ±0.01	-32.4 ±0.21	99.13 ± 1.2	88.6 ±1.37	2.01 ±0.03
One month	135.4 ±2.46	0.235 ±0.003	-32.4 ±0.90	98.01 ±0.73	71.23 ±2.1	1.78 ±2.01
Two months	130.5 ±1.7	0.245 ±0.01	-32.3 ±1.01	97.85 ±0.83	66.61 ±0.47	1.66 ±0.32
Three months	130.0 ±0.72	0.26 ±0.009	-33.6 ±0.96	96.40 ±0.20	64.36 ±0.55	1.60 ±0.45

Table 3.25 B-NLCs in liquid dispersion stability study for three months at room temperature.

B-NLCs	PS (nm)	PDI	ZP (mV)
Day 0	147.4 ±0.28	0.231 ±0.23	-34.4 ±0.87
One month	151.4 ±3.71	0.209 ±0.01	-35.5 ±0.85
Two months	144.1 ±0.98	0.235 ±0.01	-38.5 ±2.17
Three months	142.8 ±0.62	0.23 ±0.001	-35.6 ±0.91

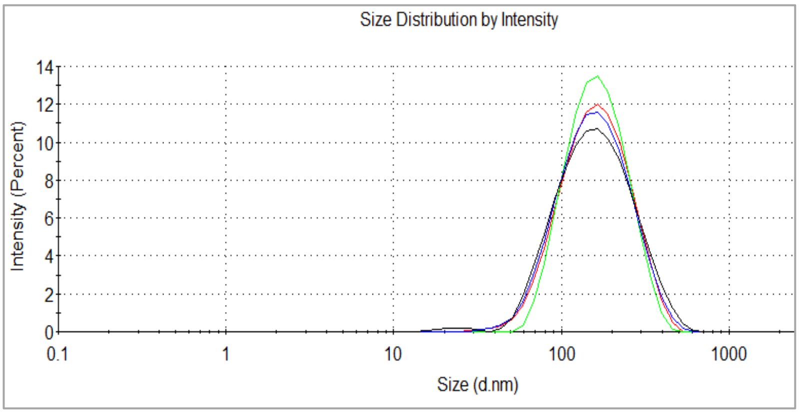

(a)

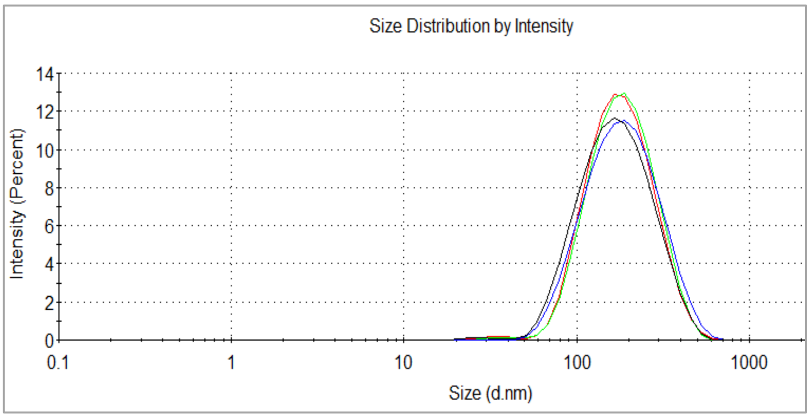

(b)

Figure 3.55 Stability study for up to three months at room temperature showing particle size and particles distribution for (a) overlay graph for DTX-NLC (b) overlay graph for B-NLC. Data are mean, N=3.

3.5.11.3. Long-term stability

Stability studies were conducted on freeze-dried DTX-NLCs with samples stored at different storage temperature over a period of six months (-20, 4, 25 and 40°C), respectively. DTX-NLC showed good stability in terms of PS when stored at -20 °C (Figure 3.56 and 3.57), as no significant increase in PS, was observed for samples stored at -20 °C for up to the period of six months, and a slight increase in PS when DTX-NLC stored at 4°

C for up to six months. DTX-NLC PS suffered from a highly significant increase in PS when DTX-NLC stored at 25 and 40 °C at all time points, indicating that high temperature might not be suitable for storing the DTX-NLC. Interestingly, our data for PS demonstrated better results than reported by Fan *et al.,* (2014) at similar storage environments.

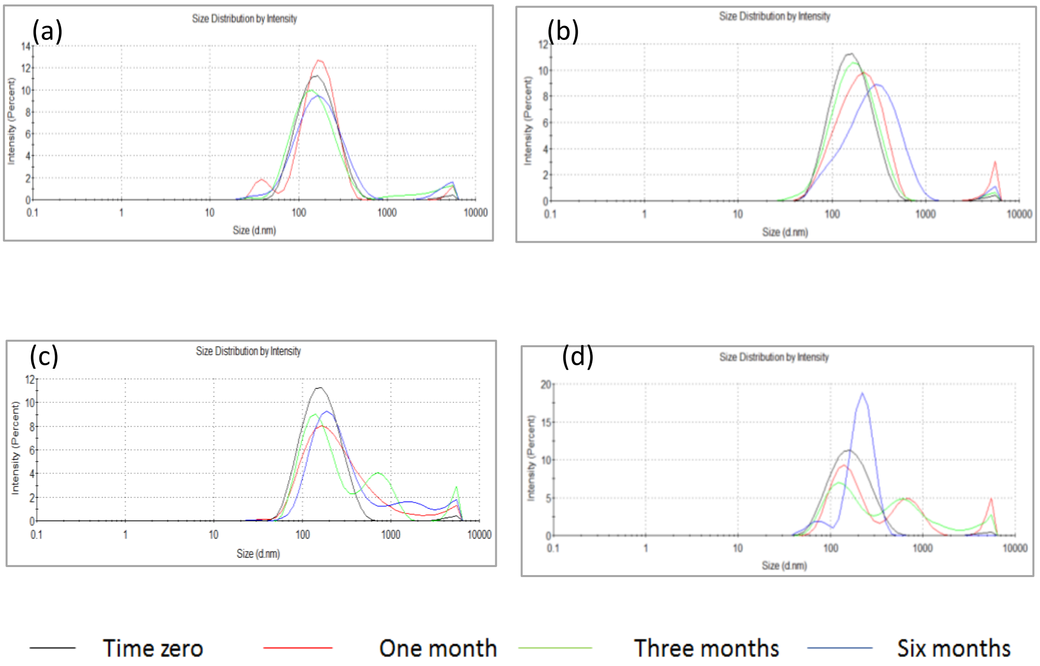

Figure 3.56 Combined graphs showing PS and PDI stability study for DTX-NLC, Stored at different temperature (a) at -20 °C, (b) at 4°C, (c) at 25°C, and (d) at 40 °C, respectively.

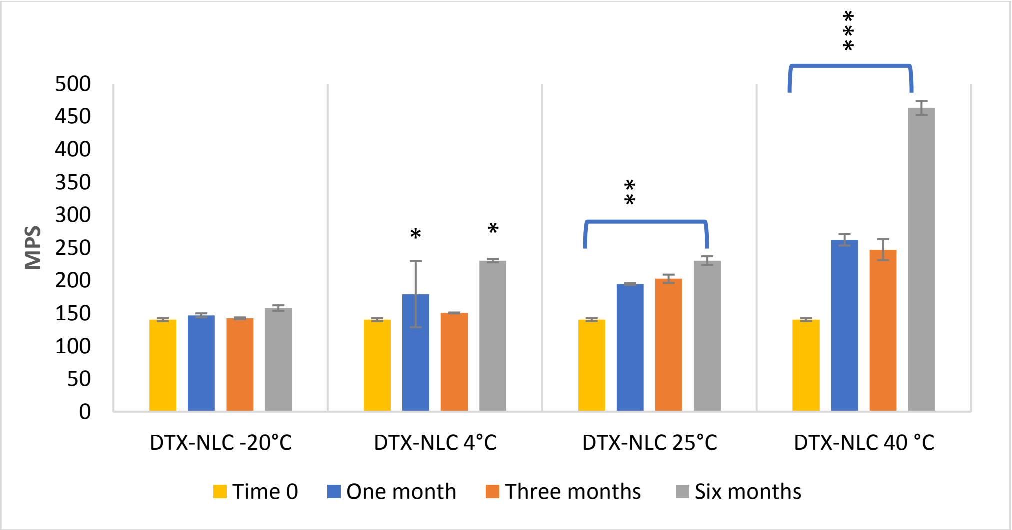

Figure 3.57 Stability study over six months and the effect of storing the DTX-NLCs at -20, 4, 25, and 40°C on PS. Data are mean ± SD, N=3, * P < 0.05, ** P < 0.001 and *** P < 0.000 refers to a significant difference when samples stored at variable temperature were compared to a fresh DTX-NLC.

Figure 3.58 a, demonstrated a significant increase in the size distribution of the PDI when DTX-NLCs were stored at -20°C, 4°C, 25 and 40 °C for up to six months. However, storing DTX-NLC at -20°C and 4°C were much preferable over higher storage temperature due to PDI > 0.5 at six months period. The ZP of DTX-NLC showed a significant increase at -20, 4, and 25 °C, which probably contributed to increasing the stability of these formulations. It was reported earlier that ZP > -30.0 mV was good for physical stability (Mukherjee *et al.,* 2008). In our experiments all DTX-NLCs stored at different temperature were characterised by a high zeta potential and/or remain unchanged as ZP was ranging from -36.1 ± 1.5 to -45.86 ± 0.5 mV during the six months period of storage (Figure 3.58 b) that suggests a good long-term physical stability as reported by Mukherjee *et al.,* (2008). and Fan *et al.,* (2014).

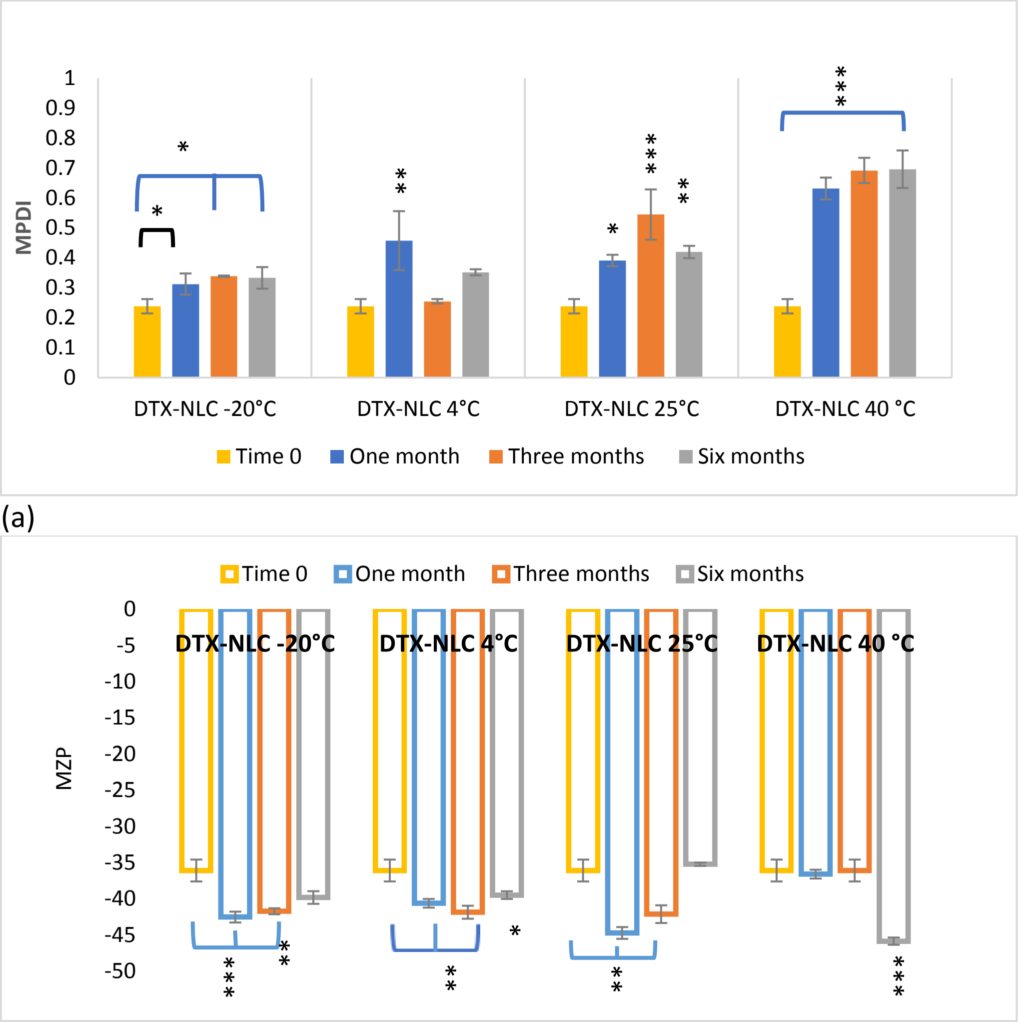

(a)

(b)

Figure 3.58 Stability study over six months and the effect of storing the DTX-NLCs at -20, 4, 25, and 40°C on (a) PDI and (b) ZP. Data are mean ± SD, N=3, * P < 0.05, ** P < 0.001 and *** P < 0.000 refers to the significant difference when samples stored at variable temperature were compared to a fresh DTX-NLC.

The %TD were maintained for up to three months, beyond that %TD was reduced by 10, 12, 12, and 20 % at the end of six month period at -20, 4, 25, and 40 °C, respectively (Figure 3.59 a). Additionally, only DTX-NLC stored at -20 °C was showing high %DL with no significant reduction for up to six months, and the % DL of DTX-NLC stored at 4 and 25 °C was slightly reduced. Notably, a drastic reduction in % DL was observed at 40°C beyond one-month storage (Figure 3.59 b).

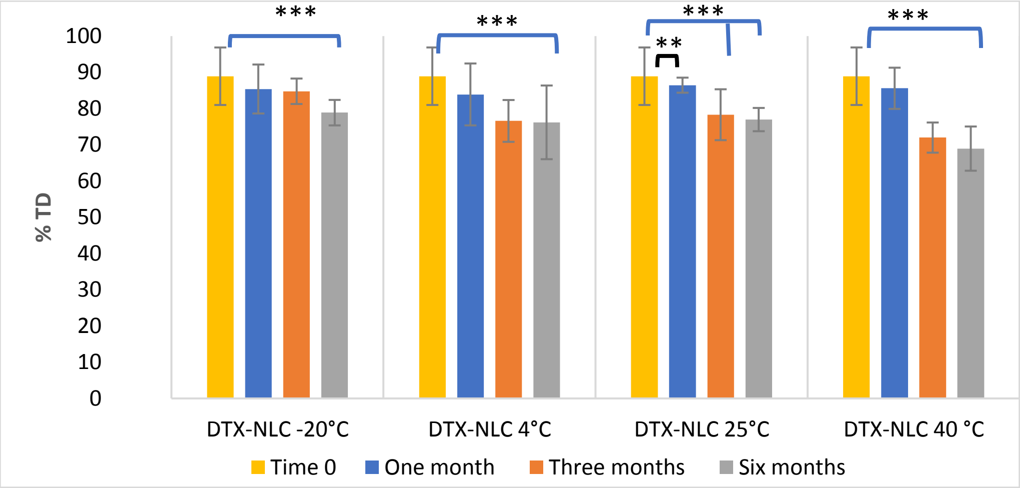

(a)

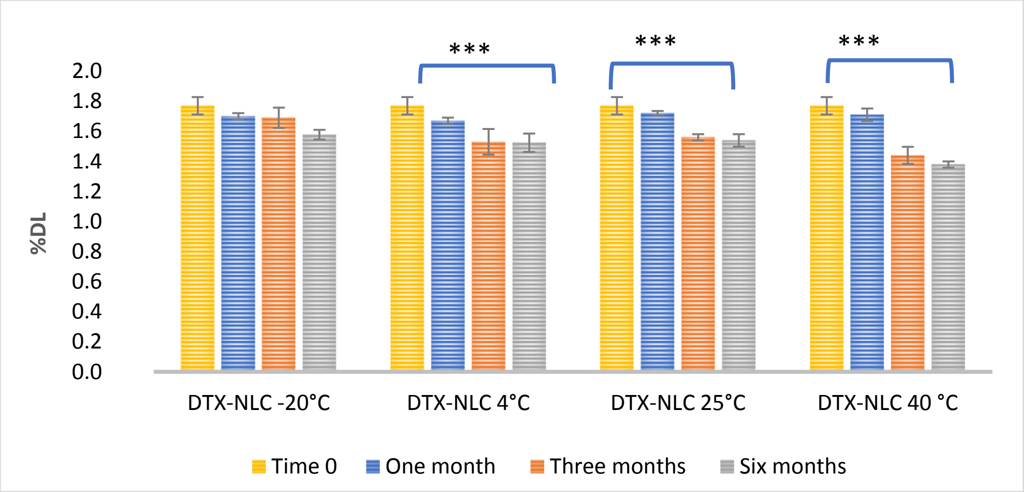

(b)

Figure 3.59 Stability study over six months and the effect of storing the DTX-NLCs at -20, 4, 25, and 40°C on (a) %TD and (b) %DL. Data are mean ± SD, N=3, * $P < 0.05$, ** $P < 0.001$ and *** $P < 0.000$ refers to the significant difference when samples stored at variable temperature were compared to a fresh DTX-NLC.

It was evident in figure 3.60 that the DTX-NLC % EE showed a high DTX entrapment within the NLCs for all examined samples, preferably DTX-NLC should be stored at -20 and 4°C due to relatively stable changes of all tested parameters during the six month period. It is worth mentioning that our finding demonstrated relatively good PS and %EE when NLCs were stored at 25°C when compared with previous literature by Li *et al.,* (2009).

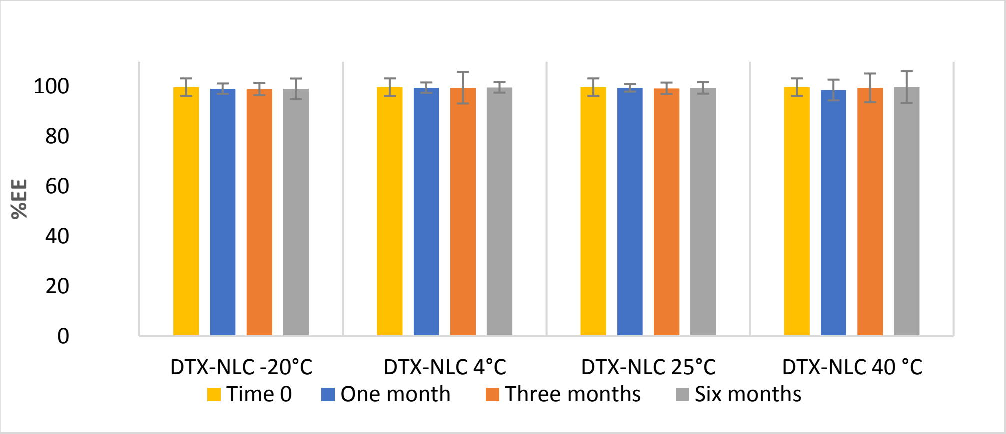

Figure 3.60 Stability study over six months and the effect of storing the DTX-NLCs at -20, 4, 25, and 40°C on % EE. Data are mean ± SD, N=3, * P < 0.05 refers to the significant difference, ** P < 0.001 and *** P < 0.000 refers to a highly significant difference when samples stored at variable temperature were compared to a fresh DTX-NLC. In this case, no significant difference was observed in all tested samples.

DTX-NLC followed a trend of Oswald ripening for all DTX-NLC stored at -20, 4, 25 and 40°C as the r^2 versus time demonstrated a relatively linear relation r^2 was ranging between 0.69-0.30 (Witayaudom and Klinkesorn, 2017), this phenomenon occurs due to small particle size accumulate and disposed into larger particle size, so the ripening increases with time (Figure 3.61 a). However, DTX-NLC stored at 40 °C apart from Oswald ripening also demonstrated coalescence and flocculation (Figure 3.61 b).

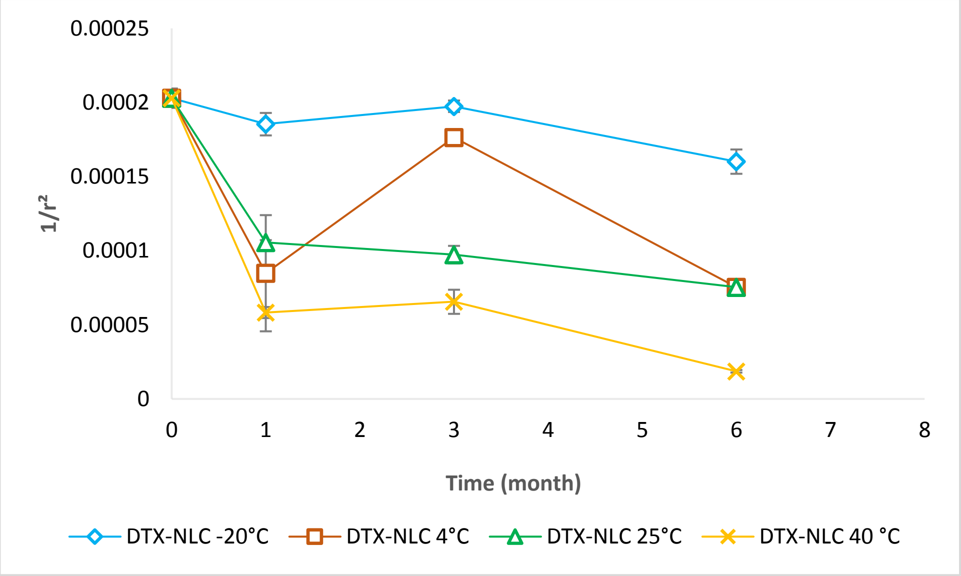

(a)

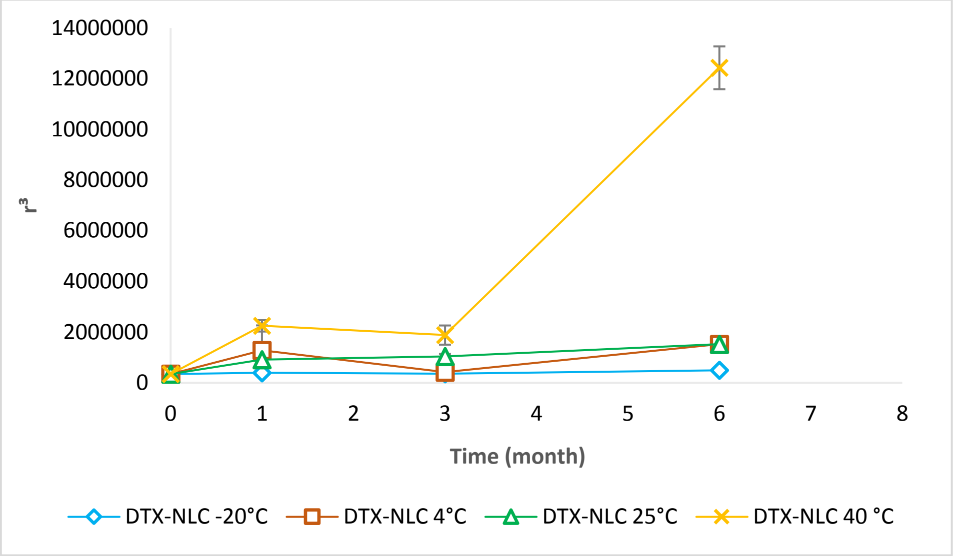

(b)

Figure 3.61 Stability study over six months and the effect of storing the DTX-NLCs at -20, 4, 25, and 40°C (a) the plot of 1/r^2 with respect to time, (b) the plot of r^3 as a function of time. Data are mean ± SD, N=3. (r) refers to the radius of NLCs.

In summary, DTX-NLCs were developed and prepared in a temperature-controlled environment and organic solvent-free preparation process. Biodegradable excipients that were acceptable for IV route administration were used for DTX-NLC fabrication, where a combination of surfactants system, solid and liquid lipids were used to produce a formulation with low PS 136 nm, uniform distribution PDI 0.23, desirable high surface charge -32 mV, drug entrapment 99%, and drug content 88 %. Stable in water and dextrose 5% physiological media with up to six months of stability at -20 °C for freeze-dried form. Followed by a successful surface modification with two PUFAs (GLA and ALA) and novel SA43-aptamer. Additionally, DTX-NLCs and surface modified NLCs were characterised for their thermal, crystalline and structural compositions.

Chapter Four

In-vitro cell lines and 3D spheroids studies

4.1. Introduction

4.1.1. Monolayer cell lines as *in-vitro* model

The use of *in-vitro* cell lines as screening models for evaluation of different drugs and compounds has great value for overcoming obstacles in the drug development and screening processes (Allen *et al.,* 2005). Using tissue culture, it is possible to study cell lines derived from humans and animals and to assess the effect of the drug on the desired target systems; and examining the mechanism of action and toxicity (Allen *et al.,* 2005).

After the development of new NLC formulations loaded with anti-cancer drug DTX, as previously detailed in chapter three, the evaluation of their efficacy and effect on cell proliferation was investigated. Specifically, this involved study of the cellular uptake, internalisation mechanism and the effect on cell cycle of the DTX and NLCs loaded with DTX and further the effect of surface modification of DTX-NLC with PUFAs (GLA and ALA) and SA43-aptamer was studied. Commercially available immortalised glioblastoma cell lines and patient-derived short-term cultures of glioblastomas grown in a monolayer were used as models for the aforementioned assays.

4.1.2. Spheroids as a 3D *in-vitro* model

Three dimensional (3D) spheroids permit the evaluation of cytotoxic therapeutics under specific conditions, which partially represent the tumour microenvironment more so than a monolayer (Hamilton, 1998). Spheroids are micro size aspherical cell groups that self-assemble to form a 3D tumour (Mehta *et al.,* 2012). Spheroids are thought to be produced by promoting cell coupling with a neighbour cell and by resisting cell–surface interactions with the tissue culture plate (Friedrich *et al.,* 2007). Spheroids have been used for studying a variety of treatments as demonstrated by Sha *et al.,* (2015) and Gao *et al.,* (2012). It is believed that tumour spheroid models will participate to economic savings in cancer research as the physiologically relevant microenvironment as they more closely represent the *in vivo* environment, hence improving the predictive drug efficacy and thereby reducing downstream animal tests (Carver *et al.,* 2014; Friedrich *et al.,* 2007). Wherever possible, 3D spheroids were used for cell proliferation and uptake assays, but where high cell numbers were required, monolayer cultures had to be used.

4.1.3. Docetaxel mechanism of action and tumoricidal effect

It is well reported that DTX exerts tumouricidal effects by disrupting microtubule assembly and stabilising the polymers against depolymerisation, hence inhibiting the microtubule dynamics (Ringel and Horwitz, 1991; Herbst and Khuri, 2003). Additionally, DTX causes impairment of mitotic progression leading to cell cycle arrest at G2/M phase (Figure 4.1), thereby inhibiting cell proliferation (Zhang and Zhang, 2013; Choi *et al.,* 2015).

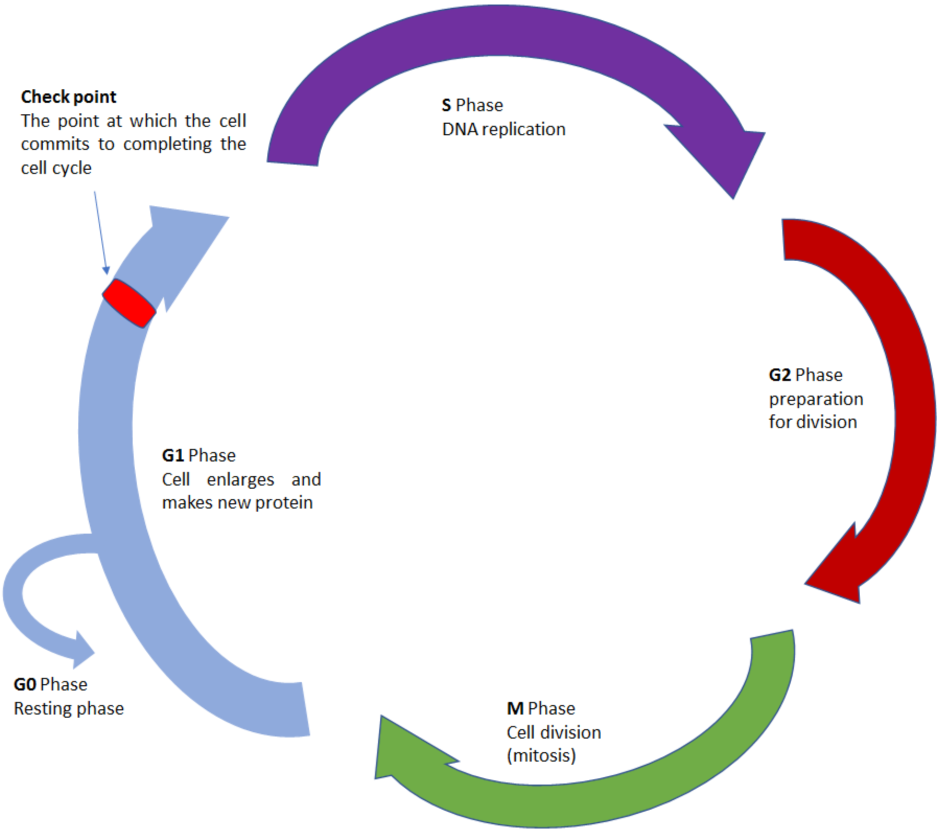

Figure 4.1 Cell cycle phase distributions.

4.2. Aim

The aim of this study was to evaluate the efficacy and toxicity of DTX-NLCs for treatment of glioblastoma and to explore the effect of surface modification DTX-NLCs (DTX-NLC, GLA-DTX-NLC, ALA-DTX-NLC, and SA43-DTX-NLC) with respect to enhanced DTX-NLC selective uptake, internalisation and toxicity.

4.2.1. Objective 1

Evaluation of the effect of DTX-NLCs on cell proliferation in monolayer U87MG glioblastoma cell lines and patient-derived short-term cultures of glioblastoma BTNW911 and compare to non- cancerous glial cell line SVG P12.

4.2.2. Objective 2

Evaluation of the effect of the presence of combined antioxidants (Vit E and AP), used during the fabrication of DTX-NLC, GLA-DTX-NLC, and ALA-DTX-NLC on cell proliferation of U87MG cell line.

4.2.3. Objective 3

Evaluation of the effect of variable ratios of GLA, ALA and SA43-aptamer functionalised DTX-NLCs on cell proliferation in monolayer U87MG glioblastoma cell lines, patient-derived short-term cultures of glioblastoma BTNW911 as compared to non- cancerous glial cell line SVG P12.

4.2.4. Objective 4

Evaluation of the cell proliferation differential effect of DTX-NLC and surface modified DTX-NLCs in U87MG glioblastoma cell lines spheroids.

4.2.5. Objective 5

Internalisation and selective uptake analysis of DTX-NLC and surface modified DTX-NLCs in monolayer U87MG glioblastoma cell lines and patient-derived short-term cultures of glioblastoma BTNW911 (FACS only) compared to non- cancerous glial cell line SVG P12 measured by fluorescence microscopy and flow cytometry respectively.

4.2.6. Objective 6

Selective uptake analysis of DTX-NLC and surface modified DTX-NLCs in spheroid U87MG glioblastoma cell line measured using flow cytometry.

4.2.7. Objective 7

Elucidation of the uptake pathway of DTX-NLCs and surface modified DTX-NLCs in monolayer U87MG glioblastoma cell lines compared to non- cancerous glial cell line SVG P12 measured by fluorescence microscopy and flow cytometer in the presence of specific pathway inhibitors.

4.2.8. Objective 8

Determine the cell cycle phase distribution following treatment with developed formulations of DTX-NLCs in monolayer U87MG glioblastoma cell lines.

4.3. Equipment and materials

4.3.1. Equipment

Class II microbiological safety cabinets (Labcaire Systems Limited, UK) were used for sterile tissue culture. Separate class II cabinets were used for immortalised cell line culture and short-term culture of patient-derived primary cells to minimise the risk of cross-contamination of cell lines. Fluorescence spectroscopy measurements were made in a plate reader (Genios Pro microtiter plate reader, Tecan, Austria) and data were analysed using GraphPad software Prism version 5.00 for Windows, (San Diego California, USA). Fluorescence imaging was captured with a Carl Zeiss fluorescence microscope (Carl Zeiss Microscopy GmbH, Germany). Fluorescence images were taken with an AxioCam MRm Zeiss camera, (Carl Zeiss Microscopy GmbH, Germany) and processed with Zen blue software (Carl Zeiss Microscopy GmbH, Germany). A benchtop flow cytometer was used for cellular uptake, internalisation mechanism and cell cycle analysis (Guava, Merck, Germany), and the data were analysed with Guava® EasyCyte software 3.1.1 (Guava, Merck, Germany), The cells were incubated in a Sanyo CO_2 incubator (Sanyo, Japan). Cells were visualised with Leica DMIL light microscope from Leica Microsystems GmbH, Germany whereas light microscope images were taken with the MShot camera, China and processed with MShot Digital Imaging System software, China. Haemocytometer slide used for cell counting was obtained from Marienfeld (Marienfeld, Germany). Bench centrifuge (ALC, Buckinghamshire, UK) at 179 x g for 5 min. All sterile culture flasks (T25 and T75 cm^3), sterile plates (6-well, 12-well, and 96-well) (Nunc™ MicroWell™), sterile centrifuge tubes (15 and 50 ml), serological pipettes and Mr Frosty™ freezing containers were purchased from Fisher Scientific, UK. Syringes were obtained and Millex® sterile syringe filters (0.45 µm and 0.22 µm pore size) were from Fisher, UK. The slides and cover slides from Fisher, UK. Non-tissue culture/ V-shaped 96 well plates were purchased from Fisher, UK.

4.3.2. Materials

The media, supplements and chemicals were obtained from the following: Eagle's minimum essential medium (EMEM) Lonza, Belgium. Foetal bovine serum (FBS), L-glutamine, sodium pyruvate, non-essential amino acid (NEAA) and phosphate buffer saline (PBS) 0.1 M pH 7.4 at 25°C (Fisher, UK). RNAse free water was from Fisher, UK. Propidium iodide, Trypsin solution 10X, Trypan blue, sucrose and agarose were purchased from Sigma Aldrich, UK. Presto blue, 16% Formaldehyde, HBSS 1X consists of (Potassium Chloride (KCl) 5.33 mM, Potassium Phosphate monobasic (KH_2PO_4) 0.441 mM, Sodium

Bicarbonate ($NaHCO_3$) 4.166 mM, Sodium Chloride (NaCl) 137.93 mM, Sodium Phosphate dibasic (Na_2HPO_4) anhydrous 0.338 mM and Other Components D-Glucose (Dextrose) 5.55 mM and Phenol Red 0.026 mM) at pH7.4, 1X TryPLE Express, ethanol, DMSO, RNAs, Nystatin and Cytochalasin B, industrial methylated spirit (IMS) were purchased from Fisher Scientific, UK. Vectashield mounting medium with DAPI was purchased from Vector Labs, UK. Accumax™ Cell Counting Solution in Dulbecco's Phosphate-Buffered Saline (DPBS) was provided by Merck Millipore, UK.

4.3.3. Cell lines

SVG P12 (human, non-cancerous foetal glial cell line) was cultured with a passage number ranging from 9-13, U87MG (human glioblastomas, grade IV cell line), was cultured with a passage number ranging from 15-23. Both cell lines were obtained from the European Collection of Cell Cultures (ECACC, UK). BTNW911 was a short-term culture derived from primary cells obtained from a 60-year-old, male grade IV glioblastomas, used at passage number 9 and 10 with written ethical consent from the BTNW (Brain Tumour North West) tissue bank (Appendix II).

4.4. Methods

All the experiments reported in this chapter were performed under sterile conditions and by using a class II laminar flow hood. All equipment, materials, pipettes, flasks were sterilised prior to place it inside the hood either by spring with 70% industrial methylated spirit (IMS) or by autoclaving and spraying with 70% IMS. Unsterile reagents were sterilised by filtering the reagents with sterile filters of pore sizes 0.22 µm. All media, PBS and media supplements were placed in the water bath at 37°C for at least 30 min before starting the experiments. Moreover, all the flasks containing cell suspension and media were sprayed with 70% IMS then placed at 37°C in a humidified incubator under 5 % CO_2 atmosphere, all these conditions were kept constant during the course of this studies, to maintain a clean, sterile and desirable environment for the cell lines and spheroids to grow properly.

4.4.1. Preparations

4.4.1.1. Media preparation

Eagle's minimum essential medium (EMEM) was used for growing U87MG, U87MG spheroids and SVG P12 cells then adding to it 1 mM sodium pyruvate, 1% non-essential amino acid (NEAA), 2 mM L-glutamine and 10% foetal bovine serum (FBS) as supplements for the cell lines. For BTNW911 the primary culture was maintained in F-12 media, and 1 mM pen-strep, 2 mM L-glutamine and 10% Foetal bovine serum (FBS) as supplements were added. The prepared media were stored at 4 °C.

4.4.1.2. Trypsin and Phosphate buffer saline (PBS)

Trypsin 1x (0.25 mM) was used to detach the adherent monolayer cells from the flasks, it was prepared by 1:10 dilution with sterile PBS (0.1 M, pH7.4) and the PBS was prepared by adding one tablet of PBS in 200 ml H_2O to give a final concentration of 0.1 M with pH7.4, then sterilised by autoclaving. Additionally, in all the experiments PBS concentration 0.1 M, pH7.4 was used for washing the adherent cells prior to detaching them by the trypsin, diluting cell suspensions for uptake, and cell cycle experiments. In the case of BTNW911, HBSS 1x (pH 7.4) and 1x TrypLE™ ready to use as advised by the supplier was used for washing and dissociation, respectively.

4.4.1.3. Agarose preparation and plate coating

For the spheroid formation, the agarose coating method was used. A 1 % agarose solution was prepared by dissolving 1 g of agarose in 100 ml sterile PBS solution (1 % w/v), and stirring at 90 °C until the solution became clear. The 1 % agarose was autoclaved and stored at room temperature until used. The 1% agarose solution was heated again and a 50 µl were placed in each 96/well/ tissue culture plates in a sterile laminar flow hood and kept inside the hood for 3 h. The plates were sealed using parafilm and covered with aluminium foil to protect from light and kept at 4 °C overnight prior to use the following day (Garanti 2016).

4.4.1.4. Coating coverslips with fibronectin

For the qualitative internalisation study coverslips pre-sterilised with 70 % IMS, were also autoclaved, washed with HBSS and placed in 12 well tissue culture plates. For each well, 5 µg/ml fibronectin diluted with HBSS was added on top of the coverslip and incubated for 24 h in a humidified incubator under 5 % CO_2 atmosphere. Then prior to the seeding day the excess fibronectin was removed by washing the coverslips two times with 1 ml of sterile PBS.

4.4.2. Cell lines thawing

The cryovial containing the frozen cells were removed from liquid nitrogen storage and thawed immediately by gently swirling the vial in a 37° C water bath, for less than 1 minute. The thawed cells were transferred to a centrifuge tube containing 1 ml (1:1, ratio media: cells) of pre-warmed complete growth medium appropriate for each cell line. The cell suspension was centrifuged at room temperature at 179 x g for 5 min. The supernatant was removed gently without disturbing the cell pellet. The cells were resuspended in 10 ml complete growth medium appropriate for each cell line in T75 flasks, or 5 ml media for T25 flasks. Moreover, all flasks were then placed at 37 °C in a humidified incubator under 5 % CO_2 atmosphere and cultured until 75-80 % confluent.

4.4.3. Cell lines sub-culturing

At 75-80 % confluency, the media were aspirated from each flask and the monolayer cells were gently washed with 2 ml PBS (0.1 M, pH7.4), then the PBS discarded. This was followed by adding 2 ml pre-warmed trypsin, incubating the flasks at 37 °C for less than 5 min until the detached cells were observed under the microscope. Flasks were placed back into the laminar flow hood and 2 ml of complete growth media was added. The cell suspension was transferred to a 15 ml tube and centrifuged at room temperature at 179 x g for 5 min. The cell pellet was resuspended in complete growth medium and an appropriate volume was transferred into new cell culture flasks depending on the split ratio/cell concentration required. For each of U87MG, SVG P12, and BTNW911 cell lines were split into (1:3, 1:3, and 1:2) ratio, respectively. All new flasks were labelled with cell type, passage number, date and split ratio and placed into the incubator.

4.4.4. Cell count and viability assessment

Cell counting was performed after the protocol in section 4.4.3. After the cell pellet was resuspended in media, a 50 µl cell suspension was transferred into 1.5 ml tube (Eppendorf), and 50 µl of trypan blue was added and mixed. Then 10 µl of the mixture were added on a hemocytometer then covered with a coverslip. A viable cell count was performed at 10 X magnification under the light microscope by counting the cells that looked bright and colourless and excluding the dead cells that had taken up the trypan blue dye, (dark blue appearance) (Louis and Siegel, 2011). The haemocytometer consists of 9 large squares with 1 mm length, and four squares were used to count the viable cells, and an average was calculated then multiplied by dilution factor and the haemocytometer factor 1 x10^4 to obtain the number of cells per 1 ml of suspension. Cells were seeded in different densities depending on the intended use and purpose of the experiment.

4.4.5. Cell line growth kinetics

To study the growth pattern of the immortalised (U87MG, SVG P12) and patient-derived short-term (BTNW911) cell lines, cell count versus time was determined using Presto Blue® dye. Cells were seeded at a density of 500, 1000, 2500, 5000 and 10000 cells/ 90 µl well in a 96 well tissue culture plate and cultured at 37 °C and 5 % CO_2 in a humidified incubator. Every 24 h, for four days, cells were stained with 10 µl Presto Blue ® dye and counted using a plate reader (section 4.3.1). For every time point, an average cell count from six wells was calculated up to four days because no experiment would last longer than this. The growth medium was changed every other day to maintain cells in a healthy environment.

4.4.6. Spheroids formation

Using the method of Garanti *et al*., (2016), U87MG were grown into spheroids by seeding 3 x 10^3 cells/100 µL in 96-well tissue culture plates that were pre-coated with 1% sterile agarose (refer to section 4.4.1.3), then 100 µl of complete EMEM media was added gently and dropwise to each well (to give a total volume of 200 µl). The plates were then transferred to a humidified incubator at 37 °C and 5 % CO_2 and were incubated for four days until the spheroids formation was complete. The spheroid formation was confirmed using an inverted light microscope.

4.4.7. Cell proliferation evaluation

To determine the effect of DTX, B-NLC, DTX-NLC, GLA-DTX-NLC, ALA-DTX-NLC and SA43-DTX-NLC on U87MG, SVG P12, BTNW911 monolayers cells and U87MG spheroids, cell proliferation was assessed by using Presto Blue® viability reagent; this protocol was adapted from Thakor *et al.,* 2017.

4.4.7.1. Cell proliferation evaluation of docetaxel-loaded nanostructured lipid carriers (DTX-NLCs) in monolayer cell lines

Cells were seeded at a density of 2500 cells/90 µl/well for U87MG and SVG P12, and 5000 cells/90 µl/well in a 96-well plate for BTNW911. The monolayer cell lines were then cultured for 24 hours prior to drug treatment at concentrations 2.5, 5, 10, 25, 50, 100, 250, 500, 1000 ng/ml from each of the formulation. Media without any cells was used as a blank and cells and media without a drug were used as a control. Presto Blue® was used to perform the proliferation assay by adding 10 µl/well of Presto Blue at 24, 48 and 72 h, after drug treatment. All plates were covered with aluminium foil and transferred to the incubator for 1 h incubation in a humidified incubator at 37 °C and 5 % CO_2, then the plate reader was used for detection of fluorescence response for Presto Blue at an excitation wavelength of 535 nm and an emission wavelength of 612nm. This experiment was repeated three times and cell proliferation that is corresponding to cell viability was calculated using equation 4.1.

$$\%\ \boldsymbol{Cell\ Viability} = \left[\frac{(\boldsymbol{Fluor.Drug\ Treatment - Fluor.Blank})}{(\boldsymbol{Fluor.Control - Fluor.Blank})}\right] \times \mathbf{100}$$

(Equation 4.1)

Mean cell viability *versus* drug concentration was plotted using the Prism5 software (GraphPad Software, USA). The concentration at which 50 % inhibition (decrease in cell proliferation) was achieved (IC_{50} value) was calculated for all tested formulations.

4.4.7.1.1. Cell proliferation evaluation of PUFA tagged docetaxel-loaded nanostructured lipid carriers

Two PUFAs (GLA and ALA) were examined as ligands for surface modification of DTX-NLCs and the effect of the ligand density was investigated on cell proliferation.

4.4.7.1.1.1. Cell proliferation evaluation of nanostructured lipid carriers composed of antioxidants and surface modified with PUFAs

A combination of two antioxidants Ascorbyl palmitate (AP) and α-Tocopherol (Vit. E) were used (0.05%, w/v of AP+ 0.02%, w/v of Vit. E), during the fabrication of DTX-NLC, which was then functionalised with GLA and ALA in two ratios 1:1/5 and 1:1/6 (FAG: PUFAs) as detailed in Chapter Three (sections 3.4.2, 3.5.6.1.1, and 3.5.6.2.1). The cell proliferation assay was performed on U87MG and SVG P12 monolayers for the same range of concentrations and incubation time detailed in section 4.4.7.1, to evaluate the presence of antioxidants effect on the cell line when treated with DTX-NLCs, GLA-DTX-NLC, and ALA-DTX-NLC formulated with the antioxidant combination. This was measured by the Presto Blue® assay and a percentage of mean cell viability was calculated as per equation 4.1, followed by measuring IC_{50} values for all tested formulations.

4.4.7.1.1.2. Cell proliferation evaluation of nanostructured lipid carriers composed of variable ratios of PUFAs as ligands

GLA-DTX-NLC and ALA-DTX-NLC were prepared with varied ligand density of PUFAs as detailed in Chapter Three (sections 3.4.2, 3.5.6.1, and 3.5.6.2) and only two ratios 1:1/5 and 1:1/6 (FAG: PUFAs) were selected for cell proliferation studies with U87MG and SVG P12 cells following the same protocol, range of concentrations and incubation time as detailed in section 4.4.7.1. Cell proliferation was measured using Presto Blue® assay and a percentage of mean cell viability was calculated as per equation 4.1, followed by determination of IC_{50} values for all the tested formulations.

4.4.7.1.2. Cell proliferation after treatment with aptamer tagged docetaxel-loaded nanostructured lipid carriers

SA43-aptamer was surface modified with DTX-NLC as detailed in Chapter Three (sections 3.4.3 and 3.5.7) and the ratio of 1:1/8 (FAG: SA43) was chosen to perform cell proliferation test with monolayer cell lines. Following the same protocol, the range of concentrations and incubation time as detailed in section 4.4.7.1. Cell proliferation was measured using Presto Blue® assay and a percentage of mean cell viability was calculated as per equation 4.1, followed by measuring IC_{50} values for the tested formulation.

4.4.7.2. Cell proliferation evaluation of docetaxel-loaded nanostructured lipid carriers in U87MG spheroids

For the proliferation evaluation of the U87MG spheroids, a 3000 cells/90 µl/well in a 96-well plate were seeded as described in section 4.4.6. The U87MG spheroids were treated with DTX, DTX-NLC, GLA-DTX-NLC, ALA-DTX-NLC and SA43-DTX-NLC and incubated with the treatment for 72 h for the same range of concentrations mentioned in section 4.4.7.1, then the spheroids were transferred gently into a new 96 well plate (the plates were not coated with agarose at this stage), with 90 µl media. After that, cell proliferation was determined as described in section 4.4.7.1.

4.4.8. Qualitative Cellular internalisation study

The mechanism of cellular internalisation for entry of fluorescence-labelled DTX-NLCs with Rhodamine 123 (R) prepared as described in chapter three section 3.4.1 was determined. R-DTX-NLC, R-GLA-DTX-NLC, R-ALA-DTX-NLC and R-SA43-DTX-NLC were evaluated in U87MG and SVG P12 cells, this method was adopted and modified from Garanti *et al.,* (2016). When cells reached 75-80% confluency they were seeded at $2.5x10^5$ /well/1 ml on a sterile pre-coated coverslip prepared as described in section 4.4.1.4. The coverslips were placed in a 12-well plate and transferred to a humidified incubator at 37 °C and 5 % CO_2 and incubated for 24 h. The plates containing the adherent monolayer cells (seeded on the coverslips) were removed from the incubator and washed twice with 1 ml/well pre-warmed PBS (0.1 M, pH7.4) followed by addition of 1 µg/ml formulations diluted with media (R-DTX-NLC, R-GLA-DTX-NLC, R-ALA-DTX-NLC and R-SA43-DTX-NLC), and incubated for 2 and 4 h, respectively. The media containing the formulations were aspirated from each well and washed three times with PBS to remove the NLCs that had not been taken up by the cells. Cells were then fixed by adding 1 ml of 4% paraformaldehyde (PFD) diluted with PBS (1:4 ratio, v/v) and then the plates were incubated at room temperature for 20 min. The PFD was removed, and each well was washed three times with PBS. Finally, mounting medium containing DAPI was used to stain the nucleus by placing one drop of mounting medium containing DAPI on the microscope slide and the coverslips containing the cells were placed facing down on the slide. The slides were sealed with transparent nail polish and stored at 4 °C in a slide box for up to 12 h. Images were captured with the Zeiss fluorescence microscope in a 63x magnification with an oil lens.

4.4.9. Quantitative uptake study

The quantitative uptake studies were performed on U87MG, SVG P12, and BTNW911 monolayer cell lines. Additionally, U87MG spheroids were evaluated for NLCs uptake. The flow cytometer was used to carry out these experiments. Formulations were labelled with R123 (R-DTX-NLC, R-GLA-DTX-NLC, R-ALA-DTX-NLC and R-SA43-DTX-NLC) as described in chapter three section 3.4.1. After a series of optimisations steps, the cell density was adjusted in this study to give no more than 500 cells/1 µl during the analysis. The acquired events were ranged from 5000-10000 events, in a medium flow rate for each sample. All samples were placed in a V-shaped, non-tissue culture 96 well plate. Non treated cells were used as a control:

4.4.9.1. Time-dependent uptake

The U87MG and SVG P12 were seeded in a 12 well tissue culture plate once they reached a confluencey of 75-80%. The seeding densities were optimised through several steps and a final density of 150000/1 ml/well and 180000/1 ml/well, respectively, it was used during this experiment. The plates were incubated for 24 h in a humidified incubator at 37 °C and 5 % CO_2 then media was aspirated and replaced with 1 µg/ml of each of the formulation (R-DTX-NLC, R-GLA-DTX-NLC, and R-ALA-DTX-NLC) diluted with media and the plates were placed back in the incubator for a time-dependent course study (0.5, 1, 2,4, 6, and 24 h). Following each designated time point the plates were removed from the incubator, and the formulation diluted with media was aspirated gently then each well was washed three times with 1 ml sterile PBS, and then cells were detached by adding 0.5 ml trypsin and placed back into the incubator. After the trypsinisation step, 0.5 ml media was added to each well, and the cell suspension was placed in a centrifuge tube and centrifuged at 179 x g for 5 min. The supernatant was removed, and the cell pellet resuspended with 0.3 ice-cold PBS. Each sample was placed in a V-shaped, non-tissue culture 96 well plates then a 30 µl of PI (50 µg/ml stock) was added prior to the analysis and each plate was placed in the flow cytometer, the same settings described in section 4.4.9. were followed. Data were expressed by plotting mean fluorescence intensity versus time.

For the BTNW911 cells, a seeding density of 180000/1m/well was used during uptake study, and one-time point 6 h was chosen to evaluate labelled formulation with 1 µg/ml R123 (R-DTX-NLC, R-GLA-DTX-NLC, R-ALA-DTX-NLC and R-SA43-DTX-NLC) and the same protocol as described above was followed.

4.4.9.2. Concentration-dependent uptake

Concentration-dependent uptake of R-DTX-NLC, R-GLA-DTX-NLC, R-ALA-DTX-NLC and R-SA43-DTX-NLC by U87MG and SVG P12 cells was assessed at four concentrations 1, 2, 3, and 5 µg/ml at 6 h following the protocol described in section 4.4.9.1.

4.4.9.3. 3D tumour spheroids uptake

Spheroids uptake analysis was performed by adopting and modifying a protocol proposed by Garanti *et al.,* (2016). On the fourth day, after the spheroids were formed properly as described in section 4.4.6, spheroids were treated with 200 µg/ 200 µl of the labelled formulations (R-DTX-NLC, R-GLA-DTX-NLC, R-ALA-DTX-NLC and R-SA43-DTX-NLC) and incubated for 6 h. Following the incubation period, the spheroids were harvested and placed in a 15 ml centrifuge tube and washed three times with 1 ml sterile PBS, then 0.75 ml of AccuMax® cell dissociation solution was added to the tubes and incubated at 37 °C for 30 min, to allow proper dissociation of the spheroids. All tubes were then centrifuged for 5 min at 179 x g and the cells resuspended in 0.3 ml ice-cold PBS and spheroids uptake was performed following the same protocol described in section 4.4.9.1.

4.4.10. Quantitative and qualitative endocytosis pathways analysis

Following the similar protocol mentioned in section 4.4.9.1. for seeding density and analysis U87MG and SVG P12 were exposed to different endocytosis inhibitors diluted with media as follows: 4˚ C used for energy-dependent endocytosis, 0.45 M sucrose used for clathrin pathway, 5 µg/ml cytochalasin B used for micropinocytosis/phagocytosis, and 5 µg/ml nystatin used caveolae/ lipid rafts pathway for 90 min. Media containing endocytic inhibitors was removed and replaced with 1 µg/ml R123-labelled formulations (R-DTX-NLC, R-GLA-DTX-NLC, R-ALA-DTX-NLC and R-SA43-DTX-NLC) diluted with media plus the three mentioned inhibitors and then incubated for a further 4 h except for samples stored at the 4˚ C. This method was adopted and modified from Doherty and McMahon (2009) and Sahay *et al.,* (2010). Samples were then prepared and analysed for internalisation and selective uptake as described in section 4.4.8. and 4.4.9. respectively.

4.4.11. Cell cycle analysis

U87MG cell cycle analyses were performed by propidium iodide (PI) staining to evaluate the DTX, DTX-NLC, GLA-DTX-NLC, ALA-DTX-NLC, and SA43-DTX-NLC effect on U87MG cell cycle. Following the optimisation process, the cells were seeded at a density 50000/well in sterile 12 well tissue culture plates, then placed in a humidified incubator at 37 °C and 5 % CO_2 for 24 h. Media was aspirated from each well and 1 ml of each sample diluted with media were placed in the well. The plates were then incubated for 24 h with the treatments in a humidified incubator at 37 °C and 5 % CO_2. Following the treatment period, the wells were washed with 1 ml PBS and detached with 0.5 ml trypsin, then incubated in a humidified incubator. The trypsin was neutralised with 0.5 ml media and the cell suspension was collected from each well and placed in a 15 ml centrifuge tube, and centrifuged at 179 x g for 5 min. The supernatant was removed and the cell pellets were resuspended and fixed by adding 6 ml of ice-cold 70% ethanol (diluted with PBS) dropwise, whilst vortexing to prevent clumping. Then the tubes were stored at -20^{o}C for at least at least 24 h. Following the storage period, the fixed samples were centrifuged at 179 x g for 5 min and washed once by adding 1 ml of ice-cold PBS to each tube, then centrifuged again at 179 x g for 5 min. The fixed cells were resuspended in 0.35 ml PBS and a 0.225 ml of the fixed cell suspension was transferred to a non-tissue culture 96 well plate/ V-shaped, then 22.5 µl of PI concentration (500µg/ml stock) was added to each well followed by 2.5 µl of RNAase (10 mg/ml stock) and incubated for 2 h at 37° C and 5 % CO_2. All plates were processed by using flow cytometry and Guava software for data analysis to determine DNA content by fluorescence intensity (488 nm) for each treated population.

4.4.12. Statistical data analysis

The statistical analysis was performed using the Kolmornov-Smirnov test for normality followed by ANOVA (with post-hoc analysis Tukey and Dunnett test) and independent-samples T test (SPSS, IBM software). The analysis of variance was statistically significant difference when (*) $P < 0.05$ (95% confidence), (**) $P < 0.001$ (99% confidence), and (***) $P < 0.000$. The data are presented as the mean ± standard deviation for N=3 experiments in triplicate (n=9).

4.5. Results and discussion

4.5.1. Cell line growth kinetics

To study the growth behaviour of SVG P12, U87MG, and BTNW911, cells were seeded and counted with respect to time, to establish the lag phase, log (exponential) phase and a plateau phase. This experiment was done using Presto Blue dye® for determining the cells number. The exponential phase is where the cell undergoes mitosis and multiply exponentially (Mather and Roberts 1998).

It is essential to study the cell behaviour in the exponential phase (Mather and Roberts 1998) since data from the exponential phase will give an indication when the cells should be treated with the drug of interest. In our case cells were seeded in 2500 cell/90 µl/ well for both U87MG and SVG P12 and 5000 cells/ 90 µl/well for BTNW911 cell lines to ensure that cells were in exponential phase within 24 h of seeding, as this was when drug treatment would commence. Cells were then treated with DTX, B-NLC, DTX-NLC, GLA-DTX-NLC, ALA-DTX-NLC and SA43-DTX-NLC during the course of the *in-vitro* evaluation. For the analysis of growth kinetics, when cells were seeded at less than 2500 cells/ 90 µl/ well, the lag phase lasted until day 3 (Appendix II). To ensure that cells were in the exponential growth phase within 24 h of seeding, as required for the DTX-NLCs treatment experiments, seeding densities of 2500 cells/ 90µl/ well were chosen for U87MG (Appendix II), SVG P12 (Appendix II) and 5000 cells/ 90µl/ well for BTNW 911 (Appendix II), which had slower growth kinetics. The double time for U87MG and SVG P12 was found to be approximately 45 h and 50 h respectively, which is in rough agreement with commercial specifications and previous reports (Aptekar *et al.,* 2015). A slightly slower doubling time of 55 h for BTNW911 was as expected for a short-term primary derived culture (Kumar *et al.,* 2014).

Additionally, the morphology of U87MG, SVG P12, and BTNW911 were observed under a light microscope during the study of growth patterns at 10 X magnification as shown in figures 4.2 a, b, and c respectively after 3 days of incubation. The data showed that U87MG and SVG P12 cell lines were more confluent than BTNW911 as primary cell lines take a longer time to grow in comparison with immortalised cell lines.

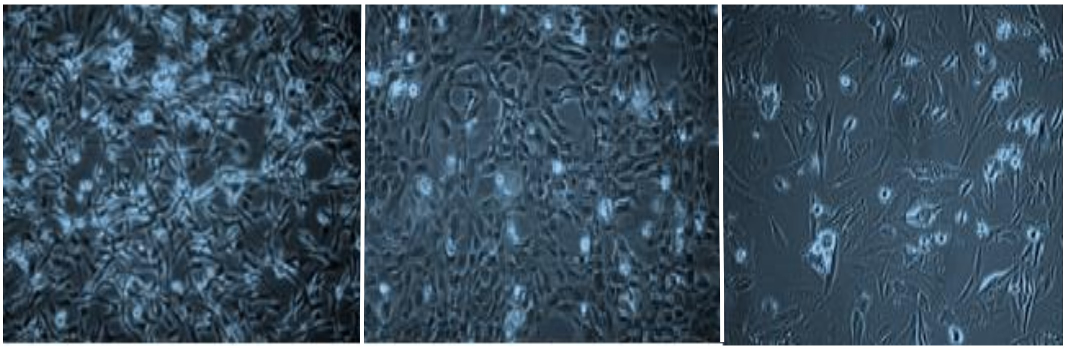
(a) (b) (c)

Figure 4.2 Images of monolayer cell lines under the microscope (a) U87MG cell line; (b) SVG P12 cell line, (c) Primary BTNW911 cell line.

4.5.2. Cell proliferation evaluation

Cell proliferation following treatment with DTX, B-NLC, DTX-NLC, GLA-DTX-NLC, ALA-DTX-NLC and SA43-DTX-NLC was studied in U87MG, SVG P12, and BTNW911 cells. The data for the IC_{50} values are listed in tables 4.1, 4.2, 4.3, 4.4, 4.5, and 4.6. In all cases, the potency of DTX-NLCs and surface modified DTX-NLCs treatments were compared to the potency of standard treatment docetaxel alone.

4.5.2.1. Cell proliferation after treatment with docetaxel-loaded nanostructured lipid carriers

DTX-NLC verses DTX

DTX-NLC showed significantly higher IC_{50} values in U87MG than DTX, at 24 and 48 h incubation time (Figure 4.3 and Table 4.1). No significant difference in IC_{50} between DTX-NLC and DTX alone was observed at 72 h which suggested that DTX-NLC was as cytotoxic as DTX alone, but there was a time-dependent delay to reach this equivalent effect, that might be attributed to the slow release of DTX from DTX-NLC at initial time in physiological pH7.4 as previously determined in Chapter three (section 3.5.10.2) where DTX-NLC released only 16 % of DTX at 8 h in comparison to the DTX solution which demonstrated 30 % release under the same conditions. Additionally, the DTX-NLC PS might lead to increasing the distance between the surface and the lipid core of the NLCs as previously reported by Xu *et al.,* (2009), since DTX is encapsulated within the NLCs, hence taking longer time for the DTX to be released from the NLCs lipid core.

A similar pattern of time-dependent toxicity effect was observed for the same treatments in SVG P12 (Figure 4.4) and BTNW 911 cells (Figure 4.5). The DTX-NLC had less toxicity towards SVG P12 at 24 and 48 h incubation when compared to the DTX on SVG P12 at similar incubation times. No significant difference was encountered at 72 h incubation of DTX-NLC with the SVG P12 cells (Figure 4.4), that signified that early time points of incubation were less toxic to the non-cancerous cells.

Our data demonstrated more efficacy towards U87MG cell line with lower IC_{50} value (24.37 ±0.74 ng/ml), and showed 33 folds reduction in IC_{50} at 48 h incubation with the treatment in comparison to previous literature reported by Singh *et al.,* (2015) where their DTX-SLN gave an IC_{50} value of (0.792 ±0.03 µg/ml) when incubated for 48 h with U87MG cell lines. These results indicate the potential use of DTX-NLC in glioblastoma therapy; encapsulating DTX within the NLCs might also be beneficial for avoidance or reduced direct interaction with the blood cells and consequently decrease the DTX haematological toxicity (Feng and Mumper, 2013).

Table 4.1 mean IC_{50} values for DTX, DTX-NLC, and B-NLC, in U87MG, SVG P12, and BTNW911 cell line at 24, 48, and 72 h. Data mean values ±SD, (N=3), and * $p < 0.05$, ** $p < 0.001$ and *** $p < 0.000$ refers to the significant difference when all formulations compared to the standard treatment DTX.

Cell line	**Time (h)**	**IC_{50} Values (ng/ml)**		
		DTX	**DTX-NLC**	**B-NLC**
U87MG	24	7.22 ±0.84	32.44 *** ±2.72	316.22 *** ± 4.65
U87MG	48	5.44 ±3.94	24.37 *** ±0.74	398.1 *** ± 6.87
U87MG	72	1.80 ±0.01	3.17 ±0.36	N/A
SVG P12	24	2.07 ±0.46	23.04 *** ±6.42	N/A
SVG P12	48	2.55 ±0.58	7.10 *** ±0.82	N/A
SVG P12	72	0.22 ±0.10	1.80 ±1.18	N/A
BTNW911	24	95.16 ±4.95	N/A	N/A
BTNW911	48	10.05 ±0.32	62.71 *** ±2.15	N/A
BTNW911	72	1.77 ±0.64	25.18 *** ±0.24	N/A

Duration of incubation

When comparing the effect of duration of incubation of DTX and DTX-NLC treatments on IC_{50}, in all cases (except SVG P12, 48 h when treated with DTX), the IC_{50} values decreased with time indicating that a longer incubation resulted in greater cytotoxic effect.

B-NLC

Above a certain concentration, the blank nanostructured lipid carrier was found to cause a significant decrease in cell proliferation as compared to the non-drug treated control cells which occurred at 0.012 % for 24 h and 0.12 % for 48 h incubation. When the original nanoparticle stock solution was diluted with media up to 99.98 and 99.88 %, respectively for U87MG cells treated with B-NLC, and all tested B-NLC concentrations were considered safe at 72 h incubation. Similarly, SVG P12 and BYNW911 demonstrated the notable effect at 24 h incubation (0.012 %) and both 48 and 72 h incubation with B-NLC were considered fairly safe for all examined concentrations. This information enabled us to ensure that all nanoparticle suspensions need to be diluted at least with 99.98 % media to ensure that all cell proliferation changes were related to the release of docetaxel, and since further dilution of DTX-NLC more than 99.98 % was reducing the cell proliferation, so this effect was considered due to DTX present in the NLCs and not due to B-NLC excipients.

The B-NLC showed a highly significant increase in IC_{50} values when compared to the DTX IC_{50} values at similar incubation times towards U87MG cell line at all time points, and undetectable cell toxicity when SVG P12 and BTNW911 cell lines were treated with B-NLC within the studied concentrations, indicating the empty nanostructured lipid carrier had significantly less cytotoxicity (high cell proliferation) compared to the DTX treatment alone.

SVG P12 verses U87MG/ BTNW 911

To assess the IC_{50} values between U87MG or BTNW911 and SVG P12 of DTX and DTX-NLC at 72 h revealed that significant increase in IC_{50} of BTNW911 in comparison to IC_{50} values of SVG P12 when both cell lines treated with DTX at 72 h ($p < 0.05$), and no significant effect in IC_{50} (potency) in U87MG cells compared to SVG P12 cells when treated with DTX at 72 h. Similarly, no significant difference in IC_{50} of U87MG and BTNW911 cell lines was observed. Interestingly, there seemed to be less efficient (2.1 % difference) in the short-term primary derived cultures (BTNW911) as compared to the U87MG cells, indicating that there are differences in the cell models that warrant further investigation. Additionally, a significant increase in IC_{50} value at 72 h incubation with DTX-NLC in comparison to the IC_{50} values of SVG P12 and U87MG cell lines ($p < 0.001$) was observed, suggesting more resistance to treatment in case of patient-derived cells BTNW911. A higher concentration or longer incubation time of DTX-NLC might be worth to try. An equal potency of DTX-NLC was observed towards both U87MG and SVG P12 due to no significant difference in IC_{50} value at 72 h incubation (Table 4.1).

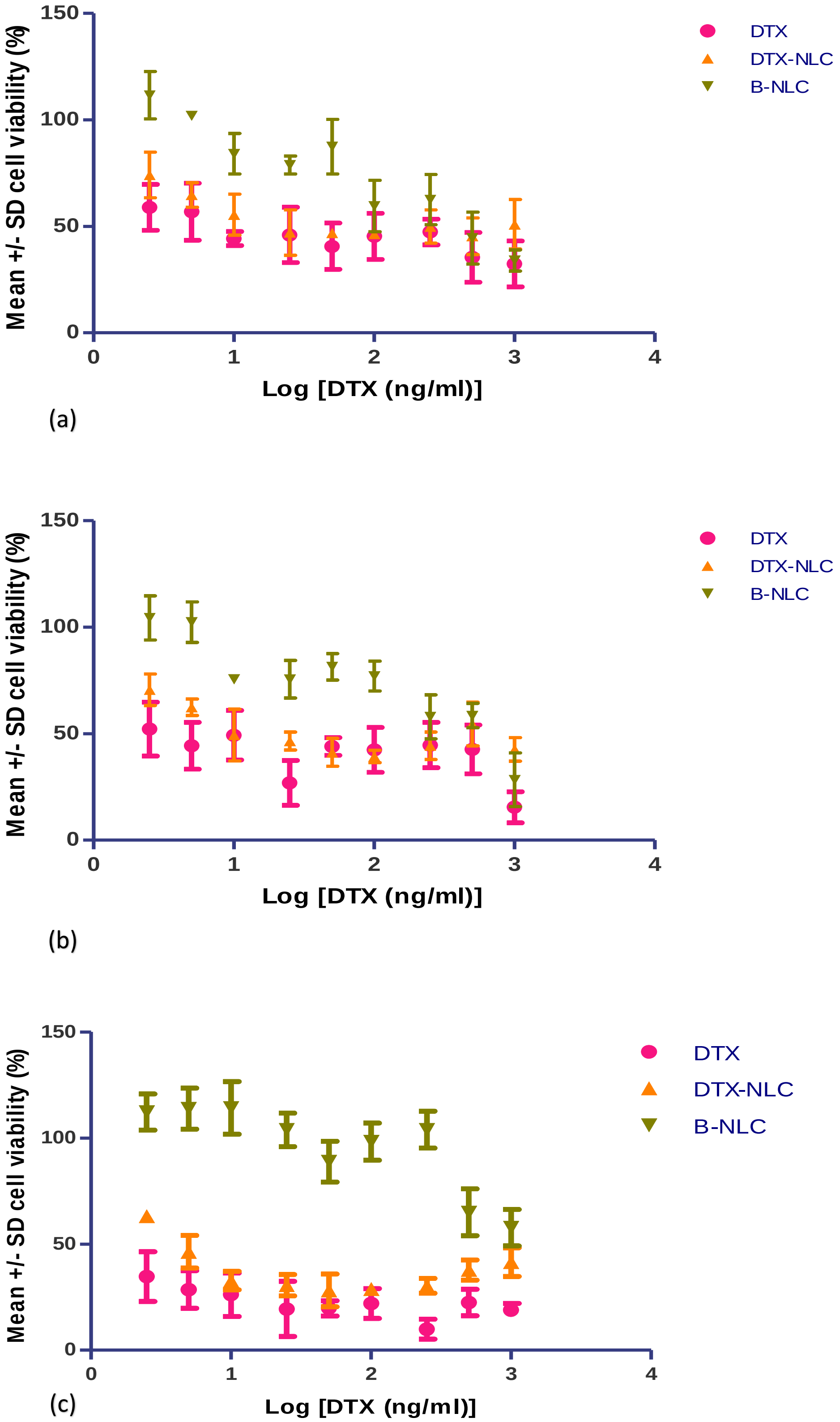

Figure 4.3 Mean percentage cell viability relative to control cells with no drug treatment for DTX, DTX-NLC, and B-NLC when incubated with U87MG cell line at (a) 24, (b) 48, and (c) 72 h. Data mean values ±SD, (N=3), and all formulations were compared to standard treatment docetaxel alone.

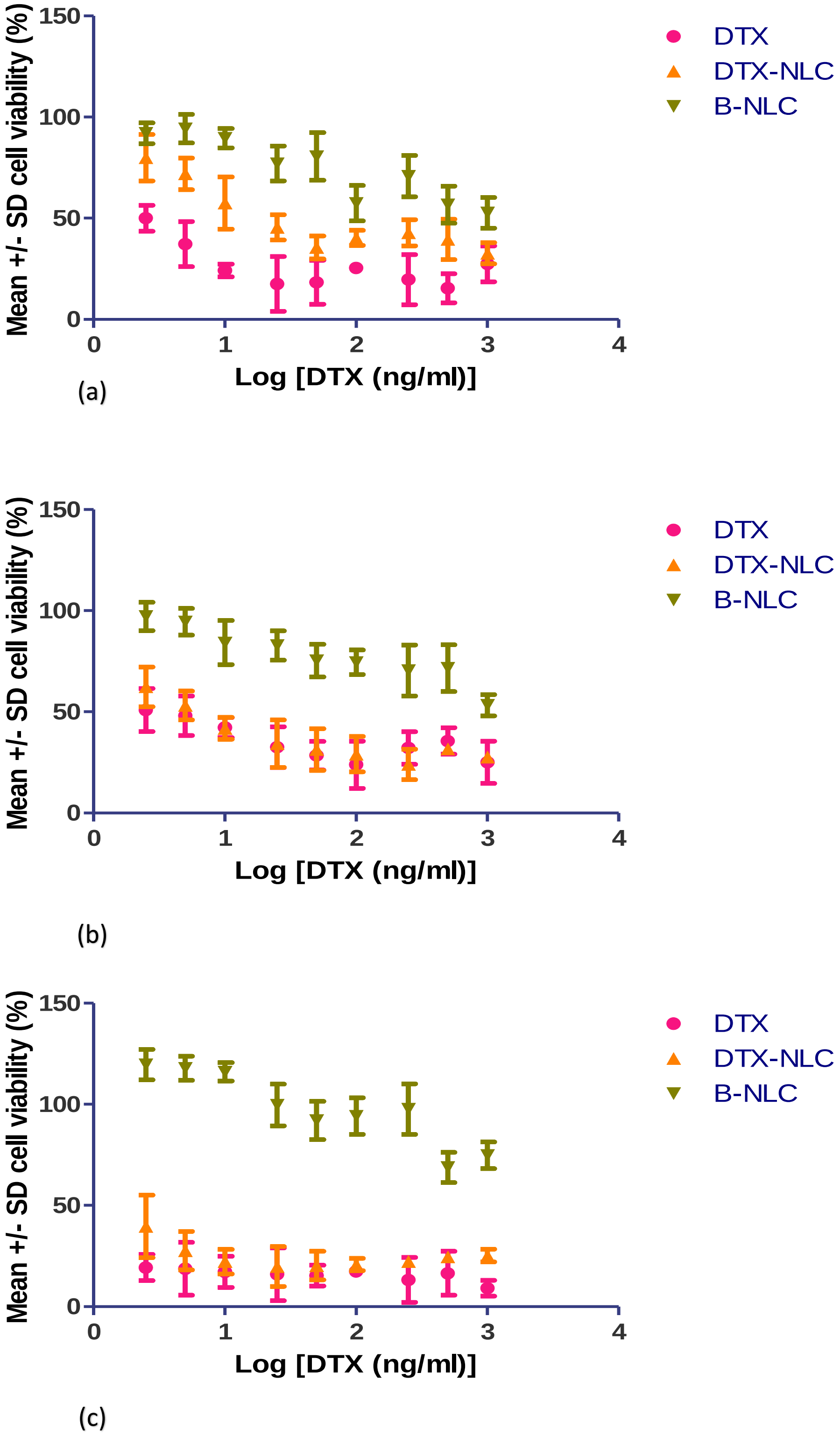

Figure 4.4 Mean percentage cell viability for DTX, DTX-NLC, and B-NLC when incubated with SVG P12 cell line at (a) 24, (b) 48, and (c) 72 h. Data mean values ±SD, (N=3), and all formulations were compared to standard treatment docetaxel alone.

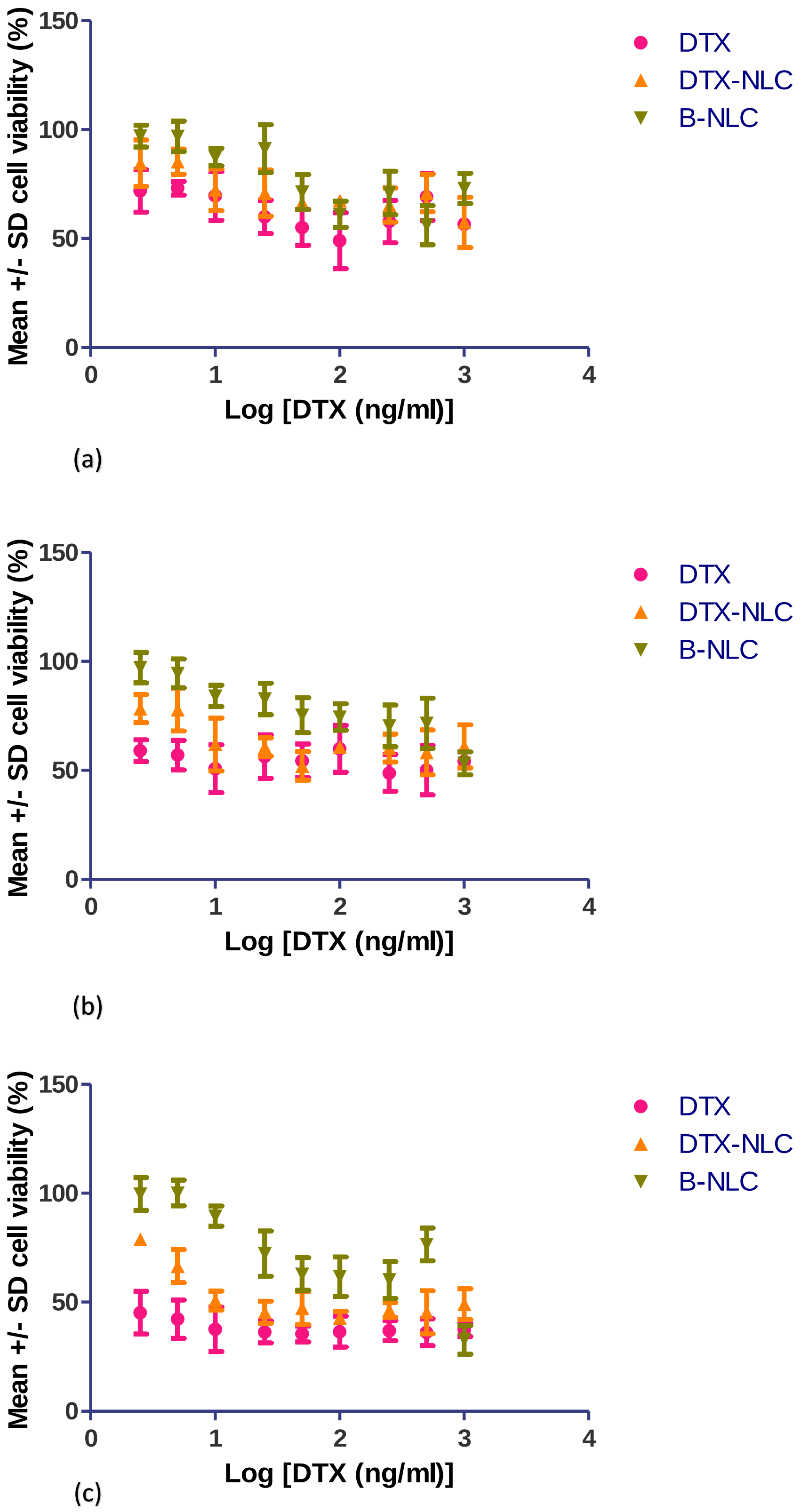

Figure 4.5 Mean percentage cell viability for DTX, DTX-NLC, and B-NLC when incubated with BTNW911 cell line at (a) 24, (b) 48, and (c) 72 h. Data mean values ±SD, (N=3), and all formulations were compared to standard treatment docetaxel alone.

4.5.2.2. Cell proliferation after treatment with PUFAs tagged docetaxel-loaded nanostructured lipid carriers

DTX-NLC was prepared with presence and absence of antioxidant combination (Vit E and AP) to preserve the surface modified DTX-NLC with PUFAs (GLA-DTX-NLC and ALA-DTX-NLC) from oxidation and to evaluate the effect of the presence of antioxidants in the formulation on cell proliferation. GLA-DTX-NLC and ALA-DTX-NLC with variable ratios of GLA and ALA were evaluated.

4.5.2.2.1. Cell proliferation after treatment with nanostructured lipid carriers composed of antioxidants and surface modified with PUFAs

DTX-NLCs were first evaluated for their effect on cell proliferation prior to the surface modification with PUFAs.

DTX-NLC with and without antioxidants verses DTX

A delayed effect on cell proliferation was noted when DTX-NLC were prepared with antioxidants on both U87MG and SVG P12 cells (Table 4.2) especially at initial incubation time in comparison to DTX and DTX-NLC (without antioxidants). No IC_{50} values could be determined at 24 h incubation, and a highly significant increase in IC_{50} at 48 h followed by similar potency to DTX at 72 h incubation was observed for, DTX-NLC (with antioxidants) indicating that the formulations with antioxidants might exhibit longer time to release DTX, and the antioxidants acted as a barrier that caused a delayed effect on cell proliferation. Similar behaviour was observed with SVG P12 cells treatment (Table 4.2).

Table 4.2 Mean IC_{50} values for DTX and DTX-NLC (prepared with and without antioxidants combination) in U87MG and SVG P12 following 24, 48, and 72 h incubations. Data mean values ±SD, (N=3). * $p < 0.05$ and *** $p < 0.000$ refers to the significant difference when all formulations compared to the standard treatment DTX.

Cell lines	**Time (h)**	**IC_{50} Values (ng/ml)**		
		DTX	**DTX-NLC With antioxidants**	**DTX-NLC Without antioxidants**
U87MG	24	7.22 ±0.84	N/A	32.44 *** ±2.72
U87MG	48	5.44 ±3.94	39.80 *** ±0.30	24.37 *** ±0.74
U87MG	72	1.80 ±0.01	3.41 ±0.49	3.17 ±0.36
SVG P12	24	2.07 ±0.46	99.95 ±0.07	23.04 *** ±6.42
SVG P12	48	2.55 ±0.58	3.68 ±0.45	7.10 *** ±0.82
SVG P12	72	0.22 ±0.10	3.35 ±0.54	1.80 ±1.18

GLA-DTX-NLCs verses DTX

Two ratios of GLA (1:1/5 and 1:1/6, FAG: GLA) were used to prepare GLA-DTX-NLCs (DTX-NLCs were prepared with antioxidants prior to surface modification). Table 4.3 summarises the effect of the IC$_{50}$ values. Both GLA-DTX-NLCs displayed a time-dependent increase in toxicity towards U87MG, with low potency towards U87MG (high IC$_{50}$) observed at 24 h incubation in comparison to DTX, followed by similar cytotoxicity effect for both ratios as the DTX effect at 48 and 72 h incubation. It is worth noting that GLA-DTX-NLC displayed more potency than DTX-NLC at 24 and 48 h incubation as indicated by low IC$_{50}$ values (Tables 4.2 and 4.3). GLA has been previously reported for its tumoricidal effect towards U87MG cell lines (Leaver *et al.,* 2002b). It was reported by Das (2004) that antioxidants especially Vit E might block the tumoricidal effect of the PUFAs (GLA and ALA) as it functions as a lipid peroxidase inhibitor (blocking the PUFAs mechanisms of action), and consequently decrease the inhibitory effect of the PUFAs *in-vitro* (Das 2004; Menendez *et al.,* 2001). Thus, similar ratios of GLA-DTX-NLCs were examined towards U87MG and SVG P12 when DTX-NLCs were not incorporated with antioxidants (section 4.5.2.2.2).

Table 4.3 Mean IC$_{50}$ values for formulations prepared with antioxidants combination GLA-DTX-NLC (1:1/5), GLA-DTX-NLC (1:1/6), ALA-DTX-NLC (1:1/5), and ALA-DTX-NLC (1:1/6) in U87MG following 24, 48, and 72 h incubations. Data mean values ±SD, (N=3). * $p < 0.05$ and *** $p < 0.000$ refers to the significant difference when all formulations compared to the standard treatment DTX.

Cell line	**Time (h)**	**IC$_{50}$ Values (ng/ml)**				
		DTX	**GLA-DTX-NLC (1:1/5)**	**GLA-DTX-NLC (1:1/6)**	**ALA-DTX-NLC (1:1/5)**	**ALA-DTX-NLC (1:1/6)**
U87MG	24	7.22 ±0.84	100.37 *** ±0.54	158 *** ±0.52	39.81 *** ±0.14	62.79 *** ±0.51
U87MG	48	5.44 ±3.94	8.33 ±3.81	7.94 ±0.17	9.77 ±0.48	24.86 *** ±0.54
U87MG	72	1.80 ±0.01	3.88 ±2.21	1.25 ±0.48	2.51 ±0.12	3.38 ±0.52

ALA-DTX-NLC verses DTX

Like GLA, ALA was studied in two ratios (1:1/5 and 1:1/6, FAG: ALA), were used to prepare ALA-DTX-NLCs (DTX-NLCs were prepared with antioxidants prior to surface modification). A higher ratio of FAG: ALA (1:1/5) in the ALA-DTX-NLC exhibited a similar effect on U87MG proliferation as the DTX at 48 and 72 h, while lower ratio demonstrated a delayed effect (Table 4.3). That could be either due to the presence of antioxidants in the DTX-NLC (prior to surface modification) or due to ligand density. Previous reports have shown that an intermediate ligand density provided a statistically significant improvement in cell binding in comparison with higher and lower ligand densities in nanoparticles (Elias *et al.,* 2013). Overall, it was decided not to continue with the fabrication of DTX-NLCs in the presence of antioxidants for PUFAs functionalisation and rather carry out the process in the environment of nitrogen, as the presence of antioxidants increased the IC_{50} values

4.5.2.2.2. Cell proliferation after treatment with nanostructured lipid carriers composed of variable ratios of PUFAs

DTX-NLCs were prepared and surface modified with variable ratios of PUFAs (GLA and ALA). No antioxidants were used, instead, the entire process of surface functionalisation was carried out under a nitrogen environment to protect GLA-DTX-NLC and ALA-DTX-NLC from oxidation and their effect on cell proliferation was evaluated.

GLA-DTX-NLC verses DTX

The GLA-DTX-NLC with high ligand density (1:1/5 FAG: GLA ratio) demonstrated good efficacy with low cell proliferation of U87MG cells as indicated by similar IC_{50} values to DTX alone at all time points (Figure 4.6 and Table 4.4). Low ligand density GLA-DTX-NLC (1:1/6 FAG: GLA ratio) exhibited a significant increase in IC_{50} at 24 h incubation, followed by similar activity as DTX and GLA-DTX-NLC (1:1/5 FAG: GLA ratio) at 48 and 72 h incubation (Table 4.4). Lower cell toxicity was observed against the SVG P12 at 24 and 48 h incubation when the data was compared with the DTX at similar time points (Figure 4.7) as revealed by significant increase in IC_{50} values at incubation time of 24 and 48 h, while no significant effect could be seen at 72 h incubation time when data were compared with the DTX IC_{50} values at similar incubation time points. Notably lower ligand density (1:1/6 FAG: GLA ratio) of GLA-DTX-NLC demonstrated low activity towards SVG P12 owing to the significant increase in IC_{50} values at all time point when compared with DTX alone (Table 4.4). This is in line with previous reports which have shown that PUFAs have a limited effect on normal cells and high cytotoxicity towards cancerous cell lines (Horia and Watkins 2005). High ligand concentration can lead to efficient binding to the target because of high avidity (Cao *et al.,* 2018; Elias *et al.,* 2013). Therefore, GLA-DTX-NLC with high ligand density (1:1/5 FAG: GLA ratio) which has not only displayed good activity but also has low PS and fairly uniform particle size distribution (Section 3.5.6.1) was further evaluated with patient-derived cells BTNW911.

Table 4.4 Mean IC_{50} values for GLA-DTX-NLC (1:1/5), GLA-DTX-NLC (1:1/6), ALA-DTX-NLC (1:1/5), and ALA-DTX-NLC (1:1/6) in U87MG and SVG P12 following 24, 48, and 72 h incubations. Data mean values ±SD, (N=3). * $p < 0.05$ and *** $p < 0.000$ refers to the significant difference when all formulations compared to the standard treatment DTX.

Cell line	**Time (h)**	**IC_{50} Values (ng/ml)**				
		DTX	**GLA-DTX-NLC (1:1/5)**	**GLA-DTX-NLC (1:1/6)**	**ALA-DTX-NLC (1:1/5)**	**ALA-DTX-NLC (1:1/6)**
U87MG	24	7.22 ±0.84	5.46 ±0.93	10 * ±0.13	19.95 ** ±0.55	11.59 ±1.39
U87MG	48	5.44 ±3.94	4.5 ±0.57	4.46 ±0.43	10.23 ±1.54	2.85 ±0.32
U87MG	72	1.80 ±0.01	3.06 ±0.52	3.54 ±0.65	6.30 ** ±0.43	2.58 ±0.19
SVG P12	24	2.07 ±0.46	11.82 * ±1.58	39.81*** ±2.54	79.43 *** ±4.34	10.56 * ±1.79
SVG P12	48	2.55 ±0.58	5.13 * ±0.43	12.58 ** ±1.67	3.16 ±1.23	3.17 ±0.36
SVG P12	72	0.22 ±0.10	1.85 ±0.77	6.30 ** ±0.98	1.41 ** ±0.76	1.12 ±0.12

ALA-DTX-NLC verses DTX

It was interesting to note that IC_{50} values for ALA-DTX-NLC (1:1/6 FAG: ALA ratio) demonstrated no significant difference from DTX IC_{50} values when incubated at 24, 48, and 72 h, respectively (Figure 4.6). This suggested that low ligand density in case of ALA-DTX-NLC was as effective as the DTX treatment alone in toxicity towards U87MG cells and the data did not seem to exhibit a time-dependent effect on the cytotoxicity. It has been reported earlier by Elias *et al.,* (2013) that high ligand density does not always mean high binding to cells, thus it was important to evaluate variable ligand ratios. ALA-DTX-NLC (1:1/5 FAG: ALA ratio) exhibited less toxicity towards U87MG and SVP12 at 24 and 72 h of incubation (Table 4.4). In case of SVG P12, ALA-DTX-NLC (1:1/6 FAG: ALA ratio) was as effective as DTX alone (no significant difference in IC_{50}) at 48 h and 72 h (Figure 4.7). Meanwhile, ALA-DTX-NLC (1:1/6 FAG: ALA ratio) showed a significant increase in IC_{50} value at 24 h when the SVG P12 cells were treated in comparison to the IC_{50} value of DTX at the same time point (Figure 4.7). This indicates the less favourable effect of the conjugation of ALA with DTX-NLC due to increased toxicity of ALA-DTX-NLC (1:1/6 FAG: ALA ratio) towards non-cancerous cells as demonstrated at 48 and 72 h of incubation with the treatment (Figure 4.7). Therefore, ALA-DTX-NLC (1:1/6 FAG: ALA ratio) was chosen for the further test with patient-derived cell line BTNW911 as it exhibited higher efficacy against U87MG cells and demonstrated a low PS and fairly uniform particles distribution (Section 3.5.6.2).

BTNW911 versus GLA-DTX-NLC/ ALA-DTX-NLC

For BTNW 911 cells, the ALA-DTX-NLC (1:1/6) was significantly more cytotoxic than DTX at 24 h and 48 h (significantly lower IC_{50}), but at 72 h DTX was more effective (Figure 4.8 and Table 4.5). To our knowledge, the ALA surface modified NPs had not been tested before for the treatment of glioblastoma cells. ALA conjugated with Doxorubicin (DOX) have been reported in the literature for the treatment of breast cancer cell lines (MCF-7) by Huan *et al*., (2009), which were reported to show more cytotoxicity towards MCF-7 cells than free DOX. Interestingly GLA-DTX-NLC (1:1/5 FAG: GLA ratio) exhibited significantly lower IC_{50} than DTX alone at 24 h and similar potency as DTX at 48 h, followed by less activity towards BTNW911 cell lines at 72 h when compared with DTX alone (Table 4.5 and Figure 4.8). A delayed toxicity effect for the DTX alone, and sustained the desirable toxicity effect of both GLA-DTX-NLC and ALA-DTX-NLC was observed at all time point when treated with BTNW911 cells (Figure 4.8). This could be associated with cell resistance to some chemotherapeutic treatments. High activity of PUFAs towards BTNW911 cells might be attributed to the particular composition of PUFAs as it has been previously indicated that the certain fatty acids result in increased sensitivity to chemotherapy, especially in tumour lines that are resistant to chemotherapy, and cause high efficacy of cytotoxicity to a tumour (Horia and Watkins 2005).

In the literature, GLA has been reported to have a tumoricidal effect towards glioblastoma cells with lower toxicity towards non-cancerous cells (Das 2007; Das 2004; Bakshi *et al.,* 2003), it was interesting for us to see similar results when GLA was conjugated with the DTX-NLC.

Table 4.5 Mean IC_{50} values for GLA-DTX-NLC (1:1/5) and ALA-DTX-NLC (1:1/6) in BTNW911 following 24, 48, and 72 h incubations. Data mean values ±SD, (N=3). * p < 0.05 and *** p < 0.000 refers to the significant difference when all formulations compared to the standard treatment DTX.

Cell line	**Time (h)**	**IC_{50} Values (ng/ml)**		
		DTX	**GLA-DTX-NLC (1:1/5)**	**ALA-DTX-NLC (1:1/6)**
BTNW911	24	95.16 ±4.95	13.89 *** ±1.21	6.82 *** ±0.45
BTNW911	48	10.05 ±0.32	12.51 ±0.45	6.27 * ±0.28
BTNW911	72	1.77 ±0.64	10.55 *** ±0.76	5.97 *** ±0.48

Overall, GLA-DTX-NLC and ALA-DTX-NLC displayed similar activity towards U87MG at 24 h and highly significant low IC_{50} than DTX-NLC demonstrating their higher potency.

ALA-DTX-NLC demonstrated higher potency than GLA-DTX-NLC when U87MG were treated for 48 h incubation, and both formulations displayed higher activity than DTX-NLC at 48 h. However, GLA-DTX-NLC and ALA-DTX-NLC exhibited similar activity towards U8MG at 72 h, as no significant difference in IC_{50} was observed.

GLA-DTX-NLC and ALA-DTX-NLC displayed similar activity towards SVG P12 at 24 h due to no significant difference observed in IC_{50} values, though DTX-NLC demonstrated lower toxicity towards SVG P12 at 24 and 48 h. Interestingly, GLA-DTX-NLC exhibited less toxicity towards SVG P12 at 48 h than the ALA-DTX-NLC, as clearly observed by a significant increase in IC_{50} of GLA-DTX-NLC when compared to ALA-DTX-NLC. All the three formulations showed no significant effect on activity towards SVG P12 at 72 h.

For BTNW911 cell lines, ALA-DTX-NLC displayed higher activity (significantly low IC_{50}) than both DTX-NLC and GLA-DTX-NLC at all time points, and GLA-DTX-NLC exhibited more potency with significantly lower IC_{50} than DTX-NLC at all time points on treatment with BTNW911 cells.

In summary, it was obvious that surface modification with both GLA and ALA increased the potency of the DTX-NLC as observed by a decrease in IC_{50} for every incubation regardless of duration and in every cell line. Also, the cell proliferation was reduced with increasing incubation time for all treatments.

Since we obtained more potency with DTX-NLC when it was surface modified with PUFAs, therefore GLA-DTX-NLC (1:1/5 FAG: GLA ratio) and ALA-DTX-NLC (1:1/6 FAG: ALA ratio) were chosen for more detailed study for cellular internalisation, selective uptake, endocytosis pathway study and cell cycle analysis, to further investigate the effect of conjugation of DTX-NLC with GLA and ALA as ligands.

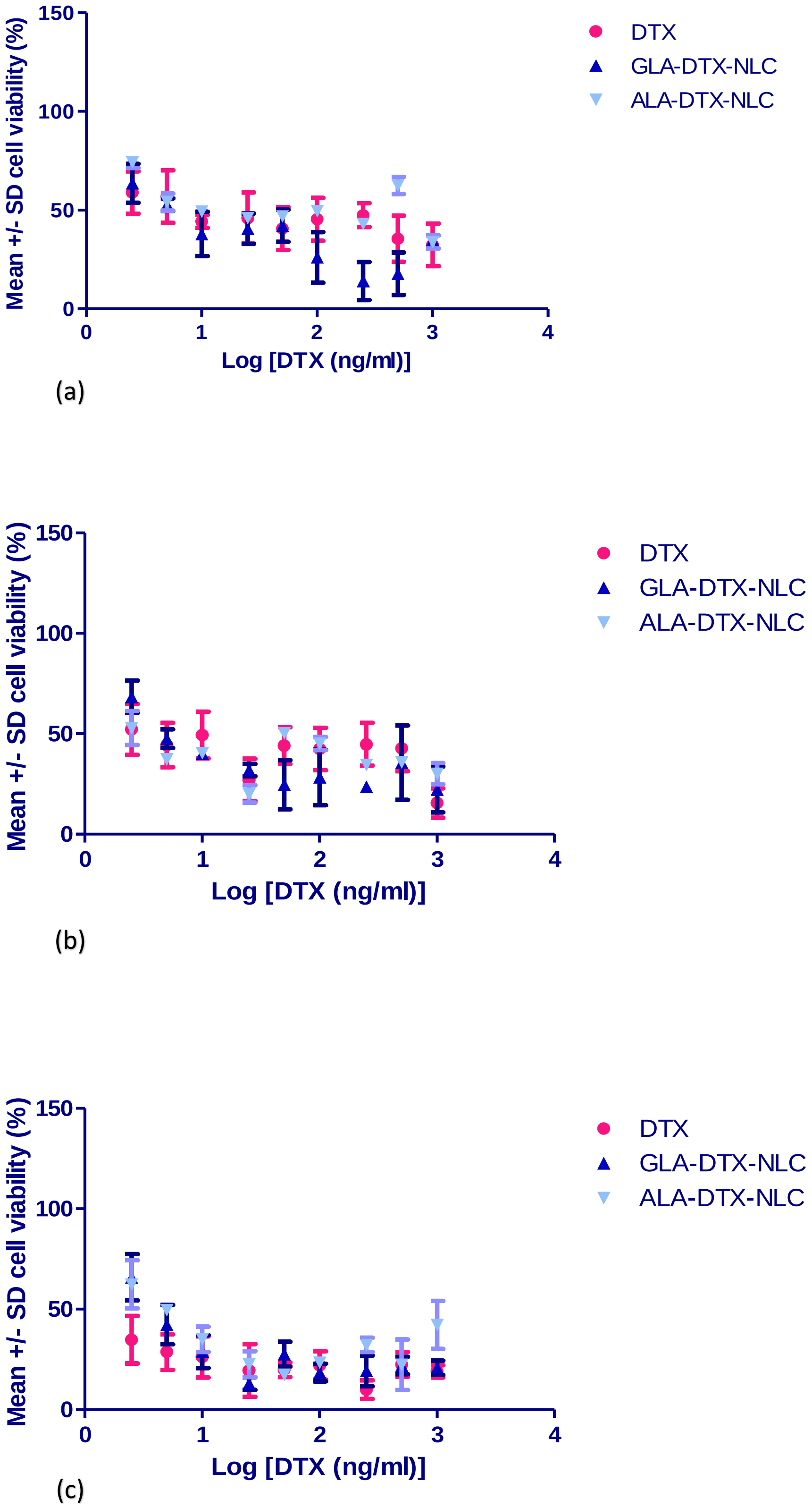

Figure 4.6 Mean percentage cell viability for DTX, GLA-DTX-NLC, and ALA-DTX-NLC when incubated with U87MG cell line at (a) 24, (b) 48, and (c) 72 h. Data mean values ±SD, (N=3), and all formulations were compared to standard treatment docetaxel alone.

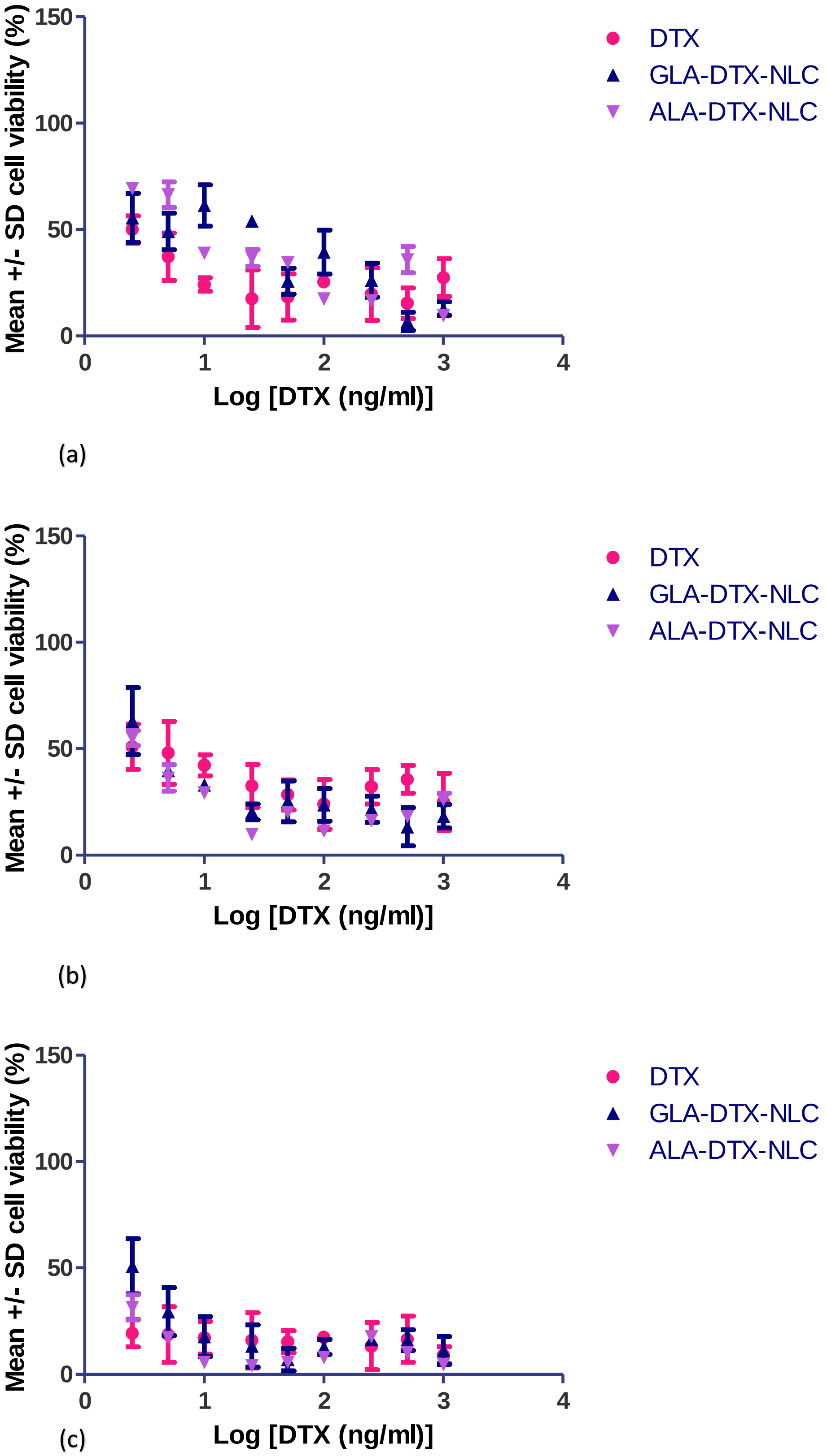

(a)

(b)

(c)

Figure 4.7 Mean percentage cell viability for DTX, GLA-DTX-NLC, and ALA-DTX-NLC when incubated with SVG P12 cell line at (a) 24, (b) 48, and (c) 72 h. Data mean values ±SD, (N=3), and all formulations were compared to standard treatment docetaxel alone.

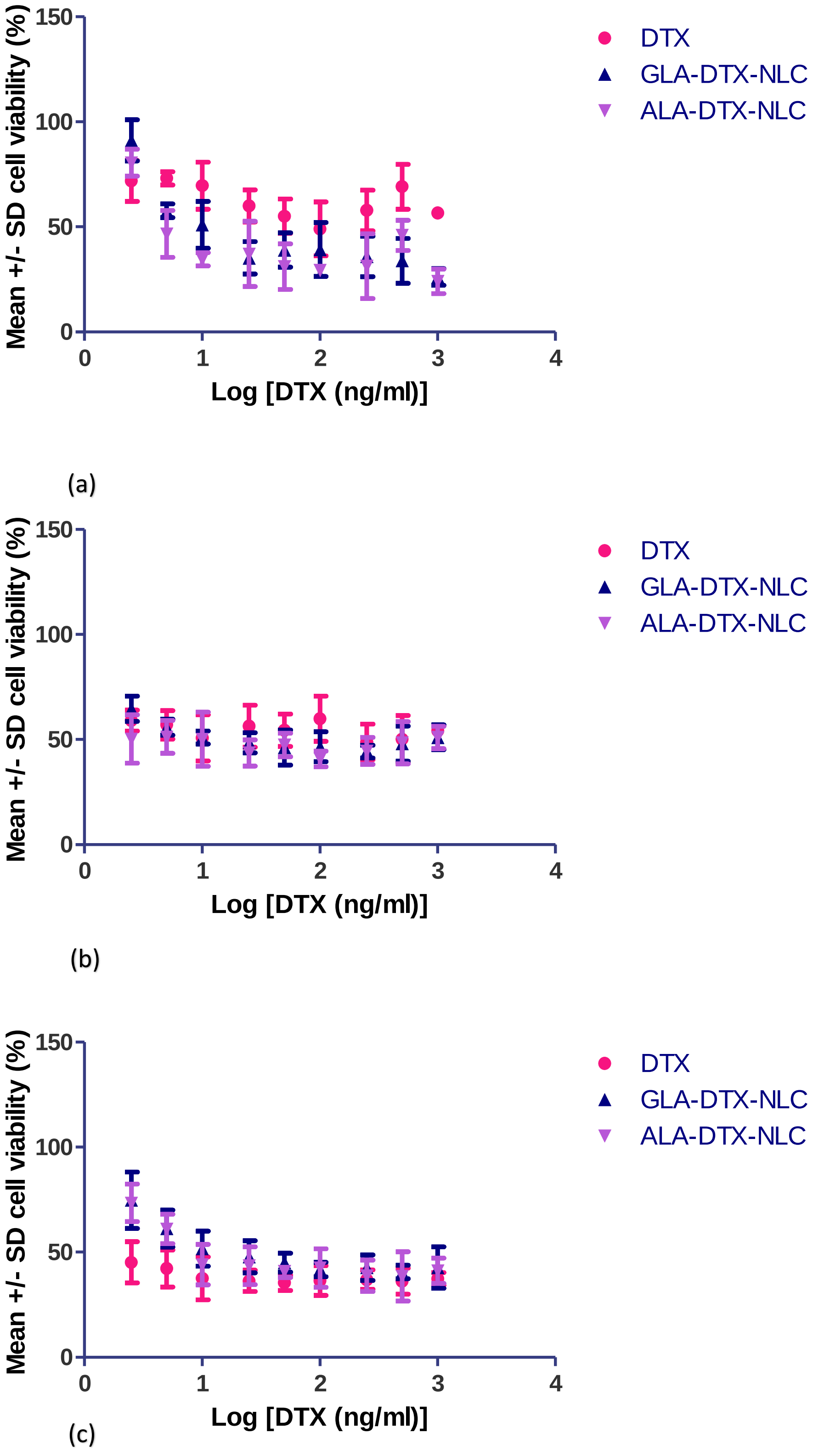

Figure 4.8 Mean percentage cell viability for DTX, GLA-DTX-NLC, and ALA-DTX-NLC when incubated with BTNW911 cell line at (a) 24, (b) 48, and (c) 72 h. Data mean values ±SD, (N=3), and all formulations were compared to standard treatment docetaxel alone.

4.5.2.3. Cell proliferation after treatment with aptamer tagged docetaxel-loaded nanostructured lipid carriers

SA43-DTX-NLC verses DTX

Interestingly SA43-DTX-NLC exhibited significantly lower potency (higher IC_{50} values) as compared with DTX IC_{50} (Table 4.6) when incubated for 24, 48, and 72 h in U87MG cell lines (Figure 4.9). A similar observation was made for SVGp12 (Figure 4.10) and BTNW 911 cells (Figure 4.11). In addition, it could be seen that conjugating the SA43 ligand to the DTX-NLC decreased potency in every cell line for nearly every duration of incubation. That might be attributed to the delayed release of DTX from the SA43-DTX-NLC. Though there are no previous reports on SA43-aptamer conjugated NPs, and our study is the first report on application of the SA43- aptamer as a ligand conjugated with DTX-NLC for selective glioblastoma therapy, previous reports on other aptamers conjugated to docetaxel-loaded NPs Chen *et al.,* (2016), have shown a similar slow release of DTX from DTX-apt-NPs, owing to hydrophobic core and hydrophilic shell of the NPs acting as a barrier. Additionally, slow release of DTX from SA43-DTX-NLC could be due to low solubility, hence causing low toxicity or plausibly due to SA43-aptamer binding to the U87MG, resulting in slow diffusion of DTX into the cells. Aptekar *et al.,* (2015) reported SA43-aptamer alone was not a therapeutic aptamer, but it displayed a selective uptake with differentiation between glioblastoma (U87MG) and non-cancerous cells (SVG P12), which is important for all anti-cancer treatments to exhibit a less or no toxicity towards the non-cancerous cells. Consequently, the SA43-DTX-NLC was further studied for cell uptake, and cell cycle analysis to evaluate the impact of conjugation of SA43 on the DTX-NLC.

Table 4.6 Mean IC_{50} values for SA43-DTX-NLC (1:1/8) in U87MG, SVG P12, and BTNW911 following 24, 48, and 72 h incubations. Data mean values ±SD, (N=3). * $p < 0.05$ and *** $p < 0.000$ refers to the significant difference when all formulations compared to the standard treatment DTX.

Cell line	**Time (h)**	**IC_{50} Values (ng/ml)**	
		DTX	**SA43-DTX-NLC**
U87MG	24	7.22 ±0.84	86.02 *** ±5.26
U87MG	48	5.44 ±3.94	16.87 *** ±0.97
U87MG	72	1.80 ±0.01	5.31 ** ±0.53
SVG P12	24	2.07 ±0.46	101.33 *** ±1.52
SVG P12	48	2.55 ±0.58	99.04 *** ±1.73
SVG P12	72	0.22 ±0.10	26.09 *** ±1.80
BTNW911	24	95.16 ±4.95	N/A
BTNW911	48	10.05 ±0.32	79.24 *** ±0.72
BTNW911	72	1.77 ±0.64	15.42 *** ±0.37

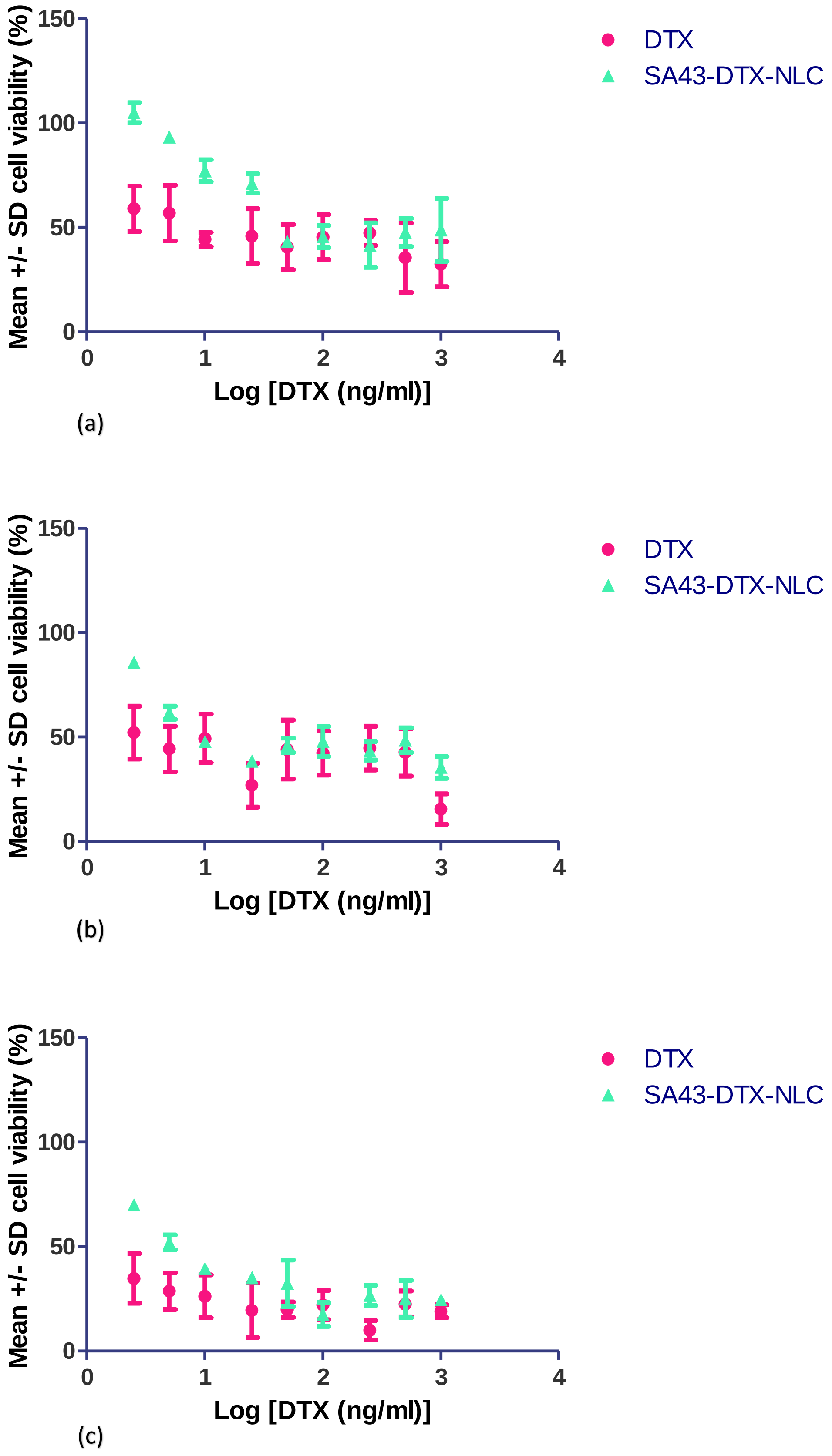

Figure 4.9 Mean percentage cell viability for DTX and SA43-DTX-NLC when incubated with U87MG cell line at (a) 24, (b) 48, and (c) 72 h. Data mean values ±SD, (N=3), and all formulations were compared to standard treatment docetaxel alone.

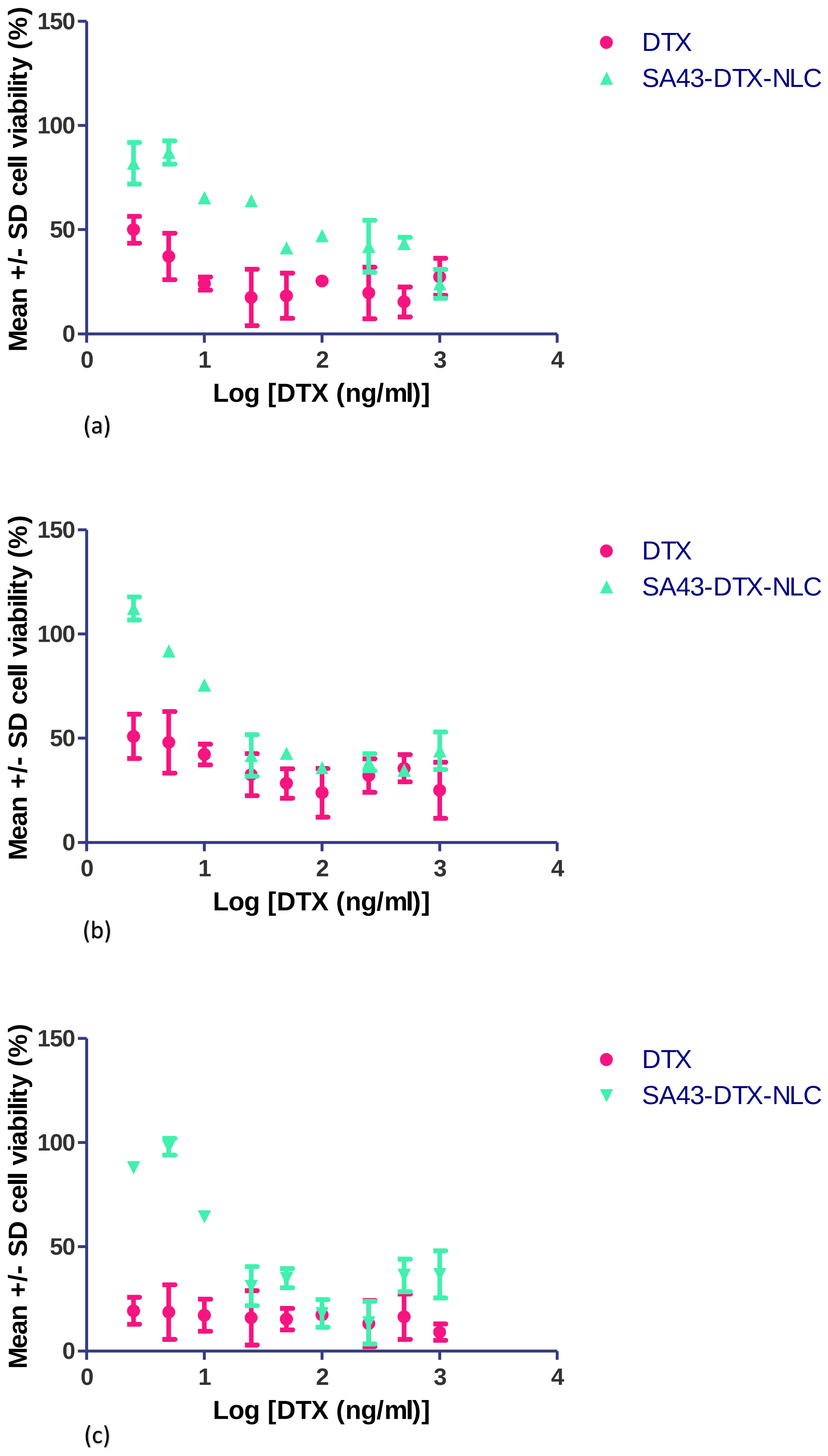

(a)

(b)

(c)

Figure 4.10 Mean percentage cell viability for DTX and SA43-DTX-NLC when incubated with SVG P12 cell line at (a) 24, (b) 48, and (c) 72 h. Data mean values ±SD, (N=3), and all formulations were compared to standard treatment docetaxel alone.

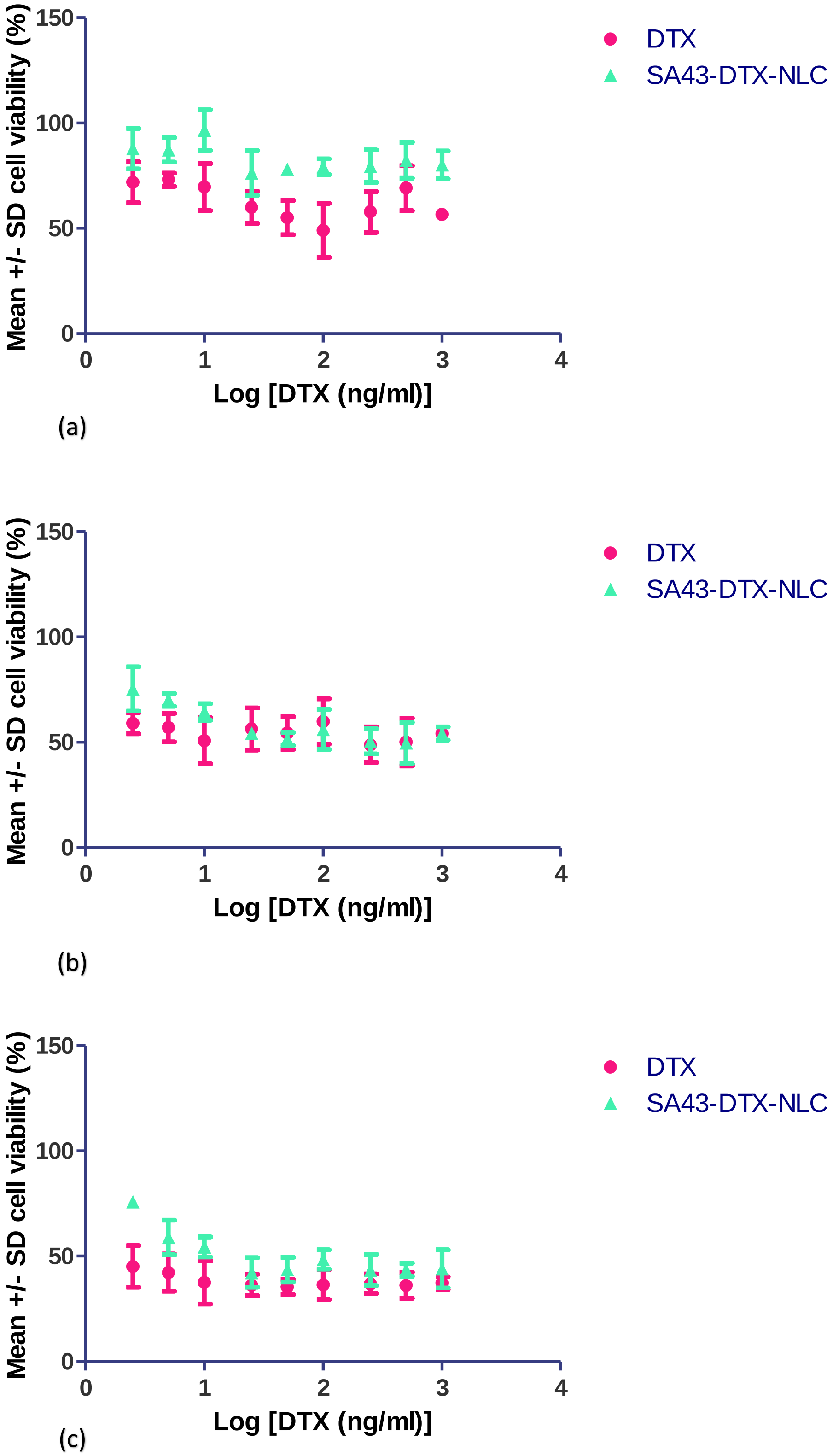

(a)

(b)

(c)

Figure 4.11 Mean percentage cell viability for DTX and SA43-DTX-NLC when incubated with BNTW911 cell line at (a) 24, (b) 48, and (c) 72 h. Data mean values ±SD, (N=3), and all formulations were compared to standard treatment docetaxel alone.

4.5.2.4. Cell proliferation evaluation in 3D U87MG spheroids

A 3D tumour spheroid has been used as a tool to evaluate the NPs efficacy (Gao *et al.,* 2012). In this experiment, from a morphological point of view, when U87MG spheroids were treated with DTX there was no reduction in the spheroids size/dimension at all tested concentrations (Figure 4.12 a), spheroids diameter was ranging between 500-510 µm, while the untreated spheroids were around 450-500 µm in diameter (Figure 4.12 a). When spheroids were treated with DTX-NLC they demonstrated a slight reduction in the spheroids diameter at higher concentration, around 490-350 µm (Figure 4.12 b), due to higher uptake of the NLCs as demonstrated by Gao *et al.,* (2014b), that contributed to transport the capsulated DTX within the NLC to the core of spheroids, which in turn increases the growth-inhibition, and consequently reduces the U87MG spheroids diameter.

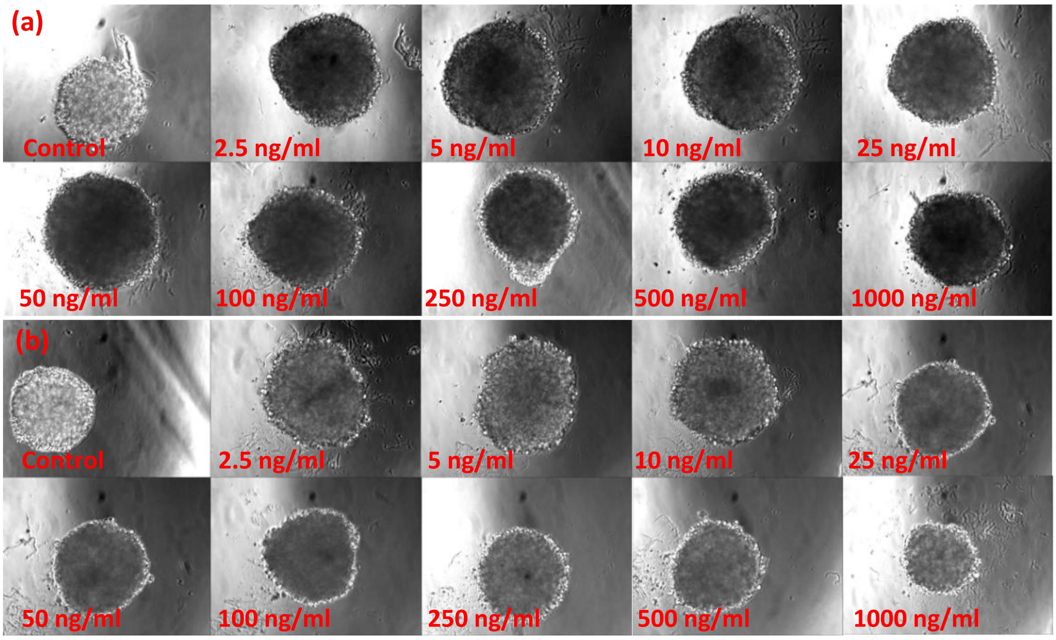

Figure 4.12 showing U87MG spheroids morphology when treated at a range of concentration between 2.5-1000 ng/ml and incubated for 72 h. with (a) DTX, (b) DTX-NLC. Data are N=3, and all formulations compared with the control untreated U87MG spheroids.

In addition, a slight reduction was also encountered with the GLA-DTX-NLC treated spheroids ranging between 480-490 µm in diameter (Figure 4.13 a), and a higher reduction in diameter was notable when spheroids were treated with ALA-DTX-NLC as the spheroids diameters were ranging 380-450 µm (Figure 4.13 b) that might be attributed to the high inhibitory-growth effect of PUFAs especially GLA on glioblastoma spheroids as reported by Leaver *et al.,* (2002).

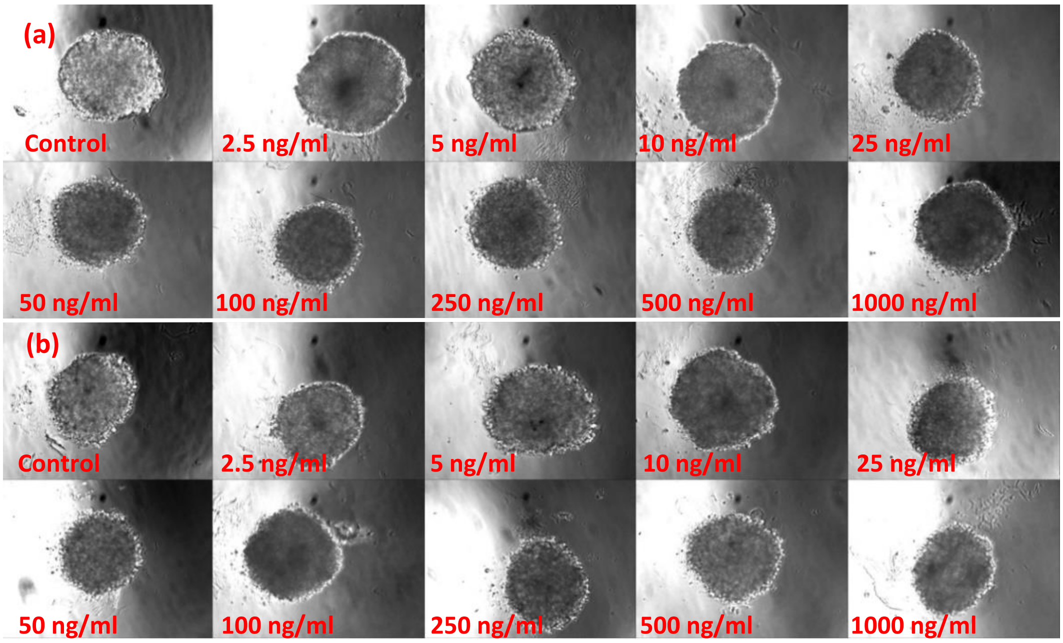

Figure 4.13 showing U87MG spheroids morphology when treated at a range of concentration between 2.5-1000 ng/ml and incubated for 72 h. with (a) GLA-DTX-NLC, (b) ALA-DTX-NLC. Data are N=3, and all formulations compared with the control untreated U87MG spheroids.

Finally, the U87MG spheroids that were treated with SA43-DTX-NL exhibited little reduction in the diameter. The spheroids diameter, in this case, was ranging between 490-450 µm (Figure 4.14).

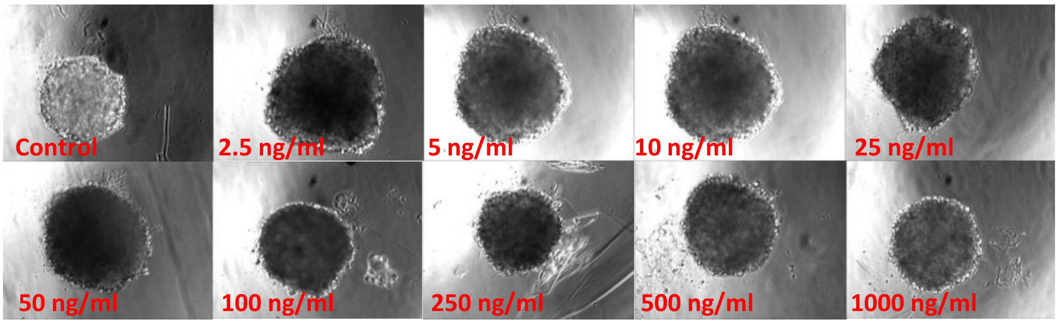

Figure 4.14 showing U87MG spheroids morphology when treated at a range of concentration between 2.5-1000 ng/ml and incubated for 72 h. with SA43-DTX-NLC. Data are N=3, and all formulations compared with the control untreated U87MG spheroids.

DTX-NLC showed higher efficacy (Figure 4.15 a) with a highly significant reduction in the IC_{50} value when compared to the DTX at 72 h incubation time (Table 4.7). This might be attributed to fact that DTX transportation to the spheroid core was extremely difficult as previously demonstrated by Gao *et al.,* (2014b). The direct contact of DTX with the spheroids, might harm the cells and cause cell death, which makes the transportation of DTX from the surface of dead cells to the core of tumour spheroid impossible (Gao *et al.,* 2014a). Therefore, the proposed encapsulation of DTX within the NLCs might be the reason for enhancing DTX-NLC uptake and consequently, DTX-NLC exhibited high potency and penetration in the spheroids core, as further demonstrated in section 4.5.4.3. Interestingly GLA-DTX-NLC demonstrated less toxicity towards U87MG spheroids, with a significant increase in IC_{50} when compared to DTX at similar incubation time. This might suggest that the DTX that was released from the GLA-DTX-NLC was taking a long time to reach the spheroids core resulting in slower penetration and causing less toxic action (Figure 4.15 b). While ALA-DTX-NLC and SA43-DTX-NLC exhibited no significant difference in toxicity towards U87MG spheroids when compared to DTX as shown in figures 4.15 c and d, and indicated in table 4.7. Both formulations were as toxic as the DTX alone, probably due to reaching of the released DTX from the formulations to the spheroids core at a similar rate as the DTX. Cells on the surface of spheroids are likely to be killed quicker than the cells deeper in the spheroid Gao *et al.,* (2014b). A longer incubation time with the treatments might be favourable, as different formulations are exhibiting a variable reaction when incubated with the spheroids due to drug taking a long time to penetrate the spheroid. Previous reports by Kim *et al.,* (2010) demonstrated that penetration of doxorubicin a well known anti-cancer drug was limited to the periphery of the spheroids and could not diffuse through the spheroid more than the outer few cell layers.

Table 4.7 Mean IC_{50} values for DTX, DTX-NLC, GLA-DTX-NLC, ALA-DTX-NLC, and SA43-DTX-NLC in U87MG spheroids following 72 h incubation. Data mean values ±SD, (N=3), and *** $p < 0.000$ refers to the significant difference when all formulations compared to the standard treatment DTX.

		IC_{50} Values (ng/ml)				
		DTX	**DTX-NLC**	**GLA-DTX-NLC**	**ALA-DTX-NLC**	**SA43-DTX-NLC**
U87MG Spheroids	Time 72 (h)	12.74 ±0.83	3.60 *** ±0.53	37.42 *** ±2.17	10.02 ±0.39	14.9 ±1.55

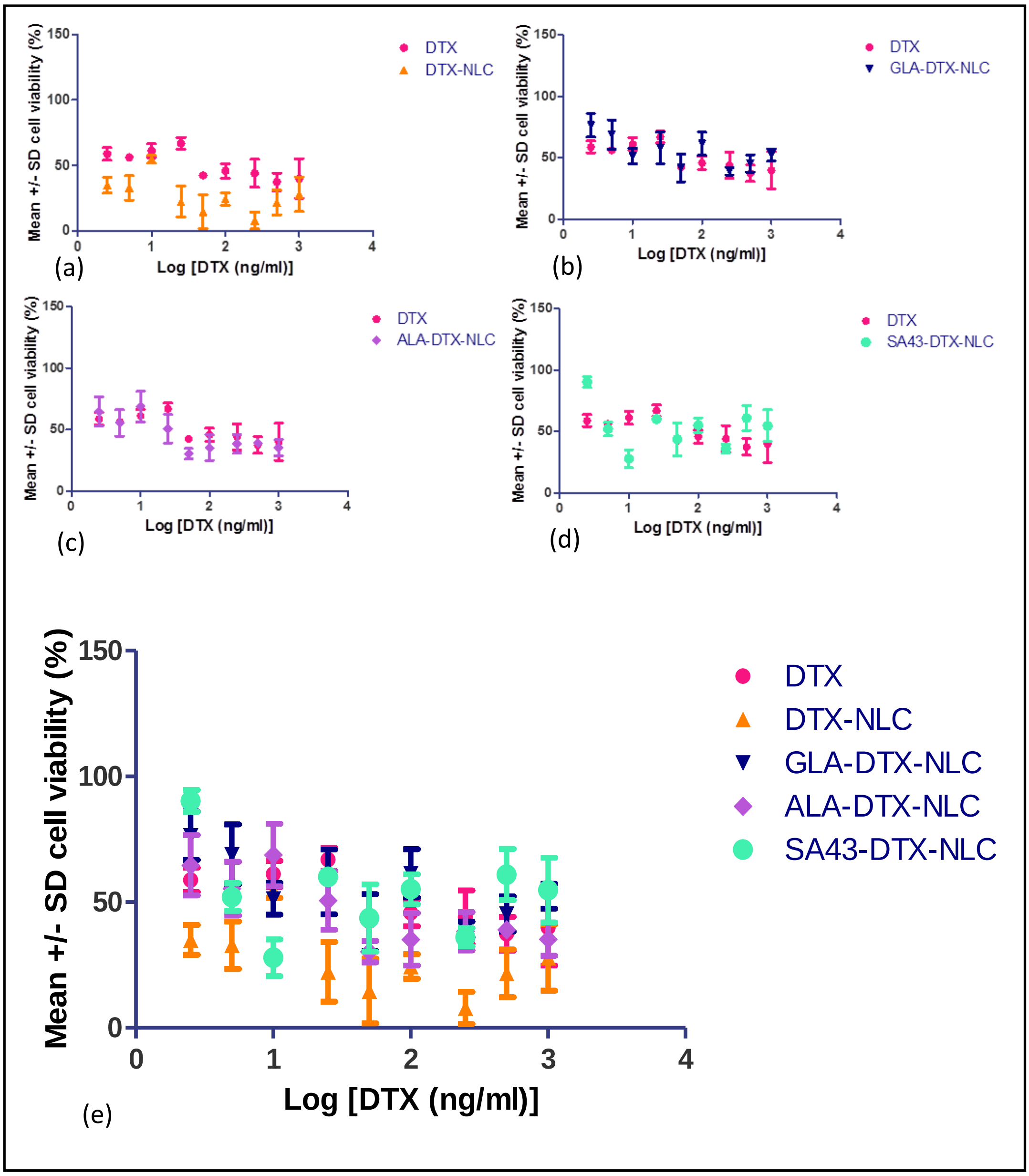

Figure 4.15 Mean percentage cell viability for (a) DTX and DTX-NLC, (b) DTX and GLA-DTX-NLC, (c) DTX and ALA-DTX-NLC, (d) DTX and SA43-DTX-NLC, and (e) % cell viability overlay of DTX, DTX-NLC, GLA-DTX-NLC, ALA-DTX-NLC, and SA43-DTX-NLC when incubated with U87MG spheroids cell line at 72 h. Data mean values ±SD, (N=3), and all formulations were compared to standard treatment docetaxel alone.

4.5.3. Qualitative internalisation study

Visualisation of the cellular internalisation of DTX-NLCs was studied for R-DTX-NLC and surface-modified R-DTX-NLC in U87MG glioblastomas and non-cancerous brain cells SVG P12 by incubating the cells with the proposed formulations for 2 and 4 h as described in section 4.4.8. Cells do not fluoresce, therefore observation of fluorescent dye was due to the internalisation of examined formulations (Martins *et al.,* 2012).

R-DTX-NLC

The internalisation study of the R-DTX-NLC was an important step to be able to visualise the delivered treatment and the localisation of the anti-cancer loaded NLCs within the cells. R-DTX-NLC demonstrated a high internalisation at both time points due to a high intensive green fluorescence colour mostly around the nucleus (stained with DAPI blue fluorescence dye) that referred to the R-DTX-NLC being internalised inside the U87MG cell line that was encapsulated with Rhodamine 123 (green fluorescence dye) (Figure 4.16 b and c). While SVG P12 showed less intense green colour at both time points mostly in the cytoplasm, that might suggest a lower uptake of the R-DTX-NLC with the non-cancerous cells (Figure 4.16 e and f), which was also indicated by a further quantitative study using the flow cytometer as detailed in section 4.5.4.1 (Figure 4.22). This finding is in agreement with previously published papers by Singh *et al.,* (2015) and Martins *et al.,* (2012) where lipidic NPs were evaluated with U87MG cell lines. Additionally, low particle size might play a role in the R-DTX-NLC uptake (R-DTX-NLC PS 136.8 nm), in collaboration with previous report Albanese *et al.,* (2012) whereby, the particle size had a positive impact on cellular uptake of the free surface formulation.

R-GLA-DTX-NLC

When R-GLA-DTX-NLC was treated with both the cell lines, higher internalisation with U87MG cell lines was observed as compared to SVG P12, especially at 2 h incubation time (Figure 4.17 b). As previously reported, GLA alone demonstrated less uptake with the non-cancerous cells (Das 2004), and consequently, it would show less internalisation (Figure 4.17 e and f) when conjugated with our DTX-NLCs as our results suggested. Moreover, this data was in line with our finding from a quantitative study using the flow cytometer as detailed in section 4.5.4.1 (Figure 4.22).

R-ALA-DTX-NLC

Interestingly, R-ALA-DTX-NLC also displayed similar behaviour with both the cell lines (Figure 4.18) as the internalisation behaviour of R-DTX-NLC. It was proposed by Elsherbiny *et al.,* (2013) that long chain fatty acids are transported inside the cells by intracellular lipid binding proteins named fatty acid binding protein (FABPs), which are present in most tissues, that might explain the higher internalisation of DTX-NLC conjugated with PUFAs.

R-SA43-DTX-NLC

R-SA43-DTX-NLC showed more selectivity towards the U87MG cell lines when compared with the internalisation at similar time points with SVG P12 (Figure 4.19). As previously reported by Aptekar *et al.,* (2015) the SA43-aptamer selectively binds to Ku 70 and Ku 80 and as a result of overexpression of Ku 70 and Ku 80 in cancer tissues which could serve as a useful strategy for targeting to glioblastoma cells. Thus, when the SA43-aptamer was conjugated to the R-DTX-NLC it enhanced its selectivity towards the glioblastoma U87MG rather than the SVG P12 (non-cancerous brain cells).

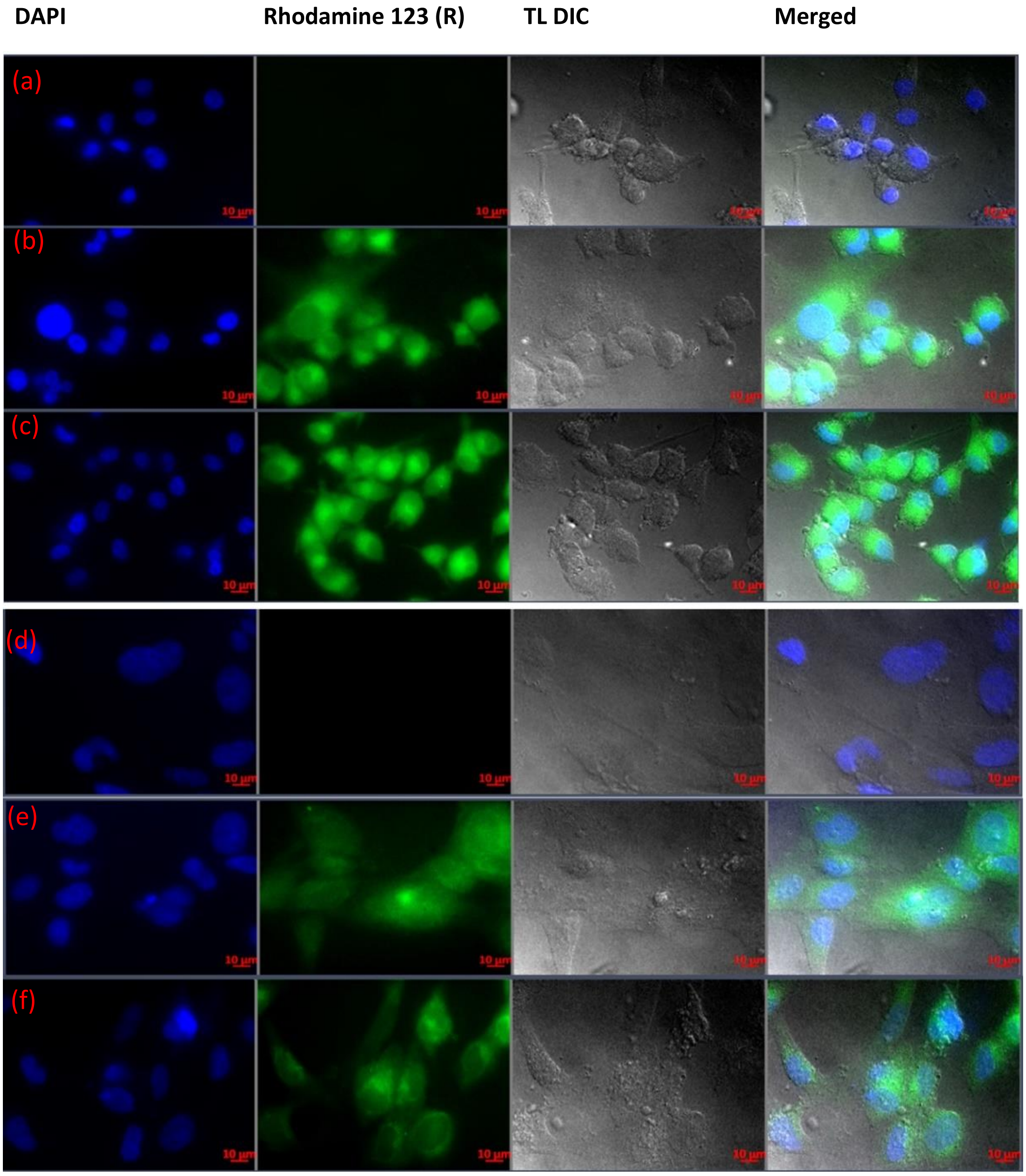

Figure 4.16 Cellular internalisation, where the blue colour refers to the stained nucleus with a fluorescence dye (DAPI) and the green fluorescence dye refers to the R-DTX-NLC (Rhodamine 123 (R) loaded within the DTX-NLC). (a) U87MG control untreated cells only stained with DAPI, (b) U87MG incubated for 2 h with R-DTX-NLC and the nuclei were stained with DAPI, (c) U87MG incubated for 4 h with R-DTX-NLC and the nuclei were stained with DAPI, (d) SVG P12 control untreated cells only stained with DAPI. (e) SVG P12 incubated for 2 h with R-DTX-NLC and the nuclei were stained with DAPI, (f) SVG P12 incubated for 4 h with R-DTX-NLC and the nuclei were stained with DAPI. Data are N=3.

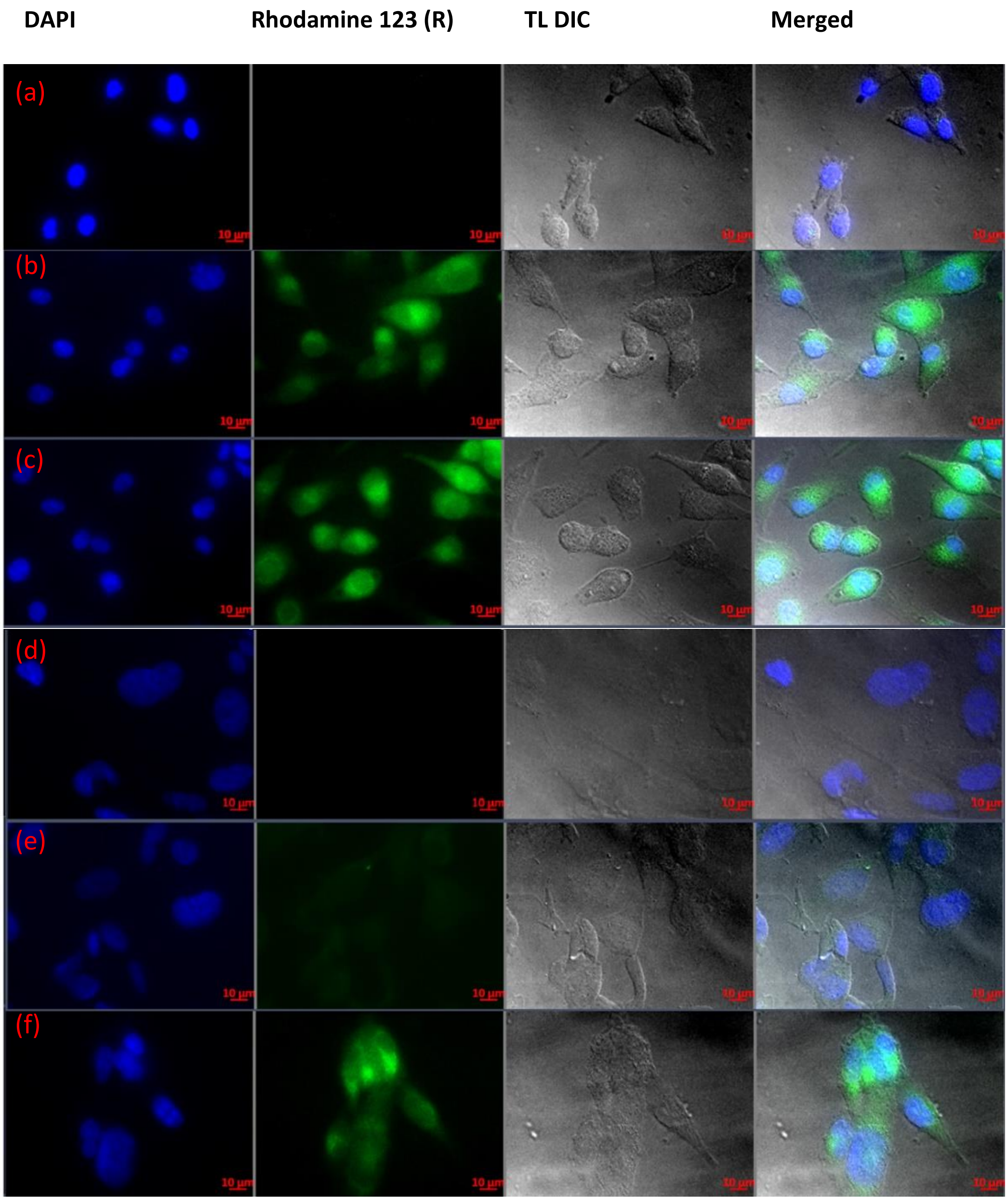

Figure 4.17 Cellular internalisation, where the blue colour refers to the stained nucleus with a fluorescence dye (DAPI) and the green fluorescence dye refers to the R-GLA-DTX-NLC (Rhodamine 123 (R) loaded within the DTX-NLC). (a) U87MG control untreated cells only stained with DAPI, (b) U87MG incubated for 2 h with R-GLA-DTX-NLC and the nuclei were stained with DAPI, (c) U87MG incubated for 4 h with R-GLA-DTX-NLC and the nuclei were stained with DAPI, (d) SVG P12 control untreated cells only stained with DAPI. (e) SVG P12 incubated for 2 h with R-GLA-DTX-NLC and the nuclei were stained with DAPI, (f) SVG P12 incubated for 4 h with R-GLA-DTX-NLC and the nuclei were stained with DAPI. Data are N=3.

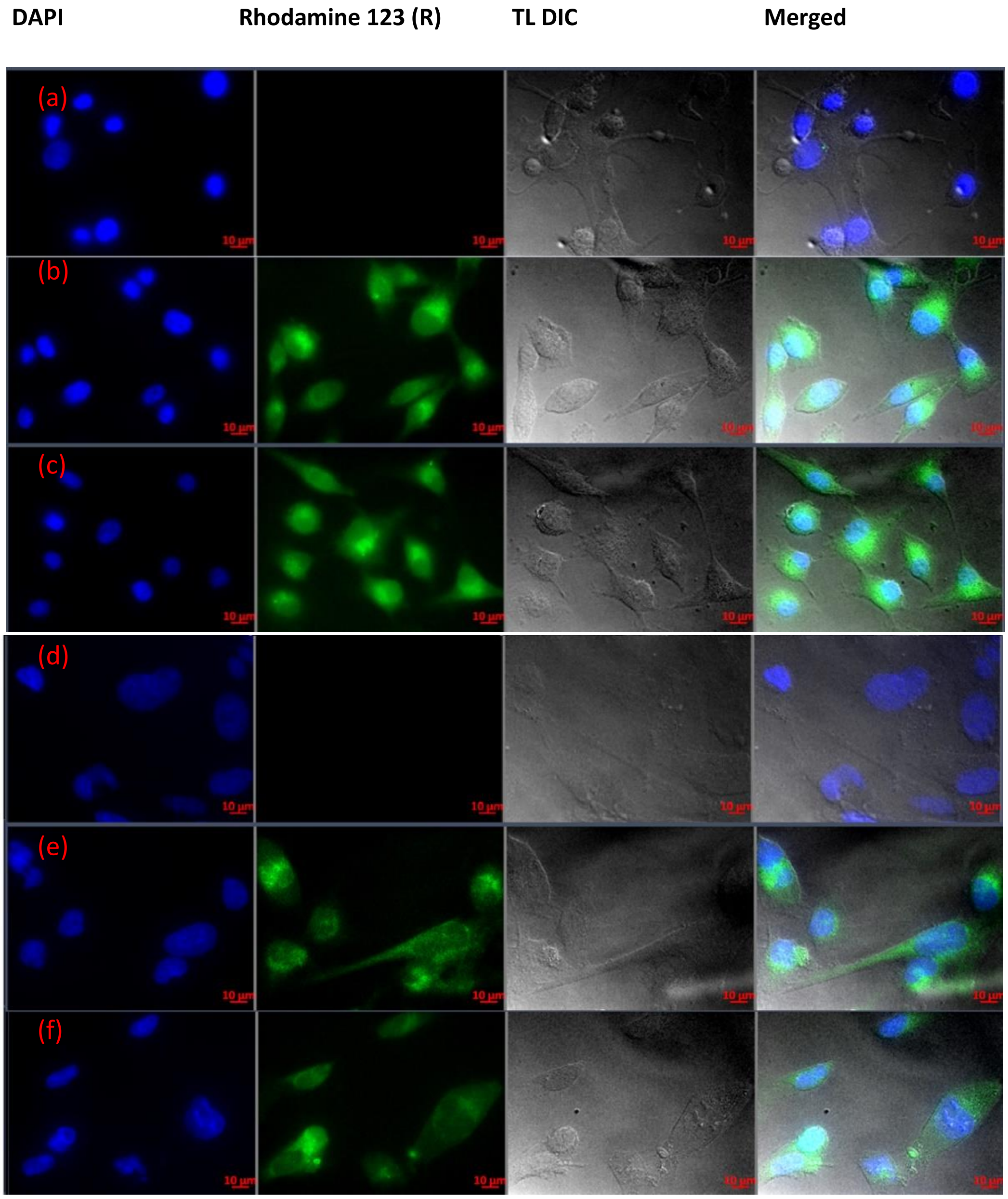

Figure 4.18 Cellular internalisation, where the blue colour refers to the stained nucleus with a fluorescence dye (DAPI) and the green fluorescence dye refers to the R-ALA-DTX-NLC (Rhodamine 123 (R) loaded within the DTX-NLC). (a) U87MG control untreated cells only stained with DAPI, (b) U87MG incubated for 2 h with R-ALA-DTX-NLC and the nuclei were stained with DAPI, (c) U87MG incubated for 4 h with R-ALA-DTX-NLC and the nuclei were stained with DAPI, (d) SVG P12 control untreated cells only stained with DAPI. (e) SVG P12 incubated for 2 h with R-ALA-DTX-NLC and the nuclei were stained with DAPI, (f) SVG P12 incubated for 4 h with R-ALA-DTX-NLC and the nuclei were stained with DAPI. Data are N=3.

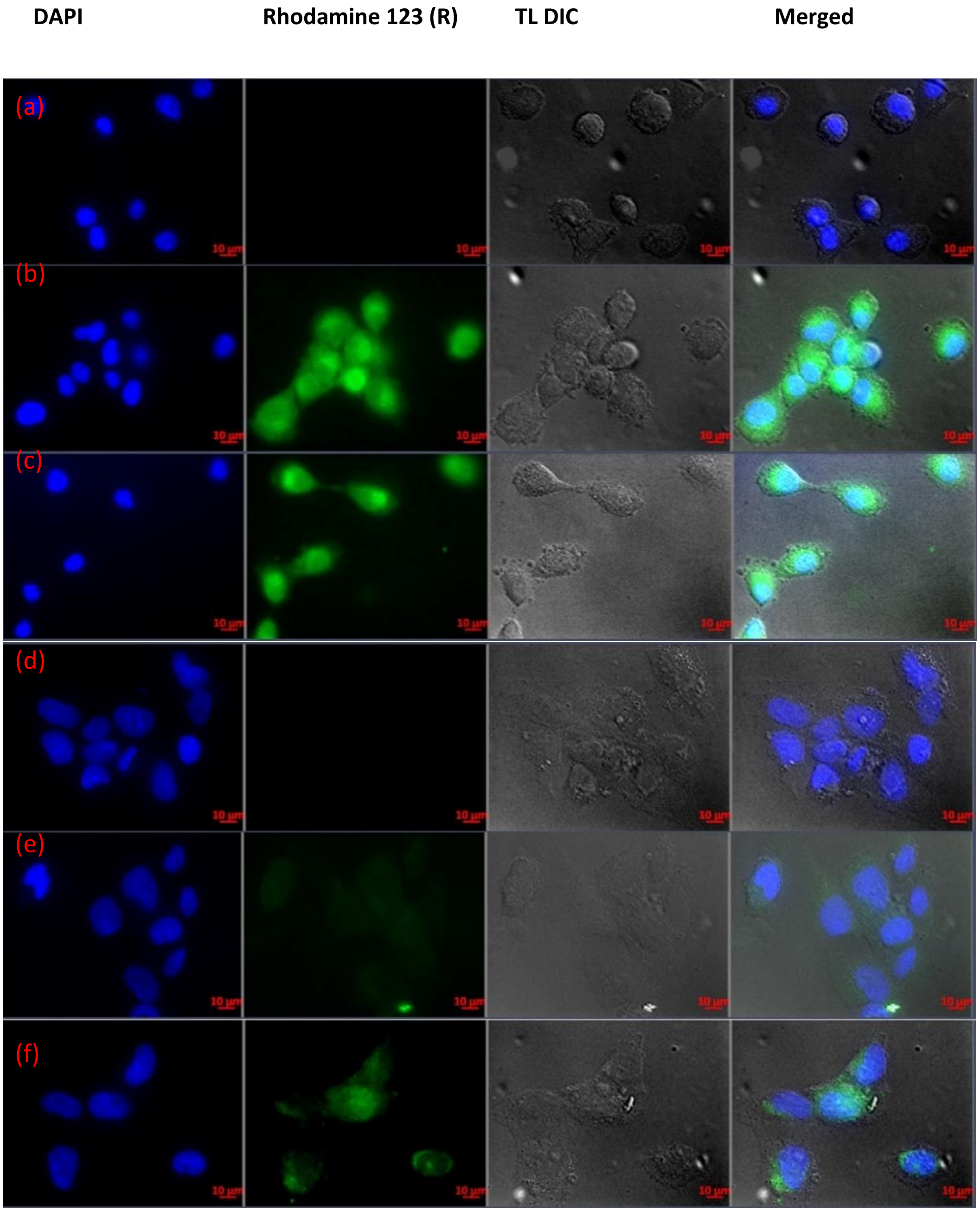

Figure 4.19 Cellular internalisation, where the blue colour refers to the stained nucleus with a fluorescence dye (DAPI) and the green fluorescence dye refers to the R-SA43-DTX-NLC (Rhodamine 123 (R) loaded within the DTX-NLC). (a) U87MG control untreated cells only stained with DAPI, (b) U87MG incubated for 2 h with R-SA43-DTX-NLC and the nuclei were stained with DAPI, (c) U87MG incubated for 4 h with R-SA43-DTX-NLC and the nuclei were stained with DAPI, (d) SVG P12 control untreated cells only stained with DAPI. (e) SVG P12 incubated for 2 h with R-SA43-DTX-NLC and the nuclei were stained with DAPI, (f) SVG P12 incubated for 4 h with R-SA43-DTX-NLC and the nuclei were stained with DAPI. Data are N=3.

4.5.4. Quantitative uptake study

In order to confirm the quantitative uptake of DTX-NLCs formulations in cell lines and 3D U87MG spheroids, time and concentration-dependent, the study was conducted as detailed below:

4.5.4.1. Time-dependent uptake

Time-dependent quantitative uptake of all R-DTX-NLCs was performed in U87MG and SVG P12 cells, and the results are presented in two ways. First by studying the linear relationship (line of best fit) between the mean fluorescence intensity (MFI) and the time, for all proposed DTX-NLC formulations that were encapsulated with a fluorescence Rhodamine 123 (R) dye. The uptake rate of R-DTX-NLC, R-GLA-DTX-NLC and R-ALA-DTX-NLC followed this order from higher to lower uptake rate R-ALA-DTX-NLC > R-GLA-DTX-NLC > R-DTX-NLC when U87MG were treated and incubated at different time intervals (Figure 4.20 a, c, e). In contrast, for the SVG P12, results demonstrated the following order from highest to lowest cell uptake R-DTX-NLC > R-GLA-DTX-NLC > R-ALA-DTX-NLC (4.20 b, d, f). These results suggest that the increase in the U87MG cell uptake and the reduction of SVG P12 uptake, though the uptake of U87MG was improved once the DTX-NLC were surface modified with PUFAs, but the efficacy of GLA-DTX-NLC and ALA-DTX-NLC was as effective as DTX alone, that might be attributed to the slow release of DTX from both formulations as they exhibited approximately 12% of DTX release at initial time and followed by very slow release profile where more than 40 % was released at 24 h as (section 3.5.10.2). It is worth mentioning that high U87MG uptake for surface modified formulation with PUFAs (ALA and GLA), might be attributed due to the higher binding to FABPs receptors (Elsherbiny *et al.,* 2013). Figure 4.20 demonstrates the uptake behaviour over a period of time, where all three tested formulations exhibited a highly significant increase in U87MG uptake ($p < 0.001$) due to the lipophilic nature of the formulations (Yuan *et al.,* 2008) over the SVG P12 uptake.

SVG P12 demonstrated slower cellular uptake in comparison to the U87MG cells as shown in figure 4.18 when the data are presented secondly as a gradient for MFI over time. Additionally, both R-ALA-DTX-NLC and R-GLA-DTX-NLC showed a highly significant increase in uptake by the U87MG cells when compared to the bare R-DTX-NLC under the same conditions (Figure 4.21).

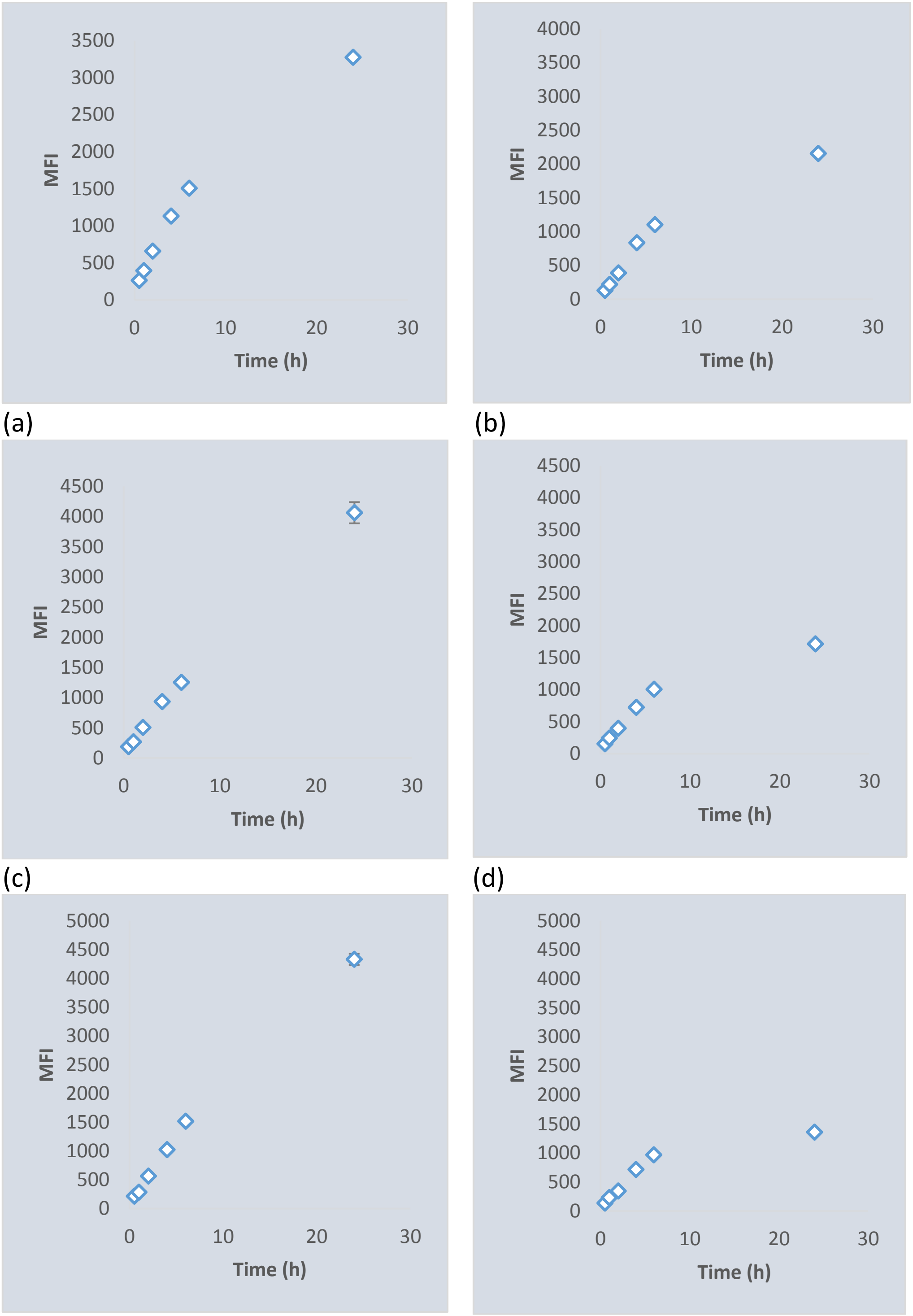

(a) (b) (c) (d) (e) (f)

Figure 4.20 Standard plots of best fit demonstrating the time-dependent uptake of cell lines treated with DTX-NLC and surface modified DTX-NLC formulations (Rhodamine 123 (R) loaded within the DTX-NLC). (a) R-DTX-NLC incubated with U87MG, (b) R-DTX-NLC incubated with SVG P12, (c) R-GLA-DTX-NLC incubated with U87MG, (d) R-GLA-DTX-NLC incubated with SVG P12, (e) R-ALA-DTX-NLC incubated with U87MG, (f) R-ALA-DTX-NLC incubated with SVG P12. Data are mean and ±SD, (N=3).

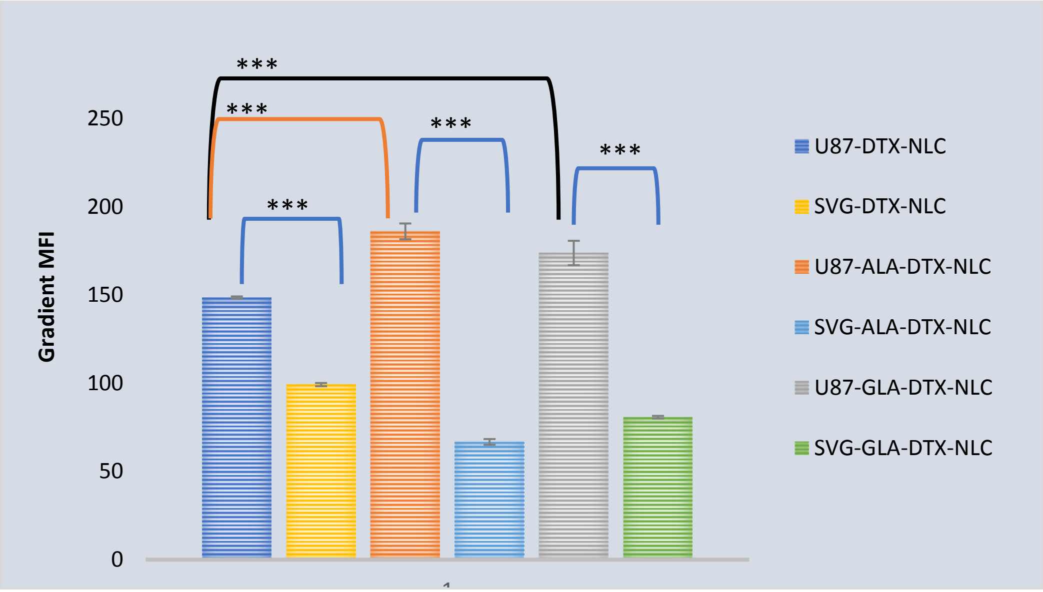

Figure 4.21 Gradient MFI demonstrating the time-dependent uptake of U87MG and SVG P12 cell lines treated with R-DTX-NLC, R-ALA-DTX-NLC, and R-GLA-DTX-NLC formulations. Data are mean and ± SD, (N=3). *** p < 0.001, refers to the significant difference.

The MFI for the uptake was demonstrated over a time interval in U87MG and SVG P12 cells treated with R-DTX-NLC, R-ALA-DTX-NLC and R-GLA-DTX-NLC formulations at 0.5, 1, 2, 4, 6, and 24 h (Figure 4.22). U87MG cells displayed an early uptake starting at 0.5 h and showed maximum uptake at 24 h for all examined formulations. Notably, figure 4.22 also show a distinguished lower uptake of all the tested formulations by SVG P12 cells. Furthermore, the uptake MFI at 2 and 4 h incubation time results were in line with our qualitative uptake findings, when the fluorescence microscopy was used to perform the cellular internalisation on both cell lines (section 4.5.3).

The flow cytometer histograms display the cellular uptake of R-DTX-NLC (Figure 4.23 a, b), R-GLA-DTX-NLC (Figure 4.24 a, b), and R-ALA-DTX-NLC (Figure 4.24 c, d) indicating an increase in cell uptake with time, as evidenced by the shift in the fluorescence intensities to the right over time for both glioblastoma U87MG cell lines and the non-cancerous brain cell lines SVG P12. The results suggest high-intensity histogram peak shifting with ($p < 0.001$) when U87MG cell lines were treated with R-GLA-DTX-NLC and R-ALA-DTX-NLC, respectively. A similar concept was previously reported by Martins *et al.,* (2012) and Garanti *et al.,* (2016). A much lower flow cytometer histogram peaks were observed when SVG P12 were treated with the same formulations under the same conditions (Figure 4.24 b and c).

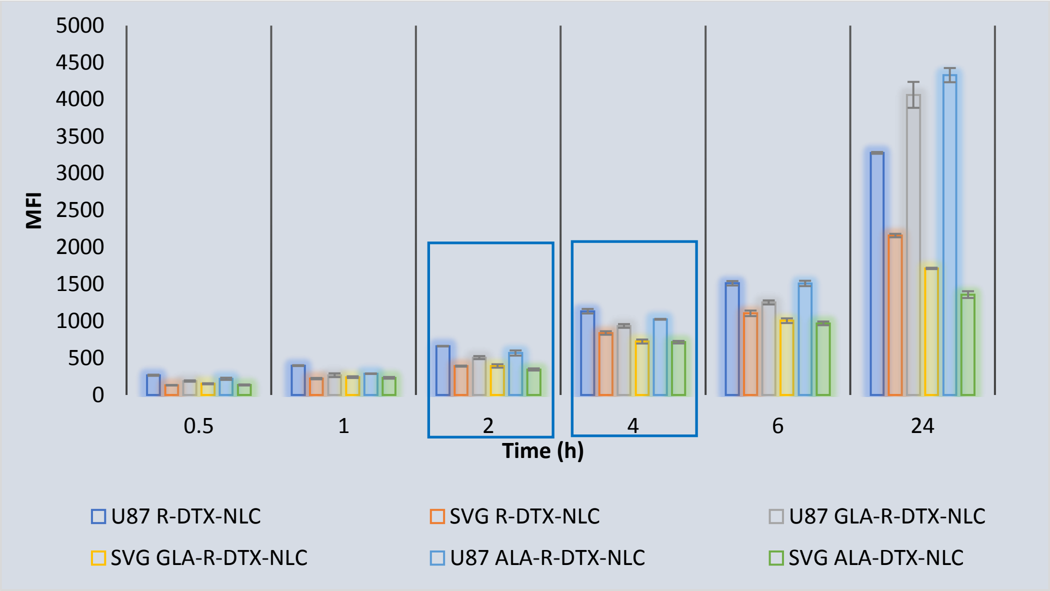

Figure 4.22 MFI over time-dependent uptake of U87MG and SVG P12 cell lines treated with R-DTX-NLC, R-ALA-DTX-NLC, and R-GLA-DTX-NLC formulations at (0.5, 1, 2, 4, 6, and 24) hr. Data are mean and ± SD, (N=3).

All the acquired results from the section 4.5.3 and the results that are presented, and discussed in this section show significant higher uptake by cancerous cells when the NLCs were surface modified over a lower uptake by the non-cancerous cells, which is a much-desired quality in the anti-cancer drug delivery. Thus surface modification of NPs with different ligands demonstrated enhanced internalisation and higher uptake in glioblastoma cell lines as previously reported by Gao *et al.,* (2014a) and Singh *et al.,* (2015). Also, for other cell lines as indicated by Zhang and Zhang, (2013). The affinity of both the PUFAs to bind to cells through lipid binding protein FABPs (Elsherbiny *et al.,* 2013) could be the plausible reason for higher cellular uptake of GLA-DTX-NLC and ALA-DTX-NLC.

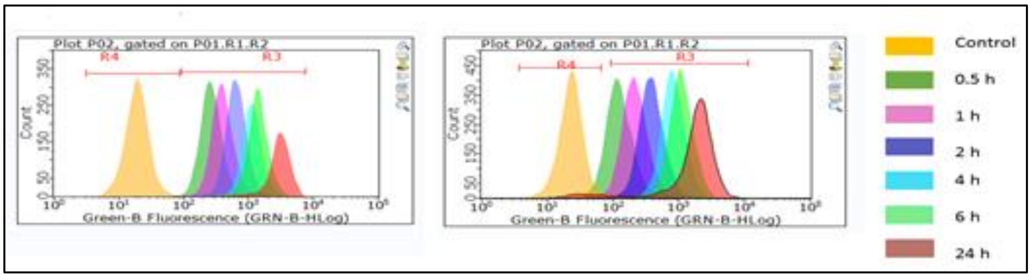

(a) (b)

Figure 4.23 Flow cytometer histograms for the time-dependent uptake when R-DTX-NLC were incubated for (0.5, 1, 2, 4, 6, and 24) h with (a) U87MG cell lines, (b) SVG P12 cell lines. R4 representing a region around the untreated control cells, and R3 representing a region around the shifted peaks as the fluorescence intensity increases the peaks shifting more to the right over time as evidence of increased uptake with time. Data are N=3.

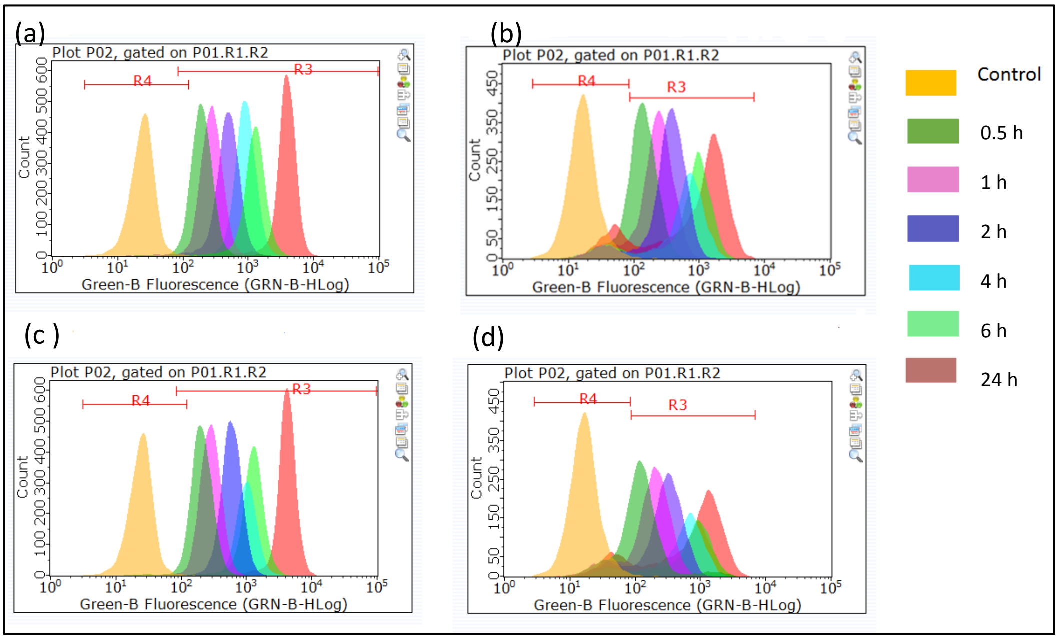

Figure 4.24 Flow cytometer histograms for the time-dependent uptake when cell lines incubated for (0.5, 1, 2, 4, 6, and 24) h with (a) U87MG cell lines, incubated with R-GLA-DTX-NLC (b) SVG P12 cell lines incubated with R-GLA-DTX-NLC. (c) U87MG cell lines, incubated with R-ALA-DTX-NLC (d) SVG P12 cell lines incubated with R-ALA-DTX-NLC R4 representing a region around the untreated control cells, and R3 representing a region around the shifted peaks as the fluorescence intensity increases the peaks shifting more to the right over time as evidence of increased uptake with time. Data are N=3.

4.5.4.2. Concentration-dependent uptake

U87MG and SVG P12 cell lines

A four-level concentration (1, 2, 3, and 5 µg/ml) uptake was performed at 6 h to establish the dose-dependent uptake by the U87MG cell lines. The U87MG cells showed a very significant increase in the uptake when the cells were treated with R-GLA-DTX-NLC at 2 and 3 µg/ml concentration, likewise the cell uptake was significantly increased when treated with 1, 2, and 3 µg/ml concentration of R-ALA-DTX-NLC and furthermore, the U87MG displayed a very significant increase in the cell uptake at all concentrations levels 1, 2, 3, and 5 µg/ml when the cells were treated with R-SA43-DTX-NLC; the R-DTX-NLC was considered as control in this study and all the formulations uptake was compared with it (Figure 4.25). In addition, uptake by the non-cancerous brain cells SVG P12 was evaluated under the same conditions. Figure 4.26 demonstrates a significant reduction in the SVG P12 uptake when treated with 1 µg/ml of R-GLA-DTX-NLC and R-ALA-DTX-NLC, respectively.

No significant difference was obtained when the cells were treated with 2 µg/ml of R-GLA-DTX-NLC and R-SA43-DTX-NLC. Furthermore, when the concentration of the R-ALA-DTX-NLC was increased to 2 µg/ml the SVG P12 uptake was significantly increased. Similar findings were obtained when the R-GLA-DTX-NLC has increased to 3 and 5 µg/ml, as a significant increase in the SVG P12 uptake was noticeable (Figure 4.26). In contrast, the R-SA43-DTX-NLC exhibited either no significant difference in the uptake at 2 and 3 µg/ml or a significant reduction at 5 µg/ml when incubated with SVG P12 cell lines suggesting high selectivity of R-SA43-DTX-NLC towards the glioblastomas U87MG cell lines as compared to SVG P12. SA43-aptamer has demonstrated higher selectivity towards the U87MG cell line due to Ku 70 and Ku 80 overexpression in glioblastoma cells, and higher binding of SA43 to both proteins, and lower uptake with the SVG P12 cell line (Aptekar *et al.,* 2015). Consequently, when this aptamer was conjugated to R-DTX-NLC it enhanced its uptake by U87MG cells over SVG P12 cells. This quality would solve a major obstacle in the anti-cancer loaded NLC delivery to the cancer cells. A similar concept of concentration-dependent uptake evaluation was reported by Gao *et al.,* (2014a).

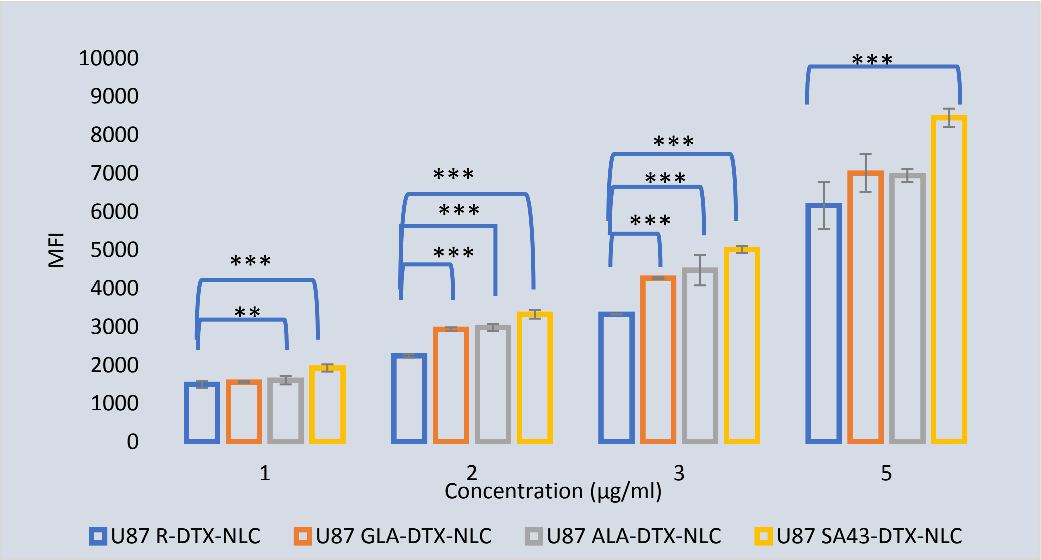

Figure 4.25 MFI demonstrating the concentration-dependent uptake of U87MG cell lines treated with R-DTX-NLC, R-ALA-DTX-NLC, R-GLA-DTX-NLC, and R-SA43-DTX-NLC formulations. Data are mean and ± SD, (N=3). * p < 0.05, refers to a significant difference when formulations were compared to R-DTX-NLC as the control in this case.

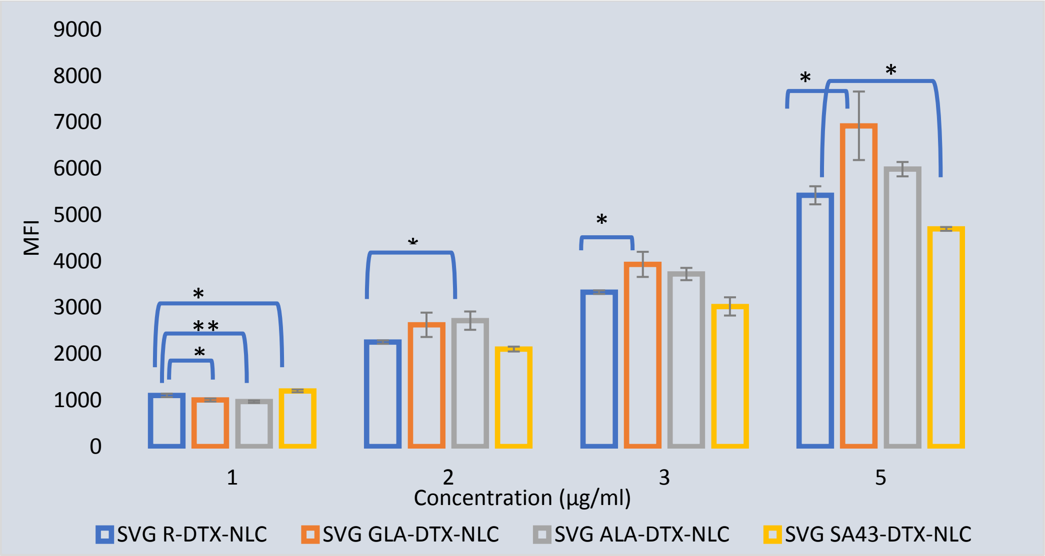

Figure 4.26 MFI demonstrating the concentration-dependent uptake of SVG P12 cell lines treated with R-DTX-NLC, R-ALA-DTX-NLC, R-GLA-DTX-NLC, and R-SA43-DTX-NLC formulations. Data are mean and ± SD, (N=3). * $p < 0.05$, refers to a significant difference when formulations were compared to R-DTX-NLC as the control in this case.

The flow cytometer histograms displayed in figures 4.27 a, b, 4.28 a, b, c, d and 4.29 a, b for both cell line also indicated the concentration-dependent cell uptake as evidenced by the shift in the fluorescence intensities to the right over different concentration levels for both glioblastoma U87MG cell lines and the non-cancerous brain cell lines SVG P12. The four formulations R-DTX-NLC, R-GLA-DTX-NLC, R-ALA-DTX-NLC and R-SA43-DTX-NLC all exhibited high intense fluorescence, histogram shifts when U87MG were treated, in comparison with less intensive histogram peaks when the SVG P12 were treated under the same conditions.

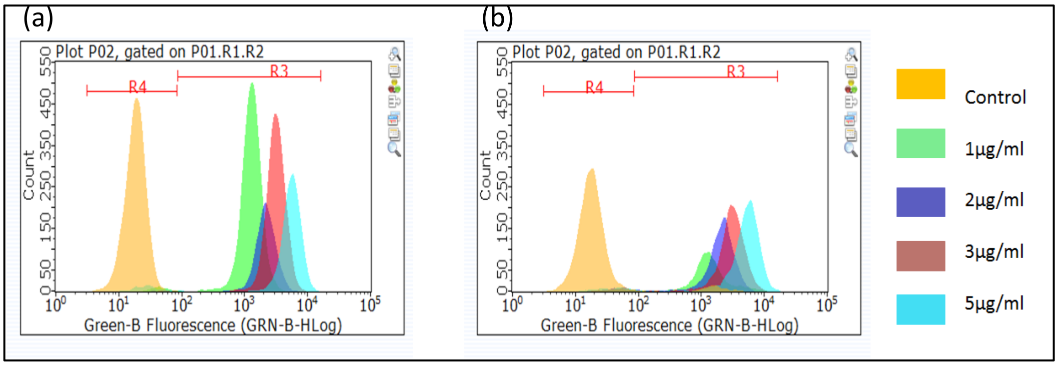

Figure 4.27 Flow cytometer histograms for the concentration-dependent uptake when R-DTX-NLC were incubated with 1, 2, 3, and 5 µg/ml (a) U87MG cell lines, (b) SVG P12 cell lines. R4 representing a region around the untreated control cells, and R3 representing a region around the shifted peaks as the fluorescence intensity increases the peaks shifting more to the right when the concentration was increased as evidence of increased uptake with the concentration. The control, in this case, was the untreated cell lines. Data are N=3.

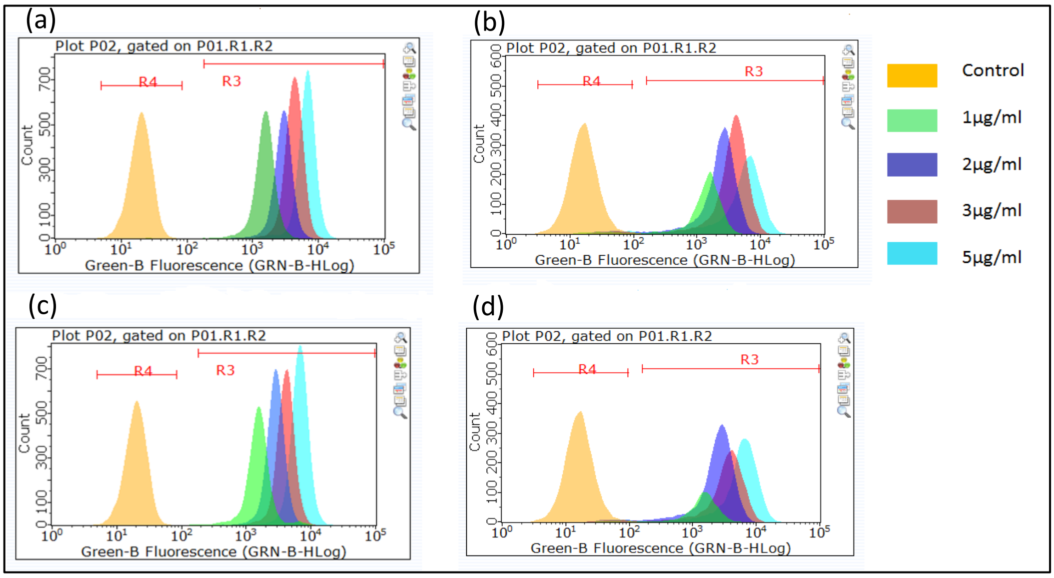

Figure 4.28 Flow cytometer histograms for the concentration-dependent uptake when incubated with 1, 2, 3, and 5 µg/ml (a) U87MG cell lines treated with R-GLA-DTX-NLC, (b) SVG P12 cell lines treated with R-GLA-DTX-NLC. (c) U87MG cell lines treated with R-ALA-DTX-NLC, (d) SVG P12 cell lines treated with R-ALA-DTX-NLC. R4 representing a region around the untreated control cells, and R3 representing a region around the shifted peaks as the fluorescence intensity increases the peaks shifting more to the right when the concentration was increased as evidence of increased uptake with the concentration. The control, in this case, was the untreated cell lines. Data are N=3.

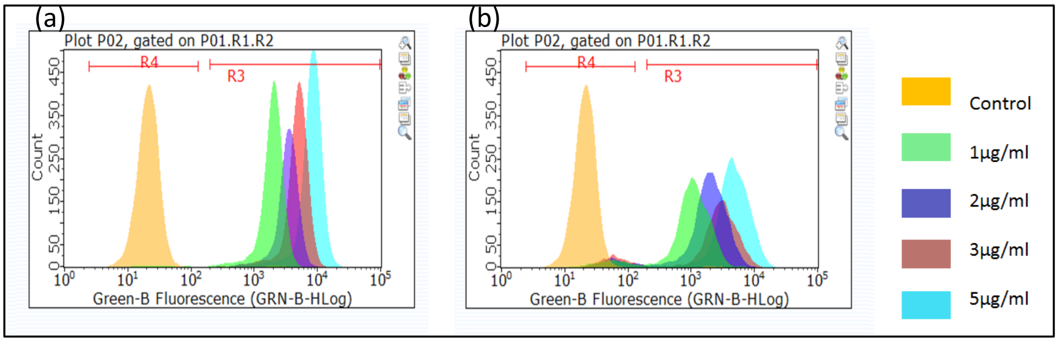

Figure 4.29 Flow cytometer histograms for the concentration-dependent uptake when R-SA43-DTX-NLC were incubated with 1, 2, 3, and 5 µg/ml (a) U87MG cell lines, (b) SVG P12 cell lines. R4 representing a region around the untreated control cells, and R3 representing a region around the shifted peaks as the fluorescence intensity increases the peaks shifting more to the right when the concentration was increased as evidence of increased uptake with the concentration. The control, in this case, was the untreated cell lines. Data are N=3.

Cells derived from patients (BTNW911 cell line)

BTNW911 cell lines were treated with four formulations R-DTX-NLC, R-GLA-DTX-NLC, R-ALA-DTX-NLC and R-SA43-DTX-NLC at 1 µg/ml for 6 h incubation time, to study the quantitative cell uptake. The MFI indicated a highly significant increase in the cell uptake ($p < 0.001$) when treated with R-DTX-NLC, in contrast to a lower cell uptake when the

BTNW911 were treated with the surface modified formulations under the same conditions (Figure 4.30). Though there was no noticeable difference in the peak shifting position of the flow cytometer histograms were laid on top of each other for all the four formulations. It is also worth mentioning that R-GLA-DTX-NLC and R-ALA-DTX-NLC showed significantly lower peak size than R-DTX-NLC formulation (Figure 3.31).

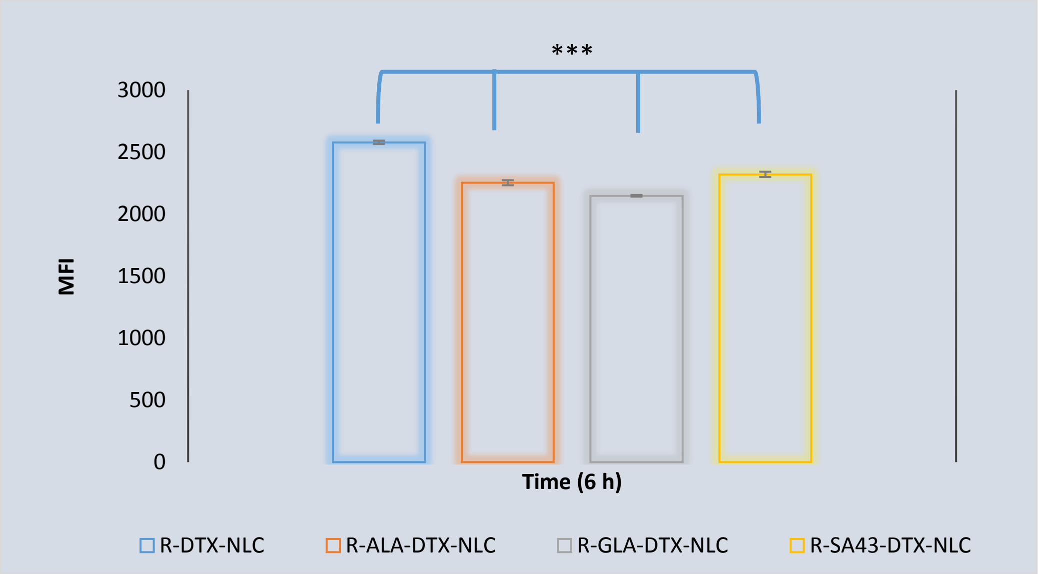

Figure 4.30 MFI demonstrating the BTNW911 uptake with one level concentration of 1 µg/ml of R-DTX-NLC, R-ALA-DTX-NLC, R-GLA-DTX-NLC, and R-SA43-DTX-NLC formulations at 6 h incubation time. Data are mean and ± SD, (N=3). *** $p < 0.001$, refers to a very significant difference when formulations were compared to R-DTX-NLC as the control in this case.

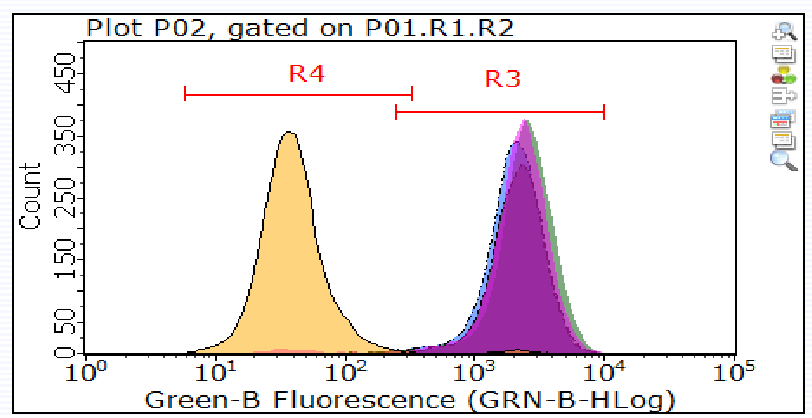

Figure 4.31 Flow cytometer histograms of the BTNW911 uptake with one level concentration 1 µg/ml of R-DTX-NLC, R-ALA-DTX-NLC, R-GLA-DTX-NLC, and R-SA43-DTX-NLC formulations 🟩 🟦 🟪 🟥, respectively. At 6 h incubation time. R4 representing a region around the untreated control cells, and R3 representing a region around the shifted peaks as the fluorescence intensity increases the peaks shifting more to the right when the cells were incubated with different formulation at one concentration as evidence of increased uptake with different types of unmodified and surface modified R-DTX-NLCs. The control, in this case, was the untreated cell lines 🟨 . Data are N=3.

4.5.4.3. Spheroids uptake

3D U87MG spheroids were prepared to evaluate the uptake of four formulations R-DTX-NLC, R-GLA-DTX-NLC, R-ALA-DTX-NLC and R-SA43-DTX-NLC at one level concentration of 1 µg/ml for 6 h incubation time. A quantitative uptake evaluation was performed using the flow cytometer as described in section 4.4.9.3. The data obtained as flow cytometer histograms (Figure 4.33) showed two populations of cell uptake, one was designated as early uptake that was thought to be the uptake by the cells on the surface of the spheroids and the second was thought to be due to the late uptake phase which was indicated by the uptake of the cells in the core of the spheroids. Due to the fact that spheroids consist of shell and core cells so it was assumed in this experiment that the cells in the core of the spheroids will take a longer time to be penetrated with the treatment, hence the data were expressed as early and late uptake as shown in figure 4.33. The MFI indicated a highly significant increase in the cellular late uptake phase ($p < 0.001$) when the spheroids were treated with R-DTX-NLC, that might be due to the high lipophilicity nature of this formulation in comparison to the other three formulations and that would explain the high potency of this formulation when examined for its antiproliferative effect in the 3D U87MG spheroids. A lower late uptake was shown when the spheroids were treated with the surface modified formulations under the same conditions (Figure 4.32), that might suggest that the surface modification of the DTX-NLC were not contributing to higher spheroids uptake due to their inability to transport to the inner core of spheroid cells. This correlates with a similar finding reported by Gao *et al.,* (2012b) whereby different formulations were uptaken by the spheroid cells in variable intensity. Additionally, R-ALA-DTX-NLC demonstrated a highly significant increase in the early uptake phase when compared with all three other formulations. Although there was no remarkable difference in the peak shifting position in the flow cytometer histograms for all the four formulations when the peaks were laid on top of each other (Figure 3.33).

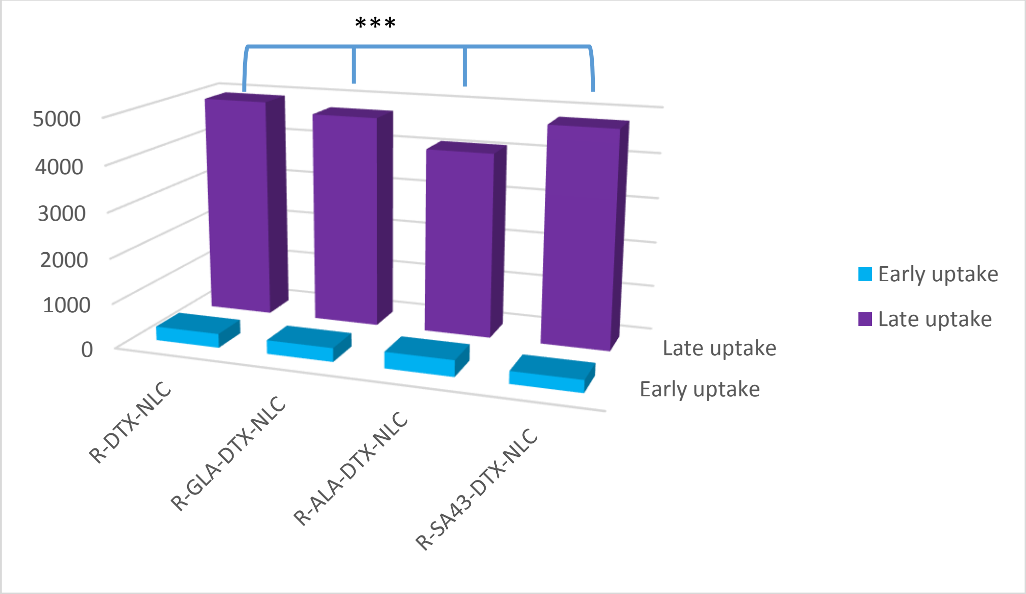

*Figure 4.32 MFI demonstrating the 3D U87MG spheroids uptake at 1 µg/ml of R-DTX-NLC, R-ALA-DTX-NLC, R-GLA-DTX-NLC, and R-SA43-DTX-NLC formulations at 6 h incubation time. Data are mean and ± SD, (N=3). *** $p < 0.001$, refers to a very significant difference when formulations were compared to R-DTX-NLC as the control in this case.*

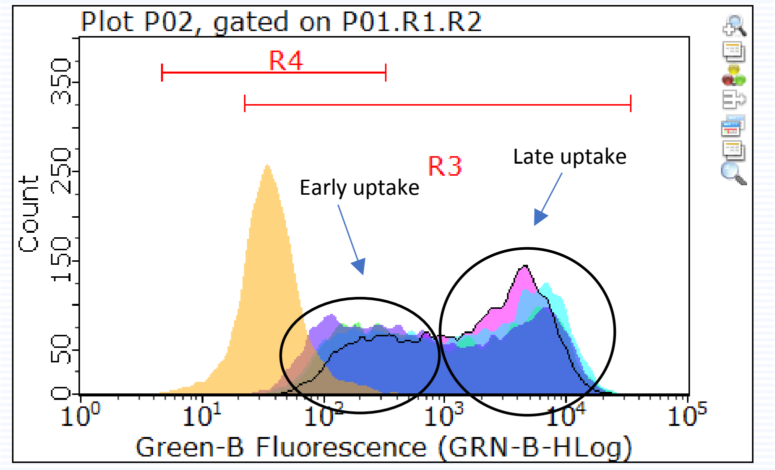

Figure 4.33 Flow cytometer histograms of the 3D U87MG spheroids uptake at 1 µg/ml of R-DTX-NLC, R-ALA-DTX-NLC, R-GLA-DTX-NLC, and R-SA43-DTX-NLC formulations 🟦 🟩 🟦 🟪, respectively at 6 h incubation time. R4 representing a region around the untreated control cells, and R3 representing a region around the shifted peaks as the fluorescence intensity increases the peaks shifting more to the right when the cells were incubated with different formulation at one concentration as evidence of increased uptake with different types of unmodified and surface modified R-DTX-NLCs. The control, in this case, was the untreated cell lines 🟨. Data are N=3.

4.5.5. Quantitative and qualitative endocytosis pathways analysis

It is well known that the endocytosis is a general mechanism for the internalisation and trafficking of NPs and other extracellular particles into the cells by different, and multiple pathways (Sahay *et al.,* 2010). In this study, four formulations were examined for their mechanism of internalisation in U87MG and SVG P12 cells, where the cells were exposed to several endocytosis inhibitors in order to distinguish the pathways each formulation exhibited to gain entry into the cells (section 4.4.10). The data were acquired and analysed for both qualitative and quantitative studies by using fluorescence microscopy for capturing and analysing the images and the flow cytometer to quantify the MFI, additionally, any peak fluorescence shifting towards the right was considered as evidence for cellular pathway mechanism, respectively.

R-DTX-NLC, R-GLA-DTX-NLC, R-ALA-DTX-NLC, and R-SA43-DTX-NLC showed less fluorescence intensity under the microscope, when treated and incubated at 4 °C for 2 and 4 h incubation time in both cell lines and examined under the same conditions; indicating that for all four formulations, the uptake was thought to be an active energy-dependent transport as evidenced by low uptake at 4 °C (Figures 4.34 b, c, 4.35 b, c, 4.38 b, c, 4.39 b, c, 4.42 b, c, 4.43 b, c, 4.46 b, c, 4.47 b, c). Moreover, the MFI results when the four formulations incubated at 4 °C with both cell lines (Figures 4.36, 4.40, 4.44, and 4.48) demonstrated a significant reduction in the MFI as compared to the incubation of same formulations at 37 °C. These results were in line with previous reports (Aptekar *et al.,* 2015, Wong *et al.,* 2017). Figures 4.37 c, d, 4.43 c, d, 4.47 c, d, 4.49 c, d, respectively, also display the peak locations of the four formulations incubated at 4 °C was close to the peaks position of the untreated control cells vs. the peak positions of the similar formulations when incubated at 37 °C that was further to the right side. As previously explained by Kam *et al.,* (2006) and Thurn *et al.,* (2011), if the uptake process was hindered by incubating the treatment at a lower temperature (4 °C rather than 37 °C) indicates the uptake mechanism is the energy-dependent endocytosis process. In addition, to further determine whether clathrin-mediated pathway has a role for the internalisation of the four formulations, both cell lines were incubated with 0.45 M sucrose, pre- and during the incubation of cell lines with the four formulations. Any disruption of the uptake process when the cells are incubated under hypertonic environment suggest that NPs were internalised through clathrin-mediated pathway Sahay *et al.,* (2010). Our findings indicate that clathrin pathway is one of the pathways that all four formulations exhibited to gain entry in both the cell line due to the fact that less fluorescence intensity was notable under the microscope (Figures 4.34 d, 4.35 d, 4.38

d, 4.39 d, 4.42 d, 4.43 d, 4.46 d, and 4.47 d) especially for SVG P12 cell lines and a highly significant reduction in MFI was displayed when both cells lines were incubated with the four formulations in the presence of sucrose vs the MFI of four formulations incubated without inhibitor (Figure 4.36). Additionally, the flow cytometer histograms for both cell lines also suggested a disruption in uptake, due to lower peaks intensity when compared to control untreated cell lines (Figures 4.37 a, b, 4.41 a, b, 4.45 a, b, 4.59 a, b). From these results, we gathered that clathrin-mediated pathway might strongly be one of the internalisation pathways that all four formulations exhibited. To assess the internalisation of all four formulations through caveolae/ lipid rafts pathway, both cell lines were treated with 5 µg/ml nystatin pre- and during treatment with the formulations. Nystatin disrupts the cholesterol distribution, it binds to cholesterol moiety and thus disrupts lipid raft in the cell membrane by directly inserting into the membrane and sequestering cholesterol into complexes and thus inhibit entry of molecule via caveolae-mediated endocytosis (Kam *et al.,* 2006).

Both cell lines were characterised by low fluorescence intensity under the microscope (Figures 4.34 f, 4.35 f, 4.38 f, 4.39 f, 4.42 f, 4.43 f, 4.46 f, and 4.47 f) with very noticeable results for SVG P12, and further confirmation that caveolae/ lipid rafts pathway might be another uptake pathway of all the four formulations. Similar results were also obtained with a significant reduction in MFI of both cell lines U87MG and SVG when pretreated with nystatin before treatment with the formulations.

To clarify the involvement of micropinocytosis/phagocytosis in all four formulations uptake, both cell lines were treated with cytochalasin B (Cyto. B) pre- and during incubation of cell lines with the four formulations. Cytochalasin B depolymerises actin filaments which are important for the structure formation needed to enclose molecules. These actin filaments internalise particulate via macropinocytosis or phagocytosis. Thus, disruption of actin filament by cytochalasin B reduce the cell internalisation of the molecule (Martin *et al.,* 2012). The data obtained from the fluorescence microscopy suggested lower fluorescence intensity when both cell lines were incubated with Cyto. B (Figures 4.34 d, 4.35 d, 4.38 d, 4.39 d, 4.42 d, 4.43 d, 4.46 d, and 4.47 d). Additionally, the MFI acquired from the flow cytometer revealed a very significant reduction in the MFI of the cells when incubated with Cyto. B in both cell lines when compared with MFI of untreated cells with the Cyto. B. The data clearly suggests that micropinocytosis/phagocytosis was one of the pathways that were involved in all four formulations of uptake mechanisms. Interestingly all the three pathways clathrin-, caveolae- and macropinocytosis contributed internalisation of NLCs. This is in line with previous reports where lipid nanoparticles have shown to be internalised by more than one pathway (Thurn *et al.,* 2011).

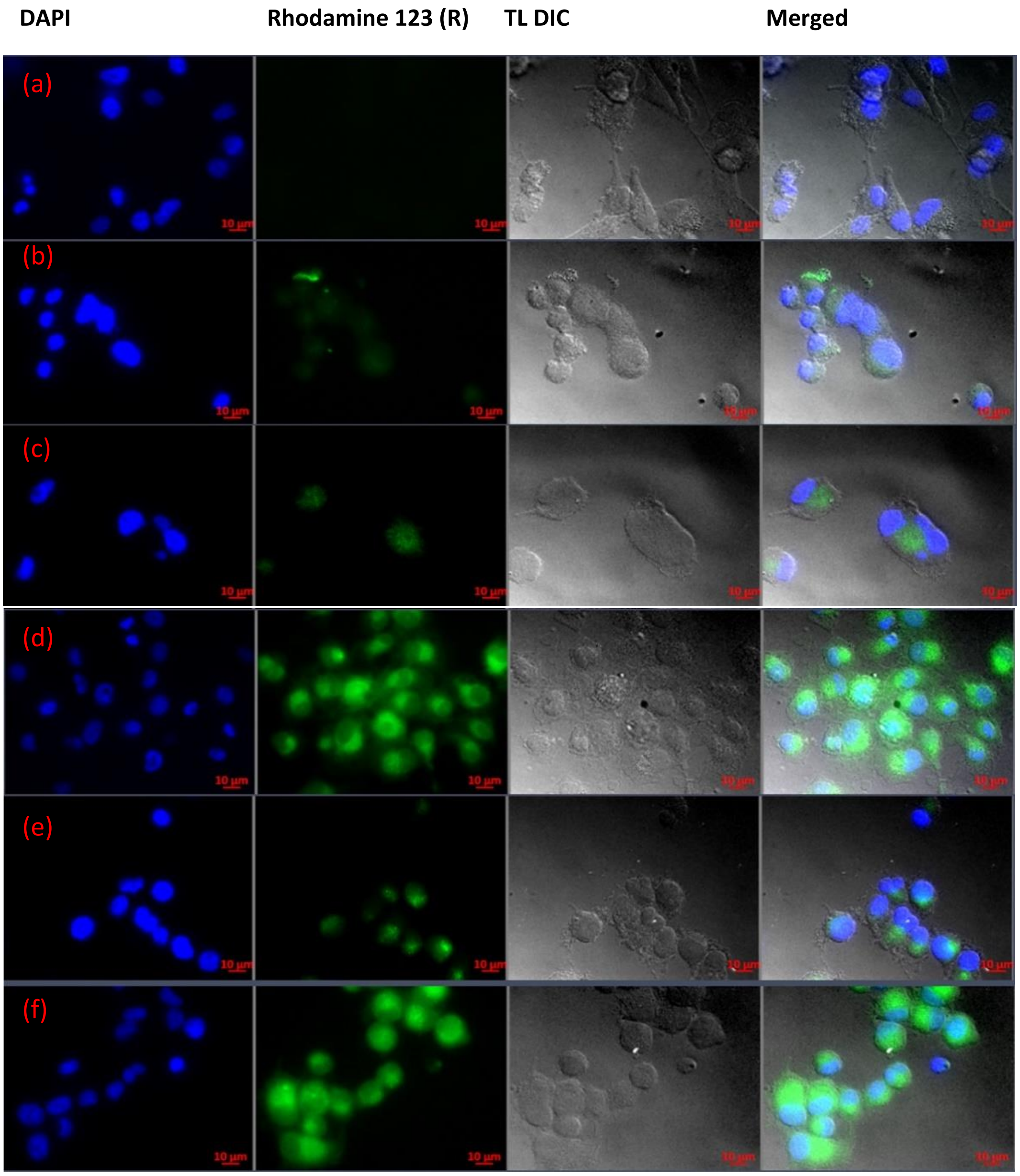

Figure 4.34 Endocytosis pathways evaluations by fluorescence microscopy imaging, where the blue colour refers to the stained nucleus with a fluorescence dye (DAPI) and the green fluorescence dye refers to the R-DTX-NLC (Rhodamine 123 (R) loaded within the DTX-NLC). (a) U87MG control untreated cells only stained with DAPI, (b) U87MG incubated for 2 h with R-DTX-NLC at 4 °C and the nuclei were stained with DAPI, (c) U87MG incubated for 4 h with R-DTX-NLC at 4 °C and the nuclei were stained with DAPI, (d) U87MG incubated with sucrose pre and during incubation with R-DTX-NLC for 4 h at 37 °C, (e) U87MG incubated with Cyto. B (cytochalasin B) pre and during incubation with R-DTX-NLC for 4 h at 37 °C, (f) U87MG incubated with Nystatin pre and during incubation with R-DTX-NLC for 4 h at 37 °C. Data are N=3.

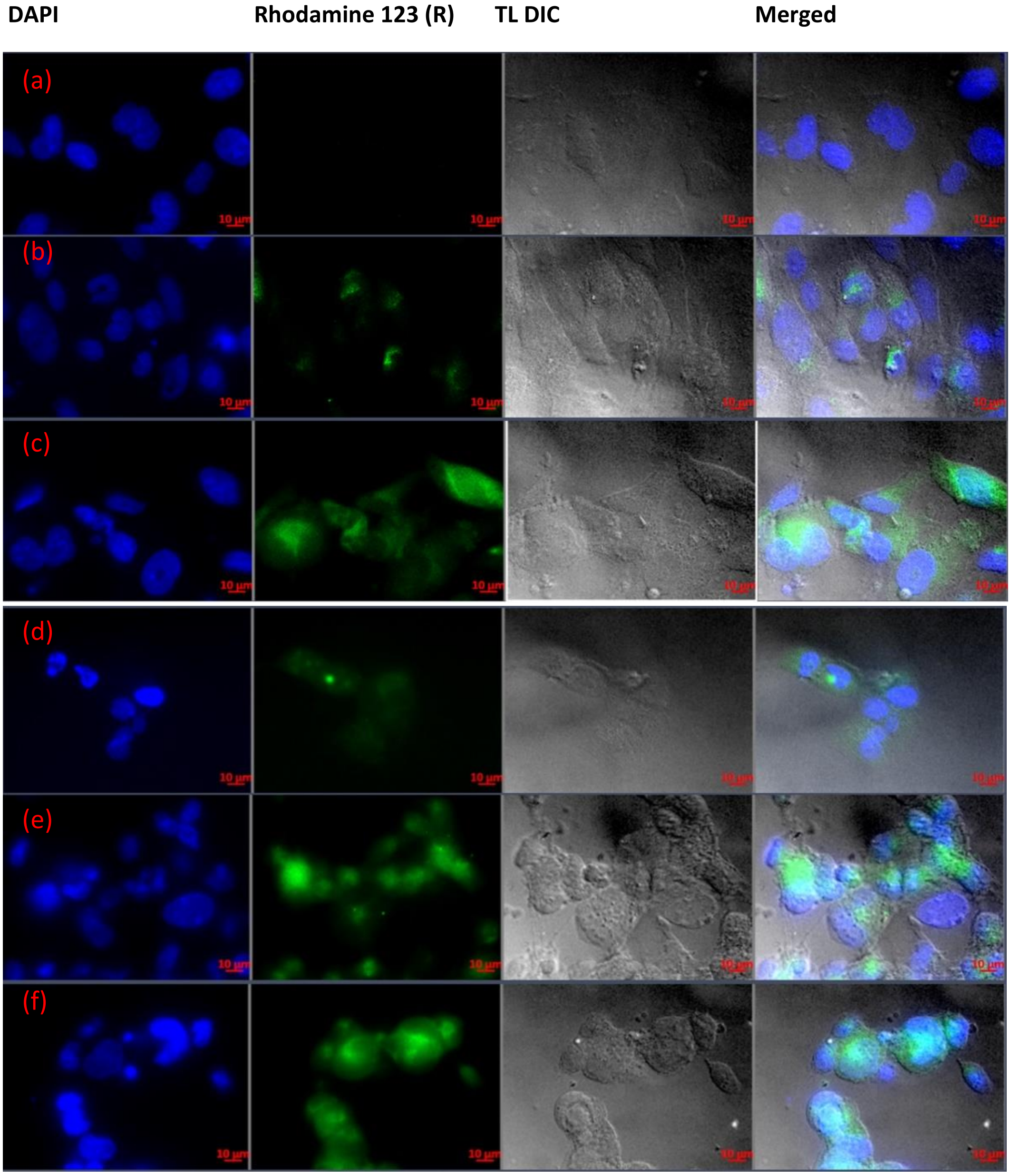

Figure 4.35 Endocytosis pathways evaluations by fluorescence microscopy imaging, where the blue colour refers to the stained nucleus with a fluorescence dye (DAPI) and the green fluorescence dye refers to the R-DTX-NLC (Rhodamine 123 (R) loaded within the DTX-NLC). (a) SVG P12 control untreated cells only stained with DAPI, (b) SVG P12 incubated for 2 h with R-DTX-NLC at 4 °C and the nuclei were stained with DAPI, (c) SVG P12 incubated for 4 h with R-DTX-NLC at 4 °C and the nuclei were stained with DAPI, (d) SVG P12 incubated with sucrose pre- and during incubation with R-DTX-NLC for 4 h at 37 °C, (e) SVG P12 incubated with Cyto. B (cytochalasin B) pre- and during incubation with R-DTX-NLC for 4 h at 37 °C, (f) SVG P12 incubated with Nystatin pre and during incubation with R-DTX-NLC for 4 h at 37 °C. Data are N=3.

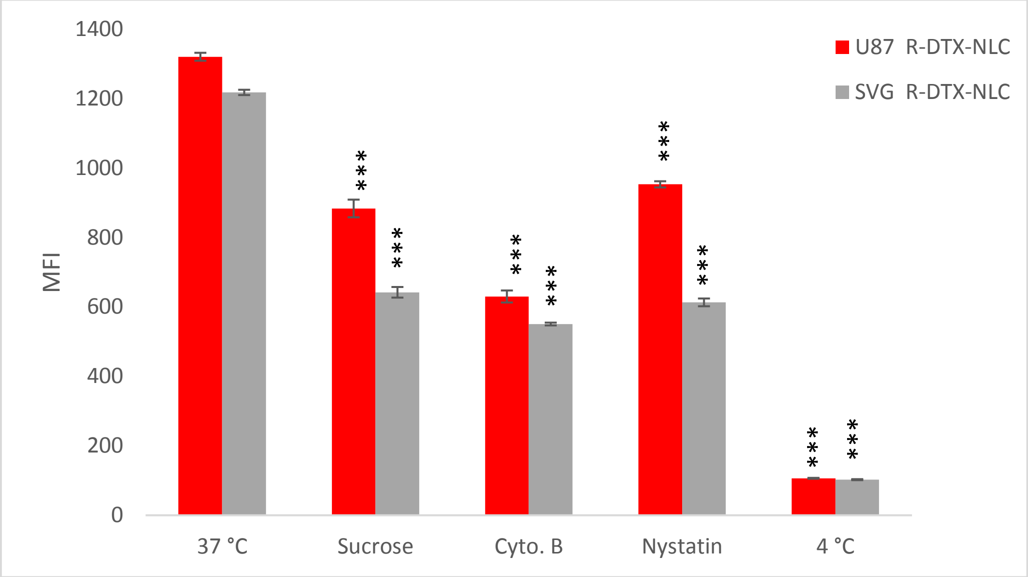

*Figure 4.36 MFI for U87MG and SVG P12 cell lines treated with endocytosis pathways inhibitors pre and during incubation with R-DTX-NLC. Data are mean and ± SD, (N=3). *** p < 0.000, refers to a very significant difference when all data were compared to R-DTX-NLC incubated at 37 °C, as the control in this case.*

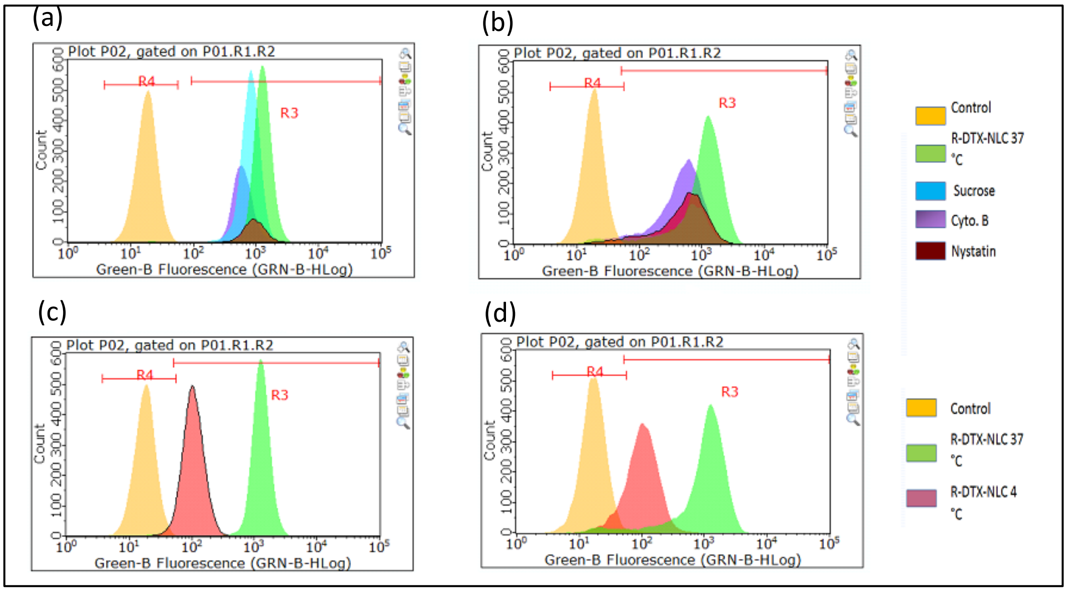

Figure 4.37 Flow cytometer histograms for U87MG and SVG P12 cell lines treated with endocytosis pathways inhibitors pre and during incubation with R-DTX-NLC where (a) U87MG treated with sucrose, Cyto. B, and Nystatin, (b) SVG P12 treated with sucrose, Cyto. B and Nystatin, (c) U87MG incubated with R-DTX-NLC at 4 °C and 37 °C, (d) SVG P12 incubated with R-DTX-NLC at 4 °C and 37 °C. T control, in this case, is the untreated cell lines. Data are N=3.

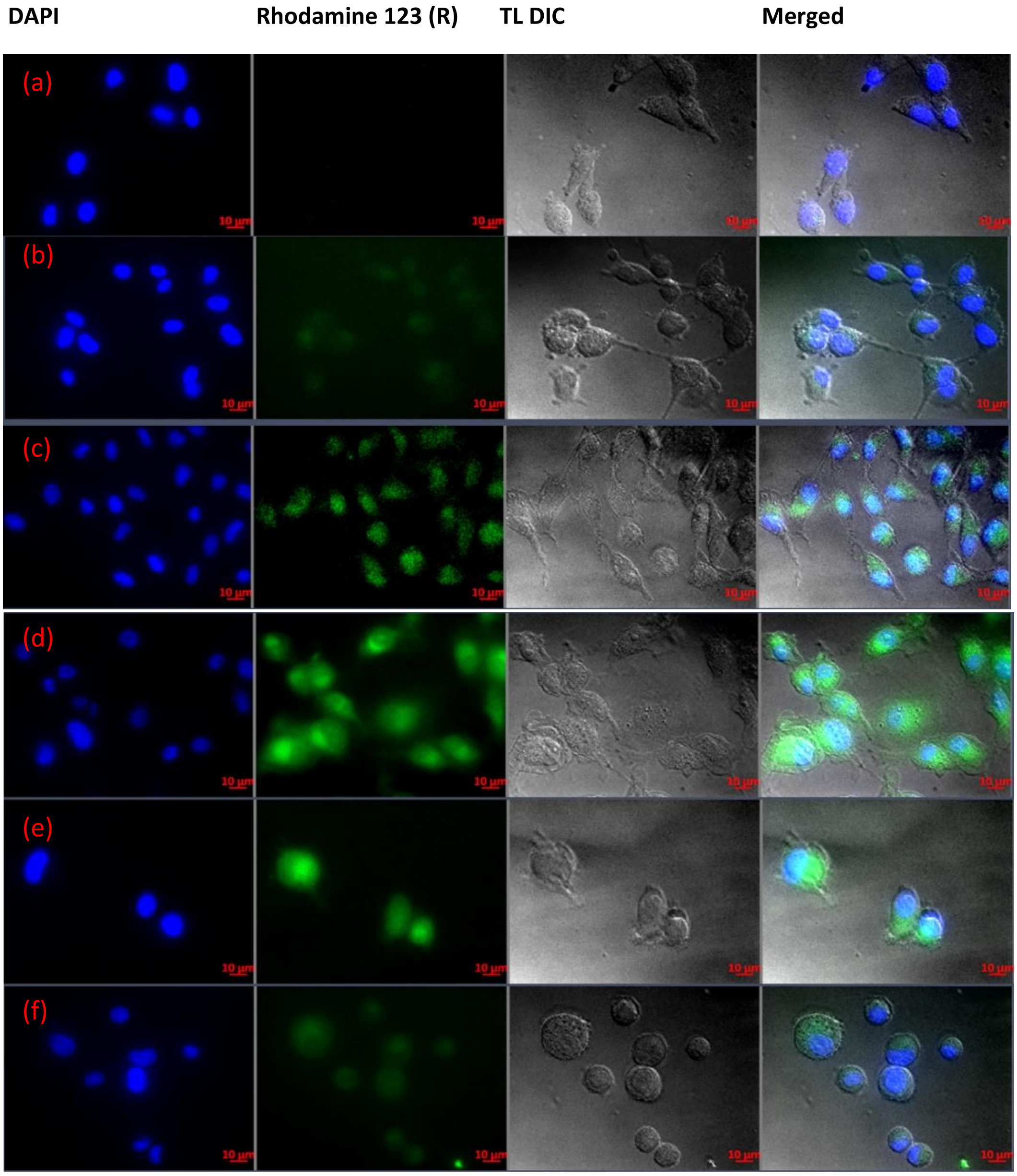

Figure 4.38 Endocytosis pathways evaluations by fluorescence microscopy imaging, where the blue colour refers to the stained nucleus with a fluorescence dye (DAPI) and the green fluorescence dye refers to the R-GLA-DTX-NLC (Rhodamine 123 (R) loaded within the DTX-NLC). (a) U87MG control untreated cells only stained with DAPI, (b) U87MG incubated for 2 h with R-GLA-DTX-NLC at 4 °C and the nuclei were stained with DAPI, (c) U87MG incubated for 4 h with R-GLA-DTX-NLC at 4 °C and the nuclei were stained with DAPI, (d) U87MG incubated with sucrose pre- and during incubation with R-GLA-DTX-NLC for 4 h at 37 °C, (e) U87MG incubated with Cyto. B (cytochalasin B) pre- and during incubation with R-GLA-DTX-NLC for 4 h at 37 °C, (f) U87MG incubated with Nystatin pre and during incubation with R-GLA-DTX-NLC for 4 h at 37 °C. Data are N=3.

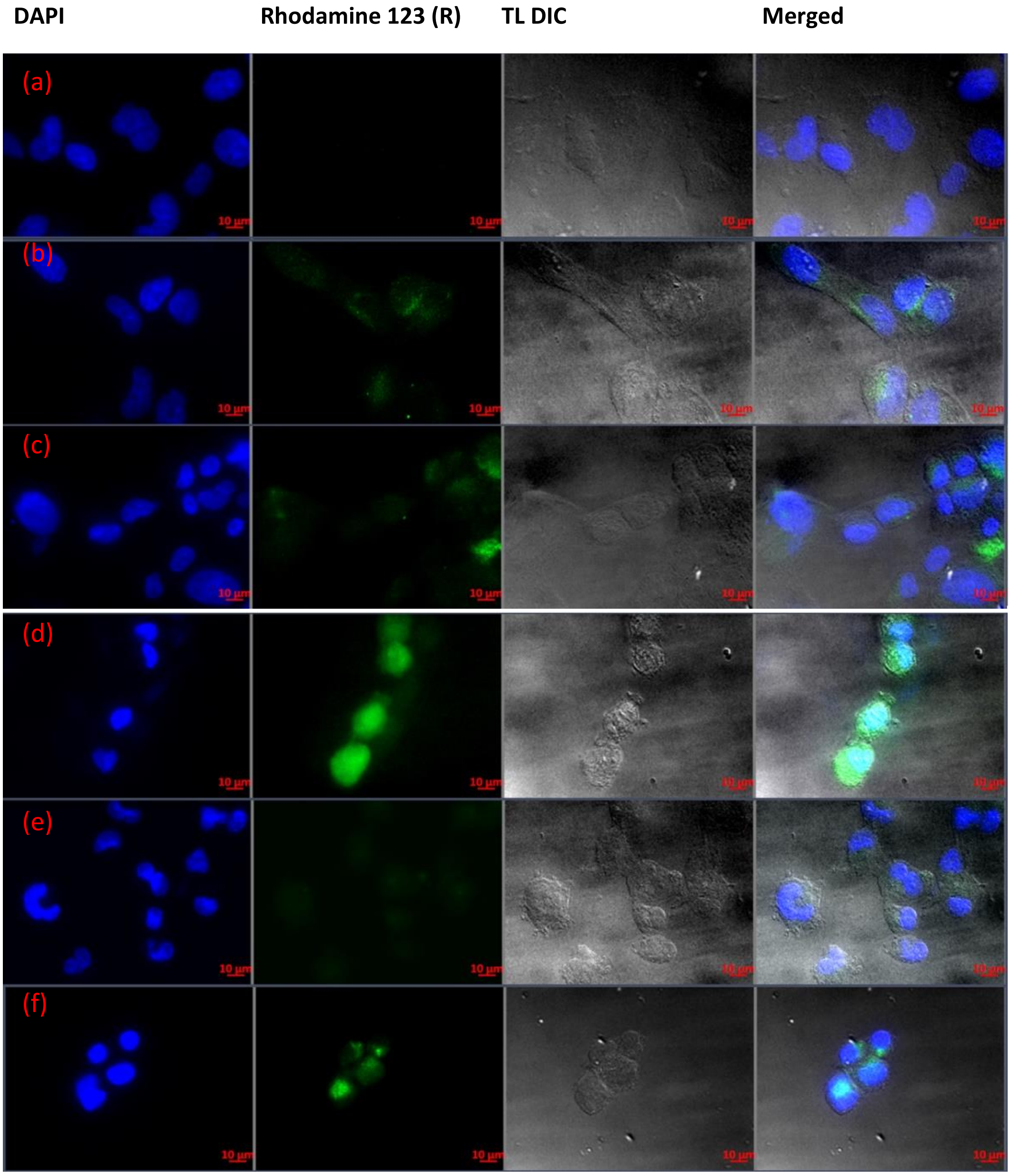

Figure 4.39 Endocytosis pathways evaluations by fluorescence microscopy imaging, where the blue colour refers to the stained nucleus with a fluorescence dye (DAPI) and the green fluorescence dye refers to the R-GLA-DTX-NLC (Rhodamine 123 (R) loaded within the DTX-NLC). (a) SVG P12 control untreated cells only stained with DAPI, (b) SVG P12 incubated for 2 h with R-GLA-DTX-NLC at 4 °C and the nuclei were stained with DAPI, (c) SVG P12 incubated for 4 h with R-GLA-DTX-NLC at 4 °C and the nuclei were stained with DAPI, (d) SVG P12 incubated with sucrose pre- and during incubation with R-GLA-DTX-NLC for 4 h at 37 °C, (e) SVG P12 incubated with Cyto. B (cytochalasin B) pre- and during incubation with R-GLA-DTX-NLC for 4 h at 37 °C, (f) SVG P12 incubated with Nystatin pre and during incubation with R-GLA-DTX-NLC for 4 h at 37 °C. Data are N=3.

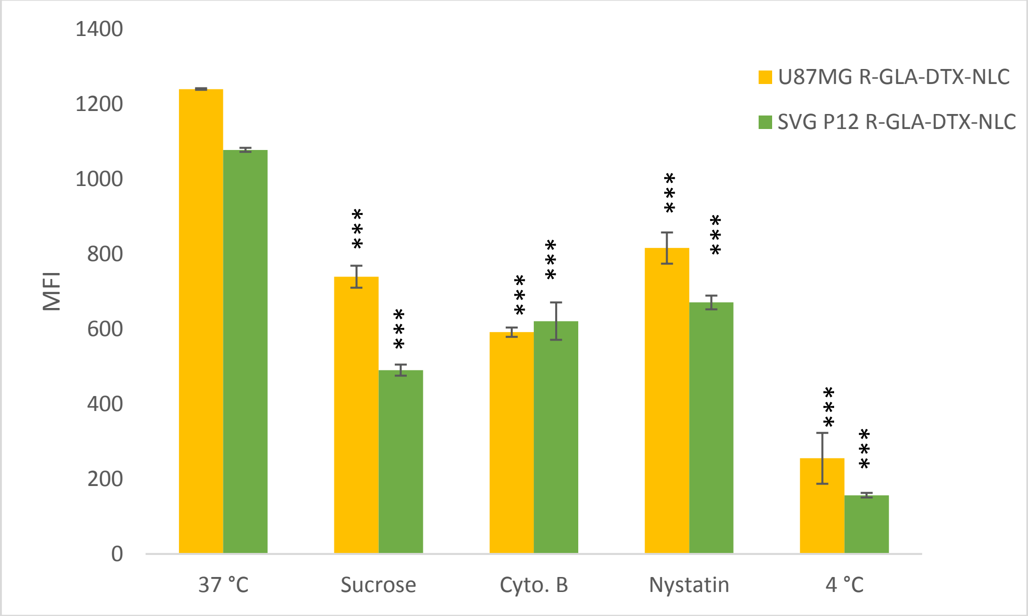

*Figure 4.40 MFI for U87MG and SVG P12 cell lines treated with endocytosis pathways inhibitors pre and during incubation with R-GLA-DTX-NLC. Data are mean and ± SD, (N=3). *** p < 0.000, refers to a very significant difference when all data were compared to R-GLA-DTX-NLC incubated at 37 °C, as the control in this case.*

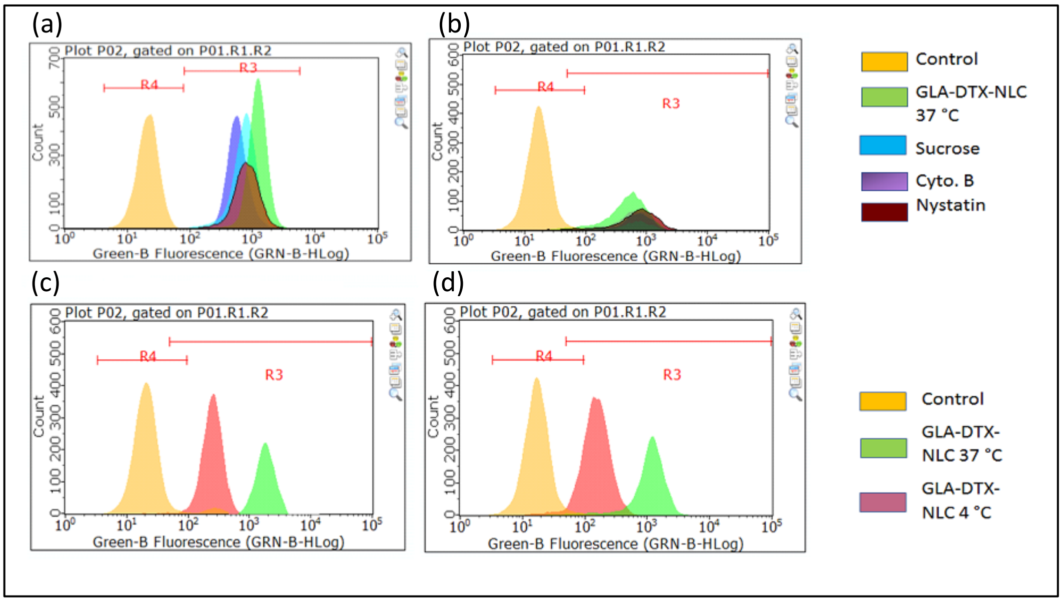

Figure 4.41 Flow cytometer histograms for U87MG and SVG P12 cell lines treated with endocytosis pathways inhibitors pre and during incubation with R-GLA-DTX-NLC where (a) U87MG treated with sucrose, Cyto. B, and Nystatin, (b) SVG P12 treated with sucrose, Cyto. B and Nystatin, (c) U87MG incubated with R-GLA-DTX-NLC at 4 °C and 37 °C, (d) SVG P12 incubated with R-GLA-DTX-NLC at 4 °C and 37 °C. T control, in this case, is the untreated cell lines. Data are N=3.

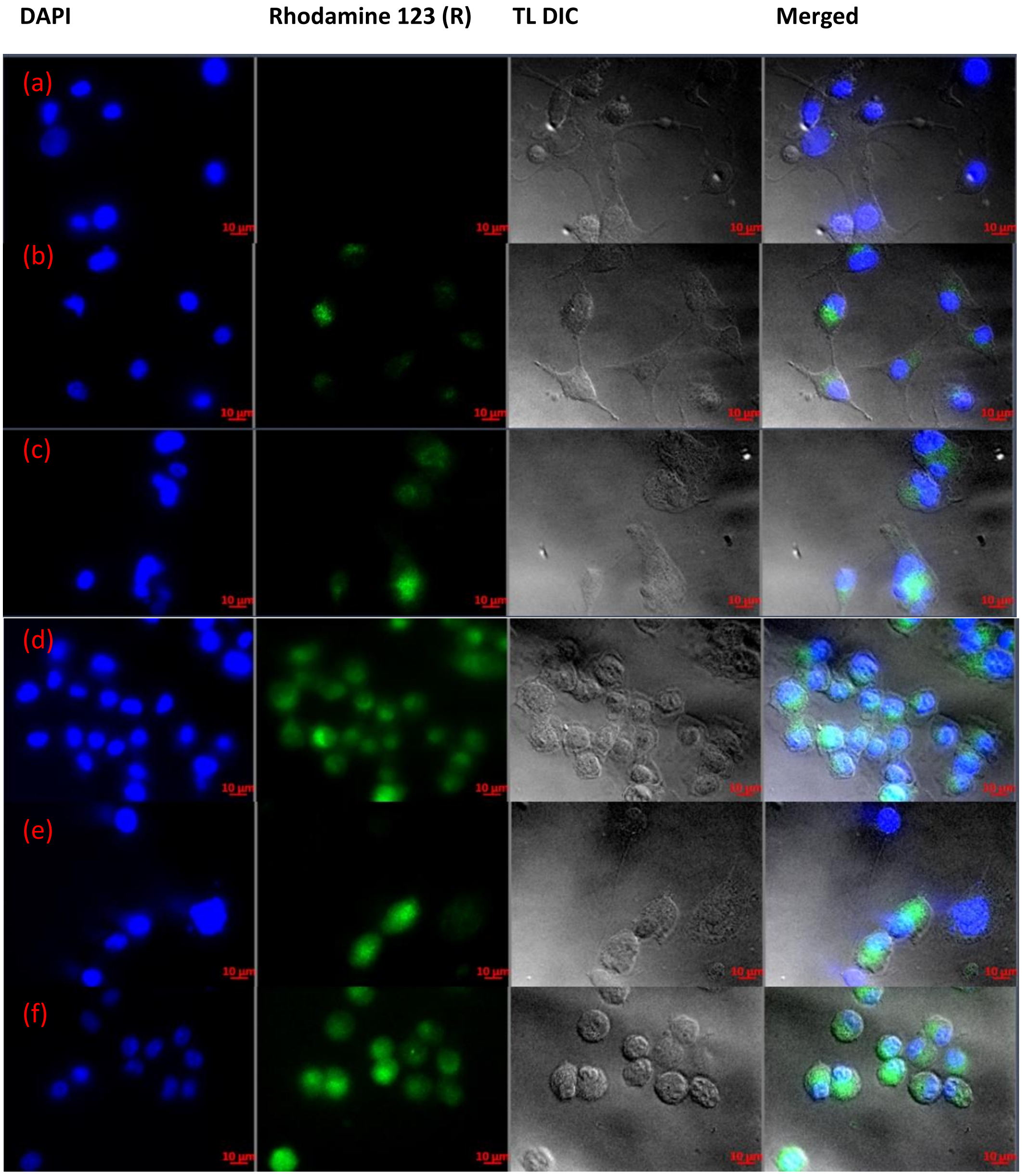

Figure 4.42 Endocytosis pathways evaluations by fluorescence microscopy imaging, where the blue colour refers to the stained nucleus with a fluorescence dye (DAPI) and the green fluorescence dye refers to the R-ALA-DTX-NLC (Rhodamine 123 (R) loaded within the DTX-NLC). (a) U87MG control untreated cells only stained with DAPI, (b) U87MG incubated for 2 h with R-ALA-DTX-NLC at 4 °C and the nuclei were stained with DAPI, (c) U87MG incubated for 4 h with R-ALA-DTX-NLC at 4 °C and the nuclei were stained with DAPI, (d) U87MG incubated with sucrose pre- and during incubation with R-ALA-DTX-NLC for 4 h at 37 °C, (e) U87MG incubated with Cyto. B (cytochalasin B) pre- and during incubation with R-ALA-DTX-NLC for 4 h at 37 °C, (f) U87MG incubated with Nystatin pre- and during incubation with R-ALA-DTX-NLC for 4 h at 37 °C. Data are N=3.

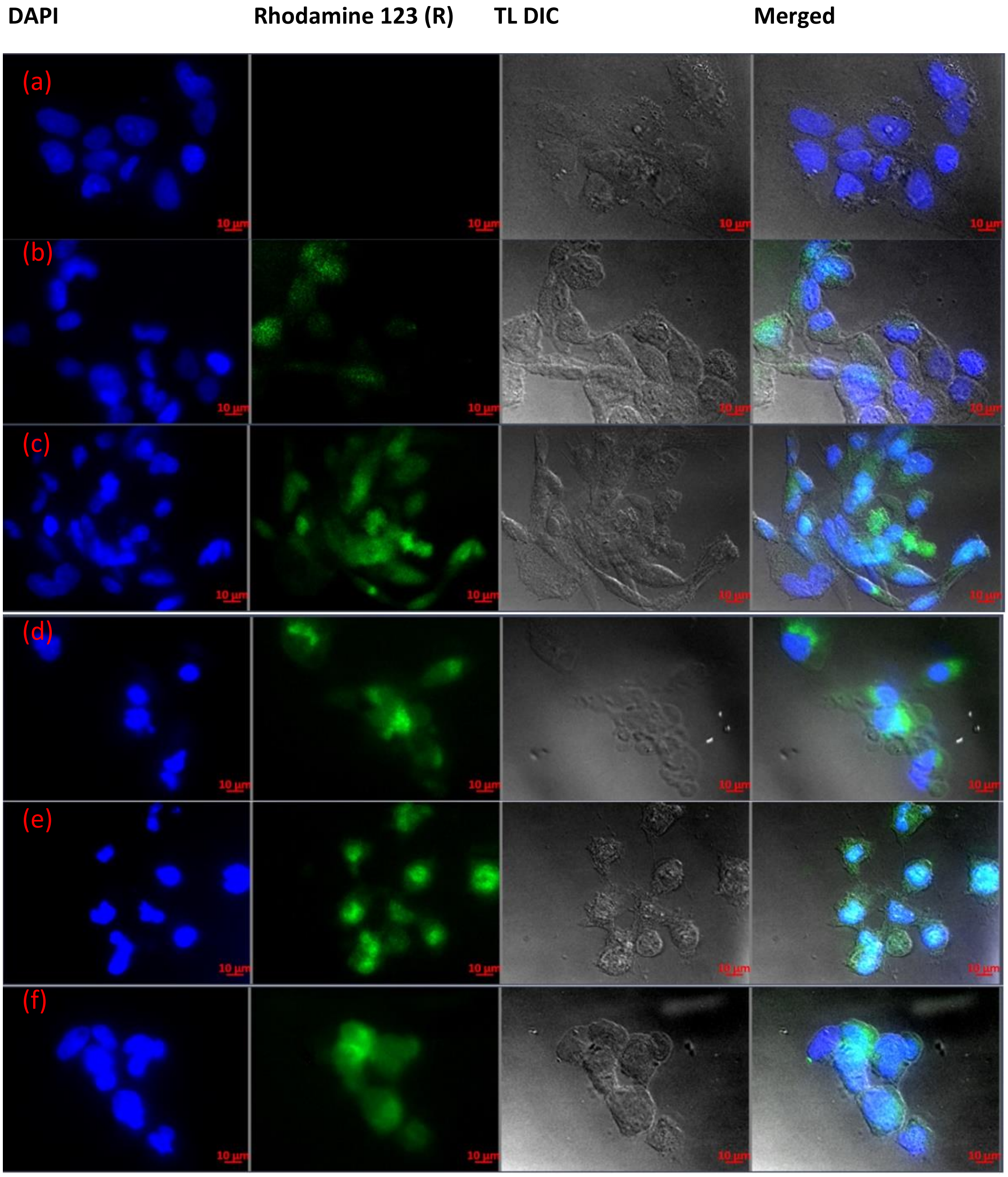

Figure 4.43 Endocytosis pathways evaluations by fluorescence microscopy imaging, where the blue colour refers to the stained nucleus with a fluorescence dye (DAPI) and the green fluorescence dye refers to the R-ALA-DTX-NLC (Rhodamine 123 (R) loaded within the DTX-NLC). (a) SVG P12 control untreated cells only stained with DAPI, (b) SVG P12 incubated for 2 h with R-ALA-DTX-NLC at 4 °C and the nuclei were stained with DAPI, (c) SVG P12 incubated for 4 h with R-ALA-DTX-NLC at 4 °C and the nuclei were stained with DAPI, (d) SVG P12 incubated with sucrose pre- and during incubation with R-ALA-DTX-NLC for 4 h at 37 °C, (e) SVG P12 incubated with Cyto. B (cytochalasin B) pre- and during incubation with R-ALA-DTX-NLC for 4 h at 37 °C, (f) SVG P12 incubated with Nystatin pre and during incubation with R-ALA-DTX-NLC for 4 h at 37 °C. Data are N=3.

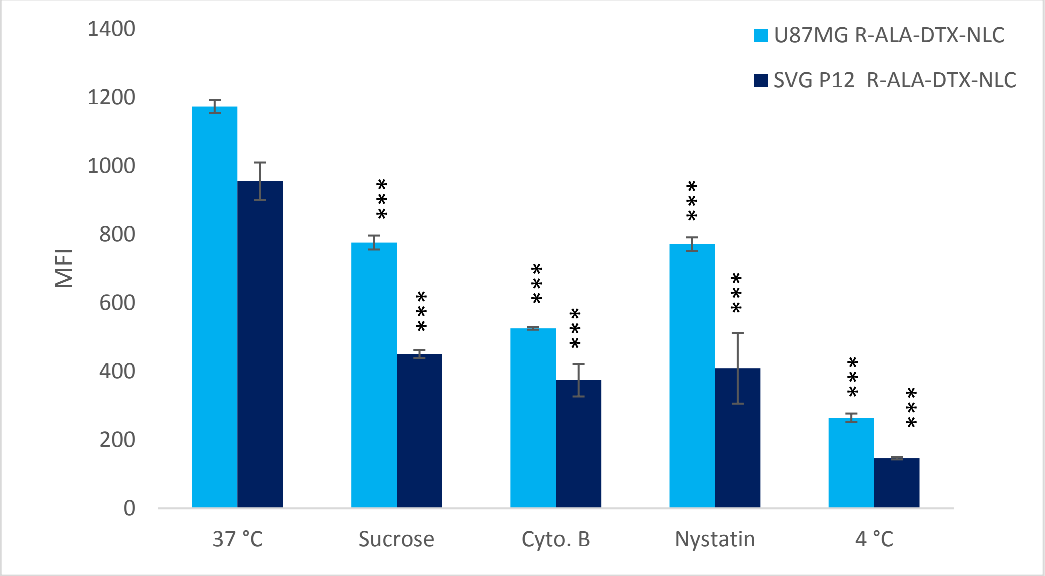

*Figure 4.44 MFI for U87MG and SVG P12 cell lines treated with endocytosis pathways inhibitors pre and during incubation with R-ALA-DTX-NLC. Data are mean and ± SD, (N=3). *** p < 0.000, refers to a very significant difference when all data were compared to R-ALA-DTX-NLC incubated at 37 °C, as the control in this case.*

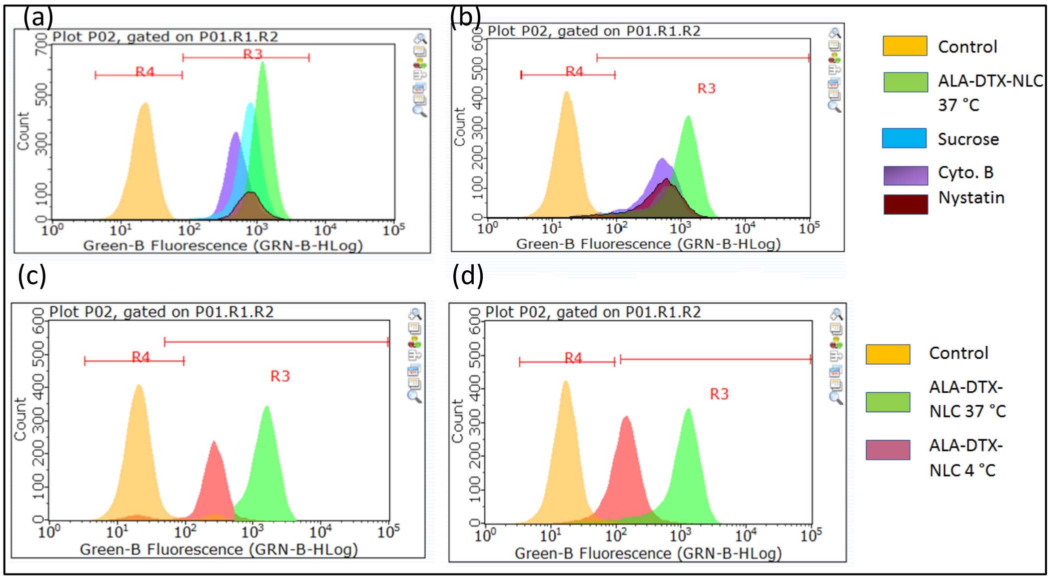

Figure 4.45 Flow cytometer histograms for U87MG and SVG P12 cell lines treated with endocytosis pathways inhibitors pre and during incubation with R-ALA-DTX-NLC where (a) U87MG treated with sucrose, Cyto. B, and Nystatin, (b) SVG P12 treated with sucrose, Cyto. B and Nystatin, (c) U87MG incubated with R-ALA-DTX-NLC at 4 °C and 37 °C, (d) SVG P12 incubated with R-ALA-DTX-NLC at 4 °C and 37 °C. T control, in this case, is the untreated cell lines. Data are N=3.

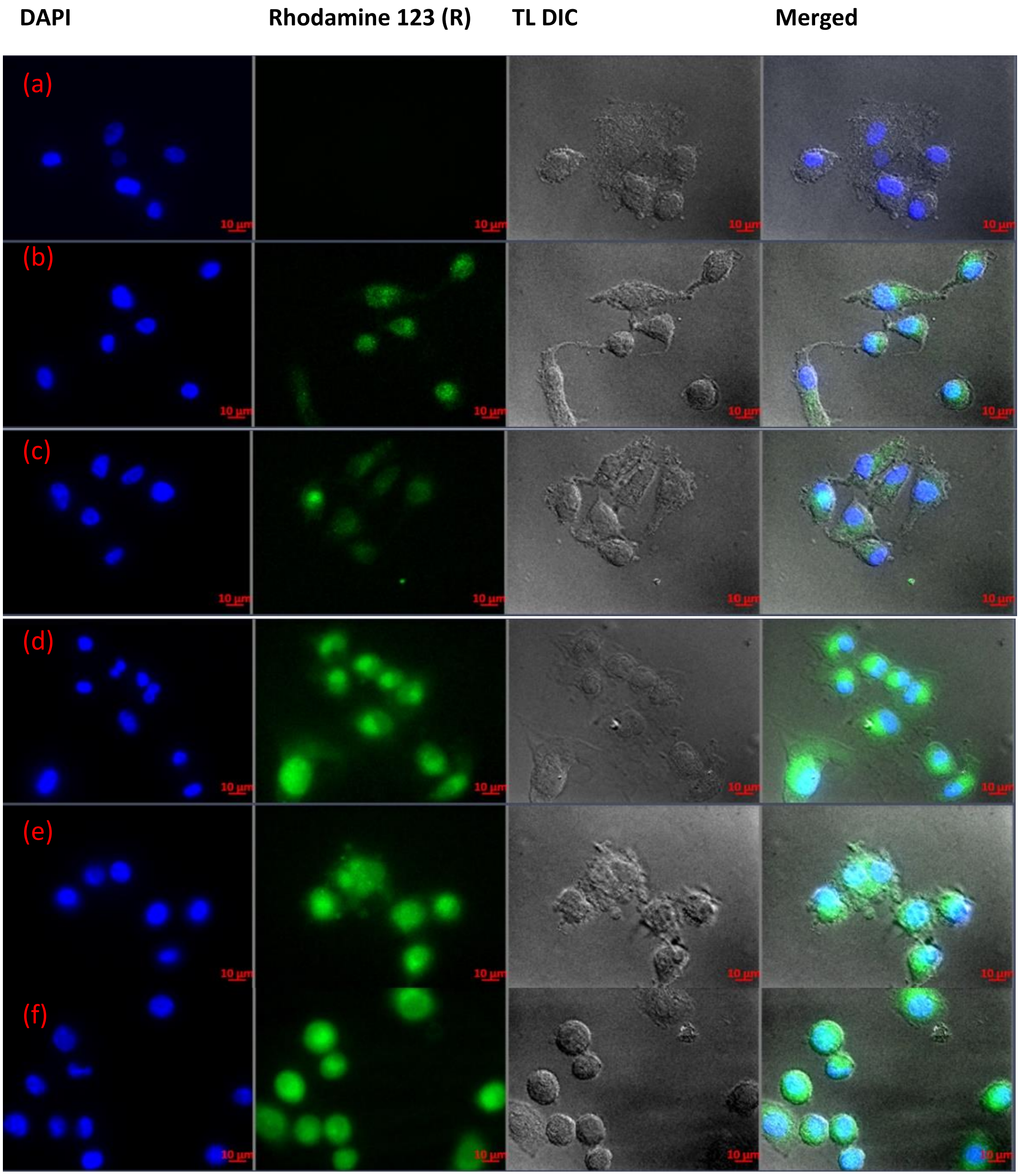

Figure 4.46 Endocytosis pathways evaluations by fluorescence microscopy imaging, where the blue colour refers to the stained nucleus with a fluorescence dye (DAPI) and the green fluorescence dye refers to the R-SA43-DTX-NLC (Rhodamine 123 (R) loaded within the DTX-NLC). (a) U87MG control untreated cells only stained with DAPI, (b) U87MG incubated for 2 h with R-SA43-DTX-NLC at 4 °C and the nuclei were stained with DAPI, (c) U87MG incubated for 4 h with R-SA43-DTX-NLC at 4 °C and the nuclei were stained with DAPI, (d) U87MG incubated with sucrose pre- and during incubation with R-SA43-DTX-NLC for 4 h at 37 °C, (e) U87MG incubated with Cyto. B (cytochalasin B) pre- and during incubation with R-SA43-DTX-NLC for 4 h at 37 °C, (f) U87MG incubated with Nystatin pre and during incubation with R-SA43-DTX-NLC for 4 h at 37 °C. Data are N=3.

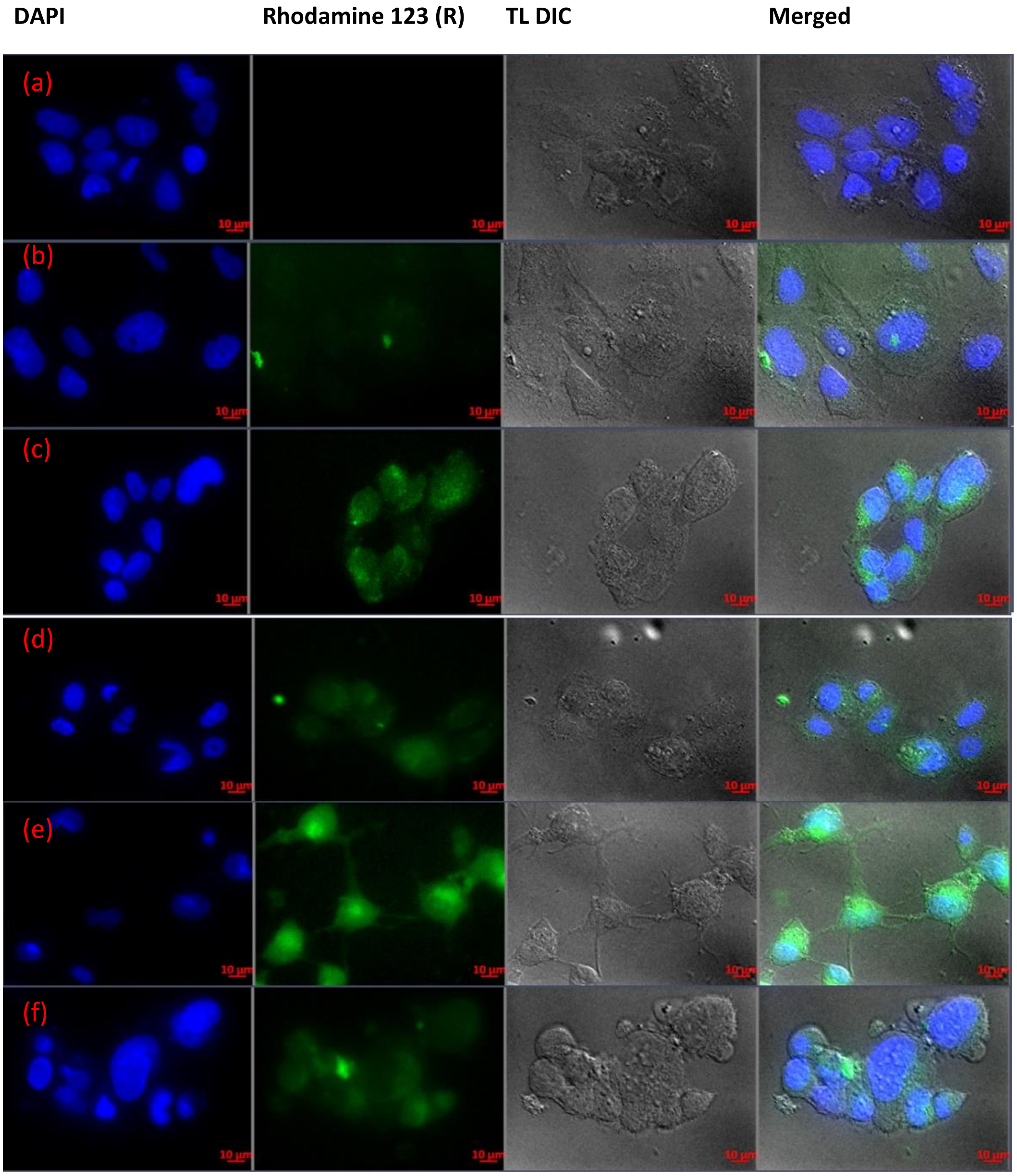

Figure 4.47 Endocytosis pathways evaluations by fluorescence microscopy imaging, where the blue colour refers to the stained nucleus with a fluorescence dye (DAPI) and the green fluorescence dye refers to the R-SA43-DTX-NLC (Rhodamine 123 (R) loaded within the DTX-NLC). (a) SVG P12 control untreated cells only stained with DAPI, (b) SVG P12 incubated for 2 h with R-SA43-DTX-NLC at 4 °C and the nuclei were stained with DAPI, (c) SVG P12 incubated for 4 h with R-SA43-DTX-NLC at 4 °C and the nuclei were stained with DAPI, (d) SVG P12 incubated with sucrose pre- and during incubation with R-SA43-DTX-NLC for 4 h at 37 °C, (e) SVG P12 incubated with Cyto. B (cytochalasin B) pre- and during incubation with R-SA43-DTX-NLC for 4 h at 37 °C, (f) SVG P12 incubated with Nystatin pre and during incubation with R-SA43-DTX-NLC for 4 h at 37 °C. Data are N=3.

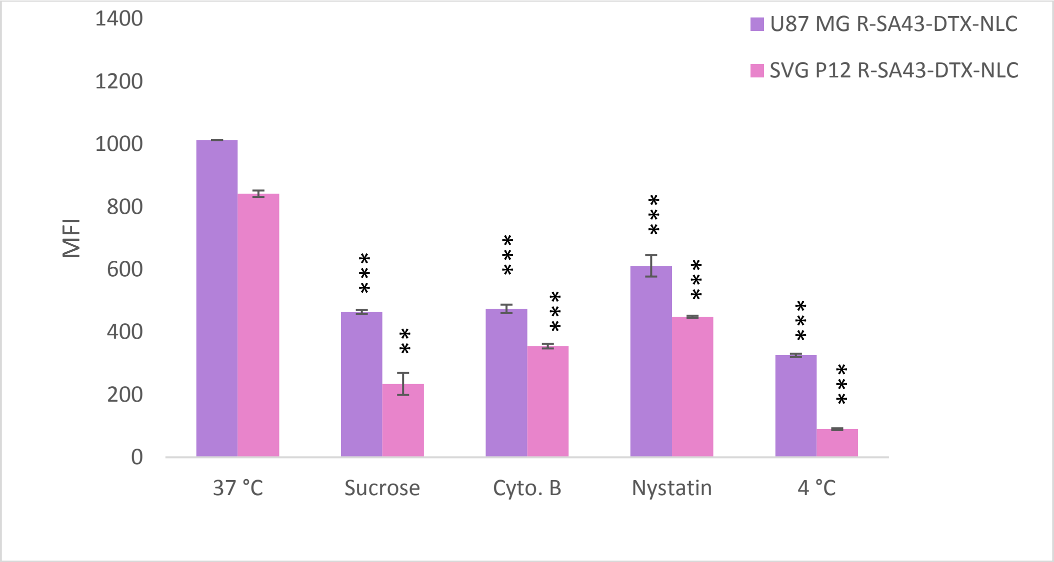

*Figure 4.48 MFI for U87MG and SVG P12 cell lines treated with endocytosis pathways inhibitors pre and during incubation with R-SA43-DTX-NLC. Data are mean and ± SD, (N=3). *** p < 0.000, refers to a very significant difference when all data were compared to R-SA43-DTX-NLC incubated at 37 °C, as the control in this case.*

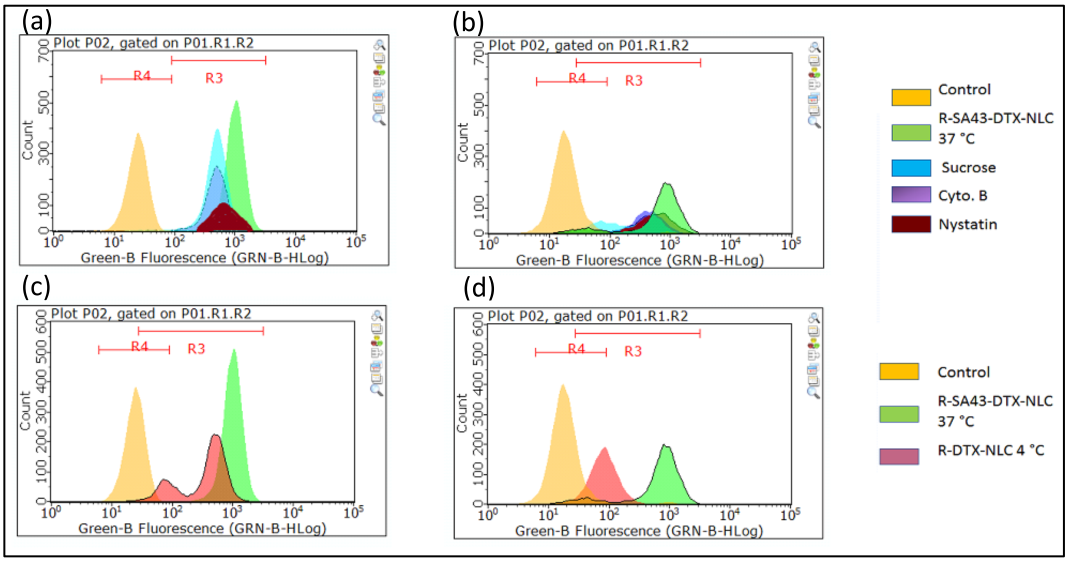

Figure 4.49 Flow cytometer histograms for U87MG and SVG P12 cell lines treated with endocytosis pathways inhibitors pre and during incubation with R-SA43-DTX-NLC where (a) U87MG treated with sucrose, Cyto. B, and Nystatin, (b) SVG P12 treated with sucrose, Cyto. B and Nystatin, (c) U87MG incubated with R-SA43-DTX-NLC at 4 °C and 37 °C, (d) SVG P12 incubated with R-SA43-DTX-NLC at 4 °C and 37 °C. The control, in this case, is the untreated cell lines. Data are N=3.

4.5.6. Cell cycle analysis

The cell cycle distribution of DTX-NLC, GLA-DTX-NLC, ALA-DTX-NLC, and SA43-DTX-NLC was performed to understand whether the NLCs loaded with DTX will follow the same pattern of DTX G2/M cell cycle arrest phase. DTX is a well-known mitotic inhibitor, and it can suppress cell growth by inducing G2/M cell cycle arrest (Choi *et al.,* 2015). Following 24 h treatment of glioblastoma U87MG cell line with the above-mentioned formulations and DTX (Figures 4.50 and 4.51), the results demonstrated the distribution of the formulations into a different cell cycle phases with a very significant reduction in G0/G1 phase when all formulations and DTX were compared to the G0/G1 phase of untreated U87MG as a control (Figure 4.51). The following order from higher to lower % cells in G0/G1 phase (Figures 4.50 and 4.51) U87MG untreated, ALA-DTX-NLC, DTX, DTX-NLC, GLA-DTX-NLC, and SA43-DTX-NLC (61.0, 20.43, 16.31, 10.54, 9.27, and 5.0 %), respectively. Phase S exhibited the order from higher to lower % cells in S phase (Figure 4.50), ALA-DTX-NLC, U87MG untreated, GLA-DTX-NLC, DTX-NLC, DTX, and SA43-DTX-NLC (9.84, 8.24, 5.74, 4.17, 4.09, and 3.18 %) respectively, with a very significant difference in the S phase cell cycle distribution when all formulation and DTX were compared to the untreated U87MG cell line as a control. In addition, the G2/M phase which taxanes are widely known display was encountered in high % in DTX-NLC and all surface modified DTX-NLC over a very significant reduction in the G2/M phase of the untreated U87MG as a control. The G2/M phase quantification is presented in figure 4.47 and followed the order from higher to the lowest G2/M phase, SA43-DTX-NLC, DTX-NLC, GLA-DTX-NLC, DTX, ALA-DTX-NLC, and untreated U87MG cell line (91.62, 85.26, 84.13, 79.49, 69.69, and 29.24%), respectively. It is worth noting that SA43-DTX-NLC was showed the highest percent of G2/M cell cycle phase population amongst all other examined formulations and DTX, demonstrating that when the DTX-NLC was conjugated with SA43-aptamer it caused a concomitant increase in the G2/M phase, so consequently strong cell division and growth inhibition, and eventually faster cell arrest would be connected to the presence of the SA43-aptamer on the surface of the DTX-NLCs. Furthermore, GLA-DTX-NLC and DTX-NLC also demonstrated similar findings as for the SA43-DTX-NLC with slightly lower percent distribution in G2/M phase than the SA43-DTX-NLC indicating that DTX-NLC surface modification with GLA had a similar effect as the DTX-NLC, and did not enhance the cell arrest due to no significant difference in G2/M phase between the two formulations. In contrast, ALA-DTX-NLC contributed less to effect on cell inhibition when the DTX-NLC was surface modified with ALA due to a highly significant reduction in G2/M phase by ALA-DTX-NLC when compared to the G2/M phase arrest by DTX-NLC. At this point, it was highly remarkable to notice the effect of the presence of SA43-aptamer in boosting the cell inhibition, rather than the presence of PUFAs on the surface of the DTX-NLC, suggesting the SA43-DTX-NLC exhibited higher cell arrest in G2/M phase through breaking of the double-strain DNA and in theory damaging of the chromosome (Ree *et al.,* 2006). It is also safe to say that all examined formulation followed DTX pattern as a drug-induced G2/M cell cycle arrest was demonstrated by all the formulations (figures 4.50 and 4.51).

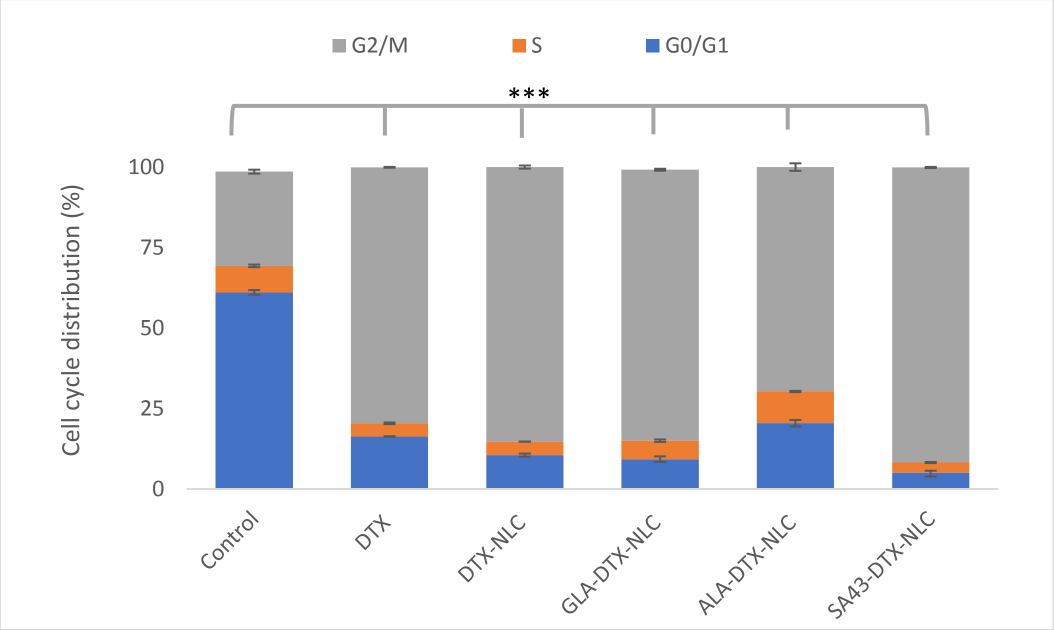

Figure 4.50 Percentage cell cycle distribution for U87MG cell lines following 24 h incubation with DTX, DTX-NLC, GLA-DTX-NLC, ALA-DTX-NLC, and SA43-DTX-NLC formulations. Data are mean and ± SD, (N=3). *** p < 0.000, refers to a very significant difference when formulations were compared to untreated U87MG as the control in this case.

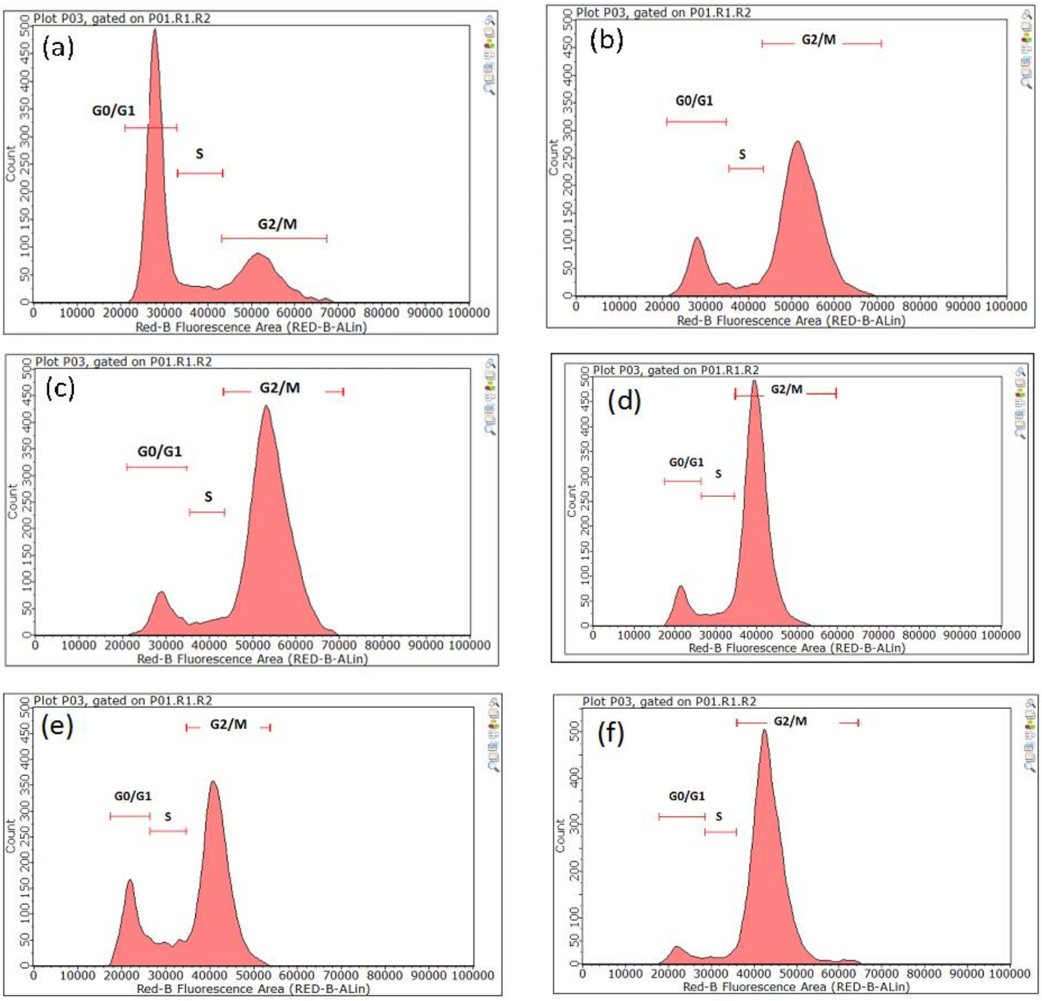

Figure 4.51 showing flow cytometer histograms for U87MG cell cycle following 24 h incubation with (a) control U87MG untreated cell lines (b) DTX (c) DTX-NLC (d) GLA-DTX-NLC (e) ALA-DTX-NLC, and (f) SA43-DTX-NLC. Data are N=3.

In summary, surface modification of DTX-NLC with PUFAs (GLA and ALA) improved the potency of DTX-NLC towards U87MG cell lines and demonstrated activity as good as DTX alone. ALA-DTX-NLC and GLA-DTX-NLC also exhibited more efficacy towards patient-derived BTNW911 cells at all time points in comparison to DTX-NLC.

Cellular internalisation and uptake were improved when DTX-NLC were surface modified with PUFAs and SA43-aptamer at all studied time points. In addition, SA43-DTX-NLC showed higher selectivity towards U87MG cell line than SVG P12. It was observed that the mechanism of cell uptake was through active transport due to binding SA43 to Ku 70 and Ku 80, and PUFAs ability to bind FABPs and the endocytosis was involved for internalisation through multiple pathways; and all four formulations exhibited cell cycle arrest at G2/M phase, with a very significant increase in G2/M phase for the SA43-DTX-NLC.

Chapter Five

3D *In-vitro* BBB model for evaluation of NLCs permeability

5.1. Introduction

5.1.1. *In-vitro* BBB model and their role in CNS drug delivery system

BBB models, especially tri-culture, represents the closest *in-vitro* model to the *in-vivo* neurovascular unit (Nakagawa *et al.,* 2007). The advantages of the *in vitro* models compared to the *in vivo* models are lower cost, a lower amount of compound required for quantitation of BBB permeability, higher throughput capacity, and the lower number of animals required for downstream drug testing if early screens are more physiologically relevant (Lundquist *et al.,* 2002). Hence *in-vitro* BBB model was investigated to establish as a proper and reliable model that can mimic all BBB functionalities for permeability, transport study and potential compound interaction with the BBB (Nielsen *et al.,* 2011; Kumar *et al.,* 2014; Bicker *et al.,* 2014). Nakagawa *et al.,* (2007) discovered that tri-culture models gave the highest TEER values when cells were seeded on a transwell insert, grown on the apical membrane to form a tri-culture. In this chapter we have used a tri-culture (3D *in-vitro* BBB model) that was established, characterised and validated in-house by Dr Alder research group (Kumar *et al*., 2014), where three primary cell lines of human origin were used in the reconstruction of all three BBB components for screening NPs, aptamers, and different compounds and evaluating their permeability through the 3D *in-vitro* BBB model (Kumar *et al.,* 2014).

5.1.2. Multidrug resistance

Multidrug resistance (MDR) also known as a drug efflux transporter called P-gp or MDR1 is highly expressed in the BBB. The P-gp pumps out the drug and compounds from the brain back to the blood side against concentration gradients, which comprises a substantial barrier in the treatment of CNS and malignant diseases (Kim 2002). In this study, we propose to encapsulate DTX a P-gp substrate (Loscher and Potschka, 2005) into NLCs to increase the DTX concentration in the brain (basolateral side of the 3D *in-vitro* BBB model) by using P-gp inhibitors Solutol® HS15 and Labrasol as surfactants during the fabrication of the DTX-NLCs. Furthermore, functionalisation of the DTX-NLCs with PUFAs ligands may potentially suppress the expression of the P-gp as indicated by Raghava and Lakshmi, (2012); thus, overcoming the DTX-NLCs efflux mechanisms.

5.2. Aim and objectives

The aim of this study was to evaluate the permeability of the developed DTX-NLC and surface modified DTX-NLCs with PUFAs (GLA-DTX-NLC and ALA-DTX-NLC), and selective aptamer SA43-DTX-NLC through a 3D *in-vitro* BBB model, and to investigate their potential uptake by glioblastoma U87MG cells on the basolateral (brain) side of the transwell after passing through the BBB model for assessment of their potential in targeted delivery for treatment of glioblastoma.

5.2.1. Objective 1

Fluorescence labelled formulations R-DTX-NLCs, R-GLA-DTX-NLC and R-ALA-DTX-NLC, and R-SA43-DTX-NLC were evaluated for apparent permeability by measuring transendothelial resistance (TEER) and appearance of fluorescence of NLCs on the basolateral side of a 3D *in-vitro* BBB model of three primary cell lines of human origin.

5.2.2. Objective 2

DTX-NLC and DTX solution were assessed for apparent permeability through the BBB model and DTX concentration was quantified by a validated HPLC method that was developed for this purpose (Chapter two section 2.5.3.3).

5.2.3. Objective 3

3D BBB model in the presence of U87MG on the basolateral side was used for examining the BBB permeability and glioblastomas uptake of fluorescence labelled formulations R-DTX-NLCs, R-GLA-DTX-NLC and R-ALA-DTX-NLC, and R-SA43-DTX-NLC through analysis using the flow cytometer.

5.2.4. Objective 4

Determination of the P-gp efflux pump activity for DTX-NLCs, GLA-DTX-NLC and ALA-DTX-NLC, and SA43-DTX-NLC through the BBB model.

5.3. Equipment and materials

5.3.1. Equipment

EVOM-2 purchased from (Merck Millipore, Oxford, UK), Tecan GENios Pro® plate reader (Tecan, Theale, UK). Humidified incubator supplied with 5 % CO_2 (Thermo Scientific Nunc, UK). Benchtop flow cytometer (Guava, Merck), and the data were analysed with Guava ® easyCyte software 3.1.1. (Guava, Merck). Benchtop centrifuge, at 179 x g for 5 min (ALC, Buckinghamshire, UK). Benchtop centrifuge was used for 30 min at 16300 x g (Spectrafuge 24D, Jencons-Pls, UK). (Agilent HPLC 1260 Infinity, Agilent Technologies, USA).

5.3.2. Materials

Fibronectin, Phosphate buffered saline (PBS) 0.1 M (pH7.4), and all plastic-ware including tissue culture flasks, well plates, centrifuge tubes, and 1.5 ml tubes were purchased from Fisher Scientific, Leicestershire, UK. Foetal bovine serum (FBS), L-glutamine, sodium pyruvate, non-essential amino acid (NEAA) and phosphate buffer saline (PBS). RNAase free water from Fisher, UK. Propidium iodide (PI), Trypsin solution 10X, Trypan blue, and Evans blue dye (EBD) were purchased from Sigma Aldrich, the UK and all lab consumables were purchased from Sigma, Dorset, UK. Human serum (HS), Endothelial basal media (EBM-2)/(EGM-2), Astrocyte basal media (ABM-2)/(AGM-2) kit and Eagle’s minimum essential medium (EMEM), Hank’s balanced salt solution (HBSS) were purchased from Lonza, UK. Pericyte medium (PM), was purchased from Caltag Medsystems. Non-tissue culture 96 well plate/ V-shaped was purchased and TryPLE Express were from Fisher, UK. Insert 6.5 mm transwell polystyrene with 8.0 µm pore polycarbonate membrane TC-treated sterile items were purchased from VWR, UK.

5.3.3. Cell lines

Human microvascular endothelial cells (HMBEC), human brain vascular pericytes (HBVP) and human astrocytes (HA) were purchased from (Sciencell, Buckingham, UK), passage number (p2-8) was used. U87MG (human glioblastoma cell line) grade IV, passage number used 15-23 were obtained from the European Collection of Cell Cultures (ECACC, UK).

5.4. Methods

All the experiments in this chapter were performed under sterile conditions and by using a class II laminar flow hood in a primary lab as described in chapter four section 4.4.

Additionally, similar protocols mentioned in chapter four for cell line thawing (section 4.4.2), subculturing (section 4.4.3), and cell counting (section 4.4.4) were followed in experiments reported in this chapter, where the only difference was PBS was used for washing instead of the HBSS, and TryPLE Express was used to detach the primary cell lines instead of the trypsin.

5.4.1. Preparations

5.4.1.1. Media preparation

Endothelial basal media (EBM-2) was used for culturing HBMEC by using Endothelial Growth Media-2 Single quotes (EGM-2) kit, plus 2% human serum (HS), Astrocyte basal media (ABM-2) was used for culturing NHA by using Astrocyte Growth Media-2 Single quotes (AGM-2) kit, plus 3% HS, For HBVP culturing, Pericyte medium (PM), Pericyte Growth Supplement (PGS) and penicillin/streptomycin solution (P/S), plus 2% of HS, a detailed growth supplement summarised in chapter two (section 2.3.2).

5.4.1.2. Coating inserts

The plates were sprayed with 70% IMS and placed inside sterile laminar flow hood, the inserts were washed with HBSS, 0.5 ml in each insert was added, and incubated for 30 min by placing the plates in 37 °C humidified incubator under 5 % CO_2 atmosphere. And the HBSS was aspirated from each insert gently then replaced with fibronectin placed on the apical side of the insert then the plates were incubated for 24 h in 37 °C humidified incubator under 5 % CO2.

5.4.2. Tri-culture on transwell for 3D BBB model

Prior to establishing the Tri-culture on transwell for 3D BBB model, the three primary cell lines were grown until reached confluency 85-90%, to develop a fully validated human cell line *in-vitro* BBB model (Kumar *et al.,* 2014). The inserts were coated prior to the seeding day as described in section 5.4.1.2. based on the primary cell lines characterisation, growth kinetics, and protocol established by Kumar *et al.,* (2014), the NHA and HBVP were seeded on the apical outer part of the insert. The inserts were incubated for 4 h inside the hood, following the incubation period the inserts were placed in the plate, and 200 µl of media was added to the apical side and 600 µl of media was added to the basolateral side. The plates were transferred into 37 °C humidified incubator under 5 % CO_2 for 48 h incubation followed by seeding HBMEC on the apical inner part of the insert, 600 µl of media was added to the basolateral side. The plates were then incubated for 48 h at 37 °C in a humidified incubator under 5 % CO_2 to form a tri-culture model.

5.4.3. Testing the integrity of the 3D *in-vitro* BBB model

There are several methods to determine the barrier properties of *in-vitro* models. The para-cellular permeability was monitored using a trans-endothelial electrical resistance (TEER) EVOM-2 instrument, which is the most widely used method to determine TEER on endothelial cells as mono-culture (Nakagawa *et al.,* 2007) or as previously reported for tri-culture (Kumar *et al.,* 2014; Esposito *et al.,* 2016). For the measurement of TEER, two electrodes were used, one being placed in the upper and the other in the lower chamber, and the results were expressed in Ohm/cm^2 (Nakagawa *et al.,* 2007). In this experiment, the TEER measurement was performed by recording at least three readings from different positions in each transwell for up to 14 days (Kumar *et al.,* 2014).

Another way to test the integrity of the BBB model was by using Evans blue dye (EBD) as an inert negative control, which is too large for paracellular transport (Kumar *et al.,* 2014) by adding 1 µg/ml of EBD on apical side of the inserts, and incubated for up to 15 min at 37 °C humidified incubator under 5 % CO_2, and then 100 µl was sampled from the basolateral side of the insert and the absorption was measured at 595 nm using the plate reader. The EBD unknown concentration was calculated by plotting a standard curve generated from known concentrations. The integrity of the model was tested by EBD prior to and at the end of each experiment following the model highest TEER values. The TEER was also measured at different time intervals 0.25, 0.5, 1, 2, 4, and 6 h, in the presence of EBD in the apical side and without the EBD to establish if there is any interruption in the TEER values due to the presence of the EBD.

5.4.4. Evaluation of the permeability of DTX-NLCs and surface modified DTX-NLCs across 3D *in-vitro* BBB model

DTX-NLCs and DTX-NLCs surface modified were screened for apparent permeability across the developed 3D *in-vitro* BBB model, all cell lines were arranged on a three-dimensional scaffold as described in section 5.4.2. After 48 h, the tri-cultures were measured for their TEER using the EVOM-2 across three locations on the insert for each of the models every day, until the model was ready to start the experiment on the 7-8 day when the TEER reached 260-300 Ω/ cm^2 to ensure barrier formation. A fluorescent-labelled R-B-NLC, R-

DTX-NLC, R-GLA-DTX-NLC, R-ALA-DTX-NLC, and R-SA43-DTX-NLC were diluted in media to a final concentration of 0.5 and 1 µg/ml. The tri-cultures were incubated in standard tissue culture conditions and at different time intervals 0.25, 0.5, 1, 2, 4, and 6 h, TEER was measured and a 100 µl of media from the basolateral side of the trans-well insert was sampled for each time point and replaced by 100 µl of fresh media. The fluorescence of the sampled media was measured at excitation wavelength 485 nm and emission wavelength 535 nm using the plate reader. The integrity of the barrier was tested using 1 µg/ml EBD prior to the experiment and in the end, to ensure that the model was intact during the incubation time and duration of the entire experiment. All data were obtained from three experimental replicates. The unknown concentration of Rhodamine123 (R) labelled DTX-NLCs were calculated using a standard curve that was established for each formulation, and the apparent permeability (Papp) was calculated using equation 5.1 as previously indicated by Kumar *et al.,* (2014) and Esposito *et al.,* (2016).

$$P_{app} = \left(\frac{V}{A \times C_0}\right) \times \left(\frac{dQ}{dt}\right) \qquad \textbf{\textit{Equation 5.1}}$$

where:

V = Volume of basolateral compartment (0.6 ml) (0.5 cm^3)

A = surface area of the polycarbonate membrane (0.3 cm^2)

C_0 = Final concentration of R-DTX-NLCs in the apical side (1 or 0.5 µg/ml)

dQ Change in the concentration of DTX-NLCs passing across the cell layer to the basolateral side (µg/ml)

dt = Change in time (Sec).

5.4.5. Evaluation of the permeability of DTX and DTX-NLC across 3D *in-vitro* BBB model using HPLC method

The 3D *in-vitro* BBB model was prepared as described in section 5.4.2, and the free DTX from the DTX solution and the DTX-NLC that permeated through the model into the basolateral side of the insert was quantified. In this experiment, two level concentrations were used 1 and 2 µg/ml for DTX and DTX-NLC by diluting the sample with media and placing 200 µl from each concentration into the apical side of the insert, then incubated for 6 h in 37 °C humidified incubator under 5 % CO_2. Following the incubation period, the experiment was terminated, and 0.45 ml was taken from each insert and placed in a 1.5 ml tube then 50 µl of 0.1 µg/ml PTX as internal standard (IS) was added to each tube, vortexed for 5 min, followed by adding 0.5 ml of ice-cold acetonitrile to each tube for extraction of DTX from the biological matrix, then vortexed again for 3 min. All tubes were then placed in the centrifuge, for 30 min at 16300 x g centrifugation speed as previously stated in chapter two (section 2.4.3.2.3) for sample preparation. 900 µl of the supernatant was taken from each tube and placed into an HPLC vial for HPLC analysis and quantification of DTX using the developed and validated method that previously detailed in chapter two (section 2.5.3.3), each sample was injected into the HPLC system three times, this experiment was a replica of three, after acquiring the free DTX concentration, then the Papp was calculated as per equation 5.1. The integrity of the barrier was tested using 1 µg/ml EB prior to the experiment and in the end, to ensure that the model was intact during the designated incubation period.

5.4.6. Evaluation of DTX-NLCs and surface modified DTX-NLCs uptake by U87MG monolayer following the permeability across 3D *in-vitro* BBB model

In this experiment for the quantification of Rhodamine 123 (R) labelled formulations R-DTX-NLC, R-GLA-DTX-NLC, R-ALA-DTX-NLC, and R-SA43-DTX-NLC uptake by U87MG monolayer following the permeability across 3D *in-vitro* BBB model, where the flow cytometer was used for quantification of fluorescence labelled formulations. The following protocol was adopted and several steps were modified from a previously published paper where they used mono-culture BBB model from a mouse brain endothelial Bend.3 as summarised by Lin *et al.,* (2016). In our experiment, a 3D *in-vitro* BBB model was prepared as described in section 5.4.2. The only addition to that protocol is the U87MG cells were seeded in a density of 20000 cells/ ml on the bottom of the plate (without the inserts), a day before the TEER reach to 260-290 Ω/ cm^2, followed by transferring the inserts in each well (contains U87MG monolayer), and incubated for at least 2 h in 37 °C humidified incubator under 5 % CO_2. Then 200 µl from each formulation was added at 1 µg/ml concentration once the TEER increased over 300 Ω/ cm^2. TEER was measured at different time intervals of 0.25, 1, 2, 4, and 6 h. Additionally, samples were withdrawn at 1, 2, 4, and 6 h from both apical 20 µl, then diluted with 80 µl mix media and from basolateral side of the insert a 50 µl was taken, then diluted with 50 µl mix media, without replacing the media.

The experiment was terminated after the last incubation time point (6 h) followed by measuring the fluorescence of the sampled media at excitation wavelength 485 nm and emission wavelength 535 nm using the plate reader. As for the U87MG cell line, the cells were prepared for the uptake analysis using the flow cytometer following the protocol detailed in chapter four (section 4.4.9.1). The integrity of the barrier was tested using 1 μg/ml EB prior to the experiment and in the end, to ensure that the model was intact during the incubation time. All data were obtained from three experimental replicates. The unknown concentration of Rhodamine123 (R) labelled DTX-NLCs were calculated using a standard curve that was established for each formulation, and the Papp was determined using equation 5.1. Additionally, for the fluorescence data acquired by the flow cytometer, the MFI was plotted against the incubation time and the flow cytometer histograms were examined for the peak shifting.

5.4.7. Evaluation of DTX-NLCs and surface modified DTX-NLCs effect on P-gp efflux pump using 3D *in-vitro* BBB model

The 3D *in-vitro* BBB model was prepared as described in section 5.4.2, and once the model reached maximum TEER measurements ranging between 260-300 Ω/ cm^2. The media was removed from the apical side and replaced by 200 μl of the following samples

(a) 10 μg/ml Rhodamine123 (R) at 37 °C
(b) 10 μg/ml R at 4 °C
(c) 10 μg/ml R+ 100 μM verapamil at 37 °C
(d) 10 μg/ml R+ 22 μM vinblastine at 37 °C
(e) 10 μg/ml R+ 1 μg/ml DTX-NLC at 37 °C
(f) 10 μg/ml R+ 1 μg/ml GLA-DTX-NLC at 37 °C
(g) 10 μg/ml R+ 1 μg/ml ALA-DTX-NLC at 37 °C
(h) 10 μg/ml R+ 1 μg/ml SA43-DTX-NLC at 37 °C

Then after 1 h incubation at 37 °C humidified incubator under 5 % $CO_{2,}$ 100 μl was sampled from the apical and basolateral side of each insert and analysed for the Rhodamine123 fluorescence. The fluorescence was measured at excitation wavelength 485 nm and emission wavelength 535 nm using the plate reader, and the unknown concentration of Rhodamine123 (R) was calculated using a standard curve of Rhodamine123.

5.4.8. Statistical data analysis

The statistical analysis was performed using the Kolmornov-Smirnov test for normality followed by ANOVA (with post-hoc analysis Tukey and Dunnett test) by using statistical analyses were performed using the Statistical Package for the Social Sciences SPSS Version 20 software (IBM company, USA) and the Microsoft Excel software for Microsoft office 360 (Microsoft Corporation, USA). The analysis of variance was statistically significant difference when (*) $P < 0.05$ (confidence 95%), (**) $P < 0.001$ (confidence 99%), and (***) $P < 0.000$. The data are presented as the mean ± standard deviation for N=3 experiments in triplicate (n=9).

5.5. Results and discussion

5.5.1. Cell characterisation

Primary cells morphology was observed under the light microscopy x10 magnification, on day 5 the endothelial cells HBMEC exhibited relatively higher growth and confluency in comparison with NHA and HBVP (Figure 5.1). HBMEC showed spindle-shaped morphology. The astrocytes NHA showed fibroblastic morphology with many elongated processes arising from each cell and less confluency in comparison to HBMEC and HBVP (Figure 5.1). The pericytes HBVP were observed as thin cells with elongated processes rising from each cell like a net shape (Figure 5.1), they were slow growing in comparison to the HBMEC.

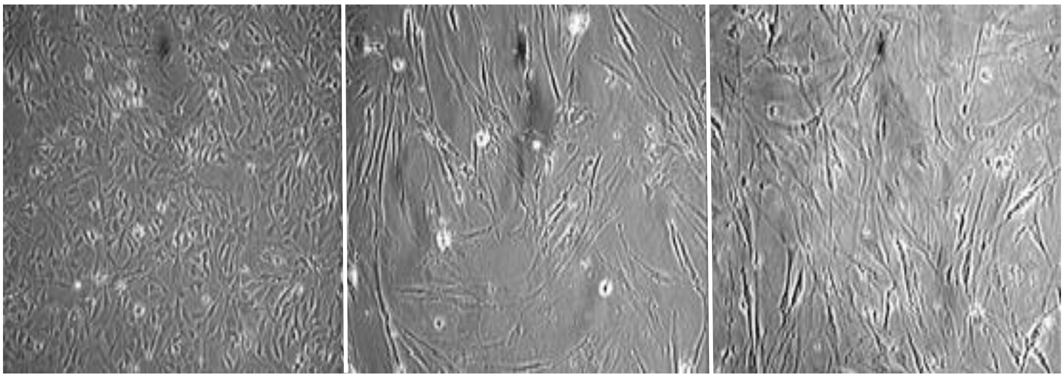

(a) (b) (c)

Figure 5.1 Light microscopy images x 10 magnification of monolayer primary cell lines (a) HBMEC cell line; (b) NHA cell line, and (c) HBVP cell line.

5.5.1. Testing the integrity of the 3D *in-vitro* BBB model

In this study, the maximum TEER obtained was 300 Ω/cm^2 on day 8, and the model was used when TEER was ranging between 260-300 Ω/cm^2 on days 7, 8, and 9 (Figure 5.2 a). Previously, the integrity of the BBB cell culture model was deemed stable and intact for assessing drug transport, when a sufficiently high TEER value 250-300 Ω/cm^2 was achieved (Esposito *et al.,* 2016; Kumar *et al*., 2014). The integrity and barrier properties of the BBB model was also tested by addition of EBD in the apical side followed by measurement of EBD appearance in the apical side and TEER values, as described in section 5.4.3. Figure 5.2 b confirmed that there was no disruption in the BBB at the designated time points, as TEER remained constant for the duration required for future experiments, and no EBD was detected by absorbance spectroscopy from media in the basolateral side, indicating that the barrier was intact and not leaky. These results demonstrated the model, as previously established by Kumar *et al.*, (2014) was validated ready for NLCs screening and permeability evaluation.

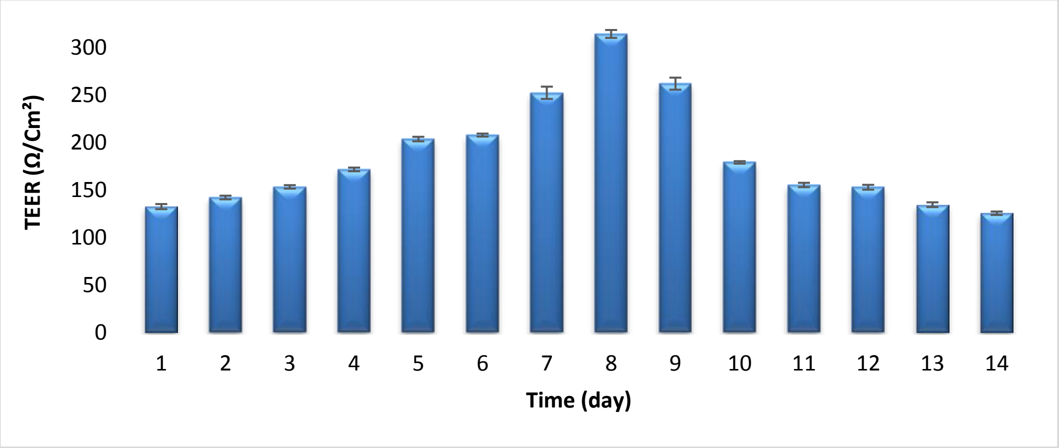

(a)

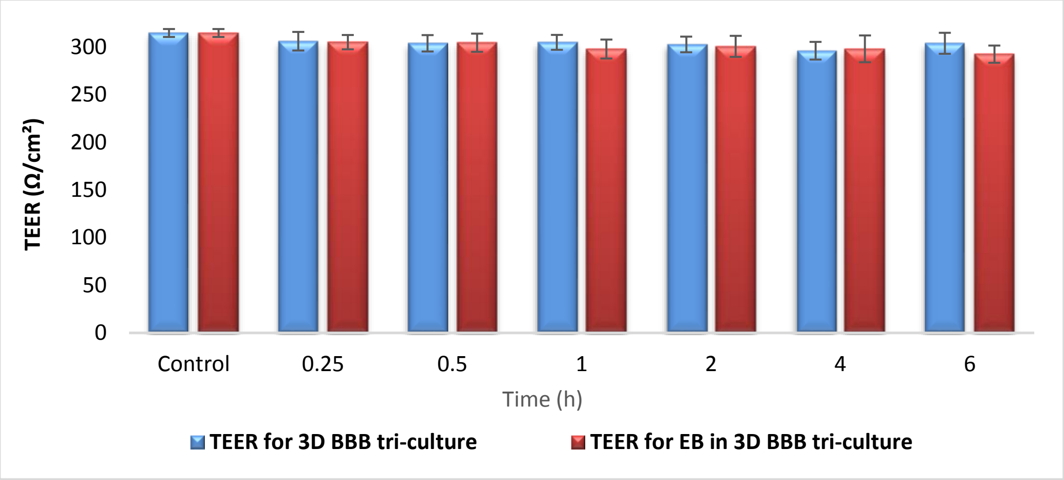

(b)

Figure 5.2 Testing the integrity of the in-vitro model (a) To establish the barrier formation TEER was measured for up to 14 days, (b) TEER measurements of the 3D in-vitro BBB model at different time intervals with and without EBD. Data are mean ± SD, (N=3).

5.5.2. Evaluation of the permeability of DTX-NLCs and surface modified DTX-NLCs across 3D *in-vitro* BBB model using fluorescence detection

As described in section 5.4.4, to test DTX-NLC and surface modified DTX-NLCs permeability, fluorescent probe Rhodamine123 (R) was encapsulated within the NLCs, and the rhodamine 123 fluorescence was used as a marker to determine whether the NLCs had permeated the BBB. Rhodamine123 is frequently used, in the case of this experiment the Rhodamine123 was encapsulated inside the NLC and was protected from efflux activity, so it was used as a fluorescent biomarker of NLC transport. Previous studies had shown that NLC did not release 40% contents until at least 2 h (Chapter three section 3.5.10.2), therefore for the duration of this experiment, rhodamine detection on the basolateral side of the BBB was indicative of permeation of the NLCs.

Each standard curve was obtained by measuring the Rhodamine 123 concentration within the NLCs by plotting a range of R-DTX-NLC, R-GLA-DTX-NLC, R-ALA-, and R-SA43-DTX-NLC concentrations vs their mean fluorescence intensity (MFI) to quantify the unknown concentration of samples that were withdrawn from the basolateral side of the insert.

The fluorescence of 0.5 µg/ml R-DTX-NLC that was sampled from the basolateral side of the insert was converted to concentration using a standard plot (Figure 5.3 a). In Figure 5.4 a, the data acquired demonstrated a permeation of R-DTX-NLC through the 3D *in-vitro* BBB model starting from early time point 0.25 h and reaching the highest concentration at 2 h. The TEER value dropped from 275.05 ±19.41 Ω/cm² (control) to maximum low of 173.33 ±12.46 Ω/cm² at 1 h, after which, TEER values started to increase and had returned to control values at 2 h, and until the termination of the experiment up to 6 h (Figure 5.4 a). This decrease and recovery in TEER could be due to the opening of the TJs facilitating passage of NLC through the *in-vitro* BBB model. It is known that tight junctions can be opened only to a limited extent (Bazzoni 2006). A similar pattern was shown when a higher concentration of 1 µg/ml R-DTX-NLC was evaluated for its permeability (Figure 5.4 b), where TEER values also dropped from 0.25 to 1 h and then returned to normal after 2 h of incubation. The fluorescence of 1 µg/ml R-DTX-NLC that was sampled from the basolateral side of the insert was converted into concentration using the standard plot shown in figure 5.3 b, and the highest concentration was obtained at 2 h, which was higher than when 0.5 µg/ml R-DTX-NLC was tested. Interestingly, the R-DTX-NLC was still showing permeability even after TEER returned to normal values following the closing of the TJ, suggesting another transport mechanism other than paracellular transport was involved. Solutol® HS15 (a PEG copolymer/surfactant) was incorporated in the preparation of the R-DTX-NLC formulation to prolong circulation time (Chen *et al.,* 2004). Permeation of the R-DTX-NLC may have continued due to the role of Solutol®HS15 as a resistance modification agent (RMA); consequently, it works as an efflux pump P-gp inhibitor to reverse the multidrug resistance (MDR) as demonstrated by Coon *et al.,* (1991). Additionally, the Papp was calculated using equation 5.1 for both concentrations (Figure 5.4 c). Higher apparent permeability (Papp values) were displayed when 0.5 µg/ml R-DTX-NLC was examined at 0.25, 0.5, 1, and 2 h than the Papp of 1 µg/ml R-DTX-NLC, when almost similar Papp was observed at 4 and 6 h of incubation for both concentration of R-DTX-NLC. Moreover, both concentrations demonstrated the same pattern, and high

Papp values correlated with when the TEER values dropped, indicating that the R-DTX-NLC has the ability to pass through the BBB *in-vitro* model. The model was considered intact due to no EBD detectable in the basolateral side of the insert during and at the end of the experiment.

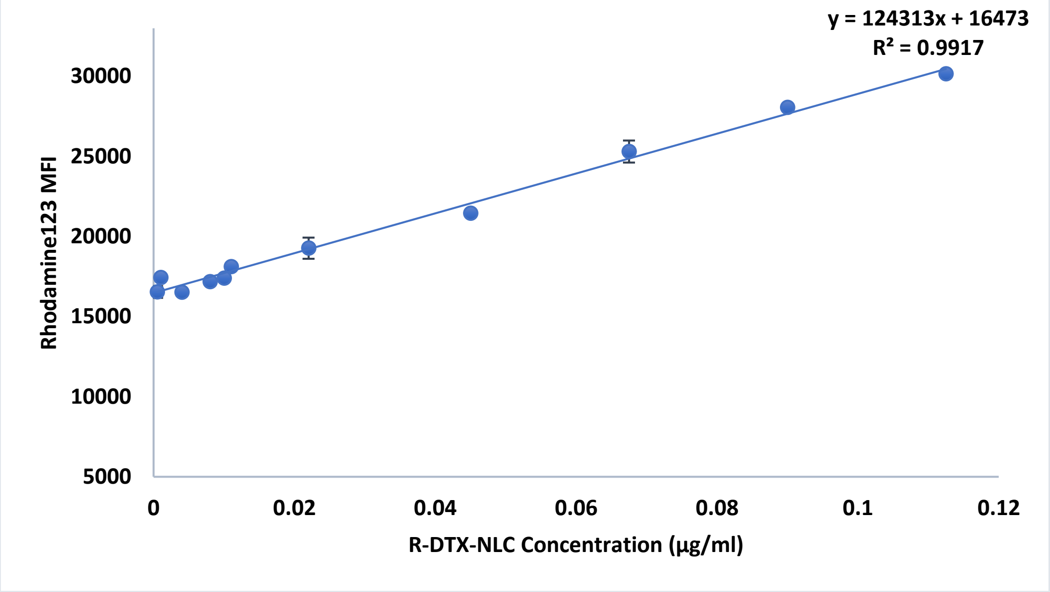

(a)

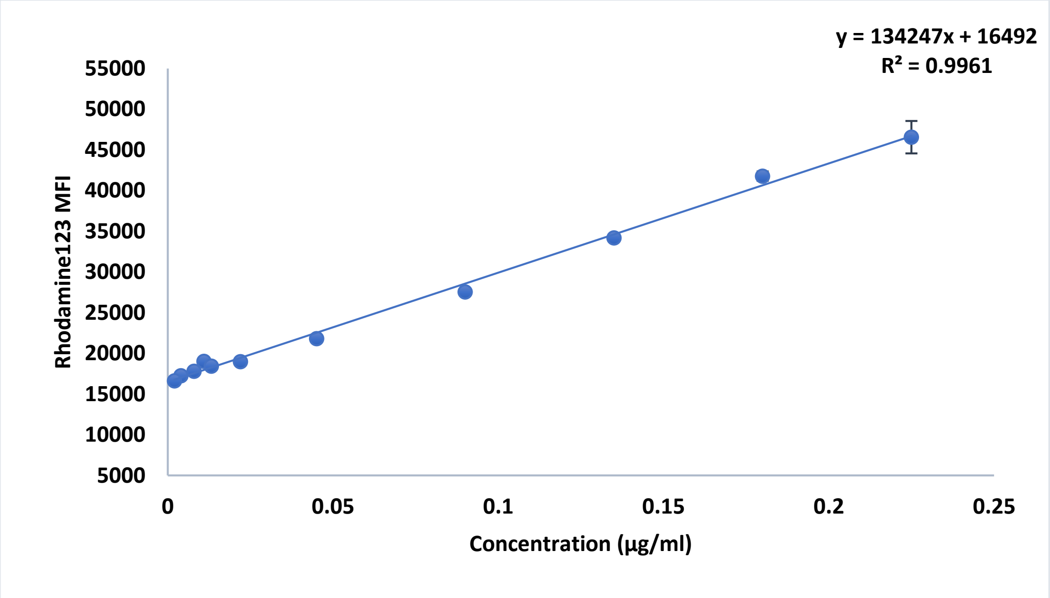

(b)

Figure 5.3 Standard calibration plot for (a) 0.5 µg/ml R-DTX-NLC (b) 1 µg/ml R-DTX-NLC. Data are mean ± SD, (N=3).

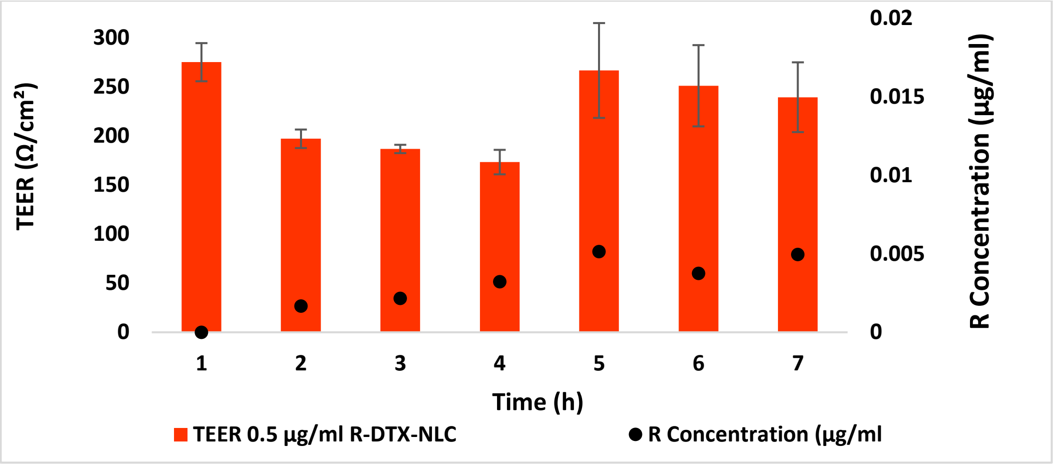

(a)

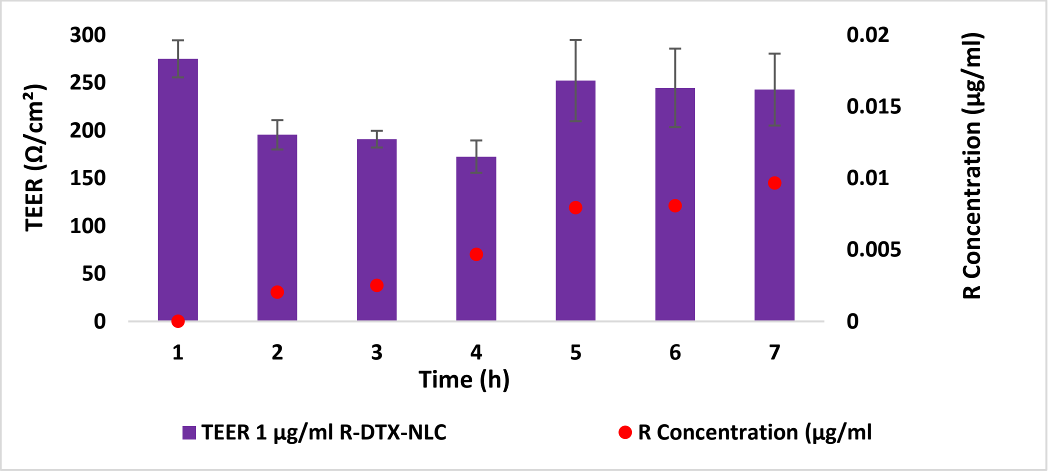

(b)

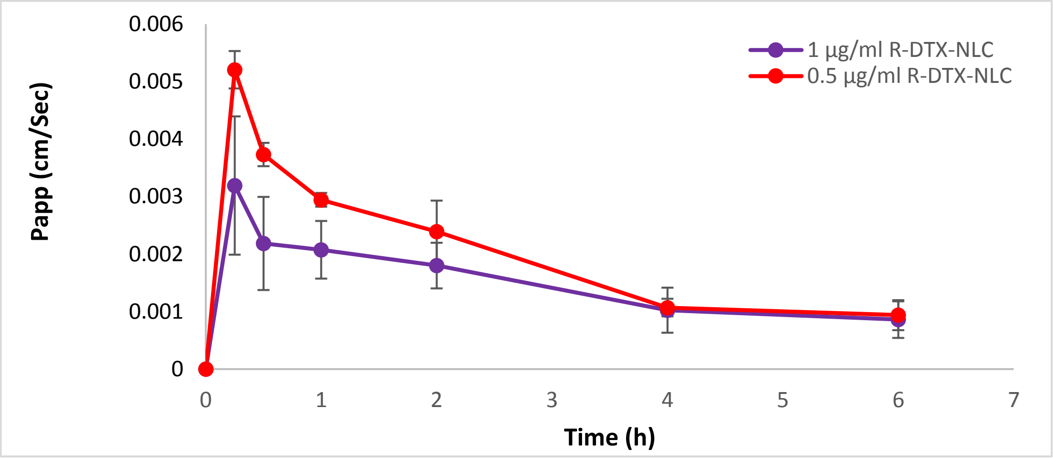

(c)

Figure 5.4 In-vitro BBB permeability of R-DTX-NLCs (a) Combo graph for the TEER measurements and fluorescence concentration for 0.5 µg/ml R-DTX-NLC, (b) Combo graph for the TEER measurements and fluorescence concentration for 1 µg/ml R-DTX-NLC, (c) scatter graph for the Papp values plotted with time of 0.5 and 1 µg/ml R-DTX-NLCs. Data are mean ± SD, (N=3).

As shown in figure 5.6 a and b, when R-GLA-DTX-NLC was evaluated at two-level concentrations, the TEER values started to drop from 286.5 ±2.5 Ω/cm² (control) to 233.5 ±0.83 Ω/cm² at 1 h for 0.5 µg/ml R-GLA-DTX-NLC (Figure 5.6 a), and, 197.44 ±31.82 Ω/cm² at 2 h, when 1 µg/ml of RGLA-DTX-NLC was examined (Figure 5.6 b). Additionally, the concentration of 0.5 and 1 µg/ml R-GLA-DTX-NLC that were sampled from the basolateral side of the inserts was calculated from fluorescence measurements using the standard plots shown in figure 5.5 a and b, respectively. The highest concentrations were displayed for both the tested concentrations of R-GLA-DTX-NLCs at the 6 h time point. The fluorescence permeated from 1 µg/ml R-GLA-DTX-NLC was two-fold higher than the maximum fluorescence shown when 1 µg/ml bare R-DTX-NLCs without surface modification was examined at 6 h incubation time. This indicates that when the formulation was functionalised with GLA it caused a higher permeation of the R-GLA-DTX-NLC through the BBB model. The Papp values for both concentrations 0.5 and 1 µg/ml R-GLA-DTX-NLC (Figure 5.6 c) exhibited low permeability at the early time point, followed by reaching the highest value at 1 h incubation, then the Papp values were reduced at 4 and 6 h of incubation. It was reported in literature that upon administration of GLA reactive oxygen species (ROS) were generated (Leaver *et al.,* 2002a), that led to the suppression of P-gp expression, and eventually to P-gp inhibition (Yuan *et al.,* 2008), which in turn caused efflux pump inhibition and which explains the high fluorescence level of R-GLA-DTX-NLC that was permeating through the 3D *in-vitro* BBB model, even when the TEER values returned to normal values, demonstrating the termination of the transit opening for the TJ period. Another mechanism for the permeation of R-GLA-DTX-NLC through the BBB model might be due to GLA on the surface of the NLC binding to the brain FABP7 receptors (Elsherbiny *et al.,* 2013; Shimizu *et al.,* 1997). Fatty acids have the ability to enter the brain by passive diffusion and proteins-mediated transport by the membrane-associated proteins, like fatty acid transport proteins and fatty acid translocases (CD36) as indicated by Chen *et al.,* (2008), this was further studied in section 5.5.5.

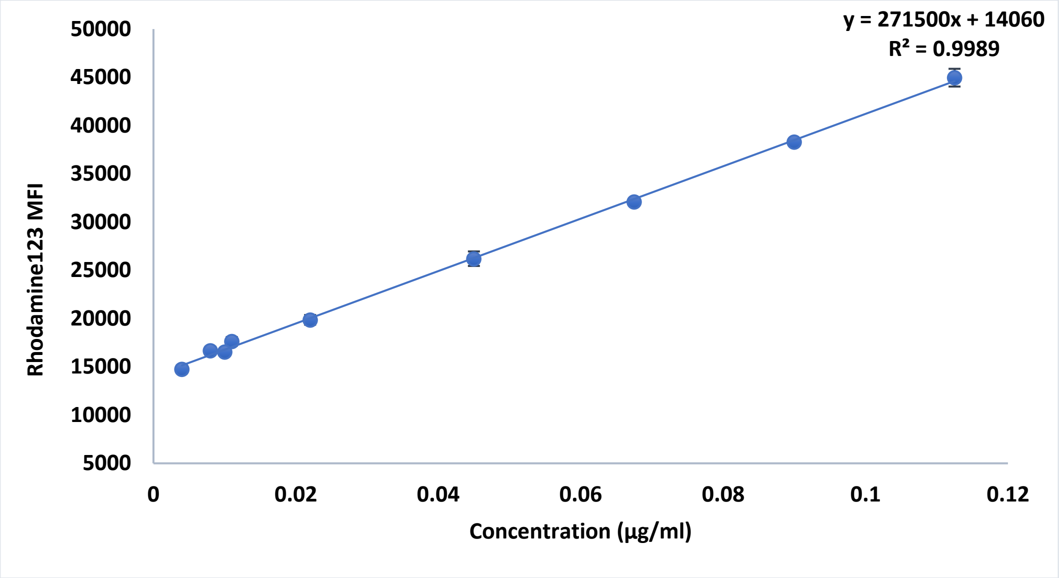

(a)

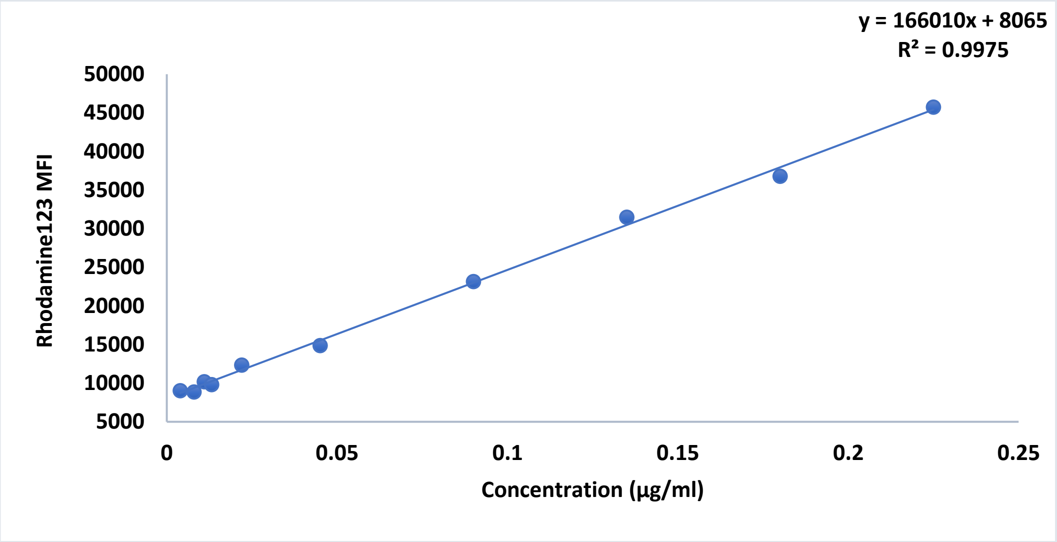

(b)

Figure 5.5 Standard calibration plot for (a) 0.5 µg/ml R-GLA-DTX-NLC (b) 1 µg/ml R-GLA-DTX-NLC. Data are mean ± SD, (N=3).

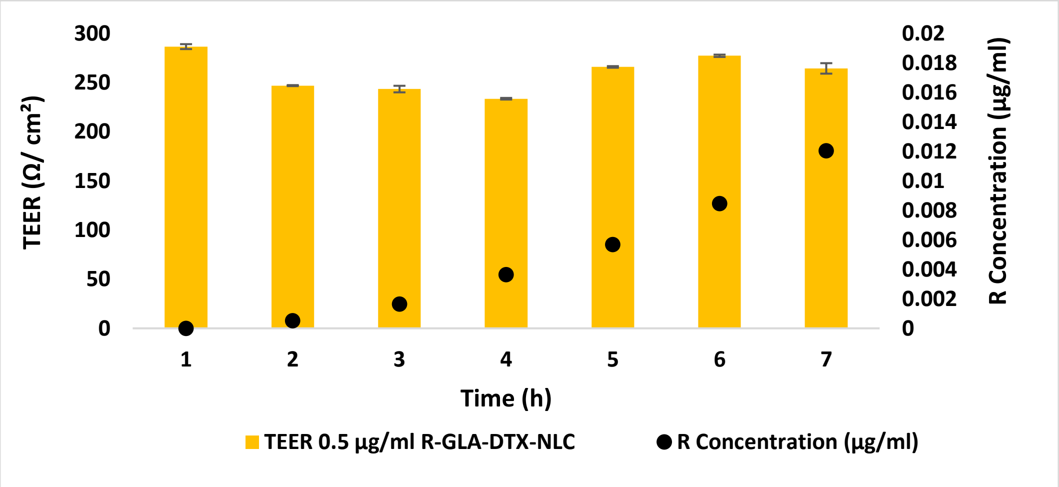

(a)

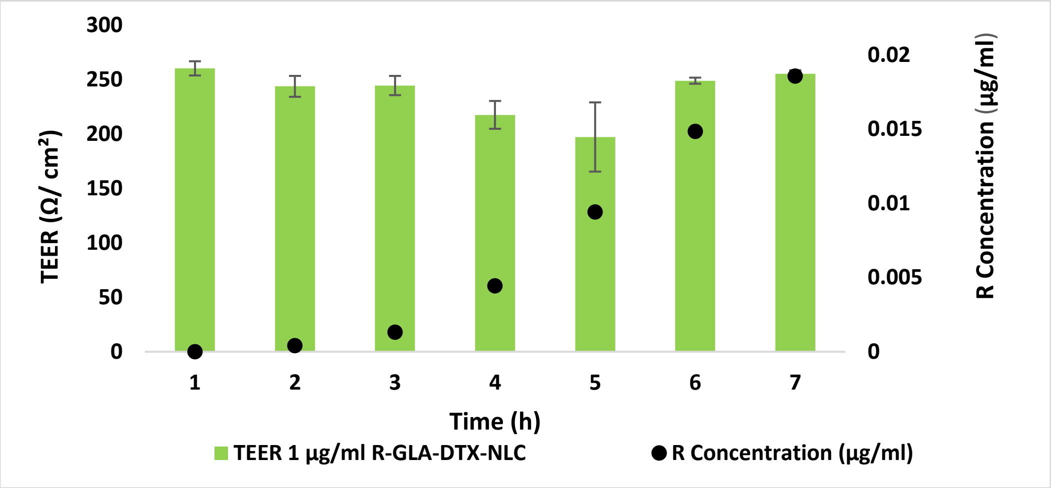

(b)

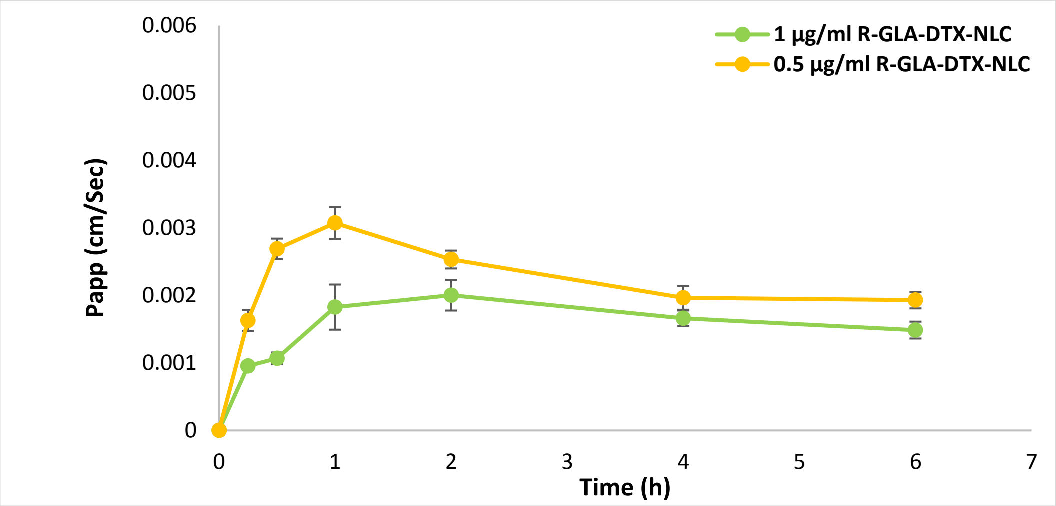

(c)

Figure 5.6 In-vitro BBB permeability of R-GLA-DTX-NLCs (a) Combo graph for the TEER measurements and fluorescence concentration for 0.5 µg/ml R-GLA-DTX-NLC, (b) Combo graph for the TEER measurements and fluorescence concentration for 1 µg/ml R-GLA-DTX-NLC, (c) scatter graph for the Papp values plotted with time of 0.5 and 1 µg/ml R-GLA-DTX-NLCs. Data are mean ± SD, (N=3).

Figure 5.8 a and b represents R-ALA-DTX-NLC permeation through the 3D *in-vitro* BBB model through the transient opening of the TJ, indicated by the reduction in the TEER values from 286.5 ±2.5 Ω/cm² for the control to 243.66 ±0.33 Ω/cm² at 1 h, when incubated with 0.5 µg/ml R-ALA-DTX-NLC (Figure 5.8 a); and to 243.11 ±4.14 Ω/cm² at 2 h when 1 µg/ml R-ALA-DTX-NLC was incubated (Figure 5.8 b). The permeation of fluorescence-tagged ALA-DTX-NLCs concentration of 0.5 and 1 µg/ml R-ALA-DTX-NLCs that were sampled from the basolateral side of the insert was calculated using the standard plots shown in figure 5.7 a and b, respectively. The highest concentrations of

0.5 and 1 µg/ml R-ALA-DTX-NLCs permeation were exhibited at 6 h incubation (Figure 5.8 a, b). Additionally, the calculated Papp values for both tested concentrations of R-ALA-DTX-NLCs showed high apparent permeability at an early time point followed by a reduction in the Papp values when the higher concentration was examined at 1 h, and until the termination of the experiment at 6 h incubation time, while at a lower concentration the Papp reached the highest level at 2 h incubation followed by lower Papp values at 4 and 6 h incubation time (Figure 5.8 c). Similar mechanisms that were discussed for the permeation of R-GLA-DTX-NLCs might be exhibited by R-ALA-DTX-NLCs permeation as well, due to the fact that they are both PUFAs and might bind to similar receptors. To the best of our knowledge, both R-GLA-DTX-NLCs and R-ALA-DTX-NLCs are newly developed NLCs for brain-targeted therapy, and no previous reports have been reported for the permeation of these NLCs through a 3D *in-vitro* BBB model.

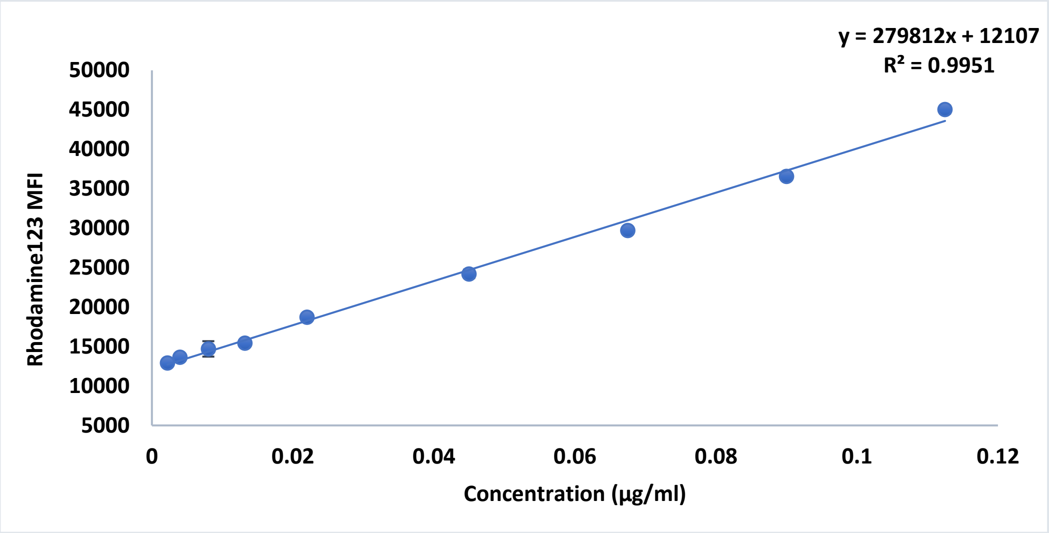

(a)

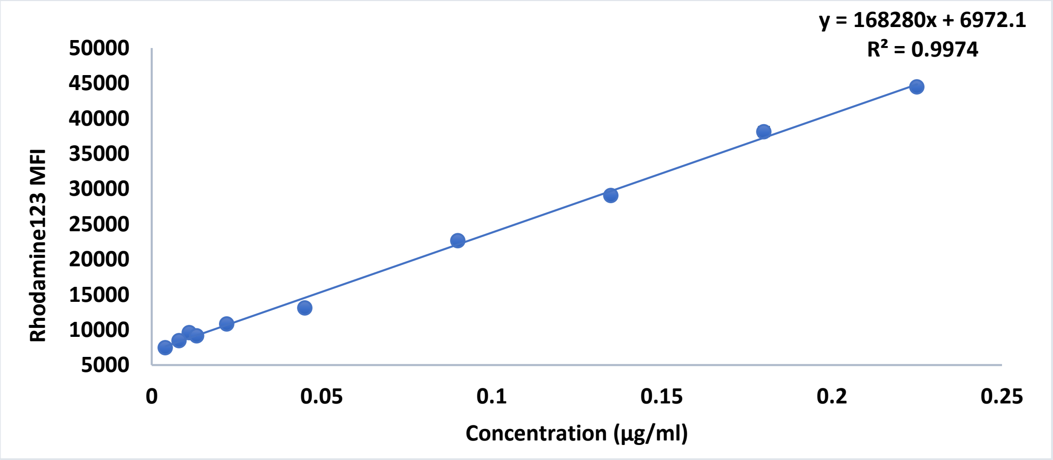

(b)

Figure 5.7 Standard calibration plot for (a) 0.5 µg/ml R-ALA-DTX-NLC (b) 1 µg/ml R-ALA-DTX-NLC. Data are mean ± SD, (N=3).

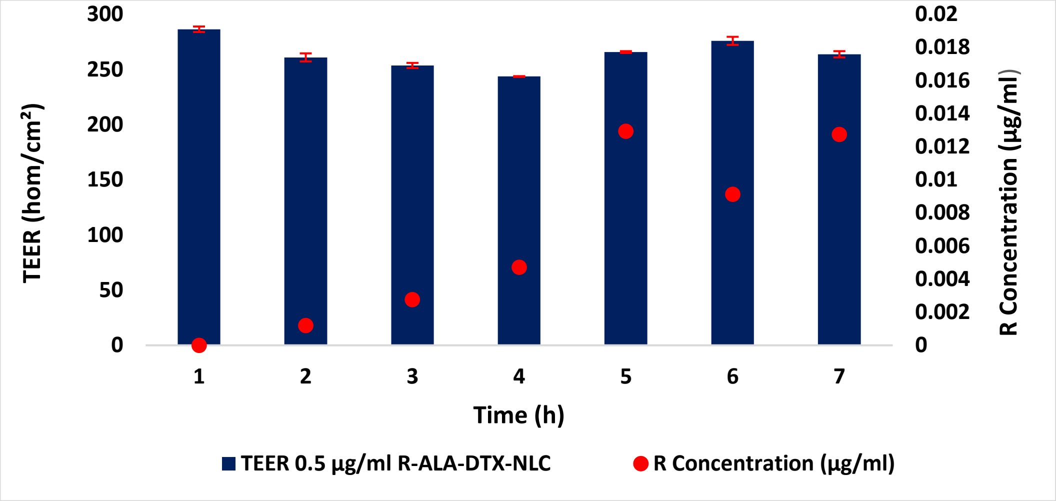

(a)

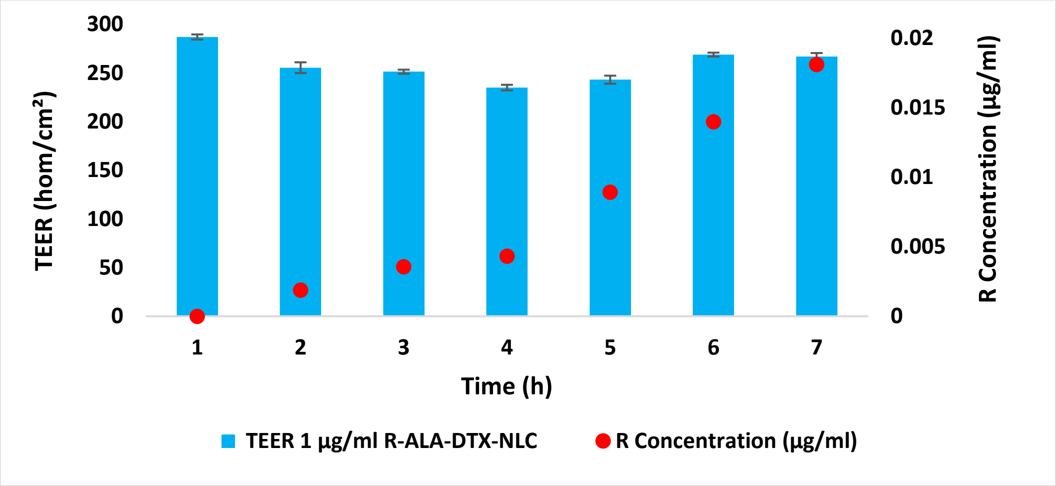

(b)

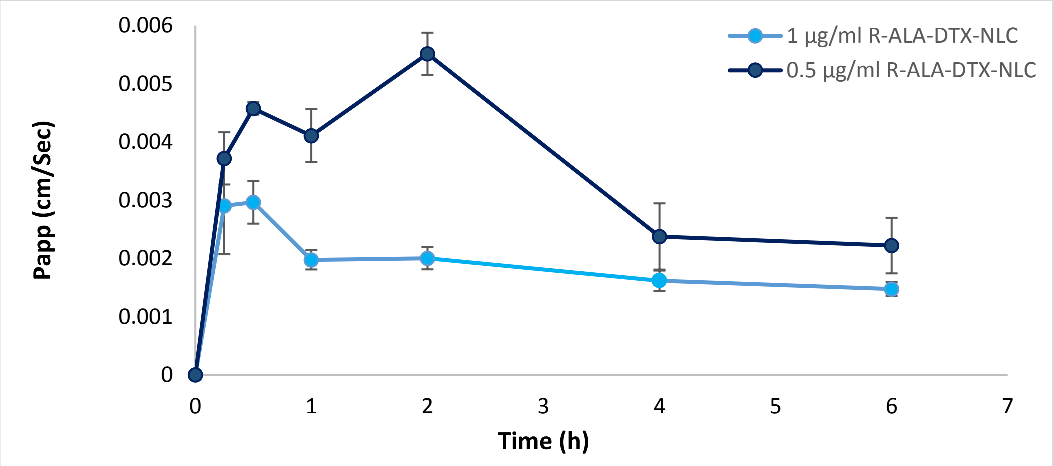

(c)

Figure 5.8 In-vitro BBB permeability of R-ALA-DTX-NLCs (a) Combo graph for the TEER measurements and fluorescence concentration for 0.5 µg/ml R-ALA-DTX-NLC, (b) Combo graph for the TEER measurements and fluorescence concentration for 1 µg/ml R-ALA-DTX-NLC, (c) scatter graph for the Papp values plotted with time of 0.5 and 1 µg/ml R-ALA-DTX-NLCs. Data are mean ± SD, (N=3).

To test the permeability of the R-DTX-NLC after functionalisation with selective SA43-aptamer, one level concentration was examined at 1 µg/ml R-SA43-DTX-NLC. A drop in the TEER values was observed from 294.77 ±5.17 Ω/cm² for the control to 255.33 ±24.09 Ω/cm² at 4 h incubation time (Figure 5.10 a). These values indicated that the BBB took a longer time to recover when it was incubated with R-SA43-DTX-NLC, as compared to the other three formulations discussed earlier (R-DTX-NLC, R-GLA-DTX-NLC, and R-ALA-DTX-NLC). Additionally, the calculated concentration was higher after 6 h incubation time, as calculated by using the standard plot in figure 5.9 for R-SA43-DTX-NLC. Interestingly, the Papp values calculated for 1 µg/ml R-SA43-DTX-NLC at different time intervals indicated a lower Papp (Figure 5.10 b), and a different pattern compared to the other three formulations, where the highest Papp was achieved at 0.5 h and remained almost constant until the termination of the experiment at 6 h. The free SA43-aptamer has previously been evaluated for its permeation through the 3D *in-vitro* BBB model, where a temporary drop in the TEER values indicated the transit opening of the TJ, and an apparent permeability of $4.32 \pm 3.90 \times 10^{-9}$ cm/min was reported (Aptekar *et al.,* 2015). Aptekar *et al.,* (2015) found staining of patient glioblastomas tissue sections revealed that SA43 aptamer binding to endothelial cells was variable, therefore the process of permeability was uncertain as to whether it was transcellular or via an endothelial specific protein. While the mechanism of the SA43-aptamer passing through the BBB is still unknown at this stage, several mechanisms might be involved in crossing through the BBB, that could be attributed to transcellular transport, or the variable binding to endothelial cells may suggest that the aptamer is able to bind to endothelial specific ligands within the cell (Aptekar *et al.,* 2015).

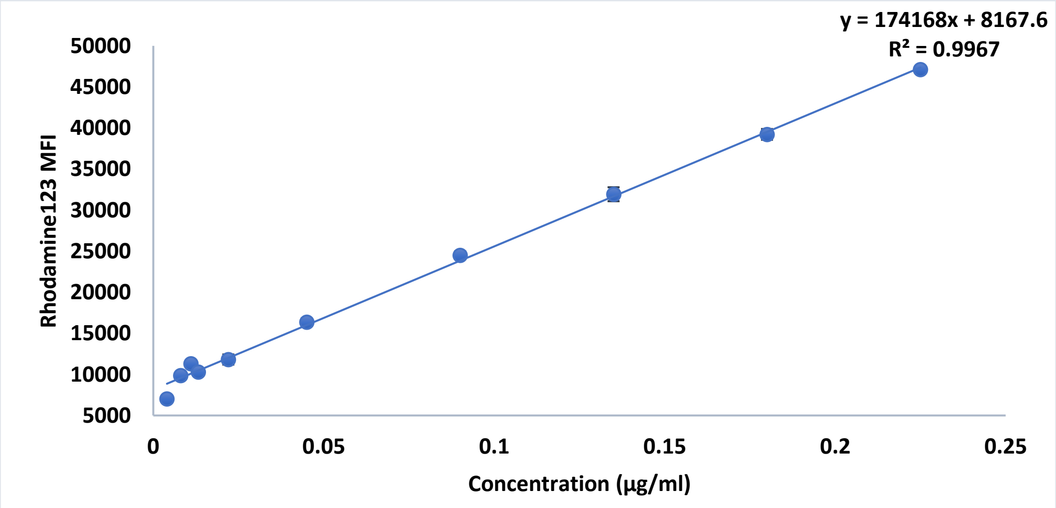

Figure 5.9 Standard calibration plot for 1 µg/ml RSA43-DTX-NLC. Data are mean ± SD, (N=3).

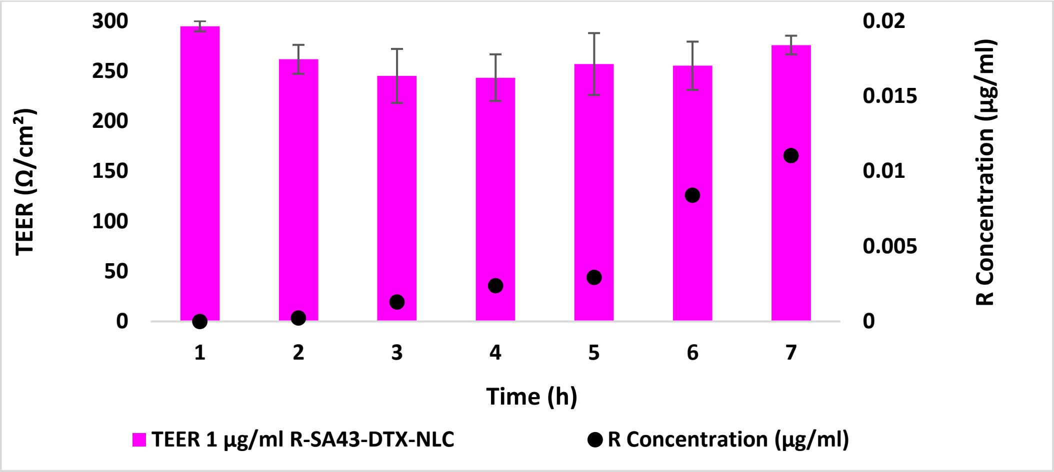

(a)

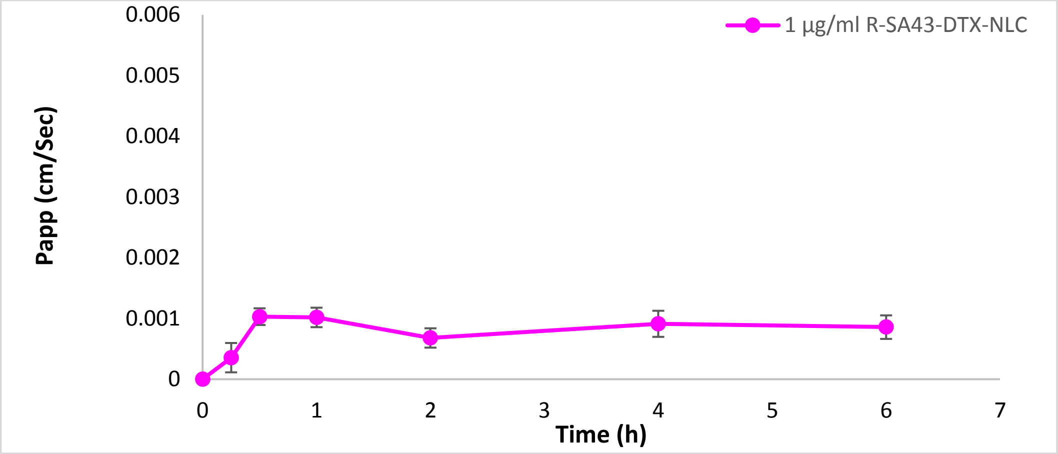

(b)

Figure 5.10 In-vitro BBB permeability of R-SA43-DTX-NLCs (a) Combo graph for the TEER measurements and fluorescence concentration for 1 µg/ml R-SA43-DTX-NLC, (b) scatter graph for the Papp values plotted with respect to time for the evaluation of 1 µg/ml R-SA43-DTX-NLCs. Data are mean ± SD, (N=3).

There was no significant difference in the Papp values of all the four formulations when compared with one another at 1 h incubation time at of concentration 1 µg/ml as demonstrated the Papp values were 2x 10^{-3}, 1.8x 10^{-3}, 1.9x 10^{-3}, 1.02x 10^{-3} cm/Sec for R-DTX-NLC, R-GLA-DTX-NLC, R-ALA-DTX-NLC, and SA43-DTX-NLC, respectively. Furthermore, no significant difference was exhibited when 0.5 µg/ml concentration of R-DTX-NLC, R-GLA-DTX-NLC, and R-ALA-DTX-NLC was evaluated, the Papp were 2.9x 10^{-3}, 3x10^{-3}, and 4.1x 10^{-3} cm/Sec, respectively. Though significantly higher concentrations permeated to the basolateral side for R-GLA-DTX-NLC and R-ALA-DTX-NLC in comparison to the R-DTX-NLC at 6 h incubation, indicating that both PUFA surface modified formulations enhanced the permeation of R-DTX-NLC. From this data, we can establish, that all four formulations permeated through the BBB model in a similar manner at the examined time point (1 h) for each designated concentration. In this study, the Papp is not a time-dependent or concentration-dependent variable as demonstrated in figures 5.4c, 5.6 c, 5.8 c, and 5.10 b, as higher Papp values were shown for lower concentration 0.5 µg/ml when R-DTX-NLC, R-GLA-DTX-NLC, and R-ALA-DTX-NLC were evaluated.

All four formulations displayed permeation through the BBB model that might be due to the transient opening of the TJs allowing the NLCs to pass through the BBB model by paracellular diffusion, as previously reported some molecules have the ability to diffuse through the BBB, by passing through the TJ (Patel *et al.,* 2013; Kumar *et al.,* 2014). In addition to the transient opening of the TJ, there are different mechanisms for the NLCs penetration across the BBB, it might be attributed to the type of surfactants that were used for the fabrication of the NLCs that facilitated the passage through the BBB. As indicated by a previous study that the size and surface charge of NPs had no influence on BBB permeation, and it was the surfactant that affected the BBB permeation (Voigt *et al.,* 2014). Soy lecithin (Lipoid S75), was used for fabrication of the SLN reported by Manjunath and Venkateshwarlu (2006), for enhancing the BBB uptake. Likewise, for Solutol® HS15 (Singh *et al.,* 2013). These two surfactants were used for the fabrication and development of the NLCs which could have contributed to BBB permeation of NLCs. Also, the lipophilicity of the NLCs might contribute to their ability to pass through the 3D *in-vitro* BBB model as indicated in literature lipidic particles with low molecular weight drugs can pass the BBB by trans-cellular diffusion (Patel *et al.,* 2013). Moreover, enhancing of NPs phagocytosis by monocytes can be considered as an unconventional approach to deliver NPs-loaded drugs to the brain, after phagocytosis of NPs may transport their cargo into the brain (Afergan *et al.,* 2008). The mechanism for BBB permeability and uptake of NPs was thought to be receptor-mediated endocytosis by the brain capillary endothelial cells, followed by transcytosis (Gabathuler, 2010). The PUFAs functionalised NLCs (R-GLA-DTX-NLC and R-ALA-DTX-NLC) might permeate through the BBB model through binding to FABP7 receptors (Elsherbiny *et al.,* 2013; Shimizu *et al.,* 1997). Moreover, Fatty acids have the ability to enter the brain by passive diffusion and proteins-mediated transport by the membrane-associated proteins, like fatty acid transport proteins and fatty acid translocases (CD36) as indicated by Chen *et al.,* (2008). As far as we know the SA43 may have the ability to bind to endothelial specific ligands that might lead to R-SA43-DTX-NLC permeation through the BBB, in addition to other mentioned mechanisms listed above for the NLCs permeability through the BBB model. The model was considered intact during evaluation of all four formulations, due to no EBD detectable in the basolateral side of the insert during and at the end of the experiment.

5.5.3. Evaluation of the permeability of DTX and DTX-NLC across 3D *in-vitro* BBB model using HPLC method

DTX-NLC is a newly developed carrier aimed for targeted delivery and enhances therapeutic for the treatment of glioblastoma, therefore the evaluation of its permeability through the BBB is a necessary and essential step at this stage as previously recommended by Doan *et al.,* (2002) and Kikuchi *et al.,* (2013). Additionally, there are few reports of *in-vitro* models for testing the permeability of different compounds using the HPLC method for quantification, a monoculture model established from HBMEC, and tri-culture cultivated from rat primary cell lines as detailed by Moradi-Afrapoli *et al.,* (2016), likewise a tri-culture *in-vitro* BBB model of rat origin was also used by Jahne *et al.,* (2014). As described in section 5.5.2 DTX-NLCs showed high permeation through the 3D *in-vitro* BBB model established from all human origin primary cells, due to the high Papp values quantified using fluorescence labelled DTX-NLCs. The gold standard for separation and quantification of compounds in the pharmaceutical industry is HPLC with an appropriate detection technique such as UV or tandem mass spectrometry. We have developed and validated a specific HPLC-UV method for quantification of DTX in a biological matrix comprising of a mixture of culture media used in the in *in-vitro* BBB model. Experiments as described in section 5.4.5, for the DTX and DTX-NLCs were repeated using a different method of quantification (HPLC-UV) and evaluated for permeation through the BBB model at two level concentrations. Formulations used in this study were not labelled with a fluorescence marker. Compared to the higher sensitivity of fluorescence, there was concern that detection of DTX on the basolateral side of the model would be lower than the LOD for the HPLC method (Chapter two, Section 2.5.3.3.7). Therefore, DTX-NLCs were studied at 1 and 2 µg/ml concentrations. Figure 5.11 showed the TEER values dropping from 330.33 ±13.38 Ω/cm² (control) to 296.66 ±7.76 and 309.66 ±5.13, Ω/cm² at 0.25 and 1 h respectively, when incubated with 1 µg/ml DTX-NLC, then the TEER values returned to normal values following 2 h incubation. When 2 µg/ml DTX-NLC was evaluated the TEER values took a longer time to recover. TEER values for the control 330.33 ±13.38, then reduced to 308.66 ±9.50, 299 ±18.08, and 300.88 ±19.29 Ω/cm² at 0.25, 1, and 2 h incubation that indicated the transient opening of the TJ (Figure 5.11 a). The similar pattern was notable when 1 µg/ml of DTX solution was evaluated through the model as the TEER values were 333.33 ±10.38 Ω/cm² for the control and followed by dropping at 0.25 and 1 h incubation, 303.66 ±1.52 and 299.33 ±4.04 Ω/cm², respectively. While, when

2 µg/ml DTX solution was tested TEER values 333.33 ±10.38 Ω/cm^2 for the control, were followed by fluctuation in the TEER, till it decreased to 290.66 ±5.03 Ω/cm^2 at final incubation time (6 h) as shown in figure 5.11 b. It would seem that the BBB model did not recover and TEER values remained decreased even at 6 h after adding a high concentration of DTX, though the integrity of the model was still intact, as measured by EBD evaluation at the end of the experiment. The model was considered intact when there is no detectable EBD in the basolateral side of the insert. This unbalanced and variation in the TEER values might be attributed to the fact that DTX at higher concentration might cause toxicity to the tri-culture cells.

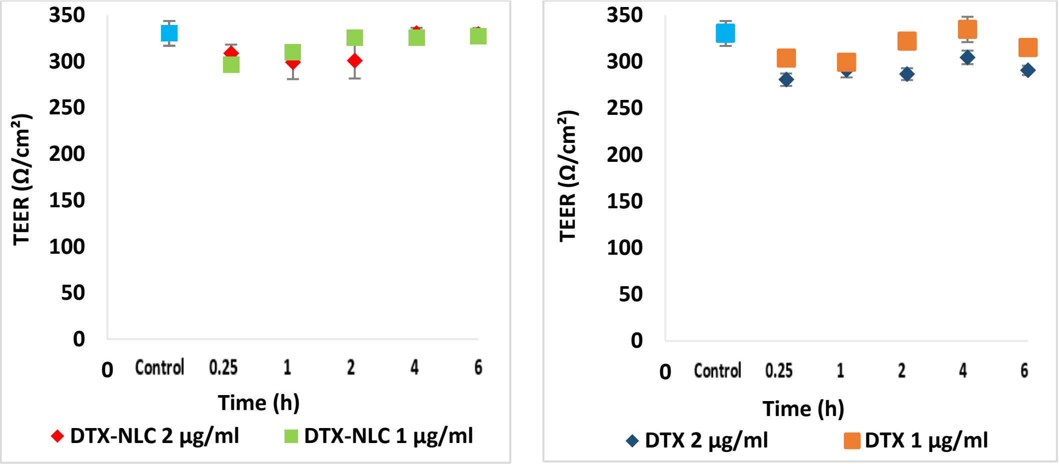

(a) (b)

Figure 5.11 TEER measurements over 6 h (a) for 1 and 2 µg/ml DTX-NLC, (b) 1 and 2 µg/ml DTX solution, where the control is the tri-culture cell lines without treatment. Data are mean ± SD, (N=3).

DTX exhibited a high potency and toxicity in normal and cancerous cell lines as we previously determined in Chapter Four (Section 4.5.2.1), and it would appear that the BBB model lost barrier function when it came into direct contact with the DTX alone. The Papp values for 1 µg/ml for DTX-NLC and DTX after 6 h incubation period was 40 x10^{-3} and 25x 10^{-3} cm/Sec respectively, showing a highly significant difference between the two treatments. When 2 µg/ml of DTX-NLC and DTX were examined there was no significant difference between the Papp. DTX is a CNS negative drug (P-gp substrate) (Loscher and Potschka, 2005), but our data indicated the ability of DTX to pass through the BBB on prolonged incubation, though that high concentration of DTX damaged the stability of the BBB model, leading to loss of integrity.

To our knowledge, no previous reports have been published for testing the permeation of DTX through a 3D *in-vitro* BBB model. Our data indicated that the permeability is not a concentration-dependent variable as also shown in section 5.5.2 when two level concentration were examined with a fluorescence labelled DTX-NLCs. Additionally, the higher values of Papp that were acquired after quantifying DTX from the biological matrix by HPLC showed a more efficient way and better method to determine the actual Papp values. due to a high extraction recovery % as the extraction recovery was ranging between 100.02 and 90.03 % as detailed earlier in chapter two (section 2.5.3.3.5).

5.5.4. Evaluation of DTX-NLCs and surface modified DTX-NLCs uptake by U87MG monolayer following the permeability across 3D *in-vitro* BBB model

To explore the fate of four formulations, R-DTX-NLC, R-GLA-DTX-NLC, R-ALA-DTX-NLC, and R-SA43-DTX-NLC after passing through the 3D *in-vitro* BBB model as detailed in section 5.5.2, we propose to determine these four formulations uptake by a glioblastoma U87MG monolayer. In addition, to evaluate the effect of the presence of U87MG with the 3D *in-vitro* BBB model, the TEER, concentration by fluorescence quantification from the basolateral side and Papp were calculated. As summarised in section 5.4.6, the U87MG cells were seeded on the bottom of the plate then the tri-culture BBB model was introduced to glioblastoma cells once the TEER values were high enough ranging between 260-290 Ω/ cm^2.

The TEER was 297.66 ±24.2 Ω/cm^2 for the control (untreated cells), then followed by a maximum drop in the TEER values to 253.66 ±7.96Ω/cm^2 at 1 h, when R-DTX-NLC 1 µg/ml was incubated. The TEER gradually returned close to the control values (Figure 5.12 a). A similar pattern was displayed by both R-GLA-DTX-NLC and R-ALA-DTX-NLC, the lowest TEER value was obtained after 1 h incubation for 1 µg/ml R-ALA-DTX-NLC and R-GLA-DTX-NLC (Figure 5.12 b and c). While for the R-SA43-DTX-NLC the TEER measurements indicated that the BBB model exhibited a longer time to retain normal TEER values as the TEER values were 261.77 ±14.43, 243.4 ±23.29, 257 ±30.94, and 255.33 ±24.09 Ω/cm^2 when incubated for 0.25, 1, 2, and 4 h, respectively (Figure 5.12 d). All four formulations indicated a change in the TEER values (Figure 5.12 e) which in turn proposed that they interact with the TJs proteins in the endothelial barrier causing them to open transiently and might suggest the permeation of those formulations through the paracellular diffusion as discussed in details in section 5.5.2. When comparing the four ligands there was no significant difference between them as to which caused the largest decrease in TEER. Moreover, the TEER values were not significantly affected by the presence of

U87MG cells in the BBB model due to the virtually similar pattern were shown when the four formulation tested with the absence of the U87MG in the BBB model as detailed in section 5.2.2. This may be explained by the fact that BBB cells were not grown in the presence of the U87MG glioblastomas. *In vivo*, glioblastoma is known to grow behind intact BBB, as well as causing a leaky BBB in nearby vessels (On *et al.,* 2013). The focus of this thesis was to improve the permeability of CNS therapeutics, therefore the intact BBB model was grown in the absence of U87MG cells, and the 3D insert was only exposed to the glioblastoma U87MG monolayer for 2 h during the experiment, to ensure that compounds from the glioblastoma secretome did not disrupt the barrier, skewing the apparent permeability of test formulations.

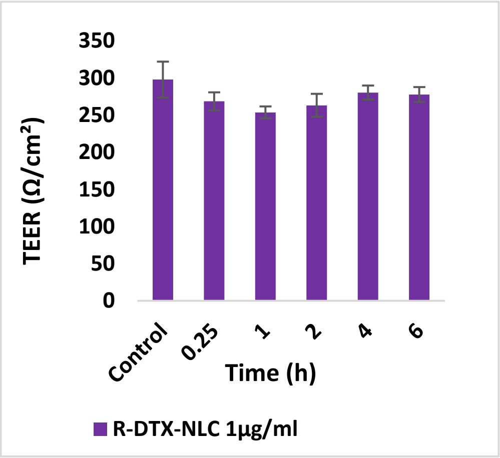

(a)

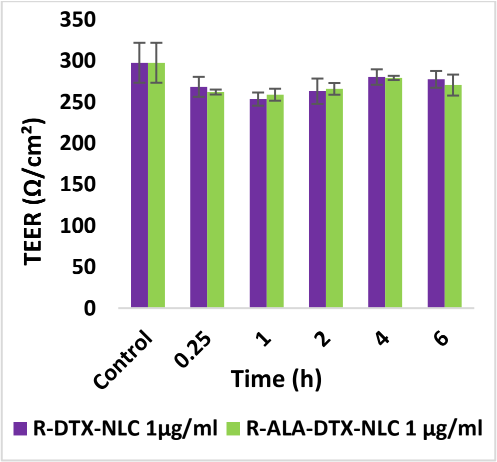

(b)

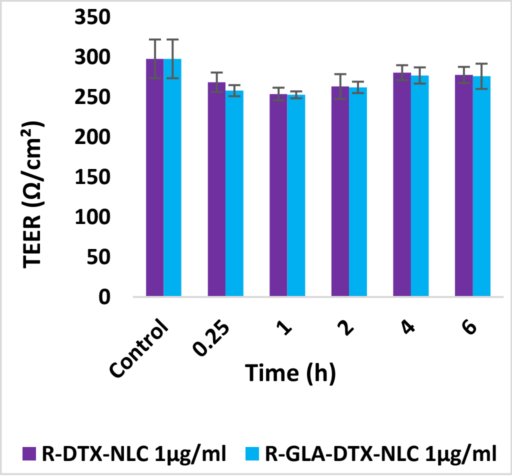

(c)

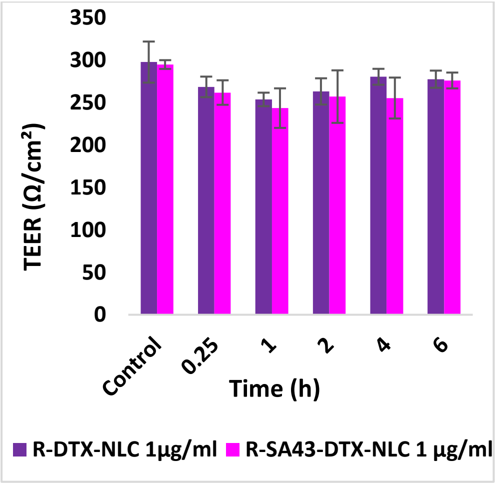

(d)

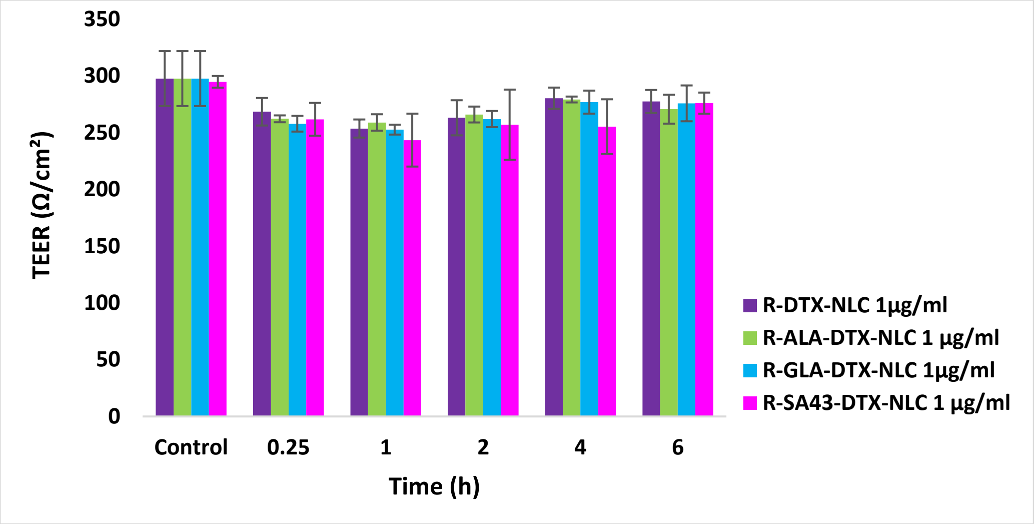

(e)

Figure 5.12 TEER measurements over 6 h time intervals for (a) 1 µg/ml R-DTX-NLC, (b) 1 µg/ml R-DTX-NLC and R-GLA-DTX-NLC, (c) 1 µg/ml R-DTX-NLC and R-ALA-DTX-NLC,(d) 1 µg/ml R-DTX-NLC and R-SA43-DTX-NLC, and (e) combined data for 1 µg/ml R-DTX-NLC, R-GLA-DTX-NLC, R-ALA-DTX-NLC, and R-SA43-DTX-NLC . Data are mean ± SD, (N=3).

In addition to measuring the TEER values, we quantified the concentration for the samples that were collected from the basolateral side of the insert,reading fluorescence values from the standard plot shown in figures 5.13 a, b, c, and d for the R-DTX-NLC, R-GLA-DTX-NLC, R-ALA-DTX-NLC, and R-SA43-DTX-NLC, respectively (Figure 5.14).

The concentration of DTX-NLCs permeated in the presence of the U87MG in the 3D *in-vitro* BBB model was significantly higher than the fluorescence concentration examined with BBB model in absence of the U87MG cells for all the all four formulations R-DTX-NLC, R-GLA-DTX-NLC, R-ALA-DTX-NLC, and R-SA43-DTX-NLC, respectively at 1 µg/ml (figures 5.4 b, 5.6 b, 5.8 b, and 5. 10).

Data showed a higher concentration passing through the BBB model, with a slight increase with respect to time, and R-SA43-DTX-NLC fluorescence concentration showed a highly significant difference in comparison to R-DTX-NLC and R-GLA-DTX-NLC, and no significant difference when compared with R-ALA-DTX-NLC at 1 h incubation time. All formulations demonstrated a permeation through the BBB model even when the TEER returned to normal values, leading to the conclusion that there may be different mechanisms that enable the permeability of the NLCs through the BBB model.

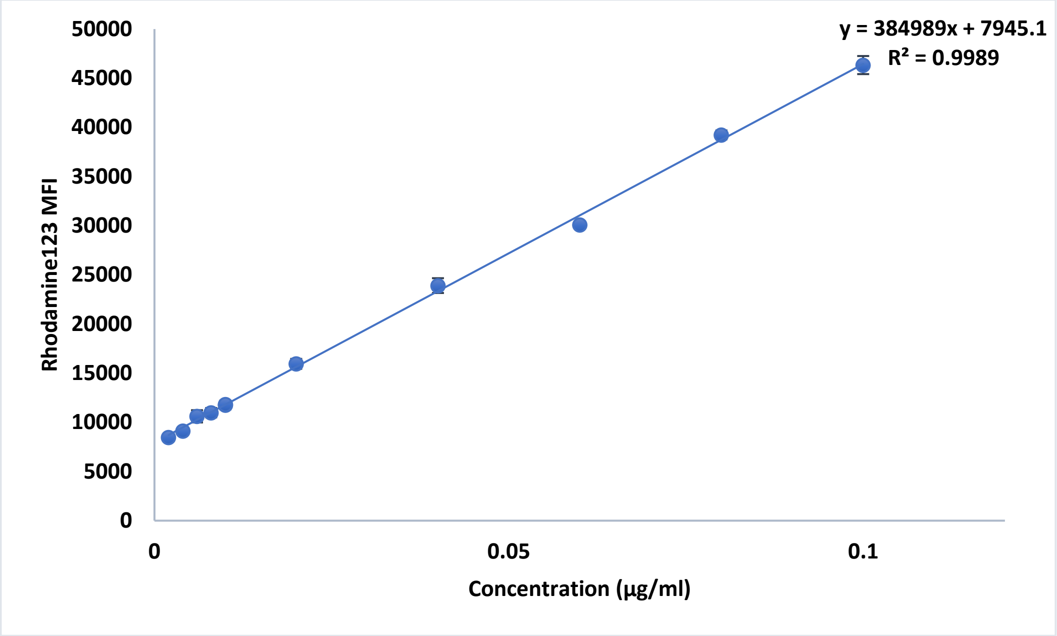
y = 384989x + 7945.1
R² = 0.9989
Rhodamine123 MFI
50000
45000
40000
35000
30000
25000
20000
15000
10000
5000
0
0
0.05
0.1
Concentration (µg/ml)

(a)

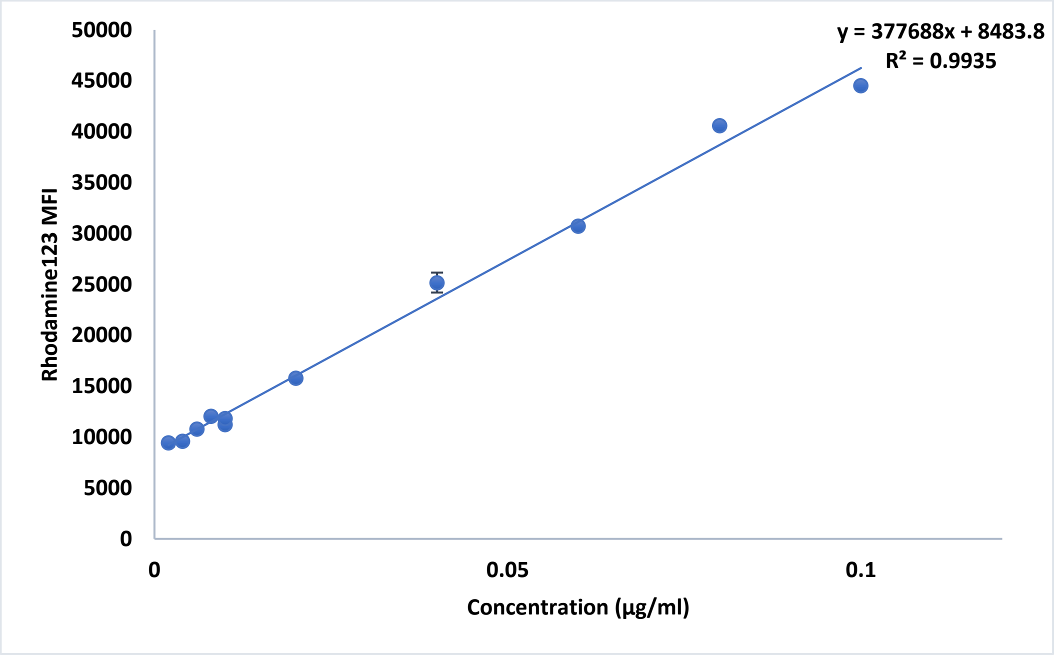
y = 377688x + 8483.8
R² = 0.9935
Rhodamine123 MFI
50000
45000
40000
35000
30000
25000
20000
15000
10000
5000
0
0
0.05
0.1
Concentration (µg/ml)

(b)

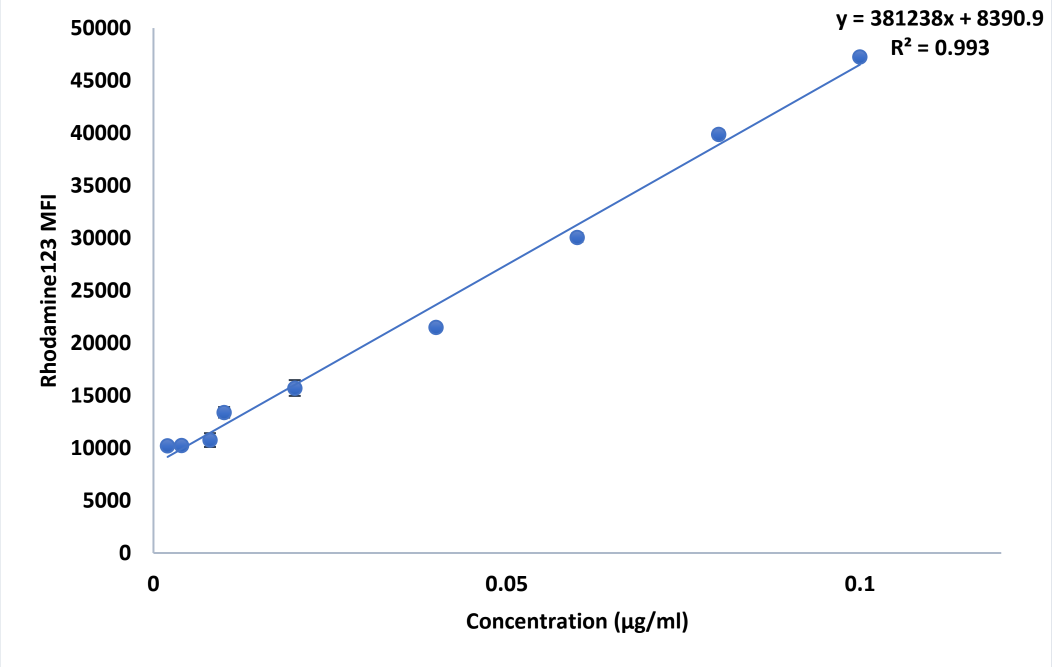

(c)

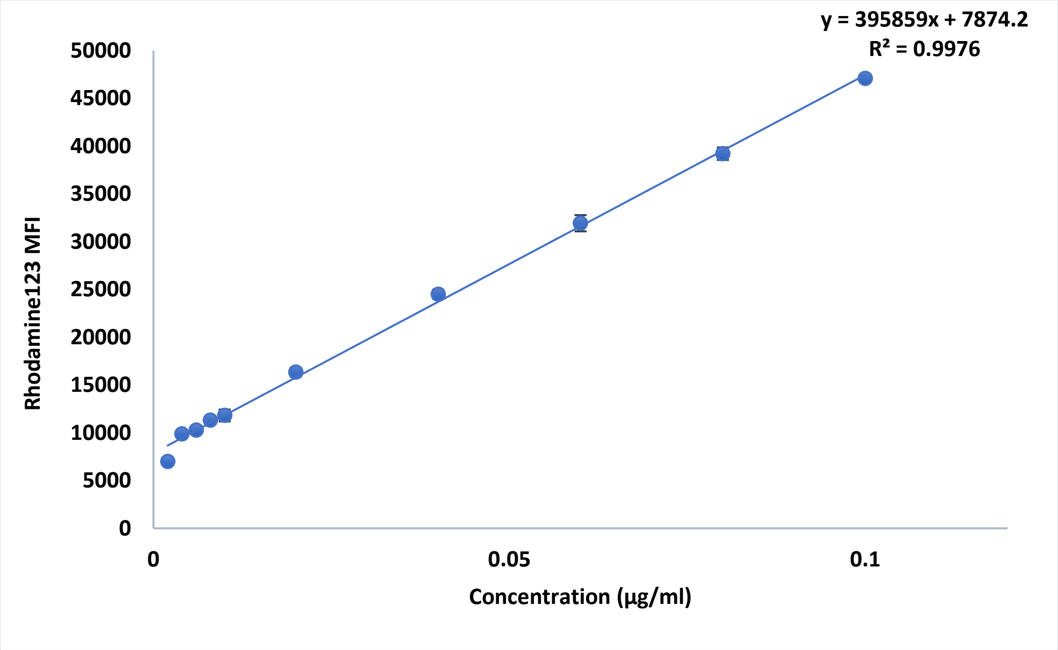

(d)

Figure 5.13 Standard calibration plots 1 µg/ml of (a) R-DTX-NLC, (b) R-GLA-DTX-NLC, (c)R-ALA-DTX-NLC, and (d) R-SA43-DTX-NLC. Data are mean ± SD, (N=3).

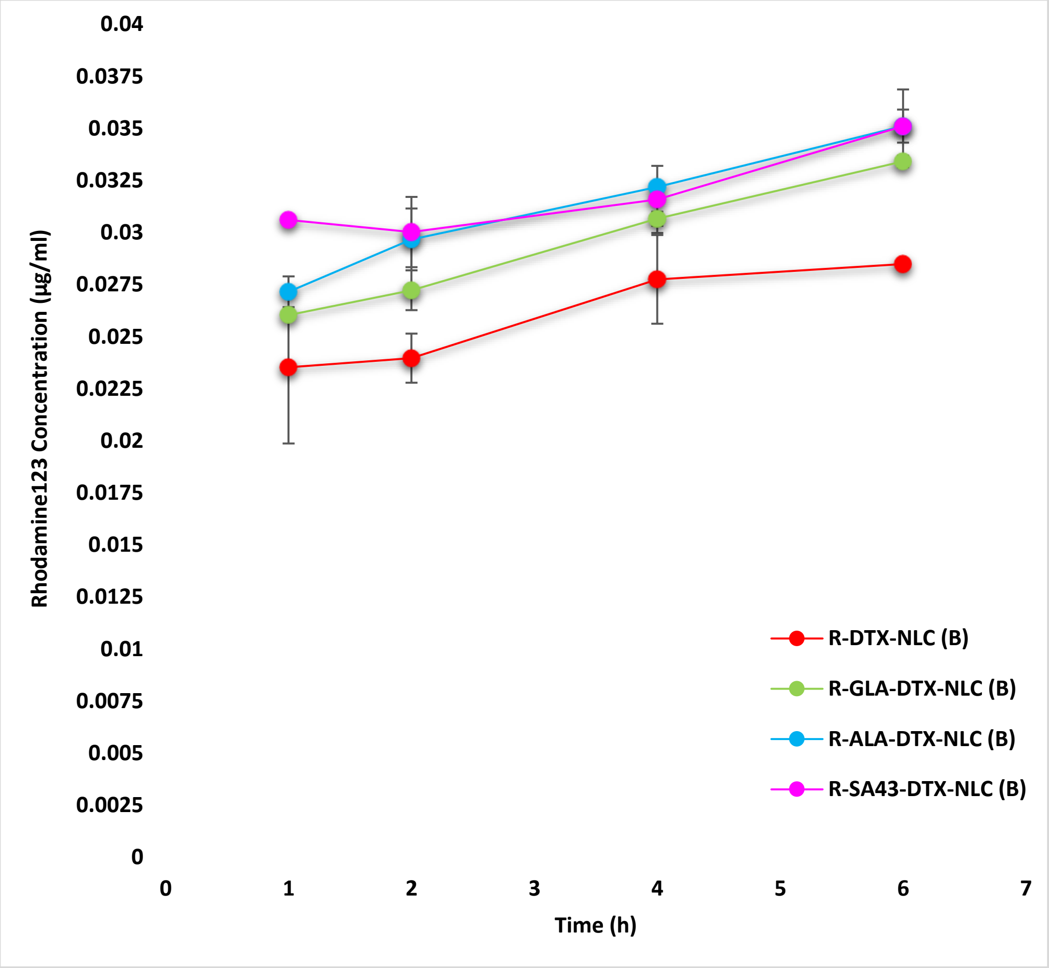

Figure 5.14 Fluorescence concentrations for 1 µg/ml of R-DTX-NLC, R-GLA-DTX-NLC, R-ALA-DTX-NLC, and R-SA43-DTX-NLC, respectively, that were sampled from basolateral side (B) of the insert at 1, 2, 4, and 6 h. Data are mean ± SD, (N=3).

The apparent permeability for all formulations was calculated using equation 5.1 and plotted with respect to time (Figure 5.15), the Papp indicated a higher value at 1 h incubation time for all four formulations, additionally, the Papp of R-SA43-DTX-NLC was significantly higher then Papp of R-DTX-NLC, and no significant difference between R-SA43-DTX-NLC when compared with R-GLA-DTX-NLC and R-ALA-DTX-NLC. Furthermore, a significant increase in Papp was displayed when R-GLA-DTX-NLC and R-ALA-DTX-NLC were compared with R-DTX-NLC at 1 h incubation time. The Papp values were high at 1 h incubation then started to reduce over time. From this results we gather that the Papp values were high due to the opening of the TJ and it was reduced when the TEER values returned close to normal values indicating the close of the TJ gap, and due to the fact that the TEER values of R-SA43-DTX-NLC took longer time to return to normal values than the other three formulations, suggesting that the TJ took long time to close and led to the increase of R-SA43-DTX-NLC permeation and resulted in high Papp value at 1 h incubation (Figure 5.15).

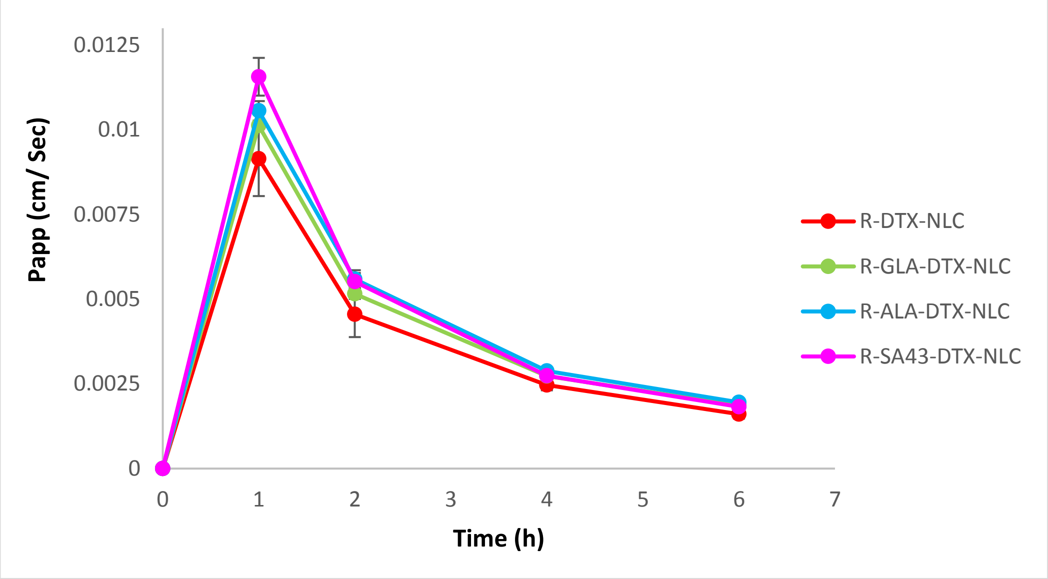

Figure 5.15 Expressing the for the Papp values in a scatter graph plotted with respect to different time intervals, for 1 µg/ml of R-DTX-NLC, R-GLA-DTX-NLC, R-ALA-DTX-NLC, and R-SA43-DTX-NLC. Papp was calculated for samples collected from the basolateral side of the insert for each formulation at 1, 2, 4, and 6 h. Data are mean ± SD, (N=3).

To determine the uptake of all four formulations by U87MG after passing through the BBB model the U87MG cells were collected from the bottom of the plate after 6 h incubation with the four formulations, then samples were prepared and analysed using the flow cytometer to quantify the amount of the formulations that were uptaken by U87MG. The MFI indicated no significant difference when all four formulations were compared with each other (Figure 5.16 a), suggesting that the ligands attached to the surface of the NLCs might need to be increased to enhance the uptake of the formulation after passing the BBB model. There was an enhanced rate of permeation of the NLCs when it was surface modified with the SA43-aptamer. The flow cytometer histograms in figures 5.16 b and c showed the peak shifting towards the right side, due to U87MG uptake in all four formulations R-DTX-NLC, R-GLA-DTX-NLC, R-ALA-DTX-NLC, and R-SA43-DTX-NLC, respectively.

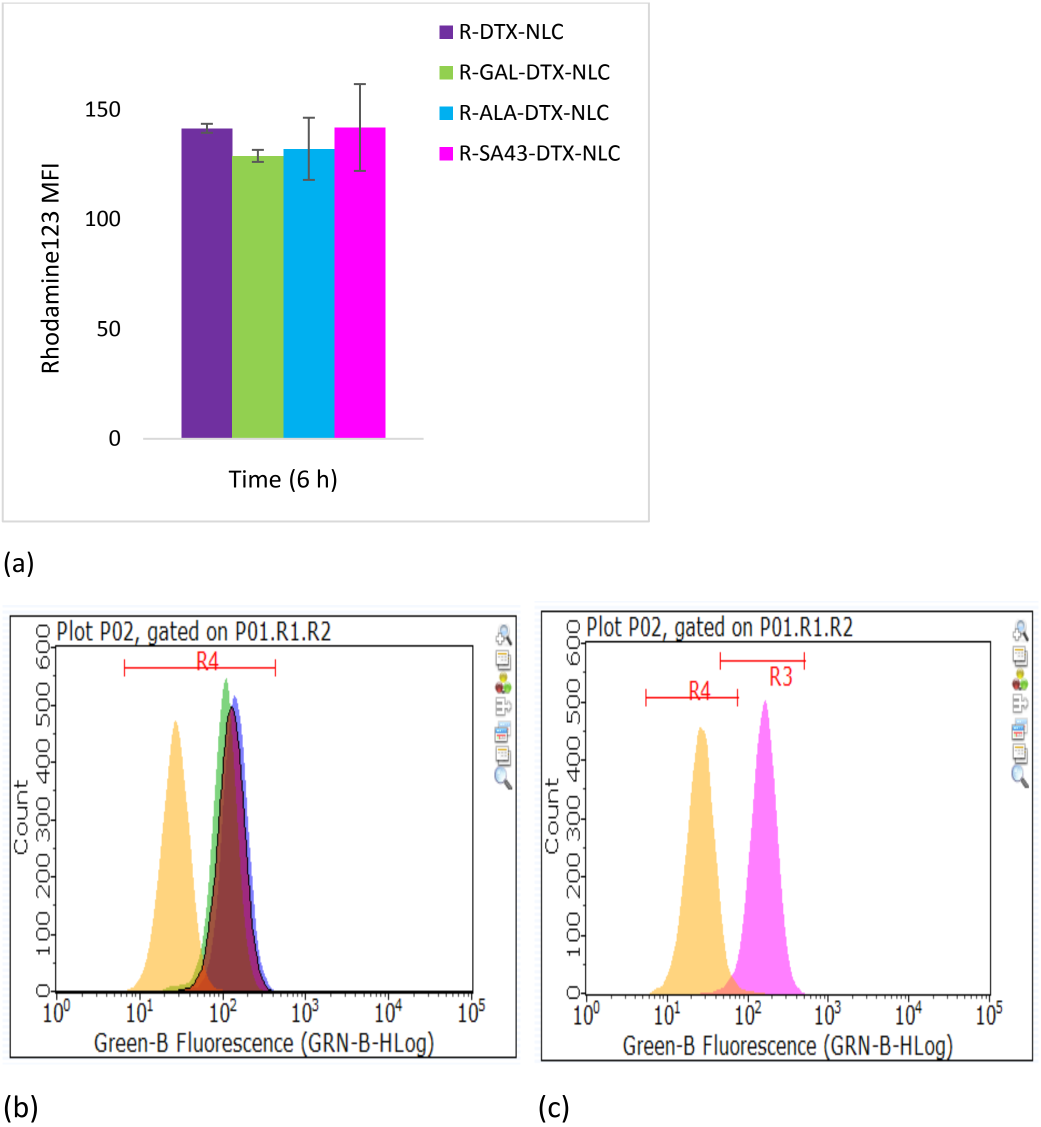

Figure 5.16 U87MG uptake data following penetration through the BBB model (a) MFI at 6 h incubation with 1 µg/ml R-DTX-NLC, R-GLA-DTX-NLC, R-ALA-DTX-NLC, and R-SA43-DTX-NLC, respectively. Data are mean ± SD, (N=3), (b) flow cytometer histograms demonstrating the U87MG uptake, and peak shifts for 6 h incubation time of 🟨 🟩 🟥 🟪 control (untreated U87MG cells), and 1 µg/ml of R-DTX-NLC, R-GLA-DTX-NLC, and R-ALA-DTX-NLC, respectively and (c) flow cytometer histograms demonstrating the U87MG uptake, and peak shifts for 6 h incubation time of 🟨 control (untreated U87MG cells) and 🟪 1 µg/ml of R-SA43-DTX-NLC, respectively. Data are (N=3).

Generally, Papp was considered high in case Papp > 60 × 10^{-6} cm/min according to Amidon *et al.,* (1995); Esposito *et al.,* (2016) and Kumar *et al.,* (2014). It is worth mentioning that GB cells exhibit overexpression of vascular endothelial growth factor (VEGF), which is an angiogenesis factor. VEGF might be related to the increase in the paracellular permeability in a BBB model (Miao *et al.,* 2014; Dwyer *et al.,* 2012). The brain tumour barrier model might be causing the leaky conditions of the endothelial cells, which in turn increase the permeability (Kumar *et al.,* 2014). In our case, the increase in paracellular permeability might lead to the excess NLCs permeating through the BBB model in the presence of the U87MG cells, suggesting the existence of glioblastoma promotes endothelial permeability in brain microvascular endothelial cells as previously demonstrated by Dwyer *et al.,* (2012). Additionally, other mechanisms might be involved in higher permeation of R-GLA-DTX-NLC and ALA-DTX-NLC, such as the capacity to promote the NLCs to bind to the brain FABP7 receptors. PUFAs (GLA and ALA) have been reported to bind to these receptors (Elsherbiny *et al.,* 2013; Shimizu *et al.,* 1997). The ability of SA43-aptamer to bind to Ku 70 and Ku 80 and also to bind to endothelial specific ligands within the cell (Aptekar *et al.,* 2015) might cause the higher permeability of this three formulation through the BBB model in presence of U87MG more than the permeability that have been shown to same formulation when tested in the same model without the presence of U87MG, glioblastoma induce permeability, through its receptor CXCR2 on brain endothelial (Dwyer *et al.,* 2012).

5.5.5. Evaluation of DTX-NLCs and surface modified DTX-NLCs effect on P-gp efflux pump using 3D *in-vitro* BBB model

For the purpose of evaluating the efflux inhibition potential of DTX-NLC, GLA-DTX-NLC, ALA-DTX-NLC, and SA43-DTX-NLC, rhodamine 123 efflux pump activity in the presence and absence of the four formulations relative to verapamil and vinblastine were evaluated, as detailed in section 5.4.7. Rhodamine123 (R) a well known cell-permeable and was used for examining membrane transport, Rhodamine 123 is a P-gp substrate efflux transport (Yang *et al.,* 2015). was used in 10 µg/ml concentration in combination with all samples. A standard plot of R was generated to quantify its concentration in the basolateral side of the insert.

Efflux activity of R was significantly reduced when incubated at 4° C compared to R concentration when incubated at 37 °C. Additionally, when efflux activity of 10 µg/ml R (no P-gp inhibitors) was compared to 10 µg/ml R concentration in the presence of P-gp inhibitors verapamil and vinblastine, a significantly higher concentration of R, was measured on the basolateral side, confirming verapamil and vinblastine effect as P-gp inhibitor (Figure 5.17) these results were in line with previous research by Yang *et al.,* (2015) and Wilhelm *et al.,* (2011).

A significantly lower concentration of R was seen when DTX-NLC formulation was incubated with 10 µg/ml R at 37 °C suggesting that DTX-NLC, might be not an active efflux inhibitor, or might need longer incubation time to display its effect. Some NPs in the literature have been found to act as P-gp inhibitors depending on their compositions (Bansal *et al.,* 2009a). Solutol HS-15 and Labrasol have the ability to inhibit the P-gp functions and enhance drug accumulation, through their ability to insert themselves between the plasma membrane lipid tails of the lipid bilayer and fluidise the membrane. Also, they might interact with the bilayers polar head groups and modify the hydrogen bond or ionic bond forces which may add on to the inhibitory effect of P-gp inhibitors (Lo 2003). Both of these surfactants were used for the fabrication of our DTX-NLC formulation. Notably, the absence of any P-gp inhibition may be due to a lower concentration of excipients (Figure 5.17).

GLA-DTX-NLC also had a similar effect as the DTX-NLC. Some PUFAs have a role as P-gp expression suppressor as previously reported by Srivalli and Lakshmi, (2012) and Yuan *et al.,* (2008), through elevated levels of ROS, but it is known that changing gene expression needs a long time to be achieved, hence GLA-DTX-NLC did not express a notable change in the R concentration when samples were collected from the basolateral side of the BBB model. While ALA-DTX-NLC and SA43-DTX-NLC demonstrated no significant increase in R concentration when compared to the 10 µg/ml R at 37 °C (Figure 5.17), which suggest that their effect as P-gp inhibitors might appear on prolonging incubation time or considering a higher surfactants concentration for both Solutol HS-15 and Labrasol.

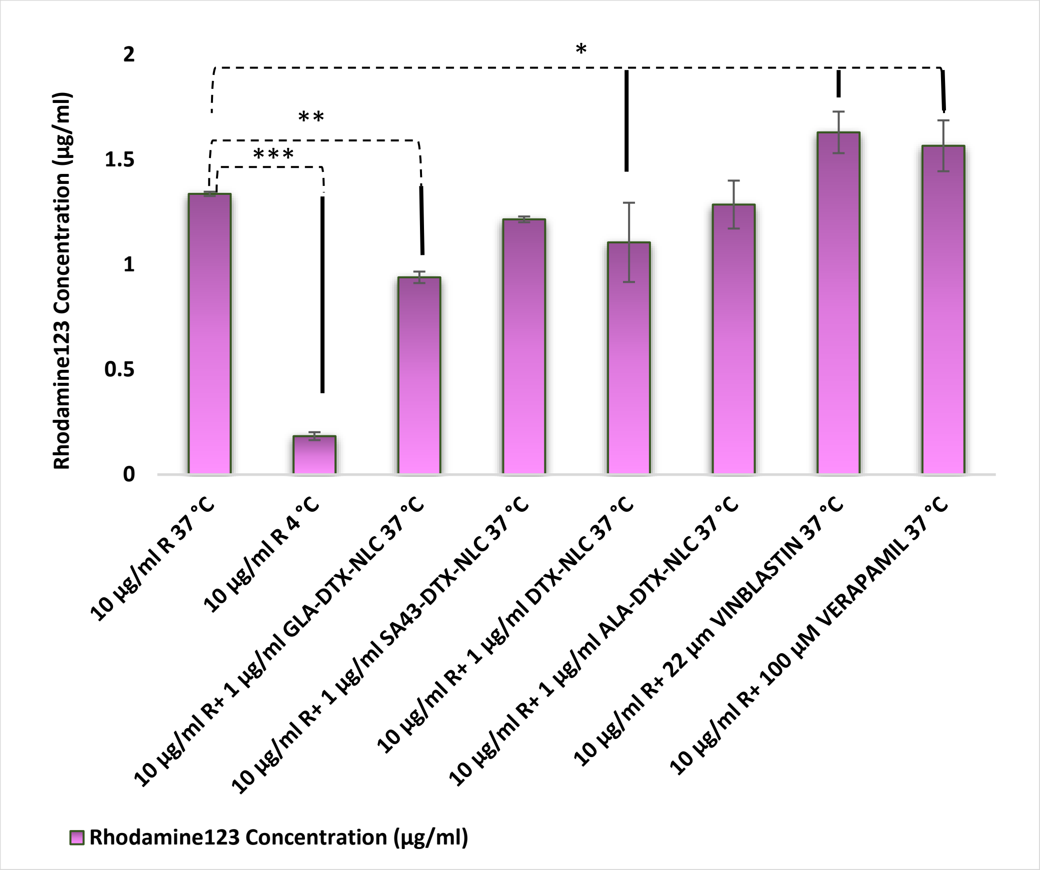

Figure 5.17 Papp values for 10 µg/ml Rhodamine123 (R) at 37 °C, 10 µg/ml R at 4 °C, 10 µg/ml R+ 100 µM verapamil at 37 °C, 10 µg/ml R+ 22 µM vinblastine at 37 °C, 10 µg/ml R+ 1 µg/ml DTX-NLC at 37 °C, 10 µg/ml R+ 1 µg/ml GLA-DTX-NLC at 37 °C, 10 µg/ml R+ 1 µg/ml ALA-DTX-NLC at 37 °C, 10 µg/ml R+ 1 µg/ml SA43-DTX-NLC at 37 °C after 1 h incubation. All samples were compared to 10 µg/ml R at 37 °C. * $P < 0.05$, ** $P < 0.001$ and *** $P < 0.000$ refers to the significant difference. Data are mean ± SD, (N=3).

In summary, the Papp suggested that ligands improved permeation of the DTX-NLC formulation due to the ability of PUFAs to enter the brain by passive diffusion and proteins-mediated transport by the membrane-associated proteins, like fatty acid transport proteins and fatty acid translocases (CD36) as indicated by Chen *et al.,* (2008), but this does not seem to have been achieved by P-gp inhibition, leading to the conclusion that the attached ligands may be masking the P-gp inhibiting groups of the NLC. The additional active transport mediated mechanism, such as receptor-mediated endocytosis, may be involved as PUFAs might enable the DTX-NLC binding to the brain FABP7 receptors, and the ability of SA43-aptamer to Bind to Ku 70 and Ku 80, thus increasing the permeability of DTX-NLC through the 3D *in-vitro* BBB model, which makes these formulations suitable as a carrier system of chemotherapeutic drug docetaxel for brain delivery and CNS therapeutics.

Chapter Six

Conclusion and future work

6.1. Conclusion

The main aim of this project was to enhance selectivity and therapeutic efficacy of an anticancer drug docetaxel (DTX) for targeting and treating glioblastomas, by examining the glioblastoma cell lines proliferation, internalisation, uptake, cell cycle distribution and permeation through 3D *in-vitro* BBB model that was set up from human origin cell lines.

This was achieved by enhancing permeation through the BBB of the poorly water-soluble drug DTX, by incorporating it into nanostructure lipid carrier (NLC) as a delivery system composed of biodegradable excipients and increasing its selective uptake by glioblastoma cells by use of novel aptamer and polyunsaturated fatty acids (PUFAs) as targeting ligands.

6.1.1. Analytical methods development and validation

- HPLC method was developed and validated for quantification of DTX from NLCs to determine total DTX content and its entrapment efficiency within the DTX-NLCs. THF 20% and 80% mobile Phase (Acetonitrile and water, 50:50), was found to be a suitable organic solvent system to completely dissolve the DTX-NLCs. Optimum chromatographic separation was achieved by a mobile phase consisting of acetonitrile and water (50:50, v/v), used at a flow rate of 1.0 ml/min. The method demonstrated high linearity in the range of 1 to 10 µg/mL with a coefficient of regression 0.9994. The minimum detectable concentration of *DTX (*LOD) was 0.013 µg/ml and the minimum concentration that the HPLC method is able to quantify (LOQ) was 0.041 µg/ml. The method was found to be highly sensitive, specific, repeatable and reproducible with accuracy ranging between 99 % to 100.6 %, All validated parameters were well within the acceptable values of the ICH and FDA guidelines.
- Moreover, HPLC methods were also developed and validated successfully for quantification of DTX released from the NLCs into the two-dissolution media. This method was used for quantifying and establishing the release kinetics of the DTX from the developed DTX-NLCs. The method revealed high linear regression with an R^2 value of 0.999, this method was precise and accurate with high specificity and sensitivity with all validated parameters well within the acceptable values of the ICH and FDA guidelines.
- Also, a new HPLC method was developed for the quantification of DTX in a biological matrix containing a mixture of three primary cell culture media consisting of proteins and human serum. Paclitaxel was used as an internal standard. Retention time for DTX and PTX were found at 7.2min and 7.7 min respectively with no interference from the biological media at these RTs. The method was found to be linear between the

concentration range of 0.05 to 2 µg/ml and was accurate, repeatable and precise with high extraction recovery ranging from 90.03-100.02 %. This method was used for quantification of DTX and DTX-NLC that permeated through the physiological 3D *in-vitro* BBB model. All validated parameters were well within the acceptable values of the ICH, FDA, and EMA guidelines. This method would be of a great value and contribution for future research as to the best of our knowledge there is no method developed for the DTX and DTX-NLC extraction and quantification in BBB culture media.

6.1.2. DTX-NLCs development, functionalisation and characterisation

- DTX loaded NLCs (DTX-NLC) were successfully developed using hot homogenisation technique using probe sonication. DTX was successfully encapsulated in the NLCs using solid lipid triglyceride Dynasan®114 (D114) with a combination of three liquid lipids to enhance DTX solubility and stabilised using a combination of surfactants that not only reduced the interfacial tension and produced stable NLCs but also act as P-gp inhibitors and would possibly improve BBB permeation.
- During development, both product and process parameters were thoroughly optimised initially using one-factor-at-a-time approach followed by 3^2 factorial design. Amongst the process parameters, the temperature was found to be a critical parameter affecting DTX stability and required to be controlled during the production of NLCs. In product parameters, lipid and surfactant concentration affected the critical quality parameters (Particle size, PDI, zeta potential, total drug, entrapment efficiency) of the DTX-NLCs and stable formulation could be identified with the response surface methodology.
- DTX-NLC was characterised by low particle size (136 nm), uniform distribution (0.23), spherical shape, high drug entrapment efficiency (99.1 %) and desirable drug release over the period of 24 h. This formulation also exhibited high zeta potential (ZP) -32 mV, which aided in its stability. DSC, XRD and FTIR confirmed the presence of the entrapped drug in an amorphous state in NLCs.
- Successful functionalisation of DTX-NLC with two PUFAs (GLA and ALA), and one novel SA43-aptamer could be achieved using EDC-NHS chemistry. It was established that the free amine group (FAG): GLA ratio of 1: 1/5, ALA ratio of 1: 1/6 and FAG: the SA43-aptamer ratio of 1:8 were the most favourable ratios for conjugation of GLA, ALA, and SA43-aptamer respectively to DTX-NLCs. To the best of our knowledge, these ligands were not previously reported for their conjugation with NLCs as ligands for treatment of glioblastoma. These surface modified DTX-NLCs would contribute to the ongoing research for the treatment of a brain tumour and specifically glioblastomas. GLA-DTX-NLC, ALA-

DTX-NLC, and SA43-DTX-NLC formulations exhibited low particle size and fairly uniform particle size distribution with high drug entrapment efficiency. FTIR spectral analysis, Raman spectroscopy and reduction of free surface amines confirmed the covalent bonding of ligands.

- DTX-NLC could be successfully lyophilised to produce a free-flowing product by using 10% trehalose as a cryo-protectant. Remarkably a low particle size could be achieved on reconstitution with only 13 nm increase in particle size from the original DTX-NLC before the lyophilisation. The freeze-dried form showed good stability for up to six months when stored at a temperature of 4 °C and -20 °C. Further, DTX-NLC in liquid dispersion form demonstrated good colloidal stability in water and dextrose 5% physiological media for up to 24 h.

6.1.3. *In-vitro* cell lines and 3D spheroids studies

- Cell proliferation studies illustrated enhanced DTX-NLCs potency by surface modification of the DTX-NLC with PUFAs when treated with U87MG glioblastoma cells. Both GLA-DTX-NLC and ALA-DTX-NLC displayed similar activity towards U87MG at 24 h and highly significant low IC_{50} value than bare DTX-NLC. ALA-DTX-NLC demonstrated higher potency than GLA-DTX-NLC when incubated for 48 h with U87MG, while both formulations displayed higher activity than DTX-NLC at 48 h. The ligand density had an impact on cell proliferation as well as the presence of antioxidants in the NLCs. The SA43-DTX-NLC displayed lower toxicity towards U87MG cell lines as compared to DTX and DTX-NLCs.
- DTX-NLC demonstrated less toxicity towards SVG P12 than DTX at 24 and 48 h respectively signifying its lower toxicity to the non-cancerous cells at early time points. GLA-DTX-NLC and ALA-DTX-NLC both showed lower cell toxicity towards SVG P12 at 24 h. Interestingly GLA-DTX-NLC exhibited less toxicity towards SVG P12 at 48 h than the ALA-DTX-NLC. However, all the three formulations showed no significant difference in their activity towards SVG P12 at 72 h. SA43-DTX-NLC exhibited the least toxicity towards SVG P12 than all the tested samples, therefore, can be considered the safest formulation to non-cancerous cells.
- When tested on patient-derived glioblastoma BTNW911 cell lines, ALA-DTX-NLC displayed higher activity (significantly low IC_{50}) than both DTX-NLC and GLA-DTX-NLC at all time points, and GLA-DTX-NLC, in turn, exhibited more potency (significantly lower IC_{50}) than DTX-NLC at all time points when treated with BTNW911 cell). Thus DTX-NLC potency increased when surface modified with PUFAs due to the tumoricidal effect of PUFAs against glioblastoma cell lines, and less toxicity towards non-cancerous cell lines SVG P12.

The SA43-DTX-NLC showed lower activity than DTX-NLCs probably due to lack of any therapeutic effect of the SA43.

- Delivery of DTX using NLCs showed favourable cytotoxicity towards the 3D U87MG spheroids than treatment with the native drug, which might be due to the higher cellular uptake of DTX-NLC by spheroid cells as confirmed from the FACS data. Interestingly GLA-DTX-NLC demonstrated less toxicity towards U87MG spheroids while ALA-DTX-NLC and SA43-DTX-NLC elicited similar potency as DTX.

- Fluorescence microscopy and FACS analysis also confirmed the preferential uptake of NLCs by glioblastoma cells in comparison to normal cells ($p<0.05$) when the DTX-NLCs were surface modified with GLA, ALA, and SA43-aptamer. The obtained data also indicate that SA43-DTX-NLC showed higher selectivity towards U87MG cell lines rather than non-cancerous brain cells SVG P12.

  The internalisation mechanisms showed both time and concentration-dependent cellular uptake when U87MG cell lines were treated with all four formulations with notably less uptake by SVG P12 cells. All four formulations were uptaken by patient-derived cell line BTNW911. Additionally, 3D U87MG spheroids demonstrated higher uptake with DTX-NLC, and surface modification of DTX-NLCs did not enhance the 3D U87MG spheroids. Longer incubation time might be required in case of 3D U87MG spheroids uptake.
- Fluorescence microscopy and FACS analysis for endocytosis pathway study demonstrated that all four formulations internalised through multiple pathways (clathrin-mediated pathway, caveolae/ lipid rafts pathway, and involvement of micropinocytosis/phagocytosis). Additionally, it was observed that the mechanism of cell uptake might be through active transport due to lower uptake of formulations at 4 °C.
- Cell cycle distribution results in U87MG cells demonstrated all examined formulations followed DTX pattern and clearly showed arrest at drug-induced G2/M phase.

6.1.4. 3D *in-vitro* BBB model for evaluation of NLCs permeability

- 3D *in-vitro* BBB model of all human cell lines illustrated high TEER value of 300 Ω/cm^2 obtained on day 8, exhibiting integrity of the model. This model was used for screening the permeability of DTX, DTX-NLC and surface modified DTX-NLCs.

  DTX-NLCs and all three surface modified DTX-NLCs demonstrated high permeation through the model, with apparent permeability ranging between $1.02x\ 10^{-3}$ - $2x\ 10^{-3}$-cm/Sec which, might be due to paracellular diffusion. Notably, when DTX-NLC was functionalised with GLA and ALA, it caused a high concentration permeation of the formulations through the BBB model that might be due to binding to the brain FABP7 receptors. SA43-DTX-NLC displayed similar permeability as DTX-NLC when studied using *in-vitro* BBB model.

- However, in the tumour presence model where a layer of U87MG was grown on the basolateral side of *in-vitro* BBB model, R-SA43-DTX-NLC, R-GLA-DTX-NLC and R-ALA-DTX-NLC fluorescence concentrations showed a highly significant increase in comparison to R-DTX-NLC (at 1h), suggesting that surface modification of the R-DTX-NLC with selective SA43-aptamer and PUFAs contributed to higher circulating concentration on the basolateral side of the 3D insert. Also, FACS data confirmed that all four formulations were uptaken by the U87MG cells after passing through the 3D *in-vitro* BBB model.
- DTX-NLC and surface modified DTX-NLCs formulations were not active P-gp inhibitors leading to the conclusion that the attached ligands might be masking the P-gp inhibiting groups of the NLC. The active transport via transcytosis might be the mechanism responsible for the permeation of the DTX-NLCs through the BBB model due to the notably lower concentration at 4°C which indicates an energy-dependent process. The receptor-mediated transcytosis, may be involved as PUFAs might enable the DTX-NLC binding to the brain FABP7 receptors, and the ability of SA43-aptamer to bind to Ku 70 and Ku 80, thus increasing the permeability of DTX-NLC through the 3D *in-vitro* BBB model, which makes these formulations suitable as a carrier system of chemotherapeutic drug DTX for brain delivery treatment.

6.1.5. General conclusion

In conclusion, we have achieved the aim of this project of using NLCs as a carrier system for delivery of chemotherapeutic drug DTX for treatment of glioblastoma and improving its potency with increased toxicity towards glioblastoma cell lines by surface modification of the DTX-NLC with PUFAs (GLA and ALA). DTX-NLC was characterised by low particle size and uniform particle distribution with negative surface charge and lyophilised formulation stable for up to six months.

All three-surface modified formulations demonstrated high uptake by glioblastoma U87MG cells, and notably less cellular uptake with non-cancerous brain cells (SVG P12), with distinguishing selectivity against glioblastoma cell line U87MG.

DTX permeability through 3D *in-vitro* BBB model could be enhanced by encapsulation of DTX within the NLCs and further, the permeation was found to increase by surface modification of DTX-NLC with ligands (GLA, ALA and SA43-aptamer). Distinctive increase in the apparent permeability through the *in-vitro* tumour model in the presence of glioblastoma (U87MG) monolayer cell lines with the BBB model followed by successful uptake by U87MG cells for all the three-surface modified DTX-NLCs, as compared to bare DTX-NLC acclaims not only their enhanced BBB permeability but also, improved cellular internalisation and selective uptake which merits their potential in future glioblastomas therapy. Our data will open the door for new carrier system that uses a selective and targeted therapy by surface modifying the nanoparticles with novel ligands comprising of polyunsaturated fatty acids and aptamer. Additionally, incorporation of docetaxel with a combination of solid and liquid lipids showed a down gradation of toxicity towards the non-cancerous brain cells while enabling the docetaxel nanoparticles to permeate through the *in-vitro* BBB model which indicates the possibility of solving the limitation of inability of docetaxel to penetrate the BBB and reduce its non-specific toxicity.

6.2. Future work

The present study involved the development of NLCs as a carrier system for chemotherapeutic drug docetaxel for enhancing its brain permeability and targeted delivery for treating glioblastomas. Several challenges still remain to be discovered to achieve more selective and higher potency within one single formulation. Additionally, further studies are required to exploit these systems for their potential use in glioblastoma therapy Given below is an outline of some of the ideas proposed for future work:

- A long-term stability study of the DTX-NLCs according to ICH guidelines would need to be carried out to explore if they have any potential for commercial application.
- Scale-up studies and understanding the effect of scale-up on critical quality attributes of the formulation.
- The present studies on cytotoxicity and selectivity are based on in vitro studies, a detailed pharmacokinetic and biodistribution are required to understand the in vivo fate of the developed nanoparticulate formulations.
- Also, efficacy studies in orthotropic glioblastomas model in nude mice would be one of essential next steps for proof of concept *in vivo* studies.
- Presently the effect of PUFAs (GLA and ALA) and the SA43-aptamer have been studied individually for enhancing drug efficacy, cellular uptake, selectivity and permeability through the 3D *in-vitro* BBB model, it would be interesting to evaluate their effectiveness as a dual ligand for dual receptor targeting to achieve better efficacy and selective targeting.

- Further studies are also required to evaluate the glioblastoma cell apoptosis mechanism for the developed NLCs and surface modified NLCs and also conduct experiments in the hypoxic chamber and evaluate the difference between non- hypoxic environments.
- Since we established that the NLCs has the ability to permeate through the 3D *in-vitro* BBB model and also up taken by glioblastoma cells after passing the model, it would worthwhile to delineate the mechanism of transport of the NLCs and surface modified NLCs across the BBB model, and deciphering whether the permeability of the NLCs and surface modified NLCs was paracellular or transcellular.
- Another aspect of future studies would be to study the systems in an advanced 3D *in-vitro* model combining BBB model with 3D tumour spheroids to better mimic *in vivo* situation.

Chapter Seven

References

Abinaya, A., Abirami, S., Nasrin, N. F. and Kalaiyarasi, R. (2017) ‘Detection and Classification of Brain Tumour Using SVM and K-NN Based Clustering’, (March), pp. 70–74.

Adamson, R. H., Lenz, J. F., Zhang, X., Adamson, G. N., Weinbaum, S. and Curry, F. E. (2004) ‘Oncotic pressures opposing filtration across non-fenestrated rat microvessels’, *Journal of Physiology*, 557(3), pp. 889–907. doi: 10.1113/jphysiol.2003.058255.

Afergan, E., Epstein, H., Dahan, R., Koroukhov, N., Rohekar, K., Danenberg, H. D. and Golomb, G. (2008) ‘Delivery of serotonin to the brain by monocytes following phagocytosis of liposomes’, *Journal of Controlled Release*. Elsevier B.V., 132(2), pp. 84–90. doi: 10.1016/j.jconrel.2008.08.017.

Agrahari, V. (2017) ‘The exciting potential of nanotherapy in brain-tumor targeted drug delivery approaches’, *Neural Regeneration Research*, pp. 197–200. doi: 10.4103/1673-5374.200796.

Albanese, A., Tang, P. S. and Chan, W. C. W. (2012) ‘The Effect of Nanoparticle Size, Shape, and Surface Chemistry on Biological Systems’, *Annual Review of Biomedical Engineering*, 14(1), pp. 1–16. doi: 10.1146/annurev-bioeng-071811-150124.

Allen, D. D., Caviedes, R., Cárdenas, A. M., Shimahara, T., Segura-Aguilar, J. and Caviedes, P. A. (2005) ‘Cell lines as in vitro models for drug screening and toxicity studies’, *Drug Development and Industrial Pharmacy*, 31(8), pp. 757–768. doi: 10.1080/03639040500216246.

Alonso, M. J. (2004) ‘Nanomedicines for overcoming biological barriers’, *Biomedicine and Pharmacotherapy*, pp. 168–172. doi: 10.1016/j.biopha.2004.01.007.

Alves, T. R., Lima, F. R. S., Kahn, S. A., Lobo, D., Dubois, L. G. F., Soletti, R., Borges, H. and Neto, V. M. (2011) ‘Glioblastoma cells: A heterogeneous and fatal tumor interacting with the parenchyma’, *Life Sciences*. Elsevier Inc., 89(15–16), pp. 532–539. doi: 10.1016/j.lfs.2011.04.022.

Amidon, G. L., Lennernäs, H., Shah, V. P. and Crison, J. R. (1995) ‘A Theoretical Basis for a Biopharmaceutic Drug Classification: The Correlation of in Vitro Drug Product Dissolution and in Vivo Bioavailability’, *Pharmaceutical Research: An Official Journal of the American Association of Pharmaceutical Scientists*, 12(3), pp. 413–420. doi: 10.1023/A:1016212804288.

Ansari, Z., Bhattacharya, T. S., Saha, A. and Sen, K. (2018) ‘Block copolymer mediated generation of bimetallic Ni-Pd nanoparticles: Raman sensors of ethyl paraben and ciprofloxacin’, *Reactive and Functional Polymers*. Elsevier, 124(November 2017), pp. 1–11. doi: 10.1016/j.reactfunctpolym.2018.01.002.

Anton, K., Baehring, J. M. and Mayer, T. (2012) ‘Glioblastoma Multiforme: Overview of Current Treatment and Future Perspectives’, *Hematology/Oncology Clinics of North America*, pp. 825–853. doi: 10.1016/j.hoc.2012.04.006.

Anton, N., Gayet, P., Benoit, J. P. and Saulnier, P. (2007) ‘Nano-emulsions and nanocapsules by the PIT method: An investigation on the role of the temperature cycling on the emulsion phase inversion’, *International Journal of Pharmaceutics*, 344(1–2), pp. 44–52. doi: 10.1016/j.ijpharm.2007.04.027.

Aptekar, S., Arora, M., Lawrence, C. L., Lea, R. W., Ashton, K., Dawson, T., Alder, J. E. and Shaw, L. (2015) ‘Selective targeting to glioma with nucleic acid aptamers’, *PLoS ONE*, 10(8). doi: 10.1371/journal.pone.0134957.

Baker, S. D., Sparreboom, A. and Verweij, J. (2006) ‘Clinical pharmacokinetics of docetaxel: Recent developments’, *Clinical Pharmacokinetics*, 45(3), pp. 235–252. doi: 10.2165/00003088-200645030-00002.

Baklaushev, V. P., Nukolova, N. N., Khalansky, A. S., Gurina, O. I., Yusubalieva, G. M., Grinenko, N. P., Gubskiy, I. L., Melnikov, P. A., Kardashova, K. S., Kabanov, A. V. and Chekhonin, V. P. (2015) ‘Treatment of glioma by cisplatin-loaded nanogels conjugated with monoclonal antibodies against Cx43 and BSAT1’, *Drug Delivery*, 22(3), pp. 276–285. doi: 10.3109/10717544.2013.876460.

Bakshi, A., Mukherjee, D., Bakshi, A., Banerji, A. K. and Das, U. N. (2003) ‘Gamma-linolenic acid therapy of human gliomas.’, *Nutrition (Burbank, Los Angeles County, Calif.)*, 19(4), pp. 305–9. Available at: http://www.ncbi.nlm.nih.gov/pubmed/15120717.

Bamrungsap, S., Zhao, Z., Chen, T., Wang, L., Li, C., Fu, T. and Tan, W. (2012) ‘Nanotechnology in therapeutics: a focus on nanoparticles as a drug delivery system’, *Nanomedicine*, 7(8), pp. 1253–1271. doi: 10.2217/nnm.12.87.

Bandyopadhyay, A., Fine, R. L., Demento, S., Bockenstedt, L. K. and Fahmy, T. M. (2011) ‘The impact of nanoparticle ligand density on dendritic-cell targeted vaccines’, *Biomaterials*, 32(11), pp. 3094–3105. doi: 10.1016/j.biomaterials.2010.12.054.

Bansal, T., Akhtar, N., Jaggi, M., Khar, R. K. and Talegaonkar, S. (2009) ‘Novel formulation approaches for optimising delivery of anticancer drugs based on P-glycoprotein modulation’, *Drug Discovery Today*, 14(21–22), pp. 1067–1074. doi: 10.1016/j.drudis.2009.07.010.

Barani, I. J. and Larson, D. A. (2015) ‘Radiation therapy of glioblastoma’, *Cancer Treat Res*, 163, pp. 49–73. doi: 10.1007/978-3-319-12048-5_4.

Barbarite, E., Sick, J. T., Berchmans, E., Bregy, A., Shah, A. H., Elsayyad, N. and Komotar, R. J. (2016) ‘The role of brachytherapy in the treatment of glioblastoma multiforme’, *Neurosurgical Review*, pp. 195–211. doi: 10.1007/s10143-016-0727-6.

Barbero, F., Russo, L., Vitali, M., Piella, J., Salvo, I., Borrajo, M. L., Busquets-Fité, M., Grandori, R., Bastús, N. G., Casals, E. and Puntes, V. (2017) ‘Formation of the Protein Corona: The Interface between Nanoparticles and the Immune System’, *Seminars in Immunology*. Elsevier, 34(September), pp. 52–60. doi: 10.1016/j.smim.2017.10.001.

Battaglia, L. and Gallarate, M. (2012) ‘Lipid nanoparticles: state of the art, new preparation methods and challenges in drug delivery’, *Expert Opinion on Drug Delivery*, 9(5), pp. 497–508. doi: 10.1517/17425247.2012.673278.

Bazzoni, G. (2006) ‘Endothelial tight junctions: Permeable barriers of the vessel wall’, *Thrombosis and Haemostasis*, 95(1), pp. 36–42. doi: 10.1160/TH05-07-0488.

Bell, H. S., Wharton, S. B., Leaver, H. a and Whittle, I. R. (1999) ‘Effects of N-6 essential fatty acids on glioma invasion and growth: experimental studies with glioma spheroids in collagen gels.’, *Journal of neurosurgery*, 91(6), pp. 989–96. doi: 10.3171/jns.1999.91.6.0989.

Bell, R. D., Sagare, A. P., Friedman, A. E., Bedi, G. S., Holtzman, D. M., Deane, R. and Zlokovic, B. V. (2007) ‘Transport pathways for clearance of human Alzheimer’s amyloid β-peptide and apolipoproteins E and J in the mouse central nervous system’, *Journal of Cerebral Blood Flow and Metabolism*, 27(5), pp. 909–918. doi: 10.1038/sj.jcbfm.9600419.

Bellavance, M.-A., Blanchette, M. and Fortin, D. (2008) ‘Recent Advances in Blood–Brain Barrier Disruption as a CNS Delivery Strategy’, *The AAPS Journal*, 10(1), pp. 166–177. doi: 10.1208/s12248-008-9018-7.

Beloqui, A., Solinís, M. Á., Rodríguez-Gascón, A., Almeida, A. J. and Préat, V. (2016) ‘Nanostructured lipid carriers: Promising drug delivery systems for future clinics’, *Nanomedicine: Nanotechnology, Biology, and Medicine*. Elsevier Inc., 12(1), pp. 143–161. doi: 10.1016/j.nano.2015.09.004.

Bergen, J. M. and Pun, S. H. (2008) ‘Analysis of the intracellular barriers encountered by nonviral gene carriers in a model of spatially controlled delivery to neurons’, *Journal of Gene Medicine*, 10(2), pp. 187–197. doi: 10.1002/jgm.1137.

Bertrand, N. and Leroux, J. C. (2012) ‘The journey of a drug-carrier in the body: An anatomo-physiological perspective’, *Journal of Controlled Release*. Elsevier B.V., 161(2), pp. 152–163. doi: 10.1016/j.jconrel.2011.09.098.

Bertrand, N., Wu, J., Xu, X., Kamaly, N. and Farokhzad, O. C. (2014) ‘Cancer nanotechnology: The impact of passive and active targeting in the era of modern cancer biology’, *Advanced Drug Delivery Reviews*, pp. 2–25. doi: 10.1016/j.addr.2013.11.009.

Bickel, U., Yoshikawa, T. and Pardridge, W. M. (2001) 'Delivery of peptides and proteins through the blood-brain barrier', *Advanced Drug Delivery Reviews*, 46(1–3), pp. 247–279. doi: 10.1016/S0169-409X(00)00139-3.

Bicker, J., Alves, G., Fortuna, A. and Falcão, A. (2014) 'Blood-brain barrier models and their relevance for a successful development of CNS drug delivery systems: A review', *European Journal of Pharmaceutics and Biopharmaceutics*, pp. 409–432. doi: 10.1016/j.ejpb.2014.03.012.

Bissery, M. C., Nohynek, G., Sanderink, G. J. and Lavelle, F. (1995) 'Docetaxel (Taxotere®): A review of preclinical and clinical experience. Part I: Preclinical experience', *Anti-Cancer Drugs*, pp. 339–355. doi: 10.1097/00001813-199506000-00001.

Blasi, P., Giovagnoli, S., Schoubben, A., Ricci, M. and Rossi, C. (2007) 'Solid lipid nanoparticles for targeted brain drug delivery', *Advanced Drug Delivery Reviews*, pp. 454–477. doi: 10.1016/j.addr.2007.04.011.

Bright, A., Renuga Devi, T. S. and Gunasekaran, S. (2010) 'Spectroscopical vibrational band assignment and qualitative analysis of biomedical compounds with cardiovascular activity', *International Journal of ChemTech Research*, 2(1), pp. 379–388.

Broadwell, R. D. (1989) 'Transcytosis of macromolecules through the blood-brain barrier: a cell biological perspective and critical appraisal', *Acta Neuropathologica*, pp. 117–128. doi: 10.1007/BF00294368.

Brodbelt, A., Greenberg, D., Winters, T., Williams, M., Vernon, S. and Collins, V. P. (2015) 'Glioblastoma in England: 2007-2011', *European Journal of Cancer*, pp. 533–542. doi: 10.1016/j.ejca.2014.12.014.

Bvg, Z. V. (2009) *Handbook of Pharmaceutical Excipients*, *Society*. doi: 10.1080/09602011003593423.

Caddeo, C., Teska, K., Sinico, C. and Kristl, J. (2008) 'Effect of resveratrol incorporated in liposomes on proliferation and UV-B protection of cells', *International Journal of Pharmaceutics*, 363(1–2), pp. 183–191. doi: 10.1016/j.ijpharm.2008.07.024.

Campbell, D. and White, J. R. (1989) '5. IR Spectroscopy and Raman Scattering', *Polymer Characterization, Physical Techniques*, pp. 0–6.

Cantor, C. and Schimmel, P. (1980) 'Biophysical chemistry part II: Techniques for the study of biological structure and function.', *New York: W.H. Freeman and Company*, pp. 618–20. doi: 10.1097/QAD.0000000000000701.

Cao, J., Zhang, Y., Wu, Y., Wu, J., Wang, W., Wu, Q. and Yuan, Z. (2018) 'The effects of ligand valency and density on the targeting ability of multivalent nanoparticles based on negatively charged chitosan nanoparticles', *Colloids and Surfaces B: Biointerfaces*, 161, pp. 508–518. doi: 10.1016/j.colsurfb.2017.11.015.

Carver, K., Ming, X. and Juliano, R. L. (2014) 'Multicellular tumor spheroids as a model for assessing delivery of oligonucleotides in three dimensions', *Molecular Therapy - Nucleic Acids*, 3, p. e153. doi: 10.1038/mtna.2014.5.

Chang, J., Jallouli, Y., Kroubi, M., Yuan, X. bo, Feng, W., Kang, C. sheng, Pu, P. yu and Betbeder, D. (2009) 'Characterization of endocytosis of transferrin-coated PLGA nanoparticles by the blood-brain barrier', *International Journal of Pharmaceutics*, 379(2), pp. 285–292. doi: 10.1016/j.ijpharm.2009.04.035.

Chen, C. T., Green, J. T., Orr, S. K. and Bazinet, R. P. (2008) 'Regulation of brain polyunsaturated fatty acid uptake and turnover', *Prostaglandins Leukotrienes and Essential Fatty Acids*, 79(3–5), pp. 85–91. doi: 10.1016/j.plefa.2008.09.003.

Chen, Y. and Liu, L. (2012) 'Modern methods for delivery of drugs across the blood-brain barrier', *Advanced Drug Delivery Reviews*, pp. 640–665. doi: 10.1016/j.addr.2011.11.010.

Chen, Y., Dalwadi, G. and Benson, H. a E. (2004) 'Drug delivery across the blood-brain barrier.', *Current drug delivery*, 1(4), pp. 361–76. Available at: http://www.ncbi.nlm.nih.gov/pubmed/16305398.

Chen, Z., Tai, Z., Gu, F., Hu, C., Zhu, Q. and Gao, S. (2016) ‘Aptamer-mediated delivery of docetaxel to prostate cancer through polymeric nanoparticles for enhancement of antitumor efficacy’, *European Journal of Pharmaceutics and Biopharmaceutics*. Elsevier B.V., 107, pp. 130–131. doi: 10.1016/j.ejpb.2016.07.007.

Chi, T. Y., Chen, G. G. and Lai, P. B. S. (2004) ‘Eicosapentaenoic acid induces fas-mediated apoptosis through a p53-dependent pathway in hepatoma cells’, *Cancer Journal*, 10(3), pp. 190–200. doi: 10.1097/00130404-200405000-00009.

Choi, J., Ko, E., Chung, H. K., Lee, J. H., Ju, E. J., Lim, H. K., Park, I., Kim, K. S., Lee, J. H., Son, W. C., Lee, J. S., Jung, J., Jeong, S. Y., Song, S. Y. and Choi, E. K. (2015) ‘Nanoparticulated docetaxel exerts enhanced anticancer efficacy and overcomes existing limitations of traditional drugs’, *International Journal of Nanomedicine*, 10, pp. 6121–6132. doi: 10.2147/IJN.S88375.

Choudhury, H., Gorain, B., Karmakar, S. and Pal, T. K. (2014) ‘Development and validation of RP-HPLC method: Scope of application in the determination of oil solubility of paclitaxel’, *Journal of Chromatographic Science*, 52(1), pp. 68–74.doi: 10.1093/chromsci/bms206.

Chung, F. L., Pan, J., Choudhury, S., Roy, R., Hu, W. and Tang, M. S. (2003) ‘Formation of trans-4-hydroxy-2-nonenal- and other enal-derived cyclic DNA adducts from n-3 and n-6 polyunsaturated fatty acids and their roles in DNA repair and human p53 gene mutation’, *Mutation Research - Fundamental and Molecular Mechanisms of Mutagenesis*, 531(1–2), pp. 25–36. doi: 10.1016/j.mrfmmm.2003.07.001.

Combs, S. E., Gutwein, S., Thilmann, C., Huber, P., Debus, J. and Schulz-Ertner, D. (2005) ‘Stereotactically guided fractionated re-irradiation in recurrent glioblastoma multiforme’, *Journal of Neuro-Oncology*, 74(2), pp. 167–171. doi: 10.1007/s11060-004-2463-y.

Conner, S. D. and Schmid, S. L. (2003) ‘Regulated portals of entry into the cell’, *Nature*, pp. 37–44. doi: 10.1038/nature01451.

Couroussé, T. and Gautron, S. (2015) ‘Role of organic cation transporters (OCTs) in the brain’, *Pharmacology and Therapeutics*. Elsevier Inc., 146, pp. 94–103. doi: 10.1016/j.pharmthera.2014.09.008.

Cui, B., Wu, C., Chen, L., Ramirez, A., Bearer, E. L., Li, W.-P., Mobley, W. C. and Chu, S. (2007) ‘One at a time, live tracking of NGF axonal transport using quantum dots’, *Proceedings of the National Academy of Sciences*, 104(34), pp. 13666–13671. doi: 10.1073/pnas.0706192104.

Cury-Boaventura, M. F., Pompéia, C. and Curi, R. (2005) ‘Comparative toxicity of oleic acid and linoleic acid on Raji cells’, *Nutrition*, 21(3), pp. 395–405. doi: 10.1016/j.nut.2004.07.007.

Dakwar, G. R., Hammad, I. A., Popov, M., Linder, C., Grinberg, S., Heldman, E. and Stepensky, D. (2012) ‘Delivery of proteins to the brain by bolaamphiphilic nano-sized vesicles’, *Journal of Controlled Release*, 160(2), pp. 315–321. doi: 10.1016/j.jconrel.2011.12.042.

Das, S., Ng, W. K. and Tan, R. B. H. (2012) ‘Are nanostructured lipid carriers (NLCs) better than solid lipid nanoparticles (SLNs): Development, characterizations and comparative evaluations of clotrimazole-loaded SLNs and NLCs?’, *European Journal of Pharmaceutical Sciences*. Elsevier B.V., 47(1), pp. 139–151. doi: 10.1016/j.ejps.2012.05.010.

Das, U. N. (2004) ‘From bench to the clinic: gamma-linolenic acid therapy of human gliomas.’, *Prostaglandins, leukotrienes, and essential fatty acids*, 70(6), pp. 539–552. doi: 10.1016/j.plefa.2003.12.001.

Das, U. N. (2007) ‘Gamma-linolenic acid therapy of human glioma-a review of in vitro, in vivo, and clinical studies.’, *Medical science monitor: international medical journal of experimental and clinical research*, 13(7), p. RA119--31. doi: 487407.

Dausse, E., Da Rocha Gomes, S. and Toulm??, J. J. (2009) 'Aptamers: a new class of oligonucleotides in the drug discovery pipeline?', *Current Opinion in Pharmacology*, pp. 602–607. doi: 10.1016/j.coph.2009.07.006.

Dawson, L. A. and Sharpe, M. B. (2006) 'Image-guided radiotherapy: rationale, benefits, and limitations', *Lancet Oncology*, 7(10), pp. 848–858. doi: 10.1016/S1470-2045(06)70904-4.

Doan, K. M. M. (2002) 'Passive Permeability and P-Glycoprotein-Mediated Efflux Differentiate Central Nervous System (CNS) and Non-CNS Marketed Drugs', *Journal of Pharmacology and Experimental Therapeutics*, 303(3), pp. 1029–1037. doi: 10.1124/jpet.102. 039255.

Doherty, G. J. and McMahon, H. T. (2009) 'Mechanisms of endocytosis.', *Annual review of biochemistry*, 78, pp. 857–902. doi: 10.1146/annurev.biochem.78.081307.110540.

Doktorovova, S., Shegokar, R., Fernandes, L., Martins-Lopes, P., Silva, A. M., Müller, R. H. and Souto, E. B. (2014a) 'Trehalose is not a universal solution for solid lipid nanoparticles freeze-drying', *Pharmaceutical Development and Technology*, 19(8), pp. 922–929. doi: 10.3109/10837450.2013.840846.

Doktorovova, S., Souto, E. B. and Silva, A. M. A. M. (2014b) 'Nanotoxicology applied to solid lipid nanoparticles and nanostructured lipid carriers - A systematic review of in vitro data', *European Journal of Pharmaceutics and Biopharmaceutics*. Elsevier B.V., 87(1), pp. 1–18. doi: 10.1016/j.ejpb.2014.02.005.

Du, P., Li, N., Wang, H., Yang, S., Song, Y., Han, X. and Shi, Y. (2013) 'Development and validation of a rapid and sensitive UPLC-MS/MS method for determination of total docetaxel from a lipid microsphere formulation in human plasma', *Journal of Chromatography B: Analytical Technologies in the Biomedical and Life Sciences*. Elsevier B.V., 926, pp. 101–107. doi: 10.1016/j.jchromb.2013.02.006.

Dwyer, J., Hebda, J. K., Le Guelte, A., Galan-Moya, E. M., Smith, S. S., Azzi, S., Bidere, N. and Gavard, J. (2012) 'Glioblastoma Cell-Secreted Interleukin-8 Induces Brain Endothelial Cell Permeability via CXCR2', *PLoS ONE*, 7(9). doi: 10.1371/journal.pone.0045562.

Elias, D. R., Poloukhtine, A., Popik, V. and Tsourkas, A. (2013) 'Effect of ligand density, receptor density, and nanoparticle size on cell targeting', *Nanomedicine: Nanotechnology, Biology, and Medicine*. Elsevier Inc., 9(2), pp. 194–201. doi: 10.1016/j.nano.2012.05.015.

Elsherbiny, M. E., Emara, M. and Godbout, R. (2013) 'Interaction of brain fatty acid-binding protein with the polyunsaturated fatty acid environment as a potential determinant of poor prognosis in malignant glioma', *Progress in Lipid Research*, 52(4), pp. 562–570. doi: 10.1016/j.plipres.2013.08.004.

EMA (2012) 'Guideline on bioanalytical method validation', *EMEA, Committee for Medicinal Products for Human Use*, 44(July 2011), pp. 1–23. doi: EMEA/CHMP/EWP/192217/2009.

Esim, O., Savaser, A., Ozkan, C. K., Bayrak, Z., Tas, C. and Ozkan, Y. (2018) 'Effect of polymer type on characteristics of buccal tablets using factorial design', *Saudi Pharmaceutical Journal*. King Saud University, 26(1), pp. 53–63. doi: 10.1016/j.jsps.2017.10.013.

Esposito, C. L., Nuzzo, S., Kumar, S. A., Rienzo, A., Lawrence, C. L., Pallini, R., Shaw, L., Alder, J. E., Ricci-Vitiani, L., Catuogno, S. and de Franciscis, V. (2016) 'A combined microRNA-based targeted therapeutic approach to eradicate glioblastoma stem-like cells', *Journal of Controlled Release*. Elsevier B.V., 238, pp. 43–57. doi: 10.1016/j.jconrel.2016.07.032.

Fan, H., Liu, G., Huang, Y., Li, Y. and Xia, Q. (2014) 'Development of a nanostructured lipid carrier formulation for increasing photo-stability and water solubility of Phenylethyl Resorcinol', *Applied Surface Science*. Elsevier B.V., 288, pp. 193–200. doi: 10.1016/j.apsusc.2013.10.006.

Fan, R. R., Wang, Y. L., Han, B., Luo, Y. F., Zhou, L. X., Peng, X. R., Wu, M., Zheng, Y. and Guo, G. (2014) 'Docetaxel load biodegradable porous microspheres for the treatment of colorectal peritoneal carcinomatosis', *International Journal of Biological Macromolecules*. Elsevier B.V., 69, pp. 100–107. doi: 10.1016/j.ijbiomac.2014.05.026.

Fanale, D., Bronte, G., Passiglia, F., Calò, V., Castiglia, M., Di Piazza, F., Barraco, N., Cangemi, A., Catarella, M. T., Insalaco, L., Listì, A., Maragliano, R., Massihnia, D., Perez, A., Toia, F., Cicero, G. and Bazan, V. (2015) 'Stabilizing versus destabilizing the microtubules: A double-edge sword for an effective cancer treatment option?', *Analytical Cellular Pathology*. doi: 10.1155/2015/690916.

Fang, G., Tang, B., Liu, Z., Gou, J., Zhang, Y., Xu, H. and Tang, X. (2014) 'Novel hydrophobin-coated docetaxel nanoparticles for intravenous delivery: In vitro characteristics and in vivo performance', *European Journal of Pharmaceutical Sciences*, 60, pp. 1–9. doi: 10.1016/j.ejps.2014.04.016.

Farokhzad, O. C., Jon, S., Khademhosseini, A., Tran, T. N. T., LaVan, D. A. and Langer, R. (2004) 'Nanoparticle-aptamer bioconjugates: A new approach for targeting prostate cancer cells', *Cancer Research*, 64(21), pp. 7668–7672. doi: 10.1158/0008-5472.

Fauzee, N. J. S., Dong, Z. and Wang, Y. L. (2011) 'Taxanes: Promising anti-cancer drugs', *Asian Pacific Journal of Cancer Prevention*, 12(4), pp. 837–851.

Feng, L. and Mumper, R. J. (2013) 'A critical review of lipid-based nanoparticles for taxane delivery', *Cancer Letters*. Elsevier Ireland Ltd, 334(2), pp. 157–175. doi: 10.1016/j.canlet.2012.07.006.

Food and Drug Administration (2001) 'Guidance for Industry: Bioanalytical Method Validation', *U.S. Department of Health and Human Services*, (May), pp. 4–10. doi: http://www.labcompliance.de/documents/FDA/FDA-Others/Laboratory/f-507 bioanalytical-4252fnl.pdf.

Forman, B. M., Chen, J. and Evans, R. M. (1997) 'Hypolipidemic drugs, polyunsaturated fatty acids, and eicosanoids are ligands for peroxisome proliferator-activated receptors and', *Proceedings of the National Academy of Sciences*, 94(9), pp. 4312–4317. doi: 10.1073/pnas.94.9.4312.

Friedrich, J., Ebner, R. and Kunz-Schughart, L. A. (2007) 'Experimental anti-tumor therapy in 3-D: Spheroids - Old hat or new challenge?', *International Journal of Radiation Biology*, 83(11–12), pp. 849–871. doi: 10.1080/09553000701727531.

Fundarò, A., Cavalli, R., Bargoni, A., Vighetto, D., Zara, G. P. and Gasco, M. R. (2000) 'Non-stealth and stealth solid lipid nanoparticles (SLN) carrying doxorubicin: Pharmacokinetics and tissue distribution after i.v. administration to rats', *Pharmacological Research*, 42(4), pp. 337–343. doi: 10.1006/phrs.2000.0695.

G. Kakadia, P. and R. Conway, B. (2014) 'Solid Lipid Nanoparticles: A Potential Approach for Dermal Drug Delivery', *American Journal of Pharmacological Sciences*, 2(5A), pp. 1–7. doi: 10.12691/ajps-2-5A-1.

Gabathuler, R. (2010) 'Approaches to transport therapeutic drugs across the blood-brain barrier to treat brain diseases', *Neurobiology of Disease*. Elsevier Inc., 37(1), pp. 48–57. doi: 10.1016/j.nbd.2009.07.028.

Gao, H., Qian, J., Yang, Z., Pang, Z., Xi, Z., Cao, S., Wang, Y., Pan, S., Zhang, S., Wang, W., Jiang, X. and Zhang, Q. (2012) 'Whole-cell SELEX aptamer-functionalised poly(ethyleneglycol)-poly(ε-caprolactone) nanoparticles for enhanced targeted glioblastoma therapy', *Biomaterials*. Elsevier Ltd, 33(26), pp. 6264–6272. doi: 10.1016/j.biomaterials.2012.05.020.

Gao, H., Yang, Z., Cao, S., Xiong, Y., Zhang, S., Pang, Z. and Jiang, X. (2014a) 'Tumor cells and neovasculature dual targeting delivery for glioblastoma treatment', *Biomaterials*, 35(7), pp. 2374–2382. doi: 10.1016/j.biomaterials.2013.11.076.

Gao, H., Zhang, S., Yang, Z., Cao, S., Jiang, X. and Pang, Z. (2014b) 'In vitro and in vivo intracellular distribution and anti-glioblastoma effects of docetaxel-loaded nanoparticles functioned with IL-13 peptide', *International Journal of Pharmaceutics*. Elsevier B.V., 466(1–2), pp. 8–17. doi: 10.1016/j.ijpharm.2014.03.012.

Gao, K., Sun, J., Liu, K., Liu, X. and He, Z. (2008) 'Preparation and characterization of a submicron lipid emulsion of docetaxel: submicron lipid emulsion of docetaxel.', *Drug development and industrial pharmacy*, 34(11), pp. 1227–37. doi: 10.1080/03639040802005057.

Gao, Y., Sun, W. and Zhang, J. (2011) 'Optimization of preparation and property studies on glycosylated albumin as drug carrier for nanoparticles', *Pharmazie*, 66(7), pp. 484–490. doi: 10.1691/ph.2011.0850.

Garanti, T. (2016) 'RGD-targeted Solid Lipid Nanoparticles Containing Asiatic Acid for the Treatment of Cancer'.

Garanti, T., Stasik, A., Burrow, A. J., Alhnan, M. A. and Wan, K.-W. W. (2016) 'Anti-glioma activity and the mechanism of cellular uptake of asiatic acid-loaded solid lipid nanoparticles', *International Journal of Pharmaceutics*. Elsevier B.V., 500(1–2), pp. 305–315. doi: 10.1016/j.ijpharm.2016.01.018.

Georgieva, J. V., Hoekstra, D. and Zuhorn, I. S. (2014) 'Smuggling drugs into the brain: An overview of ligands targeting transcytosis for drug delivery across the blood–brain barrier', *Pharmaceutics*, 6(4), pp. 557–583. doi: 10.3390/pharmaceutics6040557.

Girotra, P. and Singh, S. K. (2017) 'Multivariate Optimization of Rizatriptan Benzoate-Loaded Solid Lipid Nanoparticles for Brain Targeting and Migraine Management', *AAPS PharmSciTech*, 18(2), pp. 517–528. doi: 10.1208/s12249-016-0532-0.

Gopal, J., Abdelhamid, H. N., Huang, J. H. and Wu, H. F. (2016) 'Nondestructive detection of the freshness of fruits and vegetables using gold and silver nanoparticle mediated graphene enhanced Raman spectroscopy', *Sensors and Actuators, B: Chemical*, 224, pp. 413–424. doi: 10.1016/j.snb.2015.08.123.

Gopinath, S. C. B. (2007) 'Methods developed for SELEX', *Analytical and Bioanalytical Chemistry*, 387(1), pp. 171–182. doi: 10.1007/s00216-006-0826-2.

Göppert, T. M. and Müller, R. H. (2005) 'Adsorption kinetics of plasma proteins on solid lipid nanoparticles for drug targeting', *International Journal of Pharmaceutics*, 302(1–2), pp. 172–186. doi: 10.1016/j.ijpharm.2005.06.025.

Grant, G. a., Abbott, N. J. and Janigro, D. (1998) 'Understanding the Physiology of the Blood-Brain Barrier: In Vitro Models.', *News in physiological sciences : an international journal of physiology produced jointly by the International Union of Physiological Sciences and the American Physiological Society*, 13(December), pp. 287–293. Available at: http://www.ncbi.nlm.nih.gov/pubmed/11390805.

Gu, P. F., Xu, H., Sui, B. W., Gou, J. X., Meng, L. K., Sun, F., Wang, X. J., Qi, N., Zhang, Y., He, H. B. and

Guidelines, N. (2010) 'Carmustine implants and temozolomide for the treatment of newly diagnosed high-grade glioma', *121, NICE technology appraisal guideance*, (August), pp. 1–45.

Hamard, L., Ratel, D., Selek, L., Berger, F., van der Sanden, B. and Wion, D. (2016) 'The brain tissue response to surgical injury and its possible contribution to glioma recurrence', *Journal of Neuro-Oncology*. doi: 10.1007/s11060-016-2096-y.

Hamilton, G. (1998) 'Multicellular spheroids as an in vitro tumor model', *Cancer Letters*, 131(1), pp. 29–34. doi: 10.1016/S0304-3835(98)00198-0.

Hands, J. R., Dorling, K. M., Abel, P., Ashton, K. M., Brodbelt, A., Davis, C., Dawson, T., Jenkinson, M. D., Lea, R. W., Walker, C. and Baker, M. J. (2014) 'Attenuated Total Reflection Fourier Transform Infrared (ATR-FTIR) spectral discrimination of brain tumour severity from serum samples', *Journal of Biophotonics*, 7(3–4), pp. 189–199. doi: 10.1002/jbio.201300149.

Haque, S., Md, S., Alam, M. I., Sahni, J. K., Ali, J. and Baboota, S. (2012) 'Nanostructure-based drug delivery systems for brain targeting', *Drug Development and Industrial Pharmacy*, 38(4), pp. 387–411. doi: 10.3109/03639045.2011.608191.

He, C., Cai, P., Li, J., Zhang, T., Lin, L., Abbasi, A. Z., Henderson, J. T., Rauth, A. M. and Wu, X. Y. (2017) 'Blood-brain barrier-penetrating amphiphilic polymer nanoparticles deliver docetaxel for the treatment of brain metastases of triple negative breast cancer', *Journal of Controlled Release*. Elsevier B.V., 246, pp. 98–109. doi: 10.1016/j.jconrel.2016.12.019.

He, H., Li, Y., Jia, X. R., Du, J., Ying, X., Lu, W. L., Lou, J. N. and Wei, Y. (2011) 'PEGylated Poly(amidoamine) dendrimer-based dual-targeting carrier for treating brain tumors', *Biomaterials*, 32(2), pp. 478–487. doi: 10.1016/j.biomaterials.2010.09.002.

Hénon, G., Kemény, Z., Recseg, K., Zwobada, F. and Kövári, K. (1997) 'Degradation of α-linolenic acid during heating', *JAOCS, Journal of the American Oil Chemists' Society*, 74(12), pp. 1615–1617. doi: 10.1007/s11746-997-0087-z.

Herbst, R. S. and Khuri, F. R. (2003) 'Mode of action of docetaxel - A basis for combination with novel anticancer agents', *Cancer Treatment Reviews*, pp. 407–415. doi: 10.1016/S0305-7372(03)00097-5.

Hielscher, T. (2005) 'Ultrasonic Production of Nano-Size Dispersions and Emulsions', *Ens*, (December), pp. 14–16.

Holmes, D. (2013) 'The next big things are tiny', *The Lancet Neurology*, p. 32. doi: 10.1016/S1474-4422(12)70313-7.

Horia, E. and Watkins, B. A. (2005) 'Comparison of stearidonic acid and alpha-linolenic acid on PGE2 production and COX-2 protein levels in MDA-MB-231 breast cancer cell cultures', *J Nutr Biochem*, 16(3), pp. 184–192. doi: 10.1016/j.jnutbio.2004.11.001.

Horiba Jobin Yvon (2017) 'Raman Spectroscopy for Analysis and Monitoring', *Raman data and analysis*, pp. 1–2. Available at: http://www.horiba.com/fileadmin/uploads/Scientific/Documents/Raman/bands.pdf.

Horita, Y., Wanibuchi, M., Akiyama, Y., Suzuki, K., Omori, Y., Iihoshi, S., Ochi, S., Mikami, T. and Mikuni, N. (2016) 'Exophytic glioblastoma multiforme originating from the medulla oblongata', *Biomedical Research and Clinical Practice*, 1(2), pp. 58–61. doi: 10.15761/BRCP.1000111.

Hou, L. C., Veeravagu, A., Hsu, A. R. and Tse, V. C. K. (2006) 'Recurrent glioblastoma multiforme: a review of natural history and management options', *Neurosurgical Focus*, 20(4), p. E3. doi: 10.3171/foc.2006.20.4.2.

Huan, M. lei, Zhou, S. yuan, Teng, Z. hui, Zhang, B. le, Liu, X. you, Wang, J. pin and Mei, Q. bing (2009) 'Conjugation with α-linolenic acid improves cancer cell uptake and cytotoxicity of doxorubicin', *Bioorganic and Medicinal Chemistry Letters*, 19(9), pp. 2579–2584. doi: 10.1016/j.bmcl.2009.03.016.

ICH (1996) 'Guidance for industry : Q2B validation of analytical procedures: methodology', *International conference on harmonisation of technical requirements for registration tripartite guideline*, (November), p. 13. doi: 62 FR 27464.

Ioffe, V., Kalendarev, T., Rubinstein, I. and Zupkovitz, G. (2002) 'Reverse phase HPLC for polar lipids. Simple and selective HPLC procedures for analysis of phospholipid-based derivatives of valproic acid and various non-steroidal anti-inflammatory drugs', *Journal of Pharmaceutical and Biomedical Analysis*, 30(3), pp. 391–403. doi: 10.1016/S0731-7085(02)00220-0.

Iqbal, M. A., Md, S., Sahni, J. K., Baboota, S., Dang, S. and Ali, J. (2012) 'Nanostructured lipid carriers system: Recent advances in drug delivery', *Journal of Drug Targeting*, pp. 813–830. doi: 10.3109/1061186X.2012.716845.

Jähne, E. A., Eigenmann, D. E., Culot, M., Cecchelli, R., Walter, F. R., Deli, M. A., Tremmel, R., Fricker, G., Smiesko, M., Hamburger, M. and Oufir, M. (2014) 'Development and validation of a LC-MS/MS method for assessment of an anti-inflammatory indolinone derivative by in vitro blood-brain barrier models', *Journal of Pharmaceutical and Biomedical Analysis*. Elsevier B.V., 98, pp. 235–246. doi: 10.1016/j.jpba.2014.05.026.

Jaimes-Aguirre, L., Morales-Avila, E., Ocampo-García, B. E., Medina, L. A., López-Téllez, G., Gibbens-Bandala, B. V. and Izquierdo-Sánchez, V. (2017) 'Biodegradable poly(D,L-lactide-co-glycolide)/poly(L-γ-glutamic acid) nanoparticles conjugated to folic acid for targeted delivery of doxorubicin', *Materials Science and Engineering C*. Elsevier B.V., 76, pp. 743–751. doi: 10.1016/j.msec.2017.03.145.

Jain, A., Agarwal, A., Majumder, S., Lariya, N., Khaya, A., Agrawal, H., Majumdar, S. and Agrawal, G. P. (2010) 'Mannosylated solid lipid nanoparticles as vectors for site-specific delivery of an anti-cancer drug', *Journal of Controlled Release*, 148(3), pp. 359–367. doi: 10.1016/j.jconrel.2010.09.003.

Jain, R. K. (1994) 'Barriers to drug delivery in solid Jain, R. K. (1994). Barriers to drug delivery in solid tumors. Scientific American, 271(1), 58-65. Retrieved from http://www.ncbi.nlm.nih.gov/pubmed/8066425tumors.', *Scientific American*, 271(1), pp. 58–65. Available at: http://www.ncbi.nlm.nih.gov/pubmed/8066425.

Jiang, Y., Marinescu, V. D., Xie, Y., Jarvius, M., Maturi, N. P., Haglund, C., Olofsson, S., Lindberg, N., Olofsson, T., Leijonmarck, C., Hesselager, G., Alafuzoff, I., Fryknäs, M., Larsson, R., Nelander, S. and Uhrbom, L. (2017) 'Glioblastoma Cell Malignancy and Drug Sensitivity Are Affected by the Cell of Origin', *Cell Reports*, 18(4), pp. 977–990. doi: 10.1016/j.celrep.2017.01.003.

Kam, N. W. S., Liu, Z. and Dai, H. (2006) 'Carbon nanotubes as intracellular transporters for proteins and DNA: An investigation of the uptake mechanism and pathway', *Angewandte Chemie - International Edition*, 45(4), pp. 577–581. doi: 10.1002/anie.200503389.

Karsy, M., Gelbman, M., Shah, P., Balumbu, O., Moy, F. and Arslan, E. (2012) 'Established and emerging variants of glioblastoma multiforme: Review of morphological and molecular features', *Folia Neuropathologica*, 50(4), pp. 301–321. doi: 10.5114/fn.2012.32361.

Kasongo, K. W., Jansch, M., Müller, R. H. and Walker, R. B. (2011) 'Evaluation of the in vitro differential protein adsorption patterns of didanosine-loaded nanostructured lipid carriers (NLCs) for potential targeting to the brain', *Journal of Liposome Research*, 21(3), pp. 245–254. doi: 10.3109/08982104.2010.539186.

Kaur, S., Nautyal, U., Singh, R., Singh, S. and Devi, A. (2015) 'Nanostructure Lipid Carrier (NLC): the new generation of lipid nanoparticles', *Asian Pac. J. Health Sci.*, 2(22), pp. 76–93.

Kaye, S. B. and Vasey, P. A. (2002) 'Docetaxel in ovarian cancer: phase III perspectives and future development', *Semin. Oncol.*, 29(3 Suppl 12), pp. 22–27. Available at: www.ncbi.nlm.nih.gov/pubmed/12170448.

Keum, C. G., Noh, Y. W., Baek, J. S., Lim, J. H., Hwang, C. J., Na, Y. G., Shin, S. C. and Cho, C. W. (2011) 'Practical preparation procedures for docetaxel-loaded nanoparticles using polylactic acid-co-glycolic acid.', *International journal of nanomedicine*, 6, pp. 2225–2234. doi: 10.2147/IJN.S24547.

Khan, A., Imam, S. S., Aqil, M., Ahad, A., Sultana, Y., Ali, A. and Khan, K. (2016) 'Brain Targeting of Temozolomide via the Intranasal Route Using Lipid-Based Nanoparticles: Brain Pharmacokinetic and Scintigraphic Analyses', *Molecular Pharmaceutics*, 13(11), pp. 3773–3782. doi: 10.1021/acs.molpharmaceut.6b00586.

Khan, I., Iqbal, Z., Khan, A., Hassan, M., Nasir, F., Raza, A., Ahmad, L., Khan, A. and Akhlaq Mughal, M. (2016) 'A simple, rapid and sensitive RP-HPLC-UV method for the simultaneous determination of sorafenib & paclitaxel in plasma and pharmaceutical dosage forms: Application to pharmacokinetic study', *Journal of Chromatography B: Analytical Technologies in the Biomedical and Life Sciences*. Elsevier B.V., 1033–1034, pp. 261–270. doi: 10.1016/j.jchromb.2016.08.029.

Khan, M. K., Hunter, G. K., Vogelbaum, M., Suh, J. H. and Chao, S. T. (2009) 'Evidence-based adjuvant therapy for gliomas: current concepts and newer developments', *Indian Journal of Cancer*, 46(2), pp. 96–107. doi: 10.4103/0019-509X.49147.

Kikuchi, R., De Morais, S. M. and Kalvass, J. C. (2013) '*In vitro* P-glycoprotein efflux ratio can predict the in vivo brain penetration regardless of biopharmaceutics drug disposition classification system class', *Drug Metabolism and Disposition*, 41(12), pp. 2012–2017. doi: 10.1124/dmd.113.053868.

Kim, J. K., Park, J. S. and Kim, C. K. (2010) ‘Development of a binary lipid nanoparticles formulation of itraconazole for parenteral administration and controlled release’, *International Journal of Pharmaceutics*, 383(1–2), pp. 209–215. doi: 10.1016/j.ijpharm.2009.09.008.

Kim, R. B. (2002) ‘Drugs as P-glycoprotein substrates, inhibitors, and inducers’, *Drug Metabolism Reviews*, pp. 47–54. doi: 10.1081/DMR-120001389.

Kintzel, P. E., Michaud, L. B. and Lange, M. K. (2006) ‘Docetaxel-associated epiphora.’, *Pharmacotherapy*, 26(6), pp. 853–867. doi: 10.1592/phco.26.6.853.

König, J. (2011) ‘Uptake transporters of the human OATP family: Molecular characteristics, substrates, their role in drug-drug interactions, and functional consequences of polymorphisms’, *Handbook of Experimental Pharmacology*, pp. 1–28. doi: 10.1007/978-3-642-14541-4_1.

Koopaei, M. N., Khoshayand, M. R., Mostafavi, S. H., Amini, M., Khorramizadeh, M. R., Tehrani, M. J., Atyabi, F. and Dinarvand, R. (2014) ‘Docetaxel loaded PEG-PLGA nanoparticles: Optimized drug loading, in-vitro cytotoxicity and in-vivo antitumor effect’, *Iranian Journal of Pharmaceutical Research*, 13(3), pp. 819–834.

Kovacevic, A., Savic, S., Vuleta, G., Müller, R. H. and Keck, C. M. (2011) ‘Polyhydroxy surfactants for the formulation of lipid nanoparticles (SLN and NLC): Effects on size, physical stability and particle matrix structure’, *International Journal of Pharmaceutics*. Elsevier B.V., 406(1–2), pp. 163–172. doi: 10.1016/j.ijpharm.2010.12.036.

Kovacsics, D., Patik, I. and Özvegy-Laczka, C. (2017) ‘The role of organic anion transporting polypeptides in drug absorption, distribution, excretion and drug-drug interactions’, *Expert Opinion on Drug Metabolism & Toxicology*, 13(4), pp. 409–424. doi: 10.1080/17425255.2017.1253679.

Koziara, J. M., Lockman, P. R., Allen, D. D. and Mumper, R. J. (2004) ‘Paclitaxel nanoparticles for the potential treatment of brain tumors’, *Journal of Controlled Release*, 99(2), pp. 259–269. doi: 10.1016/j.jconrel.2004.07.006.

Kreisl, T. N. (2009) ‘Chemotherapy for Malignant Gliomas’, *Seminars in Radiation Oncology*, pp. 150–154. doi: 10.1016/j.semradonc.2009.02.003.

Kulhari, H., Kulhari, D. P., Singh, M. K. and Sistla, R. (2014) ‘Colloidal stability and physicochemical characterization of bombesin conjugated biodegradable nanoparticles’, *Colloids and Surfaces A: Physicochemical and Engineering Aspects*. Elsevier B.V., 443, pp. 459–466. doi: 10.1016/j.colsurfa.2013.12.011.

Kumar, K. N., Raju, N. A., Raju, S. S., Ramarao, B. and Mukkanti, K. (2010) ‘Estimation of docetaxel in parenterals by RP-HPLC’, *Asian Journal of Chemistry*, 22(10), pp. 7513–7518.

Kumar, S., Shaw, L., Lawrence, C., Lea, R. and Alder, J. (2014) ‘P50 * Developing a Physiologically Relevant Blood Brain Barrier Model for the Study of Drug Disposition in Glioma’, *Neuro-Oncology*, 16(suppl 6), p. vi8-vi8. doi: 10.1093/neuonc/nou249.38.

Landfester, K., Bechthold, N., Tiarks, F. and Antonietti, M. (1999) ‘Formulation and stability mechanisms of polymerizable miniemulsions’, *Macromolecules*, 32(16), pp. 5222–5228. doi: 10.1021/ma990299+.

Lasa-Saracibar, B., Estella-Hermoso de Mendoza, A., Guada, M., Dios-Vieitez, C. and Blanco-Prieto, M. J. (2012) ‘Lipid nanoparticles for cancer therapy: state of the art and future prospects.’, *Expert opinion on drug delivery*, 9(10), pp. 1245–61. doi: 10.1517/17425247.2012.717928.

Laskowitz, D. T., Thekdi, A. D., Thekdi, S. D., Han, S. K. D., Myers, J. K., Pizzo, S. V. and Bennett, E. R. (2001) ‘Downregulation of microglial activation by apolipoprotein E and apoE-mimetic peptides’, *Experimental Neurology*, 167(1), pp. 74–85. doi: 10.1006/exnr.2001.7541.

Leaver, H. A., Bell, H. S., Rizzo, M. T., Ironside, J. W., Gregor, A., Wharton, S. B. and Whittle, I. R. (2002a) ‘Antitumour and pro-apoptotic actions of highly unsaturated fatty acids in glioma', *Prostaglandins Leukotrienes and Essential Fatty Acids*, 66(1), pp. 19–29. doi: 10.1054/plef.2001.0336.

Leaver, H. A., Wharton, S. B., Bell, H. S., Leaver-Yap, I. M. M. and Whittle, I. R. (2002b) 'Highly unsaturated fatty acid induced tumour regression in glioma pharmacodynamics and bioavailability of gamma linolenic acid in an implantation glioma model: Effects on tumour biomass, apoptosis and neuronal tissue histology', *Prostaglandins Leukotrienes and Essential Fatty Acids*, 67(5), pp. 283–292. doi: 10.1054/plef.2002.0431.

Li, X., Wang, D., Zhang, J. and Pan, W. (2009) 'Preparation and pharmacokinetics of docetaxel based on nanostructured lipid carriers.', *The Journal of pharmacy and pharmacology*, 61(11), pp. 1485–1492. doi: 10.1211/jpp/61.11.0007.

Liang, Y., Diehn, M., Watson, N., Bollen, A. W., Aldape, K. D., Nicholas, M. K., Lamborn, K. R., Berger, M. S., Botstein, D., Brown, P. O. and Israel, M. A. (2005) 'Gene expression profiling reveals molecularly and clinically distinct subtypes of glioblastoma multiforme', *Proceedings of the National Academy of Sciences*, 102(16), pp. 5814–5819. doi: 10.1073/pnas.0402870102.

Lin, T., Zhao, P., Jiang, Y., Tang, Y., Jin, H., Pan, Z., He, H., Yang, V. C. and Huang, Y. (2016) 'Blood-Brain-Barrier-Penetrating Albumin Nanoparticles for Biomimetic Drug Delivery via Albumin-Binding Protein Pathways for Antiglioma Therapy', *ACS Nano*, 10(11), pp. 9999–10012. doi: 10.1021/acsnano.6b04268.

Liu, W. C., Wang, X., Zhang, X., Chen, X. and Jin, X. (2017) 'Melatonin supplementation, a strategy to prevent neurological diseases through maintaining integrity of blood brain barrier in old people', *Frontiers in Aging Neuroscience*, 9(MAY), pp. 1–6. doi: 10.3389/fnagi.2017.00165.

Lo, S. S., Huang, D., Tu, C. H., Hou, C. H. and Chen, C. C. (2009) 'Raman scattering and band-gap variations of Al-doped ZnO nanoparticles synthesized by a chemical colloid process', *Journal of Physics D: Applied Physics*, 42(9). doi: 10.1088/0022-3727/42/9/095420.

Lo, Y. L. (2003) 'Relationships between the hydrophilic-lipophilic balance values of pharmaceutical excipients and their multidrug resistance modulating effect in Caco-2 cells and rat intestines', *Journal of Controlled Release*, 90(1), pp. 37–48. doi: 10.1016/S0168-3659(03)00163-9.

Löscher, W. and Potschka, H. (2005) 'Role of drug efflux transporters in the brain for drug disposition and treatment of brain diseases', *Progress in Neurobiology*, 76(1), pp. 22–76. doi: 10.1016/j.pneurobio.2005.04.006.

Louis, D. N., Ohgaki, H., Wiestler, O. D., Cavenee, W. K., Burger, P. C., Jouvet, A., Scheithauer, B. W. and Kleihues, P. (2007) 'The 2007 WHO classification of tumours of the central nervous system', *Acta Neuropathologica*, pp. 97–109. doi: 10.1007/s00401-007-0243-4.

Louis, D. N., Perry, A., Reifenberger, G., von Deimling, A., Figarella-Branger, D., Cavenee, W. K., Ohgaki, H., Wiestler, O. D., Kleihues, P. and Ellison, D. W. (2016) 'The 2016 World Health Organization Classification of Tumors of the Central Nervous System: a summary', *Acta Neuropathologica*. Springer Berlin Heidelberg, 131(6), pp. 803–820. doi: 10.1007/s00401-016-1545-1.

Louis, K. S. and Siegel, A. C. (2011) 'Cell viability analysis using trypan blue: manual and automated methods.', *Methods in molecular biology (Clifton, N.J.)*, 740, pp. 7–12. doi: 10.1007/978-1-61779-108-6_2.

Lozano, M. V., Esteban, H., Brea, J., Loza, M. I., Torres, D. and Alonso, M. J. (2013) 'Intracellular delivery of docetaxel using freeze-dried polysaccharide nanocapsules', *Journal of Microencapsulation*, 30(2), pp. 181–188. doi: 10.3109/02652048.2012.714411.

Lundquist, S., Renftel, M., Brillault, J., Fenart, L., Cecchelli, R. and Dehouck, M.-P. (2002) 'Prediction of drug transport through the blood-brain barrier in vivo: a comparison between two in vitro cell models.', *Pharmaceutical research*, 19(7), pp. 976–981. doi: 10.1023/A:1016462205267.

Maher, E. A., Furnari, F. B., Bachoo, R. M., Rowitch, D. H., Louis, D. N., Cavenee, W. K. and DePinho, R. A. (2001) 'Malignant glioma: Genetics and biology of a grave matter', *Genes and Development*, 15(11), pp. 1311–1333. doi: 10.1101/gad.891601.

Manjunath, K. and Venkateswarlu, V. (2006) 'Pharmacokinetics, tissue distribution and bioavailability of nitrendipine solid lipid nanoparticles after intravenous and intraduodenal administration', *Journal of Drug Targeting*, 14(9), pp. 632–645. doi: 10.1080/10611860600888850.

Martin-Banderas, L., Holgado, M. a, Venero, J. L., Alvarez-Fuentes, J. and Fernández-Arévalo, M. (2011) 'Nanostructures for drug delivery to the brain.', *Current medicinal chemistry*, 18(34), pp. 5303–21. doi: 10.2174/092986711798184262.

Martins, S., Costa-Lima, S., Carneiro, T., Cordeiro-Da-Silva, A., Souto, E. B. and Ferreira, D. C. (2012) 'Solid lipid nanoparticles as intracellular drug transporters: An investigation of the uptake mechanism and pathway', *International Journal of Pharmaceutics*, 430(1–2), pp. 216–227. doi: 10.1016/j.ijpharm.2012.03.032.

Masserini, M. (2013) 'Nanoparticles for Brain Drug Delivery', *ISRN Biochemistry*, 2013, pp. 1–18. doi: 10.1155/2013/238428.Masserini, M. (2013) 'Nanoparticles for Brain Drug Delivery', *ISRN Biochemistry*, 2013, pp. 1–18. doi: 10.1155/2013/238428.

Mather, J. P. and Roberts, P. E. (1998) *Introduction to cell and tissue culture: theory and technique*, *Cell*. Available at: http://books.google.de/books?id=Cla-N2x4cRQC.Matsumura, Y. and Maeda, H. (1986) 'A new concept for macromolecular therapeutics in cancer chemotherapy: Mechanism of tumoritropic accumulation of proteins and the antitumor agent smancs', *Cancer Research*, 46(12 I), pp. 6387–6392. doi: 10.1021/bc100070g.

Medley, C. D., Bamrungsap, S., Tan, W. and Smith, J. E. (2012) 'Aptamer-Conjugated Nanoparticles for Cancer Cell Detection', *Anal Chem*, 83(3), pp. 727–734. doi: 10.1021/ac102263v.Aptamer-Conjugated.

Mehnert, W. and Mäder, K. (2001) 'Solid lipid nanoparticles: production, characterization and applications.', *Advanced drug delivery reviews*, 47(2–3), pp. 165–96. doi: 10.1016/S0169-409X(01)00105-3.

Mehta, G., Hsiao, A. Y., Ingram, M., Luker, G. D. and Takayama, S. (2012) 'Opportunities and challenges for use of tumor spheroids as models to test drug delivery and efficacy', *Journal of Controlled Release*. Elsevier B.V., 164(2), pp. 192–204. doi: 10.1016/j.jconrel.2012.04.045.

Mehta, S., Huillard, E., Kesari, S., Maire, C. L., Golebiowski, D., Harrington, E. P., Alberta, J. A., Kane, M. F., Theisen, M., Ligon, K. L., Rowitch, D. H. and Stiles, C. D. (2011) 'The Central Nervous System-Restricted Transcription Factor Olig2 Opposes p53 Responses to Genotoxic Damage in Neural Progenitors and Malignant Glioma', *Cancer Cell*, 19(3), pp. 359–371. doi: 10.1016/j.ccr.2011.01.035.

Meilakhs, A. P. and Koniakhin, S. V. (2017) 'New explanation of Raman peak redshift in nanoparticles', *Superlattices and Microstructures*. Elsevier Ltd, 110, pp. 319–323. doi: 10.1016/j.spmi.2017.08.010.

Melzig, S., Niedbalka, D., Schilde, C. and Kwade, A. (2018) 'Spray drying of amorphous ibuprofen nanoparticles for the production of granules with enhanced drug release', *Colloids and Surfaces A: Physicochemical and Engineering Aspects*. Elsevier, 536(June 2017), pp. 133–141. doi: 10.1016/j.colsurfa.2017.07.028.

Mendoza, A. E. De, Préat, V., Mollinedo, F. and Blanco-prieto, M. J. (2011) 'In vitro and in vivo ef fi cacy of edelfosine-loaded lipid nanoparticles against glioma', *Journal of Controlled Release*, 156(3), pp. 421–426. doi: 10.1016/j.jconrel.2011.07.030.

Menendez, J. A., del Mar Barbacid, M., Montero, S., Sevilla, E., Escrich, E., Solanas, M., Cortes-Funes, H. and Colomer, R. (2001) 'Effects of gamma-linolenic acid and oleic acid on paclitaxel cytotoxicity in human breast cancer cells', *European Journal of Cancer*, 37(3), pp. 402–413. doi: S0959804900004081 [pii].

Miao, Z., Dong, Y., Fang, W., Shang, D., Liu, D., Zhang, K., Li, B. and Chen, Y. H. (2014) 'VEGF increases paracellular permeability in brain endothelial cells via upregulation of EphA2', *Anatomical Record*, 297(5), pp. 964–972. doi: 10.1002/ar.22878.

Miller, D. S. (2010) 'Regulation of P-glycoprotein and other ABC drug transporters at the blood-brain barrier', *Trends in Pharmacological Sciences*. Elsevier Ltd, 31(6), pp. 246–254. doi: 10.1016/j.tips.2010.03.003.

Minniti, G., Clarke, E., Lanzetta, G., Osti, M. F., Trasimeni, G., Bozzao, A., Romano, A. and Enrici, R. M. (2011) 'Stereotactic radiosurgery for brain metastases: analysis of outcome and risk of brain radionecrosis.', *Radiation oncology (London, England)*, 6(1), p. 48. doi: 10.1186/1748-717X-6-48.

Mita, R., Coles, J. E., Glubrecht, D. D., Sung, R., Sun, X. and Godbout, R. (2007) 'B-FABP-Expressing Radial Glial Cells: The Malignant Glioma Cell of Origin?123', *Neoplasia (New York, N.Y.)*, 9(9), pp. 734–744. doi: 10.1593/neo.07439.

Modarres, H. P., Janmaleki, M., Novin, M., Saliba, J., El-Hajj, F., RezayatiCharan, M., Seyfoori, A., Sadabadi, H., Vandal, M., Nguyen, M. D., Hasan, A. and Sanati-Nezhad, A. (2018) 'In vitro models and systems for evaluating the dynamics of drug delivery to the healthy and diseased brain', *Journal of Controlled Release*. Elsevier, 273(November 2017), pp. 108–130. doi: 10.1016/j.jconrel.2018.01.024.

Modrejewski, J., Walter, J.-G., Kretschmer, I., Kemal, E., Green, M., Belhadj, H., Blume, C. and Scheper, T. (2016) 'Aptamer-modified polymer nanoparticles for targeted drug delivery', *BioNanoMaterials*, 17(1–2), pp. 43–51. doi: 10.1515/bnm-2015-0027.

Moghimi, S. M. and Szebeni, J. (2003) 'Stealth liposomes and long circulating nanoparticles: Critical issues in pharmacokinetics, opsonization and protein-binding properties', *Progress in Lipid Research*, pp. 463–478. doi: 10.1016/S0163-7827(03)00033-X.

Montet, X., Funovics, M., Montet-Abou, K., Weissleder, R. and Josephson, L. (2006) 'Multivalent effects of RGD peptides obtained by nanoparticle display', *Journal of Medicinal Chemistry*, 49(20), pp. 6087–6093. doi: 10.1021/jm060515m.

Moos, T., Nielsen, T. R., Skjørringe, T. and Morgan, E. H. (2007) 'Iron trafficking inside the brain', *Journal of Neurochemistry*, pp. 1730–1740. doi: 10.1111/j.1471-4159.2007.04976.x.

Moradi-Afrapoli, F., Oufir, M., Walter, F. R., Deli, M. A., Smiesko, M., Zabela, V., Butterweck, V. and Hamburger, M. (2016) 'Validation of UHPLC-MS/MS methods for the determination of kaempferol and its metabolite 4-hydroxyphenyl acetic acid, and application to in vitro blood-brain barrier and intestinal drug permeability studies', *Journal of Pharmaceutical and Biomedical Analysis*. Elsevier B.V., 128, pp. 264–274. doi: 10.1016/j.jpba.2016.05.039.

Mukherjee, B., Santra, K., Pattnaik, G. and Ghosh, S. (2008) 'Preparation, characterization and in-vitro evaluation of sustained release protein-loaded nanoparticles based on biodegradable polymers', *International Journal of Nanomedicine*, 3(4), pp. 487–496. doi: 10.2147/IJN.S3938.

Müller, R. (2000) 'Solid lipid nanoparticles (SLN) for controlled drug delivery: a review of the state of the art', *European Journal of Pharmaceutics and Biopharmaceutics*, 50(1), pp. 161–177. doi: 10.1016/S0939-6411(00)00087-4.

Müller, R. H., Radtke, M. and Wissing, S. A. (2002a) 'Solid lipid nanoparticles (SLN) and nanostructured lipid carriers (NLC) in cosmetic and dermatological preparations', in *Advanced Drug Delivery Reviews*. doi: 10.1016/S0169-409X(02)00118-7.

Müller, R. H., Radtke, M. and Wissing, S. A. (2002b) 'Nanostructured lipid matrices for improved microencapsulation of drugs', *International Journal of Pharmaceutics*, 242(1–2), pp. 121–128. doi: 10.1016/S0378-5173(02)00180-1.

Müller, R. H., Staufenbiel, S. and Keck, C. (2014) ‘Lipid Nanoparticles (SLN , NLC) for innovative consumer care & household products’, *Household and Personal Care Today*, 9(2), pp. 18–25.

Muro, S., Koval, M. and Muzykantov, V. (2004) ‘Endothelial endocytic pathways: gates for vascular drug delivery.’, *Current vascular pharmacology*, 2(3), pp. 281–299. doi: 10.2174/1570161043385736.

Mushtaq, A., Mukhtar, H. Bin and Shariff, A. M. (2014) ‘FTIR study of enhanced polymeric blend membrane with amines’, *Research Journal of Applied Sciences, Engineering and Technology*, 7(9), pp. 1811–1820. doi: 10.19026/rjaset.7.466.

Musumeci, T., Ventura, C. A., Giannone, I., Ruozi, B., Montenegro, L., Pignatello, R. and Puglisi, G. (2006) ‘PLA/PLGA nanoparticles for sustained release of docetaxel’, *International Journal of Pharmaceutics*, 325(1–2), pp. 172–179. doi: 10.1016/j.ijpharm.2006.06.023.

Muthu, M. S., Kulkarni, S. A., Xiong, J. and Feng, S. S. (2011) ‘Vitamin e TPGS coated liposomes enhanced cellular uptake and cytotoxicity of docetaxel in brain cancer cells’, *International Journal of Pharmaceutics*, 421(2), pp. 332–340. doi: 10.1016/j.ijpharm.2011.09.045.

Naguib, Y. W., Rodriguez, B. L., Li, X., Hursting, S. D., Williams, R. O. and Cui, Z. (2014) ‘Solid lipid nanoparticle formulations of docetaxel prepared with high melting point triglycerides: In vitro and in vivo evaluation’, *Molecular Pharmaceutics*, 11(4), pp. 1239–1249. doi: 10.1021/mp4006968.

Nakagawa, S., Deli, M. A. M. A., Nakao, S., Honda, M., Hayashi, K., Nakaoke, R., Kataoka, Y. and Niwa, M. (2007) ‘Pericytes from brain microvessels strengthen the barrier integrity in primary cultures of rat brain endothelial cells’, *Cellular and Molecular Neurobiology*, 27(6), pp. 687–694. doi: 10.1007/s10571-007-9195-4.

Nakagawa, S., Deli, M. A., Kawaguchi, H., Shimizudani, T., Shimono, T., Kittel, Á., Tanaka, K. and Niwa, M. (2009) ‘A new blood-brain barrier model using primary rat brain endothelial cells, pericytes and astrocytes’, *Neurochemistry International*, 54(3–4), pp. 253–263. doi: 10.1016/j.neuint.2008.12.002.

National Institute for Health and Clinical Excellence (2006) *Improving Outcomes for People with Brain and Other CNS Tumours*. NICE. Available at: https://www.nice.org.uk/guidance/csg10/resources/improving-outcomes-for-people-with-brain-and-other-central-nervous-system-tumours-update-27841361437.

NICE, (2016) https://www.nice.org.uk/guidance/ta121/evidence/review-decision-march-2016-2366765533.

Nielsen, P. A., Andersson, O., Hansen, S. H., Simonsen, K. B. and Andersson, G. (2011) ‘Models for predicting blood-brain barrier permeation’, *Drug Discovery Today*, pp. 472–475. doi: 10.1016/j.drudis.2011.04.004.

Nimjee, S. M., Rusconi, C. P. and Sullenger, B. A. (2005) ‘Aptamers: An Emerging Class of Therapeutics’, *Annual Review of Medicine*, 56(1), pp. 555–583. doi: 10.1146/annurev.med.56.062904.144915.

Oh, N. and Park, J. H. (2014) ‘Endocytosis and exocytosis of nanoparticles in mammalian cells’, *International Journal of Nanomedicine*, pp. 51–63. doi: 10.2147/IJN.S26592.

Ohgaki, H. and Kleihues, P. (2013) ‘The definition of primary and secondary glioblastoma’, *Clinical Cancer Research*, pp. 764–772. doi: 10.1158/1078-0432.CCR-12-3002.

Ohgaki, H., Burger, P. and Kleihues, P. (2014) ‘Definition of Primary and Secondary Glioblastoma--Response’, *Clinical Cancer Research*, 20(7), pp. 2013–2013. doi: 10.1158/1078-0432.CCR-14-0238.

Ohtsuki, S. and Terasaki, T. (2007) ‘Contribution of carrier-mediated transport systems to the blood-brain barrier as a supporting and protecting interface for the brain; importance for CNS drug discovery and development’, *Pharmaceutical Research*, pp. 1745–1758. doi: 10.1007/s11095-007-9374-5.

Olbrich, C., Kayser, O. and Müller, R. H. (2002a) ‘Enzymatic degradation of Dynasan 114 SLN - Effect of surfactants and particle size’, *Journal of Nanoparticle Research*, 4(1–2), pp. 121–129. doi: 10.1023/A:1020159331420.

Olbrich, C., Kayser, O. and Müller, R. H. (2002b) ‘Lipase degradation of Dynasan 114 and 116 solid lipid nanoparticles (SLN) - Effect of surfactants, storage time and crystallinity’, *International Journal of Pharmaceutics*, 237(1–2), pp. 119–128. doi: 10.1016/S0378-5173(02)00035-2.

Olbrich, C., Schöler, N., Tabatt, K., Kayser, O. and Müller, R. H. (2004) ‘Cytotoxicity studies of Dynasan 114 solid lipid nanoparticles (SLN) on RAW 264.7 macrophages-impact of phagocytosis on viability and cytokine production’, *Journal of Pharmacy and Pharmacology*, 56(7), pp. 883–891. doi: 10.1211/0022357023754.

On, N. H., Mitchell, R., Savant, S. D., Bachmeier, C. J., Hatch, G. M. and Miller, D. W. (2013) ‘Examination of blood-brain barrier (BBB) integrity in a mouse brain tumor model’, *Journal of Neuro-Oncology*, 111(2), pp. 133–143. doi: 10.1007/s11060-012-1006-1.

Osswald, M., Jung, E., Sahm, F., Solecki, G., Venkataramani, V., Blaes, J., Weil, S., Horstmann, H., Wiestler, B., Syed, M., Huang, L., Ratliff, M., Karimian Jazi, K., Kurz, F. T., Schmenger, T., Lemke, D., Gömmel, M., Pauli, M., Liao, Y., Häring, P., Pusch, S., Herl, V., Steinhäuser, C., Krunic, D., Jarahian, M., Miletic, H., Berghoff, A. S., Griesbeck, O., Kalamakis, G., Garaschuk, O., Preusser, M., Weiss, S., Liu, H., Heiland, S., Platten, M., Huber, P. E., Kuner, T., Von Deimling, A., Wick, W. and Winkler, F. (2015) ‘Brain tumour cells interconnect to a functional and resistant network’, *Nature*, 528(7580), pp. 93–98. doi: 10.1038/nature16071.

Ostrom, Q. T., Gittleman, H., Fulop, J., Liu, M., Blanda, R., Kromer, C., Wolinsky, Y., Kruchko, C. and Barnholtz-Sloan, J. S. (2015) ‘CBTRUS Statistical Report: Primary Brain and Central Nervous System Tumors Diagnosed in the United States in 2008-2012’, *Neuro-oncology*, 17, p. iv1-iv62. doi: 10.1093/neuonc/nov189.

Pardeike, J., Hommoss, A. and Müller, R. H. (2009) ‘Lipid nanoparticles (SLN, NLC) in cosmetic and pharmaceutical dermal products’, *International Journal of Pharmaceutics*, pp. 170–184. doi: 10.1016/j.ijpharm.2008.10.003.

Pardridge, W. M. (2002) ‘Why is the global CNS pharmaceutical market so under-penetrated?’, *Drug Discovery Today*, pp. 5–7. doi: 10.1016/S1359-6446(01)02082-7.

Pardridge, W. M. (2003) ‘BLOOD-BRAIN BARRIER DRUG TARGETING: THE FUTURE OF BRAIN DRUG DEVELOPMENT’, *Molecular Interventions*, 3(2), pp. 90–105. doi: 10.1124/mi.3.2.90.

Pardridge, W. M. (2005) ‘The blood-brain barrier: Bottleneck in brain drug development’, *NeuroRx*, pp. 3–14. doi: 10.1602/neurorx.2.1.3.

Pardridge, W. M. (2012) ‘Drug transport across the blood-brain barrier.’, *Journal of cerebral blood flow and metabolism : official journal of the International Society of Cerebral Blood Flow and Metabolism*, 32(11), pp. 1959–72. doi: 10.1038/jcbfm.2012.126.

Park, K. (2008) ‘Trojan monocytes for improved drug delivery to the brain’, *Journal of Controlled Release*, p. 75. doi: 10.1016/j.jconrel.2008.10.009.

Parodi, A., Quattrocchi, N., Van De Ven, A. L., Chiappini, C., Evangelopoulos, M., Martinez, J. O., Brown, B. S., Khaled, S. Z., Yazdi, I. K., Enzo, M. V., Isenhart, L., Ferrari, M. and Tasciotti, E. (2013) ‘Synthetic nanoparticles functionalized with biomimetic leukocyte membranes possess cell-like functions’, *Nature Nanotechnology*, 8(1), pp. 61–68. doi: 10.1038/nnano.2012.212.

Patel, D. S., Sharma, N., Patel, M. C., Patel, B. N., Shrivastav, P. S. and Sanyal, M. (2011) ‘Development and validation of a selective and sensitive LC-MS/MS method for determination of cycloserine in human plasma: Application to bioequivalence study’, *Journal of Chromatography B: Analytical Technologies in the Biomedical and Life Sciences*. Elsevier B.V., 879(23), pp. 2265–2273. doi: 10.1016/j.jchromb.2011.06.011.

Patel, Medha, Souto, Eliana and Singh, Kamalinder (2013) Advances in brain drug targeting and delivery: limitations and challenges of solid lipid nanoparticles. *Expert Opinion on Drug Delivery,* 10 (7). pp. 889-905.

Peer, D., Karp, J. M., Hong, S., Farokhzad, O. C., Margalit, R. and Langer, R. (2007) 'Nanocarriers as an emerging platform for cancer therapy.', *Nature nanotechnology*, 2(12), pp. 751–760. doi: 10.1038/nnano.2007.387.

Persohn, E., Canta, A., Schoepfer, S., Traebert, M., Mueller, L., Gilardini, A., Galbiati, S., Nicolini, G., Scuteri, A., Lanzani, F., Giussani, G. and Cavaletti, G. (2005) 'Morphological and morphometric analysis of paclitaxel and docetaxel-induced peripheral neuropathy in rats', *European Journal of Cancer*, 41(10), pp. 1460–1466. doi: 10.1016/j.ejca.2005.04.006.

Petkar, K. C., Chavhan, S. S., Agatonovik-Kustrin, S. and Sawant, K. K. (2011) 'Nanostructured Materials in Drug and Gene Delivery: A Review of the State of the Art', *Critical Reviews™ in Therapeutic Drug Carrier Systems*, 28(2), pp. 101–164. doi: 10.1615/CritRevTherDrugCarrierSyst.v28.i2.10.

Pharmaceutical press, (2012), Handbook of Pharmaceutical Excipients, NEW 7th edition. *Pharmaceutical Technology Editors.* Avilable at: http://www.pharmtech.com/handbook-pharmaceutical-excipients-new-7th-edition.

Pillai, G. (2014) 'Nanomedicines for Cancer Therapy : An Update of FDA Approved and Those under Various Stages of Development', *SOJ Pharm Pharm Sci*, 1(2), pp. 1–13. doi: 10.15226/2374-6866/1/2/00109.

Polagani, S. R., Pilli, N. R., Maddela, R., Gajula, R. and Gandu, V. (2013) 'A rapid and sensitive liquid chromatography-tandem mass spectrometric assay for cycloserine in 50µL of human plasma: Its pharmacokinetic application', *Journal of Pharmaceutical and Biomedical Analysis*. Elsevier B.V., 76, pp. 21–27. doi: 10.1016/j.jpba.2012.11.036.

Ponka, P. and Lok, C. N. (1999) 'The transferrin receptor: role in health and disease.', *The international journal of biochemistry & cell biology*, 31(10), pp. 1111–1137. doi: 10.1016/S1357-2725(99)00070-9.

Pooja, D., Kulhari, H., Singh, M. K., Mukherjee, S., Rachamalla, S. S. and Sistla, R. (2014) 'Dendrimer-TPGS mixed micelles for enhanced solubility and cellular toxicity of taxanes', *Colloids and Surfaces B: Biointerfaces*. Elsevier B.V., 121, pp. 461–468. doi: 10.1016/j.colsurfb.2014.06.059.

Price, S. J., Whittle, I. R., Ashkan, K., Grundy, P., Cruickshank, G. and Grp, U.-H. S. (2012) 'NICE guidance on the use of carmustine wafers in high grade gliomas: a national study on variation in practice', *British Journal of Neurosurgery*, 26(3), pp. 331–335. doi: Doi 10.3109/02688697.2012.673651.

Qosa, H., Miller, D. S., Pasinelli, P. and Trotti, D. (2015) 'Regulation of ABC efflux transporters at blood-brain barrier in health and neurological disorders', *Brain Research*. Elsevier, 1628, pp. 298–316. doi: 10.1016/j.brainres.2015.07.005.

Quan, Q., Kim, D.-W., Marasini, N., Kim, D. H., Kim, J. K., Kim, J. O., Yong, C. S. and Choi, H.-G. (2013) 'Physicochemical characterization and in vivo evaluation of solid self-nanoemulsifying drug delivery system for oral administration of docetaxel.', *Journal of microencapsulation*, 30(4), pp. 307–14. doi: 10.3109/02652048.2012.726280.

Radomska-Soukharev, A. (2007) 'Stability of lipid excipients in solid lipid nanoparticles', *Advanced Drug Delivery Reviews*, pp. 411–418. doi: 10.1016/j.addr.2007.04.004.

Radomska-Soukharev, A. and Müller, R. H. (2006) 'Chemical stability of lipid excipients in SLN-production of test formulations, characterisation and short-term stability', *Pharmazie*, 61(5), pp. 425–430.

Radtke, M. and Müller, R. (2001) 'Nanostructured lipid drug carriers', *New Drugs*, pp. 1–4. Available at: http://www.pharmasol-berlin.de/files/nlc.pdf.

Raghava, K. M. and Lakshmi, P. K. (2012) 'Overview of P-glycoprotein inhibitors: A rational outlook', *Brazilian Journal of Pharmaceutical Sciences*, 48(3), pp. 353–367. doi: 10.1590/S1984-82502012000300002.

Rao, B. M., Chakraborty, A., Srinivasu, M. K., Devi, M. L., Kumar, P. R., Chandrasekhar, K. B., Srinivasan, A. K., Prasad, A. S. and Ramanatham, J. (2006) 'A stability-indicating HPLC assay method for docetaxel', *Journal of Pharmaceutical and Biomedical Analysis*, 41(2), pp. 676–681. doi: 10.1016/j.jpba.2006.01.011.

Ree, A. H., Stokke, T., Bratland, Å., Patzke, S., Nome, R. V., Folkvord, S., Meza-Zepeda, L. A., Flatmark, K., Fodstad, Ø. and Andersson, Y. (2006) 'DNA damage responses in cell cycle G2 phase and mitosis - Tracking and targeting', *Anticancer Research*, 26(3 A), pp. 1909–1916.

Renehan, A. G., Booth, C. and Potten, C. S. (2001) 'What is apoptosis, and why is it important?', *BMJ (Clinical research ed.)*, 322(7301), pp. 1536–8. doi: 10.1136/bmj.322.7301.1536.

Rigo-Bonnin, R., Cobo-Sacristán, S., Gonzalo-Diego, N., Colom, H., Muñoz-Sánchez, C., Urruticoechea, A., Falo, C. and Alía, P. (2016) 'Measurement of total and free docetaxel concentration in human plasma by ultra-performance liquid chromatography-tandem mass spectrometry', *Journal of Pharmaceutical and Biomedical Analysis*, 117, pp. 140–149. doi: 10.1016/j.jpba.2015.08.025.

Ringel, I. and Horwitz, S. B. (1991) 'Studies With RP 56976 (Taxotere): A Semisynthetic Analogue of Taxol', *Journal of the National Cancer Institute*, 83(4), pp. 288–291. doi: 10.1093/jnci/83.4.288.

Rivolta, I., Panariti, A., Lettiero, B., Sesana, S., Gasco, P., Gasco, M. R., Masserini, M. and Miserocchi, G. (2011) 'Cellular uptake of coumarin-6 as a model drug loaded in solid lipid nanoparticles', *Journal of Physiology and Pharmacology*, 62(1), pp. 45–53.

Rohiwal, S. S., Tiwari, A. P., Verma, G. and Pawar, S. H. (2015) 'Preparation and evaluation of bovine serum albumin nanoparticles for ex vivo colloidal stability in biological media', *Colloids and Surfaces A: Physicochemical and Engineering Aspects*, 480, pp. 28–37. doi: 10.1016/j.colsurfa.2015.04.017.

Rusu, G. and Rusu, E. (2010) 'Evaluation of thermal and dielectric behaviour of some anionic nylon 612 copolymers', *Materials and Design*, 31(10), pp. 4601–4610. doi: 10.1016/j.matdes.2010.05.042.

Sadekar, S. and Ghandehari, H. (2012) 'Transepithelial transport and toxicity of PAMAM dendrimers: Implications for oral drug delivery', *Advanced Drug Delivery Reviews*, pp. 571–588. doi: 10.1016/j.addr.2011.09.010.

Sahay, G., Alakhova, D. Y. and Kabanov, A. V. (2010) 'Endocytosis of nanomedicines', *Journal of Controlled Release*, pp. 182–195. doi: 10.1016/j.jconrel.2010.01.036.Saltzman, W. M. (2012) 'Novel Delivery Strategies for Glioblastoma', *Cancer J.*, 18(1), pp. 1–22. doi: 10.1097/PPO.0b013e318244d8ae.

Sampath, P., Rhines, L. D., DiMeco, F., Tyler, B. M., Park, M. C. and Brem, H. (2006) 'Interstitial docetaxel (taxotere), carmustine and combined interstitial therapy: a novel treatment for experimental malignant glioma.', *Journal of neuro-oncology*, 80(1), pp. 9–17. doi: 10.1007/s11060-006-9159-4.

Sathyamoorthy, N., Rajendran, V., Naveena, V. S. H. and Dhanaraju, M. D. (2014) 'An approach for validated RP-HPLC method for the analysis of paclitaxel in rat plasma', *Journal of Applied Pharmaceutical Science*, 4(9), pp. 73–76. doi: 10.7324/JAPS.2014.40913.

Sauer, L. a, Blask, D. E. and Dauchy, R. T. (2007) 'Dietary factors and growth and metabolism in experimental tumors.', *The Journal of nutritional biochemistry*, 18, pp. 637–649. doi: 10.1016/j.jnutbio.2006.12.009.

Schaffer, H. E., Chance, R. R., Silbey, R. J., Knoll, K. and Schrock, R. R. (1991) 'Conjugation length dependence of Raman scattering in a series of linear polyenes: Implications for polyacetylene', *The Journal of Chemical Physics*, 94(6), pp. 4161–4170. doi: 10.1063/1.460649.

Schimming, R., Mason, K. a, Hunter, N., Weil, M., Kishi, K. and Milas, L. (1999) 'Lack of correlation between mitotic arrest or apoptosis and antitumor effect of docetaxel.', *Cancer chemotherapy and pharmacology*, 43(2), pp. 165–72. doi: 10.1007/s002800050879.

Schmidt, C. M., Zürn, T., Thienel, K. J. F. and Hinrichs, J. (2017) 'Development, optimization and validation of an HPLC-ELSD method for the analysis of enzymatically generated lactulose and saccharide by-products', *Food Chemistry*. Elsevier Ltd, 215, pp. 347–353. doi: 10.1016/j.foodchem.2016.07.184.Scientific, C.

Seçilmi, H. and Bardakç, B. (2011) 'Determination of Fatty Acid, C, H, N and Trace Element Composition in Grape Seed by GC/MS, FTIR, Elemental Analyzer and ICP/OES', *SDU Journal of Science*, 6(2), pp. 140–148.

Selvamuthukumar, S. and Velmurugan, R. (2012) 'Nanostructured lipid carriers: a potential drug carrier for cancer chemotherapy', *Lipids in Health and Disease*. Lipids in Health and Disease, 11(1), p. 159. doi: 10.1186/1476-511X-11-159.

Severino, P., Pinho, S. C., Souto, E. B. and Santana, M. H. A. (2012) 'Crystallinity of Dynasan®114 and Dynasan®118 matrices for the production of stable Miglyol®-loaded nanoparticles', *Journal of Thermal Analysis and Calorimetry*, 108(1), pp. 101–108. doi: 10.1007/s10973-011-1613-7.

Sha, H., Zou, Z., Xin, K., Bian, X., Cai, X., Lu, W., Chen, J., Chen, G., Huang, L., Blair, A. M., Cao, P. and Liu, B. (2015) 'Tumor-penetrating peptide fused EGFR single-domain antibody enhances cancer drug penetration into 3D multicellular spheroids and facilitates effective gastric cancer therapy', *Journal of Controlled Release*. Elsevier B.V., 200, pp. 188–200. doi: 10.1016/j.jconrel.2014.12.039.

Shabani Ravari, N., Goodarzi, N., Alvandifar, F., Amini, M., Souri, E., Khoshayand, M. R., Hadavand Mirzaie, Z., Atyabi, F. and Dinarvand, R. (2016) 'Fabrication and biological evaluation of chitosan coated hyaluronic acid-docetaxel conjugate nanoparticles in CD44+ cancer cells', *DARU, Journal of Pharmaceutical Sciences*. DARU Journal of Pharmaceutical Sciences, 24(1), pp. 1–12. doi: 10.1186/s40199-016-0160-y.

Shabir, G. (2004) 'A practical approach to validation of HPLC methods under current good manufacturing practices', *Journal of Validation Technology*, pp. 29–37.

Shabir, G. A. (2003) 'Validation of high-performance liquid chromatography methods for pharmaceutical analysis - Understanding the differences and similarities between validation requirements of the US Food and Drug Administration, the US Pharmacopeia and the International Con', *Journal of Chromatography A*, 987(1–2), pp. 57–66. doi: Pii S0021-9673(02)01536-4.

Shi, F., Zhao, J.-H., Liu, Y., Wang, Z., Zhang, Y.-T. and Feng, N.-P. (2012) 'Preparation and characterization of solid lipid nanoparticles loaded with frankincense and myrrh oil.', *International journal of nanomedicine*, 7, pp. 2033–43. doi: 10.2147/IJN.S30085.

Shimizu, F., Watanabe, T. B., Shinomiya, H., Nakamura, Y. and Fujiwara, T. (1997) 'Isolation and expression of a cDNA for human brain fatty acid-binding protein (B-FABP)', *Biochimica et Biophysica Acta*, 1354, pp. 24–28.

Singh, B., Beg, S., Lohan, S. and Kapil, R. (2013) 'Crossing Blood-Brain Barriers using Drug Delivery : A Successful Venture using Lipidic Nanostructured', *the Pharma Review*, (june), pp. 41–47.

Singh, I., Swami, R., Jeengar, M. K., Khan, W. and Sistla, R. (2015) 'p-Aminophenyl-α-d-mannopyranoside engineered lipidic nanoparticles for effective delivery of docetaxel to brain', *Chemistry and Physics of Lipids*, 188, pp. 1–9. doi: 10.1016/j.chemphyslip.2015.03.003.

Smith, M. W. and Gumbleton, M. (2006) 'Endocytosis at the blood-brain barrier: From basic understanding to drug delivery strategies', *Journal of Drug Targeting*, 14(4), pp. 191–214. doi: 10.1080/10611860600650086.

Smith, Q. R. (1996) 'Brain perfusion systems for studies of drug uptake and metabolism in the central nervous system.', *Pharmaceutical biotechnology*, 8(2), pp. 285–307. doi: 10.1007/s13398-014-0173-7.2.

Snider, J. W. and Mehta, M. (2016) 'Principles of radiation therapy', in *Handbook of Clinical Neurology*, pp. 131–147. doi: 10.1016/B978-0-12-802997-8.00008-6.

Souto, E. B., Wissing, S. A., Barbosa, C. M. and Müller, R. H. (2004) 'Evaluation of the physical stability of SLN and NLC before and after incorporation into hydrogel formulations', *European Journal of Pharmaceutics and Biopharmaceutics*, 58(1), pp. 83–90. doi: 10.1016/j.ejpb.2004.02.015.

Sparreboom, A., van Tellingen, O., Nooijen, W. J. and Beijnen, J. H. (1998) 'Preclinical pharmacokinetics of paclitaxel and docetaxel.', *Anti-cancer drugs*, 9(1), pp. 1–17. doi: 10.1097/00001813-199801000-00001.

Stoll, G., Jander, S. and Schroeter, M. (1998) 'Inflammation and glial responses in ischemic brain lesions', *Progress in Neurobiology*, pp. 149–171. doi: 10.1016/S0301-0082(98)00034-3.

Stupp, R., Mason, W., van den Bent, M. J., Weller, M., Fisher, B. M., Taphoorn, M. J. B., Belanger, K., Brandes, A. A., Marosi, C., Bogdahn, U., Curschmann, J., Janzer, R. C., Ludwin, S. K., Gorlia, T., Allgeier, A., Lacombe, D., Cairncross, G., Eisenhauer, E. and Mirimanoff, R. O. (2005) 'Radiotherapy plus Concomitant\nand Adjuvant Temozolomide for Glioblastoma', *The New England Journal of Medicine*, pp. 987–96. doi: 10.1056/NEJMoa043330.

Suchorska, B., Hamisch, C., Treuer, H., Mahnkopf, K., Lehrke, R. E., Kocher, M., Ruge, M. I. and Voges, J. (2016) 'Stereotactic brachytherapy using iodine 125 seeds for the treatment of primary and recurrent anaplastic glioma WHO° III', *Journal of Neuro-Oncology*, 130(1), pp. 123–131. doi: 10.1007/s11060-016-2214-x.

Sun, B., Luo, C., Li, L., Wang, M., Du, Y., Di, D., Zhang, D., Ren, G., Pan, X., Fu, Q., Sun, J. and He, Z. (2016) 'Core-matched encapsulation of an oleate prodrug into nanostructured lipid carriers with high drug loading capability to facilitate the oral delivery of docetaxel', *Colloids and Surfaces B: Biointerfaces*. Elsevier B.V., 143, pp. 47–55. doi: 10.1016/j.colsurfb.2016.02.065.

Sun, H., Zhu, X., Lu, P. Y., Rosato, R. R., Tan, W. and Zu, Y. (2014) 'Oligonucleotide aptamers: New tools for targeted cancer therapy', *Molecular Therapy - Nucleic Acids*, 3. doi: 10.1038/mtna.2014.32.

Tamjidi, F., Shahedi, M., Varshosaz, J. and Nasirpour, A. (2013) 'Nanostructured lipid carriers (NLC): A potential delivery system for bioactive food molecules', *Innovative Food Science and Emerging Technologies*, pp. 29–43. doi: 10.1016/j.ifset.2013.03.002.

Tan, L., Peng, J., Zhao, Q., Zhang, L., Tang, X., Chen, L., Lei, M. and Qian, Z. (2017) 'A novel MPEG-PDLLA-PLL copolymer for docetaxel delivery in breast cancer therapy', *Theranostics*, 7(10), pp. 2652–2672. doi: 10.7150/thno.19680.

Tan, Y. and Liu, C.-G. (2009) 'Self-aggregated nanoparticles from linoleic acid modified carboxymethyl chitosan: Synthesis, characterization and application in vitro.', *Colloids and surfaces. B, Biointerfaces*, 69(2), pp. 178–82. doi: 10.1016/j.colsurfb.2008.11.026.

Tao, W., Zeng, X., Liu, T., Wang, Z., Xiong, Q., Ouyang, C., Huang, L. and Mei, L. (2013) 'Docetaxel-loaded nanoparticles based on star-shaped mannitol-core PLGA-TPGS diblock copolymer for breast cancer therapy.', *Acta biomaterialia*, 9(11), pp. 8910–20. doi: 10.1016/j.actbio.2013.06.034.

Ten Tije, A. J., Verweij, J., Loos, W. J. and Sparreboom, A. (2003) 'Pharmacological effects of formulation vehicles: Implications for cancer chemotherapy', *Clinical Pharmacokinetics*, pp. 665–685. doi: 10.2165/00003088-200342070-00005.

Thurn, K. T., Arora, H., Paunesku, T., Wu, A., Brown, E. M. B., Doty, C., Kremer, J. and Woloschak, G. (2011) 'Endocytosis of titanium dioxide nanoparticles in prostate cancer PC-3M cells', *Nanomedicine: Nanotechnology, Biology, and Medicine*, 7(2), pp. 123–130. doi: 10.1016/j.nano.2010.09.004.

Thurn, K. T., Brown, E. M. B., Wu, A., Vogt, S., Lai, B., Maser, J., Paunesku, T. and Woloschak, G. E. (2007) 'Nanoparticles for Applications in Cellular Imaging', *Nanoscale Research Letters*, 2(9), pp. 430–441. doi: 10.1007/s11671-007-9081-5.

Tian, X. H., Lin, X. N., Wei, F., Feng, W., Huang, Z. C., Wang, P., Ren, L. and Diao, Y. (2011) 'Enhanced brain targeting of temozolomide in polysorbate-80 coated polybutylcyanoacrylate nanoparticles.', *International journal of nanomedicine*, 6, pp. 445–452. doi: 10.2147/IJN.S16570.

Torres, M. G., Fernández, N. G., Ortiz, P., Rapado, M., Con, M. and Acetato, P. (2007) 'Ciencias Nucleares RAMAN SPECTROSCOPY OF POLY (3-HYDROXYBUTRYRATE) MODIFIED WITH POLY (VINYL ACETATE) BY RADIATION- INDUCED COPOLYMERIZATION Ciencias Nucleares', *Nucleus*, 42, pp. 41–45.

Tosi, G., Musumeci, T., Ruozi, B., Carbone, C., Belletti, D., Pignatello, R., Vandelli, M. A. and Puglisi, G. (2016) 'The "fate" of polymeric and lipid nanoparticles for brain delivery and targeting: Strategies and mechanism of blood-brain barrier crossing and trafficking into the central nervous system', *Journal of Drug Delivery Science and Technology*. Elsevier Ltd, 32, pp. 66–76. doi: 10.1016/j.jddst.2015.07.007.

Treat, L. H., McDannold, N., Vykhodtseva, N., Zhang, Y., Tam, K. and Hynynen, K. (2007) 'Targeted delivery of doxorubicin to the rat brain at therapeutic levels using MRI-guided focused ultrasound', *International Journal of Cancer*, 121(4), pp. 901–907. doi: 10.1002/ijc.22732.

Tugarova, A. V., Mamchenkova, P. V., Dyatlova, Y. A. and Kamnev, A. A. (2018) 'FTIR and Raman spectroscopic studies of selenium nanoparticles synthesised by the bacterium Azospirillum thiophilum', *Spectrochimica Acta - Part A: Molecular and Biomolecular Spectroscopy*. Elsevier B.V., 192, pp. 458–463. doi: 10.1016/j.saa.2017.11.050.

Tunblad, K. (2004) 'Blood brain barrier transport of drugs across species wih the emphasis on health, disease and modelling'.

U. S. Food and Drug Administration/Center for Biologics Evaluation and Research (1995) 'Guideline for Industry Q2A Text on Validation of Analytical Procedures', *Food and Drug Administration*, (March), pp. 1–9.

Urbanska, K., Sokolowska, J., Szmidt, M. and Sysa, P. (2014) 'Glioblastoma multiforme - An overview', *Wspolczesna Onkologia*, pp. 307–312. doi: 10.5114/wo.2014.40559.

Valencia, P. M., Hanewich-Hollatz, M. H., Gao, W., Karim, F., Langer, R., Karnik, R. and Farokhzad, O. C. (2011) 'Effects of ligands with different water solubilities on self-assembly and properties of targeted nanoparticles', *Biomaterials*, 32(26), pp. 6226–6233. doi: 10.1016/j.biomaterials.2011.04.078.

Van Zyl, A. J. P., De Wet-Roos, D., Sanderson, R. D. and Klumperman, B. (2004) 'The role of surfactant in controlling particle size and stability in the miniemulsion polymerization of polymeric nanocapsules', *European Polymer Journal*, 40(12), pp. 2717–2725. doi: 10.1016/j.eurpolymj.2004.07.021.

Venishetty, V. K., Samala, R., Komuravelli, R., Kuncha, M., Sistla, R. and Diwan, P. V. (2013) 'Beta-Hydroxybutyric acid grafted solid lipid nanoparticles: A novel strategy to improve drug delivery to brain', *Nanomedicine: Nanotechnology, Biology, and Medicine*, 9(3), pp. 388–397. doi: 10.1016/j.nano.2012.08.004.

Venkatesh, H. S., Johung, T. B., Caretti, V., Noll, A., Tang, Y., Nagaraja, S., Gibson, E. M., Mount, C. W., Polepalli, J., Mitra, S. S., Woo, P. J., Malenka, R. C., Vogel, H., Bredel, M., Mallick, P. and Monje, M. (2015) 'Neuronal activity promotes glioma growth through neuroligin-3 secretion', *Cell*, 161(4), pp. 803–816. doi: 10.1016/j.cell.2015.04.012.

Visser, C. C., Stevanović, S., Voorwinden, L. H., Van Bloois, L., Gaillard, P. J., Danhof, M., Crommelin, D. J. A. and De Boer, A. G. (2005) 'Targeting liposomes with protein drugs to the blood-brain barrier in vitro', *European Journal of Pharmaceutical Sciences*, 25(2–3), pp. 299–305. doi: 10.1016/j.ejps.2005.03.008.

Voigt, N., Henrich-Noack, P., Kockentiedt, S., Hintz, W., Tomas, J. J. and Sabel, B. A. (2014) 'Surfactants, not size or zeta-potential influence blood-brain barrier passage of polymeric nanoparticles', *European Journal of Pharmaceutics and Biopharmaceutics*. Elsevier B.V., 87(1), pp. 19–29. doi: 10.1016/j.ejpb.2014.02.013.

Vries, H. E. de, Kuiper, J., Boer, A. G. de, Berkel, T. J. C. Van and Breimer, D. D. (1997) 'The Blood-Brain Barrier in Neuroinflammatory Diseases', *Pharmacol. Rev.*, 49(2), pp. 143–156. Available at: http://pharmrev.aspetjournals.org/content/49/2/143.

Wang, A. Z., Gu, F., Zhang, L., Chan, J. M., Radovic-Moreno, A., Shaikh, M. R. and Farokhzad, O. C. (2008) 'Biofunctionalized targeted nanoparticles for therapeutic applications', *Expert Opinion on Biological Therapy*, 8(8), pp. 1063–1070. doi: 10.1517/14712598.8.8.1063.

Wang, L. G., Liu, X. M., Kreis, W. and Budman, D. R. (1999) 'The effect of antimicrotubule agents on signal transduction pathways of apoptosis: A review', *Cancer Chemotherapy and Pharmacology*, 44(5), pp. 355–361. doi: 10.1007/s002800050989.

Wei, L., Yang, Y., Shi, K., Wu, J., Zhao, W. and Mo, J. (2016) 'Preparation and characterization of loperamide-loaded dynasan 114 solid lipid nanoparticles for increased oral absorption in the treatment of diarrhea', *Frontiers in Pharmacology*, 7(SEP), pp. 1–9. doi: 10.3389/fphar.2016.00332.

Westphal, M., Hilt, D. C., Bortey, E., Delavault, P., Olivares, R., Warnke, P. C., Whittle, I. R., Jääskeläinen, J. and Ram, Z. (2003) 'A phase 3 trial of local chemotherapy with biodegradable carmustine (BCNU) wafers (Gliadel wafers) in patients with primary malignant glioma', *Neuro-Oncology*, 5(2), pp. 79–88. doi: 10.1093/neuonc/5.2.79.

Wilhelm, I., Fazakas, C. and Krizbai, I. A. (2011) 'In vitro models of the blood-brain barrier', *Acta Neurobiol Exp (Wars)*, 71(1), pp. 113–128. doi: 10.1007/978-1-4939-0320-7_34.

Witayaudom, P. and Klinkesorn, U. (2017) 'Effect of surfactant concentration and solidification temperature on the characteristics and stability of nanostructured lipid carrier (NLC) prepared from rambutan (Nephelium lappaceum L.) kernel fat', *Journal of Colloid and Interface Science*. Elsevier Inc., 505, pp. 1082–1092. doi: 10.1016/j.jcis.2017.07.008.

Wohlfart, S., Gelperina, S. and Kreuter, J. (2012) 'Transport of drugs across the blood-brain barrier by nanoparticles', *Journal of Controlled Release*, pp. 264–273. doi: 10.1016/j.jconrel.2011.08.017.

Won, J., Oh, M. H., Oh, J. M., Kang, M. S., Choy, J. H. and Oh, S. (2008) 'Stability analysis of zinc oxide-nanoencapsulated conjugated linoleic acid and gamma-linolenic acid', *J Food Sci*, 73(8), pp. N39-43. doi: 10.1111/j.1750-3841.2008.00924.x.

Wong, N. K. Y., Shenoi, R. A., Abbina, S., Chafeeva, I., Kizhakkedathu, J. N. and Khan, M. K. (2017) 'Nontransformed and Cancer Cells Can Utilize Different Endocytic Pathways to Internalize Dendritic Nanoparticle Variants: Implications on Nanocarrier Design', *Biomacromolecules*, 18(8), pp. 2427–2438. doi: 10.1021/acs.biomac.7b00590.

Wu, J., Wang, C., Sun, J. and Xue, Y. (2011) 'Neurotoxicity of silica nanoparticles: Brain localization and dopaminergic neurons damage pathways', *ACS Nano*, 5(6), pp. 4476–4489. doi: 10.1021/nn103530b.

Xie, S., Pan, B., Wang, M., Zhu, L., Wang, F., Dong, Z., Wang, X. and Zhou, W. (2010) 'Formulation, characterization and pharmacokinetics of praziquantel-loaded hydrogenated castor oil solid lipid nanoparticles', *Nanomedicine (Lond)*, 5(5), pp. 693–701. doi: 10.2217/NNM.10.42.

Xin, H., Sha, X., Jiang, X., Zhang, W., Chen, L. and Fang, X. (2012) 'Anti-glioblastoma efficacy and safety of paclitaxel-loading Angiopep-conjugated dual targeting PEG-PCL nanoparticles', *Biomaterials*, 33(32), pp. 8167–8176. doi: 10.1016/j.biomaterials.2012.07.046.

Xu, Z., Chen, L., Gu, W., Gao, Y., Lin, L., Zhang, Z., Xi, Y. and Li, Y. (2009) 'The performance of docetaxel-loaded solid lipid nanoparticles targeted to hepatocellular carcinoma', *Biomaterials*, 30(2), pp. 226–232. doi: 10.1016/j.biomaterials.2008.09.014.

Yamini, D., Devanand Venkatasubbu, G., Kumar, J. and Ramakrishnan, V. (2014) 'Raman scattering studies on PEG functionalized hydroxyapatite nanoparticles', *Spectrochimica Acta - Part A: Molecular and Biomolecular Spectroscopy*. Elsevier B.V., 117, pp. 299–303. doi: 10.1016/j.saa.2013.07.064.

Yang, J. and Hu, J. (2015) 'Aptamer-functionalized nanoparticles for targeted drug delivery in cancer therapy', *European Journal of BioMedical Research*, 1(3), pp. 17–24. doi: 10.18088/ejbmr.1.3.2015.pp17-24.

Yang, Y. F., Xu, W., Song, W., Ye, M. and Yang, X. W. (2015) 'Transport of twelve coumarins from Angelicae Pubescentis Radix across a MDCK-pHaMDR cell monolayer - An in vitro model for blood-brain barrier permeability', *Molecules*, 20(7), pp. 11719–11732. doi: 10.3390/molecules200711719.

Yin, Y. M., Cui, F. De, Mu, C. F., Choi, M. K., Kim, J. S., Chung, S. J., Shim, C. K. and Kim, D. D. (2009) 'Docetaxel microemulsion for enhanced oral bioavailability: Preparation and in vitro and in vivo evaluation', *Journal of Controlled Release*, 140(2), pp. 86–94. doi: 10.1016/j.jconrel.2009.08.015.

Yingchoncharoen, P., Kalinowski, D. S. and Richardson, D. R. (2016) 'Lipid-Based Drug Delivery Systems in Cancer Therapy: What Is Available and What Is Yet to Come', *Pharmacological Reviews*, 68(3), pp. 701–787. doi: 10.1124/pr.115.012070.

Yoon, G., Park, J. W. and Yoon, I.-S. (2013) 'Solid lipid nanoparticles (SLNs) and nanostructured lipid carriers (NLCs): recent advances in drug delivery', *Journal of Pharmaceutical Investigation*, 43(5), pp. 353–362. doi: 10.1007/s40005-013-0087-y.

Youns, M., Hoheisel, J. D. and Efferth, T. (2011) 'Therapeutic and diagnostic applications of nanoparticles', *Current Drug Targets*, 12(3), pp. 357–365. Available at: http://www.scopus.com/inward/record.url?eid=2-s2.0-79551623194&partnerID=40&md5=2db5896b74cd1d6d3447a34a56622fbf.

Yuan, F., Dellian, M., Fukumura, D., Leunig, M., Berk, D. A., Torchilin, V. P. and Jain, R. K. (1995) 'Vascular permeability in a human tumor xenograft: Molecular size dependence and cutoff size', *Cancer Research*, 55(17), pp. 3752–3756.

Yuan, H., Miao, J., Du, Y. Z., You, J., Hu, F. Q. and Zeng, S. (2008) 'Cellular uptake of solid lipid nanoparticles and cytotoxicity of encapsulated paclitaxel in A549 cancer cells', *International Journal of Pharmaceutics*, 348(1–2), pp. 137–145. doi: 10.1016/j.ijpharm.2007.07.012.

Ze, Y., Zheng, L., Zhao, X., Gui, S., Sang, X., Su, J., Guan, N., Zhu, L., Sheng, L., Hu, R., Cheng, J., Cheng, Z., Sun, Q., Wang, L. and Hong, F. (2013) 'Molecular mechanism of titanium dioxide nanoparticles-induced oxidative injury in the brain of mice', *Chemosphere*, 92(9), pp. 1183–1189. doi: 10.1016/j.chemosphere.2013.01.094.

Zhang, J., Fan, Y. and Smith, E. (2009) 'Experimental design for the optimization of lipid nanoparticles', *Journal of Pharmaceutical Sciences*, 98(5), pp. 1813–1819. doi: 10.1002/jps.21549.

Zhang, L. and Zhang, N. (2013) 'How nanotechnology can enhance docetaxel therapy', *International Journal of Nanomedicine*, pp. 2927–2941. doi: 10.2147/IJN.S46921.

Zhang, S., Guan, J., Sun, M., Zhang, D., Zhang, H., Sun, B., Guo, W., Lin, B., Wang, Y., He, Z., Luo, C. and Sun, J. (2017) 'Self-delivering prodrug-nanoassemblies fabricated by disulfide bond bridged oleate prodrug of docetaxel for breast cancer therapy', *Drug delivery*. Informa Healthcare USA, Inc, 24(1), pp. 1460–1469. doi: 10.1080/10717544.2017.1381201

Zhang, S., Guan, J., Sun, M., Zhang, D., Zhang, H., Sun, B., Guo, W., Lin, B., Wang, Y., He, Z., Luo, C., Sun, J., Tan, L., Peng, J., Zhao, Q., Zhang, L., Tang, X., Chen, L., Lei, M. and Qian, Z. (2017) 'A novel MPEG-PDLLA-PLL copolymer for docetaxel delivery in breast cancer therapy’, *Drug delivery*. Informa Healthcare USA, Inc, 24(1), pp. 1460–1469. doi: 10.1080/10717544.2017.1381201.

Zhang, X. X., Eden, H. S. and Chen, X. (2012) ‘Peptides in cancer nanomedicine: Drug carriers, targeting ligands and protease substrates’, *Journal of Controlled Release*, pp. 2–13. doi: 10.1016/j.jconrel.2011.10.023.

Zhang, Y., Hong, H. and Cai, W. (2011) ‘Tumor-targeted drug delivery with aptamers.’, *Current medicinal chemistry*, 18(27), pp. 4185–94. doi: 10.2174/092986711797189547.

Zhou, J. and Rossi, J. J. (2011) ‘Cell-specific aptamer-mediated targeted drug delivery.’, *Oligonucleotides*, 21(1), pp. 1–10. doi: 10.1089/oli.2010.0264.

Zhuang, C., Li, N., Wang, M., Zhang, X., Pan, W., Peng, J., Pan, Y. and Tang, X. (2010) ‘Preparation and characterization of vinpocetine loaded nanostructured lipid carriers (NLC) for improved oral bioavailability’, *International Journal of Pharmaceutics*. Elsevier B.V., 394(1–2), pp. 179–185. doi: 10.1016/j.ijpharm.2010.05.005.

Zirak, M. B. and Pezeshki, A. (2015) ‘Effect of Surfactant Concentration on the Particle Size, Stability and Potential Zeta of Beta carotene Nano Lipid Carrier’, *International Journal of Current Microbiology and Applied Sciences*, 4(9), pp. 924–932.

Zlokovic, B. V. (2008) ‘The Blood-Brain Barrier in Health and Chronic Neurodegenerative Disorders’, *Neuron*, pp. 178–201. doi: 10.1016/j.neuron.2008.01.003.

Zou, L., Tao, Y., Payne, G., Do, L., Thomas, T., Rodriguez, J. and Dou, H. (2016) ‘Targeted delivery of nano-PTX to the brain tumor-associated macrophages.’, *Oncotarget*, 8(4), pp. 6564–6578. doi: 10.18632/oncotarget.14169.

Zupančič, E., Curato, C., Paisana, M., Rodrigues, C., Porat, Z., Viana, A. S., Afonso, C. A. M., Pinto, J., Gaspar, R., Moreira, J. N., Satchi-Fainaro, R., Jung, S. and Florindo, H. F. (2017) ‘Rational design of nanoparticles towards targeting antigen-presenting cells and improved T cell priming’, *Journal of Controlled Release*, 258, pp. 182–195. doi: 10.1016/j.jconrel.2017.05.014.

Appendix

- **Appendix I**
- TGA thermographs

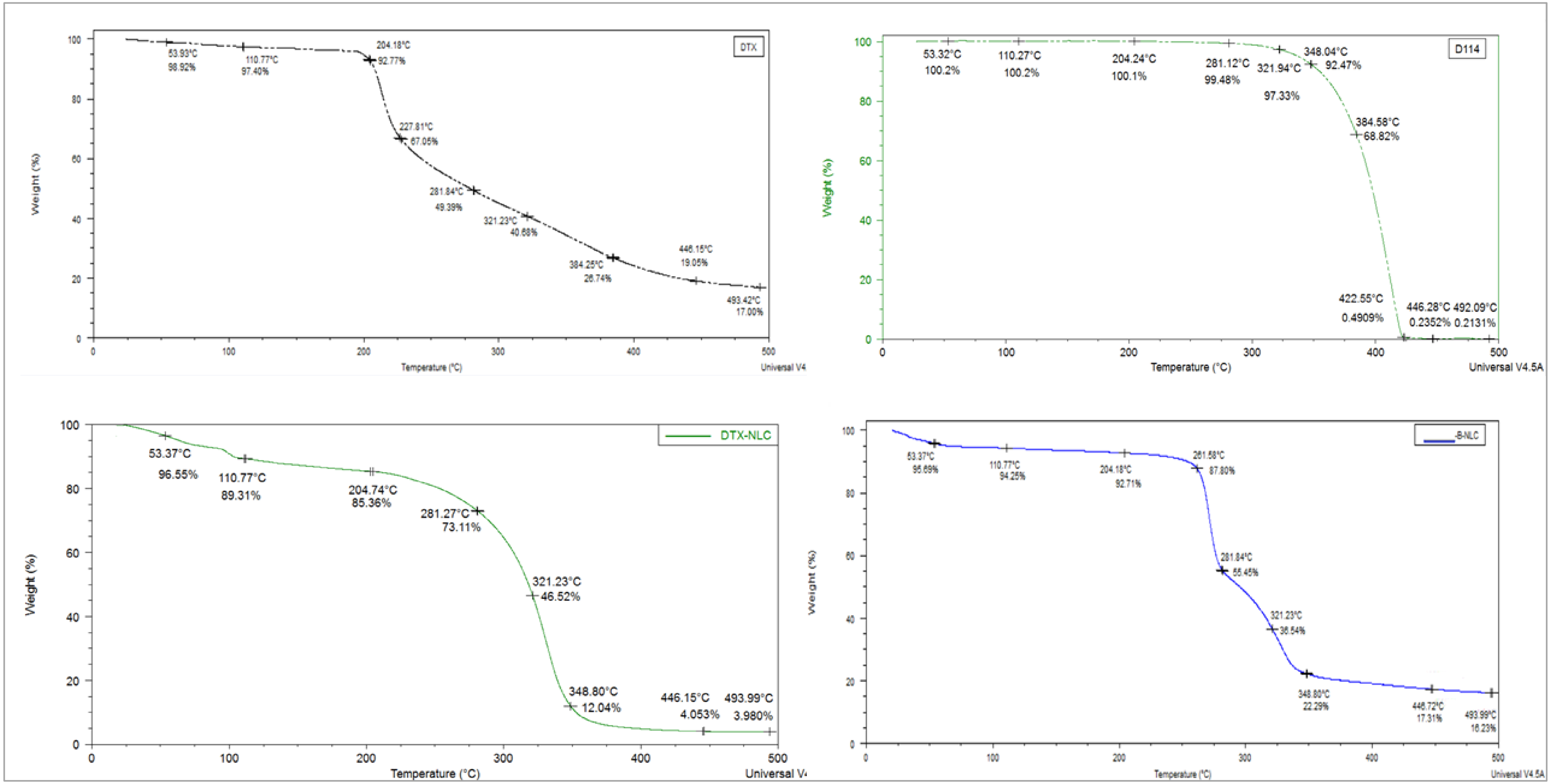

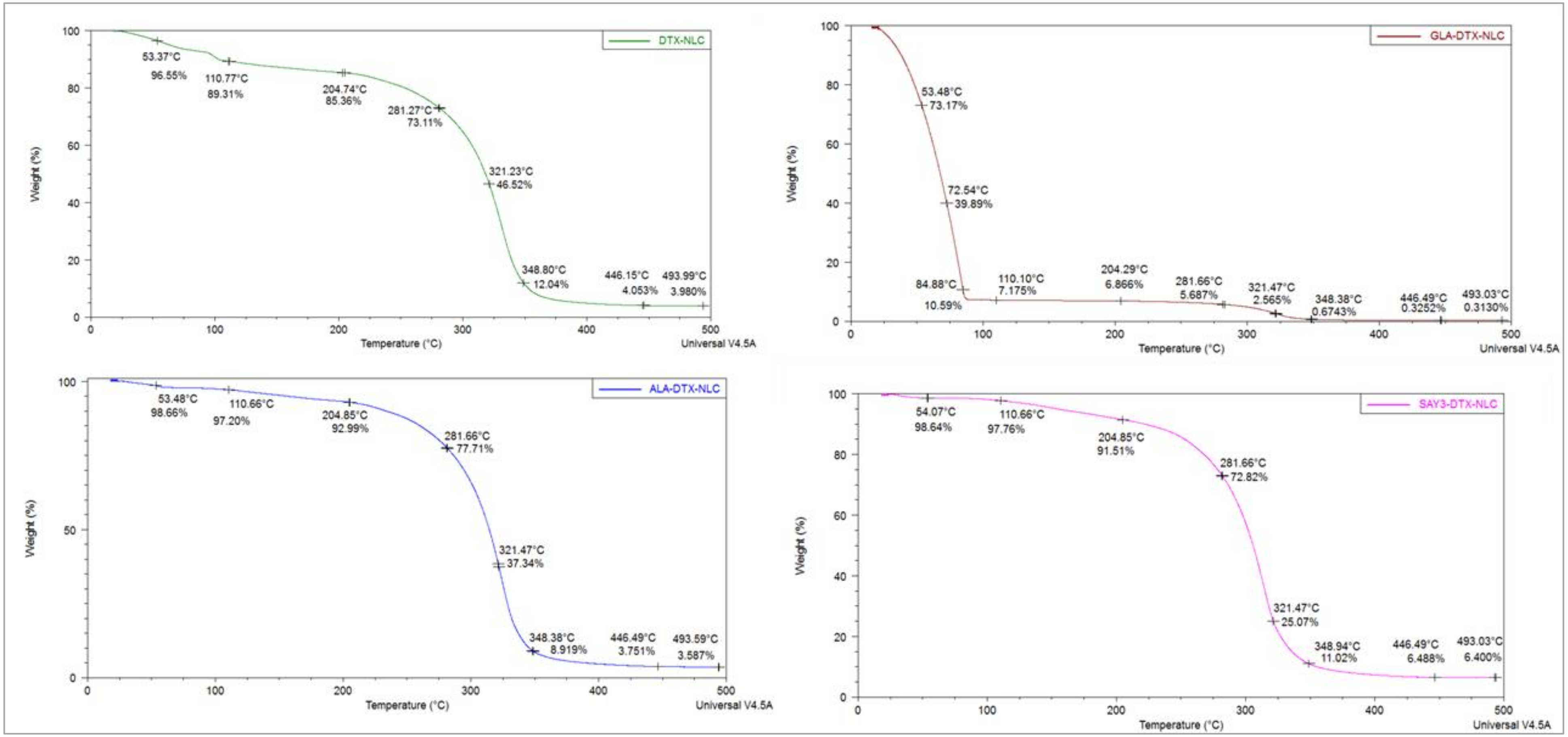
DTX-NLC
53.37°C
96.55%
110.77°C
89.31%
204.74°C
85.36%
281.27°C
73.11%
321.23°C
46.52%
348.80°C
12.04%
446.15°C
4.053%
493.99°C
3.980%
GLA-DTX-NLC
53.48°C
73.17%
72.54°C
39.89%
84.88°C
10.59%
110.10°C
7.175%
204.29°C
6.866%
281.66°C
5.687%
321.47°C
2.565%
348.38°C
0.6743%
446.49°C
0.3252%
493.03°C
0.3130%
ALA-DTX-NLC
53.48°C
98.66%
110.66°C
97.20%
204.85°C
92.99%
281.66°C
77.71%
321.47°C
37.34%
348.38°C
8.919%
446.49°C
3.751%
493.59°C
3.587%
SAY3-DTX-NLC
54.07°C
98.64%
110.66°C
97.76%
204.85°C
91.51%
281.66°C
72.82%
321.47°C
25.07%
348.94°C
11.02%
446.49°C
6.488%
493.03°C
6.400%
Weight (%)
Temperature (°C)
Universal V4.5A
0
20
40
50
60
80
100
200
300
400
500

- **FTIR spectrum**

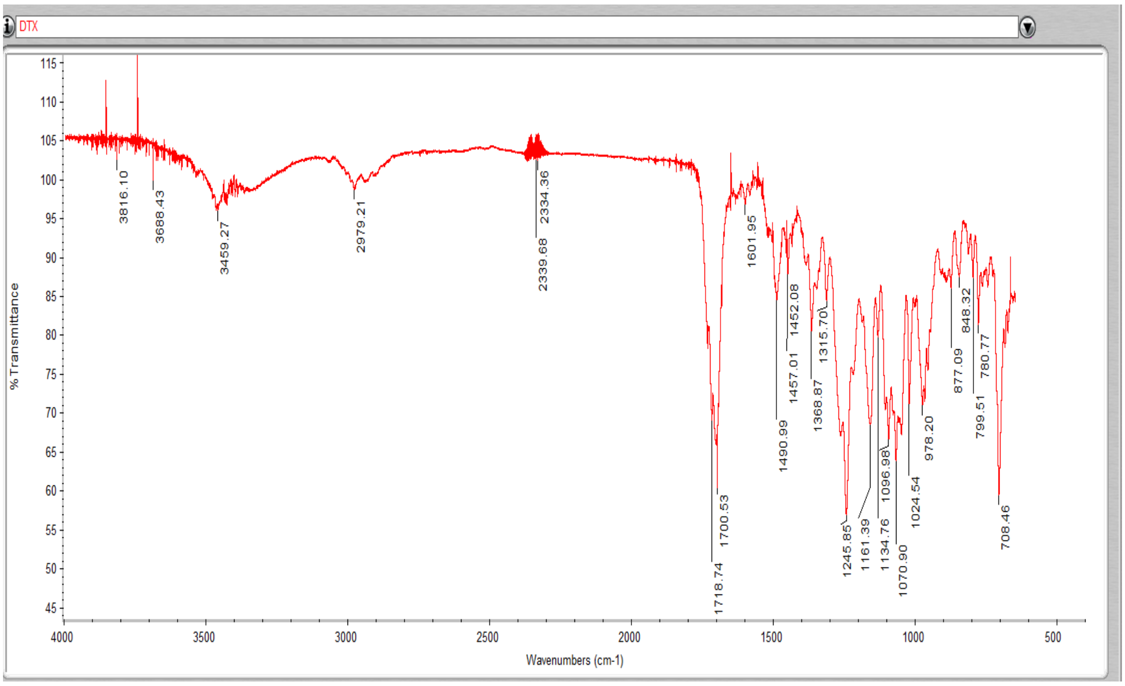

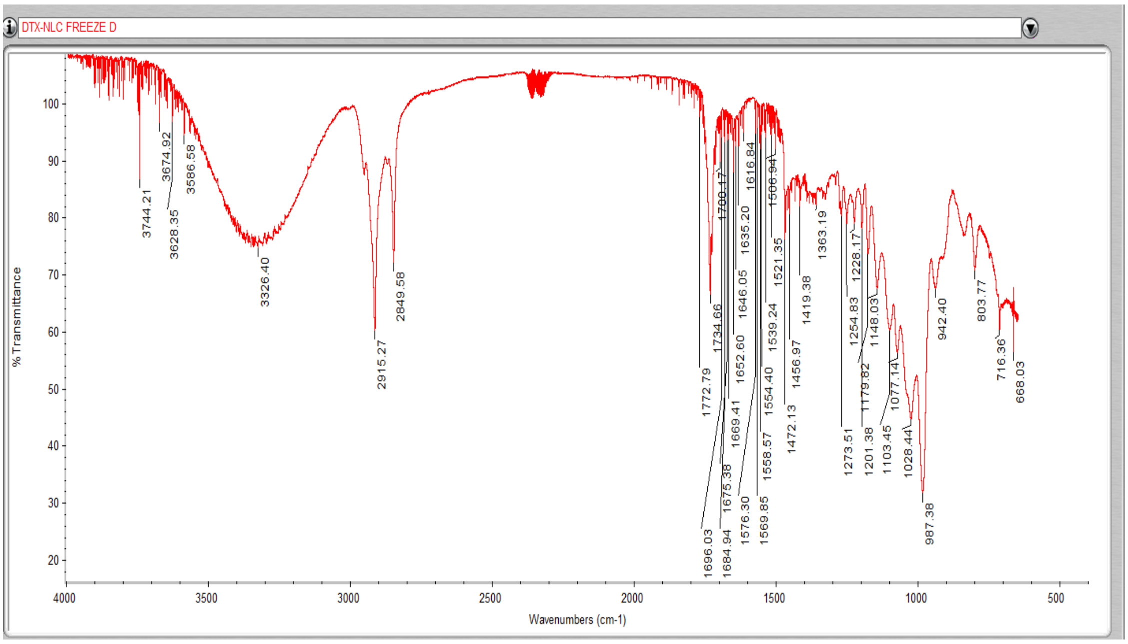

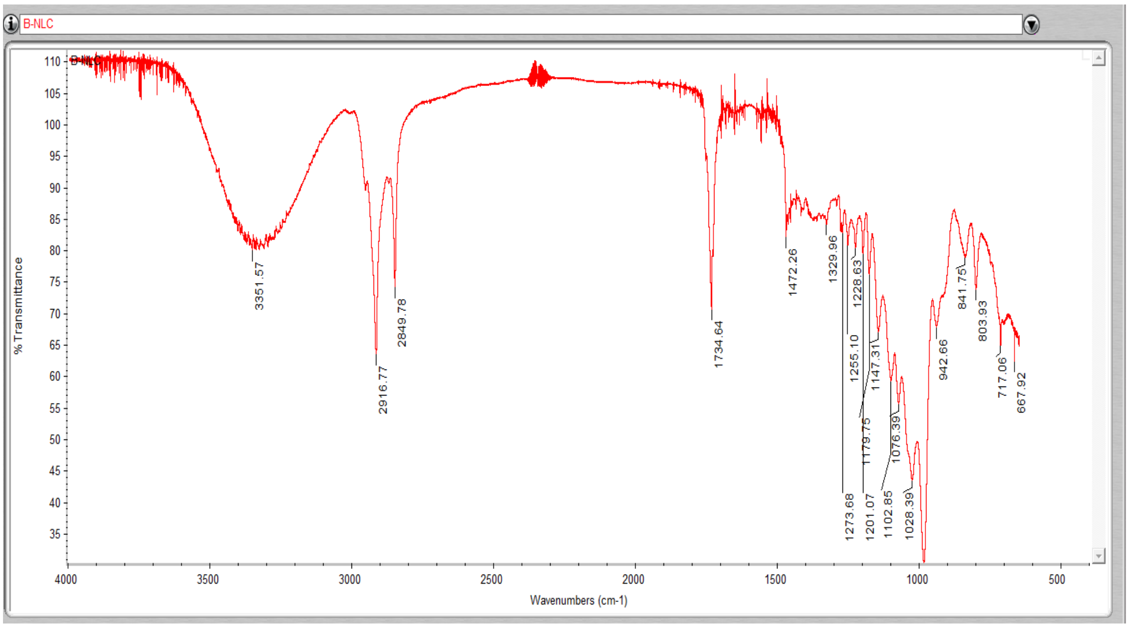
B-NLC
% Transmittance
Wavenumbers (cm-1)
110
105
100
95
90
85
80
75
70
65
60
55
50
45
40
35
4000
3500
3000
2500
2000
1500
1000
500
3351.57
2916.77
2849.78
1734.64
1472.26
1329.96
1273.68
1255.10
1228.63
1201.07
1179.75
1147.31
1102.85
1076.39
1028.39
942.66
841.75
803.93
717.06
667.92

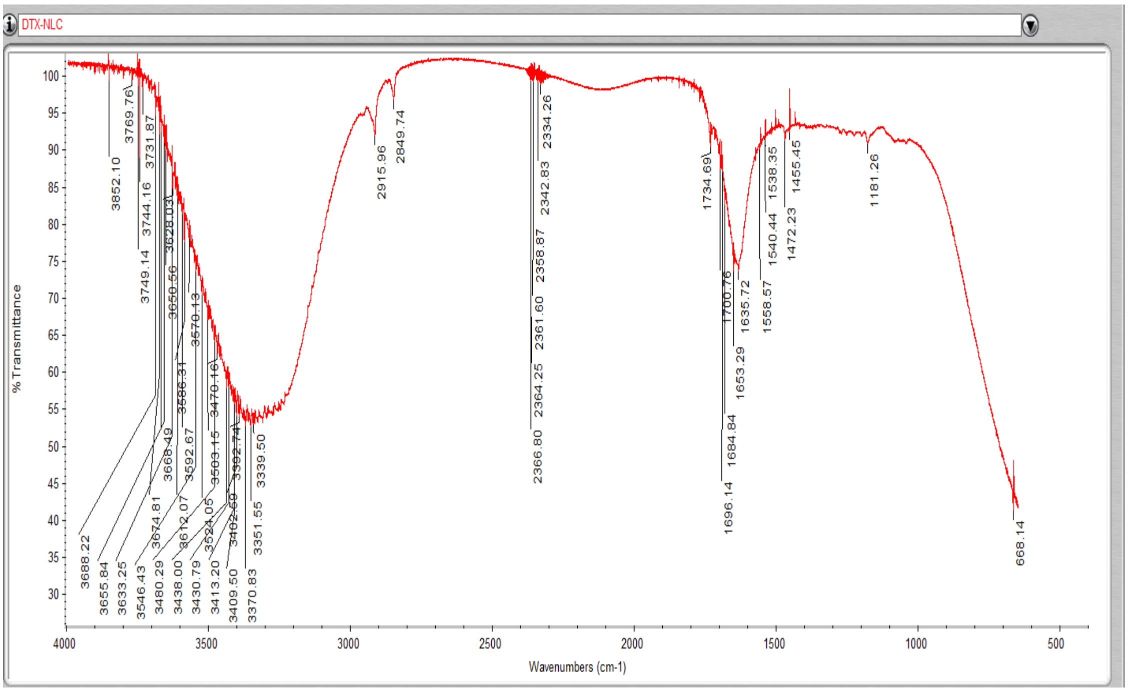
DTX-NLC
% Transmittance
Wavenumbers (cm-1)
100
95
90
85
80
75
70
65
60
55
50
45
40
35
30
4000
3500
3000
2500
2000
1500
1000
500
3852.10
3769.76
3749.14
3744.16
3731.87
3688.22
3674.81
3668.49
3655.84
3650.56
3633.25
3628.03
3612.07
3592.67
3586.31
3570.13
3546.43
3524.05
3503.15
3480.29
3470.16
3438.00
3430.79
3413.20
3409.50
3402.59
3392.74
3370.83
3351.55
3339.50
2915.96
2849.74
2366.80
2364.25
2361.60
2358.87
2342.83
2334.26
1734.69
1700.76
1696.14
1684.84
1653.29
1635.72
1558.57
1540.44
1538.35
1472.23
1455.45
1181.26
668.14

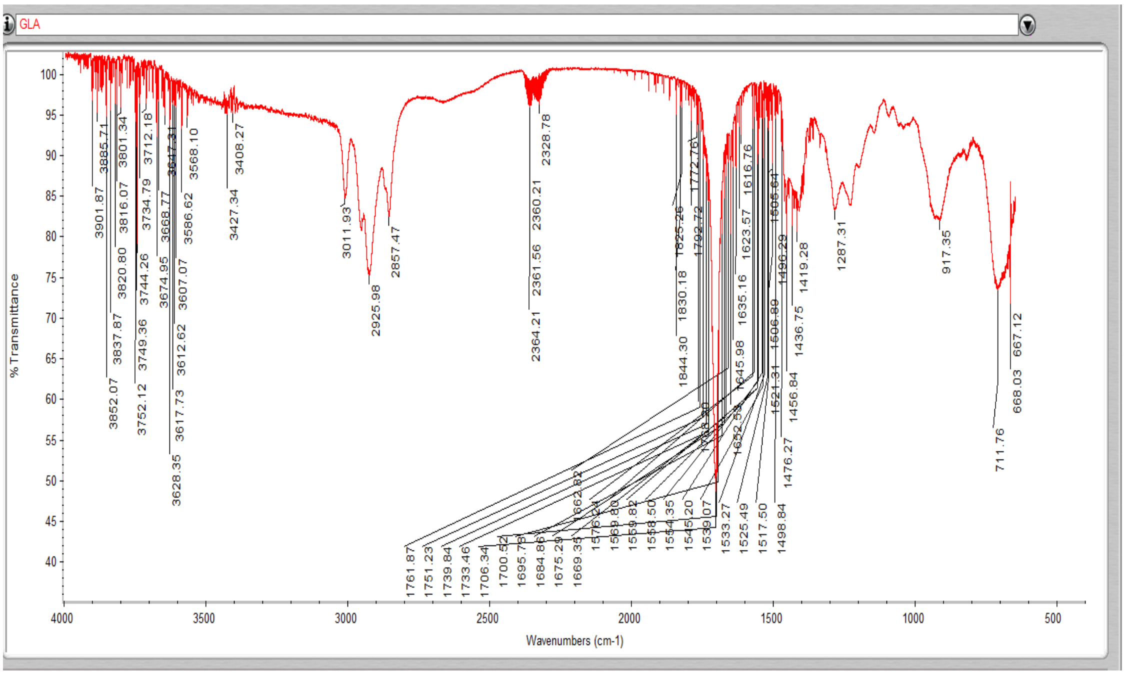
GLA
% Transmittance
Wavenumbers (cm-1)
4000
3500
3000
2500
2000
1500
1000
500
100
95
90
85
80
75
70
65
60
55
50
45
40
3901.87
3885.71
3852.07
3837.87
3820.80
3816.07
3801.34
3752.12
3749.36
3744.26
3734.79
3712.18
3674.95
3668.77
3647.31
3628.35
3617.73
3612.62
3607.07
3586.62
3568.10
3427.34
3408.27
3011.93
2925.98
2857.47
2364.21
2361.56
2360.21
2328.78
1844.30
1830.18
1825.26
1792.72
1772.76
1761.87
1751.23
1739.84
1733.46
1706.34
1700.52
1695.78
1684.86
1675.29
1669.35
1662.82
1645.98
1635.16
1623.57
1616.76
1576.24
1569.80
1559.82
1558.50
1554.35
1545.20
1539.07
1533.27
1525.49
1521.31
1517.50
1506.89
1505.64
1498.84
1496.29
1476.27
1456.84
1436.75
1419.28
1287.31
917.35
711.76
668.03
667.12

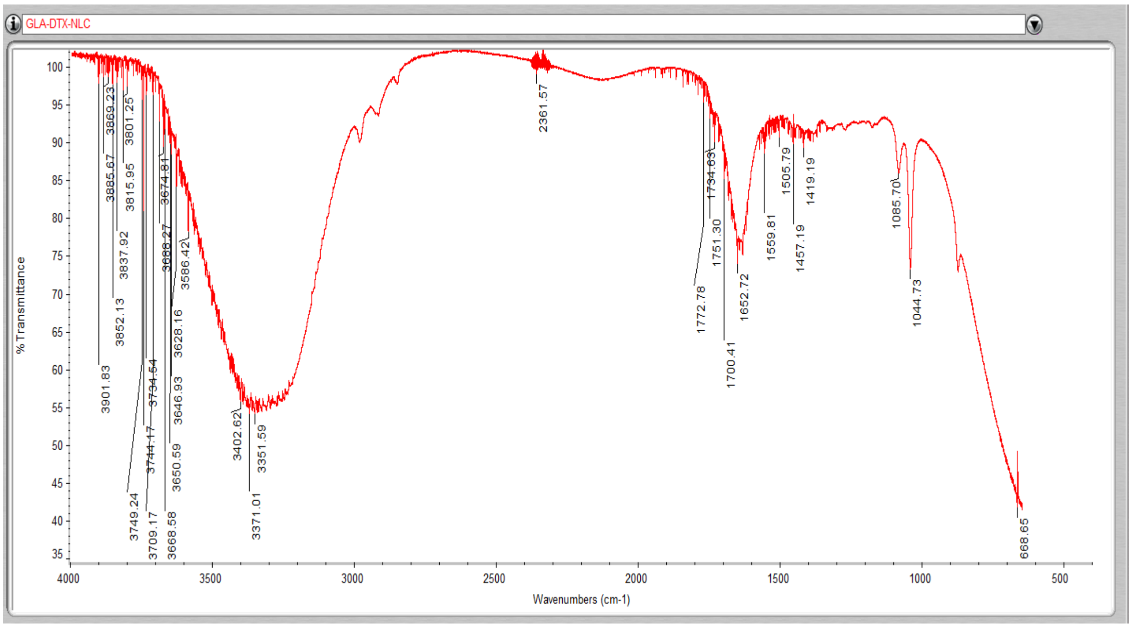
GLA-DTX-NLC
% Transmittance
Wavenumbers (cm-1)
4000
3500
3000
2500
2000
1500
1000
500
100
95
90
85
80
75
70
65
60
55
50
45
40
35
3901.83
3885.67
3869.23
3852.13
3837.92
3815.95
3801.25
3749.24
3744.17
3734.54
3709.17
3688.27
3674.81
3668.58
3650.59
3646.93
3628.16
3586.42
3402.62
3371.01
3351.59
2361.57
1772.78
1751.30
1734.63
1700.41
1652.72
1559.81
1505.79
1457.19
1419.19
1085.70
1044.73
668.65

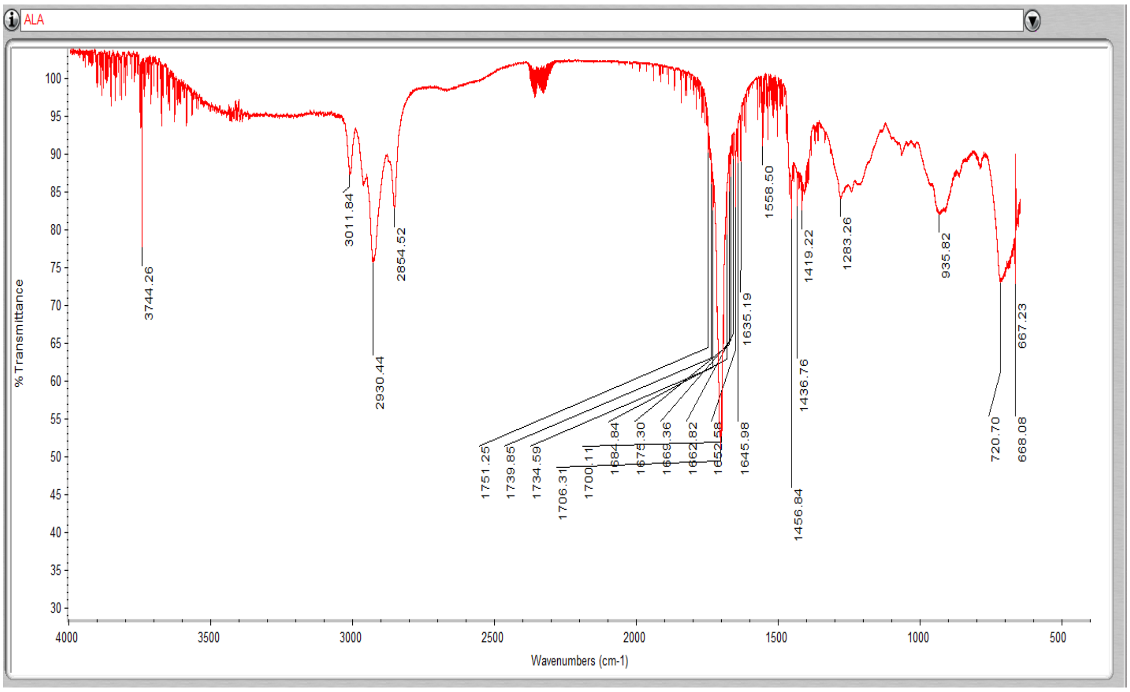
ALA
% Transmittance
100
95
90
85
80
75
70
65
60
55
50
45
40
35
30
4000
3500
3000
2500
2000
1500
1000
500
Wavenumbers (cm-1)
3744.26
3011.84
2930.44
2854.52
1751.25
1739.85
1734.59
1706.31
1700.11
1684.84
1675.30
1669.36
1662.82
1652.58
1645.98
1635.19
1558.50
1456.84
1436.76
1419.22
1283.26
935.82
720.70
668.08
667.23

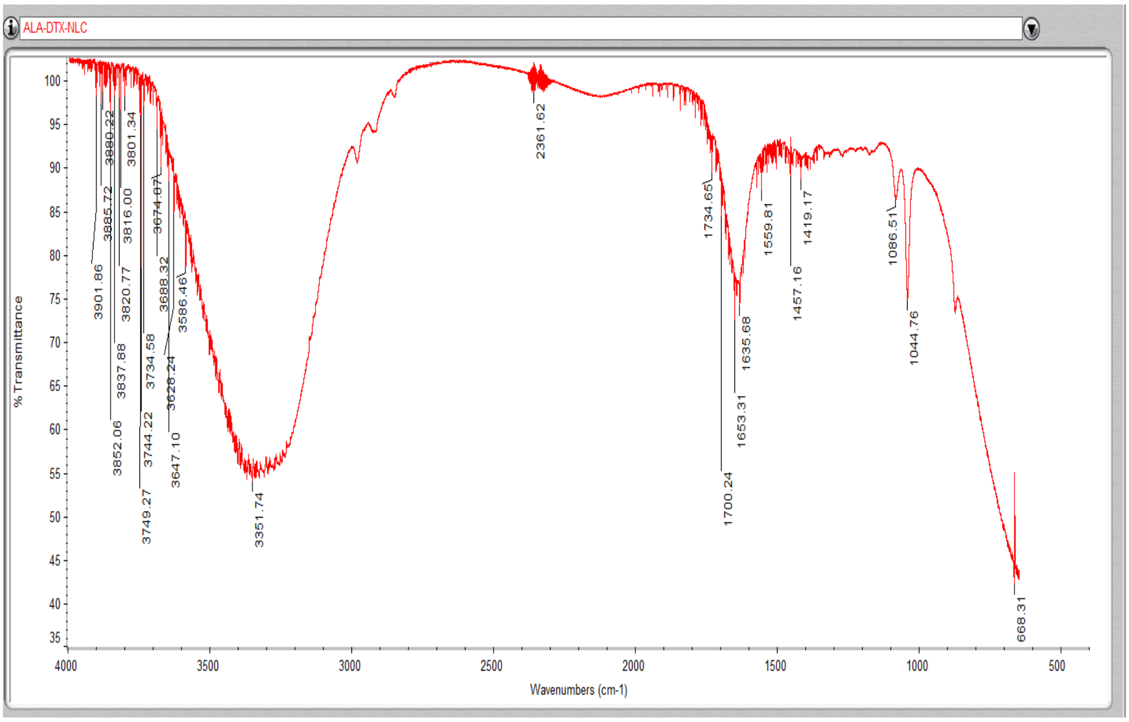
ALA-DTX-NLC
% Transmittance
100
95
90
85
80
75
70
65
60
55
50
45
40
35
4000
3500
3000
2500
2000
1500
1000
500
Wavenumbers (cm-1)
3901.86
3885.72
3880.22
3852.06
3837.88
3820.77
3816.00
3801.34
3749.27
3744.22
3734.58
3688.32
3674.07
3647.10
3628.24
3586.46
3351.74
2361.62
1734.65
1700.24
1653.31
1635.68
1559.81
1457.16
1419.17
1086.51
1044.76
668.31

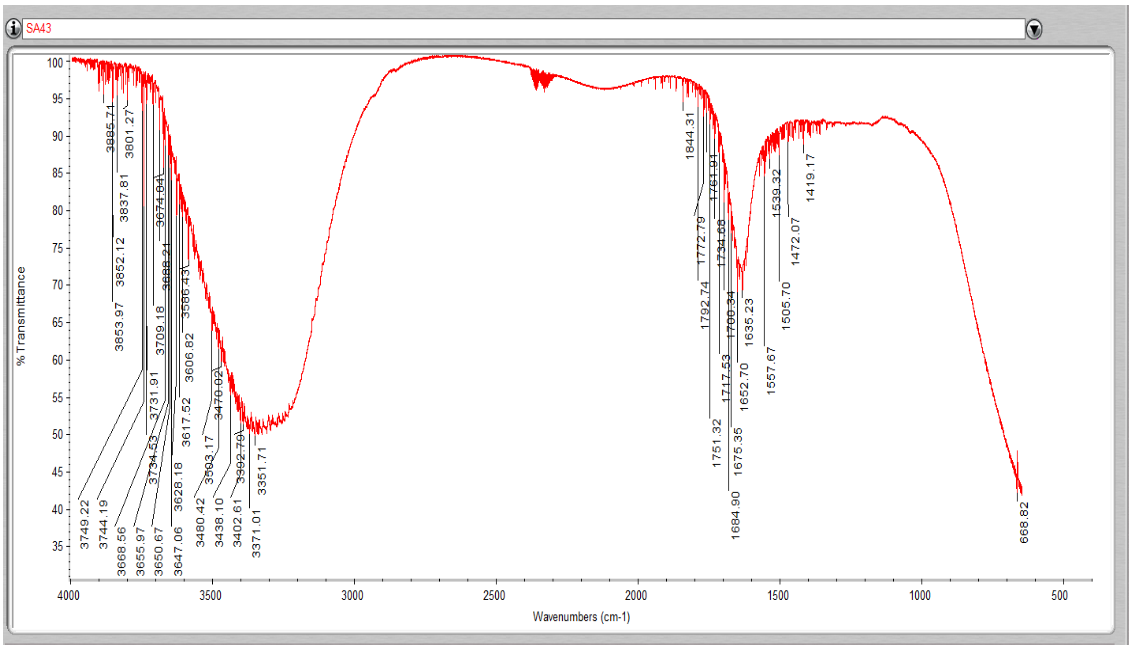
SA43
% Transmittance
100
95
90
85
80
75
70
65
60
55
50
45
40
35
3885.71
3801.27
3837.81
3852.12
3853.97
3674.04
3688.21
3709.18
3586.43
3606.82
3731.91
3617.52
3734.53
3628.18
3503.17
3470.02
3392.70
3351.71
3749.22
3744.19
3668.56
3655.97
3650.67
3647.06
3480.42
3438.10
3402.61
3371.01
1844.31
1761.91
1772.79
1734.68
1792.74
1700.34
1635.23
1717.53
1652.70
1751.32
1675.35
1684.90
1539.32
1419.17
1472.07
1505.70
1557.67
668.82
4000
3500
3000
2500
2000
1500
1000
500
Wavenumbers (cm-1)

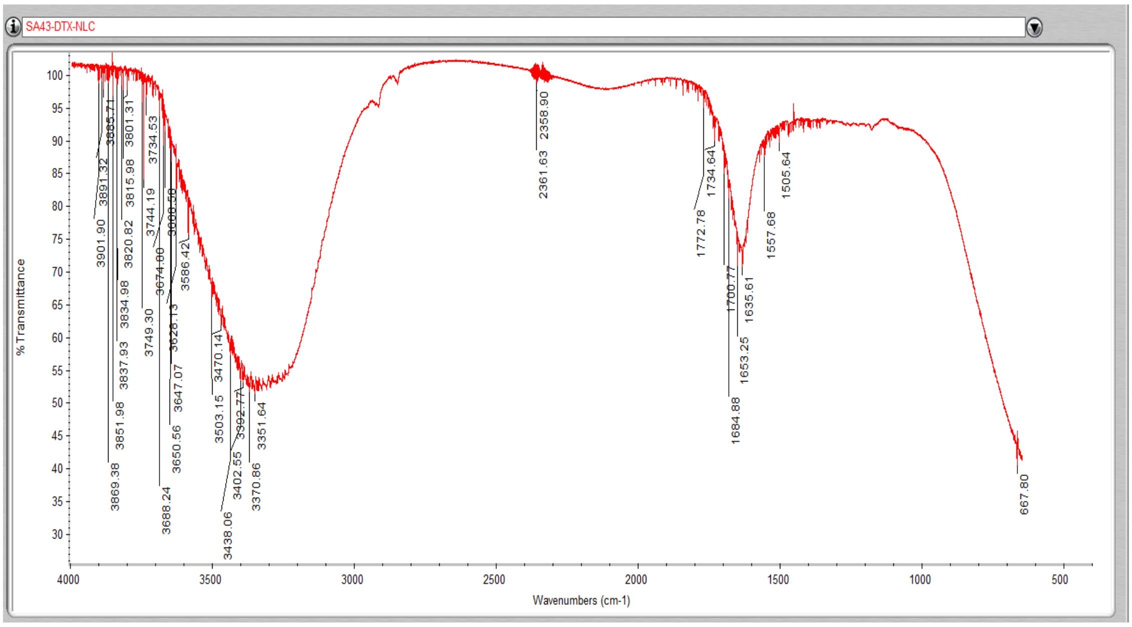
SA43-DTX-NLC
% Transmittance
100
95
90
85
80
75
70
65
60
55
50
45
40
35
30
3885.71
3891.32
3801.31
3815.98
3734.53
3901.90
3820.82
3744.19
3660.50
3674.00
3586.42
3834.98
3749.30
3628.13
3837.93
3470.14
3647.07
3851.98
3503.15
3392.77
3351.64
3650.56
3402.55
3869.38
3370.86
3688.24
3438.06
2358.90
2361.63
1734.64
1772.78
1700.77
1635.61
1653.25
1684.88
1505.64
1557.68
667.80
4000
3500
3000
2500
2000
1500
1000
500
Wavenumbers (cm-1)

- **Appendix II**

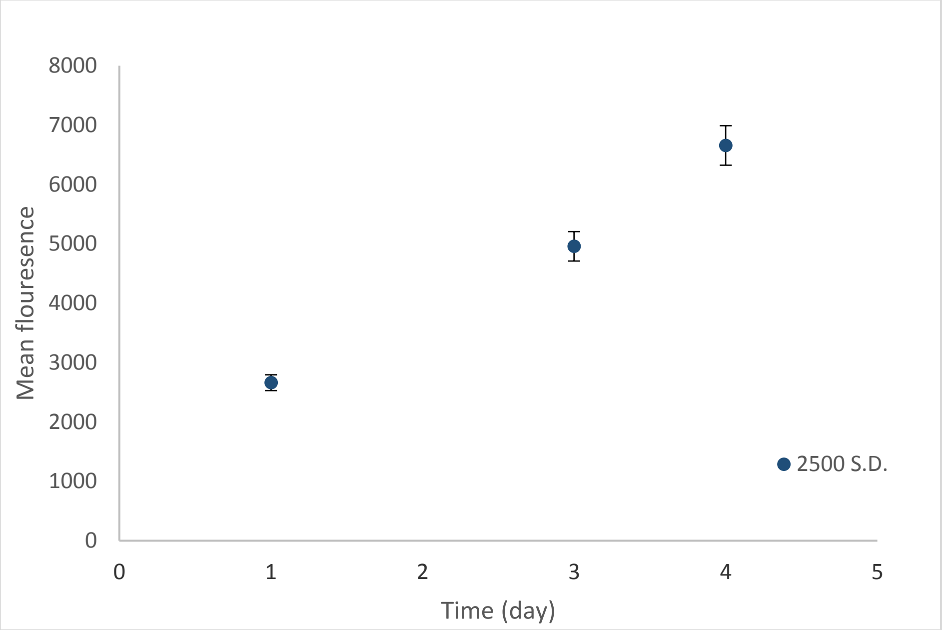

(a) U87MG cell line

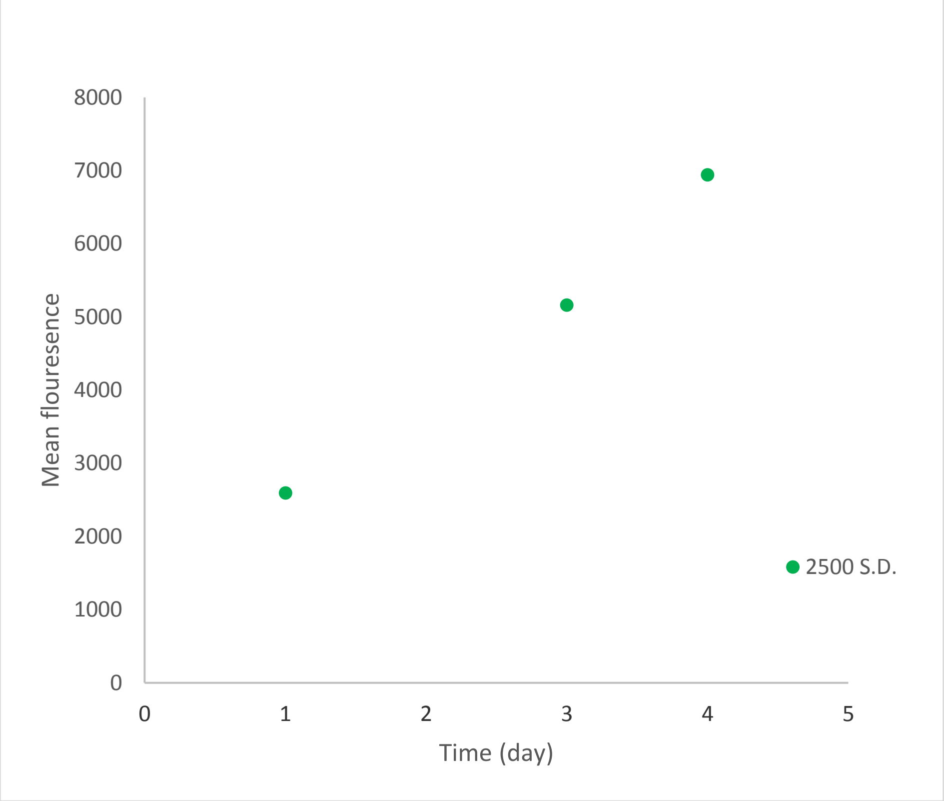

(b) SVG P12

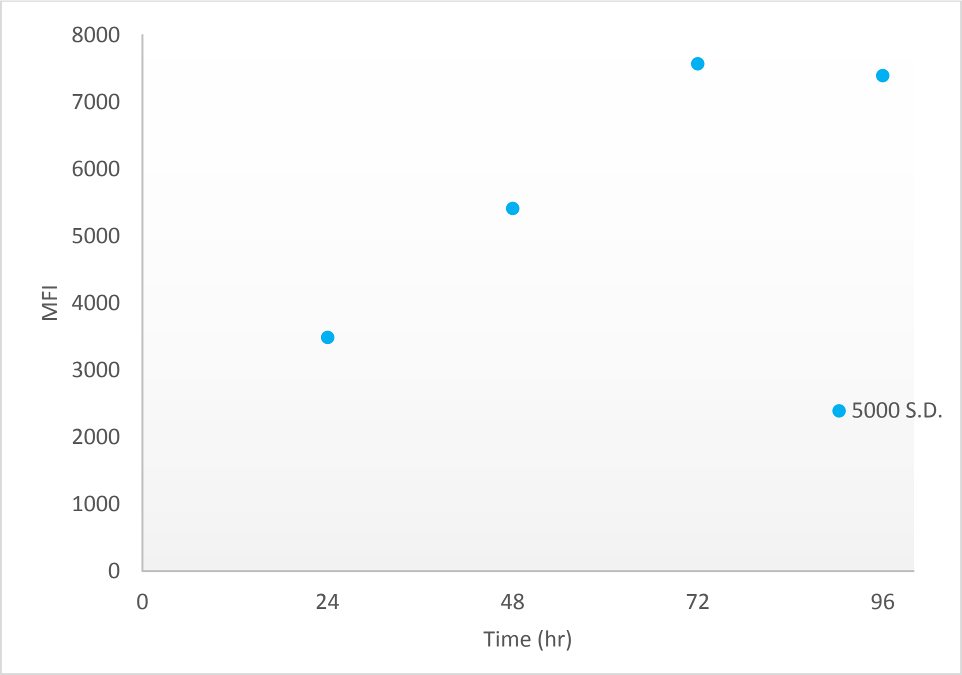

(c) BTNW911 cell line

Application for clinical samples/data from the Brain Tumour North West and the Walton Research Tissue Banks

Applicant: Duration of Project: 1 Year

Name: Tamara Akeel Abdulmunim Zwain

Address: UCLAN, Preston UK, PR1 2HE

Tel: 00447476005501
Email: taazwain@uclan.ac.uk

Student

Project Title: Developing Docetaxel lipid Nano-particle and Functionalised Lipid Nano-Particles Formulations for targeting brain tumours

Is the application for samples to support the project being made to:
Brain Tumour North West (BTNW) Tissue Bank / **Walton Research Tissue Bank (WRTB) / Joint application to both banks** (*delete as required*)

Funding:
Is the funding for the project a) external (eg funded through a grant application)
b) internal (eg funded from a researchers laboratory or institutional budget)
c) other *(please give details)*
C) Self-funded project

If the project has been submitted as a grant application for external funding?
Was the application successful? Yes / no
Was the project externally peer-reviewed? Yes / no

External Funding body: None

Details of Funding: Total £ …………… (staff …………………and consumables …………)

Research Sponsor: *Self-funded project*

Approvals:
Ethics Approval
Does the project have ethics approval? No
If yes, please supply reference number ……………….and date of approval …………..

Both Tissue Banks have generic ethical approval to supply tissue/data for projects conducted by internal applicants, without the need for further ethics approval. External researchers wishing to use tissue or data supplied by the bank need to apply to REC for individual ethical approval.

Research Governance

a) Are the applicants employed by NHS establishment(s)? no

b) Does the project involve research activity using the anonymised samples/data in an NHS establishment? no

If yes to a or b, the project may require research governance approval and applicants should consult the Research Governance Manager at their hospital

Co-applicants: **Name** **Affiliation**

Not applicable

Outline of Project

Please give a brief outline of the project under the headings below (not more than 1-3 A4 pages) or attach the external funding application

Scientific Background

Docetaxel (DTX) is a hydrophobic anticancer drug with poor water solubility and considerable systemic toxicity. This has limited its clinical application. In recent decades, the emergence of nanotechnology has provided new drug delivery systems for DTX, which can improve its water solubility, minimize the side effects and increase the tumour targeting. To improve the therapeutic potential of DTX, this study aims to develop a nanostructured lipid carrier (NLC) of DTX (DTX-NLC) that can pass the blood-brain barrier (BBB) and target glioblastoma (GBM).

Hypothesis and Study Aim

Aims:

1- To test designed DTX-NLC and functionalised DTX-NLCs with short-term culture cells

2- To study the uptake of DTX-NLC and functionalised DTX-NLCs with short-term culture cells

Plan of Project

Conducting Cytotoxicity study and uptake study for designed DTX-NLC and functionalised DTX-NLCs with short-term culture cells

(Number of cases including samples from other banks)

Five

Experimental Methodology,

Cytotoxicity study

To determine the effect of DTX, DTX-NLC, B-NLC, and functionalised DTX-NLCs on short-term culture, cell viability study will be performed. When the cells reached confluency (Figure 7) cells will be seeded at a density of 2500 cells/90 µl/well in a 96-well plate. The cells will then culture for 24 hours prior to drug treatment concentrations (2.5, 5, 10, 25, 50, 100, 250, 500, 1000) ng/ml. Presto Blue® viability reagent will be used to perform the viability assay by adding 10 µl/well of Presto Blue following 24, 48 and 72 hours of incubation of cells treated with the drug to measure the cell viability. Media without any cells was used as a blank and cells and media without a treatment were used as a control. Plate reader (Genios Pro microtiter plate reader, Tecan, Austria) was used for detection of fluorescence response for PrestoBlue at an excitation wavelength of 535 nm and an emission wavelength of 612nm. This experiment was repeated three times and a percentage of mean cell viability will be calculated using the following equation:

% Cell Viability= (fluorescence of each concentration- fluorescence of the blank/ fluorescence of the control- fluorescence of the blank) *100

A 50 % inhibition concentration (IC50) values for DTX, DTX-NLC and B-NLC were obtained and a concentration versus % mean cell viability was plotted using the Prism5 software.

Uptake study

It is proposed to analyse the cellular internalisation mechanism for entry of R123 (Rhodamine 123)-DTX-NLC and functionalised R123-DTX-NLCs into short-term culture using flow cytometry (MERKE). The samples will be incubated at variable time points at concentrations with each cell line and analysed with a Guava Flow software.

Data Analysis and Statistics

Samples will be tested for normality distribution and an SPSS software for statistical analysis will be used. One way ANOVA will be performed on samples depending on a number of groups.

Tissue Required – *Please indicate whether you require paraffin-embedded tissue, fresh frozen tissue, the cellular component of blood, plasma or serum and how many samples you require.*
Primary cells
Five

Please indicate if all samples are required at the start of the project or if further applications for samples will be made in the light of initial findings.
All samples will be needed at the beginning of the project

Please also provide a brief lay summary (maximum 200 words)

Due to previous results (unpublished data) the data have clearly demonstrated the preparation of DTX-NLC and functionalised DTX-NLCs with low particle size and uniform distribution. DTX-NLC and functionalised DTX-NLCs were characterised by high drug content and encapsulation efficiency, which exhibited more potency than DTX solution towards glioma cell lines and safety for non-cancerous cell line. DTX-NLC and functionalised DTX-NLCs have the ability to pass through the in-vitro BBB model and up-taking fast by cancerous cells.

The upcoming plan is to test DTX-NLCs and functionalised Aptamers and linolenic acids with DTX-NLC as potential targeting for brain tumour cells in short-term culture, study viability for all generated NLCs with ligands will be performed and uptake study using flow cytometer on all validated DTX-NLCs and functionalised Aptamers and linolenic acids with DTX-NLC.

For further information please contact:
BTNW Tissue Bank: Prof T Dawson email: Timothy.Dawson@lthtr.nhs.uk
Walton Research Tissue Bank: Dr C Walker email:
carol.walker@thewaltoncentre.nhs.uk

Please email completed applications to:
BTNW Tissue Bank: Prof T Dawson email: Timothy.Dawson@lthtr.nhs.uk
Walton Research Tissue Bank: Dr C Walker email:
carol.walker@thewaltoncentre.nhs.uk
Or to both for joint applications to both banks

For BTNW or WRTB use only:

Date Application Received	29/09/2017
Application Number	1709
Project Title	Developing Docetaxel lipid Nano-particle and Functionalised Lipid Nano-Particles Formulations for targeting brain tumours
Date sent to BTNW/WRTB Review Panel	29/09/2017
Names of Reviewers	Prof T P Dawson Miss E Lekka Dr N Copeland

Decision of BTNW/WRTB Committees	Approve Date: 17/10/2017

Lancashire Teaching Hospitals
NHS Foundation Trust

MATERIAL TRANSFER AGREEMENT

Lancashire Teaching Hospitals NHS Foundation Trust ("the Trust") of Sharoe Green Lane, Fulwood, Preston, PR2 9HT

will provide to: Tamara Akeel Abdulmunim Zwain
of UCLAN , Preston UK, PR1 2HE
School of pharmacy and biomedical sciences

the following material: **Samples from the BTNW tissue bank ("the Material")**
for use in the following application:
Developing Docetaxel lipid Nano-particle and Functionalized Lipid Nano-Particles Formulations for targeting brain tumours
Aims:

1- To test designed DTX-NLC and functionalised DTX-NLCs with short term culture cells
2- To study the uptake of DTX-NLC and functionalised DTX-NLCs with short term culture cells

The Trust is willing to provide the Recipient with **the Material** as described above, and the Recipient is willing to accept the same upon the terms and conditions set forth herein.

NOW, THEREFORE, the parties hereto hereby agree as follows:

1. **The Material** and any Derivatives thereof (including but not limited to recombinant constructs, cultures, subcultures, mutations or other products derived directly or indirectly from **the Material**, referred to herein as the "Derivatives") provided by The Trust remain the property of The Trust.

2. **The Material** furnished to the Recipient pursuant to this agreement and Derivatives thereof will be maintained within the sole possession and control of the Recipient and personnel associated with **the Research**. The Recipient agrees, at the Trust's request, to return or destroy unused supplies of **the Material** and confidential information to The Trust upon the discontinuance, termination or completion of **the Research**.

3. **The Material** furnished to the Recipient will be stored, accessed and processed in accordance with UK legislation relating to the use and storage of human tissue

Purpose:

4. The Recipient shall ensure that **the Material** is used only for **the Research** specified and for no other purpose.

5. **The Material** and Derivatives will not be used in therapy involving humans, and will not be distributed, transferred or sold by the Recipient to any third party for any purposes whatsoever without the prior written agreement of the Trust.

6. **The Material** and any information relating to **the Material** that may be disclosed to the Recipient by the Trust (the "Information") is being provided to and accepted by the recipient with no
representation that the use of the materials will not infringe any patent, copyright, trademark or any other proprietary right and without any warranty of merchantability or fitness for any particular purpose or any other warranty, expressed or implied.

7. The Trust and its employees or agents neither assume responsibility nor accept any liability for any damage, losses or costs (including legal fees) howsoever caused in respect of the Recipient's use of **the Materials** and make no representations in connection with **the Materials** or Derivatives or Information or their use by the Recipient and the Recipient hereby agrees to defend, indemnify and hold harmless the Trust and its employees or agents from and against any liability or claim including third party claims arising from any use of **the Material** or Derivatives by the Recipient.

Intellectual Property Rights:

8. Nothing in this agreement shall operate to transfer title to any Intellectual Property Rights ("IPR") pertaining to **the Materials** to the Recipient.

9. If use of **the Material** hereunder leads to an invention or discovery (whether or not patentable) relating to **the Material** or its Derivatives the Recipient will inform The Trust of the nature of such invention. In the event that arising intellectual property under **the Research** should be exploited by another party and the Recipient receives royalty income from said party under the terms of the third party agreement, then the Recipient shall inform the Trust of the details of such royalty income and shall pay to the Trust a reasonable percentage of such royalty income in relation to the Trust's input to the project.

Publication:

10. In any publication or dissemination of the results arising from the use of **the Material** or its Derivatives the Recipient will make due acknowledgement of its origin where there has been a significant contribution by the Trust.

Confidentiality:

11. The Recipient shall keep confidential any confidential information relating to **the Materials** which is disclosed to it by the Trust pursuant to this agreement. The Recipient shall only use such information for the purposes of **the Research** and shall not disclose it to anyone other than the personnel of the Recipient associated with **the Research**. This term shall not apply to any information which is published by the Trust.

General:

15. This agreement shall be subject to the Laws of England and the parties submit to the exclusive jurisdiction of the English courts.

16. The Contracts (Rights of Third Parties) Act 1999 shall not apply to this Agreement and no person or persons other than Parties to this Agreement shall have any rights under it, nor shall it be enforceable under that Act by any person other than the Parties to it.

Authorised Signatory of the Trust

Signed Date 23 Oct 17

Print Name: **Professor Timothy P. Dawson**
Cellular Pathology Medical
Neuropathology
GMC: 3064236

Authorised Signatory of the Recipient

Signed Date 28th/9/2017

Print Name: Tamara Zwain